frontiers | Research Topics

Global excellence in cellular neuropathology: Ukraine

Edited by
Oleg Krishtal, Elena A. Lukyanetz and Dirk M. Hermann

Coordinated by
Andrii O. Cherninskyi

Published in
Frontiers in Cellular Neuroscience
Frontiers in Physiology

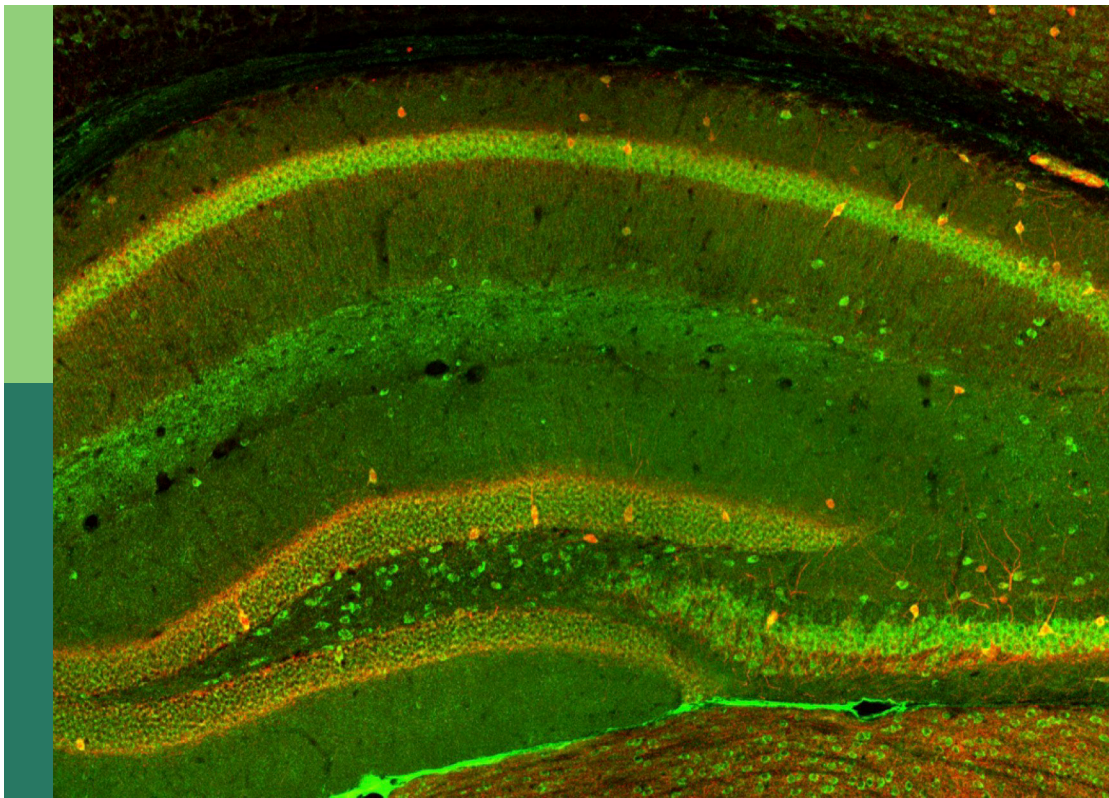

ISSN 1664-8714
ISBN 978-2-8325-4320-7
DOI 10.3389/978-2-8325-4320-7

About Frontiers

Frontiers is more than just an open access publisher of scholarly articles: it is a pioneering approach to the world of academia, radically improving the way scholarly research is managed. The grand vision of Frontiers is a world where all people have an equal opportunity to seek, share and generate knowledge. Frontiers provides immediate and permanent online open access to all its publications, but this alone is not enough to realize our grand goals.

Frontiers journal series

The Frontiers journal series is a multi-tier and interdisciplinary set of open-access, online journals, promising a paradigm shift from the current review, selection and dissemination processes in academic publishing. All Frontiers journals are driven by researchers for researchers; therefore, they constitute a service to the scholarly community. At the same time, the *Frontiers journal series* operates on a revolutionary invention, the tiered publishing system, initially addressing specific communities of scholars, and gradually climbing up to broader public understanding, thus serving the interests of the lay society, too.

Dedication to quality

Each Frontiers article is a landmark of the highest quality, thanks to genuinely collaborative interactions between authors and review editors, who include some of the world's best academicians. Research must be certified by peers before entering a stream of knowledge that may eventually reach the public - and shape society; therefore, Frontiers only applies the most rigorous and unbiased reviews. Frontiers revolutionizes research publishing by freely delivering the most outstanding research, evaluated with no bias from both the academic and social point of view. By applying the most advanced information technologies, Frontiers is catapulting scholarly publishing into a new generation.

What are Frontiers Research Topics?

Frontiers Research Topics are very popular trademarks of the *Frontiers journals series*: they are collections of at least ten articles, all centered on a particular subject. With their unique mix of varied contributions from Original Research to Review Articles, Frontiers Research Topics unify the most influential researchers, the latest key findings and historical advances in a hot research area.

Find out more on how to host your own Frontiers Research Topic or contribute to one as an author by contacting the Frontiers editorial office: frontiersin.org/about/contact

Global excellence in cellular neuropathology: Ukraine

Topic editors

Oleg Krishtal — Bogomoletz Institute of Physiology, National Academy of Sciences of Ukraine, Ukraine

Elena A. Lukyanetz — Bogomoletz Institute of Physiology, National Academy of Sciences of Ukraine, Ukraine

Dirk M. Hermann — University of Duisburg-Essen, Germany

Topic Coordinator

Andrii O. Cherninskyi — Bogomoletz Institute of Physiology, National Academy of Sciences of Ukraine, Ukraine

Citation

Krishtal, O., Lukyanetz, E. A., Hermann, D. M., Cherninskyi, A. O., eds. (2024). *Global excellence in cellular neuropathology: Ukraine*. Lausanne: Frontiers Media SA. doi: 10.3389/978-2-8325-4320-7

Table of contents

frontiers | Frontiers in Cellular Neuroscience

TYPE Editorial
PUBLISHED 08 January 2024
DOI 10.3389/fncel.2023.1354398

OPEN ACCESS

EDITED AND REVIEWED BY
Ulises Gomez-Pinedo,
Health Research Institute of Hospital Clínico San Carlos, Spain

*CORRESPONDENCE
Andrii Cherninskyi
✉ andrii.cherninskyi@biph.kiev.ua

RECEIVED 12 December 2023
ACCEPTED 21 December 2023
PUBLISHED 08 January 2024

CITATION
Cherninskyi A, Hermann DM, Lukyanetz E and Krishtal O (2024) Editorial: Global excellence in cellular neuropathology: Ukraine. *Front. Cell. Neurosci.* 17:1354398. doi: 10.3389/fncel.2023.1354398

Editorial: Global excellence in cellular neuropathology: Ukraine

Andrii Cherninskyi[1]*, Dirk M. Hermann[2], Elena Lukyanetz[3] and Oleg Krishtal[1]

[1]Department of Cellular Membranology, Bogomoletz Institute of Physiology, Kyiv, Ukraine, [2]Department of Neurology, University Hospital Essen, University of Duisburg-Essen, Essen, Germany, [3]Department of Biophysics of Ion Channels, Bogomoletz Institute of Physiology, Kyiv, Ukraine

KEYWORDS

hippocampus, epilepsy, blood-brain barrier, Alzheimer's disease, aging, nociception, cerebral ischemia, hypoxia

Editorial on the Research Topic
Global excellence in cellular neuropathology: Ukraine

Cellular neuroscience is crucial for modern biology and medicine as it focuses on understanding the fundamental building blocks of the nervous system — the cells. Insights from cellular neuroscience contribute to our understanding of neurological disorders, brain development, and the mechanisms underlying learning and memory.

This Research Topic aims to show the diversity of modern research in the field of cellular neuroscience focusing on neuropathologies that are conducted in Ukrainian institutions.

Neuroscience in Ukraine has a rich history, dating back to the establishment of St. Volodymyr University (now Taras Shevchenko National University of Kyiv) in 1834. Professor Oleksandr Valter (1818–1889), the head of the university's anatomical theater, made a significant contribution in 1842 by discovering the vasoconstrictor action of sympathetic nerves. Another notable figure from the university is Professor Volodymyr Betz (1834–1894), a globally recognized neurobiologist, anatomist, and histologist (Kushchayev et al., 2012). He is famous for discovering the giant pyramidal neurons of the primary motor cortex, later named Betz cells. Professor Vasyl Chagovets (1873–1941), also from Kyiv University, developed the electrolytic theory of biopotentials. His student, Volodymyr Pravdich-Neminsky (1879–1952), was the first to record electrophysiological potentials from the surface of the intact skull and demonstrated their origin from the brain (Neminsky, 1913). Although he initially termed these waves "electrocerebrogram," Hans Berger later proposed the term "electroencephalogram."

Presently, neuroscience research is conducted in over 30 institutions, with Bogomoletz Institute of Physiology taking a leading role. The Institute's alumni contribute significantly to research institutions worldwide. The development of neuroscience at the Institute is closely tied to Danylo Vorontsov (1886–1965) and his student Platon Kostyuk (1924–2010). In 1975, the world witnessed the first intracellular perfusion (Kostyuk et al., 1975), which allowed the replacement of the cell cytoplasm by an artificial environment, opening new avenues in the study of nerve cell physiology and biophysics. Platon Kostuyk's students and colleagues achieved several groundbreaking milestones, including the discovery of "the receptor for protons" (later named acid-sensing ion channels or ASICs) (Krishtal and Pidoplichko, 1980), the first demonstration of low-threshold calcium currents, which flow through T-channels (Kostyuk et al., 1981), the existence of ionotropic purinoreceptors (P2X) in sensory neurons (Krishtal et al., 1983), and the first recording of the electrical activity of a single nicotinic acetylcholine receptor (Derkach et al., 1987), among others.

In this Research Topic

The hippocampus stands out as one of the most extensively studied brain structures, with numerous papers dedicated to unraveling the properties of its neuronal networks. The study of Shkryl delves into the intricate spatiotemporal characteristics of calcium transients within cultured hippocampal pyramidal neurons. Employing two-dimensional fluorescence microscopy and the ratiometric dye Fura-2, the research unveils depolarization-induced Ca^{2+} transients exhibiting an asynchronous delayed rise in free Ca^{2+} concentration. Notably, diverse cellular regions display distinct resting calcium levels, with the cell nucleus exhibiting significantly lower concentrations compared to the soma, submembrane, and dendritic tree. The paper also sheds light on the different levels of involvement of ryanodine receptors in intracellular Ca^{2+} signaling across various cellular regions. In another paper, Shypshyna et al. investigate the impact of insulin on paired-pulse plasticity at glutamatergic synapses in hippocampal neurons during hyperinsulinemia, often associated with diabetes mellitus. Disruptions in insulin receptor signaling can lead to cognitive disorders linked to impaired synaptic plasticity. Results show that under normoinsulinemia, insulin enhances paired-pulse facilitation by stimulating glutamate release. Conversely, under hypoinsulinemia, insulin exhibits a limited impact on such facilitation parameters, suggesting potential insulin resistance. However, insulin's effect on neurons with paired-pulse depression indicates its capacity to restore normoinsulinemia-like conditions, including the restoration of glutamate release probability to control levels in their synapses. Pendeliuk and Melnick studied the excitatory synchronization of rat hippocampal interneurons (INs) during network activation in an *in vitro* setting. The complex nature of neural tissue has made understanding the mechanisms of INs' electrical activity synchronization challenging. Employing paired patch-clamp recordings in a simplified culture model with intact glutamate transmission, the research elevated network activity using field electric stimulation, akin to afferent processing *in situ*. The obtained data underscores that IN synchronization is primarily initiated and dominated by glutamatergic mechanisms, orchestrating various excitatory means within the neural system to support the process on a wholesale scale.

The research by Savotchenko et al. explores the pivotal role of thrombin in the initiation of early-onset seizures, particularly in the context of blood-brain barrier dysfunction observed in temporal lobe epilepsy. The study replicates the effects of blood-brain barrier disruption effects *in vitro*, examining the impact of modified blood plasma artificial cerebrospinal fluid on hippocampal neuron excitability and the role of thrombin in seizure susceptibility.

A set of papers is dedicated to the Alzheimer's disease (AD). The paper of Hanzha et al. investigates the impact of cerium dioxide nanoparticles (CNPs) on the viability of hippocampal neurons in the modeling of this disease. CNPs, known for their low toxicity and specific redox, antiradical properties, present exciting possibilities for biomedical applications, particularly in neurodegenerative diseases like AD. The results suggest that CNPs in the cultural media significantly reduce the number of dead hippocampal neurons in the presence of Aβ, emphasizing their neuroprotective properties, which may hold promise for the development of new treatments for AD. Yavorsky et al. investigated the influence of amyloid beta (Aβ) on impulse spiking in isolated CA1 hippocampal neurons, addressing one of the AD hallmarks. Findings reveal that Aβ1–42 influences AP generation differently across hippocampal neurons, with a shared effect of enhancing firing responses within a minute of Aβ1–42 application. Overall, the findings imply that prolonged exposure to Aβ1–42 in the cellular environment may lead to neuronal dysfunction due to a sustained increase in AP firing and a predisposition to this process. Amyloidosis was also the subject of the paper by Sokolik and Berchenko. The authors explored the cumulative effect of the action of miR-101 and curcumin encapsulated in a single liposome on a cellular model of AD and found it to be cumulative, which may be used for the development of more effective AD treatment.

Another topic of this Research Topic is dedicated to the aging of the nervous system. The study by Labunets et al. investigates the reactions of various brain cell types to the neurotoxin cuprizone and melatonin treatment in young and aging mice, considering the age-associated changes in inflammatory cells and their potential impact on the response to humoral/endocrine factors like melatonin. The research aims to evaluate changes in brain macrophages, astrocytes, T-cells, neural stem cells, and neurons in cuprizone-treated mice of different ages and assess the effects of exogenous melatonin. The research of Kyryk et al. explores age-related ultrastructural changes in 3D spheroids formed by adipose-derived multipotent mesenchymal stromal cells (ADSCs) from ovariectomized mice, considering the implications for cell therapy, especially in treating nervous system diseases. Their findings hold significance for potential therapeutic applications of ADSCs in treating diseases of the nervous system.

Nociception is also a big topic in Ukrainian neuroscience. Tissue acidification is known to activate primary nociceptors, leading to pain sensation, due to the activation of ASICs. According to Tkachenko et al., diminazene, a well-known antagonist of ASICs, does not suppress pH-induced activation of mechano-insensitive C-fibers. These results suggest that the excitation of afferent nerve terminals induced by mild acidification primarily involves Na^+/H^+ exchangers rather than ASICs. Another nociceptive "player" is the TRPV1 channel which is responsible for the sensation of heat. Petrushenko et al. studied the interplay between them and P2 receptors. The research investigates the dynamics of calcium transients in dorsal root ganglion neurons associated with TRPV1 channel desensitization and the impact of P2 receptor activation on this process. Anesthesia is a way to limit the sensation of pain. General anesthesia, commonly used during surgery, is known to transiently impair gastrointestinal motility, leading to postoperative ileus, which is a multifactorial condition characterized by neuromuscular failure, primarily affecting the small intestine. Despite its prevalence, there is a limited understanding of the underlying mechanisms, resulting in few effective medication options. The paper of Zholos et al. aims to provide a comprehensive overview of TRP channels, calcium signaling, and cholinergic mechanisms in the gut, detailing how general anesthetics negatively impact these processes.

Cerebral ischemia, often associated with circulatory disorders, leads to oxygen-glucose deficiency, disrupting essential pathways of cellular metabolism and causing damage to brain cells.

Mini-review by Lushnikova et al. explores the role of the mechanistic target of rapamycin (mTOR) and α-ketoglutarate signaling in maintaining cellular homeostasis in the brain under ischemic conditions. Another review by Belenichev et al. explores the involvement of heat shock proteins HSP70 in endogenous neuroprotection mechanisms, emphasizing their potential as therapeutic targets. HSP70 functions as intracellular chaperones critical for maintaining cellular proteostasis under various stress conditions. Focusing on cerebral ischemia, the review outlines HSP70's role in preventing mitochondrial dysfunction, apoptosis activation, estrogen receptor desensitization, oxidative/nitrosative stress reduction, and morpho-functional changes in brain cells suggesting the development of neuroprotective agents modulating HSP70 and HIF-1a gene expression.

The impact of hypoxia on retinal ganglion cells and their neurotransmission pathways is the focus of two papers by Dumanska and Veselovsky shedding light on crucial aspects of oxygen deficiency in ocular contexts. The authors focused on the mechanisms underlying hypoxia-induced long-term potentiation of NMDA neurotransmission in the visual retinocollicular pathway and the immediate effects of acute hypoxia on high-voltage-activated calcium currents in cultured retinal ganglion cells. Together, these studies contribute to the understanding of hypoxia-induced alterations in retinal ganglion cells, paving the way for potential interventions in ocular diseases associated with oxygen deficiency.

The study of Lisakovska et al. investigated the intricate interplay between the brain's vitamin D3 auto/paracrine system and glucocorticoid-induced neurotoxicity, aiming to elucidate the relationship between D3 status and the multifaceted disturbances associated with prolonged glucocorticoid therapy. The results highlight the importance of considering vitamin D3 supplementation in mitigating the adverse effects of such therapy on the central nervous system.

Maternal antibiotic administration (MAA) during pregnancy is a common therapeutic intervention, yet its potential impact on the cognitive and neural development of offspring remains poorly understood. Using behavioral, histological, and electron microscopy analyses, Shepilov et al. demonstrated the potential pathological consequences of MAA during specific gestational windows on cognitive behavior and early brain development in the offspring of mice. The study emphasizes the importance of considering the timing of antibiotic exposure during pregnancy in understanding its long-term effects on offspring neurodevelopment.

Finally, the paper by Storozhuk explores the therapeutic potential of cannabidiol (CBD) in treating neurological diseases, emphasizing its neuroprotective, anti-epileptic, anti-inflammatory, anxiolytic, and anti-cancer properties. CBD has gained attention for its clinical use in epilepsy treatment. However, legal restrictions on Cannabis-derived CBD in many countries pose challenges. The study discusses the potential of non-cannabis plants, particularly flax (*Linum usitatissimum*), as a natural CBD source.

Despite the ongoing Russian aggression against Ukraine, the response to the call for papers for this Research Topic exceeded the initial expectations of the editorial team: 19 papers, involving 64 co-authors from Bogomoletz Institute of Physiology, other Ukrainian research institutions, and collaborative institutions worldwide. The number of accepted papers is even greater because some of the submitted manuscripts were transferred to other sections or journals. On behalf of all the authors of this Research Topic, we would like to express our gratitude to Frontiers Media S.A. for supporting Ukrainian science during these challenging times.

Author contributions

AC: Writing—original draft. DH: Project administration, Writing—review & editing. EL: Writing—review & editing. OK: Project administration, Writing—review & editing.

Funding

The author(s) declare that no financial support was received for the research, authorship, and/or publication of this article.

Conflict of interest

The authors declare that the research was conducted in the absence of any commercial or financial relationships that could be construed as a potential conflict of interest.

The author(s) declared that they were an editorial board member of Frontiers, at the time of submission. This had no impact on the peer review process and the final decision.

Publisher's note

References

Derkach, V. A., North, R. A., Selyanko, A. A., and Skok, V. I. (1987). Single channels activated by acetylcholine in rat superior cervical ganglion. *J. Physiol.* 388, 141–151. doi: 10.1113/jphysiol.1987.sp016606

Kostyuk, P. G., Krishtal, O. A., and Pidoplichko, V. I. (1975). Effect of internal fluoride and phosphate on membrane currents during intracellular dialysis of nerve cells. *Nature*. 257, 691–693. doi: 10.1038/257691a0

Kostyuk, P. G., Veselovsky, N. S., and Fedulova, S. A. (1981). Ionic currents in the somatic membrane of rat dorsal root ganglion neurons-II. *Calcium Curr. Neurosci.* 6, 2431–2437. doi: 10.1016/0306-4522(81)90089-0

Krishtal, O. A., Marchenko, S. M., and Pidoplichko, V. I. (1983). Receptor for ATP in the membrane of mammalian sensory neurones. *Neurosci. Lett.* 35, 41–45. doi: 10.1016/0304-3940(83)90524-4

Krishtal, O. A., and Pidoplichko, V. I. (1980). A receptor for protons in the nerve cell membrane. *Neuroscience*. 5, 2325–2327. doi: 10.1016/0306-4522(80)90149-9

Kushchayev, S. V., Moskalenko, V. F., Wiener, P. C., Tsymbaliuk, V. I., Cherkasov, V. G., Dzyavulska, I. V., et al. (2012). The discovery of the pyramidal neurons: Vladimir Betz and a new era of neuroscience. *Brain* 135, 285–300. doi: 10.1093/brain/awr276

Neminsky, V. V. (1913). Ein Versuch der Registrierung der elektrischen Gehirnerscheinungen. *Zentralblatt für Physiologie* 27, 951–960.

frontiers | Frontiers in Cellular Neuroscience

TYPE Original Research
PUBLISHED 14 December 2022
DOI 10.3389/fncel.2022.1054950

OPEN ACCESS

EDITED BY
Dominique Debanne,
INSERM U1072 Neurobiologie des canaux Ioniques et de la Synapse, France

REVIEWED BY
Jean Chemin,
Centre National de la Recherche Scientifique (CNRS), France
Kaoutsar Nasrallah,
Albert Einstein College of Medicine, United States

*CORRESPONDENCE
Vyacheslav M. Shkryl
slava@biph.kiev.ua

SPECIALTY SECTION
This article was submitted to Cellular Neurophysiology, a section of the journal Frontiers in Cellular Neuroscience

RECEIVED 28 September 2022
ACCEPTED 24 November 2022
PUBLISHED 14 December 2022

CITATION
Shkryl VM (2022) The spatio-temporal properties of calcium transients in hippocampal pyramidal neurons *in vitro*.
Front. Cell. Neurosci. 16:1054950.
doi: 10.3389/fncel.2022.1054950

The spatio-temporal properties of calcium transients in hippocampal pyramidal neurons *in vitro*

Vyacheslav M. Shkryl*

Department of Biophysics of Ion Channels, Bogomoletz Institute of Physiology, NAS of Ukraine, Kyiv, Ukraine

The spatio-temporal properties of calcium signals were studied in cultured pyramidal neurons of the hippocampus using two-dimensional fluorescence microscopy and ratiometric dye Fura-2. Depolarization-induced Ca^{2+} transients revealed an asynchronous delayed increase in free Ca^{2+} concentration. We found that the level of free resting calcium in the cell nucleus is significantly lower compared to the soma, sub-membrane, and dendritic tree regions. Calcium release from the endoplasmic reticulum under the action of several stimuli (field stimulation, high K^+ levels, and caffeine) occurs in all areas studied. Under depolarization, calcium signals developed faster in the dendrites than in other areas, while their amplitude was significantly lower since larger and slower responses inside the soma. The peak value of the calcium response to the application of 10 mM caffeine, ryanodine receptors (RyRs) agonist, does not differ in the sub-membrane zone, central region, and nucleus but significantly decreases in the dendrites. In the presence of caffeine, the delay of Ca^{2+} signals between various areas under depolarization significantly declined. Thirty percentage of the peak amplitude of Ca^{2+} transients at prolonged electric field stimulation corresponded to calcium release from the ER store by RyRs, while short-term stimulation did not depend on them. 20 μM dantrolene, RyRs inhibitor, significantly reduces Ca^{2+} transient under high K^+ levels depolarization of the neuron. RyRs-mediated enhancement of the Ca^{2+} signal is more pronounced in the central part and nucleus compared to the sub-membrane or dendrites regions of the neuron. In summary, using the ratiometric imaging allowed us to obtain additional information about the involvement of RyRs in the intracellular dynamics of Ca^{2+} signals induced by depolarization or electrical stimulation train, with an underlying change in Ca^{2+} concentration in various regions of interest in hippocampal pyramidal neurons.

KEYWORDS

hippocampal neuronal culture, calcium homeostasis, ryanodine receptors, caffeine, ratiometric method, Fura-2

Introduction

The calcium ion (Ca^{2+}) is a common second messenger that regulates many physiological pathways such as secretion, fertilization, gene transcription, and apoptosis (Pozzan et al., 1994; Berridge et al., 2000). Calcium signaling in excitable cells consists of several mechanisms. In the first phase, Ca^{2+} influx across the plasma membrane after the opening of voltage-gated calcium channels (VGCCs) as a result of action potential (AP) depolarization or activation of ligand-gated channels (Berridge, 1998; Augustine et al., 2003; Bloodgood and Sabatini, 2007). Then Ca^{2+} can be released from the endoplasmic reticulum (ER) or sarcoplasmic reticulum (SR) through 1,4,5-Inositol triphosphate receptors (IP_3Rs) and/or ryanodine receptors (RyRs) expressed on the ER (or SR) membrane (Berridge, 1998, 2009; Verkhratsky, 2002; Clapham, 2007; Khakh and McCarthy, 2015).

The release of Ca^{2+} from the SR store amplified Ca^{2+} signaling and regulates a variety of cellular processes, including excitation-contraction coupling in skeletal muscle (Endo et al., 1970; Ford and Podolsky, 1970) and cardiac myocytes (Fabiato, 1983; Bers, 2002), and from the ER store calcium oscillation and gene expression in many cell types (Thorn et al., 1993; Hardingham et al., 2001), neuronal plasticity (Frenguelli and Malinow, 1996; Rose and Konnerth, 2001) and other processes. The ER is an essential intracellular organelle—one of the main functions of which is the storage of intracellular Ca^{2+}. The entry of calcium ions through VGCCs activates RyRs *via* a calcium-mediated process that obtained, at present, the generally known designation "calcium-induced calcium release," CICR (Fabiato, 1983).

In most CNS neurons, free intracellular calcium concentration ($[Ca^{2+}]_i$) changes following the opening of VGCCs (Berridge, 1998; Augustine et al., 2003; Bloodgood and Sabatini, 2007) and then is buffered with some proteins like calmodulin, calreticulin, parvalbumin, calbindin-D28k. In addition, ATP binds significant amounts of Ca^{2+} ions (Zhou and Neher, 1993; Shkryl et al., 2012a). As in other cell types, in neurons, Ca^{2+} is released from the ER through IP_3Rs and/or RyRs expressed on the ER membrane, which regulates a myriad of physiological and pathophysiological processes in it (Verkhratsky and Kettenmann, 1996; Berridge, 1998, 2002, 2009; Verkhratsky, 2002, 2005; Clapham, 2007; Khakh and McCarthy, 2015; Shkryl, 2017). The binding of Ca^{2+} to RyRs activates these channels allowing Ca^{2+} to release from the ER into the cytosol (Kuba, 1994). Activation of RyRs is linked to L-type VDCCs either *via* Ca^{2+} influx in cardiac myocytes or by direct voltage-dependent mechanical coupling in skeletal muscle (Pozzan et al., 1994; Niggli, 1999). The latter type of coupling has also been observed in neuronal cells (Chavis et al., 1996; De Crescenzo et al., 2004).

RyRs in peripheral and central neurons may amplify and prolong incoming Ca^{2+} signals *via* CICR (Holliday et al., 1991; Llano et al., 1994; Kano et al., 1995). Some studies have shown that depleting or blocking the ryanodine-sensitive Ca^{2+} stores did not significantly alter the amplitude and waveform of depolarization-induced Ca^{2+} transients and did not contribute significantly to depolarization-induced Ca^{2+} transients evoked by low-frequency activity (Garaschuk et al., 1997). However, it established that the soma of pyramidal neurons provides a reticular network of the ER and extends throughout dendrites and the entire length of the axon, including presynaptic boutons (de Juan-Sanz et al., 2017). In addition, repetitive tetanic synaptic stimulation of CA1 pyramidal cells in a slice preparation has been reported to induce Ca^{2+} release from dendritic or presynaptic ryanodine-sensitive Ca^{2+} stores (Alford et al., 1993; Tran and Stricker, 2021).

There are broadly selective drugs that are able to activate or inhibit RyRs in myocytes or neurons. The most well-known are caffeine, ryanodine, 4-chloro-m-cresol, dantrolene, ruthenium red, tetracaine, and procaine (Viero et al., 2012). Caffeine is a RyRs agonist and has been used as a pharmacological tool to study ryanodine receptor-mediated Ca^{2+} release from intracellular stores (Kong et al., 2008; Porta et al., 2011). Caffeine sensitizes RyRs to Ca^{2+} and promotes ER Ca^{2+} release at basal cytosolic Ca^{2+} levels. Another drug is RyRs-inhibitor dantrolene (Fruen et al., 1997; Fill and Copello, 2002) which in the concentration of 10 μM reduced RyRs channel open probability by 50% (Diszházi et al., 2019).

Information about the involvement of RyRs in calcium signaling in neurons is controversial, especially about where release occurs and how it interacts with the Ca^{2+} signal during short or long-term stimulation. This study aimed to obtain additional information on the involvement of ryanodine receptors in neuronal calcium signaling. Spatio-temporal properties of these signals were studied during multiple stimuli: field stimulation, high K^+, and caffeine and dantrolene at cultured rat hippocampal CA1 pyramidal neurons. We use caffeine and dantrolene to reveal RyRs. Changes in free calcium concentrations inside the cell were determined using two-dimensional fluorescence microscopy based on a charge-coupled device camera and ratiometric dye Fura-2 with dye excitation at wavelengths 340–380 nm. We analyzed two-dimensional fluorescent images of neurons spatially with temporal profiles from different areas of it. For such analysis were selected: the nucleus, sub-membrane region, central space inside of a cell, and the dendritic tree. This technique allows us to simultaneously determine the change in Ca^{2+} signals in the different regions of the neurons.

Materials and methods

All experimental procedures were performed following ethical principles of the European Convention for the protection of vertebrate animals used for experimental and other scientific

purposes (86/609/EEC; European convention, Strasburg, 1986) and were approved by the local Animal Ethics Committee of the Bogomoletz Institute of Physiology (Kyiv, Ukraine). All efforts were made to minimize the number and suffering of animals used. All experiments were performed on cultured hippocampal neurons obtained from newborn Wistar rats. Primary cultures were prepared as previously reported (Shkryl et al., 1999). Ca^{2+} imaging studies were carried out within 10–14 days of cultivation. A cover glass with cells was placed in an extracellular solution (ES) containing in mM: NaCl—140.0; KCl—2.0; $CaCl_2$—2.0; $MgCl_2$—2.0; HEPES—10.0; pH = 7.4. All chemicals were obtained from Sigma-Aldrich (St. Louis, MO).

The cells were loaded with 5 μM Fura-2 acetoxymethyl ester (Fura-2 AM) for 30 min at 37°C and 20 min for de-esterification of the dye. The values of R_{min} and R_{max} amounted to 0.44 and 9.44; F_{380}(min) = 20.7 and F_{380}(max) = 169.4; K_d(Fura-2) = 224 nM (Shkryl, 2020). The coverslip with neurons was washed and placed in an experimental chamber with two platinum electrodes used for the electric field stimulation (EFS). The stimulation was carried out according to the standard protocol by lowering two parallel platinum electrodes (20÷25 mm apart) into the chamber and passing current pulses between them (Jacobs and Meyer, 1997; Shkryl et al., 2012b). Ca^{2+} transients were also induced chemically by applying a depolarizing solution that contained 50.0 mM KCl substituting the respective amount of NaCl in ES. We used a computer-controlled perfusion system synchronized with data acquisition software.

In our study, we used a CCD camera (Olympus XM10) mounted on an Olympus IX71 inverted microscope equipped with an Olympus LUCPlanFFN 20×/0.45 lens and MT10 illumination system that included a filter wheel exchanger (340–380 nm) and 150 W xenon arc burner. For the data collection, we use Cell M software (Olympus, Japan). The acquisition speed was 30 Hz for one wave and 1.3 Hz for ratiometric use. For further data analysis, the ratio of 340–380 nm fluorescence intensity (ratio; F_{340}/F_{380}) was calculated. This is done according to the protocol described by Shkryl (Shkryl, 2020) and subtracts the background level calculated outside of cells. Dynamic changes in the ratio index assess changes in the level of free calcium.

Data analysis was performed using the IDL programming environment (ITT Visual Information Solutions). In recorded images with excitation of 340–380 nm lights, the regions of interests (ROIs) were selected. All experiments were performed at room temperature (22°C–25°C). Data are presented as mean ± SEM.

Results

In most neurons, the intracellular concentration of free calcium in the resting state is around 75 nM. This index can increase to 10 μM upon intense electrical activity of cells (Berridge et al., 2000). In particular, the calcium level in the dendrites could increase to 5 μM during the development of synaptically induced calcium waves (Pozzo Miller et al., 1996; Larkum et al., 2003). Information on the spatial distribution of the respective calcium channels and receptors is limited; however, it is clear that the molecular mechanisms and patterns of Ca^{2+} release in different regions of different neurons differ significantly (Verkhratsky, 2005). To examine changes in the intracellular calcium level in cultured pyramidal hippocampal neurons, we used 2D x-y-t ratiometric fluorescent Ca^{2+} measurements and Ca^{2+}-sensitive dye Fura-2, AM. In this series of experiments, the cells constantly perfused with ES were stimulated by EFS and by applying 50 mM KCl or 10 mM caffeine solutions.

Ca^{2+} responses in different regions of pyramidal hippocampal neuron

We analyzed Ca^{2+} signals in hippocampal pyramidal neurons in the sub-membrane, central, dendritic, and nuclear regions. **Figure 1A** illustrates representative data traces of the Fura-2 ratio (F_{340}/F_{380}; Ca^{2+} signals) increases induced by two series of 50 pulses of EFS (used to load the ER store) and followed by the application of 10 mM caffeine for 5 s to induce Ca^{2+} release from the ER stores by ryanodine receptors (RyRs). An additional EFS and 5-s application of the depolarizing solution were applied when the restoration of calcium signals to the resting level. 2D imaging of Ca^{2+} signals reveals an asynchronous delayed rise of free Ca^{2+} concentration in the nuclear compared to the sub-membrane, central or dendritic regions (**Figure 1A**). Statistical data are presented in the bottom plane of **Figure 1B**.

The value of basal free Ca^{2+} was significantly reduced in the nuclear area of the neuron, less by 15% compared to the central region (61 nM vs. 85 nM, $n = 30$; $P < 0.001$; **Figure 1Ba**). Ca^{2+} signal in the dendritic region in response to stimulation appeared faster compared to other regions (detailed below) but had the smallest amplitude during EFS, KCl depolarization, and caffeine application. The amplitude of Ca^{2+} transient in the dendritic tree of pyramidal-like neurons in response to EFS was 1.18 ± 0.09 (207 nM, $n = 19$), which was significantly smaller compared to sub-membrane—1.62 ± 0.17 (303 nM, $n = 19$; $P < 0.05$), central—1.73 ± 0.18 (329 nM, $n = 19$; $P < 0.01$), and nuclear—1.66 ± 0.17 (300 nM, $n = 19$; $P < 0.05$) regions of the cell (**Figure 1Bb**). In the dendritic tree, the amplitude of Ca^{2+} transient caused by KCl depolarization was also significantly reduced, 3.43 ± 0.41 (0.87 μM, $n = 24$) respectively to sub-membrane—4.76 ± 0.39 (1.65 μM, $n = 24$; $P < 0.05$), central—4.98 ± 0.38 (1.84 μM, $n = 24$; $P < 0.01$), and nuclear—5.06 ± 0.39 (1.81 μM, $n = 24$; $P < 0.01$) regions of studied neurons (**Figure 1Bc**). As shown in **Figure 1Bd**,

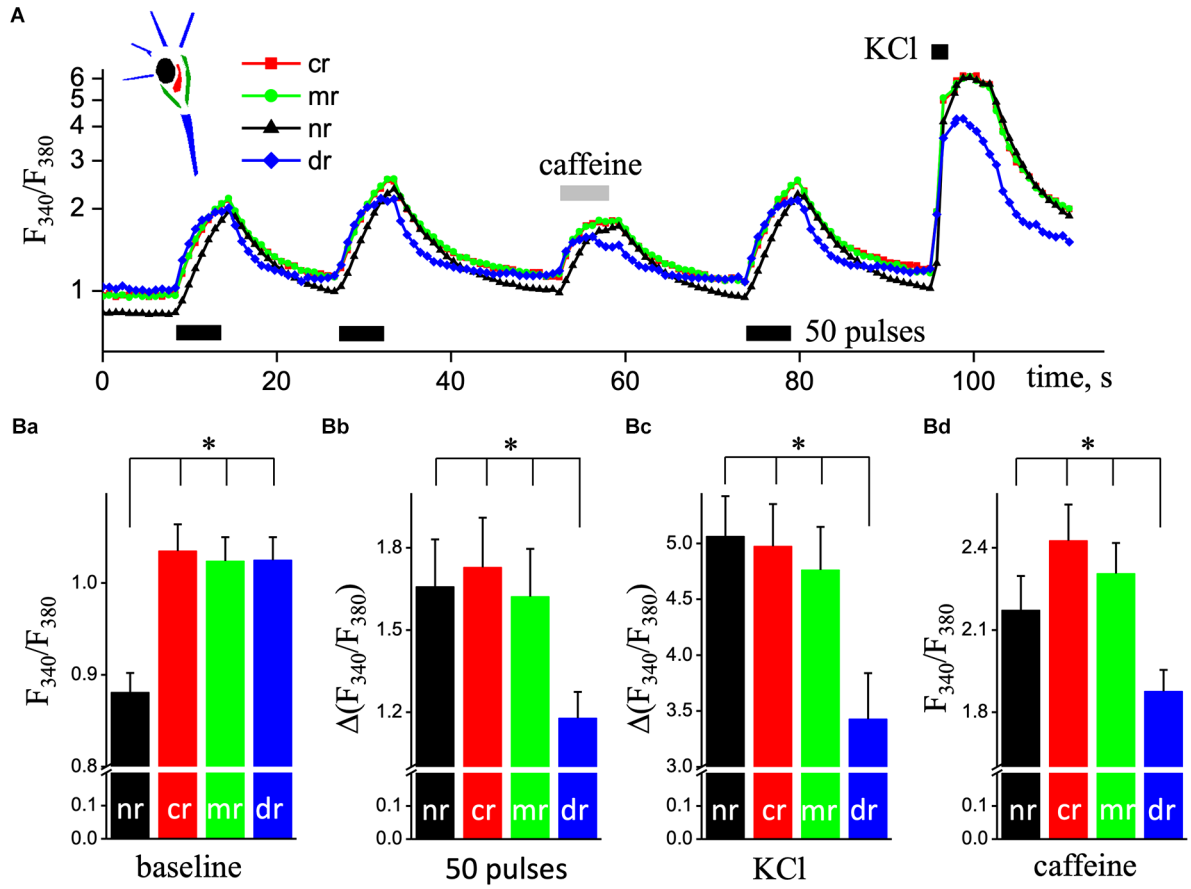

FIGURE 1
Ca^{2+} responses in different ROIs of pyramidal hippocampal neurons triggered by electrical field stimulation and application of depolarizing and caffeine solutions. **(A)** Transient increases in $[Ca^{2+}]_i$ are triggered by two series of 50 pulses of EFS (black rectangular, 9 Hz) followed by the application of caffeine (caffeine, light gray rectangular; 10 mM and 5 s) and a series of 50 pulses of EFS and depolarizing solution with 50 mM KCL (KCl, black square, 5 s). Ca^{2+} responses were recorded in the central space (cr; red squares line), sub-membrane (mr; green circles line), dendritic tree (dr; blue diamond's line), and nucleus (nr; black triangles lines) regions of cultured hippocampal neurons loaded with the fluorescent Ca^{2+} indicator Fura-2. Ratios (F_{340}/F_{380}) are presented in natural logarithmic scale. The top left corner represents a schema of neurons' area selection. The bottom panel **(B)** shows quantified responses for four studied regions in pyramidal neurons. **(Ba)** Mean value of basal Ca^{2+} levels before any stimulus; part **(Bb)** is the mean values of the amplitudes of second Ca^{2+} transients caused by EFS; part **(Bc)** is the mean values of the amplitudes of Ca^{2+} transients evoked by depolarizing solution; part **(Bd)** is the mean values of Ca^{2+} peaks evoked by 5 s application of 10 mM caffeine, as an agonist of RyRs. The black bars are data for the nucleus (nr); the red bars are data in the central space (cr); the green bars are sub-membrane regions (mr), and the blue bars are dendritic trees of neurons (dr). Results are mean ± S.E. of 30 individual cells from 10 different experiments. *$P < 0.05$.

the peak values of calcium signals induced by 10 mM caffeine (as Ca^{2+} release from the ER) were significantly reduced in the dendritic tree region to 1.88 ± 0.08 (225 nM, n = 19) from 2.31 ± 0.11 (310 nM, n = 19, $P < 0.01$) in sub-membrane, central—2.43 ± 0.13 (336 nM, n = 19; $P < 0.001$) and nuclear—2.17 ± 0.12 (283 nM, n = 19; $P < 0.05$) regions of pyramidal neurons.

Fast recording of Ca^{2+} transients

In the next series of experiments, we investigated the spatio-temporal organization of Ca^{2+} transients in the various areas of pyramidal-like neurons recorded at 30 Hz frequencies (Figure 2A). We recorded simultaneously the Ca^{2+} transients induced by ESP stimulation at excitation wavelengths 340–380 nm, which were synchronized with EFS, separated in time. The first recorded Ca^{2+} transient was with excitation wavelength at 340 nm, and then a 2 min delay produced an additional record at 380 nm with the same setting and conditions that create the F_{340}/F_{380} ratio signal (Figure 2B).

Fast 2D recording of Ca^{2+} transients under depolarization revealed an asynchronous delayed rise of free Ca^{2+} concentration. Thus, EFS caused an increase in Ca^{2+} signals that first appeared in the dendrites, then in the sub-membrane, central, and finally in the nuclear area of cells. Figure 2C shows

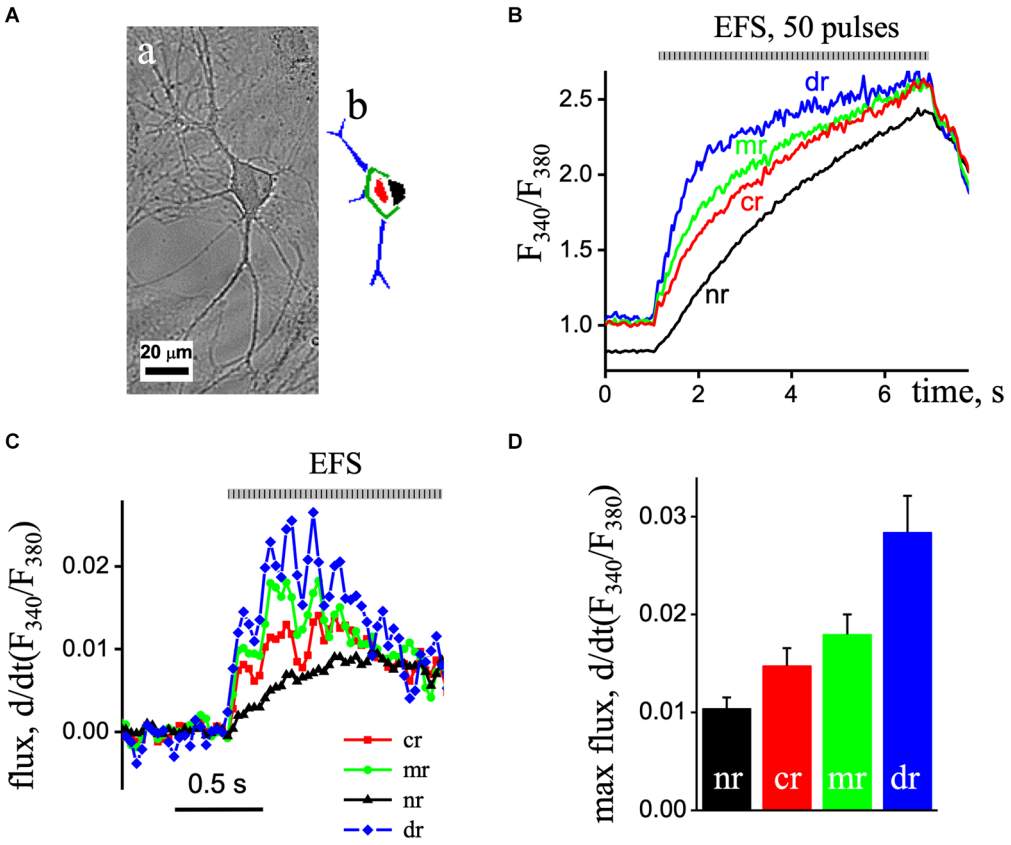

FIGURE 2
Fast recording of EPS-induced Ca^{2+} transients in a pyramidal-like hippocampal neuron. **(Aa)** The image of the cell obtained by direct illumination. **(Ab)** Different ROIs of the neuron are colored. **(B)** The imaged ratio of F340/F380 of Fura-2 loaded neuron with 50 EPS was separated as time profiles in the dendritic tree (blue line; dr), sub-membrane (green line, mr), central area (red line; cr), and nuclear (black line; nr) regions of the neuron. **(C)** d(F340/F380)/dt (s^{-1}), the first derivative of the ratio of the Ca^{2+} signal obtained in the nuclear (black triangles line), central area (red squares line), and sub-membrane (green circles line) regions of the neuron. The flux data were derived from the data presented in part **(B)**. **(D)** Mean value of the maximal flux rate obtained in the nuclear (black bar), central area (red bar), and sub-membrane (green bar) regions of the neuron.

the first derivative of the $[Ca^{2+}]_i$ signal [d(F340/F380)/dt] representing the underlying Ca^{2+} flux. The Ca^{2+} flux in the sub-membrane and central regions appeared with increasing and decreasing steps, representing the EFS-induced calcium transients. The maximum flux in the sub-membrane and central regions was observed 0.2 s after initiation and decreased with time. In the nuclear region of the neuron, the flux was delayed and reached its maximum value 0.6 s after the onset with reduced amplitude compared to other regions. The maximal flux rate was in the dendritic tree region (0.028 ± 0.004, n = 8) and reduced in the sub-membrane (0.018 ± 0.002, n = 8) and central (0.015 ± 0.004, n = 8), and minimal in nuclear aria (0.010 ± 0.001, n = 8) of the neuron (Figure 2D).

To show more detailed information about the inhomogeneity of Ca^{2+} signals in hippocampal pyramidal neurons, we studied the latency of Ca^{2+} increases for different regions of cells in one wavelength excitation mode (380 nm, 30 Hz). Figure 3 shows the dynamics of $[Ca^{2+}]_i$ increases caused by 50 pulses of EFS (3A) and 50 mM KCl solution (3B) normalized to the maximal amplitude of Ca^{2+} transients in various ROIs of the neuron. When recording in x-y-t mode (limited to 30 Hz), Ca^{2+} signals were insufficient to represent the initial phase of the Ca^{2+} signal, which was more evident during KCl-induced transients. However, we find signal delays between different ROIs at 25%, 50%, and 75% of the maximal amplitude. It is in the sub-membrane, and central regions were more pronounced and progressed during the EFS-induced Ca^{2+} transient and less during KCl depolarization, and this parameter of the difference between the dendritic tree and the sub-membrane region of interest increased up to 1 s. In the central and nuclear regions, the delay was almost independent of the type of stimulus and was around 0.2 s. Statistical data are represented in the summarized diagram in part 3C.

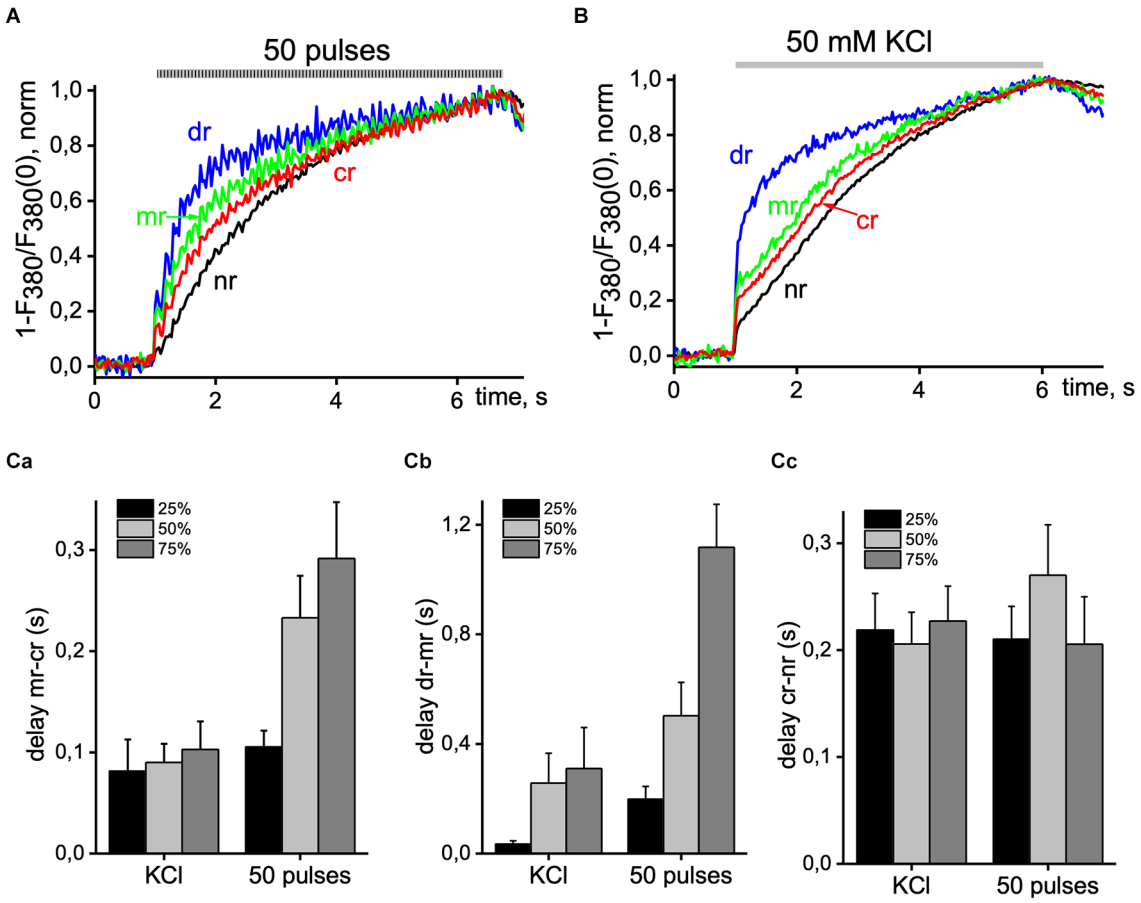

FIGURE 3
Delay of Ca^{2+} signals between distinct areas of pyramidal neurons. Normalized Ca^{2+} transients were recorded from the central (cr; red line), sub-membrane (mr; green line), nuclear (nr; black line), and dendritic tree (dr; blue line) area of the cell induced by 50 EFS pulses at 9 Hz **(A)** and 5 s application of 50 mM KCl solution **(B)**. **(C)** Summary histogram of delays between sub-membrane and central areas (mr-cr; part **a**); dendritic tree and sub-membrane areas (dr-mr; part **b**); central and nuclear areas (cr-nr; part **c**) measured at 25% (black bar), 50% (light gray bar) and 75% (dark gray bar) of maximal amplitude value with 50 pulses EFS and application of depolarizing KCl solution. Data were obtained in seven neurons in four different experiments. Ca^{2+} signals were recorded with 380 nm excitation wavelength at 33 ms per image.

RyRs mediated Ca^{2+} signal

As is well known, Ca^{2+} release from the ER occurs under conditions of the opening of the IP_3Rs and RyRs (Rizzuto and Pozzan, 2006). The IP_3Rs-mediated release of calcium from the dendrites is initiated most frequently by the action of neurotransmitters, like glutamate (Niswender and Conn, 2010), while RyRs activate by an increase of Ca^{2+} concentration in the cytosol (Shkryl and Blatter, 2013; Blatter, 2017) *via* calcium-mediated activation RyRs through CICR (Fabiato, 1983). In the following experiments, we tested the functioning of the ER stores in hippocampal pyramidal neurons. For this purpose, we activated Ca^{2+} release from the ER by applications of the RyR agonist caffeine, which often revealed an increase in cytosolic Ca^{2+} concentrations induced by caffeine. We use ESP to load the ER store.

Figure 4A shows a superimposed record that demonstrates changes in Ca^{2+} signal, recorded from a neuron under control condition (black trace) and in the presence of 10 mM caffeine (red trace). In control, the basal level of free calcium was 1.06 ± 0.03 and 1.26 ± 0.05 in the presence of caffeine. The peak amplitude of Ca^{2+} transients induced by depolarizing solution significantly decreased from 6.47 ± 0.57 (in the control) to 4.58 ± 0.31 under the application of 10 mM caffeine (Figure 4Bc; $n = 12$, $P < 0.05$). Under electrical field stimulation changing the amplitude of the caffeine depend on the duration of the stimulation. The peak amplitude of the Ca^{2+} signal induced by short (15 pulses, 9 Hz) EFS did not change appreciably, 0.54 ± 0.08 compared to 0.51 ± 0.07 (Figure 4Ba; $n = 13$). However, by a long stimulus (50 pulses, 9 Hz), this parameter significantly decreases from 2.72 ± 0.58 to 1.89 ± 0.38 (Figure 4Bb; $n = 6$, $P < 0.05$) with caffeine.

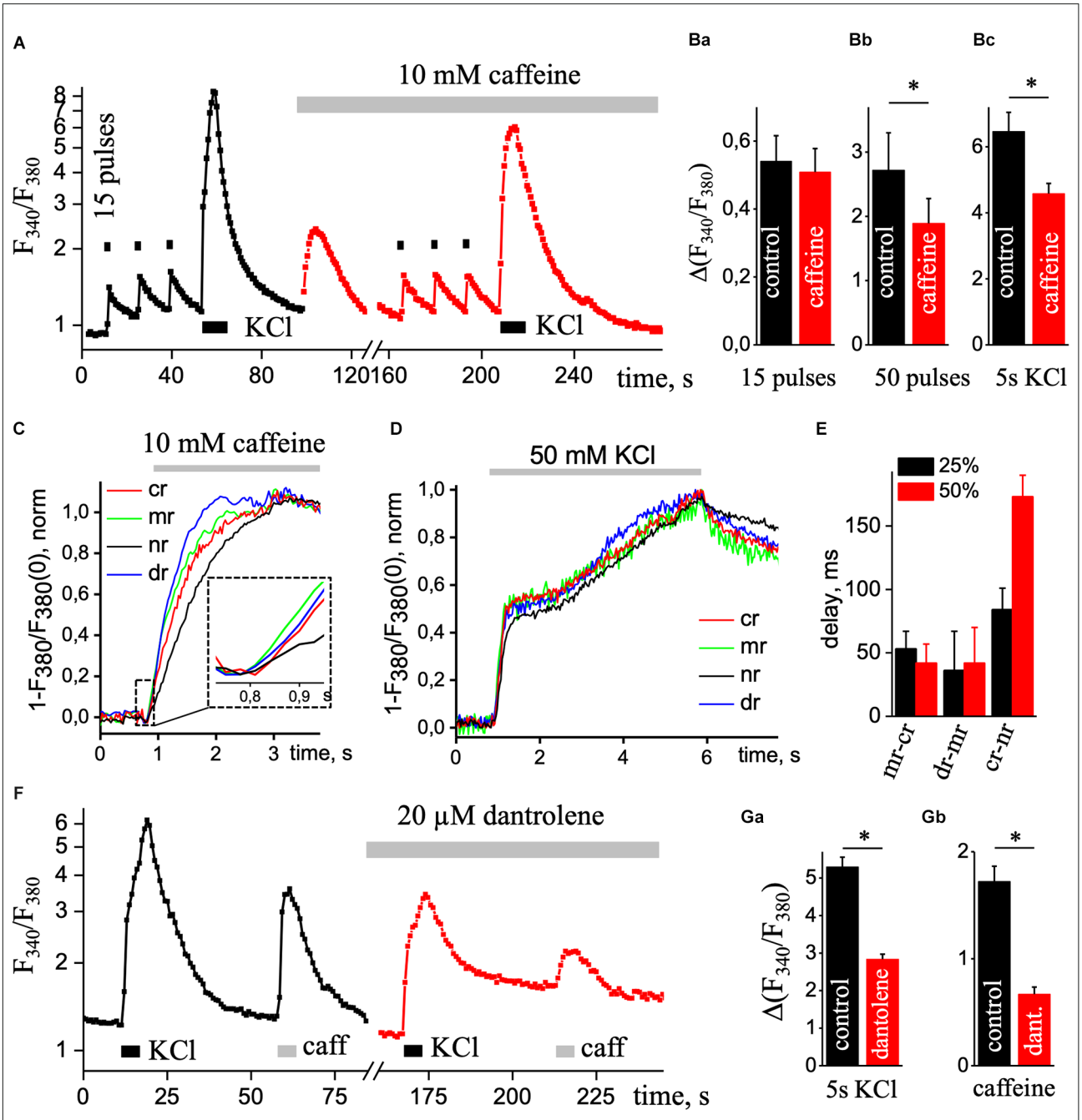

FIGURE 4
Ca^{2+} transients under the presence of caffeine. **(A)** Transient increases in $[Ca^{2+}]_i$ are triggered by three series of 15 pulses of EFS (black square; 1 s) followed by application of KCl depolarizing solution (KCl, black rectangle, 5 s) in the control condition (black square line) and repeated stimulations with continues presence of 10 mM caffeine (caffeine; red square line) to eliminate calcium release from the ER. Ca^{2+} responses were recorded in the soma without the nucleus region. The ratio (F_{340}/F_{340}) is presented on a natural logarithmic scale. **(B)** Mean values of the amplitude of the second Ca^{2+} transient caused by 15 **(a)** or 50 **(b)** pulses EFS and Ca^{2+} transient evoked by KCl solution **(c)** in control and presence of 10 mM caffeine. Normalized Ca^{2+} transients were recorded using one wavelength protocol (33 ms per image and 380 nm excitation wavelength) at different ROIs induced by the application of 10 mM caffeine **(C)** or application of KCl depolarizing solution **(D)**. A dashed line in part **(C)** contains an insert of the initial phase of caffeine-induced Ca^{2+} increase. ROIs were selected in central (cr, red line), sub-membrane (mr, green line), nuclear (nr, black line), and dendritic tree (dr, blue line) areas of the cell. **(E)** Diagram of delays between sub-membrane and central (mr-cr); dendritic tree and sub-membrane (dr-mr); central and nuclear (cr-nr) areas measured at 25% (black bar) and 50% (red bar) of the maximal amplitude in response to KCl depolarizing solution. **(F)** Transient increases in $[Ca^{2+}]_i$ are triggered by the application of KCl depolarizing solution (KCl, black rectangle, 5 s) and caffeine (caffeine, light gray rectangular; 10 mM and 5 s) in the control condition (black square line) and repeated stimulations with continues presence of 20 μM dantrolene (red square line) to reduce calcium release from the ER. Ca^{2+} responses were recorded in the soma without the nucleus region. The ratio (F_{340}/F_{340}) is presented on a natural logarithmic scale. Mean value of the amplitude of Ca^{2+} transients evoked by depolarizing solution **(Ga)** and 5 s application of 10 mM caffeine **(Gb)**. Results are mean ± S.E., $^*P < 0.05$.

The short electrical stimulation (15 pulses, 1 s) does not alter the amplitude of Ca^{2+} transients under caffeine, but the Ca^{2+} response significantly decreased under the depolarization solution or long EFS. Thus, with prolonged stimulation of the neuron, Ca^{2+} release appeared from the ER by RyRs. As we can see from normalized caffeine-induced Ca^{2+} transients (Figure 4C), a rise in signals appeared in all regions of hippocampal pyramidal neurons, but in the center and nuclear, Ca^{2+} signals were more delayed (37.5 ± 7.5 ms, $n = 4$) than in sub-membrane zone and dendritic tree. Figure 4D shows the dynamics of increases in $[Ca^{2+}]_i$ caused by 5 s application of KCl solution normalized to the maximal amplitude of the signal in various regions of interest of the neuron. Figure 4E shows the delay in different ROIs at 25% and 50% of the maximal amplitude. Under caffeine, the delay between sub-membrane and central, dendritic tree, central and nuclear regions was significantly reduced compared to control.

Additionally, we used 20 μM dantrolene to block RyRs and record high KCl-induced Ca^{2+} transients. Figure 4F shows superimposed record that demonstrates changes in Ca^{2+} signal, recorded from a neuron under control condition (black square line) and in the presence of 20 μM dantrolene (red square line). In control, the basal level of free calcium was 1.23 ± 0.03 and 1.10 ± 0.03 in the presence of dantrolene. The amplitude value of depolarizing solution-induced Ca^{2+} transients under 20 μM dantrolene significantly decreased from 5.30 ± 0.26 to 2.84 ± 0.13 (Figure 4Ga; $n = 29$, $P < 0.001$). The ER load with the presence of dantrolene was significantly decreased to 0.682 ± 0.06 from 1.72 ± 0.14 (Figure 4Gb; $n = 28$, $P < 0.01$). It further confirms the involvement of RyRs in Ca^{2+} signaling in cultured hippocampal pyramidal neurons.

Figure 5 shows representative recordings of calcium transients induced by 50 pulses of EFS in control (black line) and the presence of 10 mM caffeine (red line) in different regions

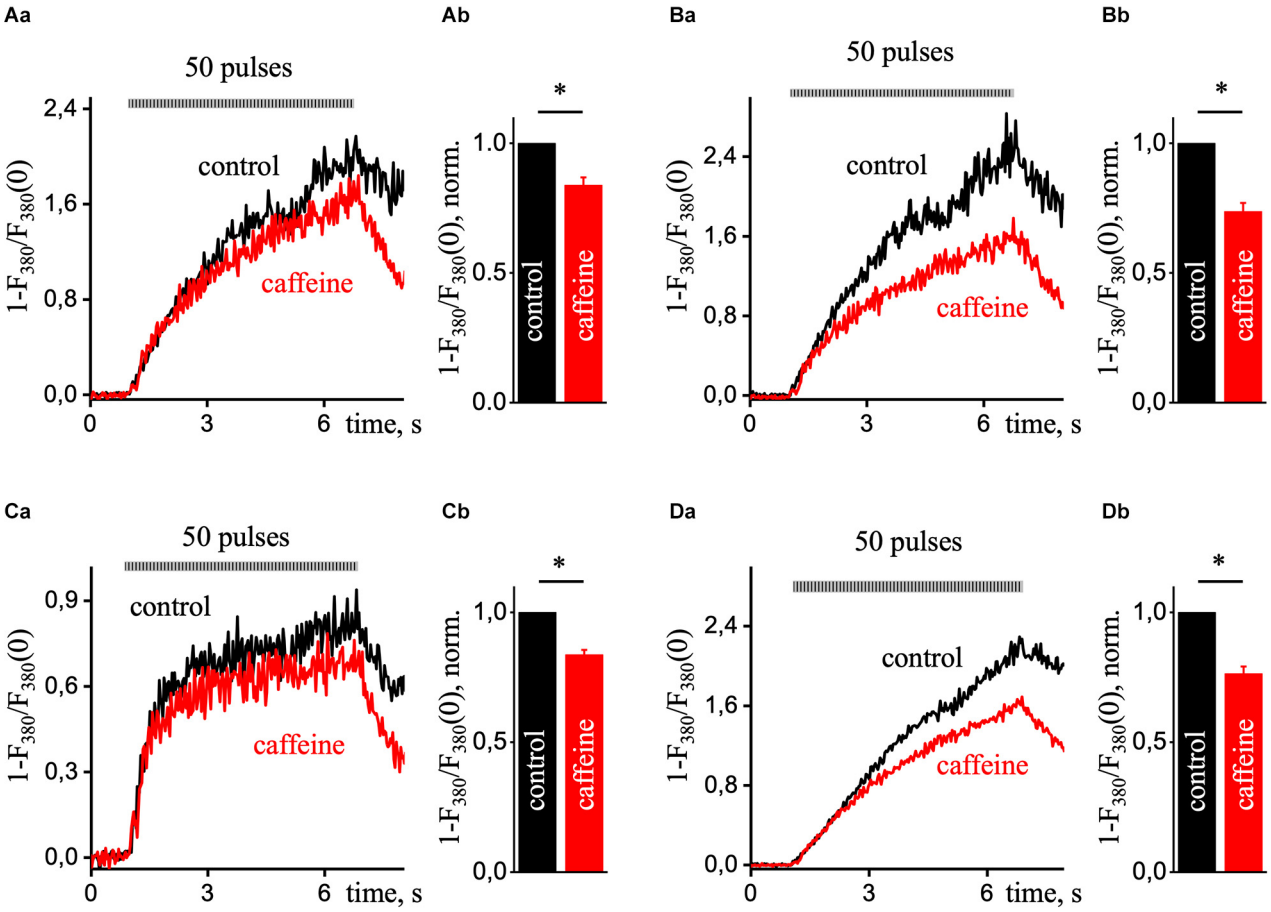

FIGURE 5
Ca^{2+} transients during prolonged electrical field stimulation in the presence of caffeine in various ROIs of hippocampal pyramidal neurons. A transient increase in intracellular $[Ca^{2+}]_i$ is induced by a series of 50 EFS pulses (9 Hz) under control conditions (black line) and in the presence of 10 mM caffeine (red line; which excludes calcium release from the ER). Each graph in part **(a)** presented Ca^{2+} responses that were recorded in the sub-membrane **(A)**, central **(B)**, dendritic tree **(C)**, and nucleus **(D)** of the cell. Normalized Ca^{2+} transients were recorded using a single wavelength protocol (33 ms per image and 380 nm excitation wavelength). Part **(b)** of each panel presents control-normalized statistics of maximal amplitude in the presence of caffeine in response to ESP. Results are mean ± S.E. $^*P < 0.05$.

of the pyramidal neuron. The calcium signals in control and caffeine had a substantial difference at the center (**Figure 5B**), although there was also a decrease in signal with caffeine in the sub-membrane (**Figure 5A**) and dendritic tree regions (**Figure 5C**) were less pronounced but significant. Data were obtained from six different experiments and compared using a paired sample *t*-test. Also, the difference between these signals in the nucleus (**Figure 5D**) was somewhat less than in the central region. It is probably due to the passive enhancement of the calcium signal by releasing Ca^{2+} from the center or neighboring ERs into the nucleus. The RyR-mediated increase in the Ca^{2+} signal presented in the periphery, the dendritic tree, and the center of the hippocampal pyramidal neuron.

Discussion

In this study, we investigated the behavior of Ca^{2+} signals in response to electrical stimulation, KCl-induced depolarization, and caffeine treatment in cultured hippocampal pyramidal neurons with a 2D imaging mode of ratiometric fluorescent microscopy.

A neuron is an excitable cell, and a fundamental principle in neuronal signal processing is the transduction of short electrical signals at the membrane into biochemical responses, resulting in longer-lasting changes in the neuronal structural and functional state (Johenning et al., 2015). The neuronal plasma membrane with channels, receptors, and pumps mediates the electrical signal propagation; the ER membrane can participate in the passive and active calcium-based signal propagation mainly along the dendritic length and soma from peripheries to the center (Shkryl, 2017; Ashhad and Narayanan, 2019). Action potentials generate widespread increases in calcium concentration inside axons and presynaptic terminals, and then they back-propagate over large regions of the dendrites (Ross, 2012). The present study shows that the level of free calcium in the resting state inside the nucleus is significantly lower compared to the center of the cell and delayed respectively to other regions of hippocampal pyramidal neurons. Fedorenko and Marchenko (2014) have shown that the nuclear membrane of hippocampal CA1 pyramidal neurons was enriched in functional inositol IP_3Rs localized in the inner nuclear membrane and is specialized to release Ca^{2+} into the nucleoplasm, which may amplify Ca^{2+} signals entering the nucleus from the cytoplasm. Our study shows that nuclear Ca^{2+} flux had the lowest amplitude compared to other studied regions. During applications of caffeine, the nuclear Ca^{2+} signal was suspended compared to the sub-membrane but appeared at the same time as the central area with almost no delay.

Localized RyR-mediated events of Ca^{2+} release occur in the soma and proximal dendrites of hippocampal pyramidal neurons in culture and acute slices (Koizumi et al., 1999; Berrout and Isokawa, 2009; Manita and Ross, 2009; Miyazaki et al., 2012). The endoplasmic reticulum localized close to the plasmalemma membrane (PM) makes a membrane domain called ER-PM junctions (EPJs). By electron microscopy, the ER at many neuronal EPJs appears as a micron-diameter, flattened vesicle less than 10 nm from the PM, a structure also called a "subsurface cistern" (Rosenbluth, 1962; Tao-Cheng, 2018). EPJs are abundant in neuronal soma (Wu et al., 2017), and neuronal soma has prominent VGCCs—and RyRs-mediated CICR (Friel and Tsien, 1992; Isokawa and Alger, 2006; Berrout and Isokawa, 2009). Our study shows that the release of calcium from the endoplasmic reticulum occurred in all regions of the neuron; the peak value of Ca^{2+} response to caffeine applications did not differ at the sub-membrane, center, and nucleus but significantly decreased in the dendrites.

Ryanodine-sensitive Ca^{2+} stores in different central neurons in the rat (including CA1 hippocampal neurons) were reported to be empty at rest and to accumulate Ca^{2+} only after its entry *via* voltage-gated Ca^{2+} channels in the plasmalemma (Brorson et al., 1991; Shmigol et al., 1994; Garaschuk et al., 1997). de Juan-Sanz et al. (2017) found evidence for Ca^{2+} release from the ER in response to a single AP or a train of 20 action potentials evoked at 20 Hz. However, recently been shown that Ca^{2+} release from the ER contributes to train-evoked Ca^{2+} elevation in pyramidal neurons (Tran and Stricker, 2021). As demonstrated in this article, the depletion of the caffeine-sensitive Ca^{2+} stores did not alter the amplitude of depolarization-induced Ca^{2+} transients evoked by low-frequency activity. However, long 5 s KCl depolarization or long train EFS (50 pulses, 9 Hz) of CA1 pyramidal cells induced Ca^{2+} release not only from dendritic ryanodine-sensitive Ca^{2+} stores, which was shown previously (Alford et al., 1993; Garaschuk et al., 1997; Tran and Stricker, 2021) but also at sub-membrane and central regions. They suggested that RyR-mediated Ca^{2+} release from presynaptic intracellular stores contributes to the activation of downstream Ca^{2+}- dependent pathways and signaling molecules, including CaMKII, which are required for LTD induction (Arias-Cavieres et al., 2018). Also, we show that the Ca^{2+} signal at the nucleus significantly depends on Ca^{2+} release from the central ER.

Neuronal dendrites play dominant roles in signal integration, neural computation, plasticity, and structurally associated adaptability (Ashhad and Narayanan, 2019). Ca^{2+} influx from the outside *via* voltage- and ligand-gated ion channels, specific synaptic activation can cause the recruitment of intracellular Ca^{2+} stores. Its results in Ca^{2+} release from the ER *via* intracellular Ca^{2+} release channels (IP_3R and RyR) in dendrites (Nakamura et al., 1999). In the present study, we have shown that calcium signals in the dendritic tree appear faster than in other regions, but the peak value of Ca^{2+} transients in this area is significantly lower than inside the soma. These differences can be explained by the fact that the diameter of the dendrites is ~1 μm, and the calcium signal in it propagates over a shorter distance, in contrast to the soma, and with a smaller

dendrite Ca^{2+} release from the ER. The diffusion of calcium inside neurons is determined not only by distance but also by the intracellular binding sites that rapidly bind free calcium ions (Matthews and Dietrich, 2015). The interplay of several systems that release Ca^{2+} into the cytosol and multiple mechanisms that buffer Ca^{2+} in the cytosol sequester Ca^{2+} in intracellular organelles and extrude Ca^{2+} across the plasmalemma provide the necessary control (Blaustein, 1988) that could be different in sub-membrane, central or dendritic tree space of the neuron.

Spontaneous, localized Ca^{2+} release events are found in cardiac myocytes [Ca^{2+} sparks; (Cheng et al., 1993)] and also reported in dendrites of hippocampal pyramidal neurons (Manita and Ross, 2009; Miyazaki and Ross, 2013). In cardiac myocytes and skeletal muscle, depolarization activates voltage-gated L-type Ca^{2+} channels in the surface membrane resulting in localized, sub-membrane increases in cytosolic Ca^{2+}. Individual Ca^{2+} release units or clusters of RyRs (Stern et al., 1999) are activated essentially simultaneously. The spatial and temporal summation of Ca^{2+} release from individual Ca^{2+} release units gives rise to whole-cell Ca^{2+} transients (Cheng et al., 1994; Hüser et al., 1996; Shkryl and Blatter, 2013). In skeletal fibers and cardiac ventricular myocytes, the extensive transverse (t) tubular network exists that assures physical proximity of surface membrane Ca^{2+} channels and clusters of RyRs in the SR throughout the entire cell volume (Soeller and Cannell, 1999). It ensures highly synchronized and spatially rather homogeneous RyRs-based Ca^{2+} release from the SR (Cannell et al., 1994; Shkryl and Blatter, 2013). In contrast, atrial cells have poorly developed or even entirely lacking t-tubular system (Hüser et al., 1996; Mackenzie et al., 2001; Smyrnias et al., 2010). Due to these ultrastructural arrangements, action potential (AP)-induced membrane depolarization activates Ca^{2+} entry through VGCCs and CICR through RyRs in the sub-membrane region. Elevation of peripheral $[Ca^{2+}]_i$ propagates *via* CICR in a Ca^{2+} wave-like fashion in centripetal direction by a diffusion-reaction process (Keizer et al., 1998; Shkryl and Blatter, 2013; Blatter, 2017). In pyramidal neurons studied here, the Ca^{2+} response to APs was likely similar to the one observed in atrial myocytes (Shkryl and Blatter, 2013; Blatter, 2017). The presence of not only RyRs but also of the high density of IP_3 receptors in hippocampal neurons (Verkhratsky and Shmigol, 1996; Berridge, 1998; Nakamura et al., 2000) makes this process more complicated, requiring not only calcium-mediated activation of RyRs in central ER but also activation IP_3Rs through the diffusion of IP_3 from the periphery cell to the central ER to activate IP_3 receptors in none sub-membrane ER (Blatter et al., 2021); and glutamate-mediated synaptic transmission could contribute a notional part of EFS-induced Ca^{2+} transient that IP_3 receptors could mediate part of the response. In experiments on freshly isolated hippocampal neurons (data not shown), the amplitude of calcium responses was significantly lower during EFS but did not differ during depolarization of solutions with a high KCl, which suggests the role of glutamate receptors in these responses.

Some limitations are present in the study. Caffeine in high concentration could chelate calcium in the lumen of the ER (Rojo-Ruiz et al., 2018) interfering with RyRs activity and reduce the caffeine-induced Ca^{2+} signal. Caffeine interacts with fluorescent calcium indicator dyes (Muschol et al., 1999). In experiments using one wavelength mode excitation, it affects the response amplitude. However, in the ratiometric mode, it is eliminated by the ratiometric. Some studies show that the Fura-2 dye limits the correct recording of Ca^{2+} (Bootman et al., 2013; Shkryl, 2020) or could be saturated with a high Ca^{2+} response, which creates an additional error in determining the actual value of the calcium concentration. Using single wavelength dye like Fluo-4 with a higher ratio of maximal to minimal fluoresce with more precision and the ability to record small Ca^{2+} events like sparks. Limitations of temporal and spatial resolution reduced the ability to reveal more detailed data on Ca^{2+} signaling in pyramidal hippocampal neurons, and fast 2D or 3D confocal microscopy is required. However, the ratiometric measurements of Fura-2 loaded neurons made it possible to achieve the required accuracy of a given signal in various areas of an individual neuron.

In summary, we demonstrate spatial dynamics of free Ca^{2+} concentration in individual rat hippocampal pyramidal neurons in culture recorded by 2D ratiometric fluorescence of Fura-2 signals. 2D imaging of Ca^{2+} transients revealed an asynchronous delayed rise of free Ca^{2+} concentration in the central area compared to near-membrane or dendritic tree regions. The nuclear response was delayed respectively to other cellular parts. Activation of ryanodine receptors by caffeine triggered a rapid rise of $[Ca^{2+}]_i$ in all four analyzed regions of interest. Using the RyR agonist caffeine as a pharmacological tool, we found that functional Ca^{2+} stores resize in the somata and peripheral and dendrites of CA1 pyramidal cells. The treatment with caffeine significantly reduces the peak amplitude of Ca^{2+} transients induced by the KCl depolarizing solution. Short electrical stimulation (1 s) was not enough to enhance the Ca^{2+} signal through CICR, but adequate at long-lasting excitation (6 s) produce calcium release from the ER store there 30% of the peak amplitude of Ca^{2+} transient corresponds to RyRs mediated calcium release.

Data availability statement

The raw data supporting the conclusions of this article will be made available by the authors, without undue reservation.

Ethics statement

All experimental procedures were performed following ethical principles of the European Convention for the protection of vertebrate animals used for experimental and other scientific

purposes (86/609/EEC; European convention, Strasburg, 1986) and were approved by the local Animal Ethics Committee of the Bogomoletz Institute of Physiology (Kyiv, Ukraine).

Author contributions

VS carried out the experiment; conceived and designed the analyses; collected the data; performed the analysis; wrote the article.

Acknowledgments

The author thanks Dr. Igor Melnick for critically reading the manuscript and Dr. Vita Hanzha for cultured hippocampal neurons preparation.

Conflict of interest

The author declares that the research was conducted in the absence of any commercial or financial relationships that could be construed as a potential conflict of interest.

Publisher's note

All claims expressed in this article are solely those of the authors and do not necessarily represent those of their affiliated organizations, or those of the publisher, the editors and the reviewers. Any product that may be evaluated in this article, or claim that may be made by its manufacturer, is not guaranteed or endorsed by the publisher.

References

Alford, S., Frenguelli, B. G., Schofield, J. G., and Collingridge, G. L. (1993). Characterization of Ca^{2+} signals induced in hippocampal CA1 neurones by the synaptic activation of NMDA receptors. *J. Physiol.* 469, 693–716. doi: 10.1113/jphysiol.1993.sp019838

Arias-Cavieres, A., Barrientos, G. C., Sánchez, G., Elgueta, C., Muñoz, P., and Hidalgo, C. (2018). Ryanodine receptor-mediated calcium release has a key role in hippocampal LTD induction. *Front. Cell Neurosci.* 12:403. doi: 10.3389/fncel.2018.00403

Ashhad, S., and Narayanan, R. (2019). Stores, channels, glue and trees: active glial and active dendritic physiology. *Mol. Neurobiol.* 56, 2278–2299. doi: 10.1007/s12035-018-1223-5

Augustine, G. J., Santamaria, F., and Tanaka, K. (2003). Local calcium signaling in neurons. *Neuron* 40, 331–346. doi: 10.1016/s0896-6273(03)00639-1

Berridge, M. J. (1998). Neuronal calcium signaling. *Neuron* 21, 13–26. doi: 10.1016/s0896-6273(00)80510-3

Berridge, M. J. (2002). The endoplasmic reticulum: a multifunctional signaling organelle. *Cell Calcium* 32, 235–249. doi: 10.1016/s0143416002001823

Berridge, M. J. (2009). Inositol trisphosphate and calcium signalling mechanisms. *Biochim. Biophys. Acta* 1793, 933–940. doi: 10.1016/j.bbamcr.2008.10.005

Berridge, M. J., Lipp, P., and Bootman, M. D. (2000). The versatility and universality of calcium signalling. *Nat. Rev. Mol. Cell Biol.* 1, 11–21. doi: 10.1038/35036035

Berrout, J., and Isokawa, M. (2009). Homeostatic and stimulus-induced coupling of the L-type Ca^{2+} channel to the ryanodine receptor in the hippocampal neuron in slices. *Cell Calcium* 46, 30–38. doi: 10.1016/j.ceca.2009.03.018

Bers, D. M. (2002). Cardiac excitation-contraction coupling. *Nature* 415, 198–205. doi: 10.1038/415198a

Blatter, L. A. (2017). The intricacies of atrial calcium cycling during excitation-contraction coupling. *J. Gen. Physiol.* 149, 857–865. doi: 10.1085/jgp.201711809

Blatter, L. A., Kanaporis, G., Martinez-Hernandez, E., Oropeza-Almazan, Y., and Banach, K. (2021). Excitation-contraction coupling and calcium release in atrial muscle. *Pflugers Arch.* 473, 317–329. doi: 10.1007/s00424-020-02506-x

Blaustein, M. P. (1988). Calcium transport and buffering in neurons. *Trends Neurosci.* 11, 438–443. doi: 10.1016/0166-2236(88)90195-6

Bloodgood, B. L., and Sabatini, B. L. (2007). Ca^{2+} signaling in dendritic spines. *Curr. Opin. Neurobiol.* 17, 345–351. doi: 10.1016/j.conb.2007.04.003

Bootman, M. D., Rietdorf, K., Collins, T., Walker, S., and Sanderson, M. (2013). Ca^{2+}-sensitive fluorescent dyes and intracellular Ca^{2+} imaging. *Cold Spring Harb. Protoc.* 2013, 83–99. doi: 10.1101/pdb.top066050

Brorson, J. R., Bleakman, D., Gibbons, S. J., and Miller, R. J. (1991). The properties of intracellular calcium stores in cultured rat cerebellar neurons. *J. Neurosci.* 11, 4024–4043. doi: 10.1523/JNEUROSCI.11-12-04024.1991

Cannell, M. B., Cheng, H., and Lederer, W. J. (1994). Spatial non-uniformities in $[Ca^{2+}]_i$ during excitation-contraction coupling in cardiac myocytes. *Biophys. J.* 67, 1942–1956. doi: 10.1016/S0006-3495(94)80677-0

Chavis, P., Fagni, L., Lansman, J. B., and Bockaert, J. (1996). Functional coupling between ryanodine receptors and L-type calcium channels in neurons. *Nature* 382, 719–722. doi: 10.1038/382719a0

Cheng, H., Cannell, M. B., and Lederer, W. J. (1994). Propagation of excitation-contraction coupling into ventricular myocytes. *Pflugers Arch.* 428, 415–417. doi: 10.1007/BF00724526

Cheng, H., Lederer, W. J., and Cannell, M. B. (1993). Calcium sparks: elementary events underlying excitation-contraction coupling in heart muscle. *Science* 262, 740–744. doi: 10.1126/science.8235594

Clapham, D. E. (2007). Calcium signaling. *Cell* 131, 1047–1058. doi: 10.1016/j.cell.2007.11.028

De Crescenzo, V., ZhuGe, R., Velázquez-Marrero, C., Lifshitz, L. M., Custer, E., Carmichael, J., et al. (2004). Ca^{2+} syntillas, miniature Ca^{2+} release events in terminals of hypothalamic neurons, are increased in frequency by depolarization in the absence of Ca^{2+} influx. *J. Neurosci.* 24, 1226–1235. doi: 10.1523/JNEUROSCI.4286-03.2004

de Juan-Sanz, J., Holt, G. T., Schreiter, E. R., de Juan, F., Kim, D. S., and Ryan, T. A. (2017). Axonal endoplasmic reticulum Ca^{2+} content controls release probability in CNS nerve terminals. *Neuron* 93, 867–881.e6. doi: 10.1016/j.neuron.2017.01.010

Diszházi, G., Magyar, Z., Mótyán, J. A., Csernoch, L., Jóna, I., Nánási, P. P., et al. (2019). Dantrolene requires Mg^{2+} and ATP to inhibit the ryanodine receptor. *Mol. Pharmacol.* 96, 401–407. doi: 10.1124/mol.119.116475

Endo, M., Tanaka, M., and Ogawa, Y. (1970). Calcium induced release of calcium from the sarcoplasmic reticulum of skinned skeletal muscle fibres. *Nature* 228, 34–36. doi: 10.1038/228034a0

Fabiato, A. (1983). Calcium-induced release of calcium from the cardiac sarcoplasmic reticulum. *Am. J. Physiol.* 245, C1–C14. doi: 10.1152/ajpcell.1983.245.1.C1

Fedorenko, O. A., and Marchenko, S. M. (2014). Ion channels of the nuclear membrane of hippocampal neurons. *Hippocampus* 24, 869–876. doi: 10.1002/hipo.22276

Fill, M., and Copello, J. A. (2002). Ryanodine receptor calcium release channels. *Physiol. Rev.* 82, 893–922. doi: 10.1152/physrev.00013.2002

Ford, L. E., and Podolsky, R. J. (1970). Regenerative calcium release within muscle cells. *Science* 167, 58–59. doi: 10.1126/science.167.3914.58

Frenguelli, B. G., and Malinow, R. (1996). Fluctuations in intracellular calcium responses to action potentials in single en passage presynaptic boutons of layer V neurons in neocortical slices. *Learn. Mem.* 3, 150–159. doi: 10.1101/lm.3.2-3.150

Friel, D. D., and Tsien, R. W. (1992). A caffeine- and ryanodine-sensitive Ca^{2+} store in bullfrog sympathetic neurones modulates effects of Ca^{2+} entry on $[Ca^{2+}]i$. *J. Physiol.* 450, 217–246. doi: 10.1113/jphysiol.1992.sp019125

Fruen, B. R., Mickelson, J. R., and Louis, C. F. (1997). Dantrolene inhibition of sarcoplasmic reticulum Ca^{2+} release by direct and specific action at skeletal muscle ryanodine receptors. *J. Biol. Chem.* 272, 26965–26971. doi: 10.1074/jbc.272.43.26965

Garaschuk, O., Yaari, Y., and Konnerth, A. (1997). Release and sequestration of calcium by ryanodine-sensitive stores in rat hippocampal neurones. *J. Physiol.* 502, 13–30. doi: 10.1111/j.1469-7793.1997.013bl.x

Hardingham, G. E., Arnold, F. J., and Bading, H. (2001). A calcium microdomain near NMDA receptors: on switch for ERK-dependent synapse-to-nucleus communication. *Nat. Neurosci.* 4, 565–566. doi: 10.1038/88380

Holliday, J., Adams, R. J., Sejnowski, T. J., and Spitzer, N. C. (1991). Calcium-induced release of calcium regulates differentiation of cultured spinal neurons. *Neuron* 7, 787–796. doi: 10.1016/0896-6273(91)90281-4

Hüser, J., Lipsius, S. L., and Blatter, L. A. (1996). Calcium gradients during excitation-contraction coupling in cat atrial myocytes. *J. Physiol.* 494, 641–651. doi: 10.1016/j.ajog.2022.10.025

Isokawa, M., and Alger, B. E. (2006). Ryanodine receptor regulates endogenous cannabinoid mobilization in the hippocampus. *J. Neurophysiol.* 95, 3001–3011. doi: 10.1152/jn.00975.2005

Jacobs, J. M., and Meyer, T. (1997). Control of action potential-induced Ca^{2+} signaling in the soma of hippocampal neurons by Ca^{2+} release from intracellular stores. *J. Neurosci.* 17, 4129–4135. doi: 10.1523/JNEUROSCI.17-11-04129.1997

Johenning, F. W., Theis, A. K., Pannasch, U., Ruckl, M., Rudiger, S., and Schmitz, D. (2015). Ryanodine receptor activation induces long-term plasticity of spine calcium dynamics. *PLoS Biol.* 13:e1002181. doi: 10.1371/journal.pbio.1002181

Kano, M., Garaschuk, O., Verkhratsky, A., and Konnerth, A. (1995). Ryanodine receptor-mediated intracellular calcium release in rat cerebellar Purkinje neurones. *J. Physiol.* 487, 1–16. doi: 10.1113/jphysiol.1995.sp020857

Keizer, J., Smith, G. D., Ponce-Dawson, S., and Pearson, J. E. (1998). Saltatory propagation of Ca^{2+} waves by Ca^{2+} sparks. *Biophys. J.* 75, 595–600. doi: 10.1016/S0006-3495(98)77550-2

Khakh, B. S., and McCarthy, K. D. (2015). Astrocyte calcium signaling: from observations to functions and the challenges therein. *Cold Spring Harb. Perspect. Biol.* 7:a020404. doi: 10.1101/cshperspect.a020404

Koizumi, S., Bootman, M. D., Bobanovic, L. K., Schell, M. J., Berridge, M. J., and Lipp, P. (1999). Characterization of elementary Ca^{2+} release signals in NGF-differentiated PC12 cells and hippocampal neurons. *Neuron* 22, 125–137. doi: 10.1016/s0896-6273(00)80684-4

Kong, H., Jones, P. P., Koop, A., Zhang, L., Duff, H. J., and Chen, S. R. (2008). Caffeine induces Ca^{2+} release by reducing the threshold for luminal Ca^{2+} activation of the ryanodine receptor. *Biochem. J.* 414, 441–452. doi: 10.1042/BJ20080489

Kuba, K. (1994). Ca^{2+}-induced Ca^{2+} release in neurones. *Jpn. J. Physiol.* 44, 613–650. doi: 10.2170/jjphysiol.44.613

Larkum, M. E., Watanabe, S., Nakamura, T., Lasser-Ross, N., and Ross, W. N. (2003). Synaptically activated Ca^{2+} waves in layer 2/3 and layer 5 rat neocortical pyramidal neurons. *J. Physiol.* 549, 471–488. doi: 10.1113/jphysiol.2002.037614

Llano, I., DiPolo, R., and Marty, A. (1994). Calcium-induced calcium release in cerebellar Purkinje cells. *Neuron* 12, 663–673. doi: 10.1016/0896-6273(94)90221-6

Mackenzie, L., Bootman, M. D., Berridge, M. J., and Lipp, P. (2001). Predetermined recruitment of calcium release sites underlies excitation-contraction coupling in rat atrial myocytes. *J. Physiol.* 530, 417–429. doi: 10.1111/j.1469-7793.2001.0417k.x

Manita, S., and Ross, W. N. (2009). Synaptic activation and membrane potential changes modulate the frequency of spontaneous elementary Ca^{2+} release events in the dendrites of pyramidal neurons. *J. Neurosci.* 29, 7833–7845. doi: 10.1523/JNEUROSCI.0573-09.2009

Matthews, E. A., and Dietrich, D. (2015). Buffer mobility and the regulation of neuronal calcium domains. *Front. Cell Neurosci.* 9:48. doi: 10.3389/fncel.2015.00048

Miyazaki, K., and Ross, W. N. (2013). Ca^{2+} sparks and puffs are generated and interact in rat hippocampal CA1 pyramidal neuron dendrites. *J. Neurosci.* 33, 17777–17788. doi: 10.1523/JNEUROSCI.2735-13.2013

Miyazaki, K., Manita, S., and Ross, W. N. (2012). Developmental profile of localized spontaneous Ca^{2+} release events in the dendrites of rat hippocampal pyramidal neurons. *Cell Calcium* 52, 422–432. doi: 10.1016/j.ceca.2012.08.001

Muschol, M., Dasgupta, B. R., and Salzberg, B. M. (1999). Caffeine interaction with fluorescent calcium indicator dyes. *Biophys. J.* 77, 577–586. doi: 10.1016/S0006-3495(99)76914-6

Nakamura, T., Barbara, J. G., Nakamura, K., and Ross, W. N. (1999). Synergistic release of Ca^{2+} from IP3-sensitive stores evoked by synaptic activation of mGluRs paired with backpropagating action potentials. *Neuron* 24, 727–737. doi: 10.1016/s0896-6273(00)81125-3

Nakamura, T., Nakamura, K., Lasser-Ross, N., Barbara, J. G., Sandler, V. M., and Ross, W. N. (2000). Inositol 1,4,5-trisphosphate (IP_3)-mediated Ca^{2+} release evoked by metabotropic agonists and backpropagating action potentials in hippocampal CA1 pyramidal neurons. *J. Neurosci.* 20, 8365–8376. doi: 10.1523/JNEUROSCI.20-22-08365.2000

Niggli, E. (1999). Localized intracellular calcium signaling in muscle: calcium sparks and calcium quarks. *Annu. Rev. Physiol.* 61, 311–335. doi: 10.1146/annurev.physiol.61.1.311

Niswender, C. M., and Conn, P. J. (2010). Metabotropic glutamate receptors: physiology, pharmacology and disease. *Annu. Rev. Pharmacol. Toxicol.* 50, 295–322. doi: 10.1146/annurev.pharmtox.011008.145533

Porta, M., Zima, A. V., Nani, A., Diaz-Sylvester, P. L., Copello, J. A., Ramos-Franco, J., et al. (2011). Single ryanodine receptor channel basis of caffeine's action on Ca^{2+} sparks. *Biophys. J.* 100, 931–938. doi: 10.1016/j.bpj.2011.01.017

Pozzan, T., Rizzuto, R., Volpe, P., and Meldolesi, J. (1994). Molecular and cellular physiology of intracellular calcium stores. *Physiol. Rev.* 74, 595–636. doi: 10.1152/physrev.1994.74.3.595

Pozzo Miller, L. D., Petrozzino, J. J., Golarai, G., and Connor, J. A. (1996). Ca^{2+} release from intracellular stores induced by afferent stimulation of CA3 pyramidal neurons in hippocampal slices. *J. Neurophysiol.* 76, 554–562. doi: 10.1152/jn.1996.76.1.554

Rizzuto, R., and Pozzan, T. (2006). Microdomains of intracellular Ca^{2+}: molecular determinants and functional consequences. *Physiol. Rev.* 86, 369–408. doi: 10.1152/physrev.00004.2005

Rojo-Ruiz, J., Rodríguez-Prados, M., Delrio-Lorenzo, A., Alonso, M. T., and García-Sancho, J. (2018). Caffeine chelates calcium in the lumen of the endoplasmic reticulum. *Biochem. J.* 475, 3639–3649. doi: 10.1042/BCJ20180532

Rose, C. R., and Konnerth, A. (2001). Stores not just for storage. intracellular calcium release and synaptic plasticity. *Neuron* 31, 519–522. doi: 10.1016/s0896-6273(01)00402-0

Rosenbluth, J. (1962). Subsurface cisterns and their relationship to the neuronal plasma membrane. *J. Cell Biol.* 13, 405–421. doi: 10.1083/jcb.13.3.405

Ross, W. N. (2012). Understanding calcium waves and sparks in central neurons. *Nat. Rev. Neurosci.* 13, 157–168. doi: 10.1038/nrn3168

Shkryl, V. M. (2017). Intracellular calcium fluxes in excitable cells. *Neurophysiology* 49, 384–392. doi: 10.1007/s11062-018-9698-2

Shkryl, V. M. (2020). Error correction due to background subtraction in ratiometric calcium measurements with CCD camera. *Heliyon* 6:e04180. doi: 10.1016/j.heliyon.2020.e04180

Shkryl, V. M., and Blatter, L. A. (2013). Ca^{2+} release events in cardiac myocytes up close: insights from fast confocal imaging. *PLoS One* 8:e61525. doi: 10.1371/journal.pone.0061525

Shkryl, V. M., Blatter, L. A., and Ríos, E. (2012a). Properties of Ca^{2+} sparks revealed by four-dimensional confocal imaging of cardiac muscle. *J. Gen. Physiol.* 139, 189–207. doi: 10.1085/jgp.201110709

Shkryl, V. M., Maxwell, J. T., Domeier, T. L., and Blatter, L. A. (2012b). Refractoriness of sarcoplasmic reticulum Ca^{2+} release determines Ca^{2+} alternans in atrial myocytes. *Am. J. Physiol. Heart Circ. Physiol.* 302, H2310–H2320. doi: 10.1152/ajpheart.00079.2012

Shkryl, V. M., Nikolaenko, L. M., Kostyuk, P. G., and Lukyanetz, E. A. (1999). High-threshold calcium channel activity in rat hippocampal neurones during hypoxia. *Brain Res.* 833, 319–328. doi: 10.1016/s0006-8993(99)01575-9

Shmigol, A., Kirischuk, S., Kostyuk, P., and Verkhratsky, A. (1994). Different properties of caffeine-sensitive Ca^{2+} stores in peripheral and central mammalian neurones. *Pflugers Arch.* 426, 174–176. doi: 10.1007/BF00374686

Smyrnias, I., Mair, W., Harzheim, D., Walker, S. A., Roderick, H. L., and Bootman, M. D. (2010). Comparison of the T-tubule system in adult rat ventricular and atrial myocytes and its role in excitation-contraction coupling and inotropic stimulation. *Cell Calcium* 47, 210–223. doi: 10.1016/j.ceca.2009.10.001

Soeller, C., and Cannell, M. B. (1999). Examination of the transverse tubular system in living cardiac rat myocytes by 2-photon microscopy and digital image-processing techniques. *Circ. Res.* 84, 266–275. doi: 10.1161/01.res.84.3.266

Stern, M. D., Song, L. S., Cheng, H., Sham, J. S., Yang, H. T., Boheler, K. R., et al. (1999). Local control models of cardiac excitation-contraction coupling. a possible role for allosteric interactions between ryanodine receptors. *J. Gen. Physiol.* 113, 469–489. doi: 10.1085/jgp.113.3.469

Tao-Cheng, J. H. (2018). Activity-dependent decrease in contact areas between subsurface cisterns and plasma membrane of hippocampal neurons. *Mol. Brain* 11:23. doi: 10.1186/s13041-018-0366-7

Thorn, P., Lawrie, A. M., Smith, P. M., Gallacher, D. V., and Petersen, O. H. (1993). Ca^{2+} oscillations in pancreatic acinar cells: spatiotemporal relationships and functional implications. *Cell Calcium* 14, 746–757. doi: 10.1016/0143-4160(93)90100-k

Tran, V., and Stricker, C. (2021). Spontaneous and action potential-evoked Ca^{2+} release from endoplasmic reticulum in neocortical synaptic boutons. *Cell Calcium* 97:102433. doi: 10.1016/j.ceca.2021.102433

Verkhratsky, A. (2002). The endoplasmic reticulum and neuronal calcium signalling. *Cell Calcium* 32, 393–404. doi: 10.1016/s0143416002001896

Verkhratsky, A. (2005). Physiology and pathophysiology of the calcium store in the endoplasmic reticulum of neurons. *Physiol. Rev.* 85, 201–279. doi: 10.1152/physrev.00004.2004

Verkhratsky, A., and Kettenmann, H. (1996). Calcium signalling in glial cells. *Trends Neurosci.* 19, 346–352. doi: 10.1016/0166-2236(96)10048-5

Verkhratsky, A., and Shmigol, A. (1996). Calcium-induced calcium release in neurones. *Cell Calcium* 19, 1–14. doi: 10.1016/s0143-4160(96)90009-3

Viero, C., Thomas, N. L., Euden, J., Mason, S. A., George, C. H., and Williams, A. J. (2012). Techniques and methodologies to study the ryanodine receptor at the molecular, subcellular and cellular level. *Adv. Exp. Med. Biol.* 740, 183–215. doi: 10.1007/978-94-007-2888-2_8

Wu, Y., Whiteus, C., Xu, C. S., Hayworth, K. J., Weinberg, R. J., Hess, H. F., et al. (2017). Contacts between the endoplasmic reticulum and other membranes in neurons. *Proc. Natl. Acad. Sci. U S A* 114, E4859–E4867. doi: 10.1073/pnas.1701078114

Zhou, Z., and Neher, E. (1993). Mobile and immobile calcium buffers in bovine adrenal chromaffin cells. *J. Physiol.* 469, 245–273. doi: 10.1113/jphysiol.1993.sp019813

frontiers | Frontiers in Cellular Neuroscience

TYPE Original Research
PUBLISHED 17 February 2023
DOI 10.3389/fncel.2023.1072750

OPEN ACCESS

EDITED BY
Ulises Gomez-Pinedo,
Health Research Institute of Hospital Clínico San Carlos, Spain

REVIEWED BY
Edwin Estefan Reza,
Monterrey Institute of Technology and Higher Education (ITESM), Mexico
Yanet Karina Gutierrez-Mercado,
University of Guadalajara, Mexico

*CORRESPONDENCE
Oleg Tsupykov
tsupykov@gmail.com

SPECIALTY SECTION
This article was submitted to Cellular Neuropathology, a section of the journal Frontiers in Cellular Neuroscience

RECEIVED 17 October 2022
ACCEPTED 30 January 2023
PUBLISHED 17 February 2023

CITATION
Kyryk V, Tsupykov O, Ustymenko A, Smozhanik E, Govbakh I, Butenko G and Skibo G (2023) Age-related ultrastructural changes in spheroids of the adipose-derived multipotent mesenchymal stromal cells from ovariectomized mice.
Front. Cell. Neurosci. 17:1072750.
doi: 10.3389/fncel.2023.1072750

Age-related ultrastructural changes in spheroids of the adipose-derived multipotent mesenchymal stromal cells from ovariectomized mice

Vitalii Kyryk[1,2], Oleg Tsupykov[1,3]*, Alina Ustymenko[1,2], Ekaterina Smozhanik[3], Iryna Govbakh[4], Gennadii Butenko[1,2] and Galyna Skibo[1,3]

[1]Cell and Tissue Technologies Department, Institute of Regenerative Medicine, National Scientific Center M.D. Strazhesko Institute of Cardiology, Clinical and Regenerative Medicine of the National Academy of Medical Sciences of Ukraine, Kyiv, Ukraine, [2]Laboratory of Pathophysiology and Immunology, D. F. Chebotarev State Institute of Gerontology of the National Academy of Medical Sciences of Ukraine, Kyiv, Ukraine, [3]Department of Cytology, Bogomoletz Institute of Physiology of the National Academy of Sciences of Ukraine, Kyiv, Ukraine, [4]Department of General Practice-Family Medicine, Kharkiv Medical Academy of Postgraduate Education, Kharkiv, Ukraine

Introduction: Adipose-derived multipotent mesenchymal stromal cells (ADSCs) are widely used for cell therapy, in particular for the treatment of diseases of the nervous system. An important issue is to predict the effectiveness and safety of such cell transplants, considering disorders of adipose tissue under age-related dysfunction of sex hormones production. The study aimed to investigate the ultrastructural characteristics of 3D spheroids formed by ADSCs of ovariectomized mice of different ages compared to age-matched controls.

Methods: ADSCs were obtained from female CBA/Ca mice randomly divided into four groups: CtrlY—control young (2 months) mice, CtrlO—control old (14 months) mice, OVxY—ovariectomized young mice, and OVxO—ovariectomized old mice of the same age. 3D spheroids were formed by micromass technique for 12–14 days and their ultrastructural characteristics were estimated by transmission electron microscopy.

Results and Discussion: The electron microscopy analysis of spheroids from CtrlY animals revealed that ADSCs formed a culture of more or less homogeneous in size multicellular structures. The cytoplasm of these ADSCs had a granular appearance due to being rich in free ribosomes and polysomes, indicating active protein synthesis. Extended electron-dense mitochondria with a regular cristae structure and a predominant condensed matrix were observed in ADSCs from CtrlY group, which could indicate high respiratory activity. At the same time, ADSCs from CtrlO group formed a culture of heterogeneous in size spheroids. In ADSCs from CtrlO group, the mitochondrial population was heterogeneous, a significant part was represented by more round structures. This may indicate an increase in mitochondrial fission and/or an impairment of the fusion. Significantly fewer polysomes were observed in the cytoplasm of ADSCs from CtrlO group, indicating low protein synthetic activity. The cytoplasm of ADSCs in spheroids from old mice had significantly increased amounts of lipid droplets compared to cells obtained from young animals. Also, an increase in the number of lipid droplets in the cytoplasm of ADSCs was observed in both the group of young and old ovariectomized mice compared with control animals of

the same age. Together, our data indicate the negative impact of aging on the ultrastructural characteristics of 3D spheroids formed by ADSCs. Our findings are particularly promising in the context of potential therapeutic applications of ADSCs for the treatment of diseases of the nervous system.

KEYWORDS

ultrastructure, spheroids, adipose-derived multipotent mesenchymal stromal cells, ovariectomy, aging

Introduction

Adipose tissue is a rich source of multipotent mesenchymal stromal cells (ADSCs). The use of ADSCs in modern medicine makes it possible to realize their multilinear potential in various pathological conditions: in the treatment of diseases of the nervous system (Ma et al., 2020; Zhou et al., 2020), endothelial dysfunction in critical limb ischemia and diabetes mellitus (Magenta et al., 2021), endocrine dysfunction (Amer et al., 2018), in coronary heart disease (Murohara et al., 2009), in plastic and reconstructive surgery of soft tissues, and the musculoskeletal system, etc.

However, it is important to note that the therapeutic success of cell therapy may depend on many factors, including the age of the donor. In a study by Liu et al. (2017), a negative effect of the age of the donor's adipose tissue on the quantity and quality of human mesenchymal adipose-derived cells was shown: both the number of colony-forming units of fibroblasts and the number of cells obtained from the stromal-vascular fraction *in vitro*, as well as the rate of their proliferation, are reduced. In addition, a violation of the migration ability of cells obtained from old donors was observed, which is explained by the reduced expression of chemokine receptors such as CXCR4 and CXCR7 (Liu et al., 2017).

Most of the pathological conditions that require cell therapy using autologous stem cells occur mainly in the elderly, so it is relevant to establish criteria for the biological safety of stem cells of adipose origin obtained in the menopausal and postmenopausal periods, which are accompanied by estrogen deficiency (Eastell et al., 2016).

The features of ADSCs are affected by both culture conditions and intercellular signals. Unlike 2D cultivation, three-dimensional (3D) culture of ADSCs in the form of spheroids, which partially mimics the conditions of the microenvironment (niche) of stem cells, can significantly improve their survival in the recipient tissue and increase the overall regenerative potential (Egger et al., 2018).

The aim of our study was to investigate the ultrastructural characteristics of multicellular three-dimensional spheroids formed by ADSCs obtained under conditions of estrogen deficiency in a model of ovariectomy in mice of different ages compared to age-matched controls. Our study aimed at establishing the mechanisms of cellular self-organization, contact intercellular signaling, extracellular matrix production, and resistance to hypoxia depending on the size of the spheroid.

Materials and methods

All animal procedures were performed in accordance with "European Convention for the protection of Vertebrate Animals Use for Experimental and Other Scientific Purposes" (Strasbourg, 1986), "European Directive 2010/63/EU on the protection of animals used for scientific purposes" and the Law of Ukraine "On protection of animals from cruelty" as well as in abidance to all principles of bioethics and biosafety regulations. The study was approved by Ethics Committee of the Institute of Genetic and Regenerative Medicine (protocol no. 9-2021 dated December 15, 2021).

Animals

Adipose tissue was obtained from young (2 months) and old (14 months) female CBA/Ca mice, which were kept under standard conditions in a vivarium of the D. F. Chebotarev State Institute of Gerontology NAMS of Ukraine under a 12:12 h light/dark cycle with access to water and food *ad libitum* (**Table 1**).

Ovariectomy modeling

Animals were anesthetized by intraperitoneal administration of 2.5% solution of 2,2,2-tribromethanol (Sigma-Aldrich, St. Louis, MO, USA) at a dose of 400 mg/kg and bilateral ovariectomy was performed under aseptic conditions using microsurgery technique. The animals of the same age which had only incisions of the abdominal cavity and isolation of the ovaries without resection (sham-operated) were used as a control group. Wounds were sutured in layers; the animals were kept under a heat lamp until the recovery from anesthesia.

TABLE 1 The distribution of animals in the experimental groups.

Experimental group	Young	Old
	The age of animals at the time of surgery (months); number (n)	
Control, sham-operated (Ctrl)	2 months ($n = 8$)	14 months ($n = 11$)
Ovariectomy (OVx)	2 months ($n = 7$)	14 months ($n = 8$)

Adipose-derived mesenchymal stromal cells isolation and culture

Murine ADSCs cultures were obtained and characterized according to standard methods (Yu et al., 2011). Two months after ovariectomy the CBA/Ca mice were euthanized by cervical dislocation under the anesthesia with 2.5% solution of 2,2,2-tribromethanol at a dose 400 mg/kg. Under sterile conditions, subcutaneous adipose tissue was isolated, minced with scissors into 1 mm^3 pieces in DMEM/F12 medium (Sigma-Aldrich, St. Louis, MO, USA) and incubated in 0.1% solution of collagenase type IA (Sigma-Aldrich, St. Louis, MO, USA) for 60 min at 37°C with constant stirring on a shaker at 100 rpm. The resulting cell suspension was washed in 10 ml DMEM medium (Sigma-Aldrich, St. Louis, MO, USA) by centrifugation at 300× *g* for 5 min. The supernatant with mature adipocytes and debris was discarded and pellet passed through a sterile cell strainer with a pore diameter of 100 μm (Greiner bio-one, Kremsmünster, Austria). Cells of the stromal-vascular fraction were cultured in a CO_2 incubator in humidified atmosphere with 5% CO_2 at a temperature of +37°C in complete nutrient medium DMEM-LG (Sigma-Aldrich, St. Louis, MO, USA) supplemented with 15% fetal bovine serum (FBS) (HyClone Laboratories Inc., South Logan, UT, USA), penicillin 100 U/ml, streptomycin 100 μg/ml (Sigma-Aldrich, St. Louis, MO, USA), 1:100 nonessential amino acids (Sigma-Aldrich, St. Louis, MO, USA). The nutrient medium was replaced in 3 days. Cells were sub-cultured to achieve 80% monolayer confluency (for 4–5 days) using 0.25% trypsin (Sigma-Aldrich, St. Louis, MO, USA) and 0.02% Versene solution (Bio-Test Laboratory, Kyiv, Ukraine).

Immunophenotyping of ADSCs

On the 2nd passage, cells were analyzed by flow cytometry with BD FACSAria cell sorter (Becton Dickinson, Franklin Lakes, NJ, USA) using anti-mouse monoclonal antibodies: CD90 APC-Cy7 (BD Biosciences, cat. no. 561401, Franklin Lakes, NJ, USA), CD105 APC (Invitrogen, cat. no. 17-1051-82, Carlsbad, CA, USA), CD73 PE (BD Biosciences, cat. no. 550741, Franklin Lakes, NJ, USA), CD44 PE (BD Biosciences, cat. no. 553134, Franklin Lakes, NJ, USA), CD45 PE (Thermo Fisher Scientific, cat. no. MA1-10233, Waltham, MA, USA), CD34 Alexa Fluor® 647 (BD Biosciences, cat. no. 560230, Franklin Lakes, NJ, USA).

Three-dimensional spheroids formed by ADSCs

After the second passage, the monolayer culture of ADSCs was transferred to a suspension state, washed from the enzyme, and 1.5 × 10^6 cells were transferred to a 5 ml PS tube with a non-adhesive surface. After the formation of the spheroids (after 24–48 h of culturing in the tube), the cells were cultured for 12–14 days in a CO_2 incubator under conditions of humidified atmosphere with 5% CO_2 at a temperature of +37°C. The nutrient medium was completely replaced every 2–3 days. On the 5–7th day, the standard medium for cultivation was replaced with medium for adipogenic induction to confirm that the obtained cultures met the minimal criteria to define ADSCs in terms of potential for directed differentiation. Adipogenic differentiation was performed using DMEM High Glucose medium (Gibco, USA) supplemented with 10% FBS, dexamethasone (1 μM), indomethacin (200 μM), 3-Isobutyl-1-methylxanthine (500 μM), and insulin (5 μg/ml), all reagents—Sigma-Aldrich, St. Louis, MO, USA. The medium was changed every 3 days and the cells were cultured for 14 days. The area of spheroids was calculated according to the formula: $S = 4 \cdot \pi R^2$, where π is a constant of 3.14; R is the radius of the sphere. To estimate the area of spheroids, we used images obtained under inverted microscope IX-71 (Olympus, Japan) using a DP20 (Olympus, Japan) camera and performed measurements using QuicjPHOTO MICRO 2.3 software (Olympus, Japan). On day 14 *in vitro* grown cultures (DIV14) ADSCs spheroids were rinsed with PBS and fixed with 4% formaldehyde. After staining with Oil Red O (Sigma-Aldrich, St. Louis, MO, USA), the cells were visualized with light microscopy IX-71 (Olympus, Japan).

Transmission electron microscopy (TEM)

The ADSCs spheroids from different experimental groups were centrifuged at 500× *g* and pellets were processed for TEM according to usual protocols (Tsupykov et al., 2016). Briefly, the culture medium was replaced with 4% formaldehyde and 2.5% glutaraldehyde (Fluka, Buchs, Switzerland) in 0.1 M phosphate buffer (PB). ADSCs spheroids were then rinsed, postfixed in 1% osmium tetroxide (Sigma-Aldrich, St. Louis, MO, USA) in 0.1 M PB, dehydrated in ascending concentrations (50%–100%) of ethanol, and then embedded in Epon 812 (Fluka, Buchs, Switzerland). Ultrathin sections (50–70 nm) were cut with a diamond knife, collected on single slot grids and then counterstained with lead citrate (Fluka, Buchs, Switzerland) and alcoholic uranyl acetate (Merck, Darmstadt, Germany). Grids were examined in JEOL 100-CX (JEOL, Japan) electron microscope operating at 80 kV.

Results

Immunophenotyping of adipose-derived multipotent mesenchymal stromal cells cultures

According to flow cytometry data, the ADSCs cultures obtained from both young and old mice expressed typical stromal markers CD44, CD90, and CD105 at a high level (≥95%). At the same time, low expression of hematopoietic markers CD34 and CD45 (<3%) was noted (**Figure 1**). In our previous study, we confirmed the potential of ADSCs from ovariectomized mice to differentiate into osteogenic and adipogenic directions (Ustymenko et al., 2019). Taking into account significant changes in adipose and bone tissue associated with hormonal changes in old age, we focused our research efforts specifically on assessing the osteogenic and adipogenic differentiation potential of adipose-derived cells. As a result, the morphology, phenotype and differentiation

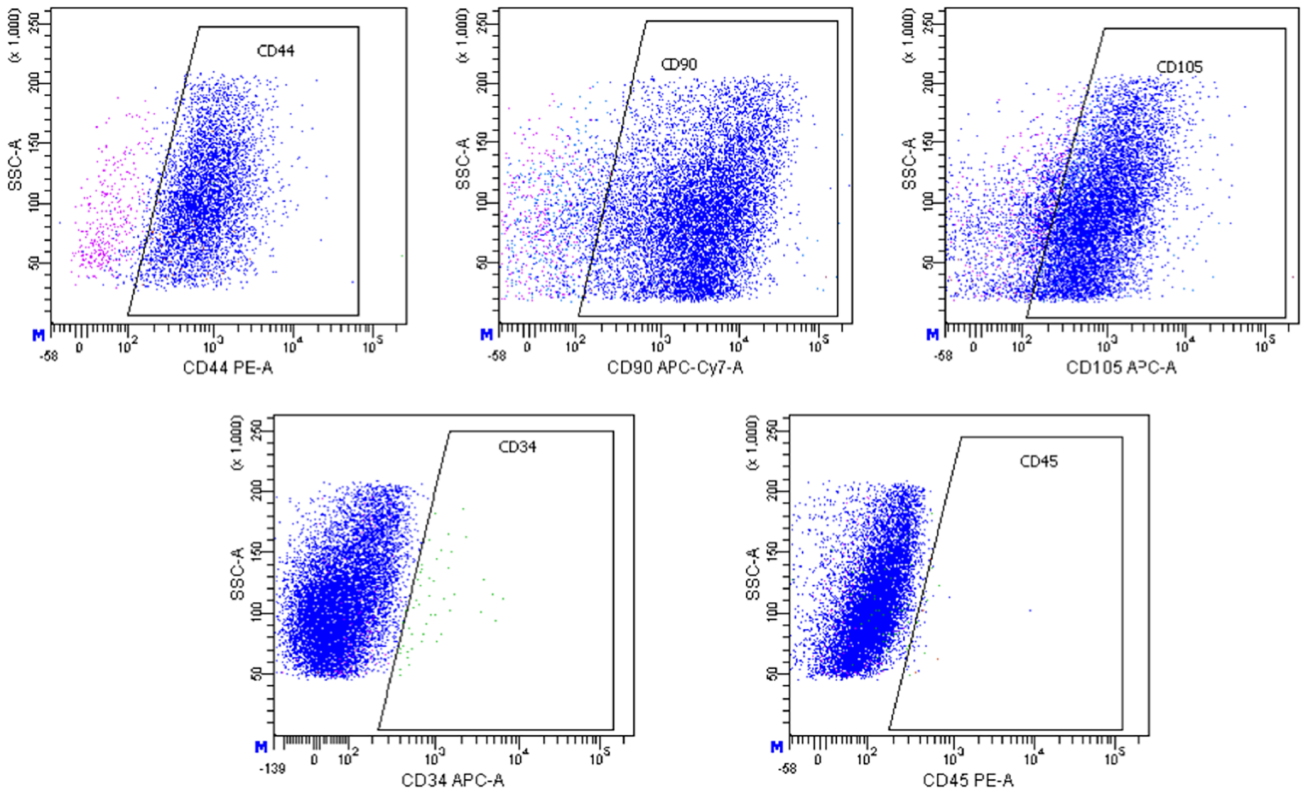

FIGURE 1
Histograms of expression of CD44, CD90, CD105, CD34, and CD45 markers in the culture of murine ADSCs from young animals according to flow cytometry, the 2nd passage.

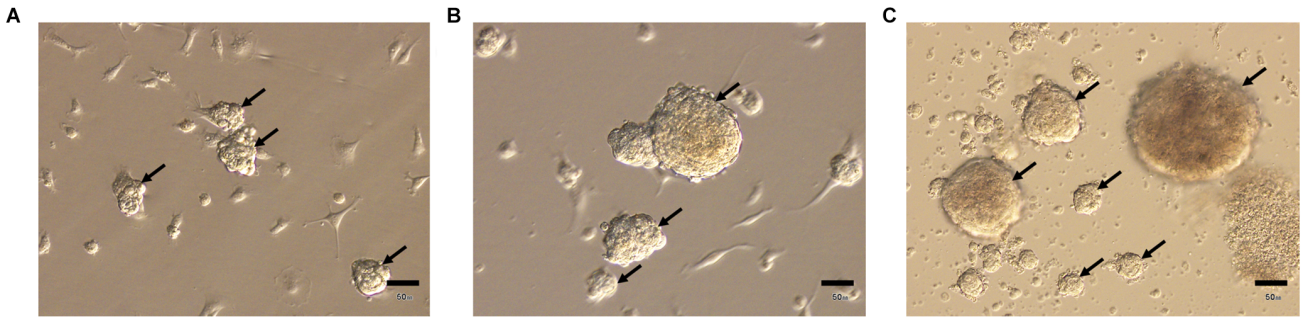

FIGURE 2
Three-dimensional spheroids (arrows) formed by ADSCs, obtained from young **(A)**, old **(B)**, and ovariectomized old **(C)** animals. Light microscopy. Scale bar—50 μm.

potential of obtained ADSCs cultures meet the minimal criteria for defining multipotent mesenchymal stromal cells according to the International Society for Cellular Therapy (ISCT) position statement (Dominici et al., 2006).

Three-dimensional spheroids formed by ADSCs

Our observations showed that ADSCs obtained from control young animals form a culture of more or less homogeneous spheres in size, the surface area of which ranges approximately from 5,000 μm^2 to 7,000 μm^2 (Figure 2A).

At the same time, ADSCs obtained from control and ovariectomized old animals are able to form a 3D-culture heterogeneous in size, the surface area of which approximately ranges from 3,000 μm^2 to 160,000 μm^2 (Figures 2B,C).

In addition, spheroids formed by ADSCs obtained from control and ovariectomized old animals exhibit enhanced adipogenic potential compared to ADSCs obtained from young mice (data not shown).

Ultrastructural analysis of spheroids from ADSCs

Results from electron microscopy showed that adipose-derived multipotent mesenchymal stromal cells (ADSCs) from young control CBA/Ca mice under non-adhesive conditions formed a culture of more or less homogeneous in size multicellular structures (from 75 μm to 95 μm in diameter)—spheroids consisted of several surface layers and an inner zone (**Figures 3A,B**).

The inner zone consisted of polygonal or round cells, embedded in an extracellular matrix (**Figure 3B**). These cells were tightly packed, with narrow extracellular spaces. In the inner area, ADSCs were attached to each other by numerous junctions, which, at high magnification, appeared as tight junctions (**Figure 3D**). ADSCs had a single, irregularly shaped and large euchromatic nuclei with one or more nucleoli (**Figures 3B,C**). Elongated electron-dense mitochondria with a regular cristae structure and a predominant condensed matrix were observed in ADSCs from CtrlY group, which could indicate high respiratory activity (**Figure 3E**). The cytoplasm had a granular appearance due to being rich in free ribosomes and polyribosomes, indicating active protein synthesis (**Figures 3E,F**). Interestingly, the rough endoplasmic reticulum cisternae were often dilatated and contained moderately electron-dense material (**Figures 3D–F**). Furthermore, transmission electron microscopy showed well-developed Golgi apparatus in the juxta-nuclear area producing large secreting granules (**Figure 3F**). A number of multivesicular bodies, a special kind of late endosomes, were also observed in ADSC cytoplasm (**Figure 3G**). Multivesicular bodies were very heterogeneous in size and morphology. Whole intracellular elements such as mitochondria were sequestered inside an autophagosome that then fused with multivesicular bodies to form amphisome (**Figure 3G**). Electron microscopy analysis revealed the process of active exocytosis on the plasma membrane of ADSCs (**Figure 3H**).

At the same time, ADSCs from old control mice (CtrlO group) formed a culture of heterogeneous in size spheroids (from 60 μm to 370 μm in diameter). Unlike spheroids formed by ADSCs from young animals, ADSCs from old mice were not tightly packed and had a wide intercellular space (**Figure 4A**). It was also difficult to clearly separate the outer and inner layers, as was observed in spheroids obtained from young mice.

Transmission electron microscopy of ADSCs from CtrlO group showed a similar ultrastructural architecture to young control, but there were some noticeable differences. In these ADSCs the mitochondrial population was heterogeneous, a significant part was represented by more round structures (**Figure 4B**). This may indicate an increase in mitochondrial fission and/or an impairment of the fusion. Mitochondria with both electron-dense condensed and enlightened matrix were presented, denoting their different respiratory activity (**Figure 4B**). Significantly fewer polysomes and ribosomes attached to the surface of rough endoplasmic reticulum were also observed in the cytoplasm of ADSCs from CtrlO group, indicating low protein synthetic activity (**Figure 4C**). In addition, the cytoplasm of ADSCs in spheroids from old mice had notably increased amounts of lipid droplets compared to cells obtained from young animals (**Figure 4D**). The cytoplasm was extremely rich in endosomal elements showing typical multilamellar and multivesicular structures (**Figure 4E**).

Electron microscopic analysis showed that ovariectomy led to changes in the ultrastructure of ADSCs in spheroids. The cytoplasm of ADSCs from young ovariectomized mice had significantly increased amounts of lipid droplets and endosomal elements compared to cells obtained from young control animals (**Figure 5A**).

Interestingly, the most prominent ultrastructural feature of the ADSCs from old ovariectomized mice was giant lipid droplets (3–4.5 μm in diameter) that probably formed by fusion or coalescence of smaller adjacent lipid droplets (**Figure 5B**). The cytoplasm was also characterized by numerous vacuolar elements.

Discussion

The issue of the impact of aging on the phenotypic and functional characteristics of stem cells is quite relevant for modern regenerative medicine. Choosing the optimal source of cells, assessing their quality, taking into account the age and health status of the donor, determine the overall effectiveness and safety of cell therapy.

The aging is associated with altered immune and metabolism dysfunctions, increased inflammation and significant changes in the physiological levels of sex hormones. Multiple pathogenic pathways induce defective adipogenesis, inflammation, aberrant adipocytokine production, and insulin resistance, leading to age-related adipose tissue dysfunction with the functional decline of adipocyte progenitors and accumulation of senescent cells (Ou et al., 2022). Under ovariectomy conditions in mice, the proliferative capacity and osteogenic potential of ADSCs are significantly impaired compared to normal animals (Wang et al., 2017). In mice after ovariectomy, enhanced adipogenic differentiation of ADSCs is likely to be the important cause for increased adipogenesis *in vivo* and subsequent obesity-like changes in body mass (Fu et al., 2014). The regenerative potential of ADSCs in conditions of age-related estrogen deficiency is also impaired. In particular, ADSCs from aged estrogen-deficient ovariectomized rats have less capacity to increase tenocyte proliferation and healing in indirect co-culture system compared with normal ADSCs (Veronesi et al., 2015).

In our previous study, it was demonstrated that there were no statistically significant differences in the expression of all typical surface markers of ADSCs in young and old mice (Ustymenko et al., 2019). This fact indicates that the immunophenotype of ADSCs and, probably, their quantity in adipose tissue do not change with age, that confirm in studies of both human and animal samples published by other researchers.

In the study of Li et al. (2021) there were no significant differences in most of the surface markers between ADSCs from 1-month-old or 20-month-old mice, implying that the adipose tissue obtained from young animals had a comparative yield of ADSCs to that of old mice under the same conditions. No significant differences were found in the expression of surface markers on ADSCs from rats aged 2-, 9- and 24 months in the study of Muñoz et al. (2020). At the same time, ADSCs derived from horses older than 5 years old exhibited several molecular alternations which markedly limit their regenerative capacity. Aged ADSCs were characterized by increased gene expression of pro-inflammatory

10.3389/fncel.2023.1072750

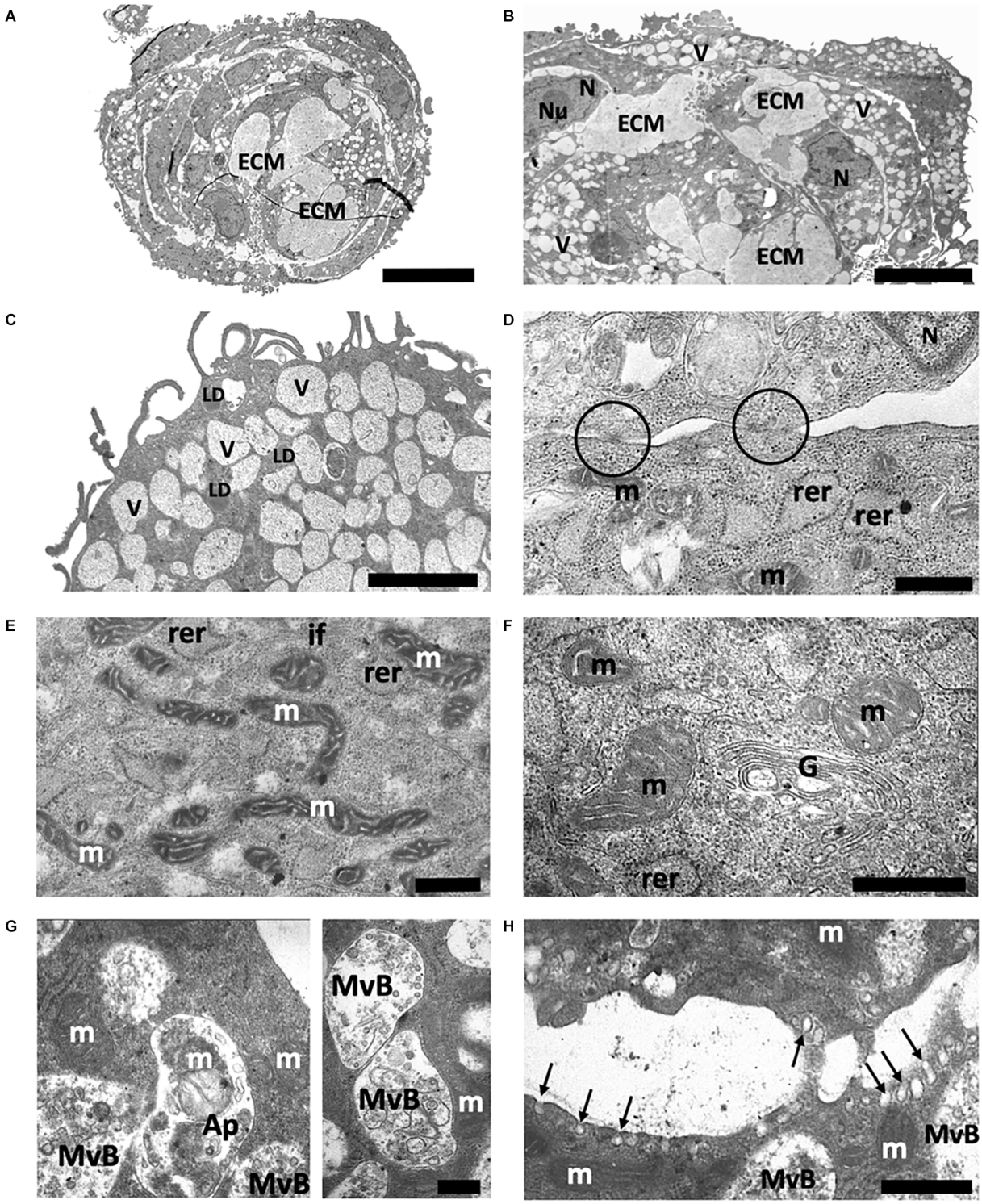

FIGURE 3
Structure of spheroids from the adipose-derived multipotent mesenchymal stromal cells from young control CBA/Ca mice. **(A)** Central section giving an overview of representative ADSCs spheroid after 14 days of culture. Spheroid consists of the dense outer zone and the inner area, where round or polygonal cells are embedded in an extracellular matrix (ECM). **(B)** Elongated cells of the outer area and a part of the inner zone of ADSCs spheroids with an extracellular matrix. The ADSCs cytoplasm is extremely rich in vacuoles (V). N—nuclei; Nu—nucleolus. **(C)** In the outer area ADSCs has many thin pseudopodia extended from the cell surface. The ADSCs cytoplasm contains a large number of vacuoles and a moderate amount of lipid droplets (LD). **(D)** Plasma membranes of adjacent adipose-derived multipotent mesenchymal stromal cells are attached by numerous junctions, which appeared as tight junctions (circles). **(E)** Detailed view of cytoplasm containing a relative high amount of elongated electron-dense mitochondria (m), rough endoplasmic reticulum (rer), and intermediate filament (if) bundles. **(F)** Well-developed Golgi apparatus (G) producing large secreting granules. **(G)** ADSC cytoplasm containing a number of late endosomal multivesicular bodies (MvB). A fragment of mitochondria is observed inside the autophagosome (Ap). **(H)** The sites of active exocytosis (arrows) on the plasma membrane. Scale bars: **(A)**—25 μm, **(B)**—15 μm, **(C)**—2 μm, **(D,E,H)**—1 μm, **(F,G)**—0.5 μm.

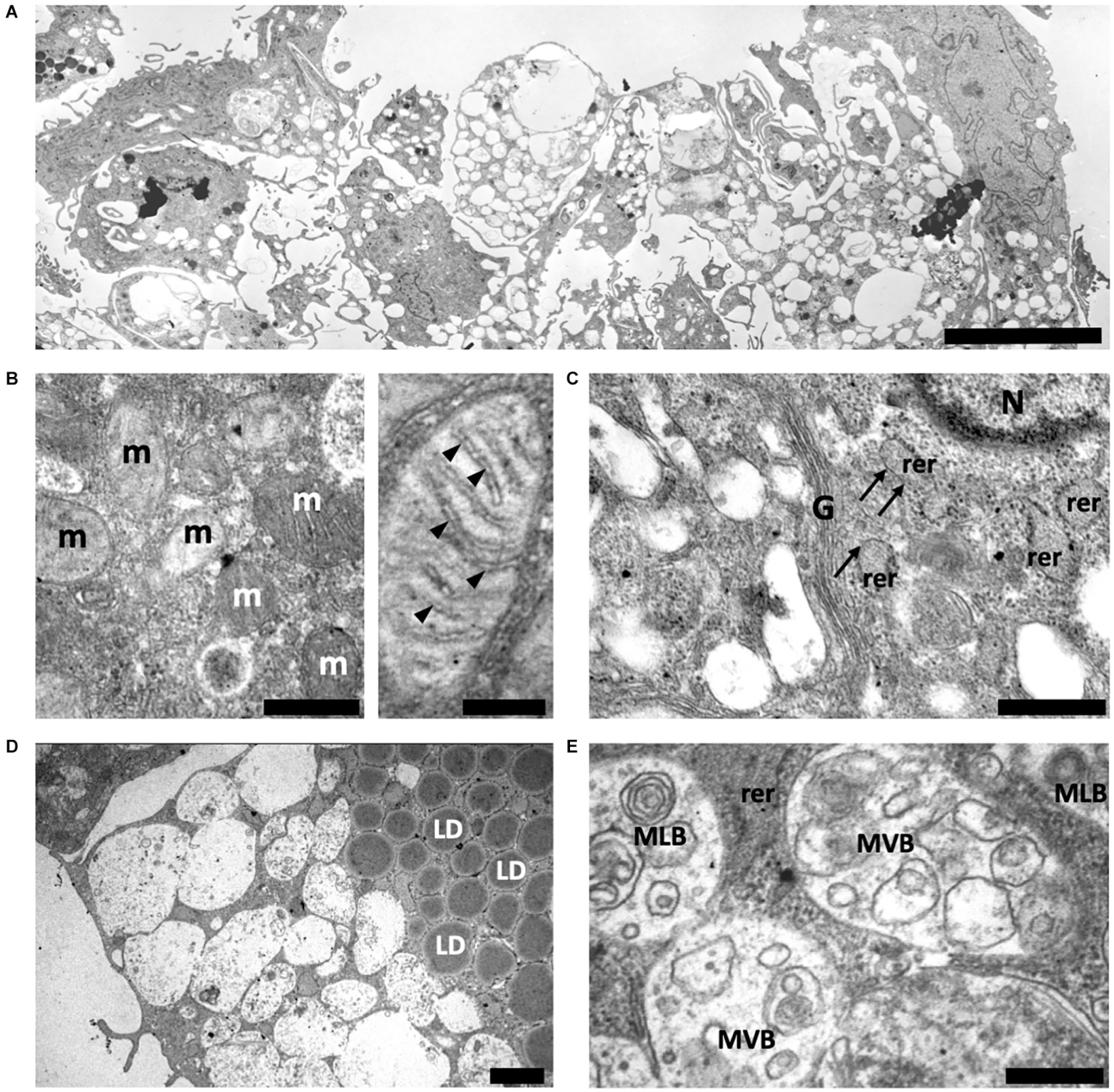

FIGURE 4
Structure of spheroids of the adipose-derived multipotent mesenchymal stromal cells from old control CBA/Ca mice. **(A)** An overview of representative ADSCs spheroid after 14 days of culture. ADSCs are not tightly packed in spheroid and had a wide intercellular space. **(B)** Left electronogram—The mitochondrial population is heterogeneous and is represented by mitochondria with both electron-dense condensed and enlightened matrix. Right electronogram—A detailed view of round mitochondrion with enlightened matrix and cristae (arrowheads) arranged perpendicular to the mitochondrial tubular axis. **(C)** The ADSCs cytoplasm contains rough endoplasmic reticulum (rer) and well-developed Golgi apparatus (G). Areas of rough endoplasmic reticulum that do not contain ribosomes are marked with arrows. N—nuclei. **(D)** A large number of lipid droplets (LD) is observed in the ADSCs cytoplasm. **(E)** Typical multivesicular (MVB) and multilamellar bodies (MLB) are observed in the ADSCs cytoplasm. Scale bars: **(A)**—15 μm, **(B)** left—0.5 μm, right—0.2 μm, **(C,D)**—1 μm, **(E)**—0.5 μm.

cytokines and miRNAs (IL-8, IL-1β, TNF-α, miR-203b-5p, and miR-16-5p), as well as apoptosis markers (p21, p53, caspase-3, caspase-9; Alicka et al., 2020).

Liu et al. (2017) showed while human ADSCs from different age populations are phenotypically similar, they present major differences at the functional level. Advancing age was found to have a significant negative effect on the adipogenic and osteogenic differentiation potentials of human ADSCs (Liu et al., 2017). Zhang et al. (2011) suggested that advanced age and comorbidity do not negatively impact isolation of ADSCs, and these stem cells retain significant capacity to acquire key endothelial cell phenotype throughout life. Chen et al. (2012) found that the doubling time of ADSCs from both age groups was maintained below 70 h and authors concluded that the

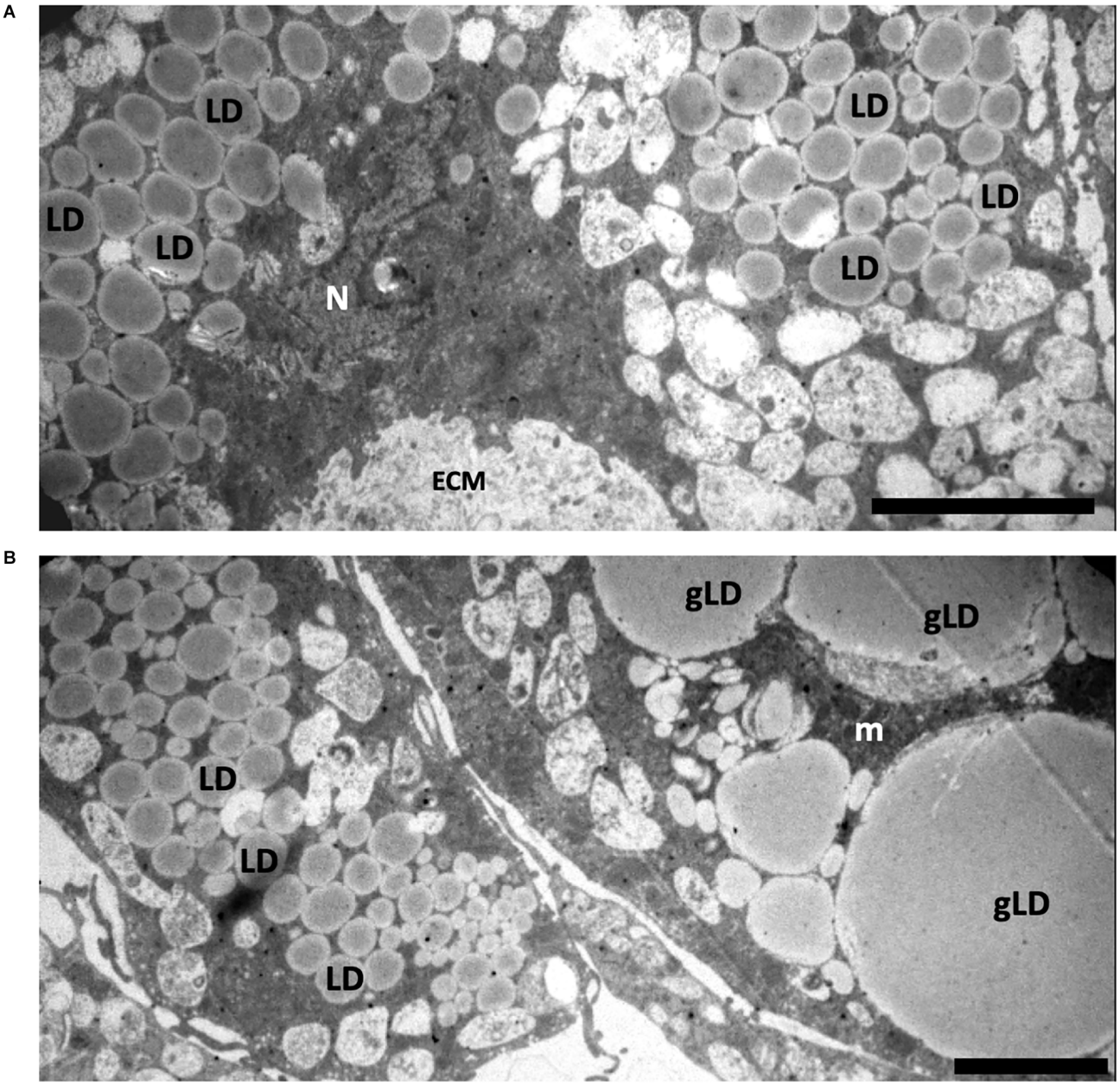

FIGURE 5
Structure of spheroids of the adipose-derived multipotent mesenchymal stromal cells from young **(A)** and old **(B)** ovariectomized CBA/Ca mice. **(A)** The cytoplasm of ADSCs from young ovariectomized mice have a large number of lipid droplets (LD) and endosomal elements. ECM—extracellular matrix. N—nuclei. **(B)** The cell cytoplasm of ADSCs from old ovariectomized mice contains giant lipid droplets (gLD). m—mitochondria. Scale bars: **(A,B)**—2 μm.

proliferation and osteogenic differentiation of ADSCs were less affected by age and multiple passages than in bone marrow-derived MSCs cultures.

The authors explain impairment of proliferative and differentiation potential by the existence of internal changes in ADSCs during aging, which is associated with senescence associated secretory phenotype (SASP) during chronic inflammation and metabolic disorders. The components of the pathologic secretory phenotype are quite heterogeneous and may depend on the cell type. In particular, it has been shown that increased levels of certain cytokines, chemokines and growth factors (IL-4, IL-13, IL-17, CCL3, CCL25 and GM-CSF) can characterize the SASP profile for ADSCs from elderly donors (Li et al., 2021).

The 3D cultivation of ADSCs in the form of spheroids, which partially simulates the conditions of the stem cells' microenvironment (niche), can significantly improve their survival in the recipient's tissue and increase the overall regenerative potential. The study of the ultrastructural characteristics of cells in the 3D spheroids is aimed at establishing the mechanisms of cell self-

organization, contact intercellular signaling, production of the extracellular matrix, resistance to hypoxia, depending on the size of the spheroid.

It has been shown that 3D spheroid culture reduces size by increasing the secretion of extracellular vesicles. This event is mediated by a decrease in actin polymerization (F-actin). Probably, the large size of ADSCs spheroid cultures from old animals in our study indicates a violation of the ability to release microvesicles into the extracellular space (Mo et al., 2018).

In the study of Li et al. (2022) scanning electron microscopy showed that surfaces of spheroids formed in simulated microgravity culture system were relatively smooth and organized in a regular, granular shape, which may be beneficial for ever exchange of nutrients and gases evenly. Lee et al. (2021) proposed method of hybridization of ADSCs spheroids with polydopamine coated single-segmented fibers to enhance viability regardless of sizes and increase their functionality by regulating the size of spheroids. Transmission electron microscopy images showed that cell-only spheroids exhibited disintegrated membranes and empty spaces. In contrast, the cell membranes in fiber incorporated spheroids were tightly bound with each other, and disconnected or empty regions were minimal (Lee et al., 2021).

Step-by-step directed differentiation of multipotent cells in 3D spheroids *in vitro* will allow to partially reproduce the physiological mechanisms of tissue formation *in vivo* and to obtain a spatially organized culture of cells capable of survival, proliferation, and differentiation into certain direction.

Baraniak and McDevitt (2012) showed that cell proliferation and differentiation potential of dissociated cells retrieved from spheroids of mesenchymal stem cells were compared to conventional adherent monolayer cultures. Cells that had been cultured within spheroids recovered morphology typical of cells cultured continuously in adherent monolayers and retained their capacity for multi-lineage differentiation potential. In fact, more robust matrix mineralization and lipid vacuole content were evident in recovered MSCs when compared to monolayers, suggesting enhanced differentiation by cells cultured as 3D spheroids (Baraniak and McDevitt, 2012).

Laschke et al. (2014) discovered that scaffolds seeded with osteogenic differentiated spheroids exhibited a markedly impaired vascularization caused by the lost ability of differentiated spheroids to form microvascular networks. This was associated with a reduced tissue incorporation of the implants and indicating the dedifferentiation of the spheroids under the given *in vivo* conditions. These findings indicate that osteogenic differentiation of ADSCs spheroids markedly impairs their vascularization capacity (Laschke et al., 2014).

In our previous study, it was shown that 3D grafts of ADSCs cultured in spheroids are able to improve bone tissue regeneration in a model of bone injury in mice. The grafts previously differentiated into osteogenic direction provide better morphological indicators of bone recovery, compared with the spheroids without prior differentiation. Intensive migration of cells from spheroids to an adhesive surface *in vitro* proves the ability of cells to survive in 3D culture. At the same time, the morphology of cells on the surface of spheroids under the influence of osteoinductive differentiation factors changes and proliferative activity decreases (Kyryk et al., 2022).

Conclusion

Thus, we can suggest that ADSCs throughout life retain a significant amount in adipose tissue and a high functional potential *in vitro*, which can be effectively used in cell therapy strategies especially in elderly patients. At the same time, our data indicate the negative impact of ovariectomy on the ultrastructural characteristics of 3D spheroids formed by ADSCs. Our findings are particularly promising in the context of vigilance for potential therapeutic applications of ADSCs from old donors.

Data availability statement

The raw data supporting the conclusions of this article will be made available by the authors, without undue reservation.

Ethics statement

The animal study was reviewed and approved by the Ethics Committee of the Institute of Genetic and Regenerative Medicine (protocol no. 9-2021 dated December 15, 2021) and performed in accordance with the European Union Directive of 22 September 2010 (2010/63/EU) for the protection of animals used for scientific purposes.

Author contributions

VK, GB, and GS: conceptualization. VK, AU, ES, IG, and OT: data collection and analysis. VK, AU, OT, and IG: writing—original draft preparation. VK, GB, and GS: writing—review and editing. ES: visualization. All authors contributed to the article and approved the submitted version.

Conflict of interest

The authors declare that the research was conducted in the absence of any commercial or financial relationships that could be construed as a potential conflict of interest.

Publisher's note

References

Alicka, M., Kornicka-Garbowska, K., Kucharczyk, K., Kępska, M., Röcken, M., and Marycz, K. (2020). Age-dependent impairment of adipose-derived stem cells isolated from horses. *Stem Cell Res. Ther.* 11:4. doi: 10.1186/s13287-019-1512-6

Amer, M. G., Embaby, A. S., Karam, R. A., and Amer, M. G. (2018). Role of adipose tissue derived stem cells differentiated into insulin producing cells in the treatment of type I diabetes mellitus. *Gene* 654, 87–94. doi: 10.1016/j.gene.2018.02.008

Baraniak, P. R., and McDevitt, T. C. (2012). Scaffold-free culture of mesenchymal stem cell spheroids in suspension preserves multilineage potential. *Cell Tissue Res.* 347, 701–711. doi: 10.1007/s00441-011-1215-5

Chen, H.-T., Lee, M.-J., Chen, C.-H., Chuang, S.-C., Chang, L.-F., Ho, M.-L., et al. (2012). Proliferation and differentiation potential of human adipose-derived mesenchymal stem cells isolated from elderly patients with osteoporotic fractures. *J. Cell. Mol. Med.* 16, 582–593. doi: 10.1111/j.1582-4934.2011.01335.x

Dominici, M., Le Blanc, K., Mueller, I., Slaper-Cortenbach, I., Marini, F., Krause, D., et al. (2006). Minimal criteria for defining multipotent mesenchymal stromal cells. The international society for cellular therapy position statement. *Cytotherapy* 8, 315–317. doi: 10.1080/14653240600855905

Eastell, R., O'Neill, T. W., Hofbauer, L. C., Langdahl, B., Reid, I. R., Gold, D. T., et al. (2016). Postmenopausal osteoporosis. *Nat. Rev. Dis. Primers* 2:16069. doi: 10.1038/nrdp.2016.69

Egger, D., Tripisciano, C., Weber, V., Dominici, M., and Kasper, C. (2018). Dynamic cultivation of mesenchymal stem cell aggregates. *Bioengineering (Basel)* 5:48. doi: 10.3390/bioengineering5020048

Fu, Y., Li, R., Zhong, J., Fu, N., Wei, X., Cun, X., et al. (2014). Adipogenic differentiation potential of adipose-derived mesenchymal stem cells from ovariectomized mice. *Cell Prolif.* 47, 604–614. doi: 10.1111/cpr.12131

Kyryk, V., Kuchuk, O., and Klymenko, P. (2022). Regenerative effects of mouse adipose-derived multipotent stromal cells in a micromass graft for the treatment of bone injury model. *Anti Aging East. Europe* 1, 73–84. doi: 10.56543/aaeeu.2022.1.1.11

Laschke, M. W., Schank, T. E., Scheuer, C., Kleer, S., Shadmanov, T., Eglin, D., et al. (2014). *In vitro* osteogenic differentiation of adipose-derived mesenchymal stem cell spheroids impairs their *in vivo* vascularization capacity inside implanted porous polyurethane scaffolds. *Acta Biomater.* 10, 4226–4235. doi: 10.1016/j.actbio.2014.06.035

Lee, J., Lee, S., Kim, S. M., and Shin, H. (2021). Size-controlled human adipose-derived stem cell spheroids hybridized with single-segmented nanofibers and their effect on viability and stem cell differentiation. *Biomater. Res.* 25:14. doi: 10.1186/s40824-021-00215-9

Li, K., Shi, G., Lei, X., Huang, Y., Li, X., Bai, L., et al. (2021). Age-related alteration in characteristics, function and transcription features of ADSCs. *Stem Cell Res. Ther.* 12:473. doi: 10.1186/s13287-021-02509-0

Li, H., Wang, C., Liu, S., Guo, Y., and Chen, J. (2022). Characterization of three-dimensional multipotent adipose-derived stem cell spheroids. *Biocell* 46, 1705–1716. doi: 10.32604/biocell.2022.018442

Liu, M., Lei, H., Dong, P., Fu, X., Yang, Z., Yang, Y., et al. (2017). Adipose-derived mesenchymal stem cells from the elderly exhibit decreased migration and differentiation abilities with senescent properties. *Cell Transplant.* 26, 1505–1519. doi: 10.1177/0963689717721221

Ma, X., Huang, M., Zheng, M., Dai, C., Song, Q., Zhang, Q., et al. (2020). ADSCs-derived extracellular vesicles alleviate neuronal damage, promote neurogenesis and rescue memory loss in mice with Alzheimer's disease. *J. Control. Release* 327, 688–702. doi: 10.1016/j.jconrel.2020.09.019

Magenta, A., Florio, M. C., Ruggeri, M., and Furgiuele, S. (2021). Autologous cell therapy in diabetes-associated critical limb ischemia: from basic studies to clinical outcomes (Review). *Int. J. Mol. Med.* 48:173. doi: 10.3892/ijmm.2021.5006

Mo, M., Zhou, Y., Li, S., and Wu, Y. (2018). Three-dimensional culture reduces cell size by increasing vesicle excretion. *Stem Cells* 36, 286–292. doi: 10.1002/stem.2729

Muñoz, M. F., Argüelles, S., Marotta, F., Barbagallo, M., Cano, M., and Ayala, A. (2020). Effect of age and lipoperoxidation in rat and human adipose tissue-derived stem cells. *Oxid. Med. Cell. Longev.* 2020:6473279. doi: 10.1155/2020/6473279

Murohara, T., Shintani, S., and Kondo, K. (2009). Autologous adipose-derived regenerative cells for therapeutic angiogenesis. *Curr. Pharm. Des.* 15, 2784–2790. doi: 10.2174/138161209788923796

Ou, M. Y., Zhang, H., Tan, P. C., Zhou, S. B., and Li, Q. F. (2022). Adipose tissue aging: mechanisms and therapeutic implications. *Cell Death Dis.* 13:300. doi: 10.1038/s41419-022-04752-6

Tsupykov, O., Ustymenko, A., Kyryk, V., Smozhanik, E., Yatsenko, K., Butenko, G., et al. (2016). Ultrastructural study of mouse adipose-derived stromal cells induced towards osteogenic direction. *Microsc. Res. Tech.* 79, 557–564. doi: 10.1002/jemt.22670

Ustymenko, A., Kyryk, V., Lutsenko, T., Tsupykov, O., and Butenko, G. (2019). Morphofunctional properties of adipose-derived multipotent mesenchymal stromal cells in vitro in ovariectomized mice of different ages. *Cell Organ Transplant.* 7, 158–167. doi: 10.22494/cot.v7i2.102

Veronesi, F., Della Bella, E., Torricelli, P., Pagani, S., and Fini, M. (2015). Effect of adipose-derived mesenchymal stromal cells on tendon healing in aging and estrogen deficiency: an *in vitro* co-culture model. *Cytotherapy* 17, 1536–1544. doi: 10.1016/j.jcyt.2015.07.007

Wang, L., Huang, C., Li, Q., Xu, X., Liu, L., Huang, K., et al. (2017). Osteogenic differentiation potential of adipose-derived stem cells from ovariectomized mice. *Cell Prolif.* 50:e12328. doi: 10.1111/cpr.12328

Yu, G., Wu, X., Kilroy, G., Halvorsen, Y.-D. C., Gimble, J. M., and Floyd, Z. E. (2011). Isolation of murine adipose-derived stem cells. *Methods Mol. Biol.* 702, 29–36. doi: 10.1007/978-1-61737-960-4_3

Zhang, P., Moudgill, N., Hager, E., Tarola, N., Dimatteo, C., McIlhenny, S., et al. (2011). Endothelial differentiation of adipose-derived stem cells from elderly patients with cardiovascular disease. *Stem Cells Dev.* 20, 977–988. doi: 10.1089/scd.2010.0152

Zhou, Z., Tian, X., Mo, B., Xu, H., Zhang, L., Huang, L., et al. (2020). Adipose mesenchymal stem cell transplantation alleviates spinal cord injury-induced neuroinflammation partly by suppressing the Jagged1/Notch pathway. *Stem Cell Res. Ther.* 11:212. doi: 10.1186/s13287-020-01724-5

frontiers | Frontiers in Cellular Neuroscience

TYPE Brief Research Report
PUBLISHED 24 February 2023
DOI 10.3389/fncel.2023.1141689

OPEN ACCESS

EDITED BY
Junhui Wang,
Mount Sinai Hospital, University of Toronto, Canada

REVIEWED BY
De-Lai Qiu,
Yanbian University, China
Dongmin Yin,
East China Normal University, China

*CORRESPONDENCE
Hanna Dumanska
✉ doomannya@gmail.com

SPECIALTY SECTION
This article was submitted to Cellular Neuropathology, a section of the journal Frontiers in Cellular Neuroscience

RECEIVED 10 January 2023
ACCEPTED 13 February 2023
PUBLISHED 24 February 2023

CITATION
Dumanska H and Veselovsky N (2023) Protein kinase C mediates hypoxia-induced long-term potentiation of NMDA neurotransmission in the visual retinocollicular pathway.
Front. Cell. Neurosci. 17:1141689.
doi: 10.3389/fncel.2023.1141689

Protein kinase C mediates hypoxia-induced long-term potentiation of NMDA neurotransmission in the visual retinocollicular pathway

Hanna Dumanska* and Nikolai Veselovsky

Department of Neuronal Network Physiology, Bogomoletz Institute of Physiology, National Academy of Science of Ukraine, Kyiv, Ukraine

The identification of processes and mechanisms underlying the early stage of hypoxic injury of the retinocollicular pathway may be beneficial for the future prevention and treatment of navigation, orientation, and visual attention impairments. Previously, we have demonstrated that short-term hypoxia led to long-term potentiation (LTP) of NMDA neurotransmission in the background of long-term depression of $GABA_A$ retinocollicular transmission. Here, we sought to obtain insight into the mechanisms of hypoxia-induced LTP of NMDA retinocollicular neurotransmission and the role of the protein kinase C (PKC) signaling pathway in it. To investigate these, we recorded pharmacologically isolated NMDA transmission in cocultivated pairs of rat retinal ganglion cells and superficial superior colliculus neurons under normoxic and hypoxic conditions, using the paired patch-clamp technique and method of fast local superfusion. We tested the involvement of the PKC by adding the potent and selective inhibitor chelerythrine chloride (ChC, 5 μM). We observed that hypoxia-induced LTP of NMDA neurotransmission is associated with the shortening of current kinetics. We also found that the PKC signaling pathway mediates hypoxia-induced LTP and associated shortening of NMDA currents. The ChC completely blocked the induction of LTP by hypoxia and associated kinetic changes. Contrary effects of ChC were observed with already induced LTP. ChC led to the reversal of LTP to the initial synaptic strength but the current kinetics remain irreversibly shortened. Our results show that ChC is a promising agent for the prevention and treatment of hypoxic injuries of NMDA retinocollicular neurotransmission and provide necessary electrophysiological basics for further research.

KEYWORDS

retinocollicular pathway, hypoxia, long-term potentiation, protein kinase C, reversal of LTP, NMDA postsynaptic currents, decay time

1. Introduction

Pathogenesis of numerous diseases and traumas as well as several physiological states are associated with hypoxia (Biddlestone et al., 2015; Luo et al., 2022). The retinocollicular pathway, as part of the visual system, is extremely sensitive to oxygen deprivation (Wong-Riley, 2010). Lesions of this pathway lead to navigation, orientation, and visual attention deficits, and also could be involved in several neurological and psychiatric disorders such as attention deficit hyperactivity disorder, and autism (Brace et al., 2015; Mathis et al., 2015; Jure, 2022). In our research, we focus on the very early hypoxia-induced processes and their mechanisms as potential therapeutic targets serving to prevent lesions of the retinocollicular visual transmission.

We have shown previously, that hypoxia induces a significant shift in excitatory-inhibitory balance toward excitation. Oxygen deprivation led to long-term potentiation (LTP) of NMDA transmission and persistent increase in the amplitude and occurrence frequency of spontaneous NMDA events in the background of long-term depression of $GABA_A$ retinocollicular transmission (Dumanska and Veselovsky, 2019). Such pathologically-induced functional alterations may reflect structural changes in NMDAR subunit composition. These receptors are extremely important in the development and refinement of the neurotransmission (Cull-Candy and Leszkiewicz, 2004; Rebola et al., 2010). The synaptic retinocollicular NMDARs contain NR2A and NR2B subunits at different developmental stages that determine the receptors distinct properties and functions (Townsend et al., 2004). The structural and functional alterations of NMDARs were observed in various pathological states and may contribute to molecular processes affecting cell survival or death (Lau and Zukin, 2007; Dewachter et al., 2009; Georgiou et al., 2010). Multiple intra and extracellular messengers, and enzymes regulate such alterations (Yaka et al., 2002; Lin et al., 2006). Among all, testing the involvement of the protein kinase C (PKC) signaling pathway in hypoxia-induced LTP of NMDA transmission seems to be the most promising prospect. Previous studies have shown that the PKC signaling pathway is involved in cellular response to hypoxia as well as in structural and functional alterations of NMDAR (Goldberg et al., 1997; Yan et al., 2000; Chen and Roche, 2007; Lee et al., 2007; Rebola et al., 2010; Kim et al., 2016). In this study, we tested the hypothesis that the protein kinase C (PKC) pathway might be involved in hypoxia-induced LTP NMDA retinocollicular transmission.

2. Materials and methods

In our experiments, we used an *in vitro* model of the visual retinocollicular pathway – primary coculture of rat retinal cells and superficial superior colliculus (SSC) neurons.

All manipulations with animals were performed in aseptic conditions in accordance with animal research regulations approved by the Ukrainian Academy of Science (in accordance with the European Convention for the Protection of Vertebrate Animals used for Experimental and other Scientific Purposes - Explanatory Report, 1986; World Medical Association Declaration of Helsinki, 1996; Convention for the Protection of Human Rights and Dignity of the Human Being with regard to the Application of Biology and Medicine: Convention on Human Rights and Biomedicine, 1997).

2.1. Coculture

The coculture was prepared as we previously described (Dumanska and Veselovsky, 2019). Briefly, the retinal and SSC tissues were obtained from pups P0-P1 of Wistar rats, both sexes. For this research we used 9 pups. After enzymatic and mechanical dissociation of the primary tissues, two suspensions of cells were placed in separate compartments of the originally-designed chamber for cocultivation in a Petri dish. The chamber consists of a silicon ring with a vertical glass baffle placed on the coverslip. One hour of incubation in a humidified atmosphere of $5 \pm 0.5\%$ CO_2 at 37 ± 0.5 C was enough for cell adhesion to the coverslip. After that, the silicon ring was removed, and the cells were stored in the incubator for further cocultivation.

2.2. Electrophysiological recordings

In the coculture, we identified synaptically connected pairs of retinal ganglion cells (RGCs) and SSC neurons by their spatial location, morphological and electrophysiological characteristics (Moriton et al., 2013; Villalobos et al., 2018). The recordings were performed from synaptically connected pairs of RGCs and SSC at room temperature (20–24°C) using the paired whole-cell patch clamp technique. Pharmacologically isolated NMDA-mediated postsynaptic currents (PSCs) were evoked in SSC neurons by generation action potentials in presynaptic RGCs. Spontaneous currents were recorded in SSC neurons in the absence of presynaptic stimulation.

In all experiments, the extracellular solution contained (in mM): NaCl 140; KCl 3; $CaCl_2$ 3; Hepes 20, and glucose 15 (Sigma-Aldrich); pH 7.4. For pharmacological isolation of NMDA currents, we added to the external solution dinitroquinoxaline-2,3(1H, 4H)-dione (DNQX, 20 μM) and bicuculline methiodide (10 μM). The internal pipette solution contained (in mM): potassium gluconate 155; EGTA 0.5; $MgCl_2$ 1 and Hepes 20 (Sigma-Aldrich); pH 7.4. We tested the involvement of the PKC by adding 5 μM of chelerythrine chloride (ChC) to the external solution. Patch pipettes were prepared from borosilicate glass capillaries (World Precision Instruments, USA) with internal tip diameters 1.0–1.5 μm.

During the electrophysiological recordings, we constantly evaluated the quality of voltage clamping by monitoring the variations of the leakage current amplitude (I_{leak}) and the time constant of the capacitive current (τ_{cap}) recorded upon applications of short (10 ms) small-amplitude hyperpolarizing rectangular stimuli (– 10 mV). The data obtained were analyzed if variations of the τ_{cap} and I_{leak} values did not exceed 20 % of the mean value.

For both types of neurons, membrane potential varied from −50 to – 70 mV. Short-term hypoxic states did not lead to statistically significant changes in membrane potential (depolarization or hyperpolarization).

Data were recorded and digitized (10 kHz) using two Axopatch-1D amplifiers (CV-4 headstages, gain: × 1/100; 5 kHz cutoff low-pass 4-pole Bessel filter), Digidata 1322A and Clampex 9.0 software (Axon Instruments).

2.3. Modulation of short hypoxic states *in vitro*

Using the method of fast local superfusion (Veselovsky et al., 1996) we applied hypoxic solutions on synaptically -connected pairs of neurons during the electrophysiological recordings to mimic short-term hypoxic states *in vitro*. This method allowed us to control the area and speed of the application. The hypoxic solutions were obtained by saturation of the external solutions with nitrogen

for 20 min just before the electrophysiological recordings. We used the next protocol for the experiments: first, we applied a normoxic external solution for 5 min – this period we called a control, then we switched to the hypoxic solution for 5 min – hypoxia, and then back to the normoxic external solution – reoxygenation.

2.4. Statistical analysis

Statistical analysis of data obtained has been done in Origin 8.5 Pro (OriginLab Corporation, USA) and Clampfit 9.0 (Axon Instruments, USA). The data is presented as mean ± SD. The decay time constants of the currents were fitted by a standard single-exponential function. We checked the normality of data sets using the Shapiro-Wilks test, the differences between two sets of values using two-sample *t*-test and the differences between the two functions using Kolmogorov-Smirnov criteria. The results of the *t*-test are represented as *t*-values (t), degrees of freedom (df), and *p*-values (p).

3. Results

In the coculture, each identified synaptically connected pair of RGCs and SSC neurons reflects a single fiber of the retinocollicular pathway (Figure 1). We examined 38 pairs of RGCs-SSC neurons. The evoked and spontaneous NMDA currents were identified by their kinetic and pharmacological characteristics (Furman and Crair, 2012).

As we have reported before (Dumanska and Veselovsky, 2019), the application of a hypoxic solution for 5 min led to the long-term potentiation (LTP) of NMDA neurotransmission (Figure 2A, $n = 8$, unpublished data). PSCs displayed single exponential deactivation time course. We observed that hypoxia-induced LTP is associated with a rapid, irreversible and statistically extremely significant shortening of evoked PSCs – the decrease in current decay time constants (Figure 2D; control 39.7 ± 2.6 ms; hypoxia 16.7 ± 2.0 ms; reoxygenation 16.4 ± 2.5 ms; $t = 85.6$, $df = 296$, $p < 0.0001$ – hypoxia compare to control; $t = 103.2$, $df = 897$, $p < 0.0001$ – reoxygenation compare to control).

To investigate the role of the PKC signaling pathway in hypoxia-induced LTP we carried out two series of experiments. In the first, we added ChC (5 μM) to the external solution during the reoxygenation, and in the second – during hypoxia. In the first case, the hypoxia application successfully induced potentiation of the evoked PSCs but the presence of ChC during reoxygenation led to the decrease of the elevated amplitudes to the basal pre-LTP level (Figure 2B, $n = 8$). The dynamic of the PSCs decay time constants represents the irreversible and statistically extremely significant decrease during hypoxia and reoxygenation (Figure 2E; control 31.1 ± 4 ms; hypoxia 19.5 ± 3.2 ms; reoxygenation in the presence of ChC 19.2 ± 2.5 ms; $t = 27.6$, $df = 296$, $p < 0.0001$ – hypoxia compare to control; $t = 46.8$, $df = 897$, $p < 0.0001$ – reoxygenation compare to control). In the second case, the presence of ChC in the hypoxic solution completely blocked the hypoxia-induced LTP of NMDA transmission (Figure 2C) and associated changes in PSCs kinetics (Figure 2F; control 32.4 ± 3.9 ms; hypoxia in the presence of ChC 32.5 ± 3.9 ms; reoxygenation 32.4 ± 3.6 ms; $t = 0.2$, $df = 296$, $p = 0.8$ – hypoxia compare to control; $t = 0$, $df = 897$, $p = 1$ – reoxygenation compare to control.

We also tested the effect of ChC on the hypoxia-induced increase of spontaneous NMDA retinocollicular activity. As with the evoked neurotransmission, we added ChC during the reoxygenation ($n = 8$), and during hypoxia ($n = 7$). In the first case, we observed the hypoxia-induced decrease of the currents decay time constants in the background of the increase in currents amplitudes. The presence of ChC during reoxygenation restored both parameters to the basic level (Figures 3A, C, F; decay time constants during control 43.7 ± 8.2 ms; hypoxia 15.6 ± 3.8 ms; reoxygenation in presence of ChC 42.8 ± 6.5 ms; $t = 18.5$, $df = 60$, $p < 0.0001$ – hypoxia compare to control; $t = 0.4$, $df = 38$, $p = 0.7$ – reoxygenation compare to control). In the second case, ChC abolished the hypoxia-induced changes of spontaneous currents amplitudes and decay time constants (Figures 3B, D, H; control 37.3 ± 4.9 ms; hypoxia in the presence of ChC 39.3 ± 5.8 ms; reoxygenation 38.5 ± 6.1 ms; $t = 1.1$, $df = 50$, $p = 0.2$ – hypoxia compare to control; $t = 0.6$, $df = 33$, $p = 0.6$ – reoxygenation compare to control). In both cases, the hypoxia-induced increase of the occurrence frequency of spontaneous events remains elevated despite the presence of ChC. The quantitative analysis of changes in the frequencies of spontaneous NMDA currents is depicted on the cumulative probability plots (Figures 3E, G).

We have also pointed out that the presence of ChC under normoxic conditions didn't induce any changes in spontaneous current amplitudes, their kinetic characteristics, distribution, or the occurrence frequency of spontaneous events.

4. Discussion

Our results show that two phenomena underlie hypoxia-induced LTP of NMDA retinocollicular neurotransmission: (1) the shortening of PSCs kinetics and (2) the involvement of the PKC signaling pathway in its induction and maintaining.

Functional NMDARs are heteromeric assemblies of NR1, NR2, and NR3 subunits. Each subunit composition of the receptor demonstrates distinct functional and electrophysiological properties (Cull-Candy and Leszkiewicz, 2004). The NR2 subunits determine such functional properties as the open probability of the receptor, its high affinity for glutamate, modulation by glycine, sensitivity to voltage-dependent block by Mg^{2+}, and current kinetics (Perin-Dureau et al., 2002; Cull-Candy and Leszkiewicz, 2004; Hatton and Paoletti, 2005; Paoletti and Neyton, 2007). The changes in NR2 subunits composition lead to changes in electrophysiological characteristics of NMDA currents and vice versa (Vicini et al., 1998; Roberts and Ramoa, 1999).

The shortening of NMDA currents in the background of hypoxia-induced elevation of amplitudes we observed might reflect changes in NMDAR subunit composition. Using decay kinetic characteristics and literature-based analysis, we considered that the decrease of the PSCs decay time constant might be caused by an increase in the NR2A/2B ratio (Vicini et al., 1998; Philpot et al., 2001; Xue et al., 2010). Because of stronger glutamate binding affinity and longer duration of currents, NR2B containing NMDARs are more permeable for calcium than NR2A containing ones (Flint et al., 1997; Vicini et al., 1998). Therefore, the

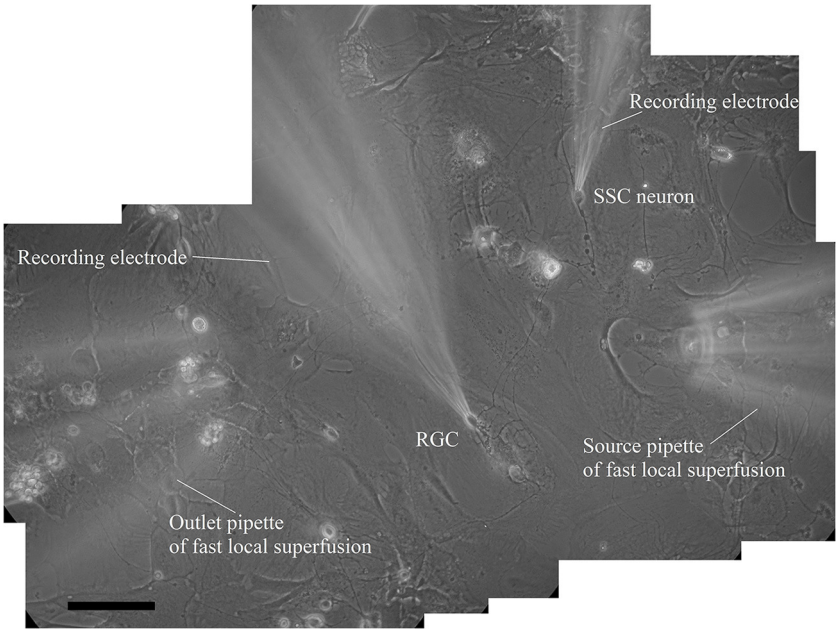

FIGURE 1
Reconstructed microphotography of synaptically connected couple of presynaptic retinal ganglion cell and postsynaptic superficial superior colliculus neuron in coculture during paired patch-clamp recording and fast local superfusion application on the 21st day *in vitro*; the scale marker corresponds to 100 μm.

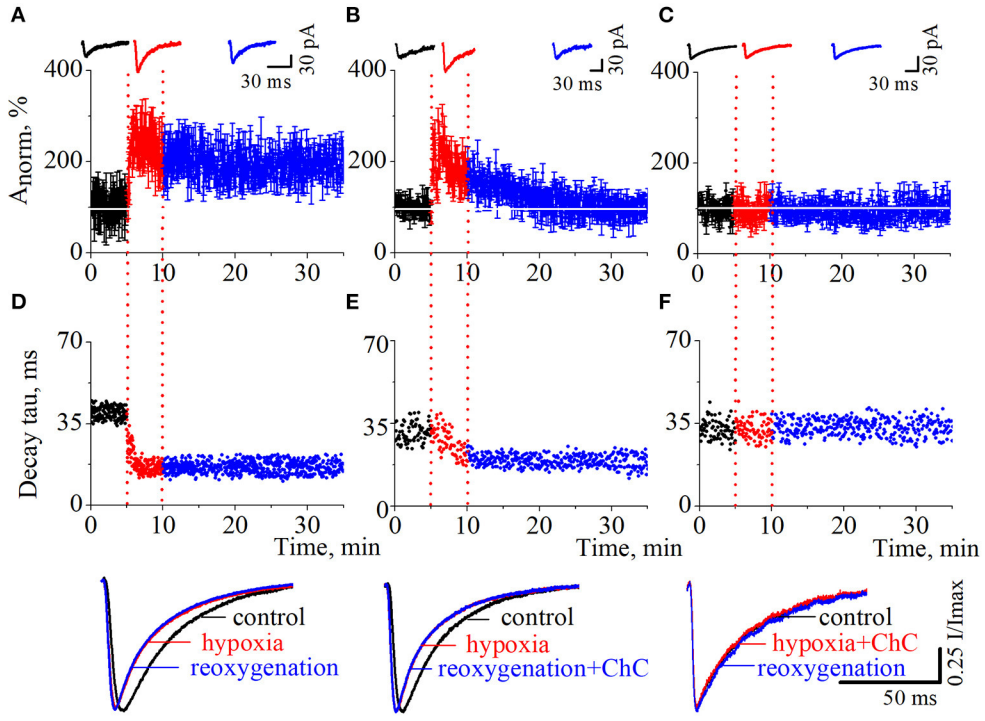

FIGURE 2
The effects of chelerythrine chloride (ChC) on hypoxia-induced LTP of NMDA synaptic neurotransmission. **(A–C)** The dynamics of the evoked postsynaptic current (PSCs) normalized average amplitudes with 5 min duration of the hypoxia application. The ChC (5 μM) was added during reoxygenation **(B)** and during hypoxia **(C)**. Representative recordings of the evoked PSCs are plotted against the corresponding period (control - black, hypoxia - red, and reoxygenation - blue) **(D–F)**. The dynamics of the currents decay time constants from **(A–C)**, respectively. Representative normalized currents are plotted bellow.

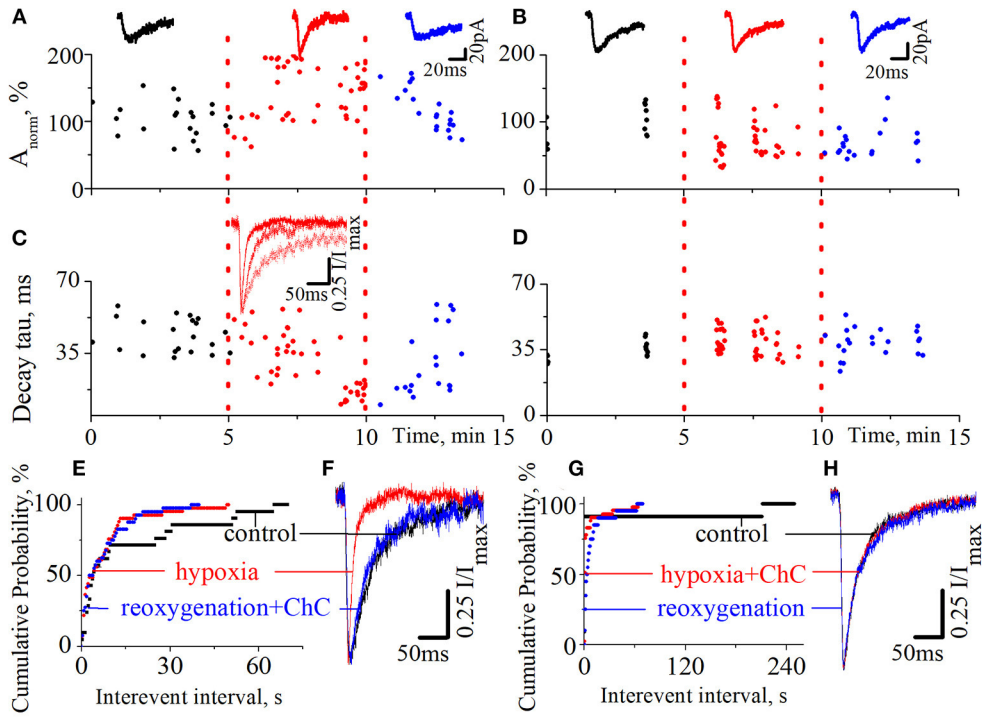

FIGURE 3
The effects of chelerythrine chloride (ChC) on the hypoxia-induced increase of spontaneous NMDA synaptic activity. **(A, B)** The dynamics of spontaneous currents normalized amplitudes with 5 min duration of hypoxia application. The ChC (5 μM) was added during reoxygenation **(A)** and during hypoxia **(B)**. The representative recordings of spontaneous currents are plotted against the corresponding period (control - black, hypoxia - red, and reoxygenation - blue) **(C, D)** The dynamics of currents decay time constants from **(A, B)**, respectively **(E, G)** The cumulative probability plots of the interevent interval of spontaneous currents from **(A, B)**, respectively **(F, H)** Normalized currents from **(A, B)**, respectively.

increase in the NR2A/2B ratio should decrease calcium influx during hypoxia-induced potentiation of NMDA retinocollicular neurotransmission. Moreover, using some statistical models, authors have declared that NR2A may not only shorten the decay time but also increase current amplitudes (Iacobucci and Popescu, 2017). In our research, there was no statistically significant synchronization between the increase in current amplitudes and the decrease in the decay time. Due to the short period of hypoxia duration, subunits changes might be associated with lateral receptor mobilization from adjacent locations, rather than with a new subunits expression (Baez et al., 2018). Overall, we tend to consider the shortening of the current kinetics as a compensatory mechanism in the background of pathologically-induced long-term plasticity as it aims to decrease calcium influx.

We also observed that the presence of ChC completely blocked hypoxia-induced LTP of NMDA retinocollicular neurotransmission and the elevation of the amplitudes of spontaneous NMDA events. ChC is the most recognized potent and specific inhibitor of PKC for isoforms α and β (Herbert et al., 1990; Chmura et al., 2000). The activity of PKC in hypoxic injury has been shown in different tissues. But the distinct role of PKC in cell response to hypoxia as well as the type of isoforms involved in it are still controversial (Skaper et al., 2001; Matsumoto et al., 2004; Bright and Mochly-Rosen, 2005). We showed that the blockade of PKC activity is able not only to prevent pathological hypoxia-induced LTP of NMDA neurotransmission but also to reverse synaptic strength from the potentiated to basal, pre-LTP level. The reversal of LTP is called depotentiation. In contrast to activity-dependent synaptic plasticity that underlies such higher cognitive processes as learning and memory, depotentiation may be responsible for forgetting or mediating degenerative disorders (Huang et al., 2001; Babür et al., 2018). Besides, depotentiation might be involved in developmental changes of synaptic transmission (Huang et al., 2001; Qi et al., 2013; Tao et al., 2019). However, there is no evidence of what role it may play in pathologically-induced LTP.

We also found that ChC blocked the initiation of hypoxia-induced shortening of NMDA evoked and spontaneous currents. It is interesting that, already induced shortening of evoked NMDA PSCs showed irreversibility despite the presence of ChC, whereas spontaneous currents showed the ability to reverse their kinetic to the initial duration. PKC activity is thought to play a key role not only in such functional changes of NMDAR as an increase in the amplitude of currents, channel open probability, and current kinetics but also in trafficking and inserting the receptors into synaptic membranes (Gerber et al., 1989; Chen and Huang, 1992; Xiong et al., 1998; Lan et al., 2001). The existence of such a difference in the reversibility of evoked and spontaneous current kinetics proves the differential regulation of synaptic and extra-synaptic NMDAR (Li et al., 2002; Hardingham and Bading,

2010). The blockade of the PKC signaling pathway didn't affect the hypoxia-induced increase in the occurrence frequency of spontaneous NMDA events.

In this study, we demonstrated that the PKC signaling pathway mediates hypoxia-induced LTP of NMDA retinocollicular neurotransmission at the expression and maintenance stages. According to the literature, PKC might affect NMDAR function directly by phosphorylation of its subunits (Lan et al., 2001; Liao et al., 2001; Zhou et al., 2021) or indirectly by interacting with molecules related to LTP including calcium/calmodulin-dependent protein kinase II (CaMKII) (Gardoni et al., 2001; Yan et al., 2011), postsynaptic density protein (PSD-95) (Wang and Peng, 2016), etc. Moreover, the PKC might act pre- or postsynaptically (Soderling and Derkach, 2000; Brager et al., 2003). Identification of precise mechanisms of PKC-mediated LTP of NMDA retinocollicular neurotransmission will reveal molecules, or complexes involved in hypoxia injury.

The physiological significance of our research can be summarized in the following, (1) hypoxia-induced LTP of NMDA retinocollicular synaptic transmission is associated with the shortening of PSCs, which is a potential cellular compensatory mechanism (2) The PKC signaling pathway mediates both hypoxia-induced LTP and associated changes in current kinetics (3) Moreover, the blockade of PKC by ChC leads to depotentiation of hypoxia-induced LTP. We consider that under pathological conditions, such depotentiation reflects the ability of the system to restore normal functioning, and ChC is a promising agent for the prevention and treatment of hypoxia-induced lesions of the retinocollicular neurotransmission (4) Our results provide the necessary electrophysiological platform for further research.

Data availability statement

The raw data supporting the conclusions of this article will be made available by the authors, without undue reservation.

Ethics statement

The animal study was reviewed and approved by the Ethics Committee of Bogomoletz Institute of Physiology National Academy of Science of Ukraine.

Author contributions

HD and NV contributed to the conception and design of the study. HD performed the experiments, analyzed the data, and prepared the manuscript. All authors read and approved the final manuscript.

Funding

This study was supported by the basic financial support from the National Academy of Science of Ukraine 0118U007353.

Acknowledgments

Partially the data were presented in abstracts at the 34th ECNP Congress, 2–5 October 2021, Lisbon, Portugal; ARVO 2021 Annual Meeting 1–7 May 2021, Virtual; FENS Regional Meeting 2021, 25–27 August, Virtual; ARVO 2022 Annual Meeting, 11–12 May, Virtual; FENS Forum 2022, 9–13 July, Paris, France. Since the presentations, we added more than 30% of the original data in this paper.

Conflict of interest

The authors declare that the research was conducted in the absence of any commercial or financial relationships that could be construed as a potential conflict of interest.

Publisher's note

References

Babür, E., Tan, B., Delibaş, S., Yousef, M., Dursun, N., Süer, C., et al. (2018). Depotentiation of long-term potentiation is associated with epitope-specific tau hyper-/hypophosphorylation in the hippocampus of adult rats. *J Mol Neurosci.* 67, 193–203. doi: 10.1007/s12031-018-1224-x

Baez, M. V., Cercato, M. C., and Jerusalinsky, D. A. (2018). NMDA receptor subunits change after synaptic plasticity induction and learning and memory acquisition. *Neural Plast.* 7, 5093048. doi: 10.1155/2018/5093048

Biddlestone, J., Bandarra, D., and Rocha, S. (2015). The role of hypoxia in inflammatory disease (review). *Int J Mol Med.* 35, 859–869. doi: 10.3892/ijmm.2015.2079

Brace, L. R., Kraev, I., Rostron, C. L., Stewart, M. G., Overton, P. G., Dommett, E. J., et al. (2015). Altered visual processing in a rodent model of attention-deficit hyperactivity disorder. *Neuroscience.* 10, 364–377. doi: 10.1016/j.neuroscience.2015.07.003

Brager, D., Cai, X., and Thompson, S. (2003). Activity-dependent activation of presynaptic protein kinase c mediates post-tetanic potentiation. *Nat Neurosci.* 6, 551–552. doi: 10.1038/nn1067

Bright, R., and Mochly-Rosen, D. (2005). The role of protein kinase C in cerebral ischemic and reperfusion injury. *Stroke.* 36, 2781–2790. doi: 10.1161/01.STR.0000189996.71237.f7

Chen, B. S., and Roche, K. W. (2007). Regulation of NMDA receptors by phosphorylation. *Neuropharmacology.* 53, 362–368. doi: 10.1016/j.neuropharm.2007.05.018

Chen, L., and Huang, L. Y. (1992). Protein kinase C reduces Mg^{2+} block of NMDA-receptor channels as a mechanism of modulation. *Nature*. 9, 521–523. doi: 10.1038/356521a0

Chmura, S. J., Dolan, M. E., Cha, A., Mauceri, H. J., and Kufe, D. W., Weichselbaum, R. R. (2000). In vitro and in vivo activity of protein kinase C inhibitor chelerythrine chloride induces tumor cell toxicity and growth delay in vivo. *Clin Cancer Res*. 6, 737–742.

Cull-Candy, S. G., and Leszkiewicz, D. N. (2004). Role of distinct NMDA receptor subtypes at central synapses. *Sci STKE*. 2004, re16. doi: 10.1126/stke.2552004re16

Dewachter, I., Filipkowski, R. K., Priller, C., Ris, L., Neyton, J., Croes, S., et al. (2009). Deregulation of NMDA-receptor function and down-stream signaling in APP[V717I] transgenic mice. *Neurobiol Aging*. 30, 241–256. doi: 10.1016/j.neurobiolaging.2007.06.011

Dumanska, H., and Veselovsky, N. (2019). Short-term hypoxia induces bidirectional pathological long-term plasticity of neurotransmission in visual retinocollicular pathway. *Exp Eye Res*. 179, 25–31. doi: 10.1016/j.exer.2018.10.014

Flint, A. C., Maisch, U. S., Weishaupt, J. H., Kriegstein, A. R., and Monyer, H. (1997). NR2A subunit expression shortens NMDA receptor synaptic currents in developing neocortex. *J Neurosci*. 17, 2469–2476. doi: 10.1523/JNEUROSCI.17-07-02469.1997

Furman, M., and Crair, M. C. (2012). Synapse maturation is enhanced in the binocular region of the retinocollicularmao prior to eye opening. *J. Neurophysiol.* 107, 3200–3216. doi: 10.1152/jn.00943.2011

Gardoni, F., Bellone, C., and Cattabeni, F., Di Luca M (2001). Protein kinase C activation modulates alpha-calmodulin kinase II binding to NR2A subunit of N-methyl-D-aspartate receptor complex. *J Biol Chem*. 276, 7609–7613. doi: 10.1074/jbc.M009922200

Georgiou, A. L., Guo, L., Cordeiro, M. F., and Salt, T. E. (2010). Changes in NMDA receptor contribution to synaptic transmission in the brain in a rat model of glaucoma. *Neurobiol Dis*. 39, 344–351. doi: 10.1016/j.nbd.2010.04.019

Gerber, G., Kangrga, I., Ryu, P. D., Larew, J. S., and Randic, M. (1989). Multiple effects of phorbol esters in the rat spinal dorsal horn. *J Neurosci*. 9, 3606–3617. doi: 10.1523/JNEUROSCI.09-10-03606.1989

Goldberg, M., Zhang, H. L., and Steinberg, S. F. (1997). Hypoxia alters the subcellular distribution of protein kinase C isoforms in neonatal rat ventricular myocytes. *J Clin Invest*. 99, 55–61. doi: 10.1172/JCI119133

Hardingham, G., and Bading, H. (2010). Synaptic versus extrasynaptic NMDA receptor signalling: implications for neurodegenerative disorders. *Nat Rev Neurosci* 11, 682–696. doi: 10.1038/nrn2911

Hatton, C. J., and Paoletti, P. (2005). Modulation of triheteromeric NMDA receptors by N-terminal domain ligands. *Neuron*. 46, 261–274. doi: 10.1016/j.neuron.2005.03.005

Herbert, J. M., Augereau, J. M., Gleye, J., and Maffrand, J. P. (1990). Chelerythrine is a potent and specific inhibitor of protein kinase C. *Biochem Biophys Res Commun*. 172, 993–999. doi: 10.1016/0006-291X(90)91544-3

Huang, C. C., Liang, Y. C., and Hsu, K. S. (2001). Characterization of the mechanism underlying the reversal of long term potentiation by low frequency stimulation at hippocampal CA1 synapses. *J Biol Chem*. 276, 48108–48117. doi: 10.1074/jbc.M106388200

Iacobucci, G. J., and Popescu, G. K. (2017). NMDA receptors: linking physiological output to biophysical operation. *Nat Rev Neurosci*. 18, 236–249. doi: 10.1038/nrn.2017.24

Jure, R. (2022). The "primitive brain dysfunction" theory of autism: the superior colliculus role. *Front Integr Neurosci*. 16, 797391. doi: 10.3389/fnint.2022.797391

Kim, H., Na, Y. R., Kim, S. Y., and Yang, E. G. (2016). Protein kinase c isoforms differentially regulate hypoxia-inducible factor-1α accumulation in cancer cells. *J Cell Biochem*. 117, 647–658. doi: 10.1002/jcb.25314

Lan, J. Y., Skeberdis, V. A., Jover, T., Grooms, S. Y., Lin, Y., Araneda, R. C., et al. (2001). Protein kinase C modulates NMDA receptor trafficking and gating. *Nat Neurosci*. 4, 382–390. doi: 10.1038/86028

Lau, C. G., and Zukin, R. S. (2007). NMDA receptor trafficking in synaptic plasticity and neuropsychiatric disorders. *Nat Rev Neurosci*. 8, 413–426. doi: 10.1038/nrn2153

Lee, J. W., Park, J. A., Kim, S. H., Seo, J. H., Lim, K. J., Jeong, J. W., et al. (2007). Protein kinase C-delta regulates the stability of hypoxia-inducible factor-1 alpha under hypoxia. *Cancer Sci*. 98, 1476–1481. doi: 10.1111/j.1349-7006.2007.00535.x

Li, B., Chen, N., Luo, T., Otsu, Y., Murphy, T. H., Raymond, L. A., et al. (2002). Differential regulation of synaptic and extra-synaptic NMDA receptors. *Nat Neurosci*. 5, 833–834. doi: 10.1038/nn912

Liao, G. Y., Wagner, D. A., Hsu, M. H., and Leonard, J. P. (2001). Evidence for direct protein kinase-C mediated modulation of N-methyl-D-aspartate receptor current. *Mol Pharmacol*. 59, 960–4. doi: 10.1124/mol.59.5.960

Lin, Y., Jover-Mengual, T., Wong, J., Bennett, M. V., and Zukin, R. S. (2006). PSD-95 and PKC converge in regulating NMDA receptor trafficking and gating. *Proc Natl Acad Sci U S A*. 103, 19902–19907. doi: 10.1073/pnas.0609924104

Luo, Z., Tian, M., Yang, G., Tan, Q., Chen, Y., Li, G., et al. (2022). Hypoxia signaling in human health and diseases: implications and prospects for therapeutics. *Signal Transduct Target Ther*. 7, 218. doi: 10.1038/s41392-022-01080-1

Mathis, C., Savier, E., Bott, J. B., Clesse, D., Bevins, N., Sage-Ciocca, D., et al. (2015). Defective response inhibition and collicular noradrenaline enrichment in mice with duplicated retinotopic map in the superior colliculus. *Brain Struct Funct*. 220, 1573–1584. doi: 10.1007/s00429-014-0745-5

Matsumoto, S., Shamloo, M., Matsumoto, E., Isshiki, A., and Wieloch, T. (2004). Protein kinase C-gamma and calcium/calmodulin-dependent protein kinase II-alpha are persistently translocated to cell membranes of the rat brain during and after middle cerebral artery occlusion. *J Cereb Blood Flow Metab*. 24, 54–61. doi: 10.1097/01.WCB.0000095920.70924.F5

Moriton, S., Komatsu, Y., Yamamori, T., and Koizumi, A. (2013). Diversity of retinal ganglion cells identified by transient GFP transfection in organotypic tissue culture of adult marmoset monkey retina. *PloS ONE* 8, e54667. doi: 10.1371/journal.pone.0054667

Paoletti, P., and Neyton, J. (2007). NMDA receptor subunits: function and pharmacology. *Curr Opin Pharmacol*.7, 39–47. doi: 10.1016/j.coph.2006.08.011

Perin-Dureau, F., Rachline, J., Neyton, J., and Paoletti, P. (2002). Mapping the binding site of the neuroprotectant ifenprodil on NMDA receptors. *J Neurosci*. 22, 5955–5965. doi: 10.1523/JNEUROSCI.22-14-05955.2002

Philpot, B. D., Sekhar, A. K., Shouval, H. Z., and Bear, M. F. (2001). Visual experience and deprivation bidirectionally modify the composition and function of NMDA receptors in visual cortex. *Neuron*. 29, 157–169. doi: 10.1016/S0896-6273(01)00187-8

Qi, Y., Hu, N. W., and Rowan, M. J. (2013). Switching off LTP: mGlu and NMDA receptor-dependent novelty exploration-induced depotentiation in the rat hippocampus. *Cereb Cortex*. 23, 932–939. doi: 10.1093/cercor/bhs086

Rebola, N., Srikumar, B. N., and Mulle, C. (2010). Activity-dependent synaptic plasticity of NMDA receptors. *J Physiol*. 588, 93–9. doi: 10.1113/jphysiol.2009.179382

Roberts, E. B., and Ramoa, A. S. (1999). Enhanced NR2A subunit expression and decreased NMDA receptor decay time at the onset of ocular dominance plasticity in the ferret. *J Neurophysiol*. 81, 2587–2591. doi: 10.1152/jn.1999.81.5.2587

Skaper, S. D., Facci, L., and Strijbos, P. J. (2001). Neuronal protein kinase signaling cascades and excitotoxic cell death. *Ann N Y Acad Sci*. 939, 11–22. doi: 10.1111/j.1749-6632.2001.tb03606.x

Soderling, T. R., and Derkach, V. A. (2000). Postsynaptic protein phosphorylation and LTP. *Trends Neurosci*.23, 75–80. doi: 10.1016/S0166-2236(99)01490-3

Tao, X., Sun, N., and Mu, Y. (2019). Development of depotentiation in adult-born dentate granule cells. *Front Cell Dev Biol*. 7, 236. doi: 10.3389/fcell.2019.00236

Townsend, M., Liu, Y., and Constantine-Paton, M. (2004). Retina-driven dephosphorylation of the NR2A subunit correlates with faster NMDA receptor kinetics at developing retinocollicular synapses. *J Neurosci*. 24, 11098–11107. doi: 10.1523/JNEUROSCI.1207-04.2004

Veselovsky, N. S., Engert, F., and Lux, H. D. (1996). Fast local superfusion technique. *Pflügers Archiv* 432, 351–354. doi: 10.1007/s004240050143

Vicini, S., Wang, J. F., Li, J. H., Zhu, W. J., Wang, Y. H., Luo, J. H., et al. (1998). Functional and pharmacological differences between recombinant N-methyl-D-aspartate receptors. *J Neurophysiol*. 79, 555–566. doi: 10.1152/jn.1998.79.2.555

Villalobos, C. A., Wu, Q., Lee, P. H., May, P. J., and Basso, M. A. (2018). Parvalbumin and GABA microcircuits in the mouse superior colliculus. *Front. Neural Circ*. 12, 35. doi: 10.3389/fncir.2018.00035

Wang, H., and Peng, R. Y. (2016). Basic roles of key molecules connected with NMDAR signaling pathway on regulating learning and memory and synaptic plasticity. *Military Med Res.* 3, 26. doi: 10.1186/s40779-016-0095-0

Wong-Riley, M. T. (2010). Energy metabolism of the visual system. *Eye Brain*. 2, 99–116. doi: 10.2147/EB.S9078

Xiong, Z. G., Raouf, R., Lu, W. Y., Wang, L. Y., Orser, B. A., Dudek, E. M., et al. (1998). Regulation of N-methyl-D-aspartate receptor function by constitutively active protein kinase C. *Mol Pharmacol*. 54, 1055–1063. doi: 10.1124/mol.54.6.1055

Xue, L., Zhang, F., Chen, X., Lin, J., and Shi, J. (2010). PDZ protein mediated activity-dependent LTP/LTD developmental switch at rat retinocollicular synapses. *Am J Physiol Cell Physiol*. 298, C1572–C1582. doi: 10.1152/ajpcell.00012.2010

Yaka, R., Thornton, C., Vagts, A. J., Phamluong, K., Bonci, A., Ron, D., et al. (2002). NMDA receptor function is regulated by the inhibitory scaffolding protein, RACK1. *Proc Natl Acad Sci U S A*. 99, 5710–5715. doi: 10.1073/pnas.062046299

Yan, J. Z., Xu, Z., Ren, S. Q., Hu, B., Yao, W., et al. (2011). Protein kinase C promotes N-methyl-D-aspartate (NMDA) receptor trafficking by indirectly triggering calcium/calmodulin-dependent protein kinase II (CaMKII) autophosphorylation. *J Biol Chem*. 286, 25187–25200. doi: 10.1074/jbc.M110.192708

Yan, S. F., Lu, J., Zou, Y. S., Kisiel, W., Mackman, N., Leitges, M., et al. (2000). Protein kinase C-beta and oxygen deprivation. A novel Egr-1-dependent pathway for fibrin deposition in hypoxemic vasculature. *J Biol Chem*. 275, 11921–11928. doi: 10.1074/jbc.275.16.11921

Zhou, M. H., Chen, S. R., Wang, L., Huang, Y., Deng, M., Zhang, J., et al. (2021). Protein kinase c-mediated phosphorylation and α2δ-1 interdependently regulate NMDA receptor trafficking and activity. *J Neurosci*. 41, 6415–6429. doi: 10.1523/JNEUROSCI.0757-21.2021

frontiers | Frontiers in Cellular Neuroscience

TYPE Brief Research Report
PUBLISHED 09 March 2023
DOI 10.3389/fncel.2023.1101006

OPEN ACCESS

EDITED BY
Dirk M. Hermann,
University of Duisburg-Essen, Germany

REVIEWED BY
Dan Z. Milikovsky,
Tel Aviv Sourasky Medical Center, Israel
Alberto Musto,
Eastern Virginia Medical School, United States

*CORRESPONDENCE
Alina Savotchenko
savrasova10@gmail.com

SPECIALTY SECTION
This article was submitted to Cellular Neuropathology, a section of the journal Frontiers in Cellular Neuroscience

RECEIVED 17 November 2022
ACCEPTED 20 February 2023
PUBLISHED 09 March 2023

CITATION
Savotchenko A, Klymenko M, Shypshyna M and Isaev D (2023) The role of thrombin in early-onset seizures.
Front. Cell. Neurosci. 17:1101006.
doi: 10.3389/fncel.2023.1101006

The role of thrombin in early-onset seizures

Alina Savotchenko[1]*, Mariia Klymenko[1], Mariia Shypshyna[2] and Dmytro Isaev[1]

[1]Department of Cellular Membranology, Bogomoletz Institute of Physiology, Kyiv, Ukraine, [2]Laboratory of Synaptic Transmission, Bogomoletz Institute of Physiology, Kyiv, Ukraine

A variety of clinical observations and studies in animal models of temporal lobe epilepsy (TLE) reveal dysfunction of blood-brain barrier (BBB) during seizures. It is accompanied by shifts in ionic composition, imbalance in transmitters and metabolic products, extravasation of blood plasma proteins in the interstitial fluid, causing further abnormal neuronal activity. A significant amount of blood components capable of causing seizures get through the BBB due to its disruption. And only thrombin has been demonstrated to generate early-onset seizures. Using the whole-cell recordings from the single hippocampal neurons we recently showed the induction of epileptiform firing activity immediately after the addition of thrombin to the blood plasma ionic media. In the present work, we mimic some effects of BBB disruption *in vitro* to examine the effect of modified blood plasma artificial cerebrospinal fluid (ACSF) on the excitability of hippocampal neurons and the role of serum protein thrombin in seizure susceptibility. Comparative analysis of model conditions simulating BBB dysfunction was performed using the lithium-pilocarpine model of TLE, which most clearly reflects the BBB disruption in the acute stage. Our results demonstrate the particular role of thrombin in seizure-onset in conditions of BBB disruption.

KEYWORDS

thrombin, blood-brain barrier, hippocampus, status epilepticus, temporal-lobe epilepsy, lithium-pilocarpine model

1. Introduction

Breakdown of the BBB is a most common feature of brain disorders, accompanied by neural and network dysfunction and degeneration (Benveniste et al., 1984; Seiffert, 2004; Tomkins et al., 2008), including epilepsy, stroke, traumatic brain injury, tumors, and neurodegenerative diseases (Brown and Davis, 2002; Davies, 2002; van Vliet et al., 2007; Stolp and Dziegielewska, 2009; Chodobski et al., 2011; Vezzani and Friedman, 2011; On et al., 2013; Wu et al., 2020). Studies on animal models of epilepsy and clinical observations among human patients reveal that the BBB has a direct role in epileptogenesis and brain damage (Mihály and Bozóky, 1984; Oby and Janigro, 2006; Friedman, 2011; Greene et al., 2022). Status epilepticus (SE) is accompanied by endothelial impairment and increased blood vessel permeability, which results in a disbalance of the neuronal environment (Obermeier et al., 2013). In particular, the ionic composition of the intercellular cerebrospinal fluid in the involved tissues is close in concentration to blood plasma (Zauner et al., 1996; Reinert et al., 2000). Such shifts in the interstitial ions can lead to changes in the impulse activity of neurons and affect the efficiency of synaptic transmission and, as a result, contribute to an increase in excitability of hippocampal neural networks (Rasmussen et al., 2020). Extravasation of blood plasma proteins into the extracellular environment of the brain in case of BBB

damage also contributes to long-term hypersynchronization of neurons in the affected areas (Seiffert, 2004; van Vliet et al., 2007). Entering the brain tissue as a consequence of traumatic brain injury thrombin is able to induce seizures (Lee et al., 1997). *In vitro* studies have shown the enhancement of thrombin activity in the brain due to pilocarpine treatment (Golderman et al., 2019). Recent findings suggest a significant increase in thrombin level in the brain following SE (Isaev et al., 2015). Moreover, intracerebral injection of thrombin may directly induce seizures (Lee et al., 1997). In this work, we simulate certain conditions of BBB breakdown *in vitro* to study the effect of thrombin in blood plasma ionic media on induction of epileptiform activity in hippocampal slices. Using the classical model of TLE we have found the resemblance in the manifestation of early-life seizures in SE-treated rats compared to seizure-like activity (SLA) due to model conditions, simulating impairment of BBB *in vitro*.

2. Materials and methods

2.1. Animals and experimental design

Experiments were conducted as per international principles of the European Convention for the protection of vertebrate animals used for experimental and other scientific purposes (European convention, Strasburg, 1986); the Law of Ukraine "On protection of animals from cruelty" and approved by the Animal Care Committee of Bogomoletz Institute of Physiology.

In our study, we use two groups of animals: control and SE-treated male Wistar rats at postnatal day (P) 21. The age was chosen based on brain sensitivity to pilocarpine (Cavalheiro et al., 1987). Hippocampal slices of control rats were subdivided into two groups: first for investigating the effect of modified blood plasma solution alone on induction of epileptiform activity (n = 17) and second—for the estimation the influence of the same solution together with 5 U/ml thrombin (n = 18) in order to mimic BBB disruption *in vitro*. Slices of SE-treated rats (n = 14) were used to compare their seizure-like activity with that of control hippocampi, induced by thrombin in blood plasma saline. For SE initiation rats were exposed to intraperitoneal injection (i.p.) of lithium chloride (127 mg/kg, 1 ml/kg) 20–22 h before administration of pilocarpine (i.p). First rats received one 40 mg/kg dose of pilocarpine with the subsequent injection of an additional 10 mg/kg dose every 30 min until the SE induction. The maximal pilocarpine concentration was 60 mg/kg per animal. We set the start of SE when the rat reached Racine stage V seizures (Racine, 1972) and terminate it at 60 min after onset by diethyl ether. Immediately after the animal fell asleep, we prepared hippocampal slices for further electrophysiological studies.

2.2. Hippocampal slice preparation

Upon anesthesia by diethyl ether and rapid decapitation, the brain was removed and placed into ice-cold carbogenated (5% CO_2 and 95% O_2) artificial cerebrospinal fluid (ACSF) containing (in mM): 119 NaCl, 2.5 KCl, 2 $CaCl_2$, 1.3 $MgCl_2$, 26 $NaHCO_3$, 1 NaH_2PO_4, and 11 glucose, pH 7.35. Isolated hippocampi were cut into 500 μm slices with a Vibroslice NVSL (World Precision Instruments Inc., Sarasota, FL, USA), and maintained in a carbogenated ACSF at room temperature for at least 1.5 h before recordings.

2.3. Electrophysiological procedure

Extracellular field potential recordings were made with glass microelectrodes containing ACSF (resistance of 1–3 MΩ) placed in the stratum pyramidale CA1. Brain slices were continuously superfused at a rate of 2–4 ml/min with carbogenated ASCF (30–32°C). Signals were digitized using an analog-to-digital converter (NI PCI-6221, National Instruments, Austin, TX, USA) and stored on a computer with WinWCP software (Strathclyde Electrophysiology Software, University of Strathclyde, Glasgow, UK).

To mimic some effects of BBB dysfunction we used an ASCF adapted to the blood plasma ionic media (in mM): 125 NaCl, 5 KCl, 1 $CaCl_2$, 0.8 $MgCl_2$, 24 $NaHCO_3$, 1.25 NaH_2PO_4, and 11 glucose, pH 7.35; Katzman and Pappius, 1973). Field potential recordings of SLA induced in blood plasma ACSF were performed on 17 slices (nine rats). Application of 5 U/ml thrombin to the blood plasma ionic media enhance seizure occurrence (18 slices, eight rats). Electrophysiological studies on hippocampal slices of SE-treated rats (14 slices, nine rats) were performed in incubation ASCF. No more than three slices per each animal were used.

2.4. Data analysis

Off-line data analysis was performed using Clampfit (Axon Instruments, CA, USA), Origin 7.5 (OriginLab, Northampton, MA, USA), and GraphPad Prism 5 (GraphPad, MA, USA) software. SLA was defined as brief, high amplitude spikes in the EEG. The Kruskal-Wallis test and *post hoc* (Dunn) were used for statistical comparison across groups. Data are shown as mean ± SEM.

3. Results

Field potential recordings were performed from the hippocampal CA1 pyramidal layer in acute slices. We did not observe SLA appearance in any of the tested slices due to ACSF perfusion (data not shown). Bath application of blood plasma ionic media led to consistent SLA in 17 slices (**Figure 1A1**). This activity persisted as long as examined solution was applied. The frequency of synchronous discharges during SLA was 1.34 ± 0.11 Hz. The amplitude of SLA was at the level 0.27 ± 0.03 mV (**Figure 1B**). Addition of 10 U/ml thrombin alone did not lead to an increase in neuronal firing in the CA3 hippocampal region of P 6–15 rats (Isaeva et al., 2012). Thrombin has evoked SLA in the presence of 7.2 mM of K^+ or 100 μM of glutamate in the extracellular solution (Maggio et al., 2008). In our study application of

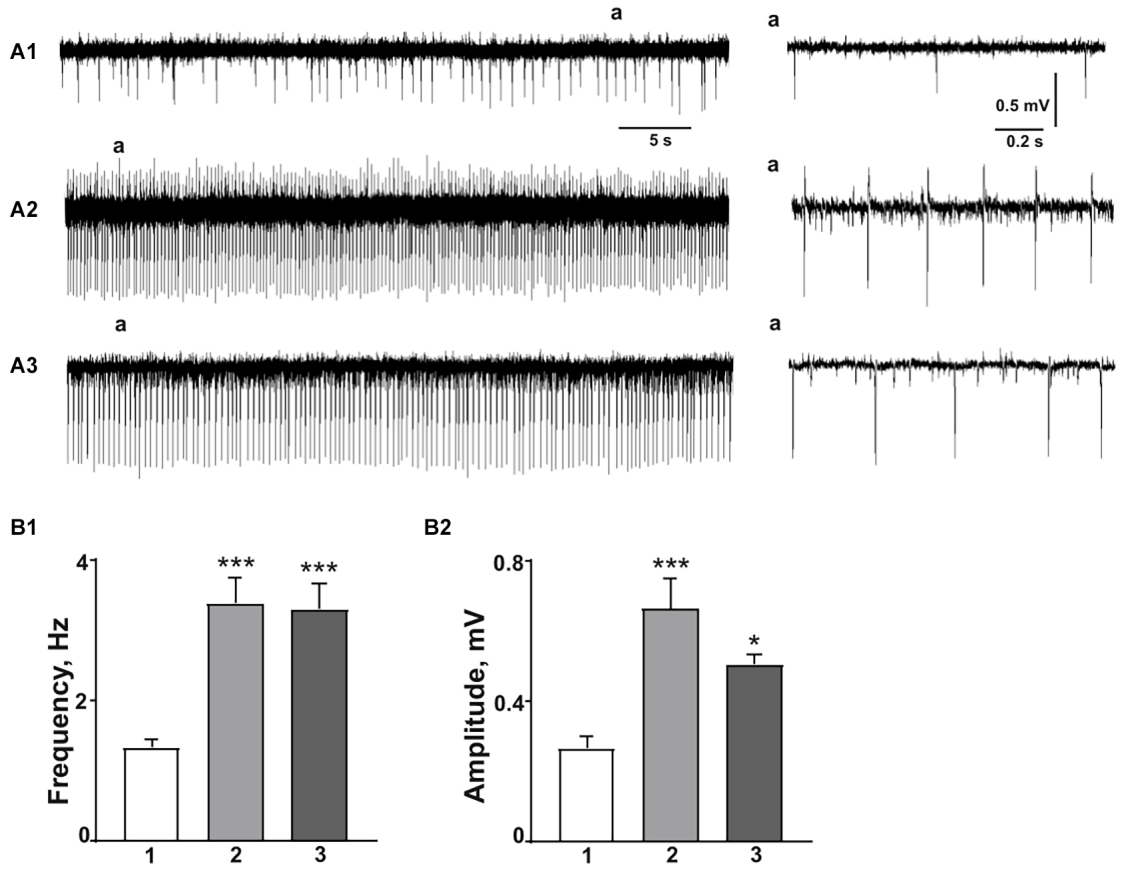

FIGURE 1
Effect of thrombin in plasma ionic media on the induction of SLA of CA1 subfield compared to Li-pilocarpine seizures. **(A1)** Extracellular field potentials recorded from CA1 pyramidal cell layer in modified to blood plasma ASCF indicate the induction to epileptiform activity. **(A2)** Application of 5U/ml thrombin produces robust SLA. **(A3)** Ictal-like events in SE-treated slices are similar to those, obtained in the presence of thrombin in blood plasma saline. Spontaneous discharges (a) shown in expanded scales in the right panel. Summary plots show the SLA frequency **(B1)** and amplitude **(B2)** during epileptiform discharges in blood plasma media (1), after the application of thrombin (2), and in SE-treated slices (3). Data presented as mean ± SEM. $^{*}P < 0.01$, $^{***}P < 0.0001$.

5 U/ml thrombin together with blood plasma ionic saline induced SLA in hippocampal CA1 pyramidal layer with the frequency of 3.39 ± 0.35 Hz and amplitude 0.66 ± 0.09 mV (n = 18, Figure 1A2). These data are in agreement with our previous report when in similar conditions the epileptiform activity in cultured hippocampal neurons was significantly enhanced (Shypshyna et al., 2021). Extracellular recordings from the slices of SE-treated rats demonstrated high-frequency oscillations with the frequency of 3.31 ± 0.35 Hz and amplitude 0.51 ± 0.03 mV (n = 14, Figure 1A3). Comparative analysis of field potentials in all experimental groups reveal significant enhancement in frequency ($H_{(2)}$ = 26.74, $P < 0.0001$; post-hoc: blood plasma media vs. thrombin—$P < 0.0001$; blood plasma media vs. SE—$P < 0.0001$, Figure 1B1) and amplitude ($H_{(2)}$ = 20.30, $P = 0.0001$; *post-hoc*: blood plasma media vs. thrombin—$P < 0.0001$; blood plasma media vs. SE—$P = 0.0011$, Figure 1B2) of SLA due to thrombin application and SE exposure. We observed non-significant decrease in amplitude of SLA in slices obtained from Li-pilocarpine-exposed epileptic rats compared to thrombin-treated slices in blood-plasma ACSF (p = 0.99, Figure 1B2).

4. Discussion

The main finding of our study is that TLE-treated slices shortly after SE induction produces similar significant increase in frequency and amplitude of SLA as blood plasma media together with thrombin.

Acute SE is induced by systemic application of muscarinic agonist, pilocarpine. *In vitro* application of pilocarpine alone did not cause epileptiform activity, but induced seizures when applied with substances that enhance BBB leakage, such as bradykinin or histamine (Uva et al., 2008). To promote an increase of BBB permeability we first perform the *in vivo* injection of lithium chloride. Subsequent administration of pilocarpine induced SE.

In our recent study, the application of serum-adapted solution increases the average action potentials frequency in neurons with spontaneous firing activity as well as tonic electrical activity in neurons. Increasing neuronal activity by blood plasma ACSF led to the development of epileptiform tonic activity in cultured hippocampal neurons (Shypshyna et al., 2021). Thrombin was shown to facilitate the effects of proconvulsants in the hippocampal slices from adult rats (Maggio et al., 2008).

We hypothesized the substantial role of BBB impairment in the initiation of seizures. Cerebrovascular damage in CNS disorders, including epilepsy is considered as a leading mechanism underlying epileptiform activity (Janigro, 1999; Seiffert, 2004; Marchi et al., 2007; Van Vliet et al., 2015). During intracerebral hemorrhage, blood compounds bleeding into the brain tissue and cause both an acute and a delayed effect on neuronal functioning (Friedman, 2011). Among the consequences of BBB damage are the changes in the intracerebral environment, when the ionic composition of the intercellular cerebrospinal fluid in the affected areas is close in concentration to blood plasma (Zauner et al., 1996; Reinert et al., 2000). Replacing the ACSF with blood plasma saline obviously affects the functioning of voltage-gated channels. Thus, increased concentrations of K^+ in extracellular solution, in addition to affecting the membrane potential and synaptic transmission, potentiate the persistent Na^+ currents in neurons (Somjen and Müller, 2000). However, such an effect contributes to the strengthening of synaptic potentials and increases the ability of neurons to recurrent synchronous discharges (Stafstrom, 2007), which we observed in our experiments. Modification of ACSF to blood plasma solution also evolves changes in Ca^{2+} and Mg^{2+} concentrations, which could neutralize the negative surface charges on the outer membrane surface and lead to the facilitation of the voltage-gated channels activation (Isaev et al., 2012). In our study, changes in the concentrations of certain ions in blood plasma media neutralized each other, which contributed to maintaining the shielding of negative charges on neural membranes at the control level. Therefore, we excluded the possibility that the epileptiform activity of the hippocampal slices in modified ACSF is related to changes in the concentrations of divalent cations.

BBB breakdown could result in penetrating and storage in the brain of toxic bloodborne molecules such as hemoglobin, albumin, thrombin, fibrinogen, iron-containing hemosiderin, plasmin, free iron, and environmental toxins (Montagne et al., 2016). Only thrombin was shown to have a potent role in the generation of early-onset SLA (Willmore et al., 1978; Lee et al., 1997; Tomkins et al., 2007). Our data are in agreement with these studies demonstrating the generation of epileptiform activity due to thrombin application in the blood plasma media. Recent findings suggest a significant increase in the thrombin level in the brain tissue caused by the enhancement of BBB permeability during pathological conditions (Woitzik et al., 2011; Isaev et al., 2015). Thrombin, through its major receptor in the neural tissue, protease-activated receptors 1 (PAR 1), produces epileptogenesis by the escalation of brain damage, induction of seizures, inflammation, and neurogenesis (Rohatgi et al., 2004).

It was shown previously that pilocarpine-induced SE may be caused by enhancement in the BBB permeability (Uva et al., 2008). It was shown the disruption of BBB shortly after SE (van Vliet et al., 2007), accompanied by the early efflux of serum proteins and disturbance in interstitial fluid homeostasis (Friedman, 2011). Later epileptic phase involved different mechanisms of propagation seizures, including activation of the innate immune system, activation of transforming growth factor beta in the response to serum albumin, extracellular accumulation of K^+ and glutamate (Cacheaux et al., 2009; David et al., 2009), etc. In our study, we demonstrate that epileptic activity in slices of pilocarpine-treated rats obtained after SE-onset have similar features as synchronous discharges due to the application of thrombin in plasma ionic media. We propose the essential role of thrombin efflux in the acute epileptiform discharges induced by pilocarpine treatment.

Data availability statement

The original contributions presented in the study are included in the article, further inquiries can be directed to the corresponding author.

Ethics statement

The animal study was reviewed and approved by European Convention for the protection of vertebrate animals used for experimental and other scientific purposes (European convention, Strasburg, 1986); the Law of Ukraine "On protection of animals from cruelty" and approved by the Animal Care Committee of Bogomoletz Institute of Physiology.

Author contributions

AS has designed the experiments, provided an elecrophysiological recordings, made statistical analysis and prepared the manuscript. MK performed experiments with Li-pilocarpine model of epilepsy and took part in disscusion of the results. MS has provided experiments with thrombin and participated in disscusion of manuscript. DI elaborated the idea of experiments, participated in summarizing results and making conclusions. All authors contributed to the article and approved the submitted version.

Conflict of interest

The authors declare that the research was conducted in the absence of any commercial or financial relationships that could be construed as a potential conflict of interest.

Publisher's note

All claims expressed in this article are solely those of the authors and do not necessarily represent those of their affiliated organizations, or those of the publisher, the editors and the reviewers. Any product that may be evaluated in this article, or claim that may be made by its manufacturer, is not guaranteed or endorsed by the publisher.

References

Benveniste, H., Drejer, J., Schousboe, A., and Diemer, N. H. (1984). Elevation of the extracellular concentrations of glutamate and aspartate in rat hippocampus during transient cerebral ischemia monitored by intracerebral microdialysis. *J. Neurochem.* 43, 1369–1374. doi: 10.1111/j.1471-4159.1984.tb05396.x

Brown, R. C., and Davis, T. P. (2002). Calcium modulation of adherens and tight junction function: a potential mechanism for blood- brain barrier disruption after stroke. *Stroke* 33, 1706–1711. doi: 10.1161/01.str.0000016405.06729.83

Cacheaux, L. P., Ivens, S., David, Y., Lakhter, A. J., Bar-Klein, G., Shapira, M., et al. (2009). Transcriptome profiling reveals TGF-β signaling involvement in epileptogenesis. *J. Neurosci.* 29, 8927–8935. doi: 10.1523/JNEUROSCI.0430-09.2009

Cavalheiro, E. A., Silva, D. F., Turski, W. A., Calderazzo-Filho, L. S., Bortolotto, Z. A., and Turski, L. (1987). The susceptibility of rats to pilocarpine-induced seizures is age-dependent. *Brain Res.* 37, 43–58. doi: 10.1016/0165-3806(87)90227-6

Chodobski, A., Zink, B. J., and Szmydynger-Chodobska, J. (2011). Blood-brain barrier pathophysiology in traumatic brain injury. *Transl. Stroke Res.* 2, 492–516. doi: 10.1007/s12975-011-0125-x

David, Y., Cacheaux, L. P., Ivens, S., Lapilover, E., Heinemann, U., Kaufer, D., et al. (2009). Astrocytic dysfunction in epileptogenesis: consequence of altered potassium and glutamate homeostasis? *J. Neurosci.* 29, 10588–10599. doi: 10.1523/JNEUROSCI.2323-09.2009

Davies, D. C. (2002). Blood- brain barrier breakdown in septic encephalopathy and brain tumours. *J. Anat.* 200, 639–646. doi: 10.1046/j.1469-7580.2002.00065.x

Friedman, A. (2011). Blood-brain barrier dysfunction, status epilepticus, seizures and epilepsy: a puzzle of a chicken and egg? *Epilepsia* 52, 19–20. doi: 10.1111/j.1528-1167.2011.03227.x

Golderman, V., Shavit-Stein, E., Gera, O., Chapman, J., Eisenkraft, A., and Maggio, N. (2019). Thrombin and the protease-activated receptor-1 in organophosphate-induced status epilepticus. *J. Mol. Neurosci.* 67, 227–234. doi: 10.1007/s12031-018-1228-6

Greene, C., Hanley, N., Reschke, C., Reddy, A., Mäe, M., Connolly, R., et al. (2022). Microvascular stabilization via blood-brain barrier regulation prevents seizure activity. *Nat. Commun.* 13:2003. doi: 10.1038/s41467-022-29657-y

Isaev, D., Ivanchick, G., Khmyz, V., Isaeva, E., Savrasova, A., Krishtal, O., et al. (2012). Surface charge impact in low-magnesium model of seizure in rat hippocampus. *J. Neurophysiol.* 107, 417–423. doi: 10.1152/jn.00574.2011

Isaev, D., Lushnikova, I., Lunko, O., Zapukhliak, O., Maximyuk, O., Romanov, A., et al. (2015). Contribution of protease-activated receptor 1 in status epilepticus-induced epileptogenesis. *Neurobiol. Dis.* 78, 68–76. doi: 10.1016/j.nbd.2015.03.026

Isaeva, E., Hernan, A., Isaev, D., and Holmes, G. L. (2012). Thrombin facilitates seizures through activation of persistent sodium current. *Ann. Neurol.* 72, 192–198. doi: 10.1002/ana.23587

Janigro, D. (1999). Blood-brain barrier, ion homeostasis and epilepsy: possible implications towards the understanding of ketogenic diet mechanisms. *Epilepsy Res.* 37, 223–232. doi: 10.1016/s0920-1211(99)00074-1

Katzman, R., and Pappius, H. M. (1973). *Brain Electrolytes And Fluid Metabolism*. Baltimore: Williams & Wilkins.

Lee, K. R., Drury, I., Vitarbo, E., and Hoff, J. T. (1997). Seizures induced by intracerebral injection of thrombin: a model of intracerebral hemorrhage. *J. Neurosurg.* 87, 73–78. doi: 10.3171/jns.1997.87.1.0073

Maggio, N., Shavit, E., Chapman, J., and Segal, M. (2008). Thrombin induces long-term potentiation of reactivity to afferent stimulation and facilitates epileptic seizures in rat hippocampal slices: toward understanding the functional consequences of cerebrovascular insults. *J. Neurosci.* 28, 732–736. doi: 10.1523/JNEUROSCI.3665-07.2008

Marchi, N., Angelov, L., Masaryk, T., Fazio, V., Granata, T., Hernandez, N., et al. (2007). Seizure-promoting effect of blood-brain barrier disruption. *Epilepsia* 48, 732–742. doi: 10.1111/j.1528-1167.2007.00988.x

Mihály, A., and Bozóky, B. (1984). Immunohistochemical localization of extravasated serum albumin in the hippocampus of human subjects with partial and generalized epilepsies and epileptiform convulsions. *Acta Neuropathol.* 65, 25–34. doi: 10.1007/BF00689824

Montagne, A., Toga, A. W., and Zlokovic, B. V. (2016). Blood-brain barrier permeability and gadolinium: benefits and potential pitfalls in research. *JAMA Neurol.* 73, 13–14. doi: 10.1001/jamaneurol.2015.2960

Obermeier, B., Daneman, R., and Ransohoff, R. M. (2013). Development, maintenance and disruption of the blood-brain barrier. *Nat. Med.* 19, 1584–1596. doi: 10.1038/nm.3407

Oby, E., and Janigro, D. (2006). The blood-brain barrier and epilepsy. *Epilepsia* 47, 1761–1774. doi: 10.1111/j.1528-1167.2006.00817.x

On, N. H., Mitchell, R., Savant, S. D., Bachmeier, C. J., Hatch, G. M., and Miller, D. W. (2013). Examination of blood-brain barrier (BBB) integrity in a mouse brain tumor model. *J. Neurooncol.* 111, 133–143. doi: 10.1007/s11060-012-1006-1

Racine, R. J. (1972). Modification of seizure activity by electrical stimulation: II. Motor seizure. *Electroencephalogr. Clin. Neurophysiol.* 32, 281–294. doi: 10.1016/0013-4694(72)90177-0

Rasmussen, R., O'Donnell, J., Ding, F., and Nedergaard, M. (2020). Interstitial ions: a key regulator of state-dependent neural activity? *Prog. Neurobiol.* 193:101802. doi: 10.1016/j.pneurobio.2020.101802

Reinert, M., Khaldi, A., Zauner, A., Doppenberg, E., Choi, S., and Bullock, R. (2000). High extracellular potassium and its correlates after severe head injury: relationship to high intracranial pressure. *Neurosurg. Focus* 8:e10. doi: 10.3171/foc.2000.8.1.2027

Rohatgi, T., Henrich-Noack, P., Sedehizade, F., Goertler, M., Wallesch, C. W., Reymann, K. G., et al. (2004). Transient focal ischemia in rat brain differentially regulates mRNA expression of protease-activated receptors 1 to 4. *J. Neurosci. Res.* 75, 273–279. doi: 10.1002/jnr.10847

Seiffert, E. (2004). Lasting blood-brain barrier disruption induces epileptic focus in the rat somatosensory cortex. *J. Neurosci.* 24, 7829–7836. doi: 10.1523/JNEUROSCI.1751-04.2004

Shypshyna, M., Savotchenko, A., Kuznetsov, K., and Veselovsky, M. (2021). The effect of thrombin in the serum-adapted ionic environment on the induction of epileptiform firing activity of hippocampal cultured neurons. *Fiziol. Zh.* 67, 3–10. doi: 10.15407/fz67.05.003

Somjen, G. G., and Müller, M. (2000). Potassium-induced enhancement of persistent inward current in hippocampal neurons in isolation and in tissue slices. *Brain Res.* 885, 102–110. doi: 10.1016/s0006-8993(00)02948-6

Stafstrom, C. E. (2007). Persistent sodium current and its role in epilepsy. *Epilepsy Curr.* 7, 15–22. doi: 10.1111/j.1535-7511.2007.00156.x

Stolp, H. B., and Dziegielewska, K. M. (2009). Role of developmental inflammation and blood-brain barrier dysfunction in neurodevelopmental and neurodegenerative diseases. *Neuropathol. Appl. Neurobiol.* 35, 132–146. doi: 10.1111/j.1365-2990.2008.01005.x

Tomkins, O., Friedman, O., Ivens, S., Reiffurth, C., Major, S., Dreier, J. P., et al. (2007). Blood-brain barrier disruption results in delayed functional and structural alterations in the rat neocortex. *Neurobiol. Dis.* 25, 367–377. doi: 10.1016/j.nbd.2006.10.006

Tomkins, O., Shelef, I., Kaizerman, I., Eliushin, A., Afawi, Z., Misk, A., et al. (2008). Blood- brain barrier disruption in post-traumatic epilepsy. *J. Neurol. Neurosurg. Psychiatry* 79, 774–777. doi: 10.1136/jnnp.2007.126425

Uva, L., Librizzi, L., Marchi, N., Noe, F., Bongiovanni, R., Vezzani, A., et al. (2008). Acute induction of epileptiform discharges by pilocarpine in the *in vitro* isolated guinea-pig brain requires enhancement of blood-brain barrier permeability. *Neuroscience* 151, 303–312. doi: 10.1016/j.neuroscience.2007.10.037

Van Vliet, E., Aronica, E., and Gorter, J. (2015). Blood-brain barrier dysfunction, seizures and epilepsy. *Semin. Cell Dev. Biol.* 38, 26–34. doi: 10.1016/j.semcdb.2014.10.003

van Vliet, E. A., da Costa Araújo, S., Redeker, S., van Schaik, R., Aronica, E., and Gorter, J. A. (2007). Blood-brain barrier leakage may lead to progression of temporal lobe epilepsy. *Brain* 130, 521–534. doi: 10.1093/brain/awl318

Vezzani, A., and Friedman, A. (2011). Brain inflammation as a biomarker in epilepsy. *Biomark. Med.* 5, 607–614. doi: 10.2217/bmm.11.61

Willmore, L. J., Sypert, G. W., and Munson, J. B. (1978). Recurrent seizures induced by cortical iron injection: a model of posttraumatic epilepsy. *Ann. Neurol.* 4, 329–336. doi: 10.1002/ana.410040408

Woitzik, J., Hohenstein, A., Hecht, N., Juettler, E., and Schilling, L. (2011). Short period of early reperfusion aggravates blood-brain barrier dysfunction during permanent focal ischemia in rats. *Transl. Stroke Res.* 2, 67–71. doi: 10.1007/s12975-010-0042-4

Wu, Y., Wu, H., Guo, X., Pluimer, B., and Zhao, Z. (2020). Blood-brain barrier dysfunction in mild traumatic brain injury: evidence from preclinical murine models. *Front. Physiol.* 11:1030. doi: 10.3389/fphys.2020.01030

Zauner, A., Bullock, R., Kuta, A. J., Woodward, J., and Young, H. F. (1996). Glutamate release and cerebral blood flow after severe human head injury. *Acta Neurochir. Suppl.* 67, 40–44. doi: 10.1007/978-3-7091-6894-3_9

frontiers | Frontiers in Cellular Neuroscience

TYPE Original Research
PUBLISHED 09 March 2023
DOI 10.3389/fncel.2023.1129991

OPEN ACCESS

EDITED BY
Chris J. McBain,
Eunice Kennedy Shriver National Institute of Child Health and Human Development (NIH), United States

REVIEWED BY
Hiroki Toyoda,
Osaka University, Japan
Jason Wester,
The Ohio State University, United States

*CORRESPONDENCE
Igor V. Melnick
✉ igorm@biph.kiev.ua

SPECIALTY SECTION
This article was submitted to Cellular Neuropathology, a section of the journal Frontiers in Cellular Neuroscience

RECEIVED 22 December 2022
ACCEPTED 20 February 2023
PUBLISHED 09 March 2023

CITATION
Pendeliuk VS and Melnick IV (2023) Excitatory synchronization of rat hippocampal interneurons during network activation *in vitro*.
Front. Cell. Neurosci. 17:1129991.
doi: 10.3389/fncel.2023.1129991

Excitatory synchronization of rat hippocampal interneurons during network activation *in vitro*

Viktoria S. Pendeliuk[1] and Igor V. Melnick[2]*

[1]Hospital of Urgent Medical Care, Department of Surgery No. 4, NAMS of Ukraine, Kiev, Ukraine, [2]Department of Biophysics of Ion Channels, Bogomoletz Institute of Physiology, NAS of Ukraine, Kiev, Ukraine

Introduction: Hippocampal interneurons (INs) are known to synchronize their electrical activity *via* mechanisms, which are poorly defined due to immense complexity of neural tissue but seem to depend on local cell interactions and intensity of network activity.

Methods: Here, synchronization of INs was studied using paired patch-clamp recordings in a simplified culture model with intact glutamate transmission. The level of network activity was moderately elevated by field electric stimulation, which is probably an analogue of afferent processing *in situ*.

Results: Even in baseline conditions, ~45% of spontaneous inhibitory postsynaptic currents (sIPSCs) resulting from firing of individual presynaptic INs coincided between cells within ±1 ms due to simple divergence of inhibitory axons. Brief network activation induced an appearance of 'hypersynchronous' (~80%) population sIPSCs occurring in response to coherent discharges of several INs with jitter ±4 ms. Notably, population sIPSCs were preceded by transient inward currents (TICs). Those were excitatory events capable to synchronize firing of INs, in this respect being reminiscent of so-called fast prepotentials observed in studies on pyramidal neurons. TICs also had network properties consisting of heterogeneous components: glutamate currents, local axonal and dendritic spikelets, and coupling electrotonic currents likely *via* gap junctions; putative excitatory action of synaptic gamma-aminobutyric acid (GABA) was not involved. The appearance of population excitatory-inhibitory sequences could be initiated and reproduced by firing of a single excitatory cell reciprocally connected with one IN.

Discussion: Our data demonstrate that synchronization of INs is initiated and dominated by glutamatergic mechanisms, which recruit, in a whole-sale manner, into supporting action other excitatory means existing in a given neural system.

KEYWORDS

synaptic transmission, GABA, glutamate, hippocampus, interneurons, synchronization, gap junctions

1. Introduction

In higher brain structures as the neocortex and hippocampus, the cells within a local group or even widely separated tend to display electrical activity synchronous in the second and millisecond time scale, which is important for physiological states such as sensory processing, sleep or arousal, and in pathological conditions as epilepsy (Engel et al., 1992;

Yuste et al., 1992; Harris and Gordon, 2015). This synchrony remains one of the most enigmatic properties of the brain, the mechanisms of which have been studied for decades. It is thought that four general processes could underlie such coherence: excitatory synapses releasing glutamate (Glu), electrotonic coupling *via* gap junctions, electrical field effects (ephaptic interactions), and changes of extracellular ions (Dudek et al., 1986); the expression of which seem to depend on the cell type, brain region, animal species, developmental age, and experimental conditions. While this classical knowledge has been mainly obtained in studies of excitatory pyramidal cells, much less is known for inhibitory interneurons (INs).

Interneurons represent a highly variable and distinct population of nerve cells in cortical structures depending on the layer location, dendritic pattern, axonal projections, and neuropeptide phenotype (Freund and Buzsaki, 1996). The subsets of INs innervate both pyramidal cells and each other in a specific manner releasing gamma-aminobutyric acid (GABA) (Pfeffer et al., 2013; Karnani et al., 2016). The latter binds to $GABA_A$ receptors opening Cl^- channels, which depresses postsynaptic electrogenesis *via* both membrane hyperpolarization and shunting effects (Miles et al., 1996; Vida et al., 2006). Moreover, INs are thought to operate like a network and synchronize their own activity *via* mechanisms to some extent distinct from those of pyramidal cells. Accordingly, to current knowledge, two specific processes might mediate this synchrony endogenously and independently of Glu neurotransmission. First, pioneering studies of Ben-Ari et al. (1989) discovered that neonatal hippocampal neurons display synchronous bursting episodes mediated by $GABA_A$ receptors, so-called giant-depolarizing potentials (GDPs). These authors have proposed that, in contrast to adult cells, GABA has an unusual depolarizing and excitatory action in connections between INs due to elevated intracellular Cl^- at that immature developmental stage (Khazipov et al., 1997; Dzhala and Staley, 2003; Sipilä et al., 2005). On the other hand, this mechanism has been also found in mature animals, in a fraction of INs expressing neuropeptide Y (Fu and van den Pol, 2007), in axo-axonic cells (Szabadics et al., 2006), and during epileptiform activity induced by convulsant drugs or tetanic electrical stimulation (Avoli et al., 1993; Michelson and Wong, 1994; Benardo, 1997; Bracci et al., 1999; Velazquez and Carlen, 1999). Second, morphological studies have found or suggested the presence of gap junctions in the dendrites of INs (Gulyás et al., 1996; Fukuda and Kosaka, 2000; Shigematsu et al., 2019), which would allow a direct transfer of electrical currents between cells facilitating the firing of action potentials (APs) and their coherence. The impact of gap junctional coupling on synchrony has been extensively studied mainly in neocortical neurons leading to high-frequency coherent oscillations of extracellular field and intracellular membrane potentials, which are observed during a range of behaviors *in vivo* or induced *in vitro* either chemically or by electrical stimulation (Steriade et al., 1993; Zhang et al., 1998; Skinner et al., 1999; Beierlein et al., 2000; Bartos et al., 2002).

The classical body of evidence indicates that excitation of individual INs is provided from external sources, in a feed-forward manner from long-ranged afferent fibers and in a feed-back (recurrent) way from local excitatory cells, both releasing Glu acting on ionotropic and metabotropic receptors, iGluR and mGluR, respectively (Miles, 1990a; McBain and Dingledine, 1993; Miles and Poncer, 1993; Geiger et al., 1997; Frerking et al., 1998; Semyanov and Kullmann, 2001; Kerlin et al., 2010; Karnani et al., 2016). It is not very surprising that the synchrony of INs can be simply induced by their near-simultaneous activation by coherent sensory input, which was demonstrated as intracellular Ca^{2+} waves synchronous within chemically-defined subsets of cortical cells (Karnani et al., 2016). Apart from this, the role of traditional Glu-ergic processes in synchronizing the activity of INs has been rarely addressed directly so far. It has been primarily due to the immense complexity in the synaptic organization of neural tissue and thus, of its electrical epiphenomena (e.g., Shigematsu et al., 2019). In particular, it is still not known with certainty how are generated those network electrical events, i.e., GDPs, epileptiform bursts, and electrical oscillations, which currently serve as models of neural synchronization. They reflect the patterned activity of thousands of nerve cells and it is difficult to isolate the activity of individual INs without interfering with excitatory cells and using respective antagonists. Thus, possibly one of the main controversies still centers around the nature of INs excitation, whether it is endo- or exogenous (i.e., dependent on iGluR). In the example of GDPs initially thought as purely GABAergic, the excitatory Glu currents within depolarizing episodes were found more recently and GDPs revealed sensitivity to blockers of iGluR (Khazipov et al., 1997; Khalilov et al., 1999). Induced epileptiform discharges were reported to persist under the blockers, when the network was made hyperexcitable (Michelson and Wong, 1994), while the blockers did affect some components of interictal- and ictal-like activity in other studies (Avoli et al., 1993; Bracci et al., 1999; Velazquez and Carlen, 1999). As for the oscillations, they were abolished by antagonists of iGluR in the study of Fisahn et al. (1998) but were resistant to them in experiments of Whittington et al. (1995). Still another limitation of existing models is that they correspond to an already high level of network activity, which could affect cellular synchrony; at the same time, the initial state often remains unknown.

In attempts to elucidate intrinsic and basic mechanisms of INs synchronization, here we present a novel and simplified approach by using low-density culture and assuming that synchrony in the hippocampus is of local character resulting from interactions of a few neighboring cells, the idea expressed by several authors (Ben-Ari et al., 1989; Khazipov et al., 1997). The correlation of spontaneous inhibitory postsynaptic currents (sIPSCs) in cell pairs was studied in the course of moderate network activation and with intact iGluR, which presumably is analogous to natural afferent processing. We demonstrate the appearance of population sIPSCs resulting from the firing of a few presynaptic INs. Population sIPSCs were preceded by transient inward currents (TICs) serving as excitatory and synchronizing network events of different natures. They consisted of dominant Glu-mediated components, coupling electrotonic currents (presumably, *via* gap junctions) and local dendritic and axonal spikelets. The latter, in its turn, represented a novel mechanism contributing to the local synchrony of synaptic inhibition.

2. Materials and methods

All animal procedures here conformed to the principles of worldwide regulations (Grundy, 2015). The experiments were carried out according to guidelines approved according to Protocol

no. 3/14 from 06.2015 from the Bogomoletz Institute of Physiology (Ukraine) and as regulated by the European Community Council Directive (2010/63/EU).

2.1. Hippocampal culture

Newborn rats (0–1 day) were anesthetized with instant decapitation. Hippocampi were dissociated enzymatically with 0.05% pronase E (Serva) and gentle trituration. Cells were plated at a density of 4–5 $\times$ 10^4 cells cm^{-2} on glass coverslips coated with a mixture of laminin/poly-L-ornithine. The feeding medium consisted of minimal essential medium (MEM), 0.6% glucose, 1 mM glutamine, 26 mM $NaHCO_3$, 0.01 mg/ml insulin, 0.1 mg/ml holo-transferrin (Sigma), and 10% horse serum (Gibco). The medium was changed 1–2 times per week. The cultures were kept at 37°C in humidified air with 5% CO_2 and after 2 weeks *in vitro* were used for experiments.

2.2. Electrophysiology

Patch-clamp recordings were made in cell-attached and whole-cell modes from pairs of neurons using two EPC-7 amplifiers (List, Germany). The extracellular solution (ACSF) contained (in mM): NaCl 140, KCl 4, $CaCl_2$ 2, $MgCl_2$ 1, HEPES 10, glucose 10. The intracellular solution contained (in mM): K-gluconate or Cs-gluconate (for postsynaptic neuron) 118, CsCl 12, $MgCl_2$ 4, Na_2ATP 4, EGTA 10, HEPES 10; pH of all solutions was 7.3. Patch pipettes had resistance 3–5 MΩ after filling with the intracellular solution. The access resistance was <25 MΩ at the beginning of an experiment and the data were discarded if it increased by >20%, series resistance compensation was not used. Liquid junction potential was measured as + 11 mV and was not corrected. The holding potential (V_m) in cell-attached mode was adjusted to zero holding current, in the whole-cell mode it was −70 mV for presynaptic cell and typically between −30 and −20 mV for postsynaptic neuron, i.e., positive to Cl^- reversal potential (theoretical $E_{Cl} = -50$ mV at 20°C). Cell identification in a pair was achieved by their sequential stimulation (50-mV depolarizing pulses, 5–40 ms in duration and 0.2 Hz frequency) and recording of either outward or inward postsynaptic responses (**Figure 1**). During initial characterization, the outward currents at V_m −30 mV (*B*, trace 3) were blocked by the application of $GABA_A$ receptor antagonist 10 μM bicuculline and were considered GABAergic inhibitory postsynaptic currents (IPSCs). Inward responses retained their direction at potentials up to 0 mV (*C*, trace 2–3) and were abolished by combined application of 50 μM APV and 10 μM CNQX (APV/CNQX), blockers of N-methyl-D-aspartate (NMDA) and non-NMDA subtypes of iGluR; they were considered as Glu-ergic excitatory postsynaptic currents (EPSCs). Similarly, using this separation by holding potential allowed us to visualize simultaneously inward sEPSCs and outward sIPSCs during the recording of spontaneous synaptic activity (e.g., **Figure 2A**).

The activation of neuronal networks was achieved by field electrical stimulation delivered to the whole coverslip by bipolar tungsten electrodes with poles separated by 10 mm and fed by constant 5–15 V voltage pulses from an isolating stimulator unit (model A365, World Precision Instruments, Sarasota, FL, USA). Stimulation protocol consisted of 3–7 trains separated by 5-s intervals, each of the trains having ten 1-ms pulses at 10 Hz frequency. The voltage of pulses was set at the lowest end and steadily increased between stimulation sessions until the minimal effects observable by the eye were noticed; among those, changes in the appearance of sIPSCs and/or their frequency were used as criteria of a positive outcome. The recordings started at 1 min after stimuli termination and continued for another 20 min; in preliminary experiments, it proved to be sufficient to cover ongoing changes before the network activity restores its baseline level. In some experiments, local extracellular stimulation of individual cells was performed. Single electrical pulses were delivered locally *via* a double-barreled micropipette with resistance 1–2 MΩ after filling with bath solution. The precision of stimulation was achieved by fine adjustment of its intensity and pipette position in close proximity to the dendrites or soma of a cell; moving the stimulating pipette a few micrometers away abolished APs, those were verified in cell-attached recording (**Figure 7E**). Membrane currents were low-pass filtered at 3 kHz, and sampled at 3–5 kHz using a computer interface (ITC-16 board, List, Germany) and TIDA acquisition software (List, Germany). The experiments were performed at room temperature (20–22°C).

Tetrodotoxin (TTX) was purchased from Sigma, and other substances such as bicuculline methiodide (BMI), D,L-2-amino-5-phosphonovaleric acid (APV), and 6-cyano-7-nitroquinoxaline-2,3-dione (CNQX) were obtained from RBI, they were dissolved in ACSF before use. Recordings were done in static bath conditions, while drug applications were performed locally by using a multibarrel system. For this, inflow and outflow pipettes (internal diameter 50 and 80 μm, respectively) were positioned with a separation of ∼400 μM between them so that an area containing a limited number of neurons (usually, <5) was covered. The procedure was initiated by applying only ACSF without drugs to obtain a steady-state level in the amplitudes of IPSCs and EPSCs. Between recordings, the bath was briefly superfused with ACSF to replenish its level.

2.3. Data analysis

Individual sIPSCs were extracted from continuous records using an event detection program (ANDATRA, Boychuk Y., Kiev). Only stable paired recordings were considered as judged from the running averages of 30 events. The detection criteria were set as reported elsewhere (Otis and Mody, 1992). Briefly, sIPSCs were inspected visually and apparent spurious and multiple detections of large events were rejected, the events with an amplitude >5 pA for miniature IPSCs and >20 pA for sIPSCs were acquired. The sIPSCs were analyzed semi-automatically. The following parameters were calculated for individual events: rise time (10–90%), peak amplitudes, and decay time constant (mono- or bi-exponential fitting using the non-linear least square method). Synaptic delay of spontaneous and evoked IPSCs was measured from the peak of presynaptic APs in cell-attached mode and inward Na^+ currents in whole-cell mode, to the onset of IPSCs (**Figures 2F, G**).

In the analysis of the correlation between sIPSCs in pair recordings, time difference histograms were plotted as described

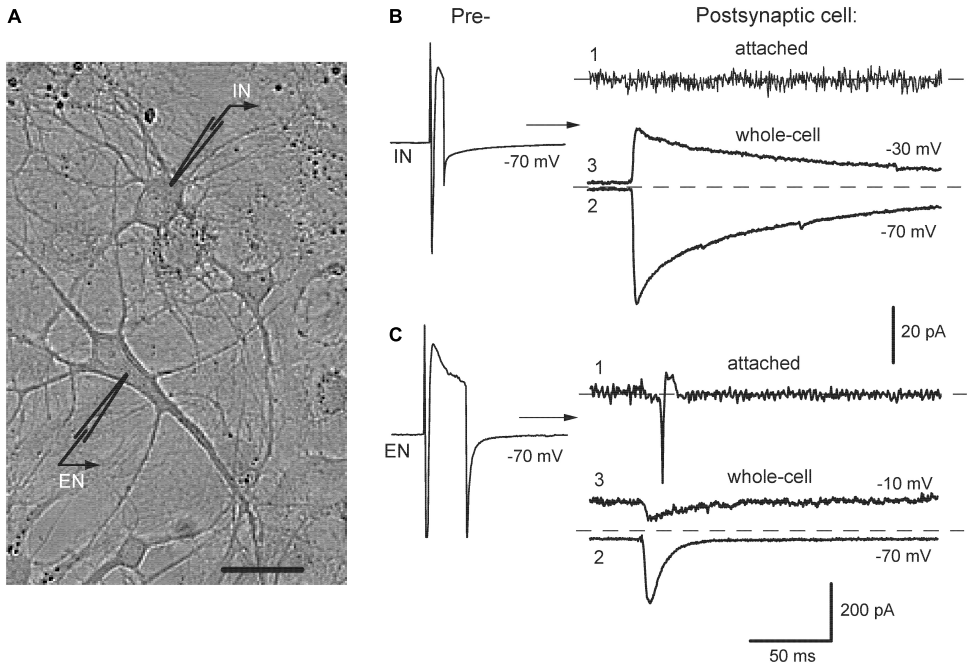

FIGURE 1
Identification of neurons in pair recordings. **(A)** A photograph of mutually connected inhibitory-excitatory neurons (IN-EN pair) in culture, bar 20 μm. **(B,C)** *Left*, stimulation of presynaptic cells to evoke inward Na^+ currents. *Right*, respective postsynaptic responses recorded consecutively in cell-attached (1) and whole-cell mode at indicated membrane potentials (2, 3). From here on, such values are designated near the traces.

elsewhere (Vincent and Marty, 1993), with minor modifications. Briefly, one of the channels was set as a reference. For each reference sIPSCs, the event closest in time was found in the partner trace and the time difference between them was entered. Because of the usually low frequency of spontaneous activity and negligible by-chance coincidence, coupled IPSCs (*C*) were readily discriminated by visual inspection from single (uncoupled) events (*U*) (e.g., Figure 2A). The value of *C* was estimated as the integral of the main peak in the histogram and *U* as an area outside of the peak. The coupling ratio was then defined as $R = C/(C + U) \times 100\%$. Results are given as mean ± SEM. Student's paired and unpaired *t*-test was used when appropriate. The probability level $P < 0.05$ was considered significant.

3. Results

3.1. Identification of neurons

The neurotransmitter phenotype of studied cells was determined in pair recordings by stimulating them sequentially and observing evoked postsynaptic responses. Figure 1 illustrates this procedure in the example of mutually connected inhibitory-excitatory neurons (*A*, designated as IN-EN). Presynaptic stimulation of IN (B, left) evoked IPSCs in EN (right) directed inwardly at −70 mV (trace 2) and outwardly at −30 mV (trace 3). These currents reversed at −48.1 ± 3.5 mV ($n = 12$), which was close to Cl^- equilibrium potential. In turn, stimulation of EN (C, left) elicited EPSCs in IN (right), the responses at −70 and −10 mV are shown (*2*, *3*). They changed their direction at −1.8 ± 2 mV ($n = 10$) indicating permeability for cations. The decay of eIPSCs was much slower than that of eEPSCs. At −30 mV, it was approximated by fast and slow components in ∼70% of cells (the reasons for this complexity of the decay phase were not studied) and the time constant of the former was 24 ± 2.7 ms ($n = 12$). The decay of eEPSCs was mainly monoexponential with tau 7.8 ± 1.2 ms ($n = 10$). This identification of synaptic currents based on their direction and decay kinetics was initially confirmed by respective antagonists and did not require their constant use in further recordings. Thus, we commonly held postsynaptic neurons at −30 or −20 mV to provide better resolution of simultaneously recorded outward IPSCs and inward EPSCs.

This identification protocol was preceded by the observation of postsynaptic responses first in cell-attached mode, which preserved intact the concentration of intracellular Cl^- (B-C, traces 1). This provided information on whether presynaptic firing could evoke APs in postsynaptic cells. Stimulation of EN reliably evoked postsynaptic spikes in EN-IN pairs as expected (C, $n = 11/12$) but none of the tested presynaptic IN-induced APs in postsynaptic cells, either in IN-EN pairs (B, $n = 8$) or in pure IN-IN pairs ($n = 7$). Similar results were also obtained in IN-IN pairs ($n = 9/10$) after network activation induced by field electrical pulses.

3.2. Baseline synchrony of spontaneous IPSCs

Neurons in culture display variable spontaneous activity ranging from random events to intensive bursting discharges; the latter is sometimes called either epileptiform or oscillatory behavior (McBain et al., 1989; Bacci et al., 1999). In our hands, the neurons

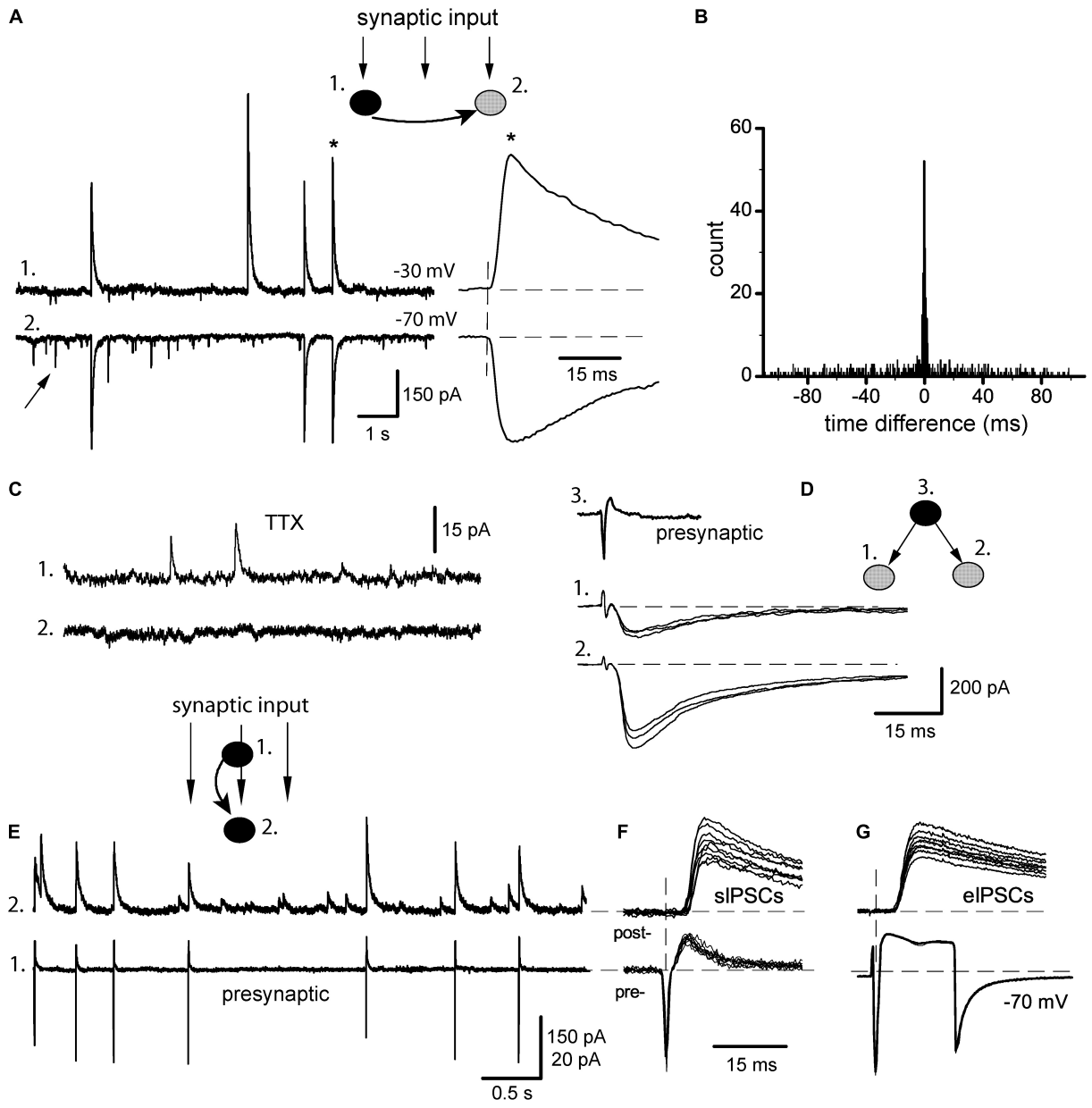

FIGURE 2
Synchrony of baseline sIPSCs. **(A)** Classical pair recording of incoming synaptic input in a pair of IN-unidentified cells (*1* and *2*, respectively), from here and below the phenotype of each pair is shown on *insets* (filled circles: INs, gray: unidentified cells). *Arrow* points on sEPSC; one of the coupled sIPSCs (*) is expanded to the right. **(B)** Respective time difference histogram. **(C)** Application of 0.5 μM TTX abolished synchrony of sIPSCs (same pair). **(D)** Stimulation of one presynaptic IN (*3*) evoked IPSCs in sequentially recorded neurons (*1*, *2*) showing the divergence of axons. **(E)** Identification of synaptic output of a given presynaptic neuron (*#1*, cell-attached mode) within a raw synaptic input impinging on postsynaptic neuron (*#2*, whole-cell mode). **(F)** Selection of APs-coupled sIPSCs. **(G)** Presynaptic stimulation with both neurons kept in whole-cell mode and recording unitary eIPSCs.

tended to show rare, isolated events at the onset of experiments, while any electrical stimulations or even inadvertent mechanical disturbances could lead to more intensive and complex patterns. Thus, the former type was assumed as a normal baseline activity of a non-stimulated network. Appropriately selected cells were recorded in pairs ($n = 15$) with at least one GABAergic neuron (Figure 2A, the phenotype of each pair is indicated on *insets*). One neuron of a pair was kept at −30 mV to display outward sIPSCs (trace 1) and their partner events were easily identified in another cell even at −70 mV (trace 2). Both sIPSCs and sEPSCs (arrow) occurred randomly with low frequency (1.8 ± 0.4 and 2.4 ± 0.6 Hz, respectively) and did not interfere with each other. Similar to evoked responses, sIPSCs had a slow bi-exponential decay in the majority of cells with a tau of fast component 21.5 ± 1.8 ms ($n = 15$ cells), while sEPSCs decayed rapidly with tau 8.2 ± 1.5 ms ($n = 15$ cells). Even in baseline conditions, many sIPSCs occurred synchronously in two cells, and coupling ratio R was calculated as 45.3 ± 2.8% (range 30–61%), with almost instantaneous precision (Figure 2A, asterisk). This corresponded to a narrow peak in time difference histograms centered at 0 ms with >95% of events

grouped within ± 1 ms (synchronization width) (Figure 2B). Such tight synchrony could be due to the firing of a common presynaptic IN with divergent axon collaterals supplying both recorded cells (Miles, 1990b; Vincent and Marty, 1993). Really, the application of 0.5 μM TTX abolished high-amplitude events and their correlation ($n = 5$, Figure 2C); only miniature IPSCs with a mean amplitude of ∼10 pA remained. This explanation was further confirmed in triple recordings ($n = 4$, Figure 2D), where stimulation of a single IN in cell-attached mode (trace 3) could evoke IPSCs in two sequentially recorded postsynaptic cells (traces 1–2). Such paired whole-cell recordings as above are a common method to study the synchrony of postsynaptic events, at the same time the real activity of presynaptic cells remains unknown. The latter can be alleviated by the approach of Vincent and Marty (1996), when presynaptic IN is found and kept in cell-attached mode, while postsynaptic neuron is recorded whole-cell (Figure 2E). As a result, sIPSCs corresponding to APs in a given presynaptic IN could be identified within a raw synaptic input. When APs-matched sIPSCs (cell 2) were aligned to respective presynaptic APs (cell 1), it gave a group of sIPSCs with small variations in their characteristics (Figure 2F). As a next step, the presynaptic neuron was ruptured and stimulated in whole-cell mode producing unitary eIPSCs (Figure 2G). Not very surprisingly, the properties of those sIPSCs and eIPSCs proved to be almost identical, as was compared in six pairs: synaptic delay 2.67 ± 0.06 vs. 2.71 ± 0.05 ms ($t = 1.76$, $P > 0.1$), rise time 2.52 ± 0.06 vs. 2.60 ± 0.04 ms ($t = 2.07$, $P > 0.05$), amplitude 156 ± 11 vs. 167 ± 14 pA ($t = 2.14$, $P > 0.05$). We checked also the possibility that the properties of eIPSCs could depend on the type of presynaptic intracellular solution based either on K^+ or Cs^+ (Vincent and Marty, 1996). In our experiments, however, using hippocampal (but not cerebellar) neurons, it was not the case. These data again support the conclusion that sIPSCs in baseline conditions were unitary events representing the synaptic output of individual INs.

3.3. Effects of network activation

Cultured neurons were briefly activated by field electrical stimulation and the effects on synchrony of sIPSCs were studied with intact synaptic transmission, i.e., without the presence of iGluR antagonists. Those have been commonly used so far in most experiments in slices to isolate inhibitory events, especially when extracellular stimulation was employed (Miles, 1990b; Miles and Poncer, 1993; Vincent and Marty, 1993; Michelson and Wong, 1994; Whittington et al., 1995; Hájos and Mody, 1997; Bartos et al., 2002). Weak stimulation induced a short-term (∼20 min) and moderate increase (<2 times) in the frequency of spontaneous events (Figure 3A, 17/25 pairs; see also Miles and Poncer, 1993). Stronger or more prolonged stimulation leads to more complex activities including epileptiform, which was seen in current-clamp mode as synchronous bursting depolarizations with APs (Figure 3B). We noticed intrinsic changes in post-stimulus sIPSCs (designated as ps-IPSCs) already after weak stimulation and focused on them (Figure 3A). The currents appeared similar to usual sIPSCs at −70 mV (Figure 3A, cell 2; Figure 4A, left) but depolarizing cells above E_{Cl} revealed that ps-IPSCs were preceded by transient inward currents (TICs) appearing as excitatory-inhibitory sequences, i.e., TICs/ps-IPSCs (Figure 3A, cell 1; Figure 4A, right). Random independent sEPSCs were also observed (Figures 3A, C, arrows). TICs had a small amplitude of 18 ± 8 pA at −30 mV (range 3–130 pA, $n = 17$) and variable shape presumably due to kinetically distinct components (Figure 3C). Some TICs could be seen even at −70 mV but mostly they were merged with the rising phase of ps-IPSCs. Interestingly, excitatory-inhibitory synaptic sequences could be also found as components within more complex bursting activity induced after stronger stimulation (Figure 3B, dashed box). Individual ps-IPSCs were highly correlated between cells and coupling ratio R increased to 81 ± 3.5% (range 64–95%; $n = 17$, $t = 9.5$, $P < 0.001$). In this case, time differences were measured using inflection points between TICs and ps-IPSCs (Figure 3C, dashed lines). Of note, ps-IPSCs in *cell 1* occurred earlier by ∼2.7 ms, a value comparable with synaptic delay. As a result, the main peak in the time difference histogram was shifted from 0 ms to the right (Figure 3D). Similar data were obtained in 11/17 pairs and six of those were of IN-EN type; in the other five pairs the histograms remained centered. Overall, the synchronization width was broader than in baseline sIPSCs and reached ± 4 ms. This type of elevated synchrony of ps-IPSCs characterized by the presence of excitatory pre-currents will be referred to below as excitatory. With a further purpose to isolate TICs and to determine how tight their link is with Cl^- currents, the application of $GABA_A$ antagonist BMI 10 μM abolished IPSCs and revealed inward currents, which occurred independently and looked similar to sEPSCs (Figure 3E, 6/6 pairs). Those were often correlated between cells and therefore could be a source of elevated synchrony of ps-IPSCs.

To get a deeper insight into the nature of ps-IPSCs, we estimated their relations with spontaneous APs recorded from presynaptic neurons kept in cell-attached mode (Figure 4A, #1) and compared then selected ps-IPSCs with single-cell evoked IPSCs. Paired segments were aligned, respectively to APs revealing strong variation in corresponding ps-IPSCs (Figure 4B, left). It was clearly distinct from the behavior of evoked responses, those reflected a real contribution of a given presynaptic IN to ps-IPSCs and, notably, contained no excitatory pre-currents (right). Another obvious difference between ps-IPSCs and eIPSCs was in their synaptic delays, 1.23 ± 0.3 vs. 2.72 ± 0.05 ms ($n = 7$, $t = 5.12$, $P < 0.01$). The smaller mean delay of ps-IPSCs was due to their broad distribution starting even from negative values, from −0.4 to 4.2 ms in a given example (Figure 4D) and from −8 ms in one extreme case. Their rise time was slower than of eIPSCs, 3.73 ± 0.23 vs. 2.53 ± 0.06 ms ($n = 7$, $t = 5.89$, $P < 0.01$), and the amplitude larger, 259 ± 21 vs. 145 ± 7 pA ($n = 7$, $t = 5.5$, $P < 0.01$). Due to low noise in attached recordings, TICs could be frequently observed also in presynaptic IN along with APs (Figure 4B, arrows). This allowed us to find paired segments, where presynaptic APs failed in a given IN but ps-IPSCs of smaller amplitudes persisted (middle). These data directly show that ps-IPSCs were population (i.e., compound) events induced by the firing of >1 presynaptic INs, most likely 2–3. Those numbers were derived from frequent observations of correlated APs in both INs at the onset of cell-attached recordings (Figure 4C) and up to three peaks were discriminated in distributions of synaptic delays (Figure 4D).

Still another important conclusion could be drawn from these observations of TICs and following APs with failures in presynaptic

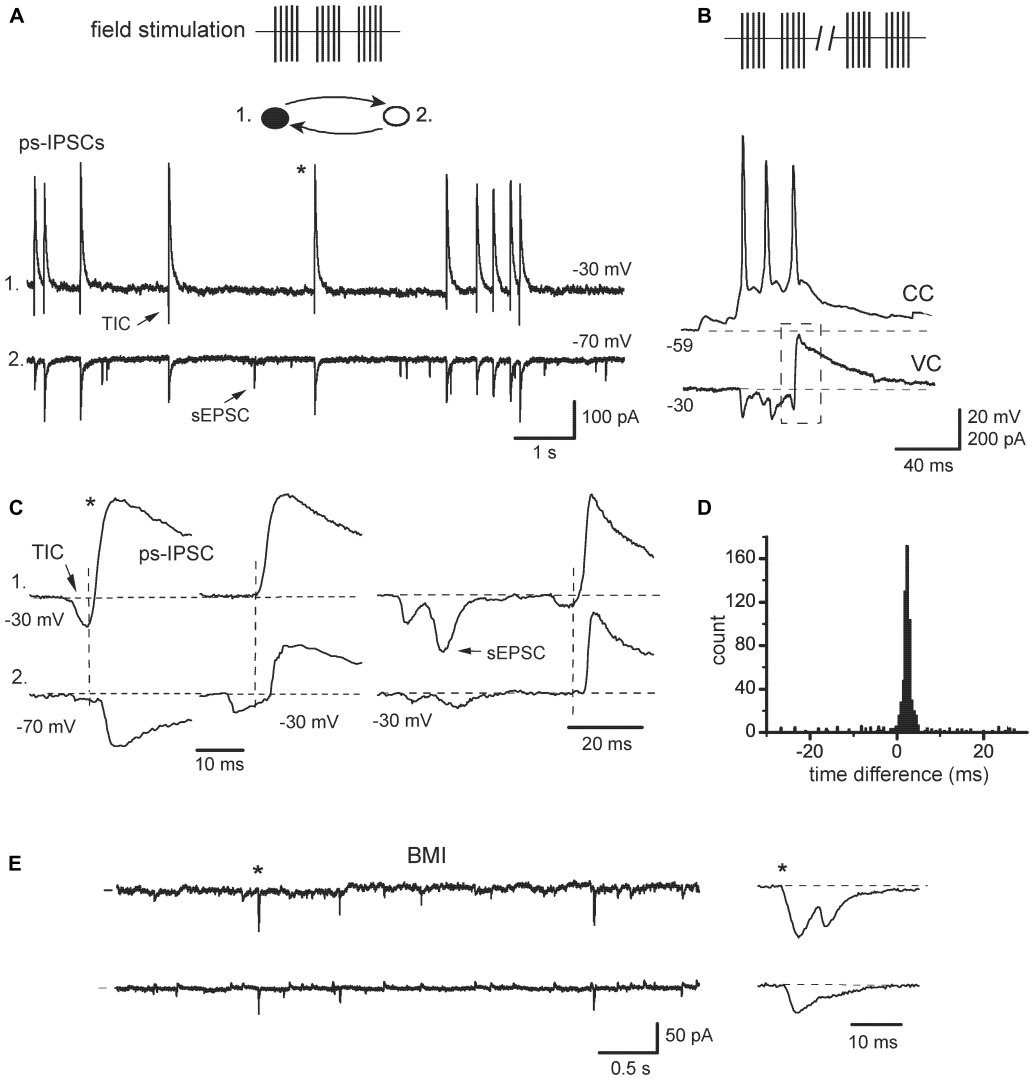

FIGURE 3
Transformation of sIPSCs after network activation. **(A)** "Hypersynchronous" sIPSCs observed after field electrical stimulation (*ps-IPSCs*), they were preceded by transient inward currents (*TIC*). *Inset*: filled circles, IN; open, EN. Random sEPSC is marked by an *arrow* [**(A,C–E)**, same recording]. **(B)** An example of epileptiform bursting episodes induced after prolonged stimulation. One cell in a pair was in current-clamp mode (*CC*) to show action potentials. The other cell was kept in a voltage-clamp (VC), which revealed an excitatory-inhibitory sequence (*dashed box*) as an intrinsic component of the bursting episode. **(C)** Different examples of sequences TIC/ps-IPSC are expanded to show the timing of the events (*vertical lines*), and *asterisk* shows the events taken from the segment in panel **(A)**. Cell #1 was constantly held at −30 mV, while cell #2 was held first at −70 and then at −30 mV. **(D)** Time difference histogram. **(E)** Application of bicuculline (BMI) blocked outward Cl^- currents and revealed synchronous excitatory currents; one of them is expanded to the *right*.

cells, namely that TICs were causal events capable to evoke APs confirming their excitatory and synchronizing role. This idea was also illustrated further with presynaptic INs kept in current-clamp mode (Figure 4E). The latter is traditional for classical microelectrode recordings and provides a link to original studies, where similar electrical events preceding APs in pyramidal cells were first described and called fast prepotentials (Spencer and Kandel, 1961, Figure 1).

The data above indicated that TICs, despite their heterogenous shape, were excitatory and synchronizing events reminiscent of sEPSCs, which prompted the question of whether they represented the same or distinct entities. To resolve this issue, ion dependency and pharmacological sensitivity of TICs were estimated. Spontaneous ps-IPSCs were recorded at different potentials and *I-V* curves were plotted for both excitatory and inhibitory parts (Figure 5A). In the majority but not all of the cells ($n = 12/17$), TICs behaved similarly to sEPSCs reversing their direction at -4.0 ± 1.3 mV ($n = 6$), which suggested permeation of both Na^+ and K^+. Interestingly, the reversal potential of the inhibitory part (-39 ± 2.5 mV, $n = 6$) was less negative than that of eIPSCs, presumably due to contamination of their rising phase with excitatory currents. The role of iGluR was tested next by applying APV and CNQX, selective antagonists of NMDA and AMPA/kainate receptor subtypes (Figure 5B). The drugs were used alone or in combination with the purpose of identifying distinct kinetic components of TICs (arrowhead and arrow). Slowly rising currents (arrowheads) with an amplitude up to A1 were modified by APV and CNQX becoming faster

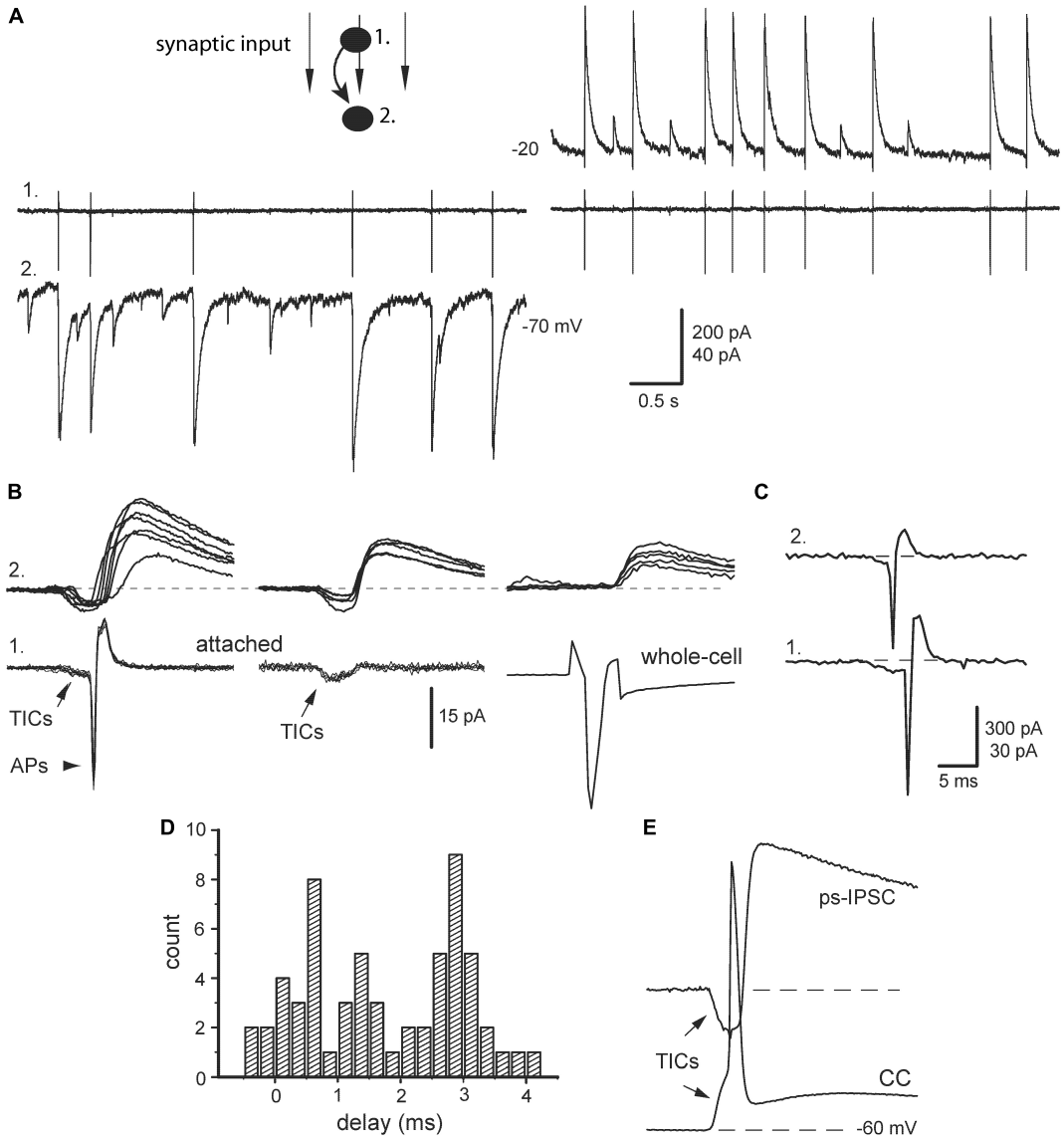

FIGURE 4
Relation of post-stimulus sIPSCs with presynaptic action potentials. **(A)** Identification of synaptic output of a given presynaptic neuron (#1, cell-attached mode) within a raw post-stimulus sIPSCs impinging on postsynaptic neuron (#2, whole-cell mode) at indicated potentials. **(B)** *Left*, paired segments were aligned, respectively to presynaptic action potentials (*APs*) with preceding TICs. *Middle*, examples of APs failures and persisting TICs. *Right*, presynaptic IN was stimulated next in whole-cell mode. **(C)** An example of correlated APs in pair of INs. **(D)** Distribution of synaptic delays [taken from panel **(A)**]. **(E)** An example of the paired segment with synchronous TICs when presynaptic IN was kept in current-clamp mode (CC).

and slower, respectively, indicating that they were mediated by both subtypes of iGluR. In contrast, faster and larger transients (arrows) behaved differently and apart from being abolished by CNQX, they revealed properties of voltage-activated channels. Namely, those events occurred in an all-or-none mode fluctuating between A1 and A2 at V_m −30 mV and suddenly disappeared with further small depolarization, at −21 mV in a given case (not shown), apparently due to channels inactivation. These features suggest that these fast transients were active electrical events (spikelets) generated locally in remote sites of a given cell. Eventually, the combined application APV/CNQX abolished all inward currents (Figure 5B, right). The blockage of TICs was accompanied by reduced synchrony of ps-IPSCs and the appearance of uncorrelated sIPSCs (Figure 5C). In the time difference histogram it was evident as a lower central peak and decreased *R*-value, 43.5 ± 2.8% vs. 79.4 ± 3.1 ($n = 12$, $t = 11.2$, $P < 0.001$; Figure 5D).

The remaining five pairs revealed partial sensitivity of their TICs to blockers of iGluR even in higher concentrations, while sEPSCs were fully abolished (Figure 6A). This was paralleled by their smaller effects on the synchrony of ps-IPSCs. In time difference histograms, the height of peaks was almost unchanged and the *R*-value decreased slightly, from 83.6 ± 5.1 to 73.2 ± 3.1% ($n = 5$, $t = 2.17$, $P > 0.05$; Figure 6B). To identify the nature of these iGluR-independent components of TICs, they were isolated pharmacologically in a mixture of APV, CNQX, and BMI appearing as fast inward transients at −60 mV (Figure 6C, left). Strong membrane depolarization to +20 or +40 mV was unable to affect

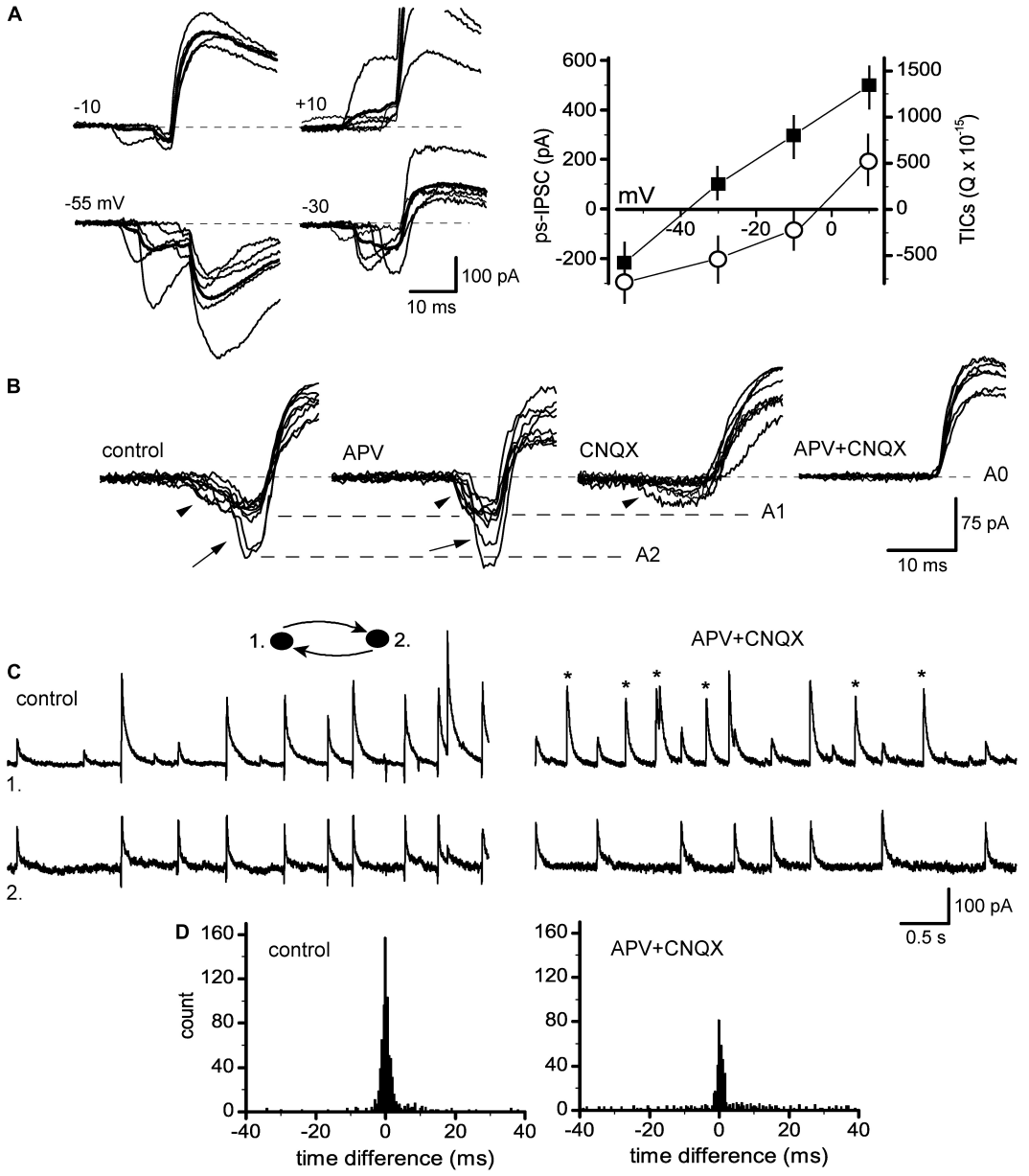

FIGURE 5
Glutamate-dependent post-stimulus sIPSCs. **(A)** TICs/ps-IPSCs sequences at different membrane potentials (*left*), lines in *thick* show averages ($n = 10$). *Right*, respective *I-V* curves plotted for both TICs (as integrals, *open circles*) and ps-IPSCs (peak amplitudes, *filled squares*). **(B)** Expanded and superimposed segments showing variety in TICs waveforms consisting of, respectively slow and small components (*arrowhead*) and fast transients (*arrow*), those fluctuated in an all-or-none way between levels *A1* and *A2*. Traces are shown in control, under APV, CNQX and in both. **(C)** Recording of ps-IPSCs in control (*left*) and under APV + CNQX (*right*), TICs were abolished and uncorrelated sIPSCs appeared (*stars*). **(D)** Respective time difference histograms.

them (middle) but the further application of 0.5 μM TTX abolished all currents (right). This insensitivity to voltage and synaptic blockers suggested that remaining TICs were passive electrotonic currents reflecting APs in nearby neurons and transmitted presumably *via* gap junctions. In support, presynaptic stimulation revealed combined chemical and electrical (arrow) responses in 3/5 pairs belonging to the IN-IN type (Figure 6D). Remarkably, no electrical coupling was observed in mixed IN-EN pairs. Passive subthreshold responses were also transmitted between connected neurons kept in current-clamp mode and the coupling ratio for DC signals was ∼1.5% (Figure 6E).

The dominant role of iGluR in the initiation and mediation of synchronized ps-IPSCs suggested a primary and causative contribution of excitatory neurons releasing Glu synaptically. This aspect was investigated in recordings from IN-EN pairs and revealed complex cell interactions beyond simple monosynaptic responses (Figure 7). Stimulation of pyramidal-like EN evoked in IN not only typical EPSCs with a short delay and no failures (A, arrow) but also, in ∼40% of pairs ($n = 4/9$), two kinds of remote synchronous responses: TIC-IPSC sequences with a delay of 40–50 ms and ∼20% of failures (*1*, *2*) and late sIPSCs appearing after 100–200 ms with ∼50% of failures (*3*). Late sIPSCs

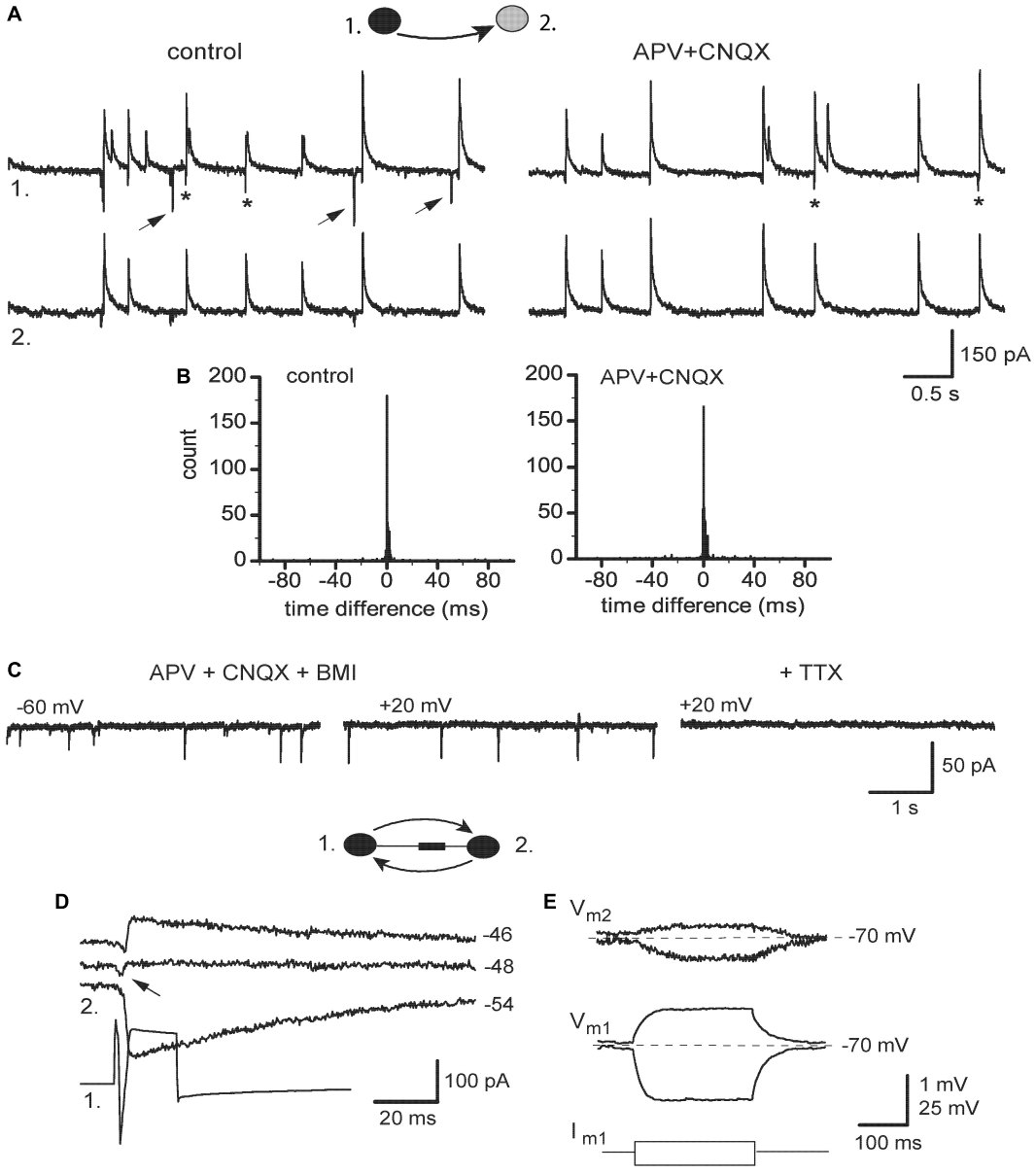

FIGURE 6
Expression of electrical coupling in ps-IPSCs weakly dependent on iGluR. **(A)** Pair recording of ps-IPSCs in control and under 100 μM APV with 20 μM CNQX. Some of the random sEPSCs are marked by *arrows*, and TICs–by *stars*. **(B)** Respective time difference histograms. **(C)** Spontaneous fast transients occurring under blockers of iGlu and $GABA_A$ receptors and insensitive to membrane potential, which were then abolished by 0.5 μM TTX. **(D)** Combined electrotonic (*arrow*) and GABAergic responses induced by presynaptic stimulation (*1*) in postsynaptic cell (*2*) in voltage-clamp mode. **(E)** Current-clamp recordings, depo- and hyperpolarizing voltage responses induced in cell 1 (V_{m1}) were passively transmitted to cell 2 (V_{m1}).

had no pre-currents and were likely due to the firing of a third cell, in accordance with data in Figure 2. Most relevant and remarkable was the finding that the activity of EN in a simple circuit could generate TIC-IPSC sequences mimicking network-induced ps-IPSCs. The analysis below demonstrates one of the ways how population events could be organized. Sequence #2 is expanded on in Figure 7C and shows temporal relations between its components: TIC occurring first and then paired IPSCs ($IPSC_a$ and $IPSC_r$). The latency between them, if measured from TIC onset (its peak was contaminated by $IPSC_a$) and thus overestimated, reached 2.0 ± 0.1 ms ($n = 4$, $P < 0.01$) being much smaller than the synaptic delay of eIPSCs (~2.7 ms). Induced TICs consisted of only fast transients occurring in an all-or-none mode and similar to spontaneous ones (Figure 5B, arrows), were classified as spikelets (SLs) generated locally in remote sites. Similarly, these SLs originated in a given IN because cell inactivation by membrane depolarization to −18 mV abolished SLs along with the simultaneous disappearance of paired IPSCs. In turn, the latter suggested that SLs were causal in initiating both $IPSC_a$ and $IPSC_r$, which specified their site of origin in the axonal tree of IN as intermediate between soma and synapses (designated as *hot spot* in Figure 7E). The axonal location of LSs helped to clarify next the origin of associated IPSCs. The $IPSC_r$ in EN was a usual recurrent IPSC in response to a spike

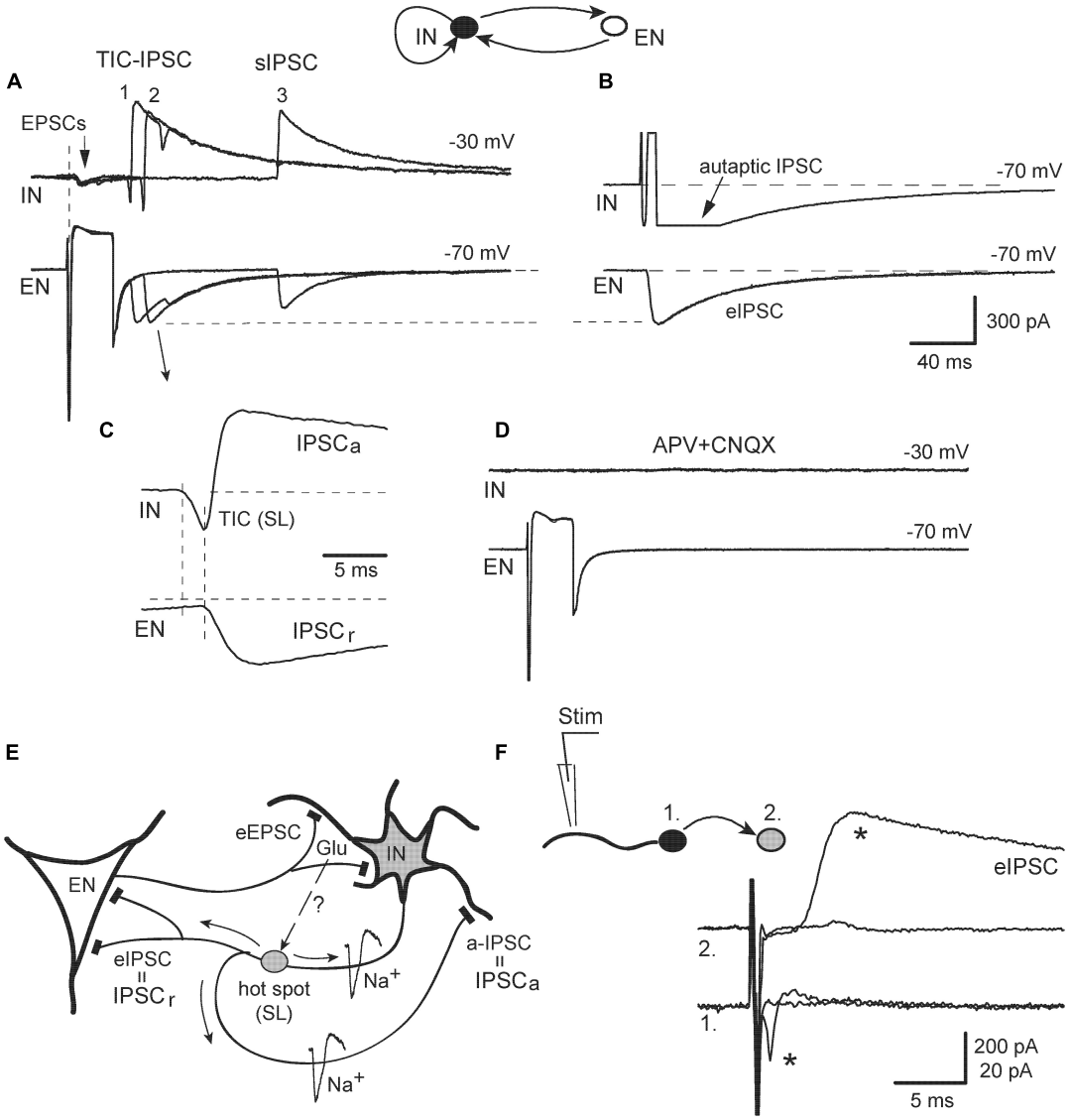

FIGURE 7
Example of the electrical behavior of excitatory-inhibitory cell circuit. **(A)** Presynaptic stimulation of EN induced three kinds of postsynaptic responses (three of them were superimposed): monosynaptic EPSCs (*arrow*), remote sequences TIC-IPSC (*1, 2*), and late sIPSC (*3*). **(B)** Stimulation of IN evoked IPSC in EN and autaptic IPSC in itself (it was blocked by BMI). **(C)** TIC-IPSC sequence #2 was expanded to show its intrinsic temporal relations (see Text for details). **(D)** The application of APV + CNQX blocked all responses. **(E)** Schema describing electrical behavior of EN-IN pair. TICs appeared as local spikelets (*SL*); they originated in axonal *hot spots* and induced both autaptic IPSC (*a-IPSC*) and *eIPSC* in EN. Putative signaling of synaptic Glu to axonal iGluR is shown by a *dashed arrow* and *question mark*. **(F)** A test of the active electrical role of the dendrites. Local extracellular stimulation of a dendrite in the IN (*1*) induced all-or-none APs (*star*) in the soma and corresponding eIPSC (*star*) in the follower cell (*2*).

in IN, either generated locally in a *hot spot* or induced by somatic stimulation (confirmed by the same amplitudes of eIPSC in panel B and $IPSC_r$ in panel A, *dashed line*). In addition to typical eIPSC, IN stimulation also induced an autaptic IPSC seen as a long tail after a depolarizing pulse (B); the $IPSC_a$ then could be explained as autaptic IPSC in response to SLs propagating back from the *hot spot* to the soma (**Figure 7E**, a-IPSC). These effects of EN stimulation were almost fully blocked by APV/CNQX confirming the dominant, but not exclusive, role of iGluR in network activation (**Figure 7D**). Some late sIPSCs (as in **Figure 7A**, #3) in a few recordings persisted under the blockers suggesting additional involvement of metabotropic GluR (Miles and Poncer, 1993).

Identification of the axonal origin of some TICs was at odds with one of the current views ascribing the origin of spikelets to the dendritic tree, as studied in pyramidal cells (Spencer and Kandel, 1961). In order to get more information on whether the dendrites of INs in our model could play an active role in electrogenesis, we stimulated the neurites of a presynaptic IN (**Figure 7F**, cell #1, kept in attached mode) locally with an extracellular pipette and simultaneously observed postsynaptic neuron (#2) in whole-cell mode. Really, active dendritic sites were found at distance of 50–70 μm from the soma stimulation which evoked, first, back-propagating APs and then corresponding eIPSC (stars). Thus, the dendrites of hippocampal INs *in vitro* were also capable to generate locally active electrical events and be the site of TICs origin.

4. Discussion

Mechanisms of interneuronal synchronization were studied in a simple model network during a dynamic transition from the rest to moderate activation with intact synaptic transmission, which presumably mimicked physiological processing *in vivo*. Resting INs fired individually and synchrony of sIPSCs did not require a special mechanism. We report that network activation resulted in the coherent firing of a few INs recruited by excitatory synchronizing currents (TICs). This was evident in the appearance of "hypersynchronous" population events, compound sIPSCs temporally preceded by TICs. The network nature of TICs was evident by their heterogeneous components, Glu-mediated currents, local dendritic and axonal spikelets, and coupling currents transmitted likely *via* gap junctions. We found then that network-driven population events could be initiated by synaptically released Glu and generated within a minimal circuit consisting of reciprocally connected excitatory and inhibitory neurons.

4.1. Divergence of inhibitory axons

Even in the resting network, a large part of sIPSCs occurred synchronously, which was abolished by TTX showing the necessary role of APs in any kind of correlated neural activity (Ben-Ari et al., 1989; Vincent and Marty, 1993; Fischer et al., 2002). In their turn, the quantal release of neurotransmitters from individual release sites is stochastic and asynchronous between cells (Ropert et al., 1990). The properties of APs-matched sIPSCs and unitary eIPSCs were similar (**Figures 2F, G**), and the firing of single INs could evoke IPSCs in several postsynaptic cells (**Figure 2D**). This suggested strongly that sIPSCs were unitary events and their correlation resulted from APs arising in a single presynaptic IN (see also, Miles, 1990b; Vincent and Marty, 1993). The latter can be achieved due to the divergence of axon collaterals of hippocampal interneurons, which are known to target many pyramidal cells and INs (Buhl et al., 1994; Gulyás et al., 1996). Obviously, this type of synchrony in sIPSCs is passive and does not require a special mechanism. Interestingly, the spontaneous firing of resting INs seemed to be driven endogenously without clear excitatory input because presynaptic APs arose from a flat baseline without preceding TICs (**Figures 2E, F**). Presynaptic APs propagated then a small distance (<150 μm) toward release sites and small fluctuations at this stage explain minimal time differences between paired sIPSCs (<1 ms).

4.2. Excitatory synchronization of interneurons

After field electrical stimulation was over, the neural behavior changed qualitatively resulting in the appearance of post-stimulus sIPSCs, the elevated synchrony of which clearly required some special mechanisms. Using currents separation by their driving force, initial excitatory components were resolved in seemingly homogenous inhibitory events. Thus, ps-IPSCs represented excitatory-inhibitory sequences (TICs/ps-IPSCs) occurring spontaneously. They were reminiscent of evoked excitatory-inhibitory responses to afferent stimulation in hippocampal slices (Alger and Nicoll, 1982; Miles and Wong, 1984; Davies and Collingridge, 1989; Lacaille, 1991). Further analysis revealed an intrinsic structure of post-stimulus sIPSCs, both parts of which were identified as population events: TICs consisting of several heterogeneous components and ps-IPSCs composed of 2–3 unitary sIPSCs. This temporal order with prior TICs and their ability to trigger APs unequivocally demonstrated that the former represented an exogenous excitatory drive to INs and a cause of increased coherence. The time width of excitatory synchronization was much broader (±4 ms) than that of baseline sIPSCs and included other processes apart from APs propagation. It was apparently determined by the kinetics of TICs and included at least one synaptic delay (e.g., **Figure 4B** left). Another peculiar feature of ps-IPSCs was displaced time difference histograms in ∼50% of IN-EN pairs (see also Vincent and Marty, 1996). We hypothesized that it was due to asymmetry in local cellular interactions during the build-up of population events, e.g., a cell with earlier and/or larger TICs in a pair could play a more active role in local boosting of synaptic inhibition. This idea was supported in the analysis of synaptic responses in EN-IN pairs (**Figure 7A**). Stimulation-induced TICs occurred first in an axonal tree of INs and initiated both recurrent and autaptic components of paired IPSCs (**Figures 7C, E**). The active and necessary role of INs was confirmed by their voltage inactivation or even destruction by a gentle pressure of the recording pipette, which abolished TIC-IPSC sequences.

Remarkably, the firing of a single EN within a minimal synaptic circuit with one IN was necessary and sufficient to induce excitatory-inhibitory sequences (**Figure 7A**), which largely mimics field electrical stimulation. This indicated a principal source of excitation for INs and highlighted a primary role of synaptically derived Glu. According to our data, the occurrence of such sequences either spontaneously in culture or evoked by afferent stimulation in slices is to be expected because they are a signature of the activity in simple but ubiquitous reciprocal circuits consisting of only ENs and INs. Relevantly, stimulation of single pyramidal cells in hippocampal slices under the presence of $GABA_A$ blockers also led to network activation and to the development of epileptiform bursting activity (Miles and Wong, 1983). Thus, the physiological sense and necessity of EN-IN circuits and of its electrical epiphenomena seem clear, to restrict neural over-excitation and promote the processing of afferent signals. While the neocortex is a brain region developmentally close to the hippocampus, recordings from EN–IN pairs therein showed simple unitary EPSPs but no signs of network activation (i.e., excitatory-inhibitory sequences) were evident (Karnani et al., 2016); the latter could be due to differences in animal species, local synaptic connectivity, etc.

Single-cell and field electrical stimulations had also two distinctions. First, TICs occurred in only one cell of a pair, which was likely due to a singular source of excitation, while numerous cells were excited by field stimulation. Second, TICs consisted of only fast transients seemingly without prior and slower Glu components (compare **Figure 5B** vs. **Figure 7C**). The reasons for this remain unclear, especially because Glu was surely released upon stimulation and evoked EPSCs *via* activation of somato-dendritic iGluR. One possibility was that Glu also diffused a long distance toward axonal iGluR concentrated within a hot

spot (**Figure 7E**, dashed arrow). The existence of both axonal and preterminal iGluR of the kainate subtype was suggested for hippocampal INs in slices (Cossart et al., 2001; Semyanov and Kullmann, 2001). Relatively slow Glu potentials would be then filtered out due to their remote electrical location and poorly detected in the soma. Overall, while the deduced schema describes the behavior of EN-IN pairs *in vitro* (**Figure 7E**), it might be not fully applicable *in situ*. More specifically, autaptic IPSCs seem to be over-expressed in culture (Mennerick et al., 1995), while their existence in slices has been only suggested but not yet proven (Miles, 1990a; Gulyás et al., 1993).

Despite the principal similarity between spontaneous excitatory-inhibitory sequences in culture and evoked afferent responses in slices, there is, however, a major distinction in their first components. The excitatory phase of afferent responses was blocked by APV/CNQX indicating that it was a simple evoked EPSP mediated solely by iGluR (Davies and Collingridge, 1989; Lacaille, 1991). In contrast, spontaneous TICs were composed of several heterogeneous components and were not limited to iGluR. This distinction is to be expected though because both electrical phenomena reflected different phases of network activity. Afferent responses induced by electrical or sensory stimulation only initiate network activity, which occurs *via* afferent fibers purely Glu-ergic in their nature. On the other hand, excitatory-inhibitory sequences occur spontaneously after stimulation is over. They show the intrinsic way of self-sustaining operation of the whole network, with its all available excitatory components. While those have been already described individually in the literature, our results suggest, however, that these means operate jointly during natural afferent processing. The network excitatory components driving the activity of INs are discussed below.

4.2.1. Ionotropic GluR

The excitatory and synchronizing drive to pairs of neurons was mainly provided by iGluR (the role of mGluR was not yet studied), which agrees with classical knowledge on excitation of individual hippocampal INs (Miles, 1990a; McBain and Dingledine, 1993; Miles and Poncer, 1993; Geiger et al., 1997; Frerking et al., 1998; Semyanov and Kullmann, 2001). All cells had TICs with Glu-mediated currents, either independent or along with other components. When in combination with local spikelets, Glu current preceded and initiated them (e.g., **Figure 5B**). In the results, synchrony in ∼2/3 of pairs was fully dependent on iGluR. The remaining cells displayed coupling currents presumably *via* gap junctions and were weakly sensitive to iGluR blockers. The reasons for the latter remain unclear; possibly other agents apart from Glu were released in the activated network and promoted the expression of gap junctions (Fischer, 2004). In terms of receptor profile, all known subtypes of iGluR participated in TICs under the presence of extracellular Mg^{2+}, i.e., AMPA/kainate and NMDA receptors. Those were activated either simultaneously (**Figure 5B**) or even individually given a large variety of TICs waveforms (see also, McBain and Dingledine, 1993). In turn, the synchrony of Glu-ergic input to INs (**Figure 3E**) was presumably mediated by divergence in axonal collaterals of excitatory cells (Miles and Wong, 1986; Miles, 1990a).

Paired recordings performed in neocortical INs have suggested the independence of their synchrony on iGluR (Tamás et al., 2000; Hu et al., 2011). Those studies, however, were focused on a distinct phenomenon, a near-synchronous correlation of APs firing observed in special conditions when both neurons in a pair were tonically/phasically depolarized *via* intracellular pipettes. It is clear, however, that *in situ* conditions such depolarization can only be produced by afferent presynaptic fibers, which necessarily release Glu on their targets.

4.2.2. Local spikelets and fast prepotentials

The majority of fast components of TICs were active electrical events (here termed as spikelets) generated locally in remote sites of recorded INs because they were affected by manipulations on given cells. Such small, transient, and all-or-none depolarizations have been known for a long time as partial spikes, spikelets, or short latency depolarizations and, as they often preceded full APs, they were widely referred to as fast prepotentials (FPPs) (Spencer and Kandel, 1961; MacVicar and Dudek, 1981; Núñez et al., 1990; Michelson and Wong, 1994). In our recordings, spikelets were analogous with classical FPPs in preceding full APs (**Figure 4E**). Two current hypotheses explained FPPs either as active events occurring in dendritic sites of impaled neurons (Spencer and Kandel, 1961; Hu et al., 1992; Steriade et al., 1993) or coupling potentials in response to the activity of nearby neurons and propagated passively to recorded cells *via* gap junctions (MacVicar and Dudek, 1981). Both scenarios were found valid here (the latter will be discussed below). Active spikelets, in turn, were often preceded and initiated by slower Glu-mediated currents (**Figure 5B**) and therefore were apparently generated in the dendrites of INs, where iGluR are located. The active role of dendrites in electrogenesis has been demonstrated for pyramidal cells, which possessed voltage-activated channels and could generate APs in response to synaptic input (Regehr et al., 1993). Similarly, the dendrites of INs were also capable to generate electrical events at some spots upon local electric stimulation, which induced back-propagating APs in the soma (**Figure 7F**; see also, Martina et al., 2000). We added complexity to this picture further and revealed that some spikelets could be initiated locally in the axonal tree of INs, as they were capable to induce postsynaptic responses (**Figures 7C, E**). Ectopic initiation of APs in axonal terminals rather than in the axon initial segment was also observed in pyramidal cells and attributed to terminal hyperexcitability induced by tetanic stimulation (Stasheff et al., 1993). Such active axonal sites could be designated as "hot spots," because they should contain an amount of iGluR to be responsive for synaptic Glu, in addition to voltage-activated Na^+ channels (**Figure 7E**). The physiological sense of local axonal spiking in INs seems clear, to restrain neural over-excitation and boost synaptic inhibition.

4.2.3. Gap junctional communication

A significant fraction of pure INs pairs (3/5) was weakly coupled electrically and displayed fast TICs due to the activity of nearby neurons transmitted passively. This did not occur in control conditions but was observed after network activation and mediated presumably *via* gap junctions (GJs). The lack of sufficiently selective pharmacological tools prevented us from more precise identification (Rouach et al., 2003). GJs allow permeation of electrical currents and small molecules and have been frequently observed along with FPPs in hippocampal neurons (MacVicar and Dudek, 1981; Michelson and Wong, 1994; Strata et al., 1997).

Solid morphological support for GJs was obtained in rats and respective specializations were demonstrated at the ultrastructural level *in situ* (Gulyás et al., 1996; Fukuda and Kosaka, 2000). However, the functional consequences of GJs in slices are somewhat controversial depending on animal species and the plane of the section. In the latter case, they could be overestimated due to stronger experimental damage and subsequent membrane fusion in coronal slicing (Gutnick et al., 1985). No coupling was observed in guinea-pig hippocampus under normal conditions, but it appeared in epileptogenic tissue (Miles, 1990b; Gulyás et al., 1993; Michelson and Wong, 1994; Zhang et al., 1998). In contrast, a high fraction of INs (50–80%) was electrically coupled in rat cortex with a DC ratio of up to 10% and up to 20% in mouse hippocampus (Gibson et al., 1999; Beierlein et al., 2000; Tamás et al., 2000; Bartos et al., 2002). Cultured neurons after 2 weeks have already repaired their experimental damage due to isolation and are advantageous in this respect. Our recordings thus agree with some of the reported studies in slices and suggest the functional expression of GJs in activated hippocampal networks. Remarkably, neural activation could be achieved non-specifically by tetanic electric stimulation or blockers of K^+ channels and once activated GJs did not require iGluR further (Michelson and Wong, 1994; Zhang et al., 1998; Skinner et al., 1999). Here too, coupling transients were induced and observed in combination with Glu currents much in the same way as active spikelets (**Figure 5B**) but they could persist thereafter even in the absence of Glu transmission (**Figures 6A, B**). Remains unclear, however, which mechanisms and neuroactive agents regulate the expression of GJs; in particular, the role of cholinergic agonists was proposed (Fischer, 2004). Clearly, further studies on this issue are warranted.

4.2.4. GABAergic depolarization

As soon as we used a novel model of synchronized activity, we also tested the relevance of a special mechanism thought to be possible in synaptic connections of INs, namely the depolarizing and excitatory action of released GABA. The latter is feasible with sufficiently elevated intracellular Cl^- level rendering reversal potential for GABA (E_{GABA}) positive to APs threshold. Such mechanism participated in network excitation and synchronous GDPs in the neonatal hippocampus but disappeared later in development after two postnatal weeks (Ben-Ari et al., 1989; Khazipov et al., 1997; Khalilov et al., 1999; Wester and McBain, 2016). On the other hand, depolarizing GABA responses are not a unique feature of immature neurons and could be also observed in adults, e.g., in some subsets of INs in baseline conditions (Szabadics et al., 2006; Fu and van den Pol, 2007) or even more importantly, during epileptiform activity induced chemically or by tetanic electrical stimulation shifting E_{GABA} to more positive values (e.g., Michelson and Wong, 1994; Staley et al., 1995; Benardo, 1997). Similarly, field electrical stimulation in our experiments (e.g., **Figures 3A, B**) might have increased postsynaptic Cl^- level and uncovered the excitatory action of GABA. Exploring such a hypothesis, however, is not a trivial technical task. It requires the following conditions: undisturbed intracellular ions in the postsynaptic neuron, its resting membrane potential, and adequate presynaptic stimulation. The first two criteria are fulfilled when keeping postsynaptic cells in attached configuration, while a third one has been routinely approximated so far by using extracellular electrical stimulation combined with the application of blockers to isolated GABA or Glu postsynaptic action. Using such an approach, conflicting conclusions were reached in young hippocampal INs (Khazipov et al., 1997; Khalilov et al., 1999) versus those in the cortex (Kirmse et al., 2015). To refine further the protocol and avoid uncertainties of extracellular stimulation (discussed in Miles, 1991), we stimulated identified presynaptic INs individually, while recording postsynaptic neurons in attached mode. No APs were induced in postsynaptic cells, both INs and ENs (**Figure 1B**, trace 1), in contrast to presynaptic stimulation of ENs (**Figure 1C**, trace 1), which was the case both in control conditions and after moderate network stimulation. These results, however, are suggestive and cannot be fully applicable to *in situ* conditions, because they did not include modest depolarizing action of HCO_3^- ions (Staley et al., 1995). Moreover, it is not excluded that stronger stimulation would increase GABA-mediated depolarization up to postsynaptic excitation.

4.4. Population IPSCs

Here we described population sIPSCs (in the text as ps-IPSCs) and identified them as a distinct type of inhibitory events arising due to the coherent firing of a few presynaptic INs. They seem to represent a necessary feature in the organization of synaptic inhibition and need to be compared with prior studies using slices. It should possibly come with no surprise that population events were not previously recognized in descriptions of sIPSPs or sIPSCs in resting neurons and under blockers of iGluR (Miles, 1990b; Otis and Mody, 1992; Hájos and Mody, 1997; Williams et al., 1998). On the other hand, the existence of population IPSPs has been tentatively presumed in highly activated networks, which was based on dissimilarities of those events with single-cell induced unitary IPSPs (Miles and Wong, 1984, Figure 8A; Fischer et al., 2002, **Figure 2**). Other lines of evidence have relied on some temporal correlations (including negative delay) between APs in INs and sIPSPs occurring in partner cells in pair recordings, those pairs, however, were not synaptically connected and thus any perceived correlations could be stochastic (Benardo, 1997, Figure 5A; Velazquez and Carlen, 1999, Figure 3A; Beierlein et al., 2000, Figures 5A, B). Similar temporal analysis was used here but in synaptically connected neurons. This verified the causal relationship between APs and sIPSCs and thus showed unambiguously the compound nature of population sIPSCs as consisting of several unitary events (**Figures 4B–D**). The peculiar feature in our recordings, however, was the association of population sIPSCs with excitatory pre-currents, which has not been regularly observed before, except for network-driven GDPs (Khalilov et al., 1999, Figure 3C left; Wester and McBain, 2016, Figure 1Eiii). The likely explanations could be the usage of sharp microelectrodes having lower amplitude and frequency resolution, recording at negative V_m when excitatory and inhibitory currents were of the same direction, and the presence of iGluR blockers in some studies. Also, it cannot be fully excluded that excitatory-inhibitory sequences were an artifact of culture, however, the

integrity of presented data strongly suggests that they correspond to the natural organization of interneuronal activity.

Data availability statement

The original contributions presented in this study are included in the article/supplementary material, further inquiries can be directed to the corresponding author.

Ethics statement

All animal procedures here conformed to the principles of world-wide regulations (Grundy, 2015). The experiments were carried out according to guidelines approved according to Protocol No. 3/14 from 06.2015 from the Bogomoletz Institute of Physiology (Ukraine) and as regulated by the European Community Council Directive (2010/63/EU).

Author contributions

VP prepared hippocampal culture and participated in electrophysiological experiments and data analysis. IM designed this project, led the experiments and data analysis, and wrote the manuscript. Both authors contributed to the article and approved the submitted version.

Funding

This work was funded on a regular basis by the National Academy of Sciences of Ukraine.

Acknowledgments

We thank Dr. Shkryl V. M. for their critical reading of the manuscript.

Conflict of interest

The authors declare that the research was conducted in the absence of any commercial or financial relationships that could be construed as a potential conflict of interest.

Publisher's note

References

Alger, B. E., and Nicoll, R. A. (1982). Feed-forward dendritic inhibition in rat hippocampal pyramidal cells studied *in vitro*. *J. Physiol.* 328, 105–123. doi: 10.1113/jphysiol.1982.sp014255

Avoli, M., Psarropoulou, C., Tancredi, V., and Fueta, Y. (1993). On the synchronous activity induced by 4-aminopyridine in the CA3 subfield of juvenile rat hippocampus. *J. Neurophysiol.* 70, 1018–1029. doi: 10.1152/jn.1993.70.3.1018

Bacci, A., Verderio, C., Pravettoni, E., and Matteoli, M. (1999). Synaptic and intrinsic mechanisms shape synchronous oscillations in hippocampal neurons in culture. *Eur. J. Neurosci.* 11, 389–397. doi: 10.1046/j.1460-9568.1999.00440.x

Bartos, M., Vida, I., Frotscher, M., Meyer, A., Monyer, H., Geiger, J. R., et al. (2002). Fast synaptic inhibition promotes synchronized gamma oscillations in hippocampal interneuron networks. *Proc. Natl. Acad. Sci. U.S.A.* 99, 13222–13227. doi: 10.1073/pnas.192233099

Beierlein, M., Gibson, J. R., and Connors, B. W. (2000). A network of electrically coupled interneurons drives synchronized inhibition in neocortex. *Nat. Neurosci.* 3, 904–910. doi: 10.1038/78809

Benardo, L. S. (1997). Recruitment of GABAergic inhibition and synchronization of inhibitory interneurons in rat neocortex. *J. Neurophysiol.* 77, 3134–3144. doi: 10.1152/jn.1997.77.6.3134

Ben-Ari, Y., Cherubini, E., Corradetti, R., and Gaiarsa, J. L. (1989). Giant synaptic potentials in immature rat CA3 hippocampal neurons. *J. Physiol.* 416, 303–325.

Bracci, E., Vreugdenhil, M., Hack, S. P., and Jefferys, J. G. (1999). On the synchronizing mechanisms of tetanically induced hippocampal oscillations. *J. Neurosci.* 19, 8104–8113. doi: 10.1523/jneurosci.19-18-08104.1999

Buhl, E. H., Halasy, K., and Somogyi, P. (1994). Diverse sources of hippocampal unitary inhibitory postsynaptic potentials and the number of synaptic release sites. *Nature* 368, 823–828. doi: 10.1038/368823a0

Cossart, R., Tyzio, R., Dinocourt, C., Esclapez, M., Hirsch, J. C., Ben-Ari, Y., et al. (2001). Presynaptic kainate receptors that enhance the release of GABA on CA1 hippocampal interneurons. *Neuron* 29, 497–508. doi: 10.1016/s0896-6273(01)00221-5

Davies, S. N., and Collingridge, G. L. (1989). Role of excitatory amino acid receptors in synaptic transmission in area CA1 of rat hippocampus. *Proc. R. Soc. Lond. B Biol. Sci.* 236, 373–384. doi: 10.1098/rspb.1989.0028

Dudek, F. E., Snow, R. W., and Taylor, C. P. (1986). Role of electrical interactions in synchronization of epileptiform bursts. *Adv. Neurol.* 44, 593–617.

Dzhala, V. I., and Staley, K. J. (2003). Excitatory actions of endogenously released GABA contribute to initiation of ictal epileptiform activity in the developing hippocampus. *J. Neurosci.* 23, 1840–1846. doi: 10.1523/jneurosci.23-05-01840.2003

Engel, A. K., König, P., Kreiter, A. K., Schillen, T. B., and Singer, W. (1992). Temporal coding in the visual cortex: New vistas on integration in the nervous system. *Trends Neurosci.* 15, 218–226. doi: 10.1016/0166-2236(92)90039-b

Fisahn, A., Pike, F. G., Buhl, E. H., and Paulsen, O. (1998). Cholinergic induction of network oscillations at 40 Hz in the hippocampus *in vitro*. *Nature* 394, 186–189. doi: 10.1038/28179

Fischer, Y. (2004). The hippocampal intrinsic network oscillator. *J. Physiol.* 554, 156–174. doi: 10.1113/jphysiol.2003.055558

Fischer, Y., Wittner, L., Freund, T. F., and Gahwiler, B. H. (2002). Simultaneous activation of gamma and theta network oscillations in rat hippocampal slice cultures. *J. Physiol.* 539, 857–868. doi: 10.1113/jphysiol.2001.013050

Frerking, M., Malenka, R. C., and Nicoll, R. A. (1998). Synaptic activation of kainate receptors on hippocampal interneurons. *Nat. Neurosci.* 1, 479–486. doi: 10.1038/2194

Freund, T. F., and Buzsaki, G. (1996). Interneurons of the hippocampus. *Hippocampus* 6, 347–470.

Fu, L. Y., and van den Pol, A. N. (2007). GABA excitation in mouse hilar neuropeptide Y neurons. *J. Physiol.* 579, 445–464. doi: 10.1113/jphysiol.2002.019356

Fukuda, T., and Kosaka, T. (2000). Gap junctions linking the dendritic network of GABAergic interneurons in the hippocampus. *J. Neurosci.* 20, 1519–1528. doi: 10.1523/jneurosci.20-04-01519.2000

Geiger, J. R., Lübke, J., Roth, A., Frotscher, M., and Jonas, P. (1997). Submillisecond AMPA receptor-mediated signaling at a principal neuron-interneuron synapse. *Neuron* 18, 1009–1023. doi: 10.1016/s0896-6273(00)80339-6

Gibson, J. R., Beierlein, M., and Connors, B. W. (1999). Two networks of electrically coupled inhibitory neurons in neocortex. *Nature* 402, 75–79. doi: 10.1038/47035

Grundy, D. (2015). Principles and standards for reporting animal experiments in The Journal of Physiology and Experimental Physiology. *J. Physiol.* 593, 2547–2549. doi: 10.1113/JP270818

Gulyás, A. I., Hájos, N., and Freund, T. F. (1996). Interneurons containing calretinin are specialized to control other interneurons in the rat hippocampus. *J. Neurosci.* 16, 3397–3411. doi: 10.1523/jneurosci.16-10-03397.1996

Gulyás, A. I., Miles, R., Hájos, N., and Freund, T. F. (1993). Precision and variability in postsynaptic target selection of inhibitory cells in the hippocampal CA3 region. *Eur. J. Neurosci.* 5, 1729–1751. doi: 10.1111/j.1460-9568.1993.tb00240.x

Gutnick, M. J., Lobel-Yaakov, R., and Rimon, G. (1985). Incidence of neuronal dye-coupling in neocortical slices depends on the plane of section. *Neuroscience* 15, 659–666. doi: 10.1016/0306-4522(85)90067-3

Hájos, N., and Mody, I. (1997). Synaptic communication among hippocampal interneurons: Properties of spontaneous IPSCs in morphologically identified cells. *J. Neurosci.* 17, 8427–8442. doi: 10.1523/jneurosci.17-21-08427.1997

Harris, A. Z., and Gordon, J. A. (2015). Long-range neural synchrony in behavior. *Annu. Rev. Neurosci.* 38, 171–194. doi: 10.1146/annurev-neuro-071714-034111

Hu, G. Y., Hvalby, O., Lacaille, J. C., Piercey, B., Ostberg, T., and Andersen, P. (1992). Synaptically triggered action potentials begin as a depolarizing ramp in rat hippocampal neurons *in vitro*. *J. Physiol.* 453, 663–687. doi: 10.1113/jphysiol.1992.sp019250

Hu, H., Ma, Y., and Agmon, A. (2011). Submillisecond firing synchrony between different subtypes of cortical interneurons connected chemically but not electrically. *J. Neurosci.* 31, 3351–3361. doi: 10.1523/jneurosci.4881-10.2011

Karnani, M. M., Jackson, J., Ayzenshtat, I., Tucciarone, J., Manoocheri, K., Snider, W. G., et al. (2016). Cooperative subnetworks of molecular similar interneurons in mouse neocortex. *Neuron* 90, 86–100. doi: 10.1016/j.neuron.2016.02.037

Kerlin, A. M., Andermann, M. L., Berezovskii, V. K., and Reid, R. C. (2010). Broadly tuned response properties of diverse inhibitory neuron subtypes in mouse visual cortex. *Neuron* 67, 858–871. doi: 10.1016/j.neuron.2010.08.002

Khalilov, I., Dzhala, V., Ben-Ari, Y., and Khazipov, R. (1999). Dual role of GABA in the neonatal rat hippocampus. *Dev. Neurosci.* 21, 310–319. doi: 10.1159/000017380

Khazipov, R., Leinekugel, X., Khalilov, I., Gaiarsa, J. L., and Ben-Ari, Y. (1997). Synchronization of GABAergic interneuronal network in CA3 subfield of neonatal rat hippocampal slices. *J. Physiol.* 498, 763–772. doi: 10.1113/jphysiol.1997.sp021900

Kirmse, K., Kummer, M., Kovalchuk, Y., Witte, O. W., Garaschuk, O., and Holthoff, K. (2015). GABA depolarizes immature neurons and inhibits network activity in the neonatal neocortex in vivo. *Nat. Commun.* 6:7750. doi: 10.1038/ncomms8750

Lacaille, J. C. (1991). Postsynaptic potentials mediated by excitatory and inhibitory amino acids in interneurons of stratum pyramidale of the CA1 region of rat hippocampal slices *in vitro*. *J. Neurophysiol.* 66, 1441–1454. doi: 10.1152/jn.1991.66.5.1441

MacVicar, B. A., and Dudek, F. E. (1981). Electrotonic coupling between pyramidal cells: A direct demonstration in rat hippocampal slices. *Science* 213, 782–785. doi: 10.1126/science.6266013

Martina, M., Vida, I., and Jonas, P. (2000). Distal initiation and active propagation of action potentials in interneuron dendrites. *Science* 287, 295–300. doi: 10.1126/science.287.5451.295

McBain, C. J., and Dingledine, R. (1993). Heterogeneity of synaptic glutamate receptors on CA3 stratum radiatum interneurons of rat hippocampus. *J. Physiol.* 462, 373–392. doi: 10.1113/jphysiol.1993.sp019560

McBain, C. J., Boden, P., and Hill, R. G. (1989). Rat hippocampal slices 'in vitro' display spontaneous epileptiform activity following long-term organotypic culture. *J. Neurosci. Methods* 27, 35–49. doi: 10.1016/0165-0270(89)90051-4

Mennerick, S., Que, J., Benz, A., and Zorumski, C. F. (1995). Passive and synaptic properties of hippocampal neurons grown in microcultures and in mass cultures. *J. Neurophysiol.* 73, 320–332. doi: 10.1152/jn.1995.73.1.320

Michelson, H. B., and Wong, R. K. S. (1994). Synchronization of inhibitory neurons in the guinea-pig hippocampus in vitro. *J. Physiol.* 477, 35–45. doi: 10.1113/jphysiol.1994.sp020169

Miles, R. (1990a). Synaptic excitation of inhibitory cells by single CA3 pyramidal cells of the guinea-pig in vitro. *J. Physiol.* 428, 61–77. doi: 10.1113/jphysiol.1990.sp018200

Miles, R. (1990b). Variation in strength of inhibitory synapses in the CA3 region of guinea-pig hippocampus in vitro. *J. Physiol.* 431, 659–676. doi: 10.1113/jphysiol.1990.sp018353

Miles, R. (1991). Tetanic stimuli induce a short-term enhancement of recurrent inhibition in the CA3 region of guinea-pig hippocampus in vitro. *J. Physiol.* 443, 669–682. doi: 10.1113/jphysiol.1991.sp018857

Miles, R., and Poncer, J. C. (1993). Metabotropic glutamate receptors mediate a post-tetanic excitation of guinea-pig hippocampal inhibitory neurons. *J. Physiol.* 463, 461–473. doi: 10.1113/jphysiol.1993.sp019605

Miles, R., and Wong, R. K. S. (1983). Single neurons can initiate synchronized population discharge in the hippocampus. *Nature* 306, 371–373. doi: 10.1038/306371a0

Miles, R., and Wong, R. K. S. (1984). Unitary inhibitory synaptic potentials in the guinea-pig hippocampus in vitro. *J. Physiol.* 431, 659–676. doi: 10.1113/jphysiol.1984.sp015455

Miles, R., and Wong, R. K. S. (1986). Excitatory synaptic interactions between CA3 neurons in the guinea-pig hippocampus. *J. Physiol.* 373, 397–418. doi: 10.1113/jphysiol.1986.sp016055

Miles, R., Tóth, K., Gulyás, A. I., Hájos, N., and Freund, T. F. (1996). Differences between somatic and dendritic inhibition in the hippocampus. *Neuron* 16, 815–823. doi: 10.1016/s0896-6273(00)80101-4

Núñez, A., García-Austt, E., and Buño, W. (1990). In vivo electrophysiological analysis of lucifer yellow-coupled hippocampal pyramids. *Exp. Neurol.* 1, 76–82. doi: 10.1016/0014-4886(90)90010-p

Otis, T. S., and Mody, I. (1992). Modulation of decay kinetics and frequency of $GABA_A$ receptor-mediated spontaneous inhibitory postsynaptic currents in hippocampal neurons. *Neuroscience* 49, 13–32. doi: 10.1016/0306-4522(92)90073-b

Pfeffer, C. K., Xue, M., He, M., Huang, Z. J., and Scanziani, M. (2013). Inhibition of inhibition in visual cortex: The logic of connections between molecularly distinct interneurons. *Nat. Neurosci.* 18, 1068–1076. doi: 10.1038/nn.3446

Regehr, W., Kehoe, J., Ascher, P., and Armstrong, C. (1993). Synaptically triggered action potentials in dendrites. *Neuron* 11, 145–151. doi: 10.1016/0896-6273(93)90278-y

Ropert, N., Miles, R., and Korn, H. (1990). Characteristics of miniature inhibitory postsynaptic currents in CA1 pyramidal neurons of rat hippocampus. *J. Physiol.* 428, 707–722. doi: 10.1113/jphysiol.1990.sp018236

Rouach, N., Segal, M., Koulakoff, A., Giaume, C., and Avignone, E. (2003). Carbenoxolone blockade of neuronal network activity in culture is not mediated by an action on gap junctions. *J. Physiol.* 553, 729–745. doi: 10.1113/jphysiol.2003.053439

Semyanov, A., and Kullmann, D. M. (2001). Kainate receptor-dependent axonal depolarization and action potential initiation in interneurons. *Nat. Neurosci.* 4, 718–723. doi: 10.1038/89506

Shigematsu, N., Nishi, A., and Fukuda, T. (2019). Gap junctions interconnect different subtypes of parvalbumin-positive interneurons in barrels and septa with connectivity unique to each subtype. *Cereb. Cortex* 29, 1414–1429. doi: 10.1093/cercor/bhy038

Sipilä, S. T., Huttu, K., Soltesz, I., Voipio, J., and Kaira, K. (2005). Depolarizing GABA acts on intrinsically bursting pyramidal neurons to drive giant depolarizing potentials in the immature hippocampus. *J. Neurosci.* 25, 5280–5289. doi: 10.1523/jneurosci.0378-05.2005

Skinner, F. K., Zhang, L., Velazquez, J. L., and Carlen, P. L. (1999). Bursting in inhibitory interneuronal networks: A role for gap-junctional coupling. *J. Neurophysiol.* 81, 1274–1283. doi: 10.1152/jn.1999.81.3.1274

Spencer, W. A., and Kandel, E. R. (1961). Electrophysiology of hippocampal neurons. IV. Fast prepotentials. *J. Neurophysiol.* 24, 272–285. doi: 10.1152/jn.1961.24.3.272

Staley, K. J., Soldo, B. L., and Proctor, W. R. (1995). Ionic mechanisms of neuronal excitation by inhibitory GABAA receptors. *Science* 269, 977–981. doi: 10.1126/science.7638623

Stasheff, S. F., Hines, M., and Wilson, W. A. (1993). Axon terminal hyperexcitability associated with epileptogenesis in vitro. I. Origin of ectopic spikes. *J. Neurophysiol.* 70, 961–975. doi: 10.1152/jn.1993.70.3.961

Steriade, M., Nunez, A., and Amzica, F. (1993). A novel slow (<1 Hz) oscillation of neocortical neurons in vivo: Depolarizing and hyperpolarizing components. *J. Neurosci.* 13, 3252–3265. doi: 10.1523/jneurosci.13-08-03252.1993

Strata, F., Atzori, M., Molnar, M., Ugolini, G., Tempia, F., and Cherubini, E. (1997). A pacemaker current in dye-coupled hilar interneurons contributes to the generation of giant GABAergic potentials in developing hippocampus. *J. Neurosci.* 17, 1435–1446. doi: 10.1523/jneurosci.17-04-01435.1997

Szabadics, J., Varga, C., Molnar, G., Olah, S., Barzo, P., and Tamás, G. (2006). Excitatory effect of GABAergic axo-axonic cells in cortical microcircuits. *Science* 311, 233–235. doi: 10.1126/science.1121325

Tamás, G., Buhl, E. H., Lörincz, A., and Somogyi, P. (2000). Proximally targeted GABAergic synapses and gap junctions synchronize cortical interneurons. *Nat. Neurosci.* 3, 366–371. doi: 10.1038/73936

Velazquez, J. L., and Carlen, P. L. (1999). Synchronization of GABAergic interneuronal networks during seizure-like activity in the rat horizontal hippocampal slice. *Eur. J. Neurosci.* 11, 4110–4118. doi: 10.1046/j.1460-9568.1999.00837.x

Vida, I., Bartos, M., and Jona, P. (2006). Shunting inhibition improves robustness of gamma oscillations in hippocampal interneuronal networks by homogenizing firing rates. *Neuron* 49, 107–117. doi: 10.1016/j.neuron.2005.11.036

Vincent, P., and Marty, A. (1993). Neighboring cerebellar Purkinje cells communicate via retrograde inhibition of common presynaptic interneurons. *Neuron* 11, 885–893. doi: 10.1016/0896-6273(93)90118-b

Vincent, P., and Marty, A. (1996). Fluctuations of inhibitory postsynaptic currents in Purkinje cells from rat cerebellar slices. *J. Physiol.* 494, 183–199. doi: 10.1113/jphysiol.1996.sp021484

Wester, J. C., and McBain, C. J. (2016). Interneurons differentially contribute to spontaneous network activity in the developing hippocampus dependent on their embryonic lineage. *J. Neurosci.* 36, 2646–2662. doi: 10.1523/jneurosci.4000-15.2016

Whittington, M. A., Traub, R. D., and Jefferys, J. G. R. (1995). Synchronized oscillations in interneuron networks driven by metabotropic glutamate receptor activation. *Nature* 373, 612–615. doi: 10.1038/373612a0

Williams, S. R., Buhl, E. H., and Mody, I. (1998). The dynamics of synchronized neurotransmitter release determined from compound spontaneous IPSCs in rat dentate granule neurons in vitro. *J. Physiol.* 510, 477–497. doi: 10.1111/j.1469-7793.1998.477bk.x

Yuste, R., Peinado, A., and Katz, L. C. (1992). Neuronal domains in developing neocortex. *Science* 257, 665–669. doi: 10.1126/science.1496379

Zhang, Y., Perez Velazquez, J. L., Tian, G. F., Wu, C. P., Skinner, F. K., Carlen, P. L., et al. (1998). Slow oscillations (= 1 Hz) mediated by GABAergic interneuronal networks in rat hippocampus. *J. Neurosci.* 18, 9256–9268. doi: 10.1523/jneurosci.18-22-09256.1998

frontiers | Frontiers in Cellular Neuroscience

TYPE Brief Research Report
PUBLISHED 16 March 2023
DOI 10.3389/fncel.2023.1131168

OPEN ACCESS

EDITED BY
Dirk M. Hermann,
University of Duisburg-Essen, Germany

REVIEWED BY
Yanet Karina Gutierrez-Mercado,
University of Guadalajara, Mexico
Olga Berchenko,
Psychiatry and Narcology of NAMS of Ukraine, Ukraine
Baskaran Stephen Inbaraj,
Fu Jen Catholic University, Taiwan

*CORRESPONDENCE
Nataliia M. Rozumna
✉ nata_nr@biph.kiev.ua

SPECIALTY SECTION
This article was submitted to Cellular Neuropathology, a section of the journal Frontiers in Cellular Neuroscience

RECEIVED 24 December 2022
ACCEPTED 02 March 2023
PUBLISHED 16 March 2023

CITATION
Hanzha VV, Rozumna NM, Kravenska YV, Spivak MYa and Lukyanetz EA (2023) The effect of cerium dioxide nanoparticles on the viability of hippocampal neurons in Alzheimer's disease modeling. *Front. Cell. Neurosci.* 17:1131168. doi: 10.3389/fncel.2023.1131168

The effect of cerium dioxide nanoparticles on the viability of hippocampal neurons in Alzheimer's disease modeling

Vita V. Hanzha[1], Nataliia M. Rozumna[1]*, Yevheniia V. Kravenska[1], Mykola Ya. Spivak[2] and Elena A. Lukyanetz[1]

[1]Department of Biophysics of Ion Channels, Bogomoletz Institute of Physiology, The National Academy of Sciences of Ukraine (NASU), Kyiv, Ukraine, [2]Danylo Zabolotny Institute of Microbiology and Virology, The National Academy of Sciences of Ukraine (NASU), Kyiv, Ukraine

The possibilities of using nanoparticle materials based on cerium dioxide (CNPs) are exciting since they are low toxic and have specific redox, antiradical properties. It can be supposed that CNPs' biomedical use is also relevant in neurodegenerative diseases, especially Alzheimer's disease (AD). AD is known as the pathologies leading to progressive dementia in the elderly. The factor that provokes nerve cell death and cognitive impairment in AD is the pathological accumulation of beta-amyloid peptide (Aβ) in the brain tissue. In our studies, we examined the impact of Aβ 1-42 on neuronal death and evaluated the potential neuroprotective properties of CNPs during AD modeling in cell culture. Our findings show that, under AD modeling conditions, the number of necrotic neurons increased from 9.4% in the control to 42.7% when Aβ 1-42 was used. In contrast, CNPs alone showed low toxicity, with no significant increase in the number of necrotic cells compared to control conditions. We further explored the potential of CNPs as a neuroprotective agent against Aβ-induced neuronal death. We found that introducing CNPs 24 h after Aβ 1-42 incubation or prophylactically incubating hippocampal cells with CNPs 24 h before amyloid administration significantly reduced the percentage of necrotic cells to 17.8 and 13.3%, respectively. Our results suggest that CNPs in the cultural media can significantly reduce the number of dead hippocampal neurons in the presence of Aβ, highlighting their neuroprotective properties. These findings suggest that CNPs may hold promise for developing new treatments for AD based on their neuroprotective properties.

KEYWORDS

hippocampus, cell culture, cerium nanoparticles, beta-amyloid, Alzheimer's disease, nanomaterials

Introduction

In recent years, new possibilities for the use of nanomaterials with several unique properties in medicine are actively studied to diagnose and treat diseases or improve the human's physiological functions. Nanomaterials have emerged as promising candidates for neuroprotection due to their unique properties, including small size, high surface area-to-volume ratio, and the ability to penetrate biological membranes. These properties enable nanomaterials to interact with cellular components, such as enzymes and

receptors, and modulate cellular signaling pathways. As a result, nanomaterials can exhibit neuroprotective effects by reducing oxidative stress, inflammation, and apoptosis. The possibilities of using nanoparticle materials based on cerium dioxide (CNPs) are especially widely studied (Lord et al., 2021; Saifi et al., 2021).

Cerium dioxide (CNPs) are a type of nanomaterial that has gained significant attention due to their unique redox properties (Yadav, 2022). CNPs can act as an antioxidant and a pro-oxidant depending on the cellular environment. Under oxidative stress conditions, CNPs can act as an antioxidant by scavenging free radicals and reducing oxidative damage. Conversely, under reducing conditions, CNPs can act as a pro-oxidant by generating reactive oxygen species (ROS) and inducing apoptosis in cancer cells (see for review Chen et al., 2013). Their characteristics, such as low toxicity and specific redox and antiradical properties, the ability to regenerate, allow to consider CNPs as a promising object for biomedical applications (Celardo et al., 2011). For example, CNPs has been shown to reduce retinal degeneration (Wong and McGinnis, 2014), protect from oxidative stress brain tissue (Heckman et al., 2013), improve outcome after mild traumatic brain Injury (Bailey et al., 2020), human skin fibroblasts (Lee et al., 2013), endothelial cells (Chen and Stephen Inbaraj, 2018), and heart (Niu et al., 2007).

It seems, CNP's biomedical use is also relevant in neurodegenerative diseases, especially Alzheimer's disease (AD) (Singh et al., 2008; D'Angelo et al., 2009; Naz et al., 2017; Zand et al., 2019). It is known that AD is one of the pathologies that leads to progressive dementia in the elderly. The hippocampus is the first area of the brain damaged by senile plaques at the course of AD. Therefore, the problems with memory, speech, and disorientation appear among the main neurobehavioral symptoms at AD (Alzheimer's Disease International [ADI], 2019). It is known that beta-amyloid peptide (Aβ) is a major component of the plaques–characteristic morphological features of AD (Haass and Selkoe, 2007). According to the "amyloid cascade" hypothesis, the factor that leads to nerve cell death and cognitive impairment is the pathological accumulation of Aβ aggregates in the brain tissue. Neurotoxicity of Aβ is manifested by impaired Ca^{2+} homeostasis, mitochondrial dysfunctions (Kravenska et al., 2016, 2020), induction of oxidative stress, excitotoxicity, inflammatory processes, intensification of apoptosis, and necrosis (Marchesi, 2011; Kravenska et al., 2016). In the context of neuroprotection, CNPs have been shown to protect neurons from oxidative stress-induced cell death. Specifically, CNPs can scavenge ROS and restore the redox balance in neurons. Additionally, CNPs can upregulate antioxidant enzymes and reduce inflammation in the brain. These mechanisms can protect neurons from neurodegeneration and promote their survival. In AD, CNPs have been investigated as a potential therapeutic agent due to their neuroprotective effects (Danish et al., 2022). CNPs have been shown to reduce Aβ-induced toxicity *in vitro* and *in vivo* by reducing oxidative stress, inflammation, and Aβ aggregation. Additionally, CNPs can penetrate the blood-brain barrier and accumulate in the brain, making them a potential candidate for delivering therapeutics to the brain (see for review Stephen Inbaraj and Chen, 2020).

In conclusion, CNPs possess unique properties that make them promising candidates for neuroprotection, especially in the context of AD. The mechanism of neuroprotection by CNPs involves scavenging ROS, restoring redox balance, and reducing inflammation in neurons. Further research is necessary to fully understand the potential of CNPs as a therapeutic agent for AD and other neurodegenerative diseases.

Our investigations aim to test the effects of CNPs on hippocampal neurons' viability during modeling AD on cell cultures.

Materials and methods

Animals

All experimental procedures followed the European Commission Directive (86/609/EEC) and ethical guidelines of the International Association for the Study of Pain and were approved by the local Animal Ethics Committee of the Bogomoletz Institute of Physiology (Kyiv, Ukraine). All efforts were made to minimize the number and suffering of animals used.

Preparation of primary dissociated hippocampal cell culture

Studies were performed on rat hippocampal culture neurons using a common technique described earlier (Lukyanetz et al., 2003a,b). To do this, a total of 12 newborn Wistar rats were used. They were decapitated, the hippocampus was isolated in a sterile and cold Petri dish, cut into several pieces each, and transferred for 10 min to a warm (36°C) enzyme solution containing 0.25% trypsin (Sigma-Aldrich, St. Louis, MO, USA). Next, the pieces of the hippocampus were washed several times with cold nutrient medium. The tissue was dispersed to homogeneous suspension using a 1 ml tip of pipetter. Using a Goryaev chamber and adding the required volume of nutrient medium, a suspension with a density of 3×10^5 cells per 1 ml was prepared. Then 200 μL of the cell suspension was applied to 20 mm × 20 mm slides, which were pre-treated with polylysine (0.05 mg/ml, Sigma-Aldrich) and laminin (0.005 mg/ml, Sigma-Aldrich). After 2 h incubation at 37°C in an atmosphere enriched with 5% CO_2, in each Petri dish was added 2 ml of nutrient medium, which included 90% of the minimum essential media (MEM, Sigma-Aldrich), 2.2 g/l $NaHCO_3$, 10% horse serum (Gibco, Cat. No. 16050130, Auckland, New Zealand), 10 μg/ml insulin and antibiotics: 50 IU/ml benzylpenicillin sodium and 50 μg/ml streptomycin sulfate. Neurons were cultured in an incubator for 2 weeks at 37°C in an atmosphere enriched with 5% CO_2. To inhibit glial cells' proliferation after 3 days *in vitro* culture was treated with 1 μM/L cytosine arabinoside (AraC) (Sigma-Aldrich) for 24 h. After that, a complete replacement of the nutrient medium of neurons was performed. Every 4 days, 400 μL of the solution of cultivating medium from the Petri dish was replaced with a fresh one. Neurons

Abbreviations: Aβ, beta-amyloid peptide; Aβ1-42, beta-amyloid peptide 1-42; AD, Alzheimer's disease; AraC, cytosine arabinoside; CNPs, nanoparticules of cerium dioxide.

were taken for the experiment on 11–13 days of cultivation (see **Supplementary Figure 1**).

Treatment of hippocampal cells with reagents. Modeling of neurodegeneration

Prolonged culturing of the central nervous system (CNS) cells *in vitro* is widely used as the AD study model (Kravenska et al., 2016; Bailey et al., 2020). In our studies, the AD model was obtained by 24 h incubation of hippocampal culture neurons with Aβ1–42-amyloid (Sigma-Aldrich, USA) at a final concentration of 2 μM. A separate group of cell cultures was co-incubated with Aβ1-42 (2 μM, 24 h) and CNPs (1: 100 dilution of 0, 1 mM stock) 24 h in different configurations of administration of active substances to study the effect of CNPs on the viability of neurons in this model of AD (see **Supplementary Figure 1C**). CNPs were obtained by the chemical method described previously in detail (Rybalko et al., 2021) from the Institute of Microbiology and Virology of NAS of Ukraine, Kyiv, Ukraine. The synthesis method enabled the preparation of cerium samples with crystallite sizes of about 3 nm. X-ray diffraction (XRD) has shown that the used samples are single-phase and correspond to cubic CeO_2. A concentrated solution of Aβ1–42-amyloid and CNPs was prepared on dimethyl sulfoxide (DMSO) and stored at −20°C. The final concentration of dimethyl sulfoxide did not exceed 0.5%. The study of the possible effect of the DMSO solvent itself on culture cells of the hippocampus of rats was carried out earlier by us. It was shown that its concentrations of 0.5% and less, when added to the culture medium for 24–48 h, did not affect the parameters of the cells in the culture and did not differ from the control group.

Detection of different types of cell death

The number of alive, cytologically normal cells and cells with manifestations of apoptosis or necrosis was evaluated using the double staining with dyes Hoechst 33258 (Sigma-Aldrich) and propidium iodide (PI, Sigma-Aldrich), **Figure 1** (left part). The first of these dyes penetrate undamaged cell membranes and stains nuclear chromatin, thus providing visualization of cytologically normal and apoptotically altered cells, which have so far remained viable (**Figure 1**). In alive cells, chromatin is distributed more evenly throughout the nucleus' volume, and Hoechst 33258 in them fluoresces faintly with blue light. In apoptotic cells, Hoechst 33258 intensity of fluorescence 3–4 times higher than in normal cells (bright blue glow), indicating condensation of chromatin and fragmentation of nuclei, which occurs during the induction of apoptosis (**Figure 1**, central image). PI cannot penetrate the intact plasma membrane and stains only the nuclei in cells with a significantly damaged plasmalemma, i.e., cells in which occurred necrotic transformation–necrosis (red color fluoresce) (**Figure 1**, right part).

A protocol was used according to the previously described technique to stain the neurons of hippocampal culture (Kravenska et al., 2016). Coverslips with control neurons or cultures treated with amyloid and/or CNPs in different configurations of administration of active substances were transferred for 10 min in a PI (final concentration 2.0 μg/ml). The cells were then fixed by immersion for 20 min in a 4% solution of paraformaldehyde, then placed for 20 min in Hoechst 33258 solution with a final concentration of 1.0 μg/ml. After each staining step, the cells were washed twice in 2.0 ml of phosphate buffer (0.1 M). All manipulations were performed at room temperature. After staining, the coverslips with cells were mounted on slides using a solution of Aqua-Poly Mount (Polysciences, Inc., Warrington, PA, USA). Fixed and mounted cells were studied using confocal microscopy.

Confocal laser scanning microscopy

The FV1000-BX61WI confocal laser scanning microscope and the software FluoView (Olympus, Japan) or Image J (National Institutes of Health, Bethesda, MD, USA) were used in the studies to obtain fluorescent images and count of neurons. The laser excitation wavelengths were 352/405 nm for Hoechst 33258 and 543 nm for PI, respectively.

Neurons were distinguished from glial cells by phase-contrast and were counted in five spatially distant areas of each sample. Each sample contained 100 to 300 cells, the number of living, apoptotic, and necrotic cells were counted. The values of every type normalized to the total cell number of the sample, and then the values of all samples were averaged for each type of cell state.

Statistical analysis

The obtained results were processed by methods of variation statistics using the program Origin 7.0 (OriginLab Corporation, Northampton, MA, USA). Numerical data are given as means ± mean error. A normal distribution characterized the results, intergroup comparison of data was performed using ANOVA analysis of variance. If intergroup differences were found, the Tukey test was used. The results were considered statistically significant at $P < 0.05$.

Results

Our research was devoted to establishing a possible neuroprotective role of CNPs on the viability of hippocampal culture neurons in the simulation of AD. To this end, five groups of experiments were conducted (see **Supplementary Figure 1**): the first—cells were cultured in control conditions; the second–the introduction of CNPs in cultural media for 24 h before the measurement; third–the introduction of amyloid Aβ1-42 in media for 24 h before the measurement; fourth–the introduction of amyloid Aβ1-42 for 24 h, and the subsequent introduction of CNPs for 24 h before the measurement; fifth–prophylactic administration of CNPs into media for 24 h before the introduction of amyloid Aβ1-42. The cells were then dual stained with two DNA-binding dyes (Hoechst and PI), and then they were investigated and counted using confocal laser scanning microscopy. The incubation duration of hippocampal cultures in all studied groups was the same. On the 11th and 12th days of cultivation, reagents were added, and on the 13th day, the samples of all 5 groups of experiments were stained

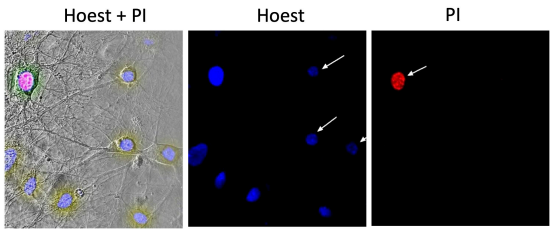

FIGURE 1
Example of a micrograph of cultured hippocampal neurons. The **(left)** part shows a phase-contrast image merged with images presented to the **(right)**; image in the **(middle)** demonstrates the fluorescence of Hoechst 33258 in neurons; **(right)** the fluorescence of propidium iodide (PI) in the necrotized neuron.

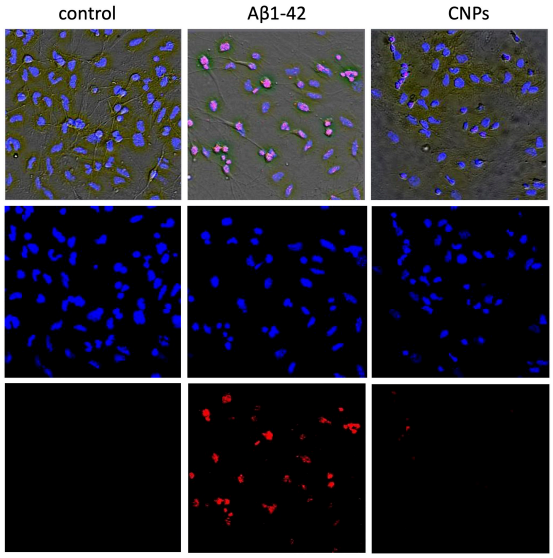

FIGURE 2
Micrographs of cultured hippocampal neurons after Aβ or CNPs incubation. The **(left)** column shows images of cells in control conditions. The next column demonstrates cells incubated with Aβ1-42 (24 h). The **(right)** column shows cells after incubation with CNPs (24 h). Above are phase-contrast images, merged with images obtained by staining with Hoechst 33258 (below in the column) and propidium iodide (PI) (lowest).

and fixed (see Supplementary Figure 1C). The study groups were carried out in quadruplicate.

In control samples of rat hippocampal cell culture, the vast majority of cells (average 84.7 ± 2.1%) did not show any pathological changes (Figure 2, left column). Figure 2 shows merged images: phase-contrast, Hoechst, and PI recorded (upper), and separately showed for Hoechst (below) and PI (lowest) stained images. The nuclei of such cells, which accumulated the Hoechst 33258, were characterized by weak blue fluorescence and had clear contours, nuclear chromatin was stained relatively evenly (Figure 2). The nuclei of a relatively small part of the neurons (5.9 ± 1.31%) in the control samples gave bright blue fluorescence. They had a pronounced fragmentation of chromatin, which was a sign of apoptotic transformation. There was also a portion of neurons in control samples (9.4 ± 1.57% on average in the group), stained with PI. They were characterized by red fluorescence, which indicated necrotic degeneration of this part of the analyzed neuronal populations. The presence of several dead cells in the control conditions is explained by their damage during culture preparation, particularly in the process of changing the culture medium.

In the second series of experiments, cells were treated with amyloid β1–42. After incubation of hippocampal cell culture samples in amyloid β1–42 medium, cytologically normal cells accounted for approximately one-third of the study population (mean 31.8 ± 3.02%). Neurons with apoptotic changes in these conditions were observed approximately five times more often than in control (25.5 ± 4.32%) (Figure 2, middle column). The group of cells with necrosis signs was also more numerous than in control samples (on average, their number was 42.7 ± 4.17%). Thus, amyloid β1–42 in the culture medium induced intensive death of hippocampal neurons: more than half of the cells of the studied sample showed pronounced pathological changes that developed in both apoptotic and necrotic scenarios.

In the third part, the introduction of CNPs showed that the proportion of living neurons averaged 81.1 ± 2.35%, apoptotic–10.1 ± 2.2%, necrotized–8.8 ± 1.34% of the total number of examined cells. Probable changes in groups of cells in comparison with control were not revealed. Therefore CNPs had a low toxic effect on cells of a hippocampus (Figure 2, right column).

The introduction of CNPs after 24 h of incubation with amyloid β1–42 ensured the preservation of a slightly larger number of alive cytological cells than under conditions of action of alone amyloid β1–42 (Figure 3, left column, Figure 4A). The relative number of cells without signs of degeneration, in this case, was more than half of the analyzed sample (average 63.7 ± 3.64%) and differed from both the control and the corresponding in the action of alone amyloid β1-42. The number of cells with apoptotic changes in this group was approximately three times greater than the control conditions. Still, this number was less than the same value in the above group of samples with the action of alone amyloid β1-42. On average, in the group, the relative number of cells with apoptosis signs was 18.5 ± 3.23% of the total (Figure 4B). The addition of CNPs provided a reduction in the number of apoptotic units by an average of 7% compared with that observed in the previous group ($P < 0.001$) (Figure 4B). The relative numbers of cells with pronounced necrotic changes in these two groups also differed approximately 2.5 times (with the introduction of CNPs after 24 h of incubation with amyloid β1-42 in the media averaged 17.8 ± 2.65%). Treatment with CNPs after the action of amyloid β1-42 suspended its pathological effect on the neurons of hippocampal culture.

After prophylactic incubation of hippocampal cells with CNPs 24 h before amyloid administration, the proportion of living neurons in the total number of cells was 79.4 ± 3.71% (approximately 2.5 times more than in the isolated action of amyloid β1-42), apoptotic–7, 3 ± 1.28%, necrotized–13.3 ± 3.61% (approximately three times less than in the isolated action of amyloid β1–42). In other words, pretreatment of cultures of CNPs hippocampal cells dramatically reduced the intensity of death of these cells due to amyloid β1–42 in both apoptotic and necrotic pathways (Figures 4B, C). Thus, in our experiments, we found that pretreatment of CNPs cultures resulted in almost complete preventing of amyloid action, which induces degeneration nerve cells. These nanoparticles also significantly reduced such negative

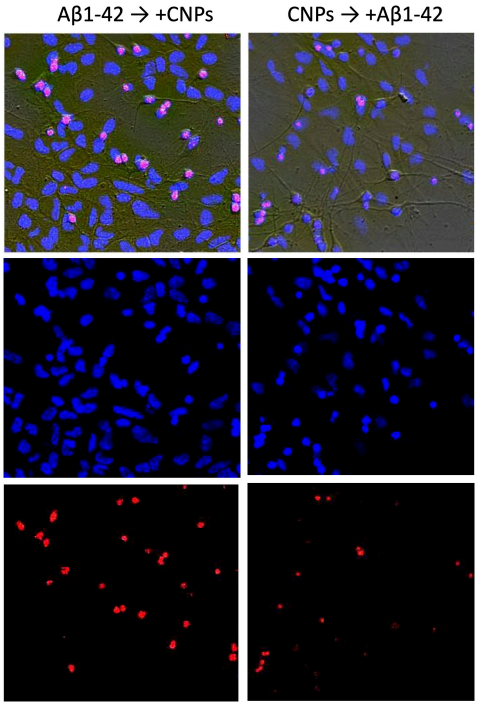

FIGURE 3
Effect of nanoparticles CNPs on the influence of Aβ on hippocampal neurons. The **(left)** column shows images of cells incubated with Aβ1-42 (24 h) and subsequent adding CNPs for the next 24 h. The **(right)** column demonstrates the images where the cells were incubated with CNPs for 24 h before introducing Aβ1-42 (incubation 24 h). Above in columns are phase-contrast images, merged with images obtained by staining with Hoechst 33258 (below in the column) and propidium iodide (PI) (lowest image in the column).

amyloid β1–42 consequences in the case of administration of CNPs after amyloid itself.

Discussion

It is known that CNPs biological activity is associated with oxygen non-stoichiometry, i.e., with the existence on the surface of nanoparticles of Ce^{3+} ions. Due to the low value of the redox potential of the pair Ce^{4+}/Ce^{3+}, near-surface cerium ions easily interact with oxygen, change their valence by 4^+, and then are reduced back to 3^+(Coelho et al., 2019). This property determines the main value of CeO_2 nanocrystals for biomedicine–the ability to participate in redox processes taking place in the body (Tarnuzzer et al., 2005). Therefore, observed in our experiments the effect of the nanoparticles CNPs, can be explained by the ability to participate in redox processes in the brain, especially in the inactivation of ROS, including free radicals (Bailey et al., 2020), which are known to be formed under the Aβ influence and lead to apoptosis or cell necrosis. Besides, after a short period, the nanoparticles can regenerate and are again able to perform an antioxidant function.

According to Heckert et al. (2008) works, the mechanism of inactivation of free radicals by cerium dioxide nanoparticles is similar to the action of superoxide dismutase. Studies of CNPs with hydrogen peroxide by X-ray photoelectron spectroscopy and

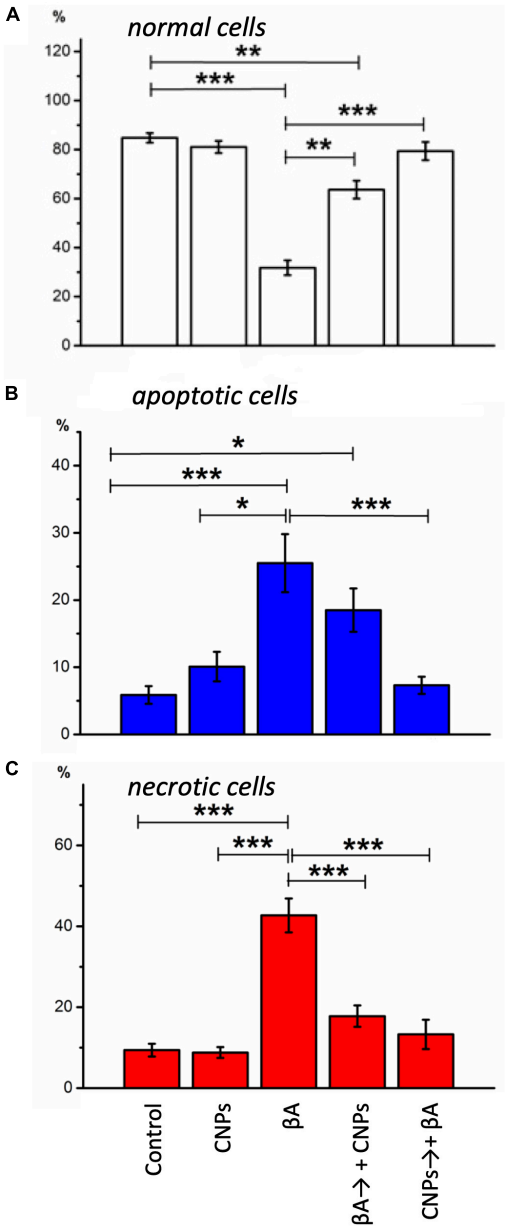

FIGURE 4
Diagrams of the relative numbers neurons of different states in distinct experimental conditions are shown. **(A)** The healthy cells; **(B)** cells with signs of apoptosis; **(C)** necrotic neurons in cells' culture are shown. The percentage of each type from the total number of neurons on the glass was calculated. Measurements were made: in control, during incubation with CNPs, with Aβ1-42, during incubation with Aβ1-42, and subsequent adding of CNPs 24 h before the measurement, prophylactic administration CNPs for 24 h before the introduction of Aβ1-42. Vertical scale–normalized values of the number of cells, %. *$P < 0.05$, **$P < 0.01$, ***$P < 0.001$.

UV spectroscopy have shown an increase in Ce^{3+} ratio: Ce^{4+} in nanoparticles is directly correlated with an increase in their ability to perform the functions of superoxide dismutase. These results convincingly confirm that the most significant factor is Ce^{3+} in the surface layer.

It should be emphasized that today the number of studies similar to ours is quite limited (Singh et al., 2008; Kwon et al., 2016;

Nelson et al., 2016). It is generally known that at the early stage of development of pathological phenomena accompanying AD, oxidation processes are disrupted. Excessive generation of ROS under the influence of β-amyloid leads to increased lipid peroxidation. The result is an intensification of apoptosis and necrotic cell death. According to Singh et al. (2008), CNPs exhibit potent antioxidant activity that depends on particle size, composition, and surface area, and can protect brain culture neurons from free radical damage and β-amyloid 1-42 toxicity. Recently, Kwon et al. (2016) highlighted CNPs therapeutic candidacy to reduce oxidative stress in AD. Their study showed that conjugated CNPs were localized predominantly in mitochondria, reducing reactive gliosis and mitochondrial damage in the AD model. These results are, to some extent, coincide with our observations.

Taking into account the obtained results, we can conclude the next: the experiments have shown that the percentage of dead neurons in control and CNPs did not differ significantly, indicating low toxicity of CNPs to the hippocampal neurons. It was found that the introduction of CNPs significantly reduces the number of dead neurons in hippocampal culture with modeled AD. Thus, on the cultural model of AD, CNPs exhibited neuroprotective properties. Thus, the use of CNPs for neurological applications is very promising, such as creating new neuroprotective drugs for the treatment and prevention of neurodegenerative diseases of the brain based on the composition of CNPs. Therefore, the presented research in this brief report was to show the presence of the cerium effect itself. In our further studies, we will investigate the mechanisms of this protective effect of cerium in detail.

Conclusion

To sum up, our study investigated the potential of cerium dioxide nanoparticles (CNPs) to protect hippocampal neurons against beta-amyloid peptide (Aβ) induced toxicity, which is a hallmark of AD. Our results show that CNPs have low toxicity and are capable of protecting hippocampal neurons from Aβ-induced necrosis. Specifically, we found that introducing CNPs either after Aβ incubation or prophylactically incubating cells with CNPs before Aβ administration significantly reduced the percentage of necrotic cells. These findings suggest that CNPs may have neuroprotective properties that hold promise for developing new treatments for AD.

However, our study has some limitations. First, we used a cell culture model, which may not fully replicate the complexity of AD pathogenesis in the human brain. Second, we focused solely on the neuroprotective properties of CNPs and did not investigate their potential therapeutic effects on cognitive function in AD animal models or humans. Further studies are needed to explore CNPs full therapeutic potential, leading to the development of effective treatments for this devastating disease.

In conclusion, our study provides evidence of the potential of CNPs as a neuroprotective agent against Aβ-induced toxicity in neurons, highlighting their exciting possibilities in developing new treatments for AD. Further studies are needed to explore CNPs' full therapeutic potential, leading to the development of effective treatments for this devastating disease.

Data availability statement

The original contributions presented in this study are included in the article/**Supplementary material**, further inquiries can be directed to the corresponding author.

Ethics statement

The animal study was reviewed and approved by the Animal Ethics Committee of the Bogomoletz Institute of Physiology (Kyiv, Ukraine).

Author contributions

NR conducted the literature review and the first draft of manuscript writing and fulfilled confocal imaging experiments and analyses. VH fulfilled cell culturing, chemical treatments, tested amyloid, and fulfilled a stain of cells and making cell samples for fluorescent analysis. YK fulfilled part of confocal imaging experiments and data analyses. MS ensured the availability of nanoparticles and advised their use in experiments. EL fulfilled supervision, project administration, the studies' conceptualization, created the study design, image processing, contributed to manuscript revisions, and translation. All authors contributed to the article and approved the submitted version.

Funding

This work was partly supported from funds of National Academy of Sciences of Ukraine to support the development of priority areas of research SRN (State Registration Number) 0120U001281.

Conflict of interest

The authors declare that the research was conducted in the absence of any commercial or financial relationships that could be construed as a potential conflict of interest.

Publisher's note

Supplementary material

The Supplementary Material for this article can be found online at: https://www.frontiersin.org/articles/10.3389/fncel.2023.1131168/full#supplementary-material

References

Alzheimer's Disease International [ADI] (2019). *World Alzheimer Report 2019*. London: Alzheimer's Disease International.

Bailey, Z. S., Nilson, E., Bates, J. A., Oyalowo, A., Hockey, K. S., Sajja, V., et al. (2020). Cerium oxide nanoparticles improve outcome after in vitro and in vivo mild traumatic brain injury. *J. Neurotrauma* 37, 1452–1462. doi: 10.1089/neu.2016.4644

Celardo, I., Pedersen, J. Z., Traversa, E., and Ghibelli, L. (2011). Pharmacological potential of cerium oxide nanoparticles. *Nanoscale* 3, 1411–1420. doi: 10.1039/c0nr00875c

Chen, B. H., and Stephen Inbaraj, B. (2018). Various physicochemical and surface properties controlling the bioactivity of cerium oxide nanoparticles. *Crit. Rev. Biotechnol.* 38, 1003–1024. doi: 10.1080/07388551.2018.1426555

Chen, S., Hou, Y., Cheng, G., Zhang, C., Wang, S., and Zhang, J. (2013). Cerium oxide nanoparticles protect endothelial cells from apoptosis induced by oxidative stress. *Biol. Trace Elem. Res.* 154, 156–166. doi: 10.1007/s12011-013-9678-8

Coelho, B. P., Gaelzer, M. M., Dos Santos Petry, F., Hoppe, J. B., Trindade, V. M. T., Salbego, C. G., et al. (2019). Dual effect of doxazosin: Anticancer activity on SH-SY5Y neuroblastoma cells and neuroprotection on an in vitro model of Alzheimer's Disease. *Neuroscience* 404, 314–325. doi: 10.1016/j.neuroscience.2019.02.005

D'Angelo, B., Santucci, S., Benedetti, E., Loreto, S. D., Phani, R., Falone, S., et al. (2009). Cerium oxide nanoparticles trigger neuronal survival in a human Alzheimer Disease model by modulating BDNF pathway. *Curr. Nanosci.* 5, 167–176. doi: 10.2174/157341309788185523

Danish, S. M., Gupta, A., Khan, U. A., Hasan, N., Ahmad, F. J., Warsi, M. H., et al. (2022). Intranasal cerium oxide nanoparticles ameliorate cognitive function in rats with Alzheimer's via anti-oxidative pathway. *Pharmaceutics* 14:756. doi: 10.3390/pharmaceutics14040756

Haass, C., and Selkoe, D. J. (2007). Soluble protein oligomers in neurodegeneration: Lessons from the Alzheimer's amyloid beta-peptide. *Nat. Rev. Mol. Cell Biol.* 8, 101–112. doi: 10.1038/nrm2101

Heckert, E. G., Karakoti, A. S., Seal, S., and Self, W. T. (2008). The role of cerium redox state in the SOD mimetic activity of nanoceria. *Biomaterials* 29, 2705–2709. doi: 10.1016/j.biomaterials.2008.03.014

Heckman, K. L., DeCoteau, W., Estevez, A., Reed, K. J., Costanzo, W., Sanford, D., et al. (2013). Custom cerium oxide nanoparticles protect against a free radical mediated autoimmune degenerative disease in the brain. *ACS Nano* 7, 10582–10596. doi: 10.1021/nn403743b

Kravenska, E. V., Ganzha, V. V., Yavorskaya, E. N., and Lukyanetz, E. A. (2016). Effect of cyclosporin a on the viability of hippocampal cells cultured under conditions of modeling of Alzheimer's Disease. *Neurophysiology* 48, 246–251. doi: 10.1007/S11062-016-9595-5/METRICS

Kravenska, Y., Nieznanska, H., Nieznanski, K., Lukyanetz, E., Szewczyk, A., and Koprowski, P. (2020). The monomers, oligomers, and fibrils of amyloid-β inhibit the activity of mitoBK(Ca) channels by a membrane-mediated mechanism. *Biochim. Biophys. Acta Biomembr.* 1862:183337. doi: 10.1016/j.bbamem.2020.183337

Kwon, H. J., Cha, M. Y., Kim, D., Kim, D. K., Soh, M., Shin, K., et al. (2016). Mitochondria-targeting ceria nanoparticles as antioxidants for Alzheimer's Disease. *ACS Nano* 10, 2860–2870. doi: 10.1021/acsnano.5b08045

Lee, S. S., Song, W., Cho, M., Puppala, H. L., Nguyen, P., Zhu, H., et al. (2013). Antioxidant properties of cerium oxide nanocrystals as a function of nanocrystal diameter and surface coating. *ACS Nano* 7, 9693–9703. doi: 10.1021/nn4026806

Lord, M. S., Berret, J. F., Singh, S., Vinu, A., and Karakoti, A. S. (2021). Redox active cerium oxide nanoparticles: Current status and burning issues. *Small* 17:e2102342. doi: 10.1002/smll.202102342

Lukyanetz, E. A., Shkryl, V. M., Kravchuk, O. V., and Kostyuk, P. G. (2003a). Action of hypoxia on different types of calcium channels in hippocampal neurons. *Biochim. Biophys. Acta* 1618, 33–38. doi: 10.1016/j.bbamem.2003.10.003

Lukyanetz, E. A., Shkryl, V. M., Kravchuk, O. V., and Kostyuk, P. G. (2003b). Effect of hypoxia on calcium channels depends on extracellular calcium in CA1 hippocampal neurons. *Brain Res.* 980, 128–134. doi: 10.1016/s0006-8993(03)02951-2

Marchesi, V. T. (2011). Alzheimer's dementia begins as a disease of small blood vessels, damaged by oxidative-induced inflammation and dysregulated amyloid metabolism: Implications for early detection and therapy. *FASEB J.* 25, 5–13. doi: 10.1096/fj.11-0102ufm

Naz, S., Beach, J., Heckert, B., Tummala, T., Pashchenko, O., Banerjee, T., et al. (2017). Cerium oxide nanoparticles: A 'radical' approach to neurodegenerative disease treatment. *Nanomedicine (Lond)* 12, 545–553. doi: 10.2217/nnm-2016-0399

Nelson, B. C., Johnson, M. E., Walker, M. L., Riley, K. R., and Sims, C. M. (2016). Antioxidant cerium oxide nanoparticles in biology and medicine. *Antioxidants (Basel)* 5:15. doi: 10.3390/antiox5020015

Niu, J., Azfer, A., Rogers, L. M., Wang, X., and Kolattukudy, P. E. (2007). Cardioprotective effects of cerium oxide nanoparticles in a transgenic murine model of cardiomyopathy. *Cardiovasc. Res.* 73, 549–559. doi: 10.1016/j.cardiores.2006.11.031

Rybalko, S., Demchenko, O., Starosyla, D., Deriabin, O., Rudenko, L., Shcherbakov, O., et al. (2021). Nanoceria can inhibit the reproduction of transmissible gastroenteritis virus: Consideration for use to prevent and treat coronavirus disease. *Mikrobiol. Z.* 83, 67–75. doi: 10.15407/MICROBIOLJ83.05.067

Saifi, M. A., Seal, S., and Godugu, C. (2021). Nanoceria, the versatile nanoparticles: Promising biomedical applications. *J. Cont. Release* 338, 164–189. doi: 10.1016/j.jconrel.2021.08.033

Singh, N., Amateis, E., Mahaney, J. E., Meehan, K., and Rzigalinski, B. A. (2008). The antioxidant activity of cerium oxide nanoparticles is size dependant and blocks Aβ1-42-induced free radical production and neurotoxicity. *FASEB J.* 22:624.2. doi: 10.1096/fasebj.22.1_supplement.624.2

Stephen Inbaraj, B., and Chen, B. H. (2020). An overview on recent in vivo biological application of cerium oxide nanoparticles. *Asian J. Pharm. Sci.* 15, 558–575. doi: 10.1016/j.ajps.2019.10.005

Tarnuzzer, R. W., Colon, J., Patil, S., and Seal, S. (2005). Vacancy engineered ceria nanostructures for protection from radiation-induced cellular damage. *Nano Lett.* 5, 2573–2577. doi: 10.1021/nl052024f

Wong, L. L., and McGinnis, J. F. (2014). Nanoceria as bona fide catalytic antioxidants in medicine: What we know and what we want to know. *Adv. Exp. Med. Biol.* 801, 821–828. doi: 10.1007/978-1-4614-3209-8_103

Yadav, N. (2022). Cerium oxide nanostructures: Properties, biomedical applications and surface coatings. *3 Biotech* 12:121. doi: 10.1007/s13205-022-03186-3

Zand, Z., Khaki, P. A., Salihi, A., Sharifi, M., Qadir Nanakali, N. M., Alasady, A. A., et al. (2019). Cerium oxide NPs mitigate the amyloid formation of α-synuclein and associated cytotoxicity. *Int. J. Nanomed.* 14, 6989–7000. doi: 10.2147/ijn.S220380

frontiers | Frontiers in Cellular Neuroscience

TYPE Original Research
PUBLISHED 20 March 2023
DOI 10.3389/fncel.2023.1133400

OPEN ACCESS

EDITED BY
Dirk M. Hermann,
University of Duisburg-Essen, Germany

REVIEWED BY
Hong Il Yoo,
Eulji University, Republic of Korea
Behnam Ghorbanzadeh,
Dezful University of Medical Sciences (DUMS), Iran

*CORRESPONDENCE
Olha Lisakovska
✉ o.lisakovskaya@gmail.com

SPECIALTY SECTION
This article was submitted to Cellular Neuropathology, a section of the journal Frontiers in Cellular Neuroscience

RECEIVED 28 December 2022
ACCEPTED 28 February 2023
PUBLISHED 20 March 2023

CITATION
Lisakovska O, Labudzynskyi D, Khomenko A, Isaev D, Savotchenko A, Kasatkina L, Savosko S, Veliky M and Shymanskyi I (2023) Brain vitamin D_3-auto/paracrine system in relation to structural, neurophysiological, and behavioral disturbances associated with glucocorticoid-induced neurotoxicity. *Front. Cell. Neurosci.* 17:1133400. doi: 10.3389/fncel.2023.1133400

Brain vitamin D_3-auto/paracrine system in relation to structural, neurophysiological, and behavioral disturbances associated with glucocorticoid-induced neurotoxicity

Olha Lisakovska[1]*, Dmytro Labudzynskyi[1], Anna Khomenko[1], Dmytro Isaev[2], Alina Savotchenko[2], Ludmila Kasatkina[3], Serhii Savosko[4], Mykola Veliky[1] and Ihor Shymanskyi[1]

[1]Department of Biochemistry of Vitamins and Coenzymes, Palladin Institute of Biochemistry, Kyiv, Ukraine, [2]Department of Cellular Membranology, Bogomoletz Institute of Physiology, Kyiv, Ukraine, [3]Research Laboratory for Young Scientists, Palladin Institute of Biochemistry, Kyiv, Ukraine, [4]Department of Histology and Embryology, Bogomolets National Medical University, Kyiv, Ukraine

Introduction: Vitamin D_3 (VD_3) is a potent para/autocrine regulator and neurosteroid that can strongly influence nerve cell function and counteract the negative effects of glucocorticoid (GC) therapy. The aim of the study was to reveal the relationship between VD_3 status and behavioral, structural-functional and molecular changes associated with GC-induced neurotoxicity.

Methods: Female Wistar rats received synthetic GC prednisolone (5 mg/kg b.w.) with or without VD_3 (1000 IU/kg b.w.) for 30 days. Behavioral, histological, physiological, biochemical, molecular biological (RT-PCR, Western blotting) methods, and ELISA were used.

Results and discussion: There was no difference in open field test (OFT), while forced swim test (FST) showed an increase in immobility time and a decrease in active behavior in prednisolone-treated rats, indicative of depressive changes. GC increased the perikaryon area, enlarged the size of the nuclei, and caused a slight reduction of cell density in CA1-CA3 hippocampal sections. We established a GC-induced decrease in the long-term potentiation (LTP) in CA1-CA3 hippocampal synapses, the amplitude of high K^+-stimulated exocytosis, and the rate of Ca^{2+}-dependent fusion of synaptic vesicles with synaptic plasma membranes. These changes were accompanied by an increase in nitration and poly(ADP)-ribosylation of cerebral proteins, suggesting the development of oxidative-nitrosative stress. Prednisolone upregulated the expression and phosphorylation of NF-κB p65 subunit at Ser311, whereas downregulating IκB. GC loading depleted the circulating pool of $25OHD_3$ in serum and CSF, elevated VDR mRNA and protein levels but had an inhibitory effect on CYP24A1 and VDBP expression. Vitamin D_3 supplementation had an antidepressant-like effect, decreasing the immobility time and stimulating active behavior. VD_3 caused a decrease in the size of the perikaryon and nucleus in CA1 hippocampal area. We found a recovery in depolarization-induced fusion of synaptic vesicles and long-term synaptic plasticity after VD_3 treatment. VD_3 diminished the intensity of oxidative-nitrosative

stress, and suppressed the NF-κB activation. Its ameliorative effect on GC-induced neuroanatomical and behavioral abnormalities was accompanied by the 25OHD3 repletion and partial restoration of the VD_3-auto/paracrine system.

Conclusion: GC-induced neurotoxicity and behavioral disturbances are associated with increased oxidative-nitrosative stress and impairments of VD_3 metabolism. Thus, VD_3 can be effective in preventing structural and functional abnormalities in the brain and behavior changes caused by long-term GC administration.

KEYWORDS

glucocorticoids, glucocorticoid-induced neurotoxicity, prednisolone, vitamin D_3, vitamin D-auto/paracrine system, oxidative-nitrosative stress, behavioral impairments

1. Introduction

Naturally occurring glucocorticoids (GCs) and their synthetic analogs, such as prednisolone and dexamethasone, are known to be widely used in medical practice due to their anti-inflammatory, desensitizing, immunosuppressive, and antiallergic properties (Cooper, 2012). However, long-term GC supplementation for the treatment of arthritis, asthma, chronic obstructive pulmonary disease and, especially now, COVID-19 increases the risk of developing a number of adverse complications, including their significant toxic effects on the central nervous system (CNS) (Alan and Alan, 2017). GC-induced neurotoxicity manifests itself in the form of impaired motor and sensory functions, emotional status, as well as integrative functions of the brain, such as memory and learning. These effects are predominantly, but not exclusively, mediated by dysfunction of the hippocampus as this structure is highly sensitive to glucocorticoids (Conrad, 2008). For example, elevated levels of GCs have been shown to cause atrophy of dendritic processes in the CA3 region, loss of hippocampal neurons, and increased neuronal damage in pathological conditions such as seizures and stroke (Patil et al., 2007; Tata and Anderson, 2010). In addition, possible mechanisms of the neurotoxic effect of GC include disruption of GR-associated signaling pathways, cross-links between transcription factors, glucocorticoid receptor (GR) polymorphisms, effects on DNA methylation and other molecular networks involved in switching between autophagy/apoptosis, mitophagy, proliferation/cell differentiation. The target effect of glucocorticoids also covers the functioning of the blood–brain barrier (BBB), astrocytes, microglia, neurons and their dendritic architecture (Obradovic et al., 2006; Fietta et al., 2009; Kim et al., 2010; Kadmiel and Cidlowski, 2013; Sorrells et al., 2014). It is known that GCs can block transendothelial transport of glucose in the CNS, as well as its uptake by hippocampal neurons and glial cells (Horner et al., 1990), thereby disrupting energy metabolism in the brain and affecting the basic functions of neurons. In addition, the negative effects of GCs may be associated with their ability to potentiate the excitotoxic effects of glutamate and reduce the inhibitory effect of GABA in the CNS (Di et al., 2009). However, there have been conflicting data from animal models showing that the glucocorticoid dexamethasone has both neuroprotective and neurotoxic effects in a dose- and time-dependent manner (Abrahám et al., 2001; Lear et al., 2014). These conflicting data raise the question of the known degree of caution in the therapeutic use of glucocorticoids.

Currently, there is no complete clarity regarding the nature of GC-associated changes in the CNS, and the molecular mechanisms underlying the development of GC-induced structural and functional abnormalities in the CNS, cognitive and behavioral disorders are poorly understood. In this regard, difficulties may arise in solving the urgent biomedical problem of finding the most effective pharmacological approaches for the correction and/or prevention of GC-induced neurotoxicity.

Vitamin D_3 (VD_3, cholecalciferol) has previously been shown to play an important role as a para- and autocrine neurosteroid that modulates multiple CNS functions, including brain development, neurotransmission, neuroprotection, and immunomodulation (Kalueff and Tuohimaa, 2007). VD_3 can easily cross the BBB (Won et al., 2015) and realize its biological action in the brain through its own vitamin D_3-auto/paracrine system (Cui et al., 2017), which consists of several major components. Vitamin D_3 receptor (VDR) is a key player that binds the hormonally active form of VD_3, 1,25-dihydroxyvitamin D_3 ($1,25(OH)_2D_3$, calcitriol). The VDR is a member of the nuclear receptor superfamily and is present in both the developing and adult brains. In the brain of adult rats, VDR is found in neurons, astrocytes (Brown et al., 2003), and oligodendrocytes (Baas et al., 2000) of various brain areas. 25-hydroxyvitamin D_3 ($25OHD_3$) is considered to be the main transport form of VD_3 and its storage metabolite delivered to body cells via vitamin D-binding protein (VDBP) (Shymanskyi et al., 2020). $1,25(OH)_2D_3$ can be synthesized and metabolized locally in the CNS from $25OHD_3$. This process is provided by 25-hydroxyvitamin D_3 1a-hydroxylase (CYP27B1), which is found in neurons and glial cells (Landel et al., 2018). Another important component of the VD_3-auto/paracrine system is 1,25-dihydroxyvitamin D_3 24-hydroxylase (CYP24A1), an enzyme that catabolizes $1,25(OH)_2D_3$ to inactive $1,24,25(OH)_3D_3$ followed by conversion to calcitroic acid. Thus, a tight balance between the VD_3 metabolism enzymes plays a pivotal role in maintaining an appropriate local level of $1,25(OH)_2D_3$ for brain function. We have previously shown that chronic administration of GCs is accompanied by the development of a profound VD_3 deficiency (Shymans'kyĭ et al., 2014). It is mainly due to impaired $25OHD_3$ synthesis in the liver as a result of a simultaneous increase

in hepatocellular necrosis and caspase-3-dependent apoptosis (Lisakovska et al., 2017). However, it remains an open question to what extent VD_3 deficiency may exacerbate glucocorticoid toxicity in the CNS.

In addition, many psychiatric and neurological diseases, including multiple sclerosis (Smolders et al., 2013), schizophrenia (Cui et al., 2021), Parkinson's disease (Fullard and Duda, 2020), diabetic peripheral neuropathy (Xiaohua et al., 2021), and other age-related neurological outcomes (Berridge, 2017) correlate with low plasma levels of $25OHD_3$, suggesting that adequate VD_3 levels may prevent, cure, or at least alleviate some mental disorders. Therefore, in the context of understanding the role of vitamin D_3 in the functioning of the CNS, both under normal and diseased conditions, it is important to establish whether chronic administration of GCs can affect the circulating pool of VD_3 and alter the ratio of the main components of the VD_3-auto/paracrine system, as well as to what consequences these changes at the molecular, cellular, functional and behavioral levels can lead to.

Given all of the above, the aim of the study was to identify the relationship between vitamin D status and behavioral, structural, functional, and molecular changes associated with neurotoxicity caused by the synthetic glucocorticoid prednisolone in experimental rats. For the fullest characterization of vitamin D status in animals, we measured the circulating pool of VD_3 (serum and cerebrospinal fluid (CSF) levels of 25-hydroxyvitamin D_3), local $25OHD_3$ content in brain tissues, and the levels of major components of VD_3-auto/paracrine system in the brain tissue—VDR, VDBP, CYP27B1, and CYP24A. To evaluate behavioral changes associated with prednisolone and vitamin D_3 administration, we performed the forced swim test (FST), open-field test (OFT), elevated plus maze (EPM), and conditioned fear test. Histological changes were examined by staining the hippocampus, cortex, thalamus, and cerebellum with hematoxylin-eosin (H&E) or toluidine blue. At a functional level, we performed recording of an array of microelectrodes of hippocampal networks to study long-term synaptic plasticity (LTP). Depolarization-induced exocytosis in isolated nerve endings of the rat brain and the rate of fusion of synaptic vesicles with plasma membranes were also detected. To complete a comprehensive study of the mechanisms of neuroprotective action of vitamin D_3 under glucocorticoid toxic load, we finally evaluated molecular changes at the level of GR, nuclear factor κB (NF-κB) p65 subunit and its phosphorylated form (at Ser 311), NF-κB inhibitor (IκB), poly(ADP-ribose)polymerase-1 (PARP-1), covalent protein modifications as the markers of oxidative-nitrosative and genotoxic stress (poly(ADP)-ribosylated (PAR), carbonylated and nitrated proteins) in brain tissue.

2. Materials and methods

2.1. Animals and general experimental design

Female Wistar rats (100 ± 5 g) were housed at the Animal Facility of the Palladin Institute of Biochemistry with free access to a standard rodent diet and drinking water *ad libitum*. Animals were kept in a temperature-controlled room and exposed to a daily 12/12 h light/dark cycle. The general scheme of animal experimental design and timescale are shown in **Figure 1**. After acclimatization for 1 week, the rats (n = 60) were randomly divided into three experimental groups: (1) the control group (n = 20); (2) the group that received the synthetic glucocorticoid prednisolone (5 mg/kg of body weight, *per os*, 30 days, n = 20); (3) the group that received prednisolone (5 mg/kg of body weight) and vitamin D_3 (1,000 IU/kg of body weight, *per os*, 30 days, n = 20). Glucocorticoid prednisolone (30 mg/ml) was purchased from Biopharma (Ukraine) and was solved in the purified water for injections for further oral administration to rats. Vitamin D_3 (cholecaciferol, Sigma-Aldrich, USA, C9756) was administered to rats as oil solution. At the end of the experimental treatment, the rats were anesthetized by intraperitoneal injection of chloral hydrate (40 mg/100 g of body weight), decapitated with a guillotine, and blood was taken from the inferior *vena cava*. The brain was quickly dissected and transferred to the appropriate buffer depending on the following procedures. All samples that were not used immediately were stored at −80°C.

2.2. Ethical statement

We performed all animal procedures in accordance with the protocols approved by the Animal Care Ethics Committee of the Palladin Institute of Biochemistry (Protocol #1, 26/01/2018), adopted on the basis of national and international directives and laws relating to animal welfare: European Convention for the protection of vertebrate animals used for experimental and other scientific purposes (Strasbourg, France; 1986), Bioethical expertise of preclinical and other scientific research conducted on animals (Kyiv, Ukraine; 2006).

2.3. Behavioral procedures

2.3.1. Open-field test (OFT)

The rats were examined in a testing apparatus (1.0 × 1.0 m polypropylene box with 0.5 m-height walls) with a floor divided into 25 equal squares. The box was illuminated with white light (60 lx) during testing. Animals were individually placed in a corner of the box and allowed to freely explore the environment for 10 min. The following parameters were evaluated: the total distance traveled (mm/10 min), the time spent on 9 internal and 16 outer arena squares.

2.3.2. Forced swim test (FST)

Forced swim test was performed according to the modified protocol described here (Slattery and Cryan, 2012). During the pretest (Day 1), rats were placed individually into the swimming cylinder (1.0 m height, 0.3 m diameter, with 0.5 m of warm water, +25°C) and left to swim for 15 min, then removed from water, dried with a towel and returned to the home cages. Twenty-four hours after the pre-test, the rats were individually forced to swim inside a vertical Plexiglas cylinder containing 0.5 m of water (+25°C). The camera was placed directly above the swimming cylinder and video recording was started before the rats were placed into the cylinder. After 5 min in the water, the rats were removed and allowed to dry for 20 min before being returned to

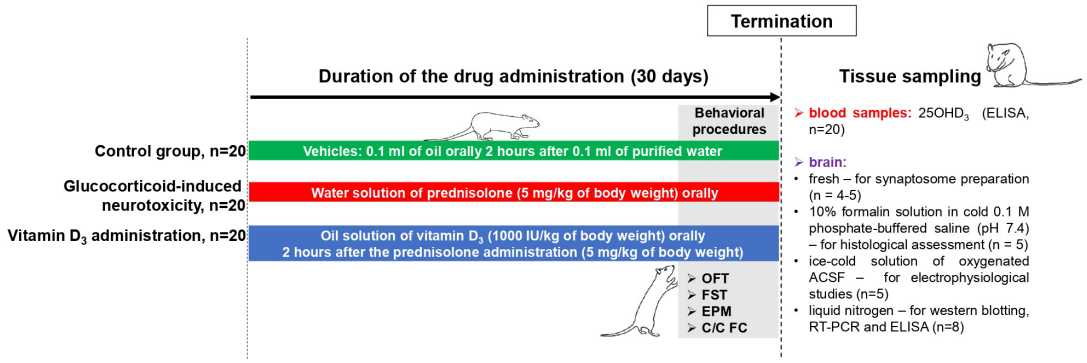

FIGURE 1
Schematic representation of the experimental design and timescale. Each experimental group included 20 animals: (1) The control group that received purified water (0.1 ml) and oil solution (0.1 ml) as vehicles; (2) the group with glucocorticoid-induced neurotoxicity, in which rats received orally the water solution of synthetic glucocorticoid prednisolone (Biopharma, Ukraine) at a dose of 5 mg/kg of body weight (30 days) and additionally oil solution (0.1 ml) as vehicle; (3) the group that received the oil solution of vitamin D_3 (Sigma-Aldrich, USA, C9756) at a dose of 1,000 IU/kg of body weight *per os* (30 days) on the background of prednisolone administration (5 mg/kg of body weight). Behavioral procedures (OFT, open-field test; FST, forced swim test; EPM, elevated plus maze; C/C FC, contextual/cued fear conditioning test) were performed during 3 days before the decapitation with the concurrent drug administration (n = 8 per group). At the end of the experimental treatment, the rats were anesthetized by an intraperitoneal injection of chloral hydrate (40 mg/100 g of body weight), decapitated with a guillotine. Blood samples were taken from the inferior *vena cava* to measure $25OHD_3$ by ELISA (n = 20 per group). The whole brain was quickly dissected and was used fresh (for synaptosome preparation, n = 4–5) or transferred into the appropriate buffer depending on the procedures: 10% formalin solution in cold 0.1 M phosphate-buffered saline (pH 7.4)—for histological assessment (n = 5 per group); an ice-cold solution of oxygenated (95% O_2, 5% CO_2) artificial cerebrospinal fluid (ACSF) solution (119 mM NaCl, 2.5 mM KCl, 2.0 mM $CaCl_2$, 1.3 mM $MgCl_2$, 26 mM $NaHCO_3$, 1.0 mM NaH_2PO_4, 11 mM glucose, pH 7.35)—for electrophysiological studies (n = 5 per group); and a liquid nitrogen—for western blotting, RT-PCR and ELISA (n = 8 per group).

their home cages. In the subsequent analysis, we defined the times for "immobile" (immobility), "mobile" (swimming), and "highly mobile" (climbing) behavior.

2.3.3. Elevated plus maze (EPM)

The EPM apparatus consisted of two opposite open arms (0.5 m × 0.1 m) and two closed arms (0.5 m × 0.1 m × 0.4 m) raised to a height of 0.5 m above the floor. The junction area of the four arms (central platform) was 0.1 m × 0.1 m. Lighting in the maze was 30 lx. For the EPM test, each animal was placed on the central platform of the maze facing one of the open arms. Total distance traveled, number of open arm entries, and time spent in open arms were assessed over a 5-min period. In the EPM, anxiety levels were measured by comparing the amount of time spent in the open arms to total time.

2.3.4. Contextual/Cued fear conditioning test

2.3.4.1. Conditioning apparatus

A conditioning box (45 cm × 45 cm × 40 cm; custom-made) with an electric grid floor was located in a sound-attenuating chamber (50 cm × 80 cm × 60 cm) to reduce external noise and visual stimulation. After each test, the conditioning box was cleaned with water containing a small amount of neutral-smelling detergent. The behavior of the rats was recorded through the side wall of the conditioning box with a camera attached to the inner roof of the chamber. The light, tone, and foot shock in the conditioning box were controlled by the custom-made software.

2.3.4.2. Contextual/Cued fear conditioning procedure

The contextual/cued fear conditioning test was performed for three consecutive days as reported previously, with some modifications (Bogovyk et al., 2017). One day prior to fear-conditioning learning (Day 1), each rat was habituated to the experimental chamber for 10 min. On Day 2 (training day), the animals were placed in the same chamber for contextual fear-conditioning training. After 60 s of free exploration, an auditory tone cue (70 dB, 10 kHz, 20 s) was presented followed by a mild foot shock (0.5 mA, 0.5 s), three tone-foot shock pairings with a 2-min interstimulus interval were applied. After the shock, the animal remained in the experimental chamber for another 60 s. On Day 3 (24 h after the previous session; testing day), the rats were subjected to a similar procedure, except that the foot shock was not given. Duration of freezing (no movement for at least 1 s) was measured during the last 20 s before the onset of an auditory tone (contextual fear conditioning) and during the tone (cued fear conditioning) twice, on the training and testing days. Spontaneous freezing refers to freezing within 20 s before the onset of an auditory tone during the training session.

2.4. Histological assessment of the structure of hippocampus, prefrontal cortex, cerebellum, and thalamus

For histological examination, rat brains were fixed in 10% formalin solution in cold 0.1 M phosphate-buffered saline (PBS, pH 7.4), dehydrated in increasing concentrations of ethanol, and embedded in paraffin (Leica-Paraplast Regular, 39601006, Leica Biosystems Inc., USA) according to the standard procedure. Paraffin sections 5 μm thick were prepared on a Thermo Microm HM 360 Rotary microtome (Microm GmbH, Germany). Sections were deparaffined in xylene and then rehydrated in decreasing concentrations of ethanol (100%, 95%, 80% and 70%) and distilled water, followed by staining for 5 min with 0.05% toluidine blue (pH 4.5) using the Nissl technique (García-Cabezas et al., 2016)

or hematoxylin and eosin (H&E; 3 min for hematoxylin and 45 s for eosin). Ten sections from hippocampus, prefrontal cortex, cerebellum, and thalamus of each animal were taken in a systematic randomized manner and covered with Histofluid coverslips (6900002, Paul Marienfeld EN, Germany). The sections were examined under a light microscope (Olympus BX 51, Japan) at ×400 magnification. Digital photographs were taken using CarlZeiss software (AxioVision SE64 Rel.4.9.1). The cells with morphological signs of cytolysis, hyperchromatosis, karyolysis, and karyopyknosis were considered affected.

2.5. Synaptosome preparation and isolation of synaptic vesicles from rat brain

Purified synaptosomes were obtained from Wistar rat brains by the differential centrifugation (Kasatkina et al., 2018) using Ficoll-400 density gradient centrifugation of crude samples. Synaptosomes were used within 2–4 h after isolation.

Synaptic vesicles (SVs) were isolated from the cerebral hemispheres according to the following method (De Lorenzo and Freedman, 1978). Crude (unpurified) synaptosomes were lysed with a buffer containing 1 mM EGTA, 10 mM Tris-HCl, pH 8.1 (3 ml/g of brain tissue) and then incubated at +4°C for 60 min. The samples were centrifuged at 20,000 *g* for 30 min, followed by the next supernatant centrifugation step at 55,000 *g* for 60 min. The last centrifugation step was carried out at 130,000 *g* (+4°C, 60 min) to obtain the SVs fraction (pellet) and the synaptosomal fraction of cytosolic proteins (supernatant). The SV pellet was resuspended in 10 mM Tris-HCl (pH 7.5). The purity of the SV fraction was assessed by measuring the activity of Na^+/K^+-ATPase, a plasma membrane marker that was not detected in the purified SV fraction.

2.6. Depolarization-induced exocytosis from isolated nerve terminals

The isolated synaptic terminals (synaptosomes) were preincubated at +37°C for 10 min and fluorescence (F) was measured on a Hitachi 650-10S spectrofluorimeter (Japan) at excitation and emission wavelengths of 490 and 530 nm (2 nm slit), respectively. High K^+ (35 mM) depolarization of the plasma membrane was achieved in Ca^{2+}-containing medium at the steady-state of acridine orange (AO) fluorescence. The traces were normalized to the similar data in the absence of synaptosomes:

$$F = F_t/F_0,$$

where F_0 is the fluorescence intensity measured upon AO quenching in the solution, and F_t is the fluorescence intensity of AO in the presence of synaptosomes.

2.7. Synaptic vesicle fusion with plasma membranes in cell-free system

We employed the octadecyl rhodamine B chloride (R18) technique to detect SV fusion with target synaptic plasma membranes. The fusion was recorded on a Hitachi 650-10S spectrofluorimeter (Japan) in a suspension of R18-labeled SVs (1 nmol/240 μg of synaptosomal protein) and unlabeled plasma membranes in a ratio of 1:8 (according to protein concentration) after addition of Ca^{2+} (Trikash et al., 2010). An increase in the fluorescence signal was recorded as a result of membrane fusion and R18 dequenching. To quantify the probe dilution during the fusion of vesicles with target membranes, the initial fluorescence signal of R18-labeled SVs (I_o) was measured. The time-dependent dequenching of the fluorescence signal (I) was recorded within 4 min after the start of testing. At the end of each experiment, $C_{12}E_8$ detergent was added to the reaction mixture at a final concentration of 0.1%, at which the maximum value (Id) of the dequenched fluorophore signal was obtained. The fusion rate at any given time is proportional to the percentage of fluorescence dequenching (%FD) and thus can be calculated as:

$$\%FD = 100\,(I - I_o) / (I_d - I_o)$$

2.8. Electrophysiology

2.8.1. Isolation of the rat hippocampal sections and slice preparation

For electrophysiological studies, experimental rats were deeply anesthetized with diethyl ether followed by decapitation. The brain was carefully removed from the skull and placed in a Petri dish filled with an ice-cold solution of oxygenated (95% O_2, 5% CO_2) artificial cerebrospinal fluid (ACSF) solution (119 mM NaCl, 2.5 mM KCl, 2.0 mM $CaCl_2$, 1.3 mM $MgCl_2$, 26 mM $NaHCO_3$, 1.0 mM NaH_2PO_4, 11 mM glucose, pH 7.35). The cerebellum was dissected with a surgical blade and a median sagittal incision was made separating the cerebral hemispheres. The hippocampus was carefully separated from the surrounding tissues and placed in a pre-prepared agar block (3.7% agar). The agar blocks with hippocampi were glued to the surface of a vibrotome plate (SYS-NVLS, World Precision Instr., USA) to ensure its reliable fixation during sectioning. The slice thickness was 400 μm. After preparation, hippocampal sections were placed in an incubation chamber with oxygenated ACSF (+26°C) for 1.5–2 h.

2.8.2. Electrophysiological studies

Extracellular recordings were performed on freshly isolated slices of the hippocampus. The slices were transferred to a submersion-type thermostatic chamber (Warner Instrument Corp., USA), where the sections were continuously perfused with oxygenated ACSF at a rate of 2–4 ml/min (+30–32°C). The stimulating and recording electrodes were placed on the slice surface at a distance of approximately 400 μm from each other. The synaptic response was induced by stimulating the Schaffer collaterals using a concentric bipolar stimulating electrode and an isolated stimulation unit (ISO-Flex, AMPI, Israel). Recording of the extracellular field potential (fEPSP) was performed from the hippocampal CA1 *striatum radiatum* layer using glass microelectrodes (resistance of 1–3 MΩ when filled with ACSF) and a patch-clamp amplifier (RK-400, Bio-Logic Science Instruments, Grenoble, France). Recordings were digitized using

an analog-to-digital converter (NI PCI-6221, National instruments, Austin, TX, USA) and stored on a computer running WinWCP software (Strathclyde Electrophysiology Software, University of Strathclyde, Glasgow, UK). For the baseline recording (0.33 Hz for 10 min), the stimulus intensity was set to elicit field excitatory postsynaptic potential (fEPSP) that was approximately 30–40% of the maximum response. To induce long-term plasticity (LTP), high-frequency tetanic stimulation (HFS) of 100 pulses at a frequency of 100 Hz was delivered at a baseline stimulation intensity. LTP was assessed by averaging the synaptic response from 30 to 40 min after HFS. LTP studies were carried out on 12 slices (7 animals) in the control group, 12 slices (6 animals) in the prednisolone-supplemented group, and 12 slices (5 animals) in the VD_3-supplemented group. No more than three slices per animal were used. Offline data analysis was performed using Prism 6 (GraphPad, La Jolla, CA, USA), and Origin 7.5 (OriginLab, Northampton, MA, USA) software. Statistical comparison of changes in synaptic response was performed by measuring the initial slope of fEPSP. For LTP analysis, data from each experiment were normalized to baseline.

2.9. RNA isolation and real-time PCR

Total RNA was isolated from rat brain using the innuPREP RNA Mini Kit (Analytik Jena AG, Germany). The mRNA concentration was determined on a DS-11 Spectrophotometer/Fluorometer (DeNovix, USA). The Maxima H Minus First Strand cDNA Synthesis Kit (Thermo Fisher Scientific Inc., USA) was used to synthesize cDNA samples for subsequent RT-PCR on a Standard real-time PCR Thermal Cycler (Analytik Jena AG, Germany). Specific primer sequences for *Vdr*, *Vdbp*, *Cyp27b1*, *Cyp24a1*, *Nf-κb*, *Iκb-alpha*, and the glyceraldehyde 3-phosphate dehydrogenase (*Gapdh*) reference gene were designed using Primer BLAST software and used at a working concentration of 10 μM:

Gene	Forward 5′→3′	Reverse 5′→3′
Vdr	TCATCCCTACTGTGTCCCGT	TGAGTGCTCCTTGGTTCGTG'
Vdbp	AAACCCTTAGGGAATGCTGC	TTTTGTCCTCAGTCGTTCCG
Cyp27b1	TGGGTGCTGGGAACTAACCC	TCGCAGACTGATTCCACCTC
Cyp24a1	TTCGCTCATCTCCCATTCGG	TTGCTGGTCTTGATTGGGGT
Gapdh	TGAACGGGAAGCTCACTGG	TCCACCACCCTGTTGCTGTA
Nf-κb	GTACTTGCCAGACACAGACGA	CTCGGGAAGGCACAGCAATA
Iκb-alpha	TGAAGTGTGGGGCTGATGTC	AGGGCAACTCATCTTCCGTG

Target genes were amplified for 60 cycles using Maxima SYBER Green/ROX qPCR Master Mix (Thermo Fisher Scientific Inc., USA). Relative mRNA expression calculations were performed according to the $2^{-\Delta\Delta Ct}$ comparison method. The expression level of each gene was normalized for GAPDH in the same samples and then calculated as a fold change compared to the control.

2.10. Western blot analysis

Using Western blotting, we measured the following protein levels in total brain tissue lysates. First, VDR was examined to evaluate the effect of chronic administration of prednisolone on the main component of the vitamin D auto/paracrine system. 3-Nitrotyrosine, carbonylated and poly(ADP)-ribosylated proteins (PAR), as well as PARP-1 attracted our attention as reliable markers of oxidative-nitrosative and genotoxic stress in brain tissue. Finally, the glucocorticoid receptor (GR), NF-κB p65 phosphorylated at Ser311, and IκB were measured to characterize the relationship of VDR and GR with NF-κB transcriptional activity. Total protein extracts were prepared from frozen brain tissue according to a standard protocol using RIPA buffer (20 mM Tris-HCl, pH 7.5; 150 mM NaCl; 1% Triton X-100; 1 mM EGTA; 0.1% SDS; 1% sodium deoxycholate; 10 mM sodium pyrophosphate) and a protease inhibitor cocktail (PIC, Sigma, USA), and then the samples were sonicated and centrifuged. The supernatants were stored at −80°C until required. Lysate samples containing 60 μg of protein were subjected to sodium dodecyl sulfate polyacrylamide gel electrophoresis (SDS-PAGE) using a 10–15% gel followed by protein transfer to a nitrocellulose membrane. The membrane was then blocked for 1 h with 5% skimmed milk diluted in Tris-buffered saline with Tween (TBST, 150 mM NaCl, 10 mM Tris-HCl, and 0.1% Tween; pH 7.5) and incubated overnight at +4°C with one of the following primary antibodies (VDR: 1:200, sc-13133, Santa Cruz; 3-nitrotyrosine: 1:2,500, #05-233, Merck Millipore; carbonylated proteins: 1:1,000, ab-178020, Abcam; poly(ADP)-ribosylated proteins: 1:1,000, 4335-MC-100_AC, Trevigen; PARP-1: 1:1,000, #9542, Cell Signaling; GR: 1:250, sc-1004, Santa Cruz; NF-κB p65 phosphorylated at Ser 311: 1:200, sc-33039, Santa Cruz; and IκB-α: 1:1,000, sc-847, Santa Cruz). Subsequently, the membrane was thoroughly rinsed and incubated for 1 h with secondary antibodies: anti-rabbit IgG (H + L)-HRP conjugate (1:4,000, #1721019, Bio-Rad) or anti-mouse IgG (Fab Specific)-Peroxidase (1:2,500, A9917, Sigma) at room temperature. Thereafter, the membrane was developed with chemiluminescent agents: p-coumaric acid (Sigma, USA) and luminol (AppliChem GmbH, Germany). Target protein immunoreactive signals were quantified by densitometry and values were adjusted for the corresponding β-actin level (1:10,000, A3854, Sigma). Immunoreactive bands were quantified using Gel-Pro Analyzer v3.1 software.

2.11. ELISA 25-hydroxyvitamin D_3 assay

Using a commercial ELISA kit «25-OH-Vitamin D_3» (Immunodiagnostics, Germany), in accordance with the manufacturer's instructions, the VD_3 status was assessed by determining the concentration of 25-hydroxyvitamin D_3 in the serum, cerebrospinal fluid and brain homogenate of rats. Cerebrospinal fluid was obtained by puncture of the atlanto-occipital space. Brain homogenates were prepared from frozen brain tissue (100 mg) that was ground in a porcelain mortar with liquid nitrogen, lysed in PBS with 1% Tween-20 (pH 7.4), then sonicated and incubated on ice for 2 h. Next, the samples were centrifuged at 14,000 *g* for 20 min at +4°C. The supernatant was

carefully collected and aliquots were stored at −20°C avoiding thawing/freezing.

2.12. Statistics

The results of all experiments were expressed as the mean ± standard deviation for at least seven rats per group. The hypothesis about the normality of data distribution was tested using the Shapiro–Wilk test. Differences between means were estimated using the ANOVA followed by Tukey's *post hoc* test. To compare difference between groups in neuronal morphometric parameters, statistical significance was determined using a two-tailed unpaired Student's *t*-test. For behavioral data, the non-parametric Kruskal–Wallis test was used, if necessary, followed by Dunn's *post hoc* test. The significance criterion was $p \leq 0.05$. Statistical analysis was performed using Origin Pro 8.5 software (OriginLab Corporation, Northampton, MA, USA). For behavioral datasets, statistical significance was analyzed using the Origin 9 and Graph Pad Prism 6 software.

3. Results

3.1. Effect of prednisolone and vitamin D_3 on brain-to-body weight ratio

The brain-to-body weight ratio is commonly used in neurotoxicity studies to estimate the presence of general morphopathological changes in the brain. As can be seen from Table 1, the administration of prednisolone slowed down the growth of rats and reduced the average body weight by 70.65% compared with the control group (Tukey's test, $p = 0.000051$), while there was no significant difference in the average brain mass between the two groups (Table 1, Tukey's test, $p > 0.05$). An assessment of the brain-to-body weight ratio revealed that GC slightly increased it by 29.04% compared with the control group (Tukey's test, $p = 0.0031$). Treatment with VD_3 enhanced mean body weight by 15.97% compared with the prednisolone group (Tukey's test, $p = 0.033$), however, it did not lead to any ameliorative effect on the brain-to-body weight ratio compared with the prednisolone group (Tukey's test, $p > 0.05$).

3.2. Vitamin D_3 status and the state of VD_3-auto/paracrine system in brain after prednisolone administration and effect of vitamin D_3 treatment

In the context of the essential role of vitamin D_3 for the CNS functioning, the question arose whether chronic GC treatment could affect the circulating VD_3 pool and alter the content of the main components of the VD_3-auto/paracrine system. First, we measured the level of 25-hydroxyvitamin D_3 as a reliable marker of VD_3 bioavailability in serum, cerebrospinal fluid, and brain homogenates. Figure 2A shows a pronounced drop in $25OHD_3$ in the serum of rats supplemented with GC (by 3.24-fold, up to 30.00 ± 3.04 nmol/L) compared with the control animals (97.23 ± 7.01 nmol/L, Tukey's test, $p = 0.000001$). In the CSF, we observed half the content of $25OHD_3$ in the prednisolone group (16.00 ± 2.05 nmol/L) than in the control group (33.00 ± 2.50 nmol/L, Figure 2A). Finally, depletion of the circulating VD_3 pool was correlated with a significant decrease in the $25OHD_3$ level in the brain tissue extracts, indicating impaired bioavailability of the VD_3-prohormone in the nervous tissue. Figure 2B demonstrates that the $25OHD_3$ level after prednisolone supplementation was 8.64 ng/g brain tissue compared to 18.60 ng/g brain tissue in the control animals, representing a 2.15-fold decrease (Tukey's test, $p = 0.022$).

Vitamin D_3 supplementation caused a partial restoration of the $25OHD_3$ content. To a greater extent, the normalizing effect concerned the serum, where the $25OHD_3$ level rose to 111.43 ± 13.17 nmol/L and there was no significant difference with the control group. In the CSF, we also observed a tendency to restore the level of $25OHD_3$, the value of which reached 22 ± 3.1 nmol/L. This is 37.5% higher than in the prednisolone group. The $25OHD_3$ level also increased in the brain extract to 12.88 ± 0.9 ng/g of tissue, which was 49% higher than in the prednisolone group (Tukey's test, $p = 0.042$), but remained still lower (by 44.4%) than in the control. Collectively, these data indicate a profound GC-induced VD_3 deficiency and depletion of the circulating VD_3 pool under the influence of prednisolone, however, vitamin D_3 treatment may partially restore the circulating VD_3 pool, suggesting that this abnormality is reversible.

Since the hormonally active form of VD_3 in different cell types exerts its biological action through specific receptors for $1,25(OH)_2D_3$ – VDR, we also examined the VDR expression in the brain at the transcriptional and translational levels (Figures 2C, D). It was shown that after prednisolone administration, the level of *Vdr* mRNA in the brain increased by 6.45 times (Tukey's test, $p = 0.000003$) (Figure 2D). We further confirmed an increase in VDR protein by western blot (Figures 2C, D), which was 41% higher than in the control group (Tukey's test, $p = 0.005$). In turn, a strong reducing effect of VD_3 on the expression of *Vdr* mRNA (by 2.14-fold, Tukey's test, $p = 0.000001$) and protein (by 3.44-fold, Tukey's test, $p = 0.000002$) was found compared with the prednisolone group.

Despite the observed disturbances in the VDR expression, the next question arises whether prednisolone is able to affect the VD_3 transport. VDBP is considered to be the major plasma transporter for all VD_3 metabolites; however, its function in the brain is not fully understood. Therefore, we examined the level of *Vdbp* mRNA and found that prednisolone caused a 42%-lowering effect (Tukey's test, $p = 0.002$) compared to the control, while VD_3 supplementation restored its level to the control value (Figure 2E).

To complete this part of the study, we focused on enzymes involved in VD_3 metabolism and considered important factors that contribute to the proper functioning of the VD_3-auto/paracrine system. As presented in Figure 2F, prednisolone induced a significant (5.46-fold, Tukey's test, $p = 0.00002$) increase in *Cyp27b1* mRNA expression in the brain compared with the control animals, which may reflect a compensatory response of the VD_3-auto/paracrine system to the lack of circulatory and brain levels of $25OHD_3$. Vitamin D_3 treatment reduced *Cyp27b1* gene expression to a level that was 9.72-fold lower than in the prednisolone group

TABLE 1 Effect of prednisolone and vitamin D_3 administration on brain-to-body weight ratios in rats (M ± m, n = 20).

Groups	Control	Prednisolone	Prednisolone + vitamin D_3
Terminal body weight (g)	241.90 ± 9.16	170.90 ± 6.64*	198.20 ± 5.39*#
Brain weight (g)	1.676 ± 0.054	1.535 ± 0.057	1.637 ± 0.052
Brain-to-body weight ratio (%)	0.699 ± 0.031	0.903 ± 0.026*	0.828 ± 0.022*

*$p < 0.05$ vs. control.
#$p < 0.05$ vs. prednisolone administration.

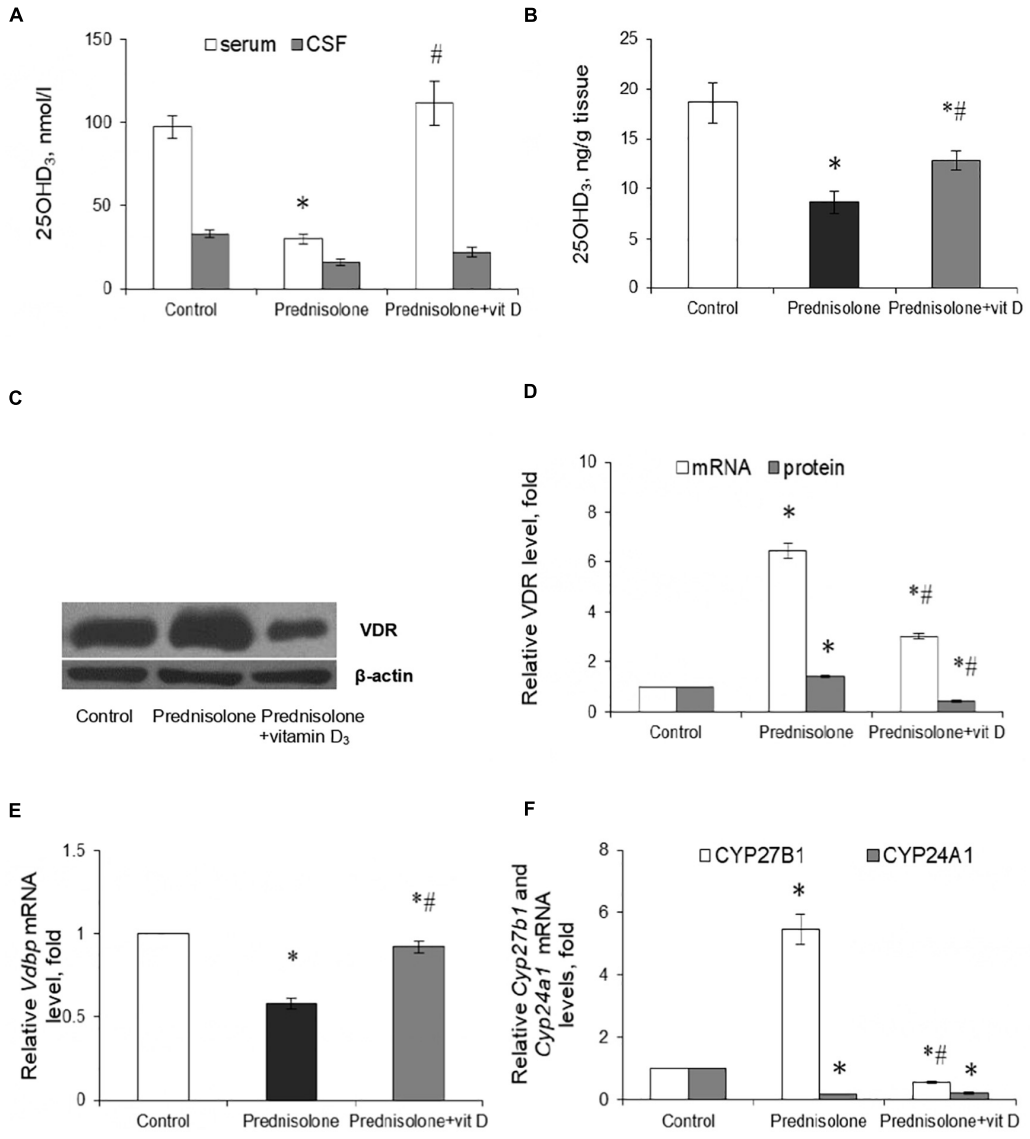

FIGURE 2
Vitamin D_3 circulating pool and the state of vitamin D_3-auto/paracrine system in the brain tissue. $25OHD_3$ concentration in the serum, cerebrospinal fluid **(A)** and brain homogenates **(B)** were measured by ELISA (n = 20). VDR protein **(C,D)** and mRNA **(D)** levels were determined by western blotting and quantitative RT-PCR respectively in rat brain tissue of three animal groups: 1—control; 2—prednisolone administration; 3—prednisolone and vitamin D_3 administration (n = 8 rats/group). Representative immunoblots are shown near the bar charts **(C)**. *Cyp27b1* **(E)** and *Cyp24a1* **(F)** mRNA levels were assessed by quantitative RT-PCR. All protein levels were normalized to β-actin and mRNA levels—to *Gapdh* expression. All data are presented as mean ± SD of three independent experiments done in triplicate; *$p < 0.05$ denotes significance compared with control, #$p < 0.05$ denotes significance compared with prednisolone administration.

(Tukey's test, p = 0.00001) and 1.79-fold lower than in the control group (Tukey's test, p = 0.0029).

Another component of the VD_3-auto/paracrine system that we examined was CYP24A1, that catalyzes the inactivation of both $25OHD_3$ and $1,25(OH)_2D_3$ (Hamamoto et al., 2006). In contrast to the effect of prednisolone on *Cyp27b1*, this glucocorticoid caused a 5.41-fold decrease in *Cyp24a1* mRNA level compared with the control group (Tukey's test, p = 0.0005), while VD_3 did not

significantly affect the level of *Cyp24A1* mRNA compared with the prednisolone group (Tukey's test, $p > 0.05$, Figure 2F).

In general, our results suggest that, despite the development of VD_3-deficiency, prednisolone elevated, most likely compensatory, the expression of such important components of the VD_3-auto/paracrine system as CYP27B1 and VDR, while the levels of mRNA transcripts of CYP24A1 and VDBP genes decreased in the brain, thus indicating an impairment of VD_3 transport and catabolism. Administration of cholecalciferol restored the circulating $25OHD_3$ pool and normalized, at least in part, the levels of key components of the VD_3-auto/paracrine system in the brain, although VD_3 24-hydroxylase remained unchanged.

3.3. Effects of prednisolone and vitamin D_3 on depressive-like behavior, locomotion and cognitive performance

To support the concept that VD_3 deficiency may be associated with behavioral abnormalities (Schoenrock and Tarantino, 2016),

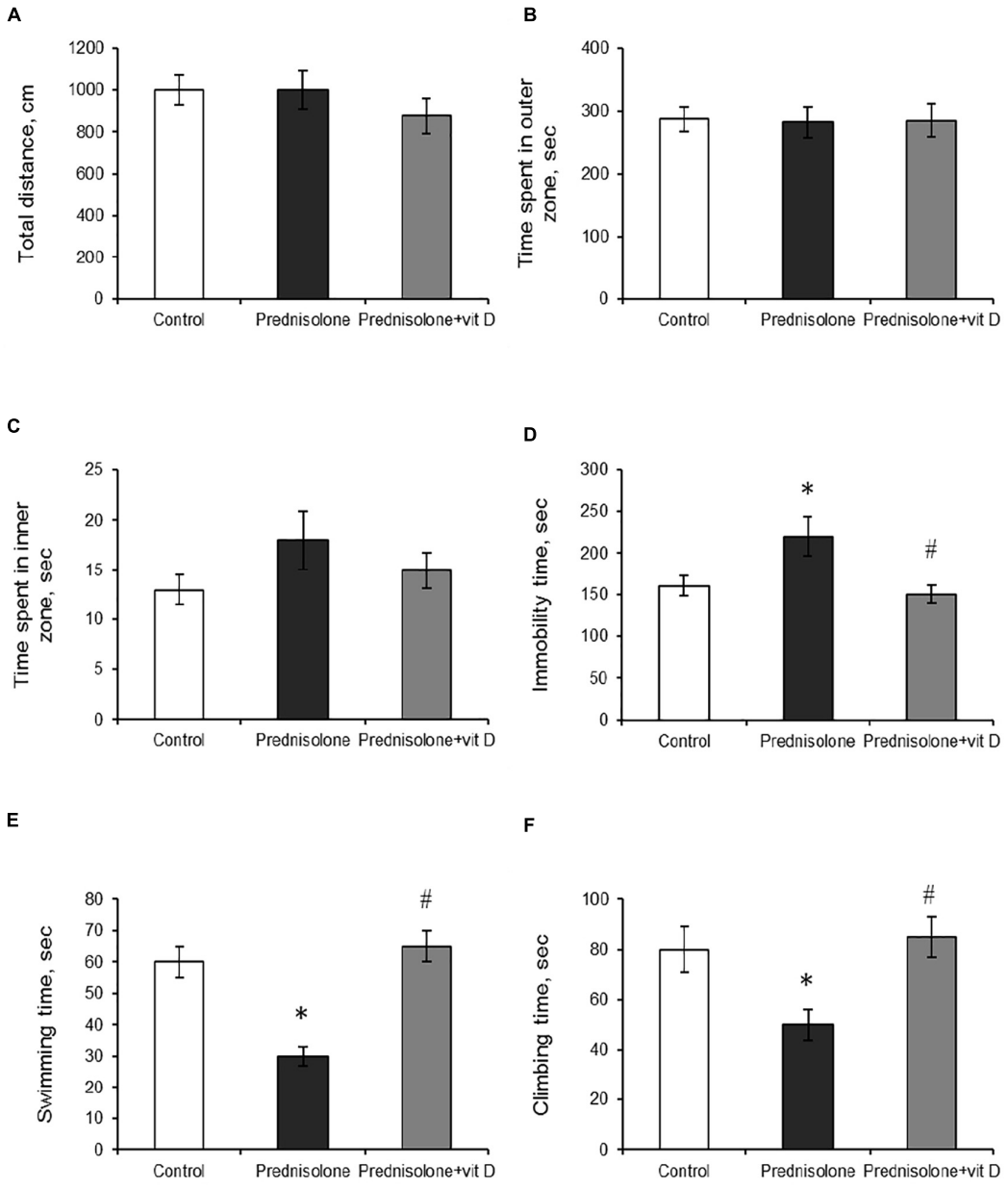

FIGURE 3
The influence of prednisolone and vitamin D_3 on the parameters of the open field (OFT) and forced swim (FST) tests. Animals from three experimental groups: 1—control; 2—prednisolone administration; 3—prednisolone and vitamin D_3 administration (n = 8 rats/group) were subjected to the OFT **(A–C)** and FST **(D–F)**. Total distance traveled **(A)**, time spent in outer **(B)** and inner **(C)** zones were calculated during the OFT. Total immobility time **(D)** and the parameters of active behavior: swimming **(E)**, and climbing **(F)** were assessed during the FST. All data are presented as mean ± SD of three independent experiments done in triplicate; $^{*}p < 0.05$ denotes significance compared with control, $^{\#}p < 0.05$ denotes significance compared with prednisolone administration.

we further estimated prednisolone-induced behavioral changes in animals that we found to exhibit significantly reduced VD_3 bioavailability. The open-field test allows to examine motor function and exploratory behavior by measuring spontaneous activity in the OFT box. Animals of all groups showed no significant difference in walking distance ($p > 0.05$) and in time spent exploring 9 inner squares and 16 outer squares ($p > 0.05$), as presented in Figures 3A–C respectively.

The forced swim test has been used to assess the presence of depression-related behaviors (Slattery and Cryan, 2012). Prednisolone-administered rats demonstrated an increase in immobility time (220 ± 15 s, Figure 3D) and a decrease in active behavior (swimming 30 ± 3 s, Figure 3E, climbing 50 ± 6 s, Figure 3F) compared with the control rats (160 ± 12 s, 60 ± 5 s, 80 ± 9 s, respectively), indicating depressive-like changes. VD_3 exerted antidepressive-like action, diminishing immobility time (150 ± 11 s) and stimulating active behavior (swimming 65 ± 5 s, climbing 85 ± 8 s) compared with the GC action.

The next task was to determine the level of anxiety in the elevated plus maze test by measuring the amount of time spent in open/closed arms. Behavior in performing this task (activity in the open arms) reflects a conflict between rodent's preference for protected areas (closed arms) and their innate motivation to explore novel environments. In the EPM test, we observed a tendency to an increased percentage of entries into the open arms (38.33 ± 5.9%, Figure 4A) and time spent in the open arms (14.92 ± 3.16%, Figure 4B) after prednisolone administration compared with the control group (21.03 ± 3.9% and 7.3 ± 1.27%, respectively). Unexpectedly, these results showed that prednisolone did not cause the anxiety-related behavioral changes. Increased time spent in the open arms and percentage of entries are conventionally interpreted as decreased anxiety-like behavior (Shoji and Miyakawa, 2021), however, another possible interpretation can be considered: an open arm study may reflect heightened anxiety and panic response to a novel situation under certain conditions. VD_3 administration reduced the percentage of entries into the open arms (13.88 ± 3.4%, $p = 0.0272$) and time

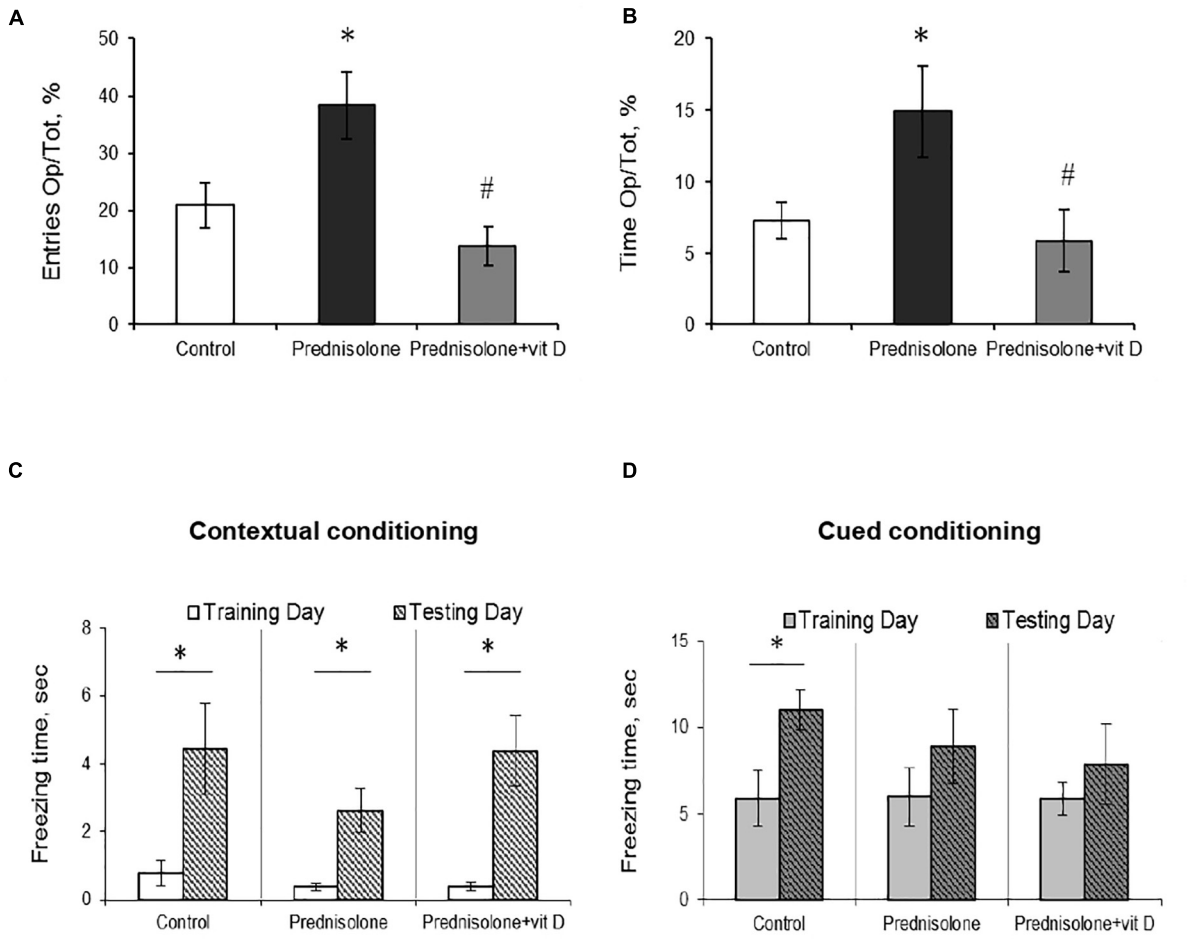

FIGURE 4
The effect of prednisolone and vitamin D_3 on the behavior in the elevated plus maze (EPM) and contextual and cued fear conditioning and memory test. Animals from three experimental groups: 1—control; 2—prednisolone administration; 3—prednisolone and vitamin D_3 administration ($n = 8$ rats/group) were subjected to the EPM **(A,B)** and contextual/cued conditioning test **(C,D)**. The percentage of entries into the open arms to the total time (Op/Tot) **(A)** and the ratio of time spent in the open arms to the total time (Op/Tot) **(B)** were measured during the EPM. Mean freezing time levels during the contextual **(C)** and cued **(D)** conditioning test were assessed after prednisolone and vitamin D_3 treatment during training and testing days. All data are presented as mean ± SD of three independent experiments done in triplicate; $^*p < 0.05$ denotes significance compared with control, $^\#p < 0.05$ denotes significance compared with prednisolone administration.

spent in the open arms (5.92 ± 2.18%, $p = 0.0306$) compared to the prednisolone-administered group. In addition, there was no meaningful difference when comparing the EPM parameters of VD_3-treated rats with the control group and the prednisolone group. Interestingly, time spent in the open arms of the EPM was positively correlated with immobility time in the FST ($r = 0.296$, $p < 0.05$) and negatively correlated with active behavior ($r = -0.382$, $p < 0.01$ for swimming).

After completion of the OFT, FST, and EPM tests, the rats were subjected to a contextual/cued fear conditioning test to assess an associative fear learning and memory. As shown in Figures 4C, D, there was no statistically significant difference in spontaneous freezing between all groups during the training day in the novel context ($p = 0.65$, Figure 4C) and after an auditory tone cue ($p = 0.99$, Figure 4D). We also did not observe significant differences between groups in the level of spontaneous freezing during the day of testing in both contextual and cued conditioning. However, we noted a tendency that the time of contextual conditioning freezing was significantly shorter in prednisolone-administered rats (2.63 ± 0.64 s vs. 4.44 ± 1.33 s in the control). A separate analysis of freezing time between each group revealed the statistically significant differences between training and testing days for three groups in contextual conditioning (Figures 4C, $p = 0.049$). However, no valuable difference was observed in cued conditioning freezing between all 3 groups (Figures 4D, $p = 0.068$).

Thus, we did not find any significant effects on locomotor activity or memory parameters (based on OFT and contextual/cued conditioning), while FST and EPM tests reflect the behavioral changes following prednisolone administration. In particular, FST demonstrated an increase in immobility time and a decrease in active behavior in glucocorticoid-treated rats, indicative of depressive-like changes. At the same time, the EPM results may point to the stimulation of anti-anxiety behavior induced by prednisolone; however, taking into consideration an increased time of immobility in the FST, we are more inclined to believe that the data obtained could reflect a panic-like reaction. Vitamin D_3 treatment diminished the immobility time and stimulated active behavior, suggesting anti-depressive effect of cholecalciferol. Exploratory behavior in the EPM was restored to control levels after VD_3 action.

3.4. Prednisolone-induced histological alterations of different brain regions and effect of vitamin D_3 in their prevention

Because lesions in the hippocampus are known to be capable of disrupting contextual fear conditioning (Chen et al., 1996), and given the observed GC-induced tendency to reduce freezing time in contextual conditioning, we first assessed the presence of histopathological changes in the hippocampus. For this purpose, histological staining with toluidine blue was carried out, followed by morphometric and statistical evaluation of the CA1–CA3 regions.

Histological examination revealed no visible signs of brain damage (neither hydropic neuronal dystrophy nor neurodegeneration) in all three groups (Figure 5A). Analysis of the morphometric parameters of pyramidal neurons in fields CA1–CA3 confirmed the presence of the following changes (Table 2). The perikaryon area increased by 55.1% in CA1, by 67.6% in CA2, and by 29.0% in the CA3 region in the prednisolone group compared with the control group (Student's t-test, $p < 0.001$). In addition, after prednisolone administration, we observed intact, but at the same time, enlarged neuronal nuclei (by 62.55, 83.45, and 49.27% in CA1, CA2, and CA3, respectively) compared with the control (Student's t-test, $p < 0.001$). The nuclei contained increased levels of euchromatin, indicating the activation of biosynthetic processes in neurons. Prednisolone also caused a slight decreasing effect on cell density in the CA1–CA3 hippocampal fields (Figure 5A). Vitamin D_3 administration led to a significant decrease in the mean areas of both the perikaryon and the nucleus in CA1 compared with the prednisolone group (by 68.12 and 73.79%, respectively, Student's t-test, $p < 0.001$), while only a slight tendency to a reduction of these parameters in CA2 and CA3 sections was found.

Histological sections of the cerebral cortex demonstrate the preservation of the general morphological structure of the prefrontal and sensorimotor cortex (Figures 5B, C). In all studied samples, pyramidal neurons and glial cells were detected in all layers of the cerebral cortex, except for the molecular layer. Structurally intact microvessels, mostly hemocapillaries, were also present. We did not reveal any signs of inflammation, leukocyte infiltration, necrosis or hemorrhage (Figures 5B, C). However, in the groups of prednisolone and VD_3, clarification of the cytoplasm was observed in large pyramidal neurons, especially in the ganglionic cell layer, probably indicating impaired functional activity of cells, inhibition of synthetic processes, and disintegration of organelles of the protein-synthesizing apparatus of neurons. We did not detect a statistically significant difference in the number of neurons in the prefrontal and sensorimotor cortex between the studied groups (Table 3). When comparing the mean area of neurons in the ganglionic layer of the cerebral cortex, there was a tendency to its increase in the prefrontal cortex after prednisolone administration compared with the control (by 13.4%, Student's t-test, $p = 0.04$). In the sensorimotor cortex, a trend toward an increase in the mean area of neurons was found after VD_3 treatment compared with the control (by 18.1%, Student's t-test, $p = 0.03$) and prednisolone (by 24.1%, Student's t-test, $p = 0.035$) groups.

Next, we studied the effect of prednisolone and cholecalciferol on the posterior thalamic nucleus. Histological evaluation did not reveal signs of dystrophic changes, necrosis or inflammation in the thalamus of all experimental groups. We also did not detect neuronal necrosis, however, single hyperchromic gliocytes and neurons were found. In general, the histological structure of the thalamic region in all the studied groups was similar (Figure 5D). These observations were confirmed by morphometric analysis, and there was no statistically significant between-group difference, as indicated in Table 4.

Finally, we found a number of morphological changes in the cerebellar cortex caused by the prednisolone action, with a slight ameliorative effect of VD_3. In general, for all experimental groups the cytoarchitecture of the cerebellar cortex was well preserved; the molecular, ganglionic, and granular layers were clearly visible (Figure 5E). In the molecular layer, single nuclei of gliocytes and processes of neurons were detected, which together formed the outer layer of the cerebellar cortex. Separate piriform neurons

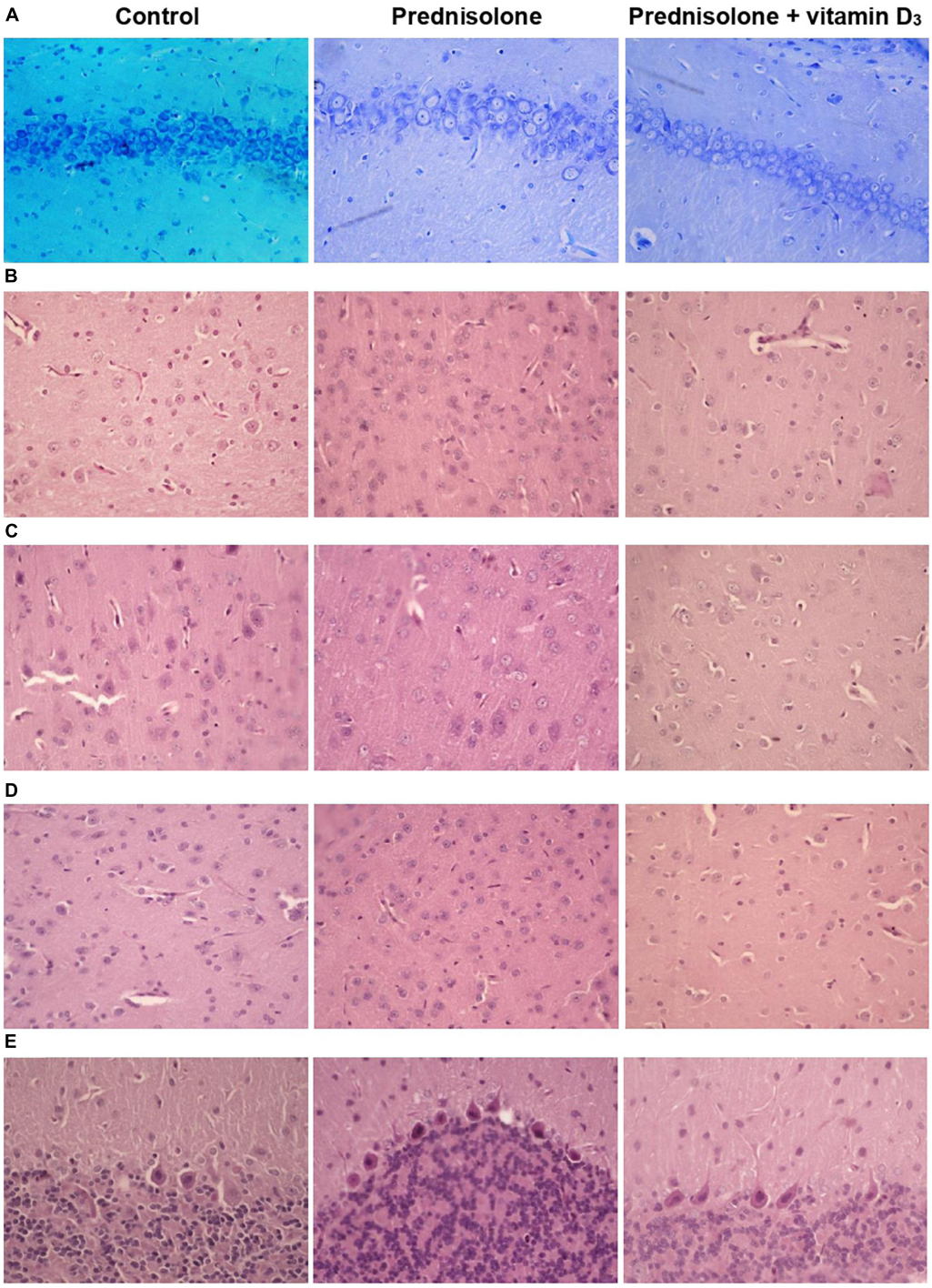

FIGURE 5
Histological examination of hippocampus, cerebral cortex, thalamus and cerebellum after prednisolone and vitamin D_3 treatment (toluidine blue or hematoxylin & eosin staining). Representative images of toluidine blue-stained 6-μm rat CA1 hippocampal sections section **(A)**, H&E-stained cerebral cortex (prefrontal cortex) **(B)**, sensory-motor cortex **(C)**, H&E-stained thalamus sections (posterior thalamic nucleus) **(D)**, and H&E-stained cerebellar cortex **(E)** from the control, prednisolone-administered and prednisolone plus vitamin D_3-administered rats (n = 5 rats/group, 400× magnification).

(Purkinje cells) in the ganglionic layer were located in a one-layered manner. The granular layer was formed by numerous small granular neurons. Thus, we did not find any neurodystrophic changes in the molecular and granular layer after prednisolone administration, while in the ganglionic layer there were strained neurons with hyperchromic staining of the cytoplasm and nuclei. Although we did not observe intergroup differences in the number of neurons and density of Purkinje cells in the cerebellar cortex (Table 5), the size of strained neurons was 43.2% and 33.2% smaller in the prednisolone group (406.1 ± 14.7 μm^2, Student's t-test, p = 0.009) and after VD_3 treatment (477.7 ± 27.8 μm^2, Student's t-test, p = 0.012), respectively, compared with the control

group (714.9 ± 48.3 μm^2). These observations indicate that neurodegenerative changes may occur under the influence of prednisolone in the cerebellar cortex.

Thus, we did not establish any valuable differences in the cytoarchitectonics of the cerebral cortex and the posterior nucleus of the thalamus between the studied groups. However, GC-induced changes were found in the hippocampus and cerebellum, namely, a decrease in cell density in the hippocampal zones, as well as a decrease in the size of neurons in the cerebellar cortex. These changes in general may indicate the onset of neurodegenerative changes under the influence of prednisolone. Vitamin D_3 partially normalized the cytoarchitecture of the hippocampus and cerebellum.

3.5. Assessment of synaptic function after prednisolone administration and effect of vitamin D_3 treatment

It is most likely that despite the absence of striking prednisolone-induced histopathological changes in the brain structures they, nevertheless, can be accompanied to some extent by impaired neuronal function. The harmful effects of GC on the brain and the impact of vitamin D_3 therapy may primarily concern some important aspects of synaptic function, such as depolarization-induced exocytosis from isolated neurons, synaptic vesicle fusion with plasma membrane of nerve terminals and changes in long-term potentiation (LTP).

First, we characterized the process of depolarization-induced exocytosis from isolated neurons and monitored vesicle-to-membrane fusion. As shown in **Figures 6A, B**, following high K^+-depolarization, the nerve endings isolated from the brain of prednisolone-administered rats demonstrated a 57.5%-decrease in exocytosis amplitude compared with the control (Tukey's test, $p = 0.00023$).

One of the reasons for the decrease in the exocytosis amplitude might be changes in the mechanisms involved in providing the fusion of synaptic vesicles with the plasma membranes of synaptic terminals. This process strictly depends on the presence of soluble cytosolic synaptic proteins and involves successive stages of interaction of synaptic vesicles with the target membrane: docking, priming, and fusion. We isolated synaptic vesicles and synaptic plasma membranes and evaluated their Ca^{2+}-triggered fusion in a cell-free system. As is seen in **Figure 6C**, synaptic vesicles from prednisolone-administered rats show a significantly lower rate of Ca^{2+}-dependent synaptic plasma membrane fusion (by 29.53%) compared to the control (Tukey's test, $p = 0.01$).

Glucocorticoids have been reported to impair cholesterol metabolism in the brain, and its level is one of the important factors influencing the rate of synaptic vesicle fusion with each other and with the synaptic plasma membrane (Gumenyuk et al., 2013). With this in mind, we studied the content of total cholesterol in synaptic membranes isolated from the cerebral hemispheres and found an increase in its level in prednisolone-supplemented animals (0.81 ± 0.07 μmol/mg protein) compared to the control level (0.65 ± 0.05 μmol/mg protein) (**Figure 6D**). Elevated synaptic plasma membrane

TABLE 2 Morphometric parameters of hippocampal neurons of CA1-CA3 fields (M ± m, $n = 5$).

Groups	Hippocampal subfields					
	CA1		CA2		CA3	
	Mean perikaryon area, μm^2	Mean area of the neuron nucleus, μm^2	Mean perikaryon area, μm^2	Mean area of the neuron nucleus, μm^2	Mean perikaryon area, μm^2	Mean area of the neuron nucleus, μm^2
Control	371.0 ± 11.1	186.1 ± 7.2	421.8 ± 10.0	196.4 ± 7.9	429.1 ± 8.3	218.6 ± 8.6
Prednisolone	575.4 ± 19.0*	302.5 ± 13.2*	707.1 ± 21.7*	360.3 ± 6.1*	553.6 ± 31.4*	326.3 ± 18.7*
Prednisolone + vitamin D_3	392.0 ± 9.8$^{\#}$	223.2 ± 6.6*$^{\#}$	646.9 ± 34.0*$^{\#}$	296.7 ± 18.4*$^{\#}$	531.7 ± 18.3*	270.4 ± 8.0*$^{\#}$

*$p < 0.001$ vs. control.
$^{\#}p < 0.001$ vs. prednisolone administration.

TABLE 3 Morphometric parameters of the cerebral cortex (test area 550 μm × 215 μm, M ± m, n = 5).

Groups	Number of neurons, units per 1 test area	Mean area of the neurons of ganglionic layer of cerebral cortex, μm^2
Prefrontal cortex		
Control	57.0 ± 5.8	362.2 ± 14.2
Prednisolone	55.7 ± 7.4	410.7 ± 25.2*
Prednisolone + vitamin D_3	50.7 ± 3.7	390.3 ± 21.5
Sensory-motor cortex		
Control	56.7 ± 2.7	487.4 ± 16.4
Prednisolone	55.0 ± 8.8	463.5 ± 40.1
Prednisolone + vitamin D_3	51.5 ± 2.9	575.5 ± 49.6*#

*$p < 0.05$ vs. control.
#$p < 0.05$ vs. prednisolone administration.

TABLE 4 Morphometric parameters of the thalamus (posterior thalamic nucleus, test area 550 μm × 215 μm, M ± m, n = 5).

Groups	Number of neurons, units per 1 test area	Mean area of the neurons, μm^2
Control	33.4 ± 3.3	388.2 ± 21.4
Prednisolone	40.8 ± 3.0	417.1 ± 20.4
Prednisolone + vitamin D_3	34.2 ± 3.2	406.9 ± 13.3

TABLE 5 Morphometric parameters of the ganglionic layer of the cerebellum (test area – width of the cortex layer 500 μm, M ± m, n = 5).

Groups	Number of neurons, units per 1 test area	Mean area of the neurons, μm^2
Control	8.0 ± 0.5	714.9 ± 48.3
Prednisolone	7.8 ± 0.4	406.1 ± 14.7*
Prednisolone + vitamin D_3	9.0 ± 0.7	477.7 ± 27.8*

*$p < 0.05$ vs. control.
#$p < 0.05$ vs. prednisolone administration.

cholesterol may indicate abnormal cholesterol metabolism associated with the administration of prednisolone and is comparable to that observed in alimentary vitamin D deficiency (Kasatkina et al., 2018).

After supplementation with VD_3, we observed an increase in mean amplitude of 103.07% compared with the prednisolone group (Tukey's test, p = 0.00002, Figure 6B), which almost reached the level of control values. Recovery of depolarization-induced release of synaptic vesicles after VD_3 treatment (Figure 6A) indicates the reversibility of prednisolone-induced changes in stimulated secretion. Contrary to our expectations, we failed to find statistically significant changes in cholesterol levels after VD_3 supplementation compared with the prednisolone group ($p > 0.5$, Figure 6D).

In the next series of experiments, we studied changes in long-term potentiation in animals in response to chronic prednisolone action and after vitamin D_3 administration. For the LTP study, we used a common tetanic stimulation protocol, which is classic for studying plasticity in the hippocampal CA1 area (100 stimuli, at a frequency of 100 Hz). In this experiment, we used sections of the septal part of the hippocampus involved in spatial memory processes. Analysis of the LTP parameters (Figure 7A) showed a decrease in fEPSP by 16.6% after GC administration compared with the control (p = 0.0025; Figure 7B) that reflects an alteration of the LTP. Vitamin D_3 treatment restored the prednisolone-induced LTP (prednisolone vs. vitamin D_3, p = 0.033) to nearly control levels (VD_3 vs. control, p = 0.56).

Thus, in relation to functional disorders, we have established a GC-induced decrease in the amplitude of high K^+-stimulated exocytosis, the rate of Ca^{2+}-dependent fusion of isolated synaptic vesicles with synaptic plasma membranes that may be partially associated with an increase in cholesterol levels in the latter. A reduced level of LTP was found in the synapses of the hippocampus. Taken together, all these impairments may underlie the observed changes in behavior after glucocorticoid loading. In turn, vitamin D_3 therapy tended to restore, at least partially, the above changes, regardless insignificant effect on cholesterol levels.

3.6. Prednisolone-induced oxidative-nitrosative stress in brain tissue and effect of vitamin D_3 treatment

Excess formation of reactive oxygen/nitrogen species (ROS/RNS) is considered to be one of the universal mechanisms leading to cell injury and CNS dysfunction (Oosthuizen et al., 2005). It is known that nitric monooxide (NO) can interact with superoxide-anion radicals to form an unstable and highly reactive peroxynitrite (ONOO-). Tyrosine residues of protein molecules are

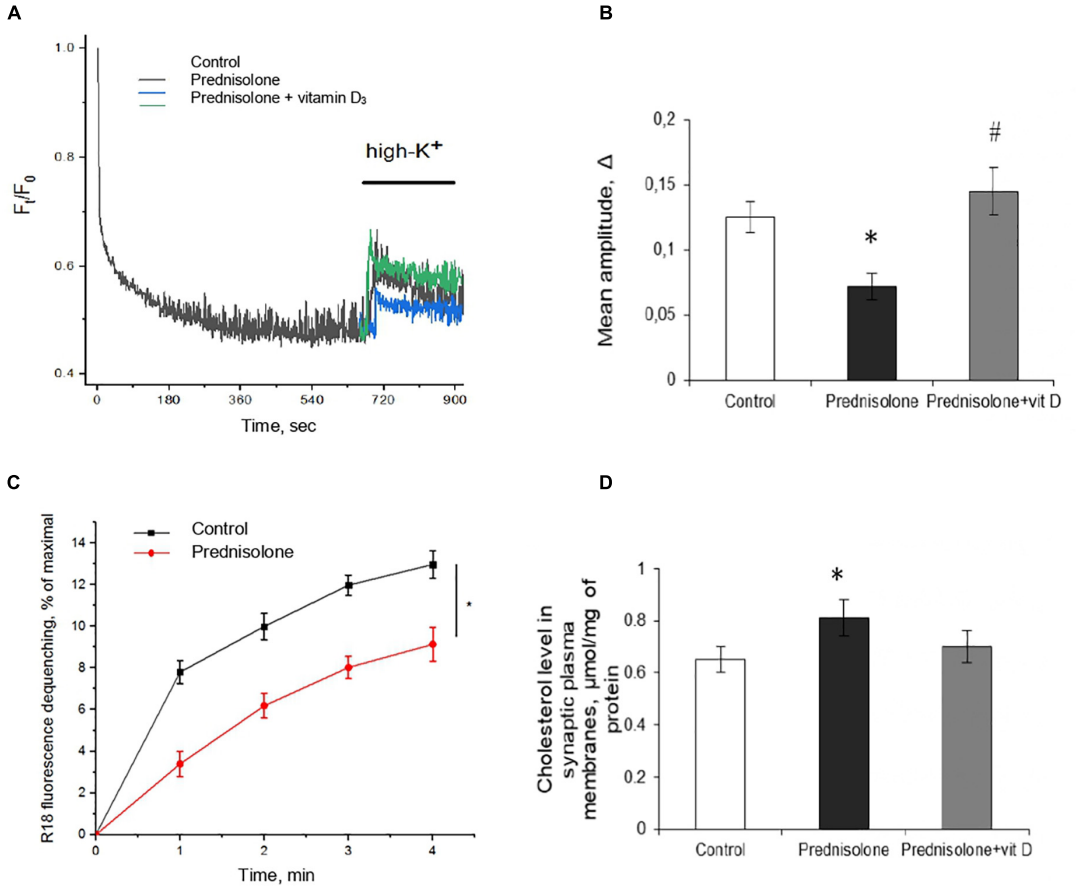

FIGURE 6
Glucocorticoid-induced disturbances of synaptic function and its correction by the vitamin D_3 supplementation. Depolarization-induced exocytosis in rat brain nerve terminals (synaptosomes) **(A)** and quantification of the mean amplitude Δ **(B)**. Nerve terminals were isolated from the control, prednisolone-treated and prednisolone plus vitamin D_3-treated rats. Spectrofluorimetric registration of pH-sensitive dye – acridine orange (AO), $n = 4$. The rate of synaptic vesicle fusion with plasma membranes in cell-free system **(C)**. Fusion was determined by monitoring of R18 fluorescence dequenching in suspension of R18-labeled synaptic vesicles and unlabeled synaptic plasma membranes upon Ca^{2+} application in control and prednisolone-administered rats, $n = 5$ (traces). Cholesterol content in synaptic plasma membranes **(D)** of control and prednisolone-treated rats ($n = 5$). All data are presented as mean ± SD of three independent experiments done in triplicate; $^{*}p < 0.05$ denotes significance compared with control, $^{\#}p < 0.05$ denotes significance compared with prednisolone administration.

sensitive targets for the action of peroxynitrite. Thus, the content of 3-nitrotyrosine can serve as a specific marker of peroxynitrite activity and the development of oxidative-nitrosative stress (Bartesaghi and Radi, 2018). We have shown that prednisolone elevated protein nitration at tyrosine residues in the brain tissue by 28% (Tukey's test, p = 0.0052) compared with the control (**Figures 8A, C**). This reflects NO-mediated protein damage that may lead to neuronal dysfunction. VD_3 administration decreased the level of nitrated proteins by 61.7% compared with the prednisolone group (Tukey's test, p = 0.0005) and by 21% compared with the control (Tukey's test, p = 0.013). This is clearly consistent with previous data on the antioxidant activity of cholecalciferol (Martín Giménez et al., 2021).

Next, we assessed the degree of oxidative modification of proteins based on the content of carbonyl groups (>C=O), which are formed within protein molecules upon ROS-mediated oxidative modifications of aminoacid residues, especially Pro, Arg, Lys, Trh, as well as a result of the interaction of macromolecules with reactive carbonyl products or reducing sugars (Hauck et al., 2019). Immunoblot analysis of carbonylated proteins did not reveal, in contrast to the level of nitrated proteins, a statistically significant difference between the three groups, as shown in **Figures 8B, D**. In our opinion, this can be explained by the augmented neutralization of nitric monooxide by superoxide anion radicals with the formation of peroxynitrite, which, in turn, can cause an increase in the content of nitrated proteins in the brain under the GC influence (**Figure 8C**).

Intensification of ROS and peroxynitrite formation, in addition to protein oxidative modification, can also lead to DNA damage, inducing the development of genotoxic stress. In turn, the appearance of single- and double-strand breaks in DNA activates one of the key enzymes of the cellular DNA repair system, PARP-1, which provides covalent modification of histone and non-histone proteins in the process of their poly(ADP)-ribosylation (Wang et al., 2019). As PARP-1 overactivation was previously reported to be detrimental in multiple types of experimental brain injury, including the impact of oxidative stress (Salech et al., 2020), the brain levels of protein poly(ADP)-ribosylation were studied. We found a significant increase (by 45%, **Figures 8E, G**) in the level of PAR after prednisolone administration (Tukey's test, p = 0.00055).

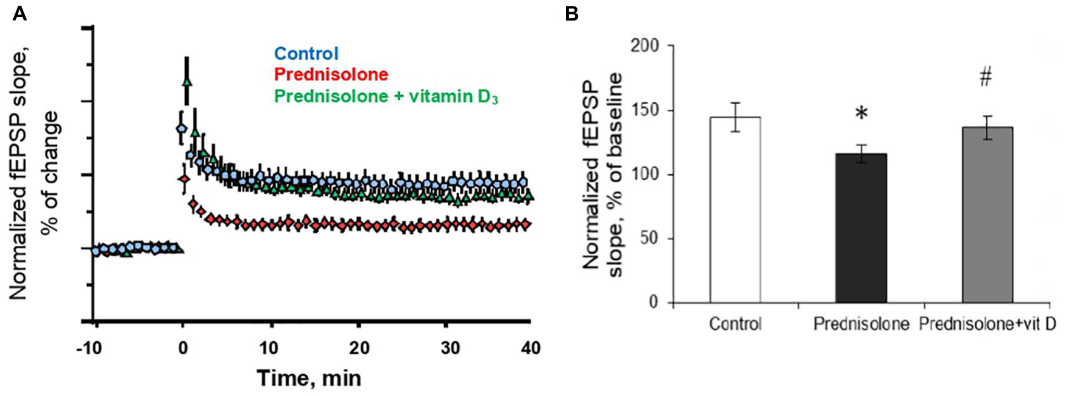

FIGURE 7
Effect of vitamin D_3 on prednisolone-induced alteration of synaptic plasticity in shaffer-collateral—CA1 synapses. fEPSP slope recorded before and after tetanic stimulation was shown **(A)** and the normalized fEPSP amplitudes was calculated **(B)** for the control, prednisolone-treated and prednisolone plus vitamin D_3-treated rats (n = 5 rats/group). All points at panel **(A)** represent the average of three consecutive responses recorded every 20 s at the indicated time points. Data are presented as mean ± SD; $^{*}p < 0.05$ denotes significance compared with control, $^{\#}p < 0.05$ denotes significance compared with prednisolone administration.

As shown in Figures 8F, H, the PARP-1 protein level did not change compared to the control (Tukey's test, p = 0.537) that, however, do not exclude an increase in the overall activity of this enzyme. Interestingly, when comparing rats supplemented with prednisolone and prednisolone plus VD_3, there were no intergroup differences in PAR (Tukey's test, p = 0.44), suggesting that VD_3 does not provide effective inhibition of this protein modification. However, VD_3 supplementation diminished PARP-1 content by 25.3% (Tukey's test, p = 0.015) compared with the prednisolone group, thus affecting protein levels rather than enzyme activity.

Collectively our data suggest that prednisolone caused the development of oxidative-nitrosative stress in brain tissue that may contribute to glucocorticoid-induced neurotoxicity. The ability of VD_3 to prevent protein nitration and to reduce PARP-1 level was established.

3.7. Effect of prednisolone and vitamin D_3 on glucocorticoid receptor level and NF-κB/IκB pathway in brain tissue

Glucocorticoids act through their particular receptor, and in rodents its expression is ubiquitous throughout the brain (Kadmiel and Cidlowski, 2013). It was important to determine whether GR is involved in prednisolone-induced neuropathological changes. Unexpectedly, we observed a significant increase (by 80%, Figures 9A, B) in the GR level after prednisolone administration compared with the control group (Tukey's test, p = 0.01). This may either reflect or contribute to impaired GR-signaling and partially explain the neurotoxic effects of long-term prednisolone administration.

Since NF-κB is reported to be a redox-sensitive transcription factor (Morgan and Liu, 2011), and in addition, GR may interact with NF-κB p65 subunit through direct protein-protein interactions (Ray and Prefontaine, 1994; Nelson et al., 2003), thus influencing its transcriptional activity, we assessed the components of the NF-κB system. Using RT-PCR (Figure 9C), we established a significant 4.23-fold increase in *Nf-κb* p65 mRNA compared with the control rats (Tukey's test, p = 0.0009). The same elevating effect was observed for the NF-κB p65 phosphorylated at Ser311 protein level, which is considered to be transcriptionally competent (Figures 9A, C). The level of phosphoNF-κB p65 was increased by 78.3% after prednisolone compared with the control group (Tukey's test, p = 0.008).

An important role in the regulation of NF-κB p65 activity belongs to the NF-κB inhibitor, which binds to NF-κB dimers and keep them inactive in the cytoplasm (Solt and May, 2008). We studied IκB expression in rat brain and found conflicting results concerning effects of GC on *IκB* mRNA (Figure 9D) and IκB protein (Figures 9A, D) levels. With a strong decrease in the gene expression of IκB under the GC action by 88.2 ± 5.5% (Tukey's test, p = 0.001), the level of IκB protein was 1.6-fold elevated compared with the control (Tukey's test, p = 0.015). This finding suggests GC-induced dysregulation of transcriptional and translational processes in nerve cells. Vitamin D_3 treatment restored the GR to control values (Figures 9A, B). In addition, VD_3 almost completely normalized *Nf-κB* mRNA expression and significantly reduced the protein content of phosphoNF-κB p65 (by 66.3% compared vs. prednisolone, and by 40% compared vs. control), suggesting VD_3 ability to counteract prednisolone-induced NF-κB activation in brain tissue. At the same time, we also observed contradictory effect of VD_3 supplementation on IκB. It increased *IκB* mRNA (by 9.4-fold compared vs. prednisolone), while decreasing IκB protein level (by 65.6% compared vs. prednisolone, and by 45% compared vs. control). This uncoordinated action of vitamin D_3 on IκB expression at transcriptional and translational levels renders the entire pattern of NF-κB activation unclear, indicating the need for further study.

To conclude, at the molecular level prednisolone caused an increase in the expression of the p65 subunit of NF-κB and an increase in its specific phosphorylation at Ser311 against the background of an increase in the IκB protein content. VD_3 diminished the intensity of oxidative-nitrosative stress, possibly by suppressing the activation of NF-κB signaling in the brain.

10.3389/fncel.2023.1133400

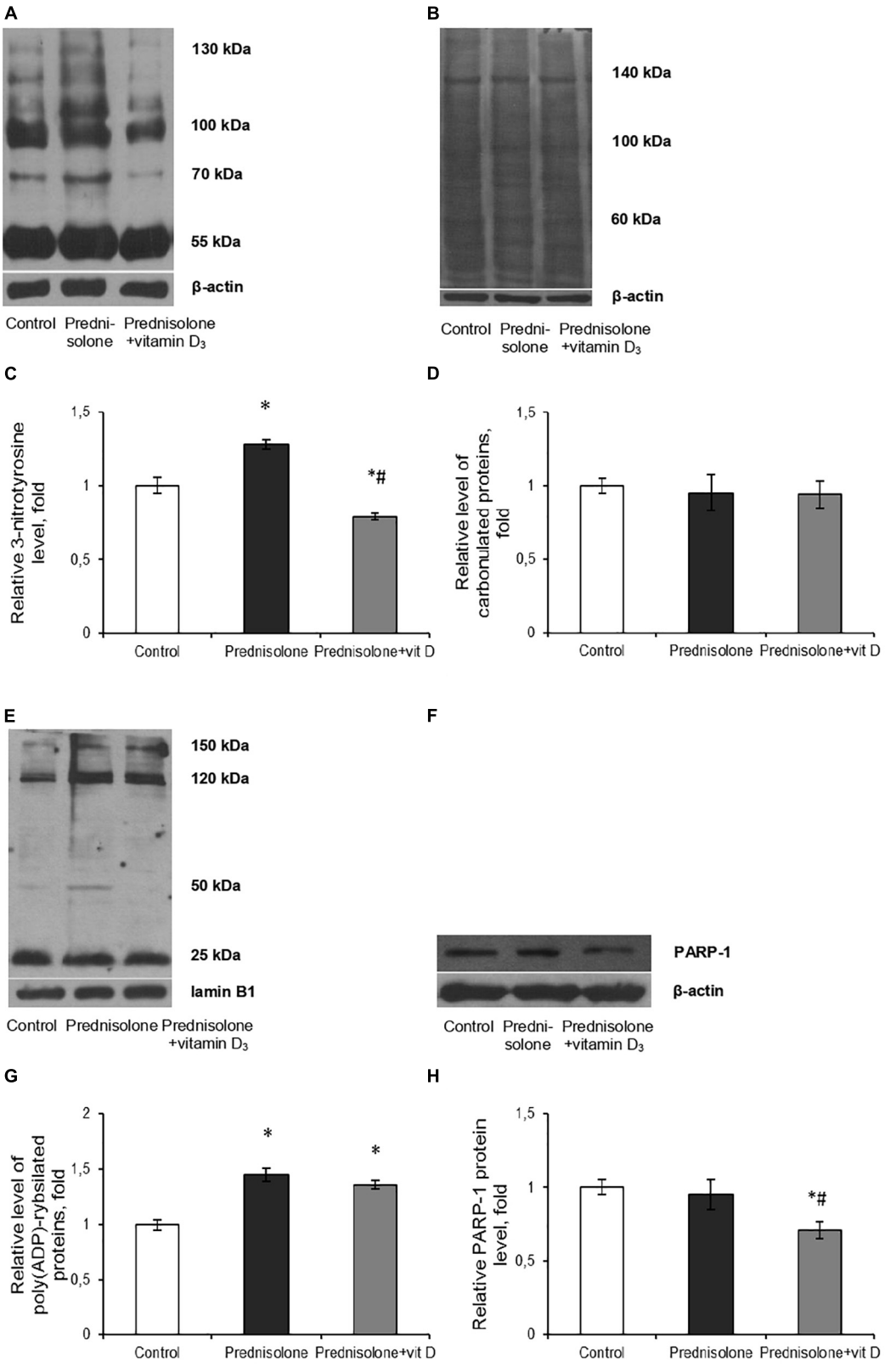

FIGURE 8
Oxidative-nitrosative stress after prednisolone and vitamin D_3 administration. Levels of 3-nitrotyrosine **(A,C)**, carbonylated proteins **(B,D)**, poly(ADP)-rybosilated proteins **(E,G)** and PARP-1 **(F,H)** were determined by western blot analysis in rat brain tissue of three animal groups: 1—control; 2—prednisolone administration; 3—prednisolone and vitamin D_3 administration (n = 8 rats/per group). Representative immunoblots are shown above the bar charts. Protein levels were normalized to β-actin and/or lamin B1. All data are presented as mean ± SD of three independent experiments done in triplicate; $^{*}p < 0.05$ denotes significance compared with control, $^{\#}p < 0.05$ denotes significance compared with prednisolone administration (one-way ANOVA, Tukey's *post-hoc* test).

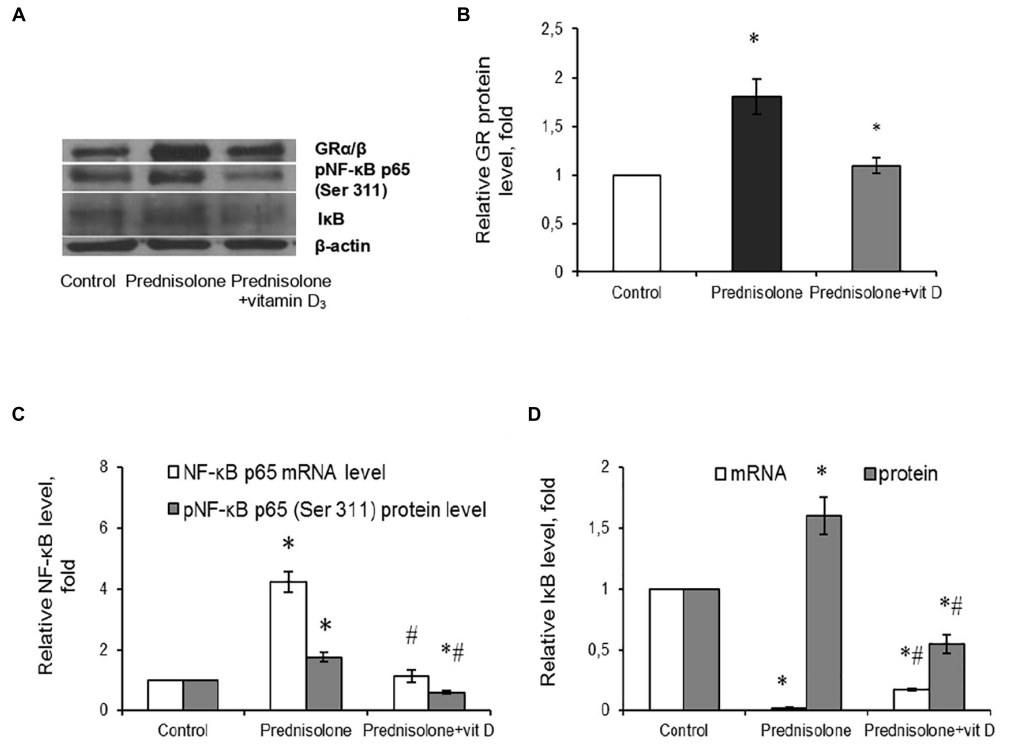

FIGURE 9
Glucocorticoid receptor level and NF-κB/IκB pathway in brain tissue after prednisolone and vitamin D_3 administration. Glucocorticoid receptor protein **(A,B)** level was determined by western blot analysis. NF-κB signaling was characterized based on the *Nf-κb p65* mRNA level **(C)**, NF-κB p65 phosphorylated at Ser 311 (Western blot) **(A,C)** and IκB protein **(A,D)** and mRNA **(D)** levels in rat brain tissue of three animal groups: 1—control; 2—prednisolone administration; 3—prednisolone and vitamin D_3 administration (n = 8 rats/group). Protein level was normalized to β-actin and mRNA levels—to *Gapdh* expression. All data are presented as mean ± SD of three independent experiments done in triplicate; $^{*}p < 0.05$ denotes significance compared with control, $^{\#}p < 0.05$ denotes significance compared with prednisolone administration (one-way ANOVA, Tukey's *post-hoc* test).

4. Discussion

A preventive approach to diminish the side effects of synthetic GCs on CNS may be achieved by using GC doses as low as possible, and by modulating the duration of the therapy, especially in high-dose courses. However, evidence has emerged, that synthetic GC neuropsychiatric sequelae often requiring psychiatric treatments that are not presently standardized. Moreover, little attention has been paid to developing possible supportive therapeutic strategies that can be applied along with the GC course. Therefore, the main scientific goal of the study was to solve the urgent medical and biological problem how to prevent and/or manage the neurotoxicity caused by long-term GC administration, in particular prednisolone, which is still widely used in clinical practice for the treatment of chronic inflammatory diseases.

Therapeutic administration of synthetic glucocorticoids may lead to adverse psychiatric effects (steroid-induced psychosis), including depressed mood, emotional lability, and even suicidality. Despite of synthetic GC therapy is frequently associated with a variety of clinical manifestations on behavior, mood and cognition, the real incidence is not presently inferable from the available literature, because few validated studies have been performed (Fietta et al., 2009). Therefore, we focused on the assessment of possible prednisolone-associated behavioral changes. Despite the fact that prednisolone is one of the most widely used synthetic glucocorticoids for the treatment of various allergic, inflammatory and autoimmune diseases, to the best of our knowledge, there have been no animal experiments focused on both prednisolone-induced behavioral changes in the brain and uncovering their functional, cellular and molecular basis.

Generally, GCs affect mood, and cognition (Keenan et al., 1996) and cause sleep disturbances (Curtis et al., 2006) in a dose- and time-dependent manner. In rodents, repeated administration of corticosterone induced depression-like behaviors (Kalynchuk et al., 2004; Zhao et al., 2008). Regarding prednisolone, there was one study on mice reporting that prednisolone (50–100 mg/kg, 7 days) caused anxiety- and depression-like behavioral alterations and impaired expression of apoptotic genes in hippocampus (Kajiyama et al., 2010). In contrast, in treatment-resistant depressed patients with fatigue and hypocortisolaemia, an augmentation of antidepressant therapy with synthetic GC prednisone may be useful and patients demonstrated significant improvement in depression (Bouwer et al., 2000).

Results from our set of behavioral experiments indicted that prednisolone did not affect locomotor activity (based on OFT) or learning and memory (based on contextual/cued conditioning). In contrast, at least one study demonstrated that a low daily dose of methylprednisolone (5 mg/kg) administered for 10-days favors aversive memory persistence in adult rats, without affecting

the exploring behavior, locomotor activity, anxiety levels, and pain perception (de Vargas et al., 2017). Herein, we found that prednisolone caused depressive-like changes in behavior (based on FST) along with possibly anti-anxiety behavior (based on EPM), if considering that the more time spent in the open arms corresponds to the lower level of anxiety. These data are in line with the finding that in patients with chronic GC treatment depressive disorder is the most frequent diagnosis, while anxiety disorder, mania or psychosis are less common (Lin et al., 2020). Moreover, depression-like behavior was induced by subcutaneous treatment of prednisolone in male mice (Aoki et al., 2022). Interestingly, there is a relationship between EPM and FST. Studies performed with selectively bred animals, found association between low exploration of the plus-maze open arms and high immobility in the FST (Keck et al., 2001; Estanislau et al., 2011). However, we found the reverse correlation between FST and EPM after prednisolone treatment: with a high immobility time in FST there was a high exploration of the plus-maze open arms in EPM. Therefore, based on possible discrepancies in the interpretation of EPM data, we are inclined to believe that changes in EPM parameters may more likely reflect a panic reaction, especially in combination with an increase in the time of immobility in the FST, than a lower level of anxiety.

As reported previously, chronic exposure to moderate/high doses of synthetic GCs may induce cumulative and potentially long-lasting effects on specific brain area morphology, such as hippocampus (Brown et al., 2004) and amygdala (Brown et al., 2008) volumes. In a study at the histological level we addressed the question of which brain areas and to what extent are affected by prednisolone. Generally, the cytoarchitectonics of the cerebral cortex and the posterior nucleus of the thalamus after prednisolone load were preserved and no valuable differences compared with the control animals were found in our trial. Previously, the influence on prefrontal cortex was found for naturally occurring glucocorticoids, however, to our knowledge there is a lack of data related to synthetic GCs. The only study we found postulated that the corticosteroid prednisolone increased amygdala and insula reactivity to food approach signals (Serfling et al., 2019). Regarding the thalamus, authors of this study (Yamazaki et al., 2021) suggested that GC administration reduced cerebral blood flow in the hippocampus and thalamus in dogs, similar to that which occurs in humans.

In contrast to cortex and thalamus, the effects of GCs on the hippocampus are well described (Höschl and Hajek, 2001). Our data confirmed previous studies revealing that prednisolone caused a slight reduction in cell density in the hippocampal areas. We additionally showed an increase in the area of the perikaryon and the size of the nuclei in CA1–CA3 areas. Such a pronounced effect of GCs on hippocampus may be explained by the high levels of GR expression in the paraventricular nucleus of the hypothalamus and in the hippocampus (Wang et al., 2013), both in glial cells and neurons, suggesting the high sensitivity of these brain structures to the GC exposure. In contrast to our expectations, we also observed a significant elevation of GR protein level in the brain, possibly, in the hippocampus, after prednisolone treatment that may contribute to GC-induced brain lesion.

Previously, it was shown that GC therapy may disrupt cerebellar development through the rapid induction of apoptosis in the cerebellar external granule layer (Noguchi, 2014). Since, clinical research also suggests the cerebellum may be particularly susceptible to GC exposure, we also performed the histological investigation of cerebellum, which is primarily responsible for the locomotor function, coordination, balance and posture control, muscle tone, and motor learning. Surprisingly, despite the fact that prednisolone did not affect locomotor activity, we found a significant decrease in the size of neurons in the cerebellar cortex. Since neuronal size is correlated with the extent of a neuron's dendritic and axonal arbor, a decrease in somal size may reflect decreased afferent and/or efferent connectivity of these cells that altogether may indicate the onset of neurodegenerative changes in the cerebellum under the influence of prednisolone.

The next studied level was to characterize functional abnormalities based on assessment of synaptic characteristics: the amplitude of exocytosis stimulated by high K^+, the rate of Ca^{2+}-dependent fusion of isolated synaptic vesicles with synaptic plasma membranes of nerve terminals and the level of LTP in CA1–CA3 hippocampal synapses. We established a GC-induced decrease in all three parameters, reflecting the impaired processes of depolarization-induced exocytosis in rat synaptosomes, altered membrane fusion and LTP. The decrease in the amplitude of high-K^+ stimulated exocytosis reflects the changes in the synaptic vesicle fusion competence and/or their readiness for release. This, in turn, affects the concentration of the neurotransmitters and their receptor activation at the post-synaptic membrane. As previously shown in a rat model of vitamin D_3 deficiency, synaptic vesicle acidification did not change and no alterations were observed at the endocytotic stage (Kasatkina et al., 2020). One of the reasons for a decreased amplitude of exocytosis, established in this study, was linked to changes in the rate of synaptic vesicle fusion with plasma membranes, which, in turn, depended on the cholesterol level in both synaptic plasma membranes and synaptic vesicles. Impaired cholesterol turnover in the brain can be one of the possible contributors to GC-associated brain disorder, since cholesterol level was markedly elevated in synaptic plasma membranes isolated from cerebral hemispheres after prednisolone action. These data are consistent with the previously shown ability of prednisone, similar to prednisolone, to cause an increased serum cholesterol even after 2 days of the treatment (Taskinen et al., 1988). Another evidence of the involvement of cholesterol impairments in the pathogenesis of GC-induced brain lesion is that defects in brain cholesterol metabolism may be implicated in the pathology of neurodegenerative diseases, such as Alzheimer's disease, Parkinson's disease, and some cognitive deficits typical of the old age. Neurons were also found to increase cholesterol synthesis in chronic myelin disease and multiple sclerosis (Berghoff et al., 2021).

The hippocampus is one of the brain regions mostly affected by stressful situations and GC treatment. A variety of physiological synaptic plasticity phenomena, which can be electrophysiologically perceived as long-term potentiation is involved in memory formation in the hippocampus (Lynch, 2004). At the same time, along with histological alterations in hippocampus, prednisolone caused a reduced fEPSP in CA1–CA3 hippocampal synapses, reflecting the interference with hippocampal electrophysiological activity, which in turn, may underlie the observed behavioral changes. Thus, our data confirmed that glucocorticoids are known to suspend the induction of LTP (Maggio and Segal, 2007). However, it was shown predominantly for naturally occurring GCs (Krugers et al., 2005). In contrast to prednisolone action on LTP, the following study demonstrated an enhanced LTP, a phenomenon that was

strengthen in hippocampal slices of rats injected with synthetic GC methylprednisolone (5 mg/kg) during 10 days (de Vargas et al., 2017), emphasizing that the influence of GC on LTP is tightly mediated by treatment doses and duration.

One of an important issue of our study was to discover the possible molecular mechanisms underlying glucocorticoid-induced brain lesion at both histological and functional levels. Growing evidence suggest that reactive oxygen and nitrogen species are one of the major contributors to the neurotoxicity induced by exogenous toxins (Singh et al., 2019). Moreover, ROS/RNS (singlet oxygen, superoxide and peroxynitrite) may modulate the effects of VD_3 by inhibiting association of $1,25(OH)_2D_3$-VDR with DNA, inducing irreversible VDR inhibition (Kröncke et al., 2002). Indeed, in the case of prednisolone load, we observed the development of oxidative-nitrosative stress in brain tissue that may contribute to glucocorticoid-induced brain damage. Oxidative-nitrosative stress was observed with a simultaneous increase in the expression and phosphorylation of the p65 NF-κB subunit, in contrast to the large pool of evidences on the inhibitory effects of GCs on NF-κB (De Bosscher et al., 2000; Nelson et al., 2003).

Since we assumed that one of the contributors that enhances the damaging effect of GCs on the brain is an abnormal VD_3 status, we examined the effect of prednisolone on the state of the VD_3-auto/paracrine system. It has been shown for the first time that prednisolone causes a profound depletion of the circulating $25OHD_3$ pool that may be associated with a decrease in VDBP, the main transport protein and vitamin D_3 depot. Previously, we showed that prednisolone may cause a decrease in $25OHD_3$, but only in serum (Lisakovska et al., 2020). A long-term vitamin D_3 deficiency in GC-administered animals strongly affected the functioning of the brain VD_3-auto/paracrine system. Elevated VDR expression, as well as CYP27B1, which converts $25OHD_3$ to the hormonally active $1,25(OH)_2D_3$, in the brain may represent, most likely, a compensatory tissue response to a decrease in the main circulating vitamin D metabolite, $25OHD_3$, in serum, and most importantly—in cerebrospinal fluid and brain tissue. Finally, an adaptive response to impaired transport and reduced levels of $25OHD_3$ and $1,25(OH)_2D_3$ in the brain also manifested in a significant decrease in catabolic enzyme CYP24A1 that might preserve a pool of hormonally active form of VD_3. Thus, the novelty of this study lies in the fact that for the first time the circulating pool of vitamin D_3 and the state of the VD_3-auto/paracrine system in the brain are characterized more thoroughly on the rodent model of chronic prednisolone administration.

Given the accumulating evidence that optimal vitamin D_3 levels are required to maintain healthy adult brain function, the logical decision was to correct the VD_3 deficiency status with vitamin D_3 supplementation to reduce brain-related manifestations of GC-induced neurotoxocity. As expected, after taking cholecalciferol, we observed a complete normalization of the $25OHD_3$ content in the serum and a partial – in the CSF and brain tissue. Our results suggest that complete repletion of the $25OHD_3$ pool in the brain, likely, takes time and requires longer treatment with higher doses of VD_3. In addition, it should be noted that serum levels of $25OHD_3$ are typically stabilized within three months after VD_3 deficiency treatment (Gani and How, 2015). Thus, we can speculate that the $25OHD_3$ level we observed in the brain and cerebrospinal fluid may still be low and insufficient for the local needs of the brain after 30 days of cholecalciferol treatment.

Among all components of the VD_3-auto/paracrine system, only the VDBP returned to the control value. This may be caused by its important role not only as the main transport protein for VD_3 metabolites, but also by its involvement in extracellular actin sequestration and activation of the complement system that makes VDBP responsible for neuroimmune homeostasis (Gomme and Bertolini, 2004). However, difficulties in explaining the changes in VDBP pattern after GC and cholecalciferol supplementation may be due to the fact that it is still unclear whether VDBP is synthesized directly in the CNS or transported from the general circulation through the BBB (Kim et al., 2021).

It is quite logical that after partial repletion of $25OHD_3$ we observed a decrease in the level of VDR mRNA and protein compared with both prednisolone and control animals that obviously, should have provided adequate calcitriol signaling. Previously, we showed the same effect of reducing VDR after the VD_3 administration against the background of prednisolone load in various tissues and organs, including bone marrow (Shymanskyi et al., 2018) and liver (Lisakovska et al., 2017), as well as kidneys (Mazanova et al., 2022) and liver (Mazanova et al., 2018) in diabetes-associated VD_3 deficiency. In addition, we revealed a marked decrease in CYP27B1 mRNA compared with prednisolone animals, most likely, in response to partially depleted pool of $25OHD_3$, thereby maintaining balance in the synthesis of the hormonally active form of VD_3. Surprisingly, the 24-hydroxylase content remained unchanged. Thus, an adequate response of the VD_3-auto/paracrine system after supplementation with VD_3 may provide adequate $25OHD_3/1,25(OH)_2D_3$-mediated functions in the brain.

The presence of VDR in the hippocampus, cortex and limbic systems of humans and rodents support an important role of VD_3 in regulating learning, memory, mood and cognitive performance (Gáll and Székely, 2021). According to our results, vitamin D_3 treatment caused anti-depressive effect and reliably restored exploratory behavior in the EPM after the development GC-induced neurotoxicity, suggesting that GC-associated behavioral changes may be reversible after restoration of VD_3 status. In support to our data, beneficial effects of vitamin D_3 on anxiety and depression-like behavior induced by unpredictable chronic mild stress by suppression of brain oxidative stress and neuroinflammation in rats was shown by Bakhtiari-Dovvombaygi et al., 2021. Moreover, it was reported that VD_3 supplementation along with increased dairy-product intake exerted a significant positive impact on physical and mental health status in psychiatric patients (Abdul-Razzak et al., 2018). However, previous studies regarding the use of VD_3 and its role in prevention and treatment of depressive disorders included small number of people to clearly assess the effectiveness and safety of vitamin D_3 as adjunctive therapy to antidepressants, as well as and its dosage range (Stefanowski et al., 2017). Therefore, our study may be considered one more evidence to support the use of vitamin D_3 as an antidepressant adjunctive therapy in different pathologies associated with VD_3 deficiency and depressive state.

In contrast to our data of no changes in OFT after VD_3 treatment, it was reported that vitamin D_3 deficiency in adult male mice results in hyperlocomotion in a novel OFT (Groves et al., 2013). However, these discrepancies can be explained by the different causes of VD_3 deficiency – induced by GC in our study and caused by vitamin D_3-deficient diet. Considering

contextual and cued conditioning, there were also no effects after cholecalciferol treatment, consistent with the finding that VD_3 status did not affect these parameters. In particular, Harms et al., 2012 showed that VD_3 deficiency does not affect the acquisition or retention of cued fear conditioning, nor does it affect the expression of latent inhibition using a fear conditioning paradigm.

At the histological level, vitamin D_3 exerted its effects predominantly on the hippocampus, influencing the size of the perikaryon and nucleus in the CA1 area, and to a lesser extent in the CA2/CA3 regions. This can be explained by a large number of VDR-expressing cells in the hippocampus (Gezen-Ak et al., 2013). Interestingly, despite the presence of VDR in the thalamus and cerebellum, no valuable effects of VD_3 on the cytoarchitectonics of the thalamus and cerebellum were found.

Not surprisingly, the most pronounced normalizing effect of VD_3 was observed at the functional level, since $1,25(OH)_2D_3$ is classified as a neurosteroid, which can alter neuronal excitability (Eyles, 2020). We found recovery of depolarization-induced synaptic vesicle fusion along with normalization of cholesterol levels after VD_3 treatment, suggesting reversibility of GC-induced changes in stimulated secretion. Vitamin D_3 has previously been shown to maintain a balanced excitatory and inhibitory neurotransmission in an animal model of VD_3-deficiency (Kasatkina et al., 2020). Furthermore, in our study, vitamin D_3 treatment restored prednisolone-induced LTP reduction, suggesting the ability of cholecalciferol to influence synaptic plasticity, consistent with the finding that optimal vitamin D_3 levels are required for LTP induction (Salami et al., 2012). Thus, our data highlight the critical role of VD_3 in restoring basic synaptic transmission and synaptic plasticity in GC-evoked brain lesion.

Vitamin D_3/VDR is known to play a protective role in diseases associated with oxidative stress and inflammation by acting on various cellular pathways through the regulation of gene expression and epigenetic modifications. One possible mechanism for the neurotropic action of VD_3 has been reported to involve ROS/RNA suppression (Sepidarkish et al., 2019). We also confirmed that against the background of chronic GC intake, vitamin D_3 showed antioxidant effects, manifested in a reduced intensity of oxidative-nitrosative stress. Our data are consistent with a study showing that calcitriol can reduce NO levels by inhibiting the expression of inducible NO synthase in the spinal cord and brain (Garcion et al., 2002). Moreover, $1,25(OH)_2D_3$ significantly affects the synthesis of cytokines in various tissues, which at the cellular level realize their action through the VDR-mediated regulation of NF-κB activity. It has been shown that VDR can physically interact with IκB-β kinase to block NF-κB activation (Chen et al., 2013). However, there is currently insufficient available research investigating the effects of VD_3 on various aspects of NF-κB functioning in the brain, especially those related to the mechanisms of GC-related neurotoxicity. Overall, in the present study, we found the ability of vitamin D_3 to suppress GC-induced activation of NF-κB signaling in the brain, which may lead to an improvement in GC-induced deleterious brain changes, thereby conferring the neuroprotective effects.

The study has the following limitations. All protein levels were measured on whole brain lysates that complicates further analysis. It was previously found that the baseline levels of the components of the VD_3-auto/paracrine system differ depending on the brain area, for example, the content of VDR and CYP24A1 mRNA is higher in hippocampal neurons than in the cortex (Gezen-Ak et al., 2013). Therefore, it can be assumed that the observed changes after taking prednisolone and VD_3 may reflect a multidirectional response from different cell types and brain regions. To solve this problem, in the following experiments we will study changes in different areas of the brain, dissecting separately the cortex, hippocampus, cerebellum and thalamus. This issue also applies to the need for brain cell typing, since the potential protective role of NF-κB in neurons must be differentiated from its potential degenerative role in glia, but this assumption definitely needs further study.

Despite the stated shortcomings, the strength of our research study lies in the comprehensive study that characterizes CNS damage after long-term exposure to the widely used GC prednisolone, manifested at the molecular, functional, histological and behavioral levels in the same animal model. The study provides insight into the possible mechanisms of glucocorticoid-associated neurotoxicity and neuroprotective action of vitamin D_3 that is important for future clinical applications. The results of this fundamental research will serve as a theoretical basis for evidence-based practical recommendations on the use of vitamin D_3 in the treatment of brain damage and cognitive dysfunctions associated with long-term GC supplementation, as well as in the treatment of other nervous and metabolic diseases accompanied by impaired VD_3 metabolism. In our opinion, the further perspective of this study should be devoted to the search for the optimal treatment duration and cholecalciferol dosage that will more fully restore the circulating pool of $25OHD_3$ in the CNS without affecting calcium metabolism and bone homeostasis.

5. Conclusion

Our findings indicate that prednisolone-induced neurotoxicity and behavioral disturbances in rats are associated with the VD_3 deficiency and alterations in the VD_3-auto/paracrine system. Replenishment of the circulating $25OHD_3$ pool and partial normalization of the VD_3-auto/paracrine system after vitamin D_3 supplementation had a neuroprotective effect. Vitamin D_3 decreased oxidative-nitrosative stress and NF-κB activation, normalized the morphometric parameters of hippocampal neurons, restored depolarization-induced fusion of synaptic vesicles with synaptic plasma membrane, as well as LTP in the hippocampus that led to an antidepressant-like effect of the treatment. Thus, vitamin D_3 may be effective in the prevention of molecular, structural, functional abnormalities and behavioral disorders caused by chronic administration of prednisolone.

Data availability statement

The original contributions presented in this study are included in the article/supplementary material, further inquiries can be directed to the corresponding author.

Ethics statement

This animal study was reviewed and approved by the Ethics Committee on controlling the rules of research work with experimental animals, Palladin Institute of Biochemistry, National Academy of Sciences of Ukraine, Kyiv, Ukraine.

Author contributions

OL and IS conceived the original idea, designed and supervised the study, interpreted data, and prepared the manuscript. IS coordinated the research group. OL, IS, DL, AK, LK, AS, and SS performed the laboratory experiments. DI, DL, and OL performed the behavioral tests. OL, DL, AS, and DI statistically analyzed the data. DI and LK contributed to the critical discussion and data analysis. MV made a substantial contribution to the general conception of the work and critically revised the manuscript. All authors read and approved the final manuscript.

Funding

This research was supported by a grant from the National Research Foundation of Ukraine (NRFU) (2020.02/0336).

Acknowledgments

We would like to acknowledge the ECNP Research Internship Program and prof. David A. Slattery from the University Hospital Frankfurt, Department of Psychiatry, Psychosomatic Medicine and Psychotherapy (Frankfurt, Germany) for the introduction into the field of behavioral neurobiology and studying how to perform behavioral tests to investigate depression- and anxiety-related changes.

Conflict of interest

The authors declare that the research was conducted in the absence of any commercial or financial relationships that could be construed as a potential conflict of interest.

Publisher's note

All claims expressed in this article are solely those of the authors and do not necessarily represent those of their affiliated organizations, or those of the publisher, the editors and the reviewers. Any product that may be evaluated in this article, or claim that may be made by its manufacturer, is not guaranteed or endorsed by the publisher.

References

Abdul-Razzak, K. K., Almanasrah, S. O., Obeidat, B. A., and Khasawneh, A. G. (2018). Vitamin D is a potential antidepressant in psychiatric outpatients. *Int. J. Clin. Pharmacol. Ther.* 56, 585–596. doi: 10.5414/CP203309

Abrahám, I. M., Harkany, T., Horvath, K. M., and Luiten, P. G. (2001). Action of glucocorticoids on survival of nerve cells: Promoting neurodegeneration or neuroprotection? *J. Neuroendocrinol.* 13, 749–760. doi: 10.1046/j.1365-2826.2001.00705.x

Alan, I. S., and Alan, B. (2017). "Side effects of glucocorticoids," in *Pharmacokinetics and adverse effects of drugs–mechanisms and risks factors*, ed. N. Malangu (London: IntechOpen). doi: 10.5772/intechopen.72019

Aoki, S., Deyama, S., Sugie, R., Ishimura, K., Fukuda, H., Shuto, S., et al. (2022). The antidepressant-like effect of resolvin E1 in repeated prednisolone-induced depression model mice. *Behav. Brain Res.* 418:113676. doi: 10.1016/j.bbr.2021.113676

Baas, D., Prüfer, K., Ittel, M. E., Kuchler-Bopp, S., Labourdette, G., Sarlième, L. L., et al. (2000). Rat oligodendrocytes express the vitamin D(3) receptor and respond to 1,25-dihydroxyvitamin D(3). *Glia* 31, 59–68. doi: 10.1002/(sici)1098-1136(200007)31:1<59::aid-glia60<3.0.co;2-y

Bakhtiari-Dovvombaygi, H., Izadi, S., Zare Moghaddam, M., Hashemzehi, M., Hosseini, M., Azhdari-Zarmehri, H., et al. (2021). Beneficial effects of vitamin D on anxiety and depression-like behaviors induced by unpredictable chronic mild stress by suppression of brain oxidative stress and neuroinflammation in rats. *Naunyn Schmiedebergs Arch. Pharmacol.* 394, 655–667. doi: 10.1007/s00210-020-02002-0

Bartesaghi, S., and Radi, R. (2018). Fundamentals on the biochemistry of peroxynitrite and protein tyrosine nitration. *Redox Biol.* 14, 618–625. doi: 10.1016/j.redox.2017.09.009

Berghoff, S. A., Spieth, L., Sun, T., Hosang, L., Depp, C., Sasmita, A. O., et al. (2021). Neuronal cholesterol synthesis is essential for repair of chronically demyelinated lesions in mice. *Cell Rep.* 37:109889. doi: 10.1016/j.celrep.2021.109889

Berridge, M. J. (2017). Vitamin D deficiency accelerates ageing and age-related diseases: A novel hypothesis. *J Physiol.* 595, 6825–6836. doi: 10.1113/JP274887

Bogovyk, R., Lunko, O., Fedoriuk, M., Isaev, D., Krishtal, O., Holmes, G. L., et al. (2017). Effects of protease-activated receptor 1 inhibition on anxiety and fear following status epilepticus. *Epilepsy Behav.* 67, 66–69. doi: 10.1016/j.yebeh.2016.11.003

Bouwer, C., Claassen, J., Dinan, T. G., and Nemeroff, C. B. (2000). Prednisone augmentation in treatment-resistant depression with fatigue and hypocortisolaemia: A case series. *Depress Anxiety* 12, 44–50. doi: 10.1002/1520-6394200012:1<44::AID-DA6<3.0.CO;2-C

Brown, E. S., Woolston, D. J., and Frol, A. B. (2008). Amygdala volume in patients receiving chronic corticosteroid therapy. *Biol. Psychiatry* 63, 705–709. doi: 10.1016/j.biopsych.2007.09.014

Brown, E. S., Woolston, D., Frol, A., Bobadilla, L., Khan, D. A., Hanczyc, M., et al. (2004). Hippocampal volume, spectroscopy, cognition, and mood in patients receiving corticosteroid therapy. *Biol. Psychiatry* 55, 538–545. doi: 10.1016/j.biopsych.2003.09.010

Brown, J., Bianco, J. I., McGrath, J. J., and Eyles, D. W. (2003). 1,25-dihydroxyvitamin D3 induces nerve growth factor, promotes neurite outgrowth and inhibits mitosis in embryonic rat hippocampal neurons. *Neurosci. Lett.* 343, 139–143. doi: 10.1016/s0304-3940(03)00303-3

Chen, C., Kim, J. J., Thompson, R. F., and Tonegawa, S. (1996). Hippocampal lesions impair contextual fear conditioning in two strains of mice. *Behav. Neurosci.* 110, 1177–1180. doi: 10.1037//0735-7044.110.5.1177

Chen, Y., Zhang, J., Ge, X., Du, J., Deb, D. K., and Li, Y. C. (2013). Vitamin D receptor inhibits nuclear factor κB activation by interacting with IκB kinase β protein. *J. Biol. Chem.* 288, 19450–19458. doi: 10.1074/jbc.M113.467670

Conrad, C. D. (2008). Chronic stress-induced hippocampal vulnerability: The glucocorticoid vulnerability hypothesis. *Rev. Neurosci.* 19, 395–411. doi: 10.1515/revneuro.2008.19.6.395

Cooper, M. S. (2012). Glucocorticoids in bone and joint disease: The good, the bad and the uncertain. *Clin. Med.* 12, 261–265. doi: 10.7861/clinmedicine.12-3-261

Cui, X., Gooch, H., Petty, A., McGrath, J. J., and Eyles, D. (2017). Vitamin D and the brain: Genomic and non-genomic actions. *Mol. Cell Endocrinol.* 453, 131–143. doi: 10.1016/j.mce.2017.05.035

Cui, X., McGrath, J. J., Burne, T. H. J., and Eyles, D. W. (2021). Vitamin D and schizophrenia: 20 years on. *Mol. Psychiatry* 26, 2708–2720. doi: 10.1038/s41380-021-01025-0

Curtis, J. R., Westfall, A. O., Allison, J., Bijlsma, J. W., Freeman, A., George, V., et al. (2006). Population-based assessment of adverse events associated with long-term glucocorticoid use. *Arthritis Rheum.* 55, 420–426. doi: 10.1002/art.21984

De Bosscher, K., Vanden Berghe, W., Vermeulen, L., Plaisance, S., Boone, E., and Haegeman, G. (2000). Glucocorticoids repress NF-kappaB-driven genes by disturbing the interaction of p65 with the basal transcription machinery, irrespective of coactivator levels in the cell. *Proc. Natl. Acad. Sci. U.S.A.* 97, 3919–3924. doi: 10.1073/pnas.97.8.3919

De Lorenzo, R. J., and Freedman, S. D. (1978). Calcium dependent neurotransmitter release and protein phosphorylation in synaptic vesicles. *Biochem. Biophys. Res. Commun.* 80, 183–192. doi: 10.1016/0006-291x(78)91121-x

de Vargas, L. D. S., Gonçalves, R., Lara, M. V. S., Costa-Ferro, Z. S. M., Salamoni, S. D., Domingues, M. F., et al. (2017). Methylprednisolone as a memory enhancer in rats: Effects on aversive memory, long-term potentiation and calcium influx. *Brain Res.* 1670, 44–51. doi: 10.1016/j.brainres.2017.06.007

Di, S., Maxson, M. M., Franco, A., and Tasker, J. G. (2009). Glucocorticoids regulate glutamate and GABA synapse-specific retrograde transmission via divergent nongenomic signaling pathways. *J. Neurosci.* 29, 393–401. doi: 10.1523/JNEUROSCI.4546-08.2009

Estanislau, C., Ramos, A. C., Ferraresi, P. D., Costa, N. F., de Carvalho, H. M., and Batistela, S. (2011). Individual differences in the elevated plus-maze and the forced swim test. *Behav. Process.* 86, 46–51. doi: 10.1016/j.beproc.2010.08.008

Eyles, D. W. (2020). Vitamin D: Brain and behavior. *JBMR Plus* 5:e10419. doi: 10.1002/jbm4.10419

Fietta, P., Fietta, P., and Delsante, G. (2009). Central nervous system effects of natural and synthetic glucocorticoids. *Psychiatry Clin. Neurosci.* 63, 613–622. doi: 10.1111/j.1440-1819.2009.02005.x

Fullard, M. E., and Duda, J. E. (2020). A review of the relationship between vitamin D and Parkinson disease symptoms. *Front. Neurol.* 11:454. doi: 10.3389/fneur.2020.00454

Gáll, Z., and Székely, O. (2021). Role of vitamin D in cognitive dysfunction: New molecular concepts and discrepancies between animal and human findings. *Nutrients* 13:3672. doi: 10.3390/nu13113672

Gani, L. U., and How, C. H. (2015). PILL series. Vitamin D deficiency. *Singapore Med. J.* 56, 433–436. doi: 10.11622/smedj.2015119

García-Cabezas, M. Á, John, Y. J., Barbas, H., and Zikopoulos, B. (2016). Distinction of neurons, glia and endothelial cells in the cerebral cortex: An algorithm based on cytological features. *Front. Neuroanat.* 10:107. doi: 10.3389/fnana.2016.00107

Garcion, E., Wion-Barbot, N., Montero-Menei, C. N., Berger, F., and Wion, D. (2002). New clues about vitamin D functions in the nervous system. *Trends Endocrinol. Metab.* 13, 100–105. doi: 10.1016/s1043-2760(01)00547-1

Gezen-Ak, D., Dursun, E., and Yilmazer, S. (2013). Vitamin D inquiry in hippocampal neurons: Consequences of vitamin D-VDR pathway disruption on calcium channel and the vitamin D requirement. *Neurol. Sci.* 34, 1453–1458. doi: 10.1007/s10072-012-1268-6

Gomme, P. T., and Bertolini, J. (2004). Therapeutic potential of vitamin D-binding protein. *Trends Biotechnol.* 22, 340–345. doi: 10.1016/j.tibtech.2004.05.001

Groves, N. J., Kesby, J. P., Eyles, D. W., McGrath, J. J., Mackay-Sim, A., and Burne, T. H. (2013). Adult vitamin D deficiency leads to behavioural and brain neurochemical alterations in C57BL/6J and BALB/c mice. *Behav. Brain Res.* 241, 120–131. doi: 10.1016/j.bbr.2012.12.001

Gumenyuk, V. P., Chunikhin, A. J., Himmelreich, N. H., and Trikash, I. O. (2013). The phenomenon of synaptic vesicle clustering as the prefusion state in the model system of exocytosis. *Gen. Physiol. Biophys.* 32, 545–558. doi: 10.4149/gpb_2013037

Hamamoto, H., Kusudo, T., Urushino, N., Masuno, H., Yamamoto, K., Yamada, S., et al. (2006). Structure-function analysis of vitamin D 24-hydroxylase (CYP24A1) by site-directed mutagenesis: Amino acid residues responsible for species-based difference of CYP24A1 between humans and rats. *Mol. Pharmacol.* 70, 120–128. doi: 10.1124/mol.106.023275/

Harms, L. R., Turner, K. M., Eyles, D. W., Young, J. W., McGrath, J. J., and Burne, T. H. (2012). Attentional processing in C57BL/6J mice exposed to developmental vitamin D deficiency. *PLoS One* 7:e35896. doi: 10.1371/journal.pone.0035896

Hauck, A. K., Huang, Y., Hertzel, A. V., and Bernlohr, D. A. (2019). Adipose oxidative stress and protein carbonylation. *J. Biol. Chem.* 294, 1083–1088. doi: 10.1074/jbc.R118.003214

Horner, H. C., Packan, D. R., and Sapolsky, R. M. (1990). Glucocorticoids inhibit glucose transport in cultured hippocampal neurons and glia. *Neuroendocrinology* 52, 57–64. doi: 10.1159/000125539

Höschl, C., and Hajek, T. (2001). Hippocampal damage mediated by corticosteroids–a neuropsychiatric research challenge. *Eur. Arch. Psychiatry Clin. Neurosci.* 251, II81–II88. doi: 10.1007/BF03035134

Kadmiel, M., and Cidlowski, J. A. (2013). Glucocorticoid receptor signaling in health and disease. *Trends Pharmacol. Sci.* 34, 518–530. doi: 10.1016/j.tips.2013.07.003

Kajiyama, Y., Iijima, Y., Chiba, S., Furuta, M., Ninomiya, M., Izumi, A., et al. (2010). Prednisolone causes anxiety- and depression-like behaviors and altered expression of apoptotic genes in mice hippocampus. *Prog. Neuropsychopharmacol. Biol. Psychiatry* 34, 159–165. doi: 10.1016/j.pnpbp.2009.10.018

Kalueff, A. V., and Tuohimaa, P. (2007). Neurosteroid hormone vitamin D and its utility in clinical nutrition. *Curr. Opin. Clin. Nutr. Metab. Care* 10, 12–19. doi: 10.1097/MCO.0b013e328010ca18

Kalynchuk, L. E., Gregus, A., Boudreau, D., and Perrot-Sinal, T. S. (2004). Corticosterone increases depression-like behavior, with some effects on predator odor-induced defensive behavior, in male and female rats. *Behav. Neurosci.* 118, 1365–1377. doi: 10.1037/0735-7044.118.6.1365

Kasatkina, L. A., Gumenyuk, V. P., Sturm, E. M., Heinemann, A., Bernas, T., and Trikash, I. O. (2018). Modulation of neurosecretion and approaches for its multistep analysis. *Biochim. Biophys. Acta Gen. Subj.* 1862, 2701–2713. doi: 10.1016/j.bbagen.2018.08.004

Kasatkina, L. A., Tarasenko, A. S., Krupko, O. O., Kuchmerovska, T. M., Lisakovska, O. O., and Trikash, I. O. (2020). Vitamin D deficiency induces the excitation/inhibition brain imbalance and the proinflammatory shift. *Int. J. Biochem. Cell Biol.* 119:105665. doi: 10.1016/j.biocel.2019.105665

Keck, M. E., Welt, T., Post, A., Müller, M. B., Toschi, N., Wigger, A., et al. (2001). Neuroendocrine and behavioral effects of repetitive transcranial magnetic stimulation in a psychopathological animal model are suggestive of antidepressant-like effects. *Neuropsychopharmacology* 24, 337–349. doi: 10.1016/S0893-133X(00)00191-3

Keenan, P. A., Jacobson, M. W., Soleymani, R. M., Mayes, M. D., Stress, M. E., and Yaldoo, D. T. (1996). The effect on memory of chronic prednisone treatment in patients with systemic disease. *Neurology* 47, 1396–1402. doi: 10.1212/wnl.47.6.1396

Kim, S. O., You, J. M., Yun, S. J., Son, M. S., Nam, K. N., Hong, J. W., et al. (2010). Ginsenoside rb1 and rg3 attenuate glucocorticoid-induced neurotoxicity. *Cell Mol. Neurobiol.* 30, 857–862. doi: 10.1007/s10571-010-9513-0

Kim, Y. J., Lê, H. G., Na, B. K., Kim, B. G., Jung, Y. K., Kim, M., et al. (2021). Clinical utility of cerebrospinal fluid vitamin D-binding protein as a novel biomarker for the diagnosis of viral and bacterial CNS infections. *BMC Infect. Dis.* 21:240. doi: 10.1186/s12879-021-05924-z

Kröncke, K. D., Klotz, L. O., Suschek, C. V., and Sies, H. (2002). Comparing nitrosative versus oxidative stress toward zinc finger-dependent transcription. Unique role for NO. *J. Biol. Chem.* 277, 13294–13301. doi: 10.1074/jbc.M111216200

Krugers, H. J., Alfarez, D. N., Karst, H., Parashkouhi, K., van Gemert, N., and Joëls, M. (2005). Corticosterone shifts different forms of synaptic potentiation in opposite directions. *Hippocampus* 15, 697–703. doi: 10.1002/hipo.20092

Landel, V., Stephan, D., Cui, X., Eyles, D., and Feron, F. (2018). Differential expression of vitamin D-associated enzymes and receptors in brain cell subtypes. *J. Steroid Biochem. Mol. Biol.* 177, 129–134. doi: 10.1016/j.jsbmb.2017.09.008

Lear, C. A., Koome, M. E., Davidson, J. O., Drury, P. P., Quaedackers, J. S., Galinsky, R., et al. (2014). The effects of dexamethasone on post-asphyxial cerebral oxygenation in the preterm fetal sheep. *J. Physiol.* 592, 5493–5505. doi: 10.1113/jphysiol.2014.281253

Lin, T. Y., Hanna, J., and Ishak, W. W. (2020). Psychiatric symptoms in Cushing's syndrome: A systematic review. *Innov. Clin. Neurosci.* 17, 30–35.

Lisakovska, O., Shymanskyi, I., Labudzynskyi, D., Mazanova, A., and Veliky, M. (2020). Vitamin D auto-/paracrine system is involved in modulation of glucocorticoid-induced changes in angiogenesis/bone remodeling coupling. *Int. J. Endocrinol.* 2020:8237610. doi: 10.1155/2020/8237610

Lisakovska, O., Shymanskyy, I., Mazanova, A., Khomenko, A., and Veliky, M. (2017). Vitamin D3 protects against prednisolone-induced liver injury associated with the impairment of the hepatic NF-κB/iNOS/NO pathway. *Biochem. Cell Biol.* 95, 213–222. doi: 10.1139/bcb-2016-0070

Lynch, M. A. (2004). Long-term potentiation and memory. *Physiol. Rev.* 84, 87–136. doi: 10.1152/physrev.00014.2003

Maggio, N., and Segal, M. (2007). Striking variations in corticosteroid modulation of long-term potentiation along the septotemporal axis of the hippocampus. *J. Neurosci.* 27, 5757–5765. doi: 10.1523/JNEUROSCI.0155-07.2007

Martín Giménez, V. M., Bergam, I., Reiter, R. J., and Manucha, W. (2021). Metal ion homeostasis with emphasis on zinc and copper: Potential crucial link to explain the non-classical antioxidative properties of vitamin D and melatonin. *Life Sci.* 281:119770. doi: 10.1016/j.lfs.2021.119770

Mazanova, A., Shymanskyi, I., Lisakovska, O., Hajiyeva, L., Komisarenko, Y., and Veliky, M. (2018). Effects of cholecalciferol on key components of vitamin D-endo/para/autocrine system in experimental type 1 diabetes. *Int. J. Endocrinol.* 2018:2494016. doi: 10.1155/2018/2494016

Mazanova, A., Shymanskyi, I., Lisakovska, O., Labudzynskyi, D., Khomenko, A., and Veliky, M. (2022). The link between vitamin D status and NF-κB-associated renal dysfunction in experimental diabetes mellitus. *Biochim. Biophys. Acta Gen. Subj.* 1866:130136. doi: 10.1016/j.bbagen.2022.130136

Morgan, M. J., and Liu, Z. G. (2011). Crosstalk of reactive oxygen species and NF-κB signaling. *Cell Res.* 21, 103–115. doi: 10.1038/cr.2010.178

Nelson, G., Wilde, G. J., Spiller, D. G., Kennedy, S. M., Ray, D. W., Sullivan, E., et al. (2003). NF-kappaB signalling is inhibited by glucocorticoid receptor and STAT6 via distinct mechanisms. *J. Cell Sci.* 116, 2495–2503. doi: 10.1242/jcs.00461

Noguchi, K. K. (2014). Glucocorticoid induced cerebellar toxicity in the developing neonate: Implications for glucocorticoid therapy during bronchopulmonary dysplasia. *Cells* 3, 36–52. doi: 10.3390/cells3010036

Obradovic, D., Gronemeyer, H., Lutz, B., and Rein, T. (2006). Cross-talk of vitamin D and glucocorticoids in hippocampal cells. *J. Neurochem.* 96, 500–509. doi: 10.1111/j.1471-4159.2005.03579.x

Oosthuizen, F., Wegener, G., and Harvey, B. H. (2005). Nitric oxide as inflammatory mediator in post-traumatic stress disorder (PTSD): Evidence from an animal model. *Neuropsychiatr. Dis. Treat.* 1, 109–123. doi: 10.2147/nedt.1.2.109.61049

Patil, C. G., Lad, S. P., Katznelson, L., and Laws, E. R. Jr. (2007). Brain atrophy and cognitive deficits in Cushing's disease. *Neurosurg. Focus* 23:E11. doi: 10.3171/foc.2007.23.3.13

Ray, A., and Prefontaine, K. E. (1994). Physical association and functional antagonism between the p65 subunit of transcription factor NF-kappa B and the glucocorticoid receptor. *Proc. Natl. Acad. Sci. U.S.A.* 91, 752–756. doi: 10.1073/pnas.91.2.752

Salami, M., Talaei, S. A., Davari, S., and Taghizadeh, M. (2012). Hippocampal long term potentiation in rats under different regimens of vitamin D: An in vivo study. *Neurosci. Lett.* 509, 56–59. doi: 10.1016/j.neulet.2011.12.050

Salech, F., Ponce, D. P., Paula-Lima, A. C., SanMartin, C. D., and Behrens, M. I. (2020). Nicotinamide, a poly [ADP-ribose] polymerase 1 (PARP-1) inhibitor, as an adjunctive therapy for the treatment of Alzheimer's disease. *Front. Aging Neurosci.* 12:255. doi: 10.3389/fnagi.2020.00255

Schoenrock, S. A., and Tarantino, L. M. (2016). Developmental vitamin D deficiency and schizophrenia: The role of animal models. *Genes Brain Behav.* 15, 45–61. doi: 10.1111/gbb.12271

Sepidarkish, M., Farsi, F., Akbari-Fakhrabadi, M., Namazi, N., Almasi-Hashiani, A., Maleki Hagiagha, A., et al. (2019). The effect of vitamin D supplementation on oxidative stress parameters: A systematic review and meta-analysis of clinical trials. *Pharmacol. Res.* 139, 141–152. doi: 10.1016/j.phrs.2018.11.011

Serfling, G., Buades-Rotger, M., Harbeck, B., Krämer, U. M., and Brabant, G. (2019). The corticosteroid prednisolone increases amygdala and insula reactivity to food approach signals in healthy young men. *Psychoneuroendocrinology* 99, 154–165. doi: 10.1016/j.psyneuen.2018.09.007

Shoji, H., and Miyakawa, T. (2021). Effects of test experience, closed-arm wall color, and illumination level on behavior and plasma corticosterone response in an elevated plus maze in male C57BL/6J mice: A challenge against conventional interpretation of the test. *Mol. Brain* 14:34. doi: 10.1186/s13041-020-00721-2

Shymans'kyĭ, I. O., Khomenko, A. V., Lisakovs'ka, O. O., Labudzyns'kyĭ, D. O., Apukhovs'ka, L. I., and Velykyĭ, M. M. (2014). The ROS-generating and antioxidant systems in the liver of rats treated with prednisolone and vitamin D3. *Ukr. Biochem. J.* 86, 111–125.

Shymanskyi, I., Lisakovska, O., Labudzynskyi, D., Mazanova, A., and Veliky, M. (2020). "Vitamin D in immune regulation and diabetes mellitus," in *Molecular nutrition, vitamins*, ed. V. B. Patel (Cambridge, MA: Academic Press), 427–446. doi: 10.1016/B978-0-12-811907-5.00013-0

Shymanskyi, I., Lisakovska, O., Mazanova, A., Labudzynskyi, D., and Veliky, M. (2018). Vitamin D3 modulates impaired crosstalk between RANK and glucocorticoid receptor signaling in bone marrow cells after chronic prednisolone administration. *Front. Endocrinol. (Lausanne)* 9:303. doi: 10.3389/fendo.2018.00303

Singh, A., Kukreti, R., Saso, L., and Kukreti, S. (2019). Oxidative stress: A key modulator in neurodegenerative diseases. *Molecules* 24:1583. doi: 10.3390/molecules24081583

Slattery, D. A., and Cryan, J. F. (2012). Using the rat forced swim test to assess antidepressant-like activity in rodents. *Nat. Protoc.* 7, 1009–1014. doi: 10.1038/nprot.2012.044

Smolders, J., Schuurman, K. G., van Strien, M. E., Melief, J., Hendrickx, D., Hol, E. M., et al. (2013). Expression of vitamin D receptor and metabolizing enzymes in multiple sclerosis-affected brain tissue. *J Neuropathol. Exp. Neurol.* 72, 91–105. doi: 10.1097/NEN.0b013e31827f4fcc

Solt, L. A., and May, M. J. (2008). The IkappaB kinase complex: Master regulator of NF-kappaB signaling. *Immunol. Res.* 42, 3–18. doi: 10.1007/s12026-008-8025-1

Sorrells, S. F., Munhoz, C. D., Manley, N. C., Yen, S., and Sapolsky, R. M. (2014). Glucocorticoids increase excitotoxic injury and inflammation in the hippocampus of adult male rats. *Neuroendocrinology* 100, 129–140. doi: 10.1159/000367849

Stefanowski, B., Antosik-Wójcińska, A. Z., and Święcicki, Ł (2017). The effect of vitamin D3 deficiency on the severity of depressive symptoms. Overview of current research. *Psychiatr. Pol.* 51, 437–454. doi: 10.12740/PP/66809

Taskinen, M. R., Kuusi, T., Yki-Järvinen, H., and Nikkilä, E. A. (1988). Short-term effects of prednisone on serum lipids and high density lipoprotein subfractions in normolipidemic healthy men. *J. Clin. Endocrinol. Metab.* 67, 291–299. doi: 10.1210/jcem-67-2-291

Tata, D. A., and Anderson, B. J. (2010). The effects of chronic glucocorticoid exposure on dendritic length, synapse numbers and glial volume in animal models: Implications for hippocampal volume reductions in depression. *Physiol. Behav.* 99, 186–193. doi: 10.1016/j.physbeh.2009.09.008

Trikash, I., Gumenyuk, V., and Lishko, V. (2010). The fusion of synaptic vesicle membranes studied by lipid mixing: The R18 fluorescence assay validity. *Chem. Phys. Lipids* 163, 778–786. doi: 10.1016/j.chemphyslip.2010.09.003

Wang, Q., Van Heerikhuize, J., Aronica, E., Kawata, M., Seress, L., Joels, M., et al. (2013). Glucocorticoid receptor protein expression in human hippocampus; stability with age. *Neurobiol. Aging* 34, 1662–1673. doi: 10.1016/j.neurobiolaging.2012.11.019

Wang, Y., Luo, W., and Wang, Y. (2019). PARP-1 and its associated nucleases in DNA damage response. *DNA Repair* 81:102651. doi: 10.1016/j.dnarep.2019.102651

Won, S., Sayeed, I., Peterson, B. L., Wali, B., Kahn, J. S., and Stein, D. G. (2015). Vitamin D prevents hypoxia/reoxygenation-induced blood-brain barrier disruption via vitamin D receptor-mediated NF-kB signaling pathways. *PLoS One* 10:e0122821. doi: 10.1371/journal.pone.0122821

Xiaohua, G., Dongdong, L., Xiaoting, N., Shuoping, C., Feixia, S., Huajun, Y., et al. (2021). Severe vitamin D deficiency is associated with increased expression of inflammatory cytokines in painful diabetic peripheral neuropathy. *Front. Nutr.* 8:612068. doi: 10.3389/fnut.2021.612068

Yamazaki, K., Yoshimura, A., Miyahara, S., Sugi, S., Itono, M., Kondo, M., et al. (2021). Evaluation of cerebral blood flow in the hippocampus, thalamus, and basal ganglia and the volume of the hippocampus in dogs before and during treatment with prednisolone. *Am. J. Vet. Res.* 82, 230–236. doi: 10.2460/ajvr.82.3.230

Zhao, Y., Ma, R., Shen, J., Su, H., Xing, D., and Du, L. (2008). A mouse model of depression induced by repeated corticosterone injections. *Eur. J. Pharmacol.* 581, 113–120. doi: 10.1016/j.ejphar.2007.12.005

frontiers | Frontiers in Cellular Neuroscience

TYPE Brief Research Report
PUBLISHED 21 March 2023
DOI 10.3389/fncel.2023.1132325

OPEN ACCESS

EDITED BY
Tommaso Pizzorusso,
Normal School of Pisa, Italy

REVIEWED BY
Marco Mainardi,
Institute of Neuroscience (CNR), Italy
Nicola Kuczewski,
Université Claude Bernard Lyon 1, France

*CORRESPONDENCE
Mariia Shypshyna
✉ shypshyna.mariia@gmail.com

SPECIALTY SECTION
This article was submitted to Cellular Neuropathology, a section of the journal Frontiers in Cellular Neuroscience

RECEIVED 27 December 2022
ACCEPTED 06 March 2023
PUBLISHED 21 March 2023

CITATION
Shypshyna M, Kolesnyk O, Fedulova S and Veselovsky N (2023) Insulin modulates the paired-pulse plasticity at glutamatergic synapses of hippocampal neurons under hypoinsulinemia.
Front. Cell. Neurosci. 17:1132325.
doi: 10.3389/fncel.2023.1132325

Insulin modulates the paired-pulse plasticity at glutamatergic synapses of hippocampal neurons under hypoinsulinemia

Mariia Shypshyna*, Oksana Kolesnyk, Svitlana Fedulova and Nickolai Veselovsky

Department of Neuronal Networks, Bogomoletz Institute of Physiology, Kyiv, Ukraine

Hypoinsulinemia is a pathological consequence of diabetes mellitus that can cause a number of complications of the central and peripheral nervous system. Dysfunction of signaling cascades of insulin receptors under insulin deficiency can contribute to the development of cognitive disorders associated with impaired synaptic plasticity properties. Earlier we have shown that hypoinsulinemia causes a shift of short-term plasticity in glutamatergic hippocampal synapses from facilitation to depression and apparently involves mechanisms of glutamate release probability reduction. Here we used the whole cell patch-clamp recording of evoked glutamatergic excitatory postsynaptic currents (eEPSCs) and the method of local extracellular electrical stimulation of a single presynaptic axon to investigate the effect of insulin (100 nM) on the paired-pulse plasticity at glutamatergic synapses of cultured hippocampal neurons under hypoinsulinemia. Our data indicate that under normoinsulinemia additional insulin enhances the paired-pulse facilitation (PPF) of eEPSCs in hippocampal neurons by stimulating the glutamate release in their synapses. Under hypoinsulinemia, insulin did not have a significant effect on the parameters of paired-pulse plasticity on neurons of PPF subgroup, which may indicate the development of insulin resistance, while the effect of insulin on PPD neurons indicates its ability to recover the form normoinsulinemia, including the increasing probability of plasticity to the control level in of glutamate release in their synapses.

KEYWORDS

hypoinsulinemia, hippocampus, glutamatergic neurotransmission, postsynaptic currents, paired-pulse plasticity

1. Introduction

Hypoinsulinemia is one of the diabetic syndromes and causes a number of complications of the central and peripheral nervous system functioning. Under type 1 diabetes mellitus this condition can manifest itself by decreased production of insulin by pancreatic β-cells caused by their massive death, and under type 2 diabetes mellitus following overstimulation of the insulin secretory machinery of the β -cell for compensation of permanent hyperglycemia. The brain is a highly insulin-sensitive organ (Zhao et al., 2004) with high expression of

insulin receptors predominantly in the hippocampus, neocortex, cerebellum, etc. (Fernandez and Torres-Alemán, 2012). Hence, many cognitive impairments associated with diabetes can also occur due to dysfunction of insulin receptor signaling cascades under hypoinsulinemia.

Recently much attention has been devoted to the role of insulin-dependent signaling in the regulation of neurogenesis and synaptic plasticity in the hippocampus and its effect on memory and learning processes. Various positive effects of insulin have been described, such as the neurotrophic action on both differentiated neurons and neuronal stem cells (Kleinridders et al., 2014), stimulation of synaptogenesis (Chiu et al., 2008) and promotion of synaptic plasticity (Huang et al., 2004; Grillo et al., 2015; Spinelli et al., 2019; Zhao et al., 2019). Insulin induces both presynaptic and postsynaptic forms of neuronal plasticity at hippocampal synapses. This hormone stimulates the proliferation and metabolism of insulin-sensitive glia (Heni et al., 2011) and therefore may affect the functional state of neurons and their synaptic connection properties. Interestingly, insulin is a modulator rather than an "inducer" of synaptic plasticity, and multiple sites of action are responsible for the effect of insulin on synaptic plasticity (Mainardi et al., 2015). Thus, dysfunction of insulin signaling pathways caused by decline of insulin levels can lead to impairment of cognitive processes under different pathological conditions.

Since hypoinsulinemia may affect the function of many insulin-sensitive organs, the primary culture of rat hippocampal neurons can be successfully used to determine the effect of insulin on the functioning of hippocampal synapses and their plasticity. Such approach allows to eliminate the numerous modulatory effects of insulin on some other organs and body systems.

The role of insulin in synaptic plasticity at hippocampus has been studied earlier (Lee et al., 2011; Mainardi et al., 2015, Zhao et al., 2019), however, the locus of short-term plasticity expression and the improving role of insulin in presynaptic release of glutamate in these neurons remain unclear, especially under conditions of previous insulin deprivation. The aim of this study was to investigate the insulin effects on modulating of paired-pulse plasticity at glutamatergic synapses of hippocampal neurons under hypoinsulinemia model.

2. Materials and methods

2.1. Ethical approval

All experimental procedures were performed in accordance with international principles of the European Convention for the protection of vertebrate animals used for experimental and other scientific purposes, Strasburg, 1986; the Law of Ukraine "On protection of animals from cruelty" and approved by the Animal Care Committee of Bogomoletz Institute of Physiology.

2.2. Hippocampal neurons culture preparation

Primary hippocampal neuronal culture from neonatal Wistar rats was prepared as described previously (Fedulova et al., 1999) with some modifications. Briefly after decapitation the rat hippocampus was removed, dissected into segments and incubated in 0.05% trypsin (type II) solution during 10 min (t = 23–25°C). Then, the hippocampal segments were washed with culturing solution containing Eagle's modified medium (MEM) 9.6 g/l, 10% horse serum, 2.2 g/l $NaHCO_3$, 103 nM insulin, penicillin 25 U/ml and streptomycin 25 μg/ml. The concentration of insulin for hippocampal neurons culturing was quite consistent with the physiological insulin levels, that can be found in brain tissues (Schechter et al., 1992; Duarte et al., 2012; Ghasemi et al., 2013). After mechanical dissociation (by Pasteur's pipettes) in culturing solution, hippocampal neurons were plated into the previously poly-L-ornithine-coated coverslips in Petri dishes at cell density approximately 30,000 cm^{-2}. Further, the neurons were incubated at 37°C at 5% CO_2 in culturing solution during 3 days, and after that 5 μM cytosine-A-D-arabinofuranoside was added for 24 h to the culture medium to reduce glia proliferation.

To simulate hypoinsulinemia, the cultured (16–20 days *in vitro*) hippocampal neurons were incubated in insulin-free media for 4 days [the time of manifestation of a significant effect of insulin deprivation on synaptic transmission according to our previous studies (Shypshyna et al., 2021)]. Electrophysiological experiments were carried out using cells after 20–24 days in culture.

2.3. Electrophysiology

Using the patch-clamp method under "whole cell" configuration and the method of local extracellular electrical stimulation of single presynaptic axon, the glutamatergic evoked excitatory postsynaptic currents (eEPSCs) in hippocampal neurons were recorded and analyzed. To obtain the best control of intracellular potential and to reduce "dendritic filtering" of eEPSCs, we performed axonal stimulation in close proximity to the soma of the postsynaptic neuron. Local electrical stimulation was performed by rectangular voltage pulses of negative polarity with a duration of 0.4 ms and frequency of 0.5 s^{-1}, that were supplied through stimulation micropipette (inner diameter of about 2 μm) filled with a standard extracellular solution and connected to the outlet of the ISO-Flex isolated output stimulator (AMPI, Israel). The amplitude of the voltage at stimulating pipette input varied from 30 to 40 V. The relationship between the output voltage (0–30 V) and the potential close to the mouth of the stimulating pipette was linear. The position of stimulating pipette was set considering the diameter zone of effective potential shift (Fedulova et al., 1999), in close (1–2 μm) proximity to the presumable axon.

To estimate the short-term plasticity a paired-pulse ratio (PPR) was calculated using the peak amplitudes of two consecutive EPSCs (interpulse interval 50 ms) by dividing the mean amplitude of the 2nd eEPSC by that of the 1st eEPSC. The period between one pair of stimuli and the next pair was 3 s, which was sufficient for full recovery of eEPSCs. The coefficients of variation values for the 1st and 2nd eEPSCs amplitudes (CV1 and CV2) were compared to estimate the average CV ratio (CV2/CV1).

All experiments were carried out at 20–22°C. Extracellular bath solution contained (in mM): NaCl 140; KCl 3; $CaCl_2$ 2; $MgCl_2$ 2; glucose 6; HEPES 20 (pH was adjusted to 7.4 with NaOH). To reduce the GABA- and glycinergic neurotransmission in culture 1 μM strychnine and 10 μM bicuculline were always added to the bath solution. The hippocampal neuron was voltage-clamped

at –70 mV. Patch pipettes from borosilicate glass (WPI, USA) with tip inner diameter 1–1.5 μm were filled with intracellular solution containing (in mM): K-gluconate 155; EGTA 0.5; $MgCl_2$ 1; HEPES 20 (pH was adjusted to 7.2 with KOH). Exchange of external solution and drugs application was performed using a rapid-change system (2 ml per min). All drugs were obtained from Sigma.

To control the series resistance and quality of voltage clamping at hippocampal neurons throughout the experiments the time constant of capacitive current in response to rectangular hyperpolarizing stimulus (10 ms duration, –10 mV amplitude) and amplitude of leakage current were monitored. Data were not included into analysis, if significant variation (>20%) of these parameters occurred during experiment.

The experimental setup was constructed by the staff of Bogomoletz Institute of Physiology, Kyiv, Ukraine. The recorded currents were filtered at 5 kHz, digitized at 10 kHz and stored in a personal computer for display and analysis using two EPC-8 amplifiers ("HEKA," Germany), DigiData 1322A analog-to-digital converter interface, and the WinWCP v3.9.6 (University of Strathclyde, UK) and pClamp 9.0 (Axon Instruments) software.

2.4. Statistical analysis

A simple binomial model was used according to the previously described methods (Sola et al., 2004) to calculate the probability of glutamate release (*p) and* the value of quantum content (*m):*

$$p = 1 - \frac{M\mathrm{CV}^2}{q\left(1 + CV^2\right)};\ m = M/q$$

where M and CV^2 are the mean and the coefficients of variation of the 1st eEPSCs in pairs under paired-pulse stimulation; q and cv^2 are the mean and the coefficients of variation of miniature synaptic currents (mEPSCs). The glutamatergic mEPSCs were measured in extracellular low Ca^{2+}/high Mg^{2+} solution (Isaacson and Walmsley, 1995) containing 0,5 mM Ca^{2+}, 10 mM Mg^{2+} and 0,25 μM TTX (Fedulova et al., 1999).

All data are presented as mean ± SEM. Statistical analysis of experimental data were performed by the paired and unpaired Student's *t*-test. In all cases, *n* refers to the number of hippocampal neurons. All data were tested for normality using the Shapiro–Wilk test. Two-way ANOVA test with *post-hoc* Bonferroni tests was used where needed (factors: culturing conditions: normo-/hypoinsulinemia, insulin effect: control/insulin addition).

3. Results

In order to determine whether insulin affects presynaptic expression of glutamatergic plasticity at hippocampal synapses under hypoinsulinemia, the standard paired-pulse plasticity paradigm was applied. Using the method of single presynaptic axon stimulation combined with whole cell patch-clamp recording we analyzed the monosynaptic glutamatergic eEPSCs under paired-pulse stimulation at 50 ms inter-stimulus intervals. The analyzed monosynaptic eEPSCs were mediated by activation of ionotropic glutamate receptors and were entirely abolished by application of 10 μM DNQX with 10 μM DL-AP5 (**Figure 1**). Addition of GABA- and glycinergic receptor blockers (1 μM strychnine and 10 μM bicuculline) did not alter the amplitude and kinetics of eEPSCs.

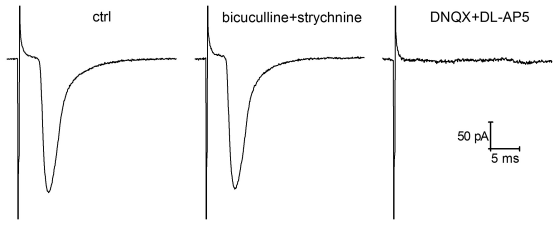

FIGURE 1
Glutamatergic evoked glutamatergic excitatory postsynaptic currents (eEPSCs) recorded in cultured hippocampal neurons following local extracellular electrical stimulation of single presynaptic axon. The represented traces of eEPSCs (averaged of 50 sweeps) demonstrate the action of GABA (gamma-aminobutyric acid)- and glycinergic neurotransmission blockers (1 μM strychnine and 10 μM bicuculline) and the effects of ionotropic glutamate receptor antagonists (10 μM DNQX and 10 μM DL-AP5) on the amplitude of eEPSCs.

In hippocampal neurons cultured at normal insulin concentration (normoinsulinemia), the paired stimulation of the single presynaptic axon usually elicited the paired-pulse facilitation (PPF) of glutamatergic eEPSCs (**Figure 2A**). Application of insulin at concentration of 100 nM for 4 min to these neurons lead to slight raising of the mean amplitudes of eEPSCs (ratio 1.1 ± 0.02, $P < 0.005$; $n = 15$) and to the increase of PPR from 1.15 ± 0.01 to 1.25 ± 0.01 ($P < 0.05$; $n = 15$), while there were no statistically significant changes in the CV ratio of eEPSCs under the insulin action (in control CV1 = –0.36 ± 0.03 and CV2 = –0.37 ± 0.03; after insulin addition CV1 = –0.33 ± 0.03 and CV2 = –0.34 ± 0.03; $P = 0.16$; $n = 15$). It should be clarified, that during the experiment the neurons of different cultures were kept in the extracellular solution before insulin application for approximately the same time. We have identified *de novo* insulin effect on paired-pulse plasticity, therefore each neural network was not reused to avoid the cumulative effect of insulin action during repeated washouts.

To verify whether insulin modulates the release probability at hippocampal synapses we estimated the amplitude and frequency of glutamatergic mEPSCs in a distinct series of experiments. Insulin did not change the amplitude of mEPSCs (**Figure 2B**), which would reflect an effect of single quanta release, but slightly increased its frequency (from 0.97 ± 0.15 to 1.86 ± 0.18 s^{-1}; $P = 0.005$; $n = 7$), that is associated with the enhancement of basal neurotransmitter release. These results are consistent with the previous reports about stimulating effect of insulin on the increase of mEPSCs frequency (Lee et al., 2011).

Use of simple binomial statistics to calculate the probability of glutamate release (p) and quantal content (m) values showed a significant increase of m approx. by 1.2 times ($P < 0.005$; $n = 15$), while p did not change significantly in insulin (0.64 ± 0.01 and 0.68 ± 0.01) (**Figure 2A**). This suggests that enhancing effect on glutamatergic eEPSCs might be realized through the mechanisms different from potentiation of presynaptic release.

To simulate hypoinsulinemia conditions, mature hippocampal cell cultures 16–20 DIV were placed into an insulin-free medium for 4 days, after that electrophysiological experiments were carried out. The experimental conditions corresponded to those described

10.3389/fncel.2023.1132325

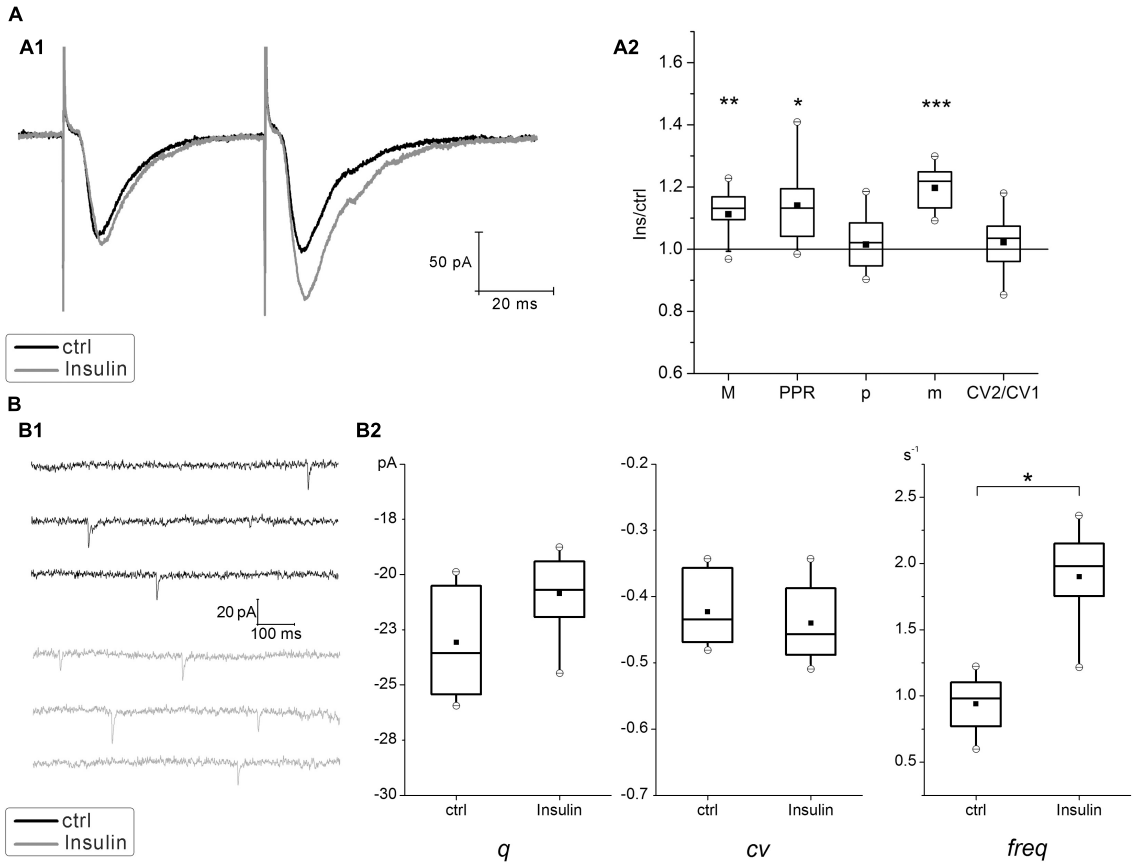

FIGURE 2
Effect of insulin on glutamatergic excitatory postsynaptic currents (EPSCs) at hippocampal neurons cultured under normoinsulinemia conditions. **(A)** Paired-pulse plasticity of evoked glutamatergic excitatory postsynaptic currents (eEPSCs) changes under insulin action. **(A1)** Sample traces of eEPSCs pairs in control (ctrl) and after 100 nM insulin application (Insulin) in the same single cell (averaged of 30 sweeps). **(A2)** The box charts show average changes of the 1st eEPSCs amplitudes (M) in the pairs, the coefficient of variation (CV), the paired-pulse ratio (PPR), the release probability (*p*) and the quantal content (*m*) after insulin addition compared with the relative parameters measured at the same synapses in control (taken as 100%). Statistical significance is indicated by: *$P < 0.05$; **$P < 0.005$; ***$P < 0.001$ compared with control (paired Student's paired *t*-test, $n = 15$). **(B)** Insulin effects on miniature EPSCs (mEPSCs). **(B1)** Sample traces of mEPSCs measured at the same neurons before (ctrl) and after (Insulin) extracellular insulin application. **(B2)** Comparison box charts of mEPSCs amplitude (quantal size, *q*), the coefficient of variation of mEPSCs (cv) and mEPSCs frequency (freq) before (ctrl) and after (Insulin) insulin addition. Statistical significance is indicated by: *$P < 0.05$ compared with control (Student's paired *t*-test, $n = 7$).

for cultures of the normoinsulinemia group. In hypoinsulinemia, glutamatergic hippocampal synapses were divided into two subgroups depending on the expression of the paired-pulse plasticity form (Figures 3A, B). In the PPF subgroup ($n = 17$) insulin application for 4–6 min did not cause significant changes in the parameters of PPR, CV2/CV1 ratio and binomial parameters *p* and *m*. In the PPD subgroup, insulin significantly increased the value of PPR from 0.77 ± 0.005 to 0.97 ± 0.006 ($P < 0.005$; $n = 16$) and decreased the CV2/CV1 ratio from 1.67 ± 0.02 to 1.3 ± 0, 01 ($P < 0,05$; $n = 16$), that may indicate an increase of release probability at glutamatergic synapses on these neurons. Additional analysis of binomial parameters confirmed these results: *p* increased by 1.3 times, while *m* did not change. In both subgroups, the insulin action on hippocampal neurons cultured under hypoinsulinemia conditions did not cause significant changes of their eEPSCs amplitudes (1st eEPSC in a pairs). We compared the 1st eEPSC in the PPF and PPD subgroups: mean values did not differ [M (PPF) = −131.5 ± 32.2 pA; M (PPD) = −100.1 ± 48.0 pA; $p = 0.6$, unpaired Student's *t*-test]. In addition, the PPR values in the PPD subgroup of hypoinsulinemia after insulin addition did not differ significantly from those measured in the control of normoinsulinemia ($p > 0.05$; two-way ANOVA), while control PPR values in normoinsulinemia and in the PPD subgroup of hypoinsulinemia significantly differed ($p < 0.05$; two-way ANOVA).

The present results are consistent with the previous data regarding presynaptic modulation of plasticity in glutamatergic synapses of hippocampal neurons under insulin action (Ferrario and Reagan, 2018), when the blockade of insulin receptors leads to a decrease in the efficiency of excitatory neurotransmission due to a decrease of presynaptic release probability of glutamate.

4. Discussion

Insulin signaling in the hippocampus has been targeted to improve impaired cognitive activity associated with diabetes mellitus and obesity (Fernandez and Torres-Alemán, 2012).

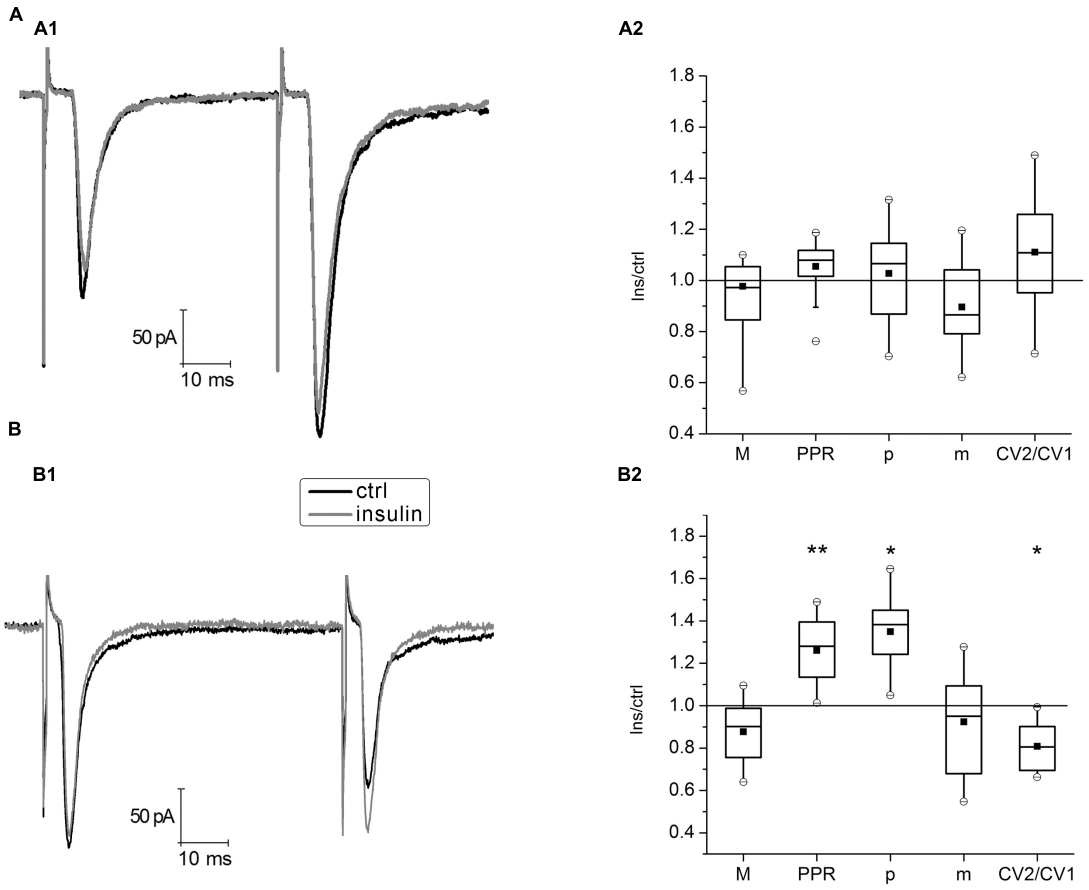

FIGURE 3
Insulin action on paired-pulse plasticity of evoked glutamatergic excitatory postsynaptic currents (eEPSCs) at glutamatergic synapses of hippocampal neurons under hypoinsulinemia. **(A)** Paired-pulse facilitation (PPF) under 100 nM insulin addition. **(A1)** Average traces of eEPSCs pairs in control (ctrl) and after insulin application (Insulin) in the same single cell. **(A2)** The box charts show average changes of PPF parameters amplitudes (M), coefficient of variation (CV), paired pulse ratio (PPR), release probability (*p*), and quantal content (*m*) (same as in **Figure 1**) under insulin action compared with those measured before insulin addition (control) at the same synapses (taken as 100%). Differences of corresponding values with those in control were not significant (Student's paired *t*-test, $P > 0.17$, $n = 17$). **(B)** Paired-pulse depression (PPD) after 100 nM insulin addition. Sample traces of eEPSCs pairs **(B1)** and summary plot of PPD parameters changes **(B2)** are presented similarly, to those in **(A)**. Statistical significance is indicated by: $*P < 0.05$; $**P < 0.005$ compared with control (Student's paired *t*-test, $n = 16$).

Insights into the underlying electrophysiological mechanisms of insulin-mediated changes in synaptic transmission and plasticity may further refine treatment efficacy. Our studies demonstrate that insulin application to hippocampal neurons cultured at normoinsulinemic conditions slightly increases the amplitude of the glutamatergic eEPSCs and, accordingly, their quantum content (*m*), while no significant changes of the release probability (*p*) were observed in these synapses. The action of insulin in this case may rather reflect its modulating effect on postsynaptic glutamate receptors and/or an increase in number of vesicles in the immediately releasable or primed pool at their presynapses. An increase of the mEPSCs frequency can also testify in favor of the latter, which is consistent with the previous reports, showing the stimulation of basal neurotransmitter release by insulin (Lee et al., 2011).

It has been suggested that insulin may target both pre- and postsynaptic membranes to affect basal synaptic transmission. For instance, it enhances the activity of postsynaptic NMDARs (N-methyl-D-aspartate receptors) in the synaptic membrane and mediates postsynaptic effects of the hormone (Skeberdis et al., 2001; van der Heide et al., 2005; Zhao et al., 2019). On the other hand, an increase in quantum content may reflect the stimulating effect of insulin on an increase in the number of releasable vesicles in these synapses, since *m* depends on *p* and *n* (the number of release sites). Apparently these changes do not affect the release probability (CV of eEPSCs and *p* did not change under insulin action).

Physiological and pathological conditions can influence insulin signaling and efficacy. For instance, patients with obesity and/or type 2 diabetes mellitus had lower insulin concentrations in the cerebrospinal fluid despite higher levels of this hormone in peripheral plasma (Heni et al., 2014). Obesity and inflammation can impair the transport of this hormone to the brain (Ketterer et al., 2011). As a result, changes in insulin signaling in the hippocampus can affect molecular mechanisms underlying synaptic plasticity and increase the risk of neurodegeneration and dementia (Kodl and Seaquist, 2008). Our previous results have shown that hypoinsulinemia causes significant weakening of synaptic activity in neural networks of cultured hippocampal neurons and decreases neurotransmitter release in their synapses (Shypshyna et al., 2021).

In order to address how insulin affects paired-pulse plasticity in the model of hypoinsulinemia, we specifically probed the effects of 100 nM insulin, as this concentration produced a robust response in the previous studies (Ghasemi et al., 2013; Zhao et al., 2019). Such insulin level is within concentration range that might occur locally in brain tissues *in vivo*. It was reported that normal physiological levels of insulin in circulating blood of adult rats is 180–240 pM (Havrankova et al., 1978, 1979). However, local accumulations of insulin can come from plasma circulation as well as activity-dependent insulin release from neurons and various glial cells (Ghasemi et al., 2013). Thus, *in vivo* insulin levels in brain tissues could be 10–100 times higher than in peripheral blood (Schechter et al., 1992; Duarte et al., 2012).

Our results have shown that against the background of hypoinsulinemia, insulin has a dual action on plasticity in hippocampal synapses. On the one hand, insulin did not have a significant effect on PPF of eEPSCs and did not change the binomial parameters p and m in these synapses; on the other hand, insulin changed PPD in the direction of increasing PPR and release probability p at these synapses.

It has been shown that PPF of eEPSCs is the most common form of paired-pulse plasticity at 50 ms interpulse interval (Debanne et al., 1996), which is the apparent reason for observing PPF under normoinsulinemia in our experiments. In addition, PPF of eEPSCs is most often observed at individual glutamatergic synapses with a low baseline release probability, whereas PPD occurred in synapses with a high release probability (Jiang et al., 2000). Therefore, we may predict the multidirectional effect of insulin on the short-term plasticity in hippocampal synapses under hypoinsulinemia depending on the baseline probability of glutamate release in them. Thus, in hypoinsulinemia, we observed both PPF and PPD, which may indicate the heterogeneity of hippocampal synapses in their resistance to insulin deprivation. Interestingly, in normoinsulinemia, insulin increased PPF, while in hypoinsulinemia such effect was not found in the PPF subgroup, whereas in the PPD subgroup, insulin appeared to decreased the PPD value. Thus, in hypoinsulinemia, the absence of insulin action on PPF neurons may indicate the development of insulin resistance, while the effect of insulin on PPD neurons indicates its ability to recover the form of plasticity to the control level in normoinsulinemia.

Thus, insulin has a modulating effect on short-term synaptic plasticity in hippocampal neurons, stimulating the glutamate release due to an increase in the quantal content in synapses of neurons under normoinsulinemia conditions. In our study under hypoinsulinemia at synapses with PPD, insulin recovered some properties of the paired-pulse plasticity to the normoinsulinemic level, including by increasing the probability of glutamate release in their synapses, but insulin did not have a significant effect on the parameters of paired-pulse plasticity at PPF synapses due to their probable insulin resistance.

Data availability statement

The raw data supporting the conclusions of this article will be made available by the authors, without undue reservation.

Ethics statement

The animal study was reviewed and approved by Animal Ethics Committee of the Bogomoletz Institute of Physiology (Kyiv, Ukraine).

Author contributions

MS carried out the experiments, conceived and designed the analyses, collected the data, performed the analysis, and wrote the article. OK carried out the experiments, collected the data, and performed the analysis. SF and NV contributed to the study design and article editing. All authors contributed to the article and approved the submitted version.

Funding

This work was funded on a regular basis by the National Academy of Sciences of Ukraine.

Conflict of interest

The authors declare that the research was conducted in the absence of any commercial or financial relationships that could be construed as a potential conflict of interest.

Publisher's note

References

Chiu, S. L., Chen, C. M., and Cline, H. T. (2008). Insulin receptor signaling regulates synapse number, dendritic plasticity, and circuit function in vivo. *Neuron* 58, 708–719. doi: 10.1016/j.neuron.2008.04.014

Debanne, D., Guérineau, N. C., Gähwiler, B. H., and Thompson, S. M. (1996). Paired-pulse facilitation and depression at unitary synapses in rat hippocampus: Quantal fluctuation affects subsequent release. *J. Physiol.* 491(Pt 1), 163–176. doi: 10.1113/jphysiol.1996.sp021204

Duarte, A. I., Moreira, P. I., and Oliveira, C. R. (2012). Insulin in central nervous system: More than just a peripheral hormone. *J. Aging Res.* 2012:384017. doi: 10.1155/2012/384017

Fedulova, S. A., Vasilyev, D. V., Isaeva, E. V., Romanyuk, S. G., and Veselovsky, N. S. (1999). Possibility of multiquantal transmission at single inhibitory synapse in cultured rat hippocampal neurons. *Neuroscience* 92, 1217–1230. doi: 10.1016/s0306-4522(99)00084-6

Fernandez, A. M., and Torres-Alemán, I. (2012). The many faces of insulin-like peptide signalling in the brain. *Nat. Rev. Neurosci.* 13, 225–239. doi: 10.1038/nrn3209

Ferrario, C. R., and Reagan, L. P. (2018). Insulin-mediated synaptic plasticity in the CNS: Anatomical, functional and temporal contexts. *Neuropharmacology* 136(Pt B), 182–191. doi: 10.1016/j.neuropharm.2017.12.001

Ghasemi, R., Haeri, A., Dargahi, L., Mohamed, Z., and Ahmadiani, A. (2013). Insulin in the brain: Sources, localization and functions. *Mol. Neurobiol.* 47, 145–171. doi: 10.1007/s12035-012-8339-9

Grillo, C. A., Piroli, G. G., Lawrence, R. C., Wrighten, S. A., Green, A. J., Wilson, S. P., et al. (2015). Hippocampal insulin resistance impairs spatial learning and synaptic plasticity. *Diabetes* 64, 3927–3936. doi: 10.2337/db15-0596

Havrankova, J., Roth, J., and Brownstein, M. J. (1979). Concentrations of insulin and insulin receptors in the brain are independent of peripheral insulin levels. Studies of obese and streptozotocin-treated rodents. *J. Clin. Invest.* 64, 636–642. doi: 10.1172/JCI109504

Havrankova, J., Schmechel, D., Roth, J., and Brownstein, M. (1978). Identification of insulin in rat brain. *Proc. Natl. Acad. Sci. U.S.A.* 75, 5737–5741. doi: 10.1073/pnas.75.11.5737

Heni, M., Hennige, A. M., Peter, A., Siegel-Axel, D., Ordelheide, A. M., Krebs, N., et al. (2011). Insulin promotes glycogen storage and cell proliferation in primary human astrocytes. *PLoS One* 6:e21594. doi: 10.1371/journal.pone.0021594

Heni, M., Schöpfer, P., Peter, A., Sartorius, T., Fritsche, A., Synofzik, M., et al. (2014). Evidence for altered transport of insulin across the blood-brain barrier in insulin-resistant humans. *Acta Diabetol.* 51, 679–681. doi: 10.1007/s00592-013-0546-y

Huang, C. C., Lee, C. C., and Hsu, K. S. (2004). An investigation into signal transduction mechanisms involved in insulin-induced long-term depression in the CA1 region of the hippocampus. *J. Neurochem.* 89, 217–231. doi: 10.1111/j.1471-4159.2003.02307.x

Isaacson, J. S., and Walmsley, B. (1995). Counting quanta: Direct measurements of transmitter release at a central synapse. *Neuron* 15, 875–884. doi: 10.1016/0896-6273(95)90178-7

Jiang, L., Sun, S., Nedergaard, M., and Kang, J. (2000). Paired-pulse modulation at individual GABAergic synapses in rat hippocampus. *J. Physiol.* 523(Pt 2), 425–439. doi: 10.1111/j.1469-7793.2000.t01-1-00425.x

Ketterer, C., Tschritter, O., Preissl, H., Heni, M., Häring, H. U., and Fritsche, A. (2011). Insulin sensitivity of the human brain. *Diabetes Res. Clin. Pract.* 93(Suppl. 1), S47–S51. doi: 10.1016/S0168-8227(11)70013-4

Kleinridders, A., Ferris, H. A., Cai, W., and Kahn, C. R. (2014). Insulin action in brain regulates systemic metabolism and brain function. *Diabetes* 63, 2232–2243. doi: 10.2337/db14-0568

Kodl, C. T., and Seaquist, E. R. (2008). Cognitive dysfunction and diabetes mellitus. *Endocr. Rev.* 29, 494–511. doi: 10.1210/er.2007-0034

Lee, C. C., Huang, C. C., and Hsu, K. S. (2011). Insulin promotes dendritic spine and synapse formation by the PI3K/Akt/mTOR and Rac1 signaling pathways. *Neuropharmacology* 61, 867–879. doi: 10.1016/j.neuropharm.2011.06.003

Mainardi, M., Fusco, S., and Grassi, C. (2015). Modulation of hippocampal neural plasticity by glucose-related signaling. *Neural Plast.* 2015:657928. doi: 10.1155/2015/657928

Schechter, R., Whitmire, J., Holtzclaw, L., George, M., Harlow, R., and Devaskar, S. U. (1992). Developmental regulation of insulin in the mammalian central nervous system. *Brain Res.* 582, 27–37. doi: 10.1016/0006-8993(92)90313-x

Shypshyna, M. S., Kuznetsov, K. I., Fedulova, S. A., and Veselovsky, M. S. (2021). Effects of artificial hypoinsulinemia on synaptic activity and plasticity of glutamatergic neurotransmission in culture of hippocampal neurons. *Fiziol. Zhurnal* 67, 3–11. doi: 10.15407/fz67.04.003

Skeberdis, V. A., Lan, J., Zheng, X., Zukin, R. S., and Bennett, M. V. (2001). Insulin promotes rapid delivery of N-methyl-D–aspartate receptors to the cell surface by exocytosis. *Proc. Natl. Acad. Sci. U.S.A.* 98, 3561–3566. doi: 10.1073/pnas.051634698

Sola, E., Prestori, F., Rossi, P., Taglietti, V., and D'Angelo, E. (2004). Increased neurotransmitter release during long-term potentiation at mossy fibre-granule cell synapses in rat cerebellum. *J. Physiol.* 557(Pt 3), 843–861. doi: 10.1113/jphysiol.2003.060285

Spinelli, M., Fusco, S., and Grassi, C. (2019). Brain insulin resistance and hippocampal plasticity: Mechanisms and biomarkers of cognitive decline. *Front. Neurosci.* 13:788. doi: 10.3389/fnins.2019.00788

van der Heide, L. P., Kamal, A., Artola, A., Gispen, W. H., and Ramakers, G. M. (2005). Insulin modulates hippocampal activity-dependent synaptic plasticity in a N-methyl-d-aspartate receptor and phosphatidyl-inositol-3-kinase-dependent manner. *J. Neurochem.* 94, 1158–1166. doi: 10.1111/j.1471-4159.2005.03269.x

Zhao, F., Siu, J. J., Huang, W., Askwith, C., and Cao, L. (2019). Insulin modulates excitatory synaptic transmission and synaptic plasticity in the mouse hippocampus. *Neuroscience* 411, 237–254. doi: 10.1016/j.neuroscience.2019.05.033

Zhao, W. Q., Chen, H., Quon, M. J., and Alkon, D. L. (2004). Insulin and the insulin receptor in experimental models of learning and memory. *Eur. J. Pharmacol.* 490, 71–81. doi: 10.1016/j.ejphar.2004.02.045

frontiers | Frontiers in Cellular Neuroscience

TYPE Original Research
PUBLISHED 13 April 2023
DOI 10.3389/fncel.2023.1132092

OPEN ACCESS

EDITED BY
Ertugrul Kilic,
İstanbul Medipol University, Türkiye

REVIEWED BY
Agenor Limon,
The University of Texas Medical Branch at Galveston, United States
Berrak Caglayan,
İstanbul Medipol University, Türkiye

*CORRESPONDENCE
Volodymyr A. Yavorsky
✉ jva@biph.kiev.ua

SPECIALTY SECTION
This article was submitted to Cellular Neuropathology, a section of the journal Frontiers in Cellular Neuroscience

RECEIVED 26 December 2022
ACCEPTED 29 March 2023
PUBLISHED 13 April 2023

CITATION
Yavorsky VA, Rozumna NM and Lukyanetz EA (2023) Influence of amyloid beta on impulse spiking of isolated hippocampal neurons. *Front. Cell. Neurosci.* 17:1132092. doi: 10.3389/fncel.2023.1132092

Influence of amyloid beta on impulse spiking of isolated hippocampal neurons

Volodymyr A. Yavorsky*, Nataliia M. Rozumna and Elena A. Lukyanetz

Department of Biophysics of Ion Channels, Bogomoletz Institute of Physiology, National Academy of Sciences of Ukraine, Kyiv, Ukraine

One of the signs of Alzheimer's disease (AD) is the formation of β-amyloid plaques, which ultimately lead to the dysfunction of neurons with subsequent neurodegeneration. Although extensive researches have been conducted on the effects of different amyloid conformations such as oligomers and fibrils on neuronal function in isolated cells and circuits, the exact contribution of extracellular beta-amyloid on neurons remains incompletely comprehended. In our experiments, we studied the effect of β-amyloid peptide (Aβ1–42) on the action potential (APs) generation in isolated CA1 hippocampal neurons in perforated patch clamp conditions. Our findings demonstrate that Aβ1–42 affects the generation of APs differently in various hippocampal neurons, albeit with a shared effect of enhancing the firing response of the neurons within a minute of the start of Aβ1–42 application. In the first response type, there was a shift of 20–65% toward smaller values in the firing threshold of action potentials in response to inward current. Conversely, the firing threshold of action potentials was not affected in the second type of response to the application of Aβ1–42. In these neurons, Aβ1-42 caused a moderate increase in the frequency of spiking, up to 15%, with a relatively uniform increase in the frequency of action potentials generation regardless of the level of input current. Obtained data prove the absence of direct short-term negative effect of the Aβ1–42 on APs generation in neurons. Even with increasing the APs generation frequency and lowering the neurons' activation threshold, neurons were functional. Obtained data can suggest that only the long-acting presence of the Aβ1–42 in the cell environment can cause neuronal dysfunction due to a prolonged increase of APs firing and predisposition to this process.

KEYWORDS

amyloid, rhythmic spiking, action potential, tonic generation, patterns of generation, perforated patch clamp, isolated hippocampal neurons

1. Introduction

Alzheimer's disease (AD) is the most common form of progressive dementia with persistent, progressive memory and cognitive impairment and plays a leading role among late-onset diseases. Multiple causes of AD have been shown, but only 3–5% of AD cases are due to genetic factors (Foidl and Humpel, 2020; Zhang et al., 2020), while other cases have a sporadic onset. Health and environmental factors play a significant role in the development of AD, for example, the effect of hypertension on the development of AD (Carnevale et al., 2016), in which high blood pressure disrupts the brain barrier,

type II diabetes, hyperinsulinemia, hypercholesterolemia, obesity; cerebrovascular damage in hypoxia and stroke, excessive activation of homocysteine, intoxication with heavy metals, including copper and iron ions (Singh et al., 2013; Becerril-Ortega et al., 2014). The treatment of AD is based on a various hypotheses, which pay attention to the mechanisms of disease development—deposition of amyloid plaques, hyperphosphorylation of tau proteins, damage of the cholinergic transmission, oxidative stress, impaired lipid metabolism, dysfunction of synapses and others.

The "amyloid" hypothesis associates the disease's development with the accumulation of senile plaques, which mainly consist of amyloid-β (Aβ) aggregates (Querfurth and LaFerla, 2010). Plaques are formed in the extracellular space between neurons under overproduction of Aβ and amyloid precursor protein (APP) by neurons. Enzymatic cleavage of APP by BACE1 and γ-secretase produces the neurotoxic peptide Aβ, which contains 37–42 amino acids. Aβ is excreted outside the neurons and can oligomerize into chains. Aβ1–42 aggregated into oligomers is considered particularly toxic (Cline et al., 2018). While tau dysfunction and tangles have been identified as more robust correlates with cognitive impairment in AD than amyloid plaques, it is still vital to study the role of plaques in the pathogenesis of this disease. Amyloid plaques are a hallmark pathological feature of AD, and their presence has been associated with the onset and progression of the disease. Thus, studying the role of amyloid plaques is still essential for a comprehensive understanding of the disease pathogenesis and for developing effective treatments. In recent studies on the role of Aβ in AD discussed the hypothesis that Aβ accumulation leads to neuronal dysfunction and cognitive impairment. The authors of the review highlight evidence from both animal models and human studies suggesting that Aβ can disrupt neuronal signaling, cause inflammation, and impair synaptic plasticity, ultimately leading to neurodegeneration (Palop and Mucke, 2016). Moreover, the hippocampus (the brain structure responsible for learning and organizing memory) is the core structure that undergoes the first and most significant changes in AD development (Morris et al., 1982; Burgess et al., 2002; Kazim et al., 2017).

Currently, the effect of excessive Aβ production on neural function and network is a highly relevant topic. According to a study by Morimoto et al. (1998), Aβ injection experiments in rat hippocampus demonstrate significant amyloid accumulation around the hippocampus, accompanied by considerable neuronal damage in the CA1 and CA4 regions, as well as the dentate gyrus. Similarly, injection of Aβ1–42 into the rhesus macaque brain resulted in intercellular accumulation of Aβ plaques and neuron death, including cholinergic neurons (Li et al., 2010). Intracellular accumulation of Aβ is also possible in the pathogenesis of AD, and in the initial stages precedes the appearance of amyloid deposits outside the cells (Gyure et al., 2001; Bossers et al., 2010; Friedrich et al., 2010). Such accumulation can cause cognitive impairment even before the stage of amyloid plaques (Billings et al., 2005) and can cause hyperexcitation of neurons (Scala et al., 2015). APP and its fragments, including Aβ, were found on the endoplasmic reticulum membranes, Golgi apparatus, endosomal, lysosomal, and mitochondrial membranes (Kravenska et al., 2020). According to the amphipathic nature of Aβ, it is possible to assume its affinity for the membrane, and therefore the possibility of penetration or attachment to the surface of membranes with the "carpet" or "detergent" effect of damage (Bharadwaj et al., 2018).

The mechanism of Aβ action is still not fully understood, with the loss of membrane integrity being the most commonly considered mechanism. It was also supposed that the Aβ peptide can form a pore in the membrane, which can lead to cell death by affecting cell potential. According to this "pore" hypothesis, the Aβ channel formed by Aβ is permeable to calcium cations in anionic lipids and acid solutions (Hirakura et al., 1999). An excessive influx of calcium through these channels can overload the cell with calcium, resulting in apoptosis and eventual cell death. Aβ in the aggregate state can also cause a decrease in membrane fluidity and, consequently, have a detrimental effect on cell function. According to another hypothesis, Aβ can cause the oxidation of neuronal lipids and leads to the excessive production of free radicals (Butterfield et al., 2001).

Hypotheses about the effect of Aβ on the neuronal generation of action potentials (APs) deal with a wide range of mechanisms acting on different organizational levels of neural networks. On the level of channel structures, studies show that Aβ is a physiological modulator of various currents due to the effect on the expression or activity of channel proteins: A-type potassium current through Kv4 channels, HCN channels, sodium Nav1.1 currents (Plant et al., 2006; Ping et al., 2015). Aβ can block the α7 and α4β2 subunits of the nicotinic acetylcholine receptor (nAChR) in hippocampal cells and cause a presynaptic increase in calcium concentration (Dougherty et al., 2003). The effect of Aβ can also be mediated through the M-current of KCNQ channels (Kv7) (Hessler et al., 2015), corresponding to the data about cholinergic deficiency in the development of AD with memory impairment when blocking cholinergic mechanisms. Intracellular calcium levels go up in transgenic models of mice with AD; such calcium loading can provoke cell death (Querfurth and LaFerla, 2010).

According to another mechanism, chronic exposure to Aβ significantly reduces the branching and length of neurites due to massive damage to synapses and thus increases neuronal bodies' input resistance and thus enhances the response to stimuli (Ghatak et al., 2019). Besides, various Aβ effects on different subcellular compartments (axon, dendrites, and mitochondria) were detected (Kravenska et al., 2016, 2020; Li et al., 2017). The indirect effect of Aβ on neurons can be developed by losing certain types of neurons, such as acetylcholinergic neurons, through inflammation, glial dysfunction, and deposition of Aβ inside blood vessels and their damage, known as cerebral amyloid angiopathy. Similarly, the specific effects of Aβ are associated with dopaminergic FS interneurons in the early stages of AD (Martorana and Koch, 2014).

The effect of Aβ is mainly classified as hyperexcitation of the neuronal network due to either increased excitability of neurons or changes in excitatory and inhibitory transmission between neurons. Damage of synaptic inhibition or excitation/inhibition balance leads to increased gamma-oscillatory activity, the formation of hypersynchronous activity in the neural network, and impaired plasticity of synaptic effects, and in turn, leads to cognitive abnormalities in AD (Mucke and Selkoe, 2012; Busche and Konnerth, 2016; Palop and Mucke, 2016). However, some studies suggest a decrease in interneuron firing under the influence of Aβ (Hazra et al., 2013) because inhibitory neurons have lost the ability to generate APs reliably, leading to hippocampal dysfunction for the APdE9 mouse model. The latter implies the amplification of

sodium leakage currents for inhibitory neurons, with a decrease in the amplitudes of APs and depolarization of the resting membrane potential (Perez et al., 2016). Another study shows that Aβ reduces the impulse activity of fast-spiking interneurons (possibly parvalbumin-positive cells), and the effect differs for various types of interneurons (Villette et al., 2010). However, the relationship between interneuronal firing deficiency with cognitive dysfunction in AD has not yet been experimentally proven. It is suggested that synaptic inhibition may lead to a deficiency of neural network deactivation, promote epileptiform activity, and reduce gamma- and theta-oscillatory activity in patients with AD (Palop and Mucke, 2016).

All these hypotheses and various responses at different organizational hierarchical levels of the nerve system create difficulties in proving the direct effect of Aβ, as there is a whole system of changes in the functioning of neural networks, which cross-initiate other changes. Common Aβ disturbances in the brain are mainly investigated at the brain slices level. In contrast, the study of effects at the single-cell level is limited. Many relationships and correlations do not show the direct effect of Aβ on individual neuron, so there is a need for particular experiments on isolated neurons that can explain the mechanisms of Aβ effects.

The study of the impulse activity of neurons in current-clamp mode was carried out previously with using the extracellular application of Aβ (Jhamandas et al., 2011; Hector and Brouillette, 2020) or the intracellular actions of Aβ through the patch-pipette solution (Fernandez-Perez et al., 2021).

However, the experiments were carried out on cultured cells or brain slices, which had limited isolation from the influence of branched neurites or synapses. These factors have a significant effect on the membrane potential fluctuations of the soma, which could not be adequately compensated in the experiments. Consequently, the shifts in the membrane potential could influence the pulse generation and lead to indirect alterations in the firing frequency.

Several studies were focused on the impact of chronic exposure to amyloid-β on neuronal activity. Although they also did not isolate neurons, these studies emphasized the need for precise control of holding potential, fixing it at −65 or −80 mV (Tamagnini et al., 2015b; Wang et al., 2016; George et al., 2021). However, the testing of neurons for intrinsic excitability were performed using a pipette solution that washed out some intercellular components of the soma, leading to possible alterations in the cell cytosol and resulting in a rapid deterioration of spiking properties.

In summary, the effect of Aβ on neurons is an enhancement in spike firing activity, which is known as hyperexcitability. Hyperexcitability is characterized by an increase in the number of repetitive APs in response to a depolarizing input current stimulus (Jhamandas et al., 2011). It was also regarded as increased excitability and loss of accommodation properties (Jhamandas et al., 2001). The firing threshold of neurons decreased in response to oligomeric Aβ treatment, resulting in the initiation of spikes at lower current stimuli, indicating a reduction in rheobase for firing (Fernandez-Perez et al., 2021). The voltage-dependent decrease in membrane conductance can explain the latter and the acute response of neurons to Aβ1–39, Aβ1–28, and Aβ1–40 by blockage of K+ channels (Good et al., 1996), as well as by an increase in membrane input resistance R_{in} (Tamagnini et al., 2015a). However, the authors imply the long-term compensatory changes due to the increased excitability that brings back resting potential and R_{in} to physiological levels. Incubation of cultured neurons with oligomeric Aβ 42 increases an action potential firing rate (George et al., 2021). Hyperexcitability was also attributed to the hyperpolarization of the action potential threshold after Aβ 500 nM treatment (Tamagnini et al., 2015b), but without any alterations in sub-threshold intrinsic properties of neurons, including membrane potential and input resistance. A lower threshold and a more prominent action potential burst were recorded on primary cultured pyramidal neurons after Aβ1–42 chronic exposure (Wang et al., 2016).

Several studies have noted the complex effects of Aβ on neuronal activity. While some suggest that Aβ initially increases neural excitability, compensatory inhibitory mechanisms may lead to hypoactivity (Hector and Brouillette, 2020). However, this is likely due to the effect of Aβ on synaptic mechanisms rather than on the neuron's soma. Another study (Spoleti et al., 2022) has shown that Aβ can impair cell excitability in CA1 hippocampal neurons in Tg2576 AD mice, that can be attributed to synaptic dysfunction in the hippocampus in this model.

There are two proposed mechanisms that suggest Aβ may increase the generation of action potentials in nerve cells. Aβ causes changes in the characteristics of APs discharges on the soma of neurons, and on the other, Aβ specifically impairs synaptic transmission (Ren et al., 2018).

Although the primary suspect for the leading role is synaptic disorder, the mechanisms must be compared and quantified since there is insufficient data on the influence of Aβ on the activity of individual neurons. Therefore, our study aimed to determine the direct effect of Aβ1–42 on APs generation in isolated neurons of the rat hippocampus by using the perforated-patch clamp experimental design and outline the effects of Aβ1–42 on neurons without synaptic influences by using the analysis based on the construction of the activation APs functions based on the data obtained on isolated neurons.

2. Materials and methods

2.1. Isolation of neurons of the CA1 zone of the hippocampus

All animal treatment and care procedures were conducted following the National Academy of Sciences of Ukraine and Bogomoletz Institute of Physiology guidelines for the care and use of laboratory animals. The method of obtaining isolated neurons of the rat hippocampus generally corresponded to the method described in our previous works (Iavors'kyi and Luk"ianets', 2013; Yavorsky and Lukyanetz, 2015). Animals (30 rats of 14-day-old) were decapitated after anesthesia with ether; the brain was quickly removed and transferred to a cold (4°C) solution A. Slices of the hippocampus 0.4–0.5 mm thick were cut with a blade and then kept for 60 min in solution B at room temperature (21–25°C), placed them on a nylon mesh in the chamber; aeration of the medium was provided by carbogen. Enzymatic treatment in solution-B with 0.1% pronase (type 23) and 0.1% trypsin ("Sigma," USA) lasted 20–35 min without changing the ambient temperature. Dispersion of hippocampal slices allowed us to obtain isolated neurons of the

required zone, which preserved the small parts of the apical and basal dendrites and had a soma with a diameter of 15–20 μm.

Solution-A contained (in mM): NaCl 120, KCl 5, HEPES 10, $MgCl_2$ 1, $CaCl_2$ 2, glucose 25. Solution-B (in mM): NaCl 125, KCl 5, NaH_2PO_4 1.25, $NaHCO_3$ 25, $MgCl_2$ 1, $CaCl_2$ 2, glucose 10. The pipette solution (in mM): $C_6H_5O_7K_3$ (tripotassium salt of citric acid) 60, KCl 20, HEPES 10, $MgCl_2$ 5; amphotericin-B, pre-dissolved in DMSO, was added to the pipette solution at a final concentration of 1 mg/ml. Caffeine (a tool to test intracellular calcium signaling), a blocker of sodium conductance quinidine, selective M1 and M2 agonists McN-A-343 and muscarinic cholinergic agonist oxotremorine, and other substances were obtained from Sigma-Aldrich, USA. Quinidine was tested as a blocker of sodium conductance, as well as two specific blockers of potassium conductance, to determine how effects on membrane conductance alter APs generation. The effects of caffeine were seen through intracellular mechanisms, through the endoplasmic depot, and through calcium mechanisms.

2.2. Electrophysiological leads and protocols

Transmembrane currents and potentials were measured using standard patch-clamp techniques under conditions of perforation of the membrane region under the action of amphotericin-B (Korn et al., 1991; Iavors'kyi and Luk"ianets', 2013; Yavorsky and Lukyanetz, 2015). Briefly, patch pipettes were filled with the pipette solution containing 5mg/ml amphotericin-B, previously dissolved in DMSO. After 5÷15 min of tight contact (more than 3GΩ) with the cell membrane, the serial resistance decreased to 4÷10 MΩ due to membrane perforation by the antibiotic. The cells were considered "healthy" and were brought into the experiment if their stable resting potential was more negative than −50 mV and the action potential showed an overshoot. Then we compensated the Ve of the amplifier to set the neuron's resting membrane potential to −80 mV. Cell activity usually became sufficiently stable about 20 min after starting the clamping, with a duration of 20–30 min for recording. The series of 4–5 ramp protocols have applied a minimum twice for the control solution, tested solution and rewashed by control solution, with 2–3 min resting interval for every cell between series. All recordings were performed at room temperature.

After the seal on the patch pipette, the isolated neurons were lifted from the surface of the experimental chamber to prevent them from touching other cells or resting at the bottom of the chamber. The neurons remained submerged in a solution with a constant laminar flow rate. Aβ1–42 was administered to the isolated neuron using an application pipette with an inner tip diameter of approximately 0.5 mm, about 4–5 mm away from the cell. Mainly, only the data from the initial application of Aβ1–42 was included in the analysis due to incomplete recovery during the washing procedure. The control and testing solutions and the isolated neuron were replaced to prepare for subsequent testing procedures. Due to our stringent selection criteria for AP firing properties, only one neuron was successfully recorded per experimental day, with numerous cells being rejected. A total of 10 records were accepted for further analysis. Changing the extracellular solution's composition was performed by switching the flow with the preservation of a constant flow rate into the chamber while pumping the existing solution with a peristaltic pump on the other side. The duration of the Aβ1–42 application did not exceed 15 min. Introducing low DMSO concentrations (0.1–0.5%) into the extracellular solution does not alter the generation parameters because DMSO was already present in the pipette solution due to the perforated patch method. The PC-ONE amplifier (Dagan Corp., USA) and the Digidata 1200 board (Axon Instruments) were controlled by the software "WinWCP" (University of Strathclyde, UK); patch pipettes were produced on a P97 puller (Sutter Instruments, USA).

Lyophilized Aβ1–42-amyloid rat (SCP0038 Sigma, USA) was diluted in dimethyl sulfoxide to get 1 mM stock solution and stored at a temperature of –20°C. Test solutions with Aβ1–42 were prepared on the day of use by adding Aβ stock into control solution-A to get concentrations from 200 nM to 10 μM and then were stored at room temperature for 1–4 h. The final concentration of dimethyl sulfoxide did not exceed 0.1%. The amyloid fibrils used in the experiments were predominant in aggregated form of Aβ1–42. Amyloid aggregation was verified by measuring thioflavin T fluorescence using a Hitachi F-4000 fluorescence spectrometer. The presence and formation of a fibrillar peptide were indicated by an increase in the fluorescence of thioflavin T (excitation at 450 nm, recording the intensity of fluorescence at 480 nm). Also, we detected the acute shift of extinction coefficient at 415 nm for solution of Aβ1–42 20 μM with thioflavin T 10 μM during the period 1–1.5 h of incubation at 37°C (absorption spectrum with NanoDrop 1000, Proteine&Label protocol, drop volume 2 μl), which may indicate Aβ fibril formation.

Reproducibility of APs generation was achieved by selecting cells with stable characteristics, unique tuning of stimulation protocols, and constant monitoring of the resting potential in neurons with stabilization of the latter at the same level. Toward the selection of protocols that characterize the regular pulse generation and control the pulsing degradation, we proposed serial testing of cells by rectangular and "ramp"-like stimuli (Iavors'kyi and Luk"ianets', 2013; Yavorsky and Lukyanetz, 2015). Test stimulation with a rectangular waveform consisted of a series of 12 rectangular stimuli at a holding resting potential of membrane −80 mV, with a duration of a single stimulus of 1 s. Neurons responded to stimulation by generating APs, which made it possible to estimate neuronal accommodation properties. Records of membrane potential from the 3rd to the 12th testing pulse were used for the analysis. The APs firing in the first and second pulse usually differed slightly from subsequent firing due to the accommodation effect. We apply ten-second resting intervals between stimuli in series. If necessary, manual adjustment of the resting potential was performed to achieve stable conditions during the long-lasting testing of neurons in the periods between stimuli. Test stimuli of triangular shape (ramp testing) lasting 5 s were repeated in series 3–5 times, with 15–20 s between stimuli.

2.3. Construction of activation functions of APs generation of neurons

The functional test for pulse generation changes in a neuron is a sensitive tool for detecting the effects of Aβ. The effect of Aβ1–42 exposure was defined as changes in the APs generation

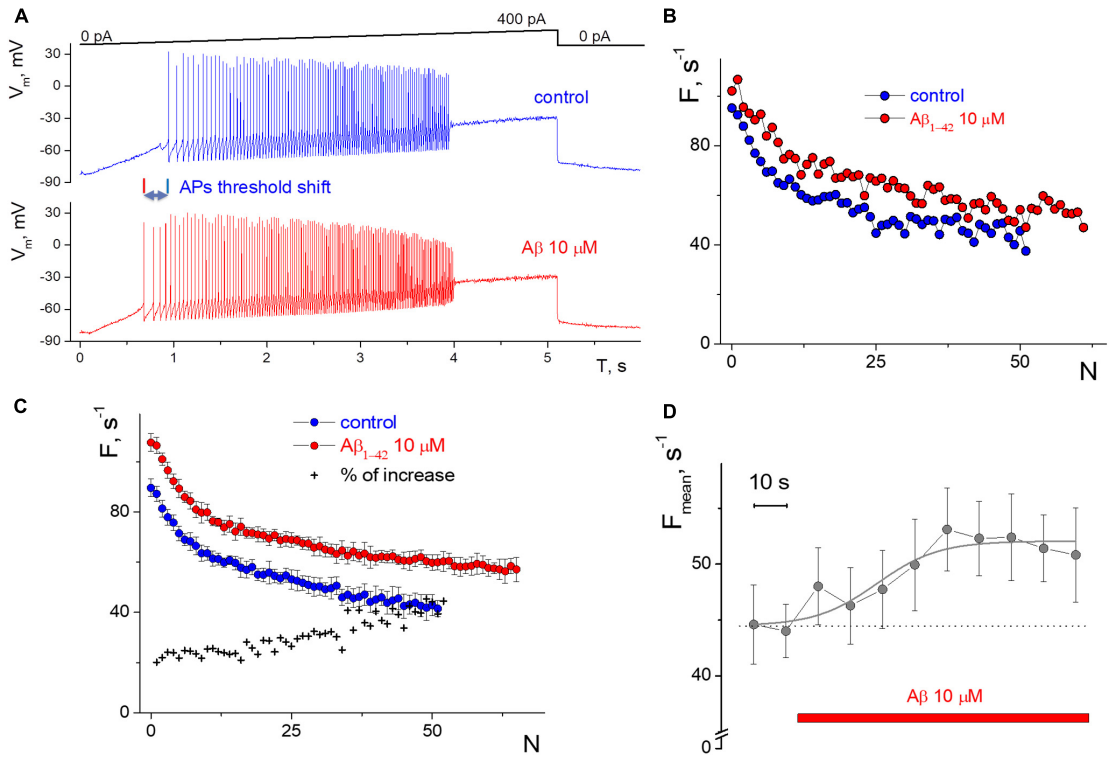

FIGURE 1
Influence of 10 μM Aβ1–42 on the induced impulse generation of a neuron compared to control. **(A)** Records of the neuronal membrane potential in control and under the Aβ1–42 action in the "ramp" protocol with a slow increase in the input current from 0 to 400 pA. **(B)** Firing frequency sequences with accommodation effect in control and 60 s after the Aβ1–42 application in the protocol with a rectangular current impulse with an amplitude of 250 pA and 1 s duration. On the abscissa axis—the ordinal number of the AP, on the *y*-axis—the instantaneous frequency of APs generation (the inverse of the interval between successive AP). **(C)** Neuron's firing frequency sequences with accommodation effect in rectangular protocol with an amplitude of 250 pA and 1 s duration, averaged over a series of 10 test impulses. Comparison of averaged control sequence and those after 6 min of the Aβ1–42 treatment, on the abscissa axis—the ordinal number of the AP, on the *y*-axis—the instantaneous frequency of APs. **(D)** The average frequency of pulse generation with a testing period of 10 s (mean ± SD over calculation interval from 0.7 to 1 s of each test impulse).

of neurons in terms of voltage recordings: the shift of the activity threshold, frequency of induced generation, number of repeated APs upon stimulation, AP half-width (Ghatak et al., 2019). However, insufficient control of the conditions under which the cell generates APs causes shortcomings in most studies' testing schemes. Thus, determining activity by the delay time of AP generation in response to the input stimulus may be uninformative without control of the initial resting potential. The shift of this potential can cause significant errors in determining the parameters of APs activity. Besides, there is absolute randomness of generation in repeated recordings. More informative is a series of tests with the same stimulus, where the input current slowly increases over the transmembrane potential level. APs time samples can be calculated from the record and converted into inter-peak intervals or instantaneous APs frequency. Furthermore, it is worth noting that membrane resistance of the neurons was not directly measured during patch-clamp recording using a specific built-in protocol. Instead, it was calculated post-hoc from recordings of ramp protocols obtained before and after the application of Aβ1–42. To calculate the membrane resistance (Rm), we utilized a linear region of the recorded membrane potential (Vm) below the impulse spiking, while discarding the area near the spiking threshold due to the non-linear rise of Vm. We fitted the linear region to a linear function, and converted the slope parameter into resistance data, assuming that slow changes in the incoming current reflect mostly passive properties of the membrane between −80 and −65 mV. However, it's important to note that the potential slope parameter is a variable, particularly when passing through the generation threshold, and may be influenced by factors such as the quality of the recording or uncontrolled leakage currents.

Also, the input resistance is not a characteristic value for a particular group of neurons but rather an individual characteristic of the neuron. It is important to note that the whole-cell configuration used for registering neuronal activity may not be optimal due to the effect of "washing out" the internal composition of the neuron in a pipette solution. This is because the whole-cell configuration involves rupturing the cell membrane, which may alter the intracellular environment and introduce confounding factors. Additionally, the pipette solution used for whole-cell recordings may differ in composition from the internal environment of the neuron, further complicating the interpretation of results. The latter causes a constant change in the pulse generation's characteristics with a "rundown" activity in a few minutes. The latter leads to the absence of a period of constancy of the excitation characteristics in that it is possible to test the Aβ. Therefore, we used a configuration of perforated patch-clamp. In this case, the washout effect is much smaller, and there is a period in which pulse generation has almost constant characteristics. Thus,

an informative method of analyzing the neuron's impulse activity is to build the APs activation functions of neurons in the protocol with a slow increase in input current ("ramp" protocol) under conditions of quality control and determination of cell generation status (Yavorsky and Lukyanetz, 2015). We determined the peak times of AP and calculated the instantaneous APs frequencies as inverse values of the APs intervals. The APs function was constructed on the graphs as a sequence of frequency values (in the ordinate) depending on the average input current at the inter-peak interval (abscissa axis). Such average current values were calculated from the input current's magnitude, which corresponds to the middle of each APs interval. Elementary linear transformations of APs functions were used to determine the frequency and input current axis shift factors. The APs function was constructed on the graphs as a sequence of frequency values (in the ordinate) depending on the average input current at the APs interval (abscissa axis). Such average current values were calculated from the input current's magnitude, corresponding to the middle of each peak interval. The multiplication factor of the APs function was set as the value that most successfully reproduced the shape of the control sequence from the Aβ-sequence after multiplying the input current values.

We evaluated the neuronal ability to generate APs in the "ramp" protocol and selected only those cells that could generate the APs in a wide range of input current intensities, usually under stimulus from 10 to 100 pA. Also, an analysis of the generation dispersion was performed. Any cell failing to meet the selection criteria was excluded. These criteria included having a well-defined body shape with no indications of swelling, a resting potential that is consistently more negative than −50 mV, action potential demonstrating an overshoot, multiple AP firing that is sustained in response to inward current stimuli, and a neuron that exhibits rhythmic firing with a relatively low coefficient of variation (CV) of interspike intervals less than 30%.

3. Results

The neuronal firing activity was studied based on the frequencies of firing rate, the ability to generate APs at low and high amplitudes of the testing current, and the rhythmicity of firing, as was described previously (Yavorskii et al., 2006; Yavorsky and Lukyanetz, 2009, 2015; Iavors'kyi and Luk"ianets', 2013). APs firing of isolated hippocampal CA1 neurons were obtained in the "ramp" protocol, the records from the fast-spiking neuron shown on **Figure 1A**. It is shown that Aβ1–42 enhances the neuronal capacity to generate action potentials in response to a broader range of stimuli. The latter means that the minimum threshold required for firing activation has decreased, and the maximum threshold for firing inhibition has increased compared to the standard firing. From the "ramp" records, we calculate the membrane resistance below the APs generation threshold by assessing the growth of membrane potential relative to the increase of input current. Neurons have Rm = 1.5 ± 0.6 GΩ in control, and Àβ1–42 elevates Rm by 16 ± 13% (mean ± SD, $n = 10$, $p = 0.0015$ for paired sample t-test), with minimal 4% and maximal 50% of the increase. The noticeable increase in Rm occurred in the first 2–3 min of Àβ1–42 application by 13 ± 15% ($n = 8$, $p = 0.02$). Washing out from Àβ1–42 reduced the Rm on average by 2 ± 19% nonsignificantly ($p = 0.3$), from a decrease of 35% to a further increase of 38%.

First, we consider the values of the instantaneous frequency of APs according to the input current stimulus intensity but previously check the signs of rhythmic firing. The selective approach was used because most tested neurons (>60%) showed a sporadic generation of APs irrespective of stimulation level. Their values of the instantaneous firing frequency formed a "cloud" of points with a significant variance on the graph, making it impossible to construct the dependence of the activation function and its analysis. For the registered "sporadic" neurons, we determined a significant variability within a series of test stimulations for the APs generation threshold (from 30 to 50 pA with repeated stimuli); also, the upper inhibition of APs generation occurred in a wide range of stimulus intensity, from 140 to 170 pA. A thorough analysis of the impulse firing of such neurons is impossible due to the low reproducibility of generation, which causes the unclear influence of external factors. It cannot be ruled out that sporadic firing activity may result from the cell's apoptotic state, damage to the cell membrane after isolation from hippocampal sections, or excess calcium entry into the cell by activating pathological processes. Therefore, we excluded such neurons from the analysis. However, according to our observations, applying Aβ1–42 affects tested "sporadic" neurons with a decrease in the average threshold of APs generation by 5–10 pA.

The study of the action of exogenous Aβ1–42 on the impulse activity of isolated neurons CA1 of the hippocampus was performed at peptide concentrations from 200 nM to 10 μM. Such concentrations are significantly higher than the mean level of Aβ in amylodopathies at 0.5 nM (Waters, 2010). However, due to the aggregation of native amyloid into fibrils and plaques, the concentration of soluble or oligomeric Aβ1–42 can increase significantly near plaques and have a more intense effect on neurons (Tamagnini et al., 2015b). In order to demonstrate the saturation of Aβ1–42 on neuronal impulse activity, concentrations deemed sufficient were used. The specific fractions of aggregated Aβ or Aβ oligomers, which can differentially affect the firing of action potentials, are insignificant as all fractions were present in abundant quantities.

Also, the selected "rhythmic" neurons in the step protocol develop a moderate or low dispersion in the APs sequence, and this rhythmicity was checked under control conditions for 3–5 min before testing. We succeeded in recording APs activity with a narrow spectrum from nine neurons; the coefficient of variation was less than 30%, even with low-intensity stimulation. The low variance also allowed us to clearly distinguish the APs sequences in control and under the influence of Aβ1–42 (**Figures 1B, C**). Neuronal resting potential undergoes only a minor hyperpolarization up to 5 mV when the replacement occurs from control to Aβ1–42 solution, as well as slow spontaneous fluctuations of the membrane potential of neurons by 2–3 mV in amplitude. We manually compensated for this potential shift to −80 mV level to achieve constant conditions for testing and avoid the influence of the holding potential level on the APs frequency.

The direct effect of 10 μM Aβ1–42 was obtained in a series of stimuli by a rectangular current pulse with an amplitude of 250 pA, 1 s duration, and an interstimulus interval of 10 s. Aβ1–42 administration for 60 s caused increasing in firing frequencies by 20–30% (**Figure 1B**), with a minimal change in firing rate at

10.3389/fncel.2023.1132092

the beginning of the stimulus. The accommodation effect of firing causes a gradual decrease in firing frequency during prolonged excitation. Accommodation shape is preserved under the influence of Aβ1–42, along with the characteristic temporal reduction in the APs firing frequencies. A further examination of the neuron firing's properties showed only slight changes in generation frequencies that occurred from the second to 6th minute of Aβ1–42 application (Figure 1C), i.e., a prime shift in APs rate arises during the first minute of Aβ1–42 application. For the represented high-rhythmic neuron, the increase in frequency at the beginning of the stimulus was 20% and rose to the end up to 40%. The latter means that Aβ1–42 may influence a bit more significantly in case of long-lasting firing when the neuron experience accommodation. The count of APs in spike trains increased at Aβ1–42 relative to control, which indicates a diverse improvement in AP firing under the influence of Aβ. Also, we assessed the effect of Aβ1–42 on stationary firing and considered the average of APs firing frequency at the end of the rectangular stimulus, taking data from 0.7 to 1 s. Figure 1D shows the temporal influence of Aβ1–42 that causes a rise in the stationary frequency of APs firing values after 60 s. The influence effect was +20.5% compared to the control when manually controlling the resting potential toward −80 mV and reflecting the central part of the overall effect of Aβ1–42 for 10 min after application. Aβ1–42 elevates or maintains the APs rate for all neurons tested, even under significant inward current stimulation conditions.

The relationship between instantaneous APs firing frequency versus input stimulating current (current injection) we defined (considered) as the APs activation function of the neuron. Figure 2A depicts the relationship between the spiking frequency and the injection current, with experimental data points accurately represented by the Nelder equation. If we consider the spike intervals (the peak-to-peak) instead of the instantaneous frequency of AP generation, the Nelder equation reflects the sum of inverse proportional and linear functions, Figure 2B. The first function reflects the threshold component of APs firing with the threshold parameter a, while the linear function shows a proportional gain of APs generation at high input current intensity. The Nelder equation gives a good approximation for all of the APs trains in ramp protocols and thus the possibility to quantitatively estimate the effects of Aβ1–42 on the spiking activity of neurons.

Under control conditions, the neuron began APs generation at a threshold current from 70 pA to more than 300 pA, with a corresponding increase in frequency from 10 s-1 to 45 s-1. Deviations of values from the primary trend of the sequence tend to be much smaller at the beginning of the stimulus (less than 5%). In comparison, the variance of values increases with intense stimulation (up to 20%). The application of 10 μM Aβ1–42 shifted the generation sequence, as seen in the scattering diagram (Figure 3A). Visually, the shift of values was observed upwards, and to the left side of the graph, so we analyzed two hypotheses about (1) an increase in firing frequencies and (2) a linear shift of sequence by input current corresponding to growth in effective depolarization. Using the Nelder equation, we estimated that a parameter (which reflects the threshold) was −56.5 pA in control, −36.0 pA at the influence of Aβ1–42, and −40.3 pA after washout. Thus, Aβ1–42 shifted the activation threshold in 20.5 pA toward the smaller values.

Detailed analysis showed that tested neurons are characterized by two types of responses to applying Aβ1–42. The shift of the

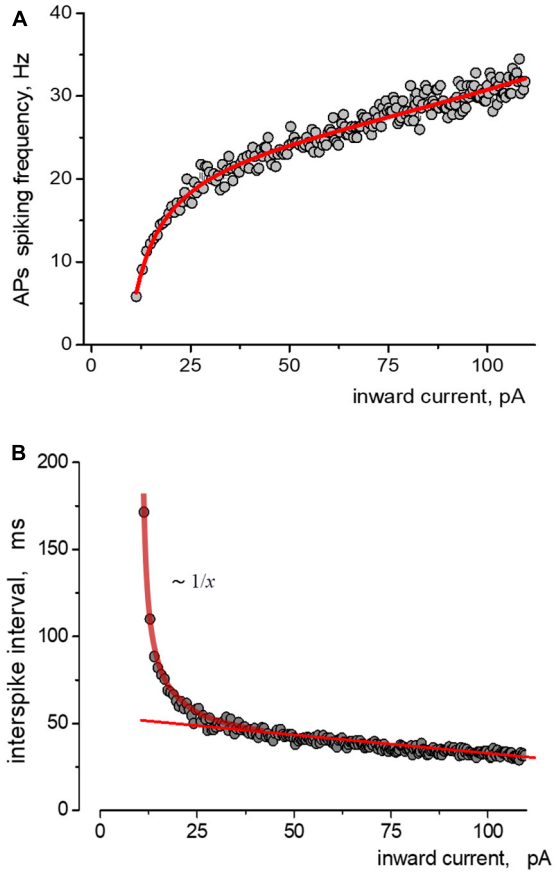

FIGURE 2
Approximations of the data obtained from induced impulse generation of a neuron. **(A)** Fitting the dependence of the frequency of spiking on stimulating inward current, where experimental data approximated by the Nelder function $y(x) = \frac{x+a}{b_0 + b_1(x+a) + b_2(x+a)^2}$ were $a = -9,1 = 0,6; b0 = 0,26 = 0,03; b1 = 0,040 + 0,001; b2 = -1,1e-4 + 1e-5$. Points and solid lines present the experimental data and their approximations, respectively. **(B)** The same data but in form of dependence of the values of interspike interval on the amplitude of stimulating inward current is presented. Experimental data are shown as points, sequence is approximated by sum of reversal function $y(x) \sim 1/x$ and a linear function.

generation threshold current towards smaller values was clearly expressed for six neurons (mean threshold 26 ± 22 pA, maximal frequency 29 ± 11 s-1, shift -41 ± 17%). AP generation under the influence of Aβ1-42 occurred at a lower stimulation intensity by the input current. At low amplitude of input current, the discrepancy in firing frequencies began much higher. For a neuron shown in Figure 3A, we observed the most significant frequency gain within the input current range from 70 to 150 pA. The effect was relatively minor for high-intensity stimulation due to the increase in the average firing frequencies. Washout from Aβ1–42 somewhat reduced the generation frequencies' value, thus partially restoring the sequence toward the control sequence data. However, washout from Aβ1–42 significantly reduced the neuron's ability to fire AP under intense stimulation, with a decrease in the suppression current threshold of AP firing by more than 20%.

In our experiments, four tested neurons had a different response to applying Aβ1–42, which was not accompanied by a shift in the firing threshold (mean threshold 15.5 ± 2.5 pA,

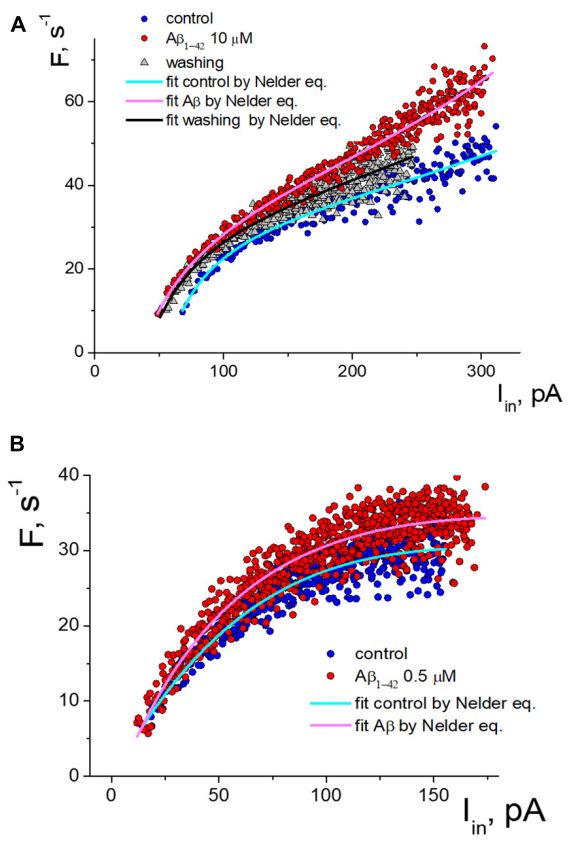

FIGURE 3
Two types of the response of pulsed generation of neurons to the application of Aβ1–42. **(A)** Change of an isolated neuron's activity function with a decrease in the generation threshold under control and Aβ1–42 10 μM, and washing with a control solution which cause partial restoration of the activation function. **(B)** Aβ1–42 increase the frequency of APs generation of neurons without threshold shift. The approximation of instantaneous frequencies under control conditions and the action of Aβ1–42 is presented based on the Nelder function.

maximal frequency 27 ± 7 s-1). An example of the activation data of such a neuron is shown in Figure 3B. For this group of neurons, Aβ1–42 caused a slight increase in the frequency of pulsed generation from 5 to 15%, with approximately the same increase in the firing frequency regardless of input current level. Under the high-intensity stimulus, a significant dispersion of the AP frequency values led to an overlap of the control sequence and the Aβ-sequence.

We define that Rm was changed similarly under Aβ1–42 for two groups of isolated neurons. In the group of neurons with firing threshold shift, Rm = 1.4 ± 0.7 GΩ in control and Aβ1–42 elevates Rm by 21 ± 15% (mean ± SD, n = 6, p = 0.01 for paired sample t-test), with minimal 7% and maximal 50% of the increase. Washing out from Aβ1–42 reduced the Rm on average by 8 ± 15%, from a decrease of 35% to a further increase of 6% (p = 0.16, insignificant). In the group of neurons with no firing threshold shift—Rm = 1.7 ± 0.5 GΩ and Aβ1–42 elevates Rm by 9 ± 6% (n = 4, p = 0.04 for paired -test), with minimal 4% and maximal 15% of the increase. Washing out from Aβ1–42 leads to multidirectional Rm changes with average nonsignificant growth by 9 ± 25%, from a decrease of 5% to an increase of 38%.

For the experimental neurons from the group with the threshold shift response, we found a clear overlay of frequency sequences in control and at Aβ1–42 when transforming Aβ-sequences by multiplying the input current values on the same coefficient (Figure 4A). We can see in the graph that both the control sequence and the Aβ-sequence nearly coincide when multiplying the input current of the Aβ-sequence (x values) by a factor of 1.37 (i.e., increase by 37%). Multiplying factors were roughly calculated for neurons as the firing threshold ratio in control and Aβ1–42 sequences. The multiplied Aβ1–42 sequence visually fully overlaps the control sequence at any input current. Accordingly, the calculated shift factor may resemble the effect of Aβ1–42 on the APs activation function of neurons, and actually, Aβ1–42 causes an uprise of the effective input current without form violation of the APs activation function. The multiplication factors diagram shows the values range from 20 to 65%, with a mean value of 41% (Figure 4B). We did not find a significant correlation between the values of the multiplying factor and the firing threshold current (Pearson r = 0.27), the maximal firing frequency (r = −0.03), the threshold current of firing suppression (r = −0.1), or the concentration values of Aβ1–42, which we used in the range from 200 nM to 10 μM. Presumably, the maximal effect of amyloid may vary between neurons depending on their type or condition or specific sensitivity to Aβ with shifting action.

We compared the effect of amyloid against several other substances on APs firing in isolated neurons (Figure 5). When stimulated with an input current of 20 pA, the voltage-sensitive sodium channel blocker quinidine 40 μM reduced the frequency of APs down to 25% during prolonged spiking but not at the beginning of the stimulation (averaged data over a series of 10 test stimuli, Figure 5A). Caffeine 10 mM, on the contrary, significantly reduced the effect of accommodation without changing the initial spiking frequency and increased the number of repeated APs upon stimulation of 40 pA (Figure 5B). Previously, we saw the remarkable effect of the epileptogenic substance pilocarpine on the firing of isolated neurons (Yavorskii et al., 2006), so we tested the effect of M1 and M2 muscarinic receptor agonists on APs function (Figures 5C, D, respectively). Under a stimulus of 20 pA, agonists show different directions of changes in APs frequencies and the slope of the APs sequence due to the accommodation effect. The M1 agonist McN-A-343 125 μM uniformly increased the APs frequency to 18–28%, while the M2 agonist oxotremorine 50 μM decreased the frequency of APs in a use-dependent manner without changing the initial APs frequency.

4. Discussion

Based on our data, it appears that Aβ1–42 has a dual effect on the impulse firing of neurons. Despite the different characteristics of these effects, they both lead to an enhancement of the firing response of neurons. This enhancement is particularly noticeable during the first minute after the application of Aβ, with a slight increase observed within 5–6 min. In conditions of perforated-patch mode, this proves the absence of direct damaging effects of significant concentrations of amyloid on neuronal functionality due to possible mechanisms of channel formation, reduced membrane fluidity, or loss of its integrity.

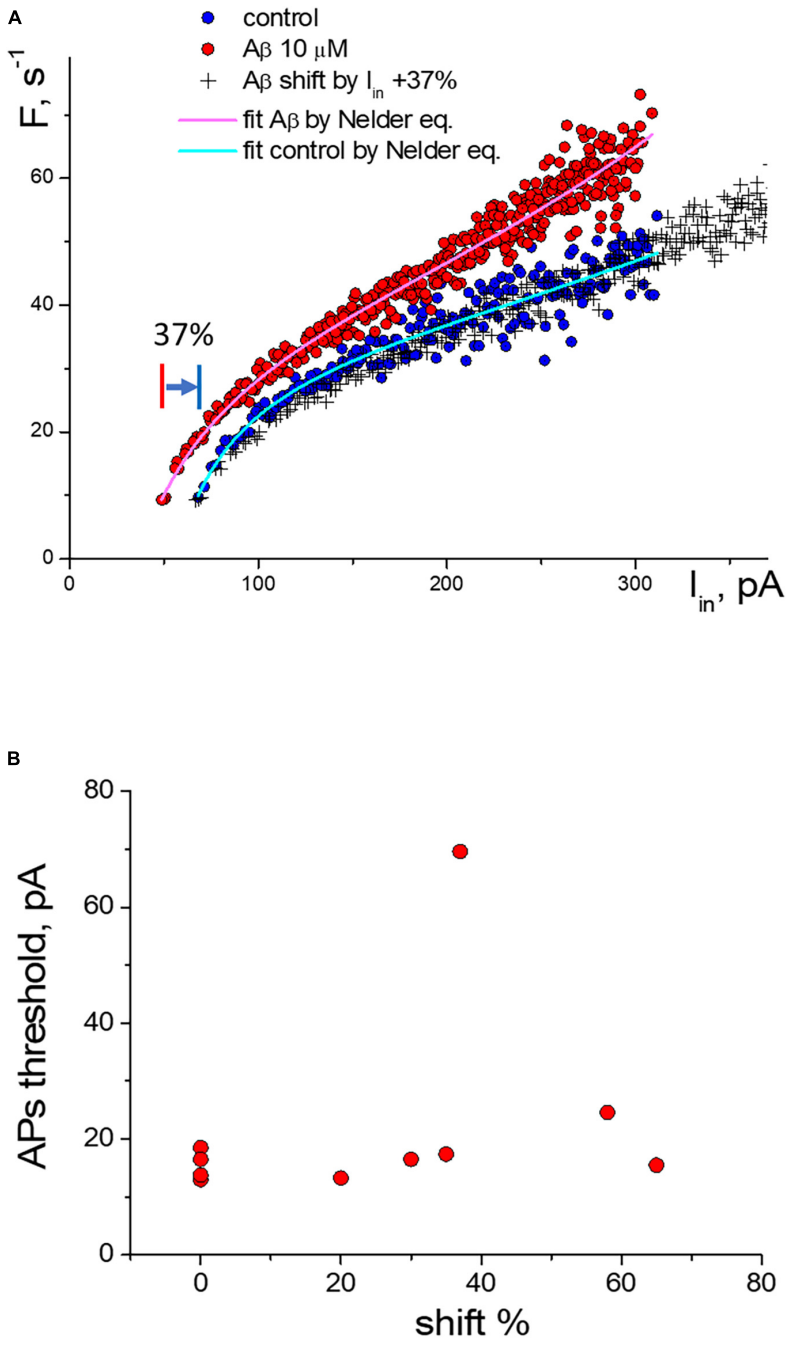

FIGURE 4
Change of the activation function of neurons along the input current's axis under the influence of Aβ1–42. **(A)** Change of the activation function at 10 μM Aβ1–42 in comparison with the control activation function: (○)—control and Aβ1–42 sequences, (+)—transformed sequence obtained by stretching the input current values by 37% (multiplication factor k = 1.37). **(B)** Statistic scattering diagram of the generation threshold levels in control (pA) vs. multiplication (stretching) coefficients in % due to Aβ1–42 action for 10 neurons.

Moreover, Aβ1–42 improves the firing capacity of neurons, and we found no restrictions of this effect for cells with a greater or lesser maximum firing frequency, activation threshold current, or suppression threshold current of AP firing. One fascinating feature of the Aβ effect is its ability to alter the activation function in neurons, resulting in a multiplied input current. Specifically, Aβ1–42 can increase the input current by 30–70%, potentially indicating a boosted membrane resistance. However, this effect may also result in a slight hyperpolarization of the potential, requiring a slightly higher stimulation threshold to reach the generation threshold.

We found that Aβ1–42 enhances impulse generation and lowers the firing threshold that can induce neuronal death at the long term influence, Figure 6. Our experiments confirm the effect of Aβ on reducing the rheobase of neuronal activation and on the increase in the frequency of firing under moderate stimulation. However, the precise mechanisms of these effects are still unknown. These secondary effects can influence and

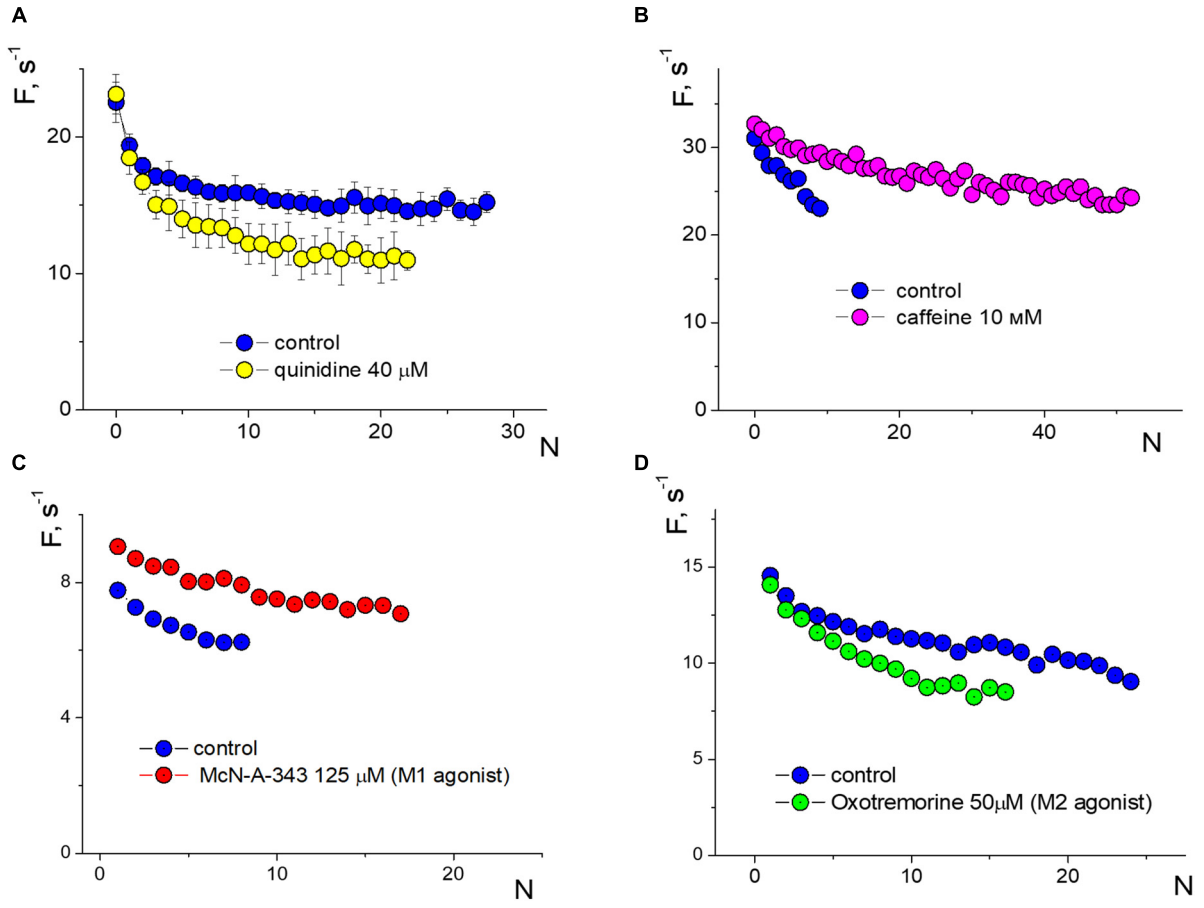

FIGURE 5
Changes in induced firing generation with accommodation effect of a neuron compared to control. Rectangular protocol applied with 1s duration. **(A)** Firing frequency sequences in control and under quinidine 40 μM, testing with an input current of 20 pA. **(B)** Firing frequency sequences in control and under caffeine 10 mM, testing with an input current of 40 pA. **(C)** Firing frequency sequences in control and under McN-A-343 125 μM, testing with an input current of 20 pA. **(D)** Firing frequency sequences in control and under oxotremorine 50 μM, testing with an input current of 20 pA.

strengthen the recorded generation, and to describe the Aβ1–42 effect accurately, it is important to establish a common understanding of the terminology used. Our research suggests that the Aβ action may be equivalent to the amplification of the input current by 20–70%, effectively enhancing the neuronal response to input stimuli without significantly changing the shape and parameters of the activation function. However, in one-third of the neurons tested, we observed a different type of reaction to Aβ1–42, which led to a slight increase in firing frequency (5–15%), regardless of the stimulation intensity. This increase in activity did not involve any shift in the threshold current of the generation or changes in the AP suppression current. Thus, we have identified two distinct mechanisms of neuronal reaction to Aβ1–42: a slight gain in firing frequency or an increase in sensitivity to the input stimulus.

The study of temporal properties of the Aβ1–42 effect has shown that it develops in a few tens of seconds with a characteristic saturation time of nearly one minute. The latter gives evidence against the hypotheses of direct Aβ action as a ligand of voltage-depended channels but permits probable action through indirect signaling pathways, similar to metabotropic effects. It is also possible that Aβ may penetrate cells and adhere to the membranes of internal compartments, such as mitochondria or the endoplasmic reticulum. If this were to occur, it may still enhance the firing capacity of neurons for a few minutes. This enhancement would be marked by a prolonged generation of action potentials

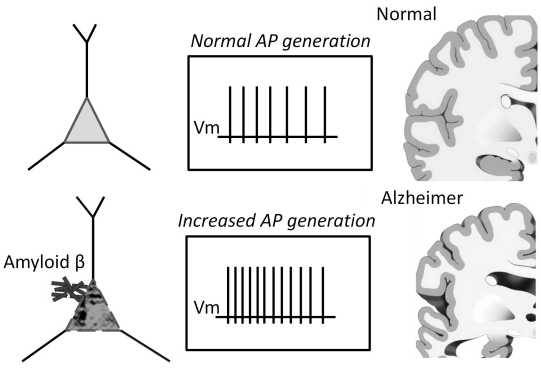

FIGURE 6
Schematic representation of the pathology of Alzheimer's disease depicting the role of increased spiking of neurons in the presence of Aβ1–42.

(APs) in response to a rectangular current pulse stimulation, with an improvement in the mechanism of rhythmogenesis in neurons that has not yet been fully established. Alternatively, it is plausible that the intracellular effects of penetrated Aβ may be compensatory and act as a programmable response of neurons through unidentified amyloid sensors.

The activation function can be a good tool for determining the pathways of influence of different substances. To conduct a comparative analysis of the activation functions of action potentials (APs) for amyloid and other substances, we can examine the direction and character of changes in the APs sequence. The absence of changes in the accommodation effect is a compelling argument that amyloid does not significantly alter sodium or calcium channels, or intracellular mechanisms of calcium signaling involved in the generation of APs. Impairment in sodium conductivity does not indicate a reduction in the amplitude of APs. Our previous research has demonstrated that additional calcium entry can significantly alter the slope of the APs sequence. In contrast, the action of Aβ1–42 is similar to that of the agonist of M1 muscarinic receptors McN-A-343 (**Figure 5C**). It is markedly different from the action of the voltage-gated sodium channel blocker quinidine, which reduces the frequency of the APs sequence by strengthening the accommodation, or from caffeine, which influences intracellular calcium signaling and leads to prolonged APs firing with low accommodation. Therefore, we can suppose that Aβ1–42 primarily affects impulse spiking through M-type (KCNQ) channels, rather than sodium or calcium channels.

The effect of Aβ1–42 is partially reversed at its high concentrations. In our experimental conditions, washing with the control solution after 10 min of Aβ application returned the APs activation function partially toward the control sequence by 20–50%. This backward effect can be considered a weak reduction of APs firing frequency at medium and high stimulus intensities. At the same time, under the condition of Aβ1–42 withdrawal, we observed impairment in the vitality of neurons with a decrease in the threshold of inhibition of generation and a general decrease in the rhythmicity of the pulse. Arrhythmia of AP generation can be a marker of irreversible degradation of neurons' impulse activity and is always observed before the loss of the neuronal ability to fire, according to our previous experiments (Iavors'kyi and Luk"ianets', 2013). The study suggests that the high concentrations of Aβ1-42 can partially reverse its effect on neurons. However, the withdrawal of Aβ1–42 leads to a decrease in the vitality of neurons, including a decrease in the threshold of inhibition of generation and a general decrease in the rhythmicity of the pulse. The arrhythmia of AP generation can be a marker of irreversible degradation of neurons' impulse activity and is always observed before the loss of the neuronal ability to fire.

The present study has demonstrated that applying Aβ1–42 to isolated neurons leads to an increase in the frequency of AP generation and a shift in the threshold for AP generation. These findings agree with previous studies showing similar effects of Aβ1–42 on neuronal function (Jhamandas et al., 2011; George et al., 2021). It has been proposed that the interaction of Aβ1-42 with neuronal membrane receptors, such as N-methyl-D-aspartate (NMDA) and alpha-7 nicotinic acetylcholine receptors, may be responsible for the observed effects (Snyder et al., 2005; Dziewczapolski et al., 2009). This hypothesis is supported by the fact that these receptors are known to be involved in regulating AP generation and synaptic plasticity. Interestingly, the present study also found that the effects of Aβ1–42 were partly reversible upon washing, indicating that the observed changes in neuronal function were not due to irreversible structural damage. This finding is consistent with previous studies that have also reported reversible effects of Aβ1–42 on neuronal function (Shankar et al., 2007; Klyubin et al., 2008; Nimmrich et al., 2008; Ferreira et al., 2015).

In conclusion, our results provide further evidence for the involvement of Aβ in the modulation of neuronal function, particularly in the regulation of AP generation. These findings have implications for our understanding of the pathophysiology of Alzheimer's disease and may provide insights into potential therapeutic targets for treating this devastating disorder.

Data availability statement

The raw data supporting the conclusions of this article will be made available by the authors, without undue reservation.

Ethics statement

This animal study was reviewed and approved by the National Academy of Sciences of Ukraine guidelines, Bogomoletz Institute of Physiology Committee for the care and use of laboratory animals.

Author contributions

VY conducted the literature review and the first draft of manuscript writing, fulfilled electrophysiological experiments and analyses. EL fulfilled conceptualization of studies, created the study design, and contributed to manuscript revisions and translation. NR prepared solutions and tested amyloid. All authors contributed to the article and approved the submitted version.

Funding

This work was partly supported from funds of National Academy of Sciences of Ukraine to support the development of priority areas of research SRN (state registration number) 0120U001281.

Acknowledgments

We thank Dr. Vyacheslav Shkryl for critically reading the manuscript. We gratefully acknowledge the free software WinWCP developed in University of Strathclyde, Glasgow.

Conflict of interest

The authors declare that the research was conducted in the absence of any commercial or financial relationships that could be construed as a potential conflict of interest.

Publisher's note

References

Becerril-Ortega, J., Bordji, K., Fréret, T., Rush, T., and Buisson, A. (2014). Iron overload accelerates neuronal amyloid-β production and cognitive impairment in transgenic mice model of Alzheimer's disease. *Neurobiol. Aging* 35, 2288–2301. doi: 10.1016/j.neurobiolaging.2014.04.019

Bharadwaj, P., Solomon, T., Malajczuk, C. J., Mancera, R. L., Howard, M., Arrigan, D. W. M., et al. (2018). Role of the cell membrane interface in modulating production and uptake of Alzheimer's beta amyloid protein. *Biochim. Biophys. Acta Biomembr.* 1860, 1639–1651. doi: 10.1016/j.bbamem.2018.03.015

Billings, L. M., Oddo, S., Green, K. N., McGaugh, J. L., and LaFerla, F. M. (2005). Intraneuronal Abeta causes the onset of early Alzheimer's disease-related cognitive deficits in transgenic mice. *Neuron* 45, 675–688. doi: 10.1016/j.neuron.2005.01.040

Bossers, K., Wirz, K. T. S., Meerhoff, G. F., Essing, A. H. W., van Dongen, J. W., Houba, P., et al. (2010). Concerted changes in transcripts in the prefrontal cortex precede neuropathology in Alzheimer's disease. *Brain* 133, 3699–3723. doi: 10.1093/brain/awq258

Burgess, N., Maguire, E. A., and O'Keefe, J. (2002). The human hippocampus and spatial and episodic memory. *Neuron* 35, 625–641. doi: 10.1016/s0896-6273(02)00830-9

Busche, M. A., and Konnerth, A. (2016). Impairments of neural circuit function in Alzheimer's disease. *Philos. Trans. R. Soc. Lond. B Biol. Sci.* 371:20150429. doi: 10.1098/rstb.2015.0429

Butterfield, D. A., Drake, J., Pocernich, C., and Castegna, A. (2001). Evidence of oxidative damage in Alzheimer's disease brain: Central role for amyloid beta-peptide. *Trends Mol. Med.* 7, 548–554. doi: 10.1016/s1471-4914(01)02173-6

Carnevale, D., Perrotta, M., Lembo, G., and Trimarco, B. (2016). Pathophysiological links among hypertension and Alzheimer's disease. *High Blood Press Cardiovasc. Prev.* 23, 3–7. doi: 10.1007/s40292-015-0108-1

Cline, E. N., Bicca, M. A., Viola, K. L., and Klein, W. L. (2018). The amyloid-β oligomer hypothesis: Beginning of the third decade. *J. Alzheimers Dis.* 64, S567–S610. doi: 10.3233/JAD-179941

Dougherty, J. J., Wu, J., and Nichols, R. A. (2003). Beta-amyloid regulation of presynaptic nicotinic receptors in rat hippocampus and neocortex. *J. Neurosci.* 23, 6740–6747.

Dziewczapolski, G., Glogowski, C. M., Masliah, E., and Heinemann, S. F. (2009). Deletion of the alpha 7 nicotinic acetylcholine receptor gene improves cognitive deficits and synaptic pathology in a mouse model of Alzheimer's disease. *J. Neurosci.* 29, 8805–8815. doi: 10.1523/JNEUROSCI.6159-08.2009

Fernandez-Perez, E. J., Muñoz, B., Bascuñan, D. A., Peters, C., Riffo-Lepe, N. O., Espinoza, M. P., et al. (2021). Synaptic dysregulation and hyperexcitability induced by intracellular amyloid beta oligomers. *Aging Cell* 20:e13455. doi: 10.1111/acel.13455

Ferreira, S. T., Lourenco, M. V., Oliveira, M. M., and De Felice, F. G. (2015). Soluble amyloid-β oligomers as synaptotoxins leading to cognitive impairment in Alzheimer's disease. *Front. Cell Neurosci.* 9:191. doi: 10.3389/fncel.2015.00191

Foidl, B. M., and Humpel, C. (2020). Can mouse models mimic sporadic Alzheimer's disease? *Neural Regen. Res.* 15, 401–406. doi: 10.4103/1673-5374.266046

Friedrich, R. P., Tepper, K., Rönicke, R., Soom, M., Westermann, M., Reymann, K., et al. (2010). Mechanism of amyloid plaque formation suggests an intracellular basis of abeta pathogenicity. *Proc. Natl. Acad. Sci. U. S. A.* 107, 1942–1947. doi: 10.1073/pnas.0904532106

George, A. A., Vieira, J. M., Xavier-Jackson, C., Gee, M. T., Cirrito, J. R., Bimonte-Nelson, H. A., et al. (2021). Implications of oligomeric amyloid-beta (oAβ(42)) signaling through α7β2-nicotinic acetylcholine receptors (nAChRs) on basal forebrain cholinergic neuronal intrinsic excitability and cognitive decline. *J. Neurosci.* 41, 555–575. doi: 10.1523/JNEUROSCI.0876-20.2020

Ghatak, S., Dolatabadi, N., Trudler, D., Zhang, X., Wu, Y., Mohata, M., et al. (2019). Mechanisms of hyperexcitability in Alzheimer's disease hiPSC-derived neurons and cerebral organoids vs isogenic controls. *Elife* 8:e50333. doi: 10.7554/eLife.50333

Good, T. A., Smith, D. O., and Murphy, R. M. (1996). Beta-amyloid peptide blocks the fast-inactivating K+ current in rat hippocampal neurons. *Biophys. J.* 70, 296–304. doi: 10.1016/S0006-3495(96)79570-X

Gyure, K. A., Durham, R., Stewart, W. F., Smialek, J. E., and Troncoso, J. C. (2001). Intraneuronal abeta-amyloid precedes development of amyloid plaques in Down syndrome. *Arch. Pathol. Lab. Med.* 125, 489–492. doi: 10.1043/0003-99852001125<0489:IAAPDO<2.0.CO;2

Hazra, A., Gu, F., Aulakh, A., Berridge, C., Eriksen, J. L., and Žiburkus, J. (2013). Inhibitory neuron and hippocampal circuit dysfunction in an aged mouse model of Alzheimer's disease. *PLoS One* 8:e64318. doi: 10.1371/journal.pone.0064318

Hector, A., and Brouillette, J. (2020). Hyperactivity induced by soluble amyloid-β oligomers in the early stages of Alzheimer's disease. *Front. Mol. Neurosci.* 13:600084. doi: 10.3389/fnmol.2020.600084

Hessler, S., Zheng, F., Hartmann, S., Rittger, A., Lehnert, S., Völkel, M., et al. (2015). β-Secretase BACE1 regulates hippocampal and reconstituted M-currents in a β-subunit-like fashion. *J. Neurosci.* 35, 3298–3311. doi: 10.1523/JNEUROSCI.3127-14.2015

Hirakura, Y., Lin, M. C., and Kagan, B. L. (1999). Alzheimer amyloid abeta1-42 channels: Effects of solvent, pH, and Congo Red. *J. Neurosci. Res.* 57, 458–466.

Iavors'kyi, V. A., and Luk"ianets', O. O. (2013). Using serial tachograms to measure the evoked impulse activity of isolated hippocampal neurons. *Fiziol. Zh.* 59, 3–10.

Jhamandas, J. H., Cho, C., Jassar, B., Harris, K., MacTavish, D., and Easaw, J. (2001). Cellular mechanisms for amyloid beta-protein activation of rat cholinergic basal forebrain neurons. *J. Neurophysiol.* 86, 1312–1320. doi: 10.1152/jn.2001.86.3.1312

Jhamandas, J. H., Li, Z., Westaway, D., Yang, J., Jassar, S., and MacTavish, D. (2011). Actions of β-amyloid protein on human neurons are expressed through the amylin receptor. *Am. J. Pathol.* 178, 140–149. doi: 10.1016/j.ajpath.2010.11.022

Kazim, S. F., Chuang, S.-C., Zhao, W., Wong, R. K. S., Bianchi, R., and Iqbal, K. (2017). Early-onset network hyperexcitability in presymptomatic alzheimer's disease transgenic mice is suppressed by passive immunization with anti-human APP/Aβ antibody and by mGluR5 blockade. *Front. Aging Neurosci.* 9:71. doi: 10.3389/fnagi.2017.00071

Klyubin, I., Betts, V., Welzel, A. T., Blennow, K., Zetterberg, H., Wallin, A., et al. (2008). Amyloid beta protein dimer-containing human CSF disrupts synaptic plasticity: Prevention by systemic passive immunization. *J. Neurosci.* 28, 4231–4237. doi: 10.1523/JNEUROSCI.5161-07.2008

Korn, S. J., Bolden, A., and Horn, R. (1991). Control of action potentials and Ca2+ influx by the Ca(2+)-dependent chloride current in mouse pituitary cells. *J. Physiol.* 439, 423–437. doi: 10.1113/jphysiol.1991.sp018674

Kravenska, E. V., Ganzha, V. V., Yavorskaya, E. N., and Lukyanetz, E. A. (2016). Effect of cyclosporin a on the viability of hippocampal cells cultured under conditions of modeling of Alzheimers disease. *Neurophysiology* 48, 246–251.

Kravenska, Y., Nieznanska, H., Nieznanski, K., Lukyanetz, E., Szewczyk, A., and Koprowski, P. (2020). The monomers, oligomers, and fibrils of amyloid-β inhibit the activity of mitoBK(Ca) channels by a membrane-mediated mechanism. *Biochim. Biophys. Acta Biomembr.* 1862:183337. doi: 10.1016/j.bbamem.2020.183337

Li, W., Wu, Y., Min, F., Li, Z., Huang, J., and Huang, R. (2010). A nonhuman primate model of Alzheimer's disease generated by intracranial injection of amyloid-β42 and thiorphan. *Metab. Brain Dis.* 25, 277–284. doi: 10.1007/s11011-010-9207-9

Li, W., Xu, Z., Xu, B., Chan, C. Y., Lin, X., Wang, Y., et al. (2017). Investigation of the subcellular neurotoxicity of amyloid-beta using a device integrating microfluidic perfusion and chemotactic guidance. *Adv. Healthc. Mater.* 6:1600895. doi: 10.1002/adhm.201600895

Martorana, A., and Koch, G. (2014). Is dopamine involved in Alzheimer's disease? *Front. Aging Neurosci.* 6:252. doi: 10.3389/fnagi.2014.00252

Morimoto, K., Yoshimi, K., Tonohiro, T., Yamada, N., Oda, T., and Kaneko, I. (1998). Co-injection of beta-amyloid with ibotenic acid induces synergistic loss of rat hippocampal neurons. *Neuroscience* 84, 479–487. doi: 10.1016/s0306-4522(97)00507-1

Morris, R. G., Garrud, P., Rawlins, J. N., and O'Keefe, J. (1982). Place navigation impaired in rats with hippocampal lesions. *Nature* 297, 681–683. doi: 10.1038/297681a0

Mucke, L., and Selkoe, D. J. (2012). Neurotoxicity of amyloid β-protein: Synaptic and network dysfunction. *Cold Spring Harb. Perspect. Med.* 2:a006338. doi: 10.1101/cshperspect.a006338

Nimmrich, V., Grimm, C., Draguhn, A., Barghorn, S., Lehmann, A., Schoemaker, H., et al. (2008). Amyloid beta oligomers (A beta(1-42) globulomer) suppress

spontaneous synaptic activity by inhibition of P/Q-type calcium currents. *J. Neurosci.* 28, 788–797. doi: 10.1523/JNEUROSCI.4771-07.2008

Palop, J. J., and Mucke, L. (2016). Network abnormalities and interneuron dysfunction in Alzheimer disease. *Nat. Rev. Neurosci.* 17, 777–792.

Perez, C., Ziburkus, J., and Ullah, G. (2016). Analyzing and modeling the dysfunction of inhibitory neurons in Alzheimer's disease. *PLoS One* 11:e0168800. doi: 10.1371/journal.pone.0168800

Ping, Y., Hahm, E. T., Waro, G., Song, Q., Vo-Ba, D. A., Licursi, A., et al. (2015). Linking abeta42-induced hyperexcitability to neurodegeneration, learning and motor deficits, and a shorter lifespan in an Alzheimer's model. *PLoS Genet.* 11:e1005025. doi: 10.1371/journal.pgen.1005025

Plant, L. D., Webster, N. J., Boyle, J. P., Ramsden, M., Freir, D. B., Peers, C., et al. (2006). Amyloid beta peptide as a physiological modulator of neuronal 'A'-type K+ current. *Neurobiol. Aging* 27, 1673–1683. doi: 10.1016/j.neurobiolaging.2005.09.038

Querfurth, H. W., and LaFerla, F. M. (2010). Alzheimer's disease. *N. Engl. J. Med.* 362, 329–344. doi: 10.1056/NEJMra0909142

Ren, S. Q., Yao, W., Yan, J. Z., Jin, C., Yin, J. J., Yuan, J., et al. (2018). Amyloid beta causes excitation/inhibition imbalance through dopamine receptor. *Sci. Rep.* 8:302. doi: 10.1038/s41598-017-18729-5

Scala, F., Fusco, S., Ripoli, C., Piacentini, R., Li Puma, D. D., Spinelli, M., et al. (2015). Intraneuronal abeta accumulation induces hippocampal neuron hyperexcitability through A-type K(+) current inhibition mediated by activation of caspases and GSK-3. *Neurobiol. Aging* 36, 886–900. doi: 10.1016/j.neurobiolaging.2014.10.034

Shankar, G. M., Bloodgood, B. L., Townsend, M., Walsh, D. M., Selkoe, D. J., and Sabatini, B. L. (2007). Natural oligomers of the Alzheimer amyloid-beta protein induce reversible synapse loss by modulating an NMDA-type glutamate receptor-dependent signaling pathway. *J. Neurosci.* 27, 2866–2875. doi: 10.1523/JNEUROSCI.4970-06.2007

Singh, I., Sagare, A. P., Coma, M., Perlmutter, D., Gelein, R., Bell, R. D., et al. (2013). Low levels of copper disrupt brain amyloid-β homeostasis by altering its production and clearance. *Proc. Natl. Acad. Sci. U. S. A.* 110, 14771–14776. doi: 10.1073/pnas.1302212110

Snyder, E. M., Nong, Y., Almeida, C. G., Paul, S., Moran, T., Choi, E. Y., et al. (2005). Regulation of NMDA receptor trafficking by amyloid-beta. *Nat. Neurosci.* 8, 1051–1058. doi: 10.1038/nn1503

Spoleti, E., Krashia, P., La Barbera, L., Nobili, A., Lupascu, C. A., Giacalone, E., et al. (2022). Early derailment of firing properties in CA1 pyramidal cells of the ventral hippocampus in an Alzheimer's disease mouse model. *Exp. Neurol.* 350:113969. doi: 10.1016/j.expneurol.2021.113969

Tamagnini, F., Scullion, S., Brown, J. T., and Randall, A. D. (2015b). Intrinsic excitability changes induced by acute treatment of hippocampal CA1 pyramidal neurons with exogenous amyloid beta peptide. *Hippocampus* 25, 786–797. doi: 10.1002/hipo.22403

Tamagnini, F., Novelia, J., Kerrigan, T. L., Brown, J. T., Tsaneva-Atanasova, K., and Randall, A. D. (2015a). Altered intrinsic excitability of hippocampal CA1 pyramidal neurons in aged PDAPP mice. *Front. Cell Neurosci.* 9:372. doi: 10.3389/fncel.2015.00372

Villette, V., Poindessous-Jazat, F., Simon, A., Léna, C., Roullot, E., Bellessort, B., et al. (2010). Decreased rhythmic GABAergic septal activity and memory-associated theta oscillations after hippocampal amyloid-beta pathology in the rat. *J. Neurosci.* 30, 10991–11003. doi: 10.1523/JNEUROSCI.6284-09.2010

Wang, X., Zhang, X. G., Zhou, T. T., Li, N., Jang, C. Y., Xiao, Z. C., et al. (2016). Elevated neuronal excitability due to modulation of the voltage-gated sodium channel nav1.6 by Aβ1-42. *Front. Neurosci.* 10:94. doi: 10.3389/fnins.2016.00094

Waters, J. (2010). The concentration of soluble extracellular amyloid-β protein in acute brain Slices from CRND8 mice. *PLoS One* 5:e15709. doi: 10.1371/journal.pone.0015709

Yavorskii, V. A., Kostyuk, P. G., and Lukyanetz, E. A. (2006). Accommodation properties of isolated hippocampal neurons under conditions of an experimental model of epilepsy. *Neurophysiology.* 38, 175–181.

Yavorsky, V. A., and Lukyanetz, E. A. (2009). Interspike model of neuronal impulse activity. *Fiziol. Zh.* 55:135.

Yavorsky, V. A., and Lukyanetz, E. A. (2015). Using the serial ramp recordings for rapid testing of the generating ability of impulse activity of isolated hippocampal neurons. *Fiziol. Zh.* 61, 19–27. doi: 10.15407/fz61.03.019

Zhang, L., Chen, C., Mak, M. S., Lu, J., Wu, Z., Chen, Q., et al. (2020). Advance of sporadic Alzheimer's disease animal models. *Med. Res. Rev.* 40, 431–458. doi: 10.1002/med.21624

frontiers | Frontiers in Cellular Neuroscience

TYPE Systematic Review
PUBLISHED 17 April 2023
DOI 10.3389/fncel.2023.1131683

OPEN ACCESS

EDITED BY
Oleg Krishtal,
National Academy of Sciences of Ukraine, Ukraine

REVIEWED BY
Kinga Szydlowska,
Polish Academy of Sciences, Poland
Thiago Heck,
Regional University of Northwestern Rio Grande do Sul State, Brazil
Galyna Grigorievna Skibo,
National Academy of Sciences of Ukraine, Ukraine

*CORRESPONDENCE
Olena G. Aliyeva
✉ aliyeva1eg@gmail.com

SPECIALTY SECTION
This article was submitted to Cellular Neuropathology, a section of the journal Frontiers in Cellular Neuroscience

RECEIVED 26 December 2022
ACCEPTED 28 March 2023
PUBLISHED 17 April 2023

CITATION
Belenichev IF, Aliyeva OG, Popazova OO and Bukhtiyarova NV (2023) Involvement of heat shock proteins HSP70 in the mechanisms of endogenous neuroprotection: the prospect of using HSP70 modulators.
Front. Cell. Neurosci. 17:1131683.
doi: 10.3389/fncel.2023.1131683

Involvement of heat shock proteins HSP70 in the mechanisms of endogenous neuroprotection: the prospect of using HSP70 modulators

Igor F. Belenichev[1], Olena G. Aliyeva[2]*, Olena O. Popazova[3] and Nina V. Bukhtiyarova[4]

[1]Department of Pharmacology and Medical Formulation With Course of Normal Physiology, Zaporizhzhia State Medical University, Zaporizhzhia, Ukraine, [2]Department of Medical Biology, Parasitology and Genetics, Zaporizhzhia State Medical University, Zaporizhzhia, Ukraine, [3]Department of Histology, Cytology and Embryology, Zaporizhzhia State Medical University, Zaporizhzhia, Ukraine, [4]Department of Clinical Laboratory Diagnostics, Zaporizhzhia State Medical University, Zaporizhzhia, Ukraine

This analytical review summarizes literature data and our own research on HSP70-dependent mechanisms of neuroprotection and discusses potential pharmacological agents that can influence HSP70 expression to improve neurological outcomes and effective therapy. The authors formed a systemic concepts of the role of HSP70-dependent mechanisms of endogenous neuroprotection aimed at stopping the formation of mitochondrial dysfunction, activation of apoptosis, desensitization of estrogen receptors, reduction of oxidative and nitrosative stress, prevention of morpho-functional changes in brain cells during cerebral ischemia, and experimentally substantiated new target links for neuroprotection. Heat shock proteins (HSPs) are an evolutionarily integral part of the functioning of all cells acting as intracellular chaperones that support cell proteostasis under normal and various stress conditions (hyperthermia, hypoxia, oxidative stress, radiation, etc.). The greatest curiosity in conditions of ischemic brain damage is the HSP70 protein, as an important component of the endogenous neuroprotection system, which, first of all, performs the function of intracellular chaperones and ensures the processes of folding, holding and transport of synthesized proteins, as well as their degradation, both under normoxic conditions and stress-induced denaturation. A direct neuroprotective effect of HSP70 has been established, which is realized through the regulation the processes of apoptosis and cell necrosis due to a long-term effect on the synthesis of antioxidant enzymes, chaperone activity, and stabilization of active enzymes. An increase in the level of HSP70 leads to the normalization of the glutathione link of the thiol-disulfide system and an increase in the resistance of cells to ischemia. HSP 70 is able to activate and regulate compensatory ATP synthesis pathways during ischemia. It was found that in response to the cerebral ischemia formation, HIF-1a is expressed, which initiates the launch of compensatory mechanisms for energy production. Subsequently, the regulation of these processes switches to HSP70, which "prolongs" the action of HIF-1a, and also independently maintains the expression of mitochondrial NAD-dependent malate dehydrogenase activity, thereby maintaining the activity of the

malate-aspartate shuttle mechanism for a long time. During ischemia of organs and tissues, HSP70 performs a protective function, which is realized through increased synthesis of antioxidant enzymes, stabilization of oxidatively damaged macromolecules, and direct anti-apoptotic and mitoprotective action. Such a role of these proteins in cellular reactions during ischemia raises the question of the development of new neuroprotective agents which are able to provide modulation/protection of the genes encoding the synthesis of HSP 70 and HIF-1a proteins. Numerous studies of recent years have noted the important role of HSP70 in the implementation of the mechanisms of metabolic adaptation, neuroplasticity and neuroprotection of brain cells, so the positive modulation of the HSP70 system is a perspective concept of neuroprotection, which can improve the efficiency of the treatment of ischemic-hypoxic brain damage and be the basis for substantiating of the feasibility of using of HSP70 modulators as promising neuroprotectors.

KEYWORDS

heat shock proteins, CNS, ischemia, hypoxia, neuroprotection, HIF-1a, HSP70 modulators

1. Introduction

Currently, a significant amount of information has been accumulated on almost all links of the pathological process triggered by ischemic damage, however, there are significant gaps regarding the mechanisms of endogenous neuroprotection that require further study (Belenichev et al., 2015a; Sheng et al., 2018; Kim et al., 2020a).

It is known that the response to any damage in the body is the activation of its own system of cytoprotection. Thus, ischemic circulatory disorders in the brain lead to the development of hypoxic stress and the launch of adaptive mechanisms of endogenous neuroprotection. Numerous studies have established a large number of intracellular signaling molecules that affect the survival of neurons after ischemia, among them: tumor necrosis factor-α (TNF-α), nuclear factor kappa B (NF-κB), hypoxia-inducible factor 1 (HIF-1), inducible nitric oxide synthase (iNOS), etc. (Ginsberg, 2016).

One of the most studied cytoprotective factors is the HSPs (heat shock proteins) family (Kim et al., 2019). One of the primary reactions of the genome in response to stress of various origins is the induction of HSPs, which are named according to their molecular weights. There is a class of proteins (chaperones), whose main function is to restore the correct tertiary structure of damaged proteins, as well as the formation and dissociation of protein complexes. Many chaperones are HSPs, that is, proteins whose expression begins in response to an increase in temperature or other cellular stresses (Deka and Saha, 2018; Kaur and Asea, 2019; Kim et al., 2019, 2020a).

Heat shock proteins are an evolutionarily integral part of the functioning of all cells, as evidenced by their high degree of homology and presence in all existing organisms (Clerico et al., 2019).

Heat shock proteins were first detected in *Drosophila melanogaster* as a result of incubation at elevated temperatures. Therefore, the synthesis of these proteins was originally considered a temperature-dependent process. Gradually, in many studies, an increase in the level and expression of HSPs was noted in various experimental stress models that did not depend on temperature conditions (UV irradiation, heavy metals, inflammation, ischemia, etc.) (Kampinga and Craig, 2010; Rosenzweig et al., 2019; Zhang et al., 2022).

Heat shock proteins act as intracellular chaperones that support cell proteostasis under normal and various stress conditions (hyperthermia, hypoxia, oxidative stress, radiation, etc.). According to the molecular weight HSPs are usually classified into six subfamilies: HSPH (HSP110), HSPC (HSP90), HSPA (HSP70), DNAJ (HSP40), HSPB [small HSPs (sHSPs)], and the chaperonin families: HSPD/E (HSP60/HSP10) and CCT [cytosolic chaperonin TCP1 ring complex (TRIC)]. Although the overall task of these proteins in maintaining cellular life remains common, the function and tissue specificity of HSPs differ between groups under physiological and stress conditions (Deka and Saha, 2018; Kim et al., 2019).

Eukaryotes often express several members of the HSP70 family, the main isoforms of which are found in all cellular compartments: Hsp72 (HSPA1A) and related HSP70 (Hsc70/HSPA8), in the cytosol and nucleus, BiP (Grp78/HSPA5) in the endoplasmic reticulum, and mtHSP70 (Grp75/mortalin/HSPA9) in mitochondria. HSP70, as an important component of the endogenous neuroprotection system, is the greatest curiosity in conditions of ischemic brain damage. Hsp70 performs the function of intracellular chaperon and plays an important role in the protection of cells from stress, by binding to unfolded proteins and preventing them from aggregating. Additionally, Hsp70 is involved in the folding, holding and transport of newly synthesized proteins, and in the repair of damaged proteins. Hsp70 is also involved in the regulation of gene expression, and in the regulation of protein degradation (Giffard and Yenari, 2004; Kim et al., 2018; Rosenzweig et al., 2019). The cytosolic isoforms, HSP70 and HSP72, are partially functionally redundant, but HSP72 transcription is highly sensitive to stress, and cytosolic HSP70 is constitutively expressed (Nitika et al., 2020). In the endoplasmic reticulum and mitochondria, members of the HSP70 family are believed to

perform specific functions and have unique substrates, while BiP plays a key role in folding and quality control of proteins in the endoplasmic reticulum, and mtHSP70 takes part in the import and export of proteins from mitochondria (Evans et al., 2010). Such a role of these proteins in cellular reactions during ischemia raises the question of the development of new neuroprotective agents which are able to provide modulation/protection of the genes encoding the synthesis of HSP70 proteins. HSP70 plays a protective role in damage to the nervous system, it acts as a chaperone and protects neurons from protein aggregation and excitotoxicity, inhibits neuroapoptosis, neuroinflammation, and exhibits an antioxidant effect. A number of studies have shown the neuroprotective effects of HSP70 caused by an increase in its expression by drugs. These studies substantiate brain protection strategies during ischemia and neurodegeneration.

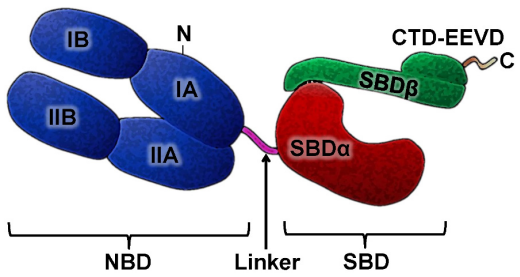

FIGURE 1
HSP70 structure. The HSP70 family members has a highly conserved N-terminal nucleotide-binding domain (NBD) and C-terminal substrate-binding domain SBD and in its structure. NBD and SBD are connected by a linker. The SBD domain is subdivided into a sandwich subdomain (SBDα) and α-helical lid subdomain (SBDβ) followed by unstructured C-terminal domain (CTD), which in many cytosolic Hsp70s is often ends with a charged EEVD motif.

2. The role of HSP70 proteins in the mechanisms of endogenous neuroprotection

It is known that the family of HSP70 includes: inducible/stress block HSP72/HSP70i, constitutive/physiological protein HSP73/HSP70, glucose-regulated protein 78 (GRP78) and GRP75, which plays a critical role in maintenance of cellular homeostasis, constitutive endoplasmic protein GRP73, and inducible heme oxygenase-1 (HO-1) involved in bilirubin metabolism (Kim et al., 2020a; Demyanenko et al., 2021). The constitutive form of HSP70 is equally present in all subcellular compartments and is involved in the operation of cell life support systems under normoxic conditions. On the contrary, the inducible form of HSP70 appears in cells in response to stress, including during ischemic stroke (Belenichev and Litvinenko, 2017; Pavlov et al., 2017a; Craig, 2018; Dukay et al., 2019; Rosenzweig et al., 2019).

First of all, HSP70 is considered as a chaperone protein that provides powerful cell proteostasis. The chaperone function of HSP70 is to interact with damaged, denatured, with subsequent determination of their fraction (Clerico et al., 2019). The appearance and accumulation of damaged proteins in the cell increases the expression of HSP70. After thermal injury causing denaturation of all proteins, the concentration of HSP70 can be up to 20% of all cytoplasmic proteins. The action of HSP70 leads to the formation of thermotolerance – the phenomenon of adaptation to elevated temperatures and an increase in the temperature threshold of sensitivity due to the stabilization of protein molecules with HSP70 during initial, less intense heating (Ramos et al., 2017). HSP70 proteins are necessary for cell repair and survival under stressful conditions, their amount correlates with the severity of various pathological conditions, such as ischemia, inflammation, autoimmune processes, malignant tumors, bacterial and viral infections, and neurodegenerative diseases (Ortan et al., 2018; Kim et al., 2020b). The participation of HSP70 in the mechanisms of holding, folding, and refolding of improperly assembled proteins, as well as the disaggregation and elimination of denatured proteins accumulating under stress conditions, protects the membranes of organelles, primarily mitochondria, and the cells themselves from damage (Aufricht, 2005; Belenichev, 2013; Clerico et al., 2015; Mayer and Gierasch., 2019).

The HSP70 family is known to be very conserved during evolution. The molecular structure of HSP70 has two functional domains: an N-terminal nucleotide binding domain (NBD) and a C-terminal substrate binding domain (SBD), which are connected by a linker. The NBD is subdivided into four subdomains (IA, IB in the lobe I and IIA, IIB in the lobe II), and there is a gap between the two lobes, which is the ATP binding site. SBD is subdivided into a β-sandwich subdomain (SBDβ) and an α-helical subdomain (SBDα), followed by a variable length C-terminal tail [C-terminal domain (CTD)]. The N-terminal NBD provides an ATP/ADP pocket for ATP binding, which is critical for the ATPase reaction necessary for folding and release of proteins. The SBD domain is a pocket for peptide binding (**Figure 1**).

To maintain the chaperone activity of HSP70, the presence of co-chaperones HSP40 and HSP10, which are hydrophobic regions of proteins and regulate the ATP/ADP exchange, is necessary. The HSP70/HSP40 complex ensures the *de novo* assembly of the synthesized protein chain, its transportation into cell organelles and subsequent refolding, preventing interprotein aggregation, maintaining the activity of polypeptides and the degradation of proteins that cannot be restored (Belenichev, 2013; Alderson et al., 2014; Ortan et al., 2018; Mayer and Gierasch, 2019; Kim et al., 2020a).

In response to ischemia, a sharp increase in the level of HSP70 is recorded, while its highest concentration is observed in vital parts of cells: nuclear, perinuclear space, mitochondria, and endoplasmic reticulum, which indicates the importance of chaperone 70 in protection against death (Sharp et al., 2013). As the work of nuclear preribosomes resumes, the concentration of HSP70 in the nucleus decreases and increases in the cytoplasm of cells. Thus, the HSP70 level can be considered as a marker of cellular and tissue damage. Hyperproduction of HSP70 in cells inhibits the development of autophagy as an alternative, more "radical" mechanism of cellular response to stress (Giffard and Yenari, 2004; Sharp et al., 2013; Paul and Mahanta, 2014; Leu et al., 2017; Dukay et al., 2019).

Scientific works of recent years have established a direct cytoprotective effect of HSP70, which is implemented through the regulation of apoptosis and cell necrosis. HSP70 inhibits

the mitochondrial and cytoplasmic pathways of apoptosis. Thus, HSP70 inhibits the transition of procaspase 9 to active caspase 9 and disrupts the formation of apoptosome in the cell cytoplasm. During HSP70 overexpression, the level of the anti-apoptotic protein Bcl-2 increases, which prevents the release of cytochrome c from mitochondria and the translocation of the apoptosis-inducing factor (AIF) into the nucleus, which prevents cell apoptosis. The HSP70 protein inhibits TNFα-induced apoptosis and also effectively inhibits the development of Fas- and TRAIL (TNF-related apoptosis-inducing ligand) mediated apoptosis in various cell types. The accumulation of HSP70 in cells increases the resistance of the latter to staurosporine and doxorubicin, known inducers of apoptosis (Naka et al., 2014).

It is known that ischemia leads to the development of local inflammation, which increases the area of brain damage. In this situation, HSP70 blocks the activation of the inflammatory transcription factor NF-κB and suppresses its cytokine-mediated translocation to the nucleus (Jo et al., 2006). In *in vitro* and *in vivo* models of ischemia, HSP70 inhibits the production of pro-inflammatory cytokines (TNF-α and IL-6), inhibits the activity of matrix metalloprotein kinases (MMPs) and iNOS (Lee et al., 2004; Dukay et al., 2019). It has been established that HSP70 in the culture of astrocytes against during ischemia inhibits proapoptotic Jun N-terminal kinases (JNK) and p38 mitogen-activating protein kinase (MAPK), disrupting the signaling pathway of apoptosis (Wang et al., 2012). The works show a direct relationship between the level of expression of HSP70 and TNFα, iNOS in microglia and MMP-9 in astrocytes. Accordingly, this is another mechanism of action of HSP70 aimed at reducing the size of ischemic damage due to degradation of the extracellular matrix (Barreto et al., 2012; Lee et al., 2012; Leu et al., 2017; Kim et al., 2018).

An important role of HSP70 in the activation of endogenous evolutionarily acquired genetically determined brain defense mechanisms has been established in numerous models of ischemic pre- and postconditioning. It has been established that short-term ischemia induces the synthesis of HSP70 and significantly increases the resistance of brain and myocardial tissues to the next long-term ischemia (Nagai et al., 2010; Sakakima, 2019; Song et al., 2019; Wang et al., 2019).

Various types of cellular stress can lead not only to an increase in the intracellular content of HSP70. In some cases, stress induces HSP70 translocation to the plasma membrane and/or release of these proteins into the extracellular space, which leads to the formation of an extracellular pool of these proteins freely circulating in the body. For the first time, the release of HSP into an extracellular site was recorded in the study of nerve cells. It has been proven that HSP can be released from glial cells (Paul and Mahanta, 2014; Belenichev et al., 2015a; Kim et al., 2018).

Extracellular HSP70 plays the role of a mediator in the processes of intercellular interactions and protein transport. After HSP70 is released into the extracellular space, it can bind to the cell surface via an autocrine or paracrine mechanism. An alternative mechanism of cellular interaction involving HSP70 may be associated with membrane vesicles containing HSP70. These vesicles can be released from cells and then taken up by other cells through membrane fusion or through receptor interaction. One of the first works on this topic described that after the release of HSP70 from glia into the extracellular space, it is taken up by surrounding neurons in the axonal region. The diversity of receptors that interact with HSP70 or are indirectly activated by HSP70 indicates that these proteins interact with different cell types and perform a number of functions outside the cell (Tukaj, 2020).

In recent years, much information has emerged about the importance of extracellular HSP70 in the regulation of the inflammatory process that occurs in response to injury. As a result of cell death, HSP70 is released into the extracellular space and acts as a signal "danger molecule" by interacting with TLR2 and TLR4 receptors of macrophages, glial, and dendritic cells. Interaction with Toll-like receptors leads to the activation of NF-κB, resulting in the activation of the expression of pro-inflammatory cytokines and iNOS (Zheng et al., 2008; Sun et al., 2015; Ortan et al., 2018; Dukay et al., 2019).

In many research papers devoted to the study of the mechanisms of endogenous neuroprotection under conditions of ischemia, the resumption of the work of the glutathione unit of the thiol-disulfide system (TDS) during an increase in the level of HSP70 is noted, and the administration of exogenous HSP70 leads to an increase in the functional activity of the glutathione system in ischemic neurons of experimental animals (Hacke et al., 2008). Thus, under conditions of ischemia, HSP70 proteins mobilize antioxidant resources in neurons by increasing the level of both the cytosolic and mitochondrial pool of reduced glutathione (Lener et al., 2015). Recently, data have appeared on the role of HSP in the stabilization of HIF-1a, which, under conditions of ischemia, is responsible for ensuring the processes of proliferation, apoptosis, angiogenesis, and stabilization of protein molecules under conditions of oxidative stress. It was also shown that under conditions of hypoxia, HSP70 is displaced from the complex with HIF-1a, which, during 20–30 min of hypoxia, protects the structure of the factor from targeted proteolysis. It is likely that HSP70 is able to increase the lifetime of the HIF-1a factor under conditions before and after hypoxia and is necessary for cells to properly respond to oxygen starvation in conditions of acute cerebrovascular accident (Jo et al., 2006; Kadhim et al., 2008; Kampinga and Craig, 2010; Kityk et al., 2015; Kim et al., 2018, 2020a). Activation of microglial products in the penumbra leads to transient activation of genes encoding transcription factors (including c-Fos) in the first few minutes from the onset of a stroke. Then the second wave of expression of HSP genes (HSP70 and HSP72) starts, increasing during the first 1–2 h of the disease and decreasing on the first and second day (Jo et al., 2006; Shulyatnikova and Shavrin, 2012; Hernandez-Ontiveros et al., 2013).

It was found that in suspensions of neurons with the introduction of glutamate (100 μM) and CDNB (80 μM), an increase in the HSP70 concentration was observed with a maximum increase at 30 min of incubation and a subsequent decrease in concentration by 60 min relative to the initial level (Pavlov et al., 2017a). A significant increase in the HSP70 concentration in the cortex and hippocampus was found on the fourth day after occlusion of the common carotid arteries in animals with mild neurological disorders (according to P. McGraw) compared with the control group (non-operated animals). In the experimental group with a moderate level of neurological deficit, a multidirectional change in the concentration of HSP70 occurred – in the cortex, the content of HSP70 was higher than in the control group, while in the hippocampus, the HSP70 concentration was reduced compared to the control group. The minimum level of HSP70 was observed in the hippocampus of the experimental group

with severe neurological symptoms. In the cortex of this group, the level of HSP70 did not differ or was lower than in the control group (Belenichev et al., 2017).

Determination of the HSP70 concentration in the hippocampus at different times after occlusion of the carotid arteries showed that after 12 h a significant increase in protein concentration occurred, and after 24 h the concentration decreased, reaching a maximum by day 4 of the experiment. After 18–21 days of occlusion, the concentration of HSP70 was lower than in the control. In the cerebral cortex of animals after occlusion of the carotid arteries, the concentration of HSP70 was higher than in the control group after 12 h and after 1 day, after 4 days the protein concentration decreased but was at the level or higher than in the control group (Belenichev et al., 2017).

Experimental studies for different periods of ischemia (1 h, 6 h, 24 h, 48 h, 72 h, 120 h, and 21 days) found that during the period of the greatest ischemic damages 24–72 h, hyperproduction of lactate is observed, during the inhibition of GK – enzyme that catalyzes the first reaction of glycolysis. When assessing the dynamics of changes in the oxidative potential, a sharp inhibition of succinate dehydrogenase (SDH) (77–85%) and isocitrate (56–70%) can be noted. The restoration of these indicators begins only by the 21st day of the experiment. Attention is drawn to the initial (from the 1st to the 24th hour) increase in the activity of mitochondrial malate dehydrogenase (MDH) and cytoplasmic MDH with an increase in the level of malate (20–50%), and later (48th–72nd hour) there is a moderate reduction of its activity (10%) with a decrease in the content of malate (16–38%). Thus, we observe a pronounced inhibition of the tricarboxylic acid cycle at the citrate-succinate site. This drastic inhibition of SDH activity makes the implementation of the succinate oxidase pathway for the supply of protons to the respiratory chain problematic. The rise of malate with an increase in the activity of mMDH and cMDH in the first hours of cerebral ischemia indicates the activation of the malate-aspartate shuttle mechanism for the transport of reduced equivalents into mitochondria. The study of bioenergy indicators in the acute period of ischemia (up to 24 h) revealed the following interesting patterns: the most significant changes were in such indicators as the activity of mitochondrial and cytosolic NAD-MDH and NADP-MDH, as well as the content of HSP70 and HIF-1a. A positive correlation was established between changes in the level of malate, NAD-MDH and HSP70 [m_r = 0.821; T-2.94 (m_r is the multiple correlation coefficient; the significance of this coefficient was estimated by the value of Student's t-test with the number of degrees of freedom k = n − 3)]. It was also found that the general trend toward a decrease in malate was associated with the restoration of NADP-MDH and HIF-1a (m_r = 0.839; T-3.09). Mathematical analysis established a direct relationship between the concentration of the HSP70 protein and the level of MDH activity. The study showed that in animals with high scores according to P. McGrow (severe neurological symptoms), the content of malate and HSP70, HIF-1a is the lowest. In studies by Dery et al. it was found that one of the chaperones, the HSP90 protein, is able to bind to the PAS domain of the B factor and stabilize it. Another cellular chaperone, HSP70, recognizes another structural motif of the HIF-1a molecule, the so-called oxygen-dependent degradation domain (ODD) (Dery et al., 2005). It should be noted that the role of these protein-protein interactions is unclear; it is assumed that they are necessary for the stabilization of HIF-1a under normoxic conditions. Under hypoxic conditions, at least one of the chaperones (HSP70) is displaced from the complex with HIF-1a by the ARNT protein, which protects the factor structure from targeted proteolysis during 20–30 min of hypoxia. Thus, HSP70 is able to increase the lifetime of the HIF-1a factor under conditions before and after hypoxia and is required for cells to respond properly to oxygen deprivation. In a general assessment of the results of the study of the metabolism of the nervous tissue, general patterns can be distinguished.

We can conclude that HSP 70 and HIF-1a proteins are inevitable companions of pathobiochemical reactions that develop during ischemic brain damage. Under these conditions, they perform a protective function, which is realized through increased synthesis of antioxidant enzymes, stabilization of oxidatively damaged macromolecules, direct anti-apoptotic and mitoprotective action. Thus, in many recent studies, the important role of HSP70 in the implementation of the mechanisms of metabolic adaptation, neuroplasticity and neuroprotection of brain cells is noted, which allows the presentation of HSP70 as a promising target for neuroprotective drug (Kampinga and Craig, 2010; Kim et al., 2018; Belenichev and Aliyeva, 2019; Belenichev et al., 2022).

3. Modern strategy for neuroprotection: potential modulators of the HSP70-dependent endogenous neuroprotection

Modulation of Hsp70 chaperone activity is a promising neuroprotective strategy. We have identified several diverse pharmacological preparations and substances that can potentially modulate the HSP70 protein system.

3.1. Tamoxifen

Tamoxifen ((Z)-2-[4-(1,2-Diphenyl-1-butenyl)phenoxy]-N,N-dimethyl-ethanamine citrate) belongs to the group of selective estrogen receptor modulators (SERMs) and, depending on the dose, can exert both agonistic and antagonistic effects. Estrogen receptors (ER) are divided into α and β and belong to the family of nuclear transcription factors. Both types of ER are present in all brain cells: in adreno-, GABA-, cholinergic, and serotonergic neurons, as well as in glia. The amount of ER-β is greater in the cortex and hippocampus, and ER-α in the area of the dentate gyrus. In a state of rest, they do not show biological activity and are in contact with proteins (HSP70, HSP90, AP-1, etc.). As a result of the binding of the ligand to the receptor, the conformation of the latter occurs, followed by the release of proteins from the ER-protein complex, which opens access to binding sites on the receptor for transcription and dimerization correlates (Wakade et al., 2008; Arevalo et al., 2011; Pavlov et al., 2017b). Studies have established the ability of tamoxifen to suppress nNOS, mediated through calmodulin, which reduces the production of NO and the accumulation of its damaging product peroxynitrite (Wakade et al., 2008; Paul and Mahanta, 2014; Pavlov et al., 2017b). In addition,

tamoxifen reduces the release of excitotoxic amino acids and acts as a scavenger of free radicals, preventing lipid peroxidation. It has been shown that Tamoxifen and 4-hydroxytamoxifen did not enhance the glutamate-induced increase in intracellular calcium and the activation of NMDA receptors (Cyr et al., 2001; Zhang et al., 2007). In addition, Tamoxifen and 4-hydroxytamoxifen blocked the 17β-estradiol-induced glutamate-dependent increase in intracellular calcium concentration. At the same time, in the culture media of hippocampal neurons, Tamoxifen increased the expression of the anti-apoptotic protein bcl-2, which indicates the neuroprotective effect of the drug. Thus, Tamoxifen and 4-hydroxytamoxifen partially exhibit ER agonist properties in the brain, and in the presence of 17β-estradiol (a "pure" ER agonist) they act as competitive ER antagonists. The obtained research results justify the perspective of studying the modulatory activity of tamoxifen in relation to the HSP70 protein (Pavlov and Belenichev, 2014; **Table 1**). An important point in the antioxidant effect of Tamoxifen was its positive effect on Mn-superoxide dismutase (MnSOD), the main antioxidant enzyme in mitochondria, which regulates the opening of the mitochondrial pore by inhibiting parasitic reactions (Belenichev et al., 2012).

3.2. Melatonin

Melatonin (N-acetyl-5-methoxytryptamine) is a natural hormone of the pineal gland, and is also synthesized by many extrapineal cells: retina, kidney, intestine, ovary, endometrium, glia, astrocytes, lymphocytes, platelets, etc. The substrate for the synthesis of melatonin is serotonin, which is synthesized from tryptophan. The main function of melatonin is to regulate the organism's circadian rhythms, therefore the highest concentration of the hormone is observed in the evening hours and leads to a decrease in emotional tension, a decrease in body temperature, and the development of sleep. By reducing the secretion of gonadotropic hormones, thyrotropin, corticotropin, somatotropin and increasing the content of serotonin and GABA, melatonin normalizes circadian rhythms, increases mental and physical performance, and reduces the manifestations of stress reactions (Reiter et al., 2016; Ramos et al., 2017).

Several subtypes of melatonin receptors have been identified in the organism: membrane MTNR/MT and nuclear RZR/ROR. The density of MT1 receptors is greatest on cells of the anterior lobe of the pituitary gland and suprachiasmal nuclei of the hypothalamus, and their activation is associated with the somnogenic effect of melatonin. MT2 receptors are found in large numbers in various structures of the brain, lungs, and retina and are involved in the processes of body synchronization, the formation of emotions, pain, and neurodegeneration (Liu et al., 2016). Activation of nuclear RZR/ROR receptors provides immunomodulatory and antitumor effects of melatonin (Hernandez-Ontiveros et al., 2013; Reiter et al., 2016).

At the moment, melatonin is considered as a universal cytoprotector in pathologies of the brain and cardiovascular system. It has antioxidant, immunomodulatory, anti-ischemic, anti-apoptotic, and neuroregenerative effects (Storr et al., 2002; Koh, 2008; Lochner et al., 2013; Yu et al., 2014; Lamont et al., 2015; Srinivasan et al., 2015; Dwaich et al., 2016; **Table 1**).

The chemical structure of melatonin allows it to act as a "trap" for free radicals, the hyperproduction of which causes cell damage during ischemic brain damage (Galano et al., 2011; Srinivasan et al., 2015; Vrienda and Reiter, 2015; Ramos et al., 2017). The greatest activity of melatonin is established in relation to the nitric oxide system. By inhibiting nNOS and NO binding, melatonin reduces the level of cytotoxic peroxynitrite and other oxygen intermediates (Storr et al., 2002). The introduction of melatonin increases the activity of antioxidant enzymes: SOD, catalase and glutathione peroxidase (GPO), which reduces the severity of oxidative stress and the amount of damage to brain structures (Fischer et al., 2013; Lochner et al., 2013). *In vivo* experiments on a model of cerebral ischemia established the ability of melatonin to restore memory functions, which is associated with its synaptotropic effect, which is realized due to the restoration of signal transmission in dopaminergic, cholinergic and GABAergic synapses (Beni et al., 2004; Koh, 2008; Hernandez-Ontiveros et al., 2013; Srinivasan et al., 2015; Ramos et al., 2017). The anti-apoptotic properties of melatonin can be associated with increasing expression of apoptosis inhibitor proteins from the Bcl-2 and HSP70 family in nervous tissue, as well as inhibiting the activity of key apoptosis enzymes from the caspase family (Koh, 2008; An et al., 2016). Melatonin increases the expression of HSP70 mRNA, improves the neurological status of rats after carotid occlusion, and promotes the activation of compensatory mitochondrial-cytosolic shunts (Belenichev et al., 2017). Melatonin, due to the induction of the Nrf2 transcription factor, contributes to an increase in the expression of genes of GSH-dependent enzymes, and thus can increase the HSP70 concentration. The prospect of using melatonin as a neuroprotector is also due to its high permeability through the blood–brain barrier and low toxicity (Yu et al., 2014; Srinivasan et al., 2015; Dwaich et al., 2016; Tordjman et al., 2017).

3.3. Heat shock factor-1

Heat shock factor-1 (HSF-1) is the main transcriptional regulator of the cellular response to various types of stress conditions (hyperthermia, hypoxia, radiation, heavy metals, etc.) (Neef et al., 2011). In the absence of stress, HSF-1 is in an inactive state as a monomer connected to HSP. Activation of HSF-1 transcriptional activity is a redox-dependent process. As a result of oxidative stress, denatured proteins accumulate, which serves as a signal for the dissociation of the HSF-1/HSP complex (Xing et al., 2004; Mendillo et al., 2012; Tang et al., 2016). The latter, acting as a chaperone, restores damaged polypeptide chains or ensures their proteasomal degradation. In turn, HSF-1 homotrimerizes and is sent to the nucleus, where, connecting to the regulatory heat shock elements (HSE) in the promoter regions of DNA, it starts the process of transcription of Hsp genes. The increased expression of HSPs continues until their numbers are sufficient to block HSF-1 (Nagai et al., 2010).

In addition to the regulation of the HSP system, HSF-1 is involved in the expression of many genes under normal conditions of cell life and regulates the processes of carbohydrate metabolism,

RNA splicing, apoptosis, ubiquitinylation and protein degradation, detoxification, transport of small molecules, and intracellular signaling (Neef et al., 2011; Mendillo et al., 2012; Otsuka et al., 2016; Su et al., 2016). The administration of HSF-1 (200 μl/kg) to rats after bilateral carotid artery occlusion contributed to a significant increase in the expression of Hsp70 mRNA, HIF-1α mRNA, and HSP70 concentration, as well as to the inhibition of neuroapoptosis in the sensorimotor cortex and CA1 zone of the hippocampus (Belenichev et al., 2017; **Table 1**).

In recent works devoted to HSF-1, the ability of HSF-1 to protect neurons through HSP-independent mechanisms was revealed, while HSF-1 does not require prior trimerization to perform its neuroprotective function (Xing et al., 2004; Qu et al., 2018). The obtained data confirm the perspective of further study of the mechanisms of neuroprotective action of HSF-1 (Verma et al., 2014; Liu et al., 2019; Steurer et al., 2022).

3.4. Glutamine

Glutamine is one of the most common free amino acids in the organism and is metabolized in almost all tissues. This amino acid is synthesized in organism *de novo* by the enzyme glutamine synthetase (GS), but in conditions of cell damage, an acute deficiency of glutamine occurs, which defines it as a conditionally indispensable amino acid (Curi et al., 2005; Cioccari et al., 2015; Cruzat et al., 2018).

Glutamine is an important participant in metabolic processes, energy production, proliferation, and antioxidant protection. So, glutamine provides nitrogen transport and serves as a carbon source. As a result of hydrolysis, an amino group is released from glutamine, which is used in transamination reactions, including the synthesis of aspartic acid, alanine, and phosphoserine. Glutamine nitrogen is involved in the synthesis of purine and pyrimidine bases, which are necessary for cell proliferation and protein synthesis. As a result of the intracellular oxidation of glutamine, ATP is formed, which is of particular value in conditions of glucose and oxygen deficiency in the brain tissue (Welbourne et al., 2001; Curi et al., 2005; Xi et al., 2011; Wang et al., 2015; Dolgodilina et al., 2016; Raizel and Tirapegui, 2018; Kim et al., 2020b).

Glutamine is a precursor of two neurotransmitters: glutamic acid and gamma-aminobutyric acid, and is also used as a substrate for the synthesis of glutathione (GSH) (Tapieroa et al., 2002; Albrecht et al., 2010; Shen, 2013; Dolgodilina et al., 2016; Hayashi, 2018). In turn, GSH supports the intracellular redox potential due to the regulation of redox-dependent signaling and the activity of transcription factors, and also, due to its antioxidant activity, it stabilizes membranes and increases the transmembrane potential of cells (Wischmeyer, 2003; Roth, 2008; Zabot et al., 2014; McRae, 2017; Brovedan et al., 2018). In many research papers, attention

TABLE 1 Pharmacological characteristics of tamoxifen, melatonin, HSF-1, and glutamine.

Drug/Pharmacological group	Dose	Pharmacological effects	References
Tamoxifen/Selective estrogen receptor modulator	0.1 μM; 10 μM	*In vitro* in suspension of neurons with addition of DNIS to incubation medium, tamoxifen increases the Hsp70 level and the activity of HSH-enzymes, and decreases in the number of apoptotically changed neurons.	Belenichev et al., 2020
	1 mg/kg	Tamoxifen at this dose is an ER agonist. In a model of acute cerebral ischemia tamoxifen citrate increases the Hsp70 level in the mitochondria and cytosol of the brain, increases the level of GSH, reduces the concentration of markers of oxidative and nitrosative stress.	Pavlov and Belenichev, 2014
	1 mg/kg; 5 mg/kg	Low-dose of tamoxifen up-regulated ER-α36 expression and enhanced neuronal survival, increased neuroprotective effects by modulating activates or suppress ER-α36 in an ovariectomized ischemic stroke model.	Zou et al., 2015
	5 mg/kg	The protective effect of tamoxifen is due to the mitigation of apoptosis, gliosis and inflammation, as well as the normalization of ER levels in CA1, leading to improved cognitive outcomes 24 h after a silent hippocampal infarct.	Finney et al., 2021
Melatonin/Neuropeptide	5 mg/kg	In carotid artery occlusion, melatonin increased the cytosolic and mitochondrial HSP70 levels, increased the ATP content in the brain, reduced the level of oxidative stress markers.	Belenichev and Bila, 2019
	5 mg/kg	Melatonin prevents cell death resulting from ischemic brain injury, and that its neuroprotective effects are mediated by the activation of Raf/MEK/ERK/p90RSK cascade.	Koh, 2008
	5 mg/kg; 10 mg/kg	Melatonin plays a protective role against ischemia-reperfusion injury by inhibiting autophagy and activating the PI3K/Akt pro-survival pathway.	Zheng et al., 2014
HSF-1/Transcription factor	200 μl/kg	HSF-1 increases the expression of HSP70 and HIF-1a in neurons of the sensorimotor cortex, inhibits neuroapoptosis, activates a compensatory shunt for ATP synthesis, reduces markers of oxidative stress.	Belenichev and Bila, 2019; Belenichev et al., 2020
Glutamine/Amino acid	0.3 and 0.5 g/kg/d	Glutamine enhances the HSP70 expression by via the hexosamine biosynthetic pathway, which inhibits the NF-κB pathway.	Raizel and Tirapegui, 2018
	25 mg/kg	Glutamine increases the concentration of HSP70 in the cytosol and mitochondria, leads to a decrease in neuroapoptosis.	Belenichev and Bila, 2019
	0.75 g/kg	Glutamine has a protective effect on cerebral ischemic injury by reducing oxidative stress, inflammatory response, and promoting astrocyte proliferation, accompanied by the upregulation of HSP70.	Luo et al., 2019

is drawn to the close relationship between the concentration of glutathione and the activity of the chaperone system, primarily HSP70 (Leite et al., 2016; Liu et al., 2018; Luo et al., 2019). In view of the above, the study of the mechanisms of influence of glutamine as a neuroprotective agent is extremely relevant (Chen et al., 2008; Belenichev et al., 2015a; Madeira et al., 2018; **Table 1**).

Analyzing information from various research papers, it is possible to conclude that the problem of increasing the effectiveness of treatment of ischemic stroke remains highly relevant. Endogenous neuroprotection is considered the main direction in solving the problem of combating ischemic damage, the mechanisms of which lead to an increase in the stability of brain cells due to the activation of their own adaptation mechanisms. In this light, chaperone proteins HSP70 are of particular interest, which under conditions of ischemic stress limit protein aggregation and denaturation, support enzyme activity, and increase antioxidant potential.

Thus, the analysis of research papers data determines the perspective and expediency of the study of selected drugs and substances with the aim of establishing the mechanisms of neuroprotective action due to the effect on the expression of the HSP70.

In research has established that in response to damage, an endogenous cytoprotection program is launched, one of the main participants of which is HSP70. The function of this protein was initially associated with a chaperone effect, which consists in ensuring the folding of newly synthesized proteins, the refolding of damaged proteins, and the disposal of irreversibly damaged polypeptides. But during the last decade, studies have appeared confirming its direct antiapoptotic effect. There is also information that HSP70 takes part in the work of the HIF-1α. Under the guidance of HIF-1α, in conditions of hypoxia, the synthesis of glycolytic enzymes such as phosphofructokinase, pyruvate kinase, glyceraldehyde-3-phosphate dehydrogenase, phosphoglycerate kinase, etc. is activated, which improve energy production in conditions of oxygen deficiency. On the other hand, numerous authors speak of a close relationship between the level of HSP70 and the activity of the antioxidant TDS. Therefore, the positive modulation of the HSP70 system is a promising concept of neuroprotection that can improve the effectiveness of the treatment of cerebral strokes. The obtained results confirm the ability of the studied drugs to activate the system of endogenous neuroprotection, namely, the expression of the genes of the HIF adaptation system. By increasing the level of chaperone 70 protein, the studied drugs support the vital activity of the HIF-1α subunit and activate the synthesis of the HIF protein, which increases the expression of adaptation factors, such as: erythropoietin, vascular endothelial growth factor, glycolysis enzymes (lactate dehydrogenase, pyruvate dehydrogenase, phosphofructokinase, aldolase, etc.), and also ensures the operation of alternative energy systems in conditions of hypoxia (malate-aspartate shuttle mechanism).

The high efficiency of HSF-1 can be explained by the fact that it is a natural stress-inducible transcription factor of the HSP family. Under the conditions of accumulation of products of oxidative and nitrosative stress, trimerization of HSF-1 occurs with detachment from the latter of inactivated HSP70 molecules. The activated HSF-1 complex is transported to the nucleus and, connecting with HSE, starts the transcription process of HSP70 genes.

Regarding Tamoxifen, we assume that it interacts with estrogen receptors, resulting in detachment from the last molecules of HSP70, which subsequently acts as a cytoprotector. At the same time, the level of HSP70 mRNA expression under the influence of tamoxifen also has positive dynamics, which indicates the direct participation of the drug in the signaling and transcription of HSP70 mRNA according to the principle of feedback. Activation of SERM β-ER in the brain causes detachment from the last HSP70 proteins, which ensures the entry of these proteins into the cell and the implementation of their biological function. The mechanism of this interaction is associated with the role of HSP70 in maintaining inactive ER that are not associated with estrogens (Zhang et al., 2007; Pavlov and Belenichev, 2014; Cruzat et al., 2018; Belenichev and Bila, 2019). It is assumed that the feedback of the receptor with the steroid ligand leads to conformational changes in the receptor molecule, its release from the complex with HSPs and their entry into the cell. Also, some researchers have put forward a hypothesis about the ability of SERM to enhance the expression of HSP70 due to a stimulating effect on the protein transcription factor – HSF.

The increase of HSP70 under the influence of melatonin is explained by its effect on nuclear transcription processes. It is known that melatonin interacts with MT1 and MT2 receptors, prevents the translocation of the NF-κB factor into the nucleus, suppresses the expression of iNOS, and reduces the level of proinflammatory cytokines TNF-α, IL-1β, IL-6, etc. In addition, melatonin exhibits a powerful antioxidant effect, reduces the amount of free radicals and, as a result, prevents total DNA damage. Since glutamine acts as a precursor of glutathione synthesis, it is possible to assume that the mechanism of its action lies in the restoration of the redox ratio of GSH/GSSG forms of glutathione, which triggers the expression of adaptation genes and prevents damage to proteins, including HSP70 (Guo et al., 2007; Szyller and Bil-Lula, 2021). It is also known that glutathione directly regulates HSP70 activity (Yang et al., 2020; Zhang et al., 2022). Reduced glutathione inhibits lipid peroxidation reactions through chemical interaction and neutralization of free radicals: singlet oxygen, superoxide radical, peroxynitrite, etc.

Thus, it was established that HSF-1, melatonin, tamoxifen, and glutamine have a significant neuroprotective effect in the case of AVCC, which consists in limiting glutamate excitotoxicity, inhibiting oxidative and nitrosative stress, improving energy metabolism, HSP70 and HIF, and restoring the work of TDS. The mechanism of the neuroprotective action of the drugs is due to HSP70-mediated modulation of endogenous neuroprotection mechanisms, which leads to an increase in the level of reduced glutathione and activation of the HIF adaptation system, which increase the resistance of neurons to ischemia (Belenichev et al., 2017).

4. Possible pathways for activation of HSP70-dependent mechanisms of endogenous neuroprotection by modulators of the thiol-disulfide system

A number of authors indicate that an increase in the level of HSP70 leads to the normalization of the glutathione link of

the TDS and an increase in the resistance of cells to ischemia (Wang et al., 2012; Pavlov et al., 2017a; Santiago and Morano, 2022). The introduction of exogenous HSP70 leads to an increase in the functional activity of the glutathione system in cortical neurons of the ischemic brain of rats. That is, it was shown that HSP70, proteins with pronounced neuroprotective properties, in conditions of ischemia mobilize antioxidant resources in neurons, in particular, increase the level of both cytosolic and mitochondrial glutathione, which prevents the development of oxidative stress (Pavlov et al., 2017a). In addition, it is known that by modulating the level of endogenous reduced glutathione, it is possible to regulate the expression of HSPs in the cell (Belenichev, 2013; Verma et al., 2014). Confirmation of the perspective of using modulators of the TDS system as means of neuroprotection, which implements its mechanism mediated by increasing the level of endogenous neuroprotection factors, is also confirmed by the following. It was established that high levels of reduced glutathione reduce the activity of 20S and 26S proteasomes of the proteolytic pathway of protein degradation, thereby stabilizing the HIF-1α protein. Thus, these data confirm that depletion of the level of RG (reduced glutathione) under hypoxic conditions plays a decisive role in reducing the level of the HIF-1α protein, and conversely, a high level of RG stabilizes the HIF-1α protein in ischemic conditions (Guo et al., 2007; Wang et al., 2012; Sousa Fialho et al., 2021). The importance of glutathione adducts (S-glutathionylation reaction products) in cell signaling and promotion of ROS-induced revascularization in ischemia through increased expression of HIF-1α is noteworthy (Watanabe et al., 2016b). Modern scientific literature reports on attempts to pharmacologically activate HIF-1α (Ayrapetov et al., 2011; McRae, 2017; Li et al., 2020). Activators of HIF-1α can be divided into two groups: activators of transcription and translation of HIF-1α (gene therapy using viral vectors); and inhibitors of degradation and inactivation of HIF-1α [deferoxamine, cobalt dichloride, dimethyloxalylglycine (DMOG), etc.], however, all these studies are currently experimental in nature. New knowledge in the mechanisms of stimulation or suppression of HIF-1α in conditions of hypoxia (ischemia) will allow to expand the possibilities of using the factor as a specific target for pharmacological correction in oncological, cardiovascular, and neurodegenerative diseases (Zhang et al., 2011; Bouhamida et al., 2022; Chen et al., 2022).

We developed the concept of neuroprotection in the acute period of cerebral stroke, which consists in the pharmacological modulation of the level of glutathione – an important participant in the system of endogenous neuroprotection and neuroplasticity and the increase of glutathione – dependent mechanisms of endogenous neuroprotection. As promising modulators of the glutathione link of the TDS of the brain, we selected: selenase – an activator of GPO, glutoxim – an activator of IL-2 expression and *de novo* reduced glutathione synthesis, glutaredoxin – an important cytosolic protein of disulfide-thiol exchange, a regulator of the activity of transcription factors (NF-1, AP-1, and NF-κB), ASK-1 inhibitor of the apoptosis kinase pathway Glutaredoxin (GRx-1).

4.1. Glutaredoxin

Glutaredoxin is one of the most important enzymes in the processes of disulfide reduction and deglutathionylation. Under conditions of oxidative stress, Grx participates in the S-glutathionylation process, while when oxidative stress is reduced, it catalyzes the deglutathionylation reaction (Lu, 2013; Lu and Holmgren, 2014). Glutaredoxin carries out GSH-dependent reduction in proteins of oxidized cysteine residues (Cys – SOH, Cys – SO2H), mediated and intermolecular disulfide bonds (-S-S-) to the redox-active thiol state (Ren et al., 2017). Thiol-containing proteins are widespread in cells. These include enzymes of energy metabolism (phosphofructokinase, glyceraldehyde-3-phosphate dehydrogenase, α-ketoglutarate dehydrogenase, and I complex of respiratory enzymes), enzymes of signaling cascades (protein kinase A, protein kinase Cα, protein tyrosine phosphatase 1b, and protein phosphatase 2A), transcription factors (NF-κB, HIF1, and AP1), and many others. The oxidative shift in the redox potential of cells leads to the formation of disulfide bonds both within protein molecules and between proteins, as well as between protein and glutathione. The formation of mixed glutathione-protein disulfides (S-glutathionylation) is considered as a redox regulatory mechanism that modulates the activity of thiol proteins and related metabolic pathways, signal transduction, and gene expression (Lu and Holmgren, 2014). However, long-term accumulation of oxidized and glutathionylated proteins is associated with the activation of apoptotic pathways in the cell. In the Grx system, electrons are transferred from NADPH to glutathione reductase, then to oxidized glutathione with the formation of RG, which, in turn, reduces oxidized glutaredoxin. Substrates for Grx are disulfides and mixed disulfides (Brigelius-Flohé and Maiorino, 2013; Fisher, 2017). The reduction of disulfides catalyzed by Grx can proceed in two ways, monothiol and dithiol, with the participation of one or two Cys residues in the active site, respectively. The monothiol mechanism leading to deglutathionylation is perhaps the most general function of glutaredoxin. Glutaredoxin is an electron donor for ribonucleotide reductase, plays a role in cell differentiation/proliferation, has anti-apoptotic functions, along with the ability to reduce dihydroascorbate to ascorbate. All these reactions proceed according to the monothiol mechanism. Glutaredoxin plays an important role in the protection of cells from apoptosis using various mechanisms. For example, the value of glutaredoxin in regulating the redox status of the serine/threonine kinase Akt has been described through a GSH-dependent mechanism by dephosphorylation and inactivation of Akt. The inhibitory ability of glutaredoxin on ASK1 kinase activity is described. Glutaredoxin has an activating effect on transcription factors (Watanabe et al., 2016a; Ryu et al., 2018; **Table 2**).

Thus, glutaredoxin makes a significant contribution to the antioxidant protection of cells against the destructive effects of oxidative stress (**Figure 2**), which causes the formation of intra- and intermolecular disulfide bonds in proteins, the oxidation of functional SH-groups with the formation of sulfonic acid and the subsequent proteosomal degradation of the protein (Ren et al., 2017).

4.2. Glutoxim

According to modern concepts, the glutathione system, namely the GSH/GSSG ratio, is the most important of all known cell redox

TABLE 2 Pharmacological characteristics of glutaredoxin, glutoxim, sodium selenite, and angiolin.

Drug	Dose	Pharmacological effects	References
Glutaredoxin/Redox enzyme	0.5–1.5 μM	Transduced glutaredoxin 1 protein (PEP-1-GLRX1) increased cell viability under oxidative stress and significantly reduced intracellular reactive oxygen species and levels of DNA damage.	Ryu et al., 2018
	200 mkl/kg	Glutaredoxin enhanced the level of ATP and ADP, and also increased the expression of HSP70 and HIF-1a in the model of acute cerebral ischemia.	Belenichev et al., 2020
Glutoxim/Thiopoietin	1, 3, 6, and 100 μg/ml	Glutoxim has a immunomodulating effect on lymphocytes showing chemoattractant activity on cells and inhibiting fMLP-induced chemotaxis.	Fimiani et al., 2002
	50 mg/kg	Glutoxim increased the receptor-mediated expression of GR, GPx and GTS, increased the expression of HSP70 in the model of acute cerebral ischemia.	Belenichev et al., 2020
	60 mg/day	The use of glutoxim in patients with sepsis and septic encephalopathy did not affect mortality, but reduced the symptoms of post-septic syndrome	Kobeliatsky et al., 2021
Sodium selenite Micronutrient	50 μg/kg	Selenase activates selenium-dependent GPO, demonstrates antioxidant effect, limits the expression of iNOS and the production of cytotoxic NO derivatives.	Belenichev et al., 2017
	0.2 mg/kg	Selenium pre-treatment within the physiological dosage attenuates glutamate toxicity and hypoxia-induced cell damage *in vitro* and ameliorates ischemic brain injury *in vivo*.	Mehta et al., 2012
	0.3 mg/kg	Se increases LP, GSH, vitamin E, Ca levels, and Ca2+-ATPase activities on pentylenetetrazole-induced brain injury.	Pillai et al., 2014
Angiolin/Antiischemic, antioxidant	50–100 mg/kg	Angiolin, increases the expression of HSP70 and HIF-1a, improves the ultrastructure of neuronal mitochondria, inhibits neuroapoptosis, increases the GSH concentration and the GSH enzymes activity in various models of cerebral ischemia.	Kucherenko et al., 2018b; Belenichev et al., 2022
	50 mg/kg	Angiolin has anti-ischemic and endothelial protective effects.	Chekman et al., 2017

systems for the regulation of many cellular processes. It is known that a change in the ratio of GSH/GSSG, the redox balance of the cellular environment, is a necessary regulatory mechanism for the activation of a number of transcription factors (AP-1 and NF-κB). Analysis of the literature shows that the majority of works are devoted to the study of the influence of reduced glutathione on various aspects of the cell's vital activity, the mechanism of action of oxidized glutathione in pathological conditions is still poorly understood (Aquilano et al., 2014). Tissue hypoxia, observed in a number of pathological processes, inevitably leads to their damage. One of the main causes of damage and death of cells in conditions of hypoxia is the disruption of the ion balance maintenance systems. Inhibition of the activity of Na, K-ATPase, the main ion-transporting protein of the plasma membrane of cells, which occurs when oxygen concentration decreases, is considered one of the earliest and critical events for cell viability. In a number of works, the authors note that at the concentrations of oxidized glutathione that exist *in vivo* under oxidative stress and hypoxia, glutathionylation of the SH groups of the α-subunit of Na, K-ATPase occurs, which prevents the oxidation of these SH groups (Ballanyi, 2004). At the same time, the SH groups of Na, K-ATPases, which are important for enzymatic activity, are protected from glutathionylation due to binding to the active center of adenyl nucleotides, primarily ATP. Glutathionylation is eliminated under the action of appropriate enzyme systems (for example, glutaredoxin in the presence of NADP H). Thus, glutathionylation in the state of hypoxia protects the SH-groups of the catalytic subunit of Na, K-ATPase, essential for activity, from irreversible oxidation, while simultaneously reducing the activity of the enzyme, which normally consumes a significant amount of ATP (Ballanyi, 2004).

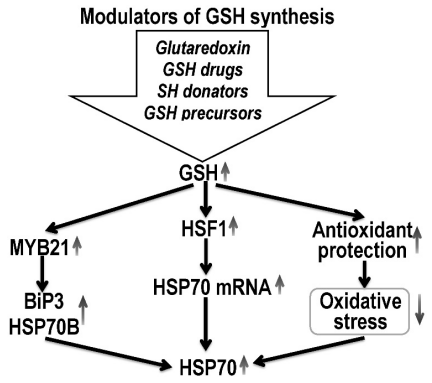

FIGURE 2
Hypothetical mechanism of HSP70 expression regulation by pharmacological glutathione modulators. Glutathione promotes HSF1 nuclear translocation and enhances the expression of HSP70 mRNA, and subsequently increases HSP70 concentration. GSH can induce HSP expression at the transcript level through the activation of its promoters. Thus, high glutathione concentrations increase the expression of myb21, which activates the promoters of the HSP gene (BiP3 HSP70B) and increase the HSP70 expression. Also, glutathione, by increasing the level of antioxidant protection against oxidative stress, increases the stability of HSP70 mRNA. The possibility of post-translational modification of HSP by S-glutathionylation is also not ruled out.

Glutoxim (glutamyl-cysteinyl-glycine-disodium) belongs to the class of thiopoietins, which modulates intracellular thiol exchange, and is currently used as an immunostimulating agent. Being an analog of endogenous oxidized glutathione, it has a fairly high bioavailability. It has immunocorrective, hemostimulating activities, increases the resistance of cells and the body as a whole in local and generalized chronic infections, increases the effectiveness of therapy in intracellular infections, eliminates the manifestations of a non-specific syndrome of chronic diseases

(Dolgodilina et al., 2016). In addition, this drug reproduces the effects of IL-2, with the help of the expression of its receptors, which can lead to a decrease in cytotoxic edema in the acute period of ischemia (Raznatovskaya, 2015). Glutoxim, like GSSG, acts as a substrate for RG and γ-glutamyl transpeptidase (γ-GT), participates in glutathionylation reactions (Townsed et al., 2008). The protection of cellular structures from the toxic effect of free radicals is due to the receptor-mediated increase in the expression of enzymes of the second phase of detoxification of xenobiotics, including glutathione reductase, glutathione peroxidase, glutathione-S-transferase, glucose-6-phosphate dehydrogenase, heme oxygenase-1, an increase in the intracellular level of reduced glutathione, due to the supply plastic material into the cell (structural amino acids) (Townsed and Tew, 2009; Townsed et al., 2009). The positive effects of the drug on LP markers are described, glutoxim reduces the level of diene conjugates and malonaldehyde against the background of an increase in the antioxidant enzymes SOD and catalase (Belenichev et al., 2020; **Table 2**). Today, the drug is successfully used in phthisiology, oncology, gastroenterology, gynecology, narcology, and toxicology, surgery (Fimiani et al., 2002; Wasinger et al., 2018).

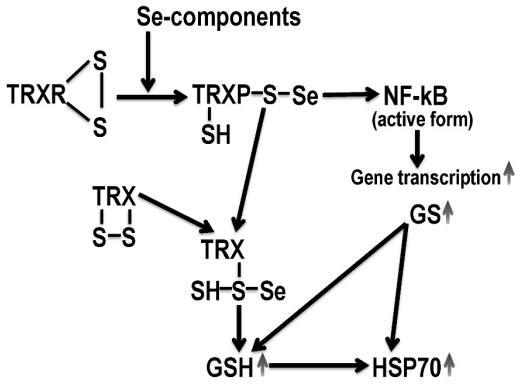

FIGURE 3
Hypothetical mechanism of selenium derivatives neuroprotection. TRX, thioredoxin; TRXR, thioredoxin reductase; GSH, reduced glutathione; GS, glutathione synthetase; NF-κB, nuclear transcription operator. Selenium derivatives activate GSH-dependent mechanisms of endogenous neuroprotection, which are mediated by an increase in HSP70 expression.

4.3. Sodium selenite

Selenium, which is part of the medicinal product, participates in energetic, metabolic reactions of the body, stimulates the conversion of methionine into cysteine and increases the synthesis of glutathione, which contributes to the overall increase in the antioxidant potential of cells (Huang et al., 2012; Weekly and Harris, 2013; Zoidis et al., 2018). Even in conditions of glutathione deficiency, selenium provides effective antioxidant protection (Tajes et al., 2013). The regulatory functions of selenium reflect the proteins and enzymes, which include a trace element. Selenium is part of GPO and thioredoxin reductase, selenoprotein P (Cardoso et al., 2012; Rahmanto and Davies, 2012). Selenium deficiency leads to a violation of cellular integrity, changes in the metabolism of thyroid hormones, and the activity of biotransforming liver enzymes (Zwolak and Zaporowska, 2012; Bera et al., 2013; Rose and Hoffmann, 2015). *In vivo*, selenoproteins bind to the endothelium of blood vessels and prevent the harmful effects of peroxynitrite. Selenium increases the activity of not only enzymes that contain selenium, but also superoxide dismutase. Selenium exhibits an anti-apoptotic effect by blocking the activation of caspase 3 and DNA fragmentation (Rahmanto and Davies, 2012; Liu et al., 2021). The ratio of reduced and oxidized glutathione is considered as the main redox system that supports the redox homeostasis of the mitochondrial matrix and protects the proteins and DNA of mitochondria from the action of reactive oxygen species. Along with glutathione, protection of cell macromolecules from reactive oxygen species, as mentioned above, is provided by selenium-dependent glutathione peroxidase and thioredoxin reductase (Richie et al., 2014). An important property of thioredoxin reductase is the regulation of redox-sensitive transcription factors. This is due to its ability to restore -SH groups of transcription factors, which are critical for binding to DNA (Pillai et al., 2014; **Figure 3**). Since all transcription factors have cysteine residues in DNA-binding domains that are highly susceptible to oxidation, thioredoxin is able to maintain them in a restored, functional state. In particular, this was established for such transcription factors as p53 and NF-κB, each of which plays a significant role in the mechanisms of proliferation and apoptosis (Mehta et al., 2012; Albensi, 2019). Thioredoxin forms an inactive complex with the N-terminal fragment of ASK-1 kinase, which regulates the process of apoptosis in the cell (Yu et al., 2014). A number of research papers determine the effectiveness of sodium selenite in myocardial infarction. Selenium compounds have an immunomodulating, radioprotective effect due to the function of glutathione peroxidase, which provides the recovery of hydroperoxides and other products of free radical reactions and regulates the release of lipoxygenase and cyclooxygenase metabolites of arachidonic acid (Koszta et al., 2012; Costa et al., 2014; Lener et al., 2015; Okuyama et al., 2015).

In studies have shown that the modulation of thiol status by the introduction of positive TDS modulators in experimentally justified doses: selenase (sodium selenite) (50 μg/kg), glutoxim (50 mg/kg), and glutaredoxin (200 μl/kg) to animals with AVCC led to less damage of the mitochondrial ultrastructure of neurons in the sensorimotor cortex, to a decrease in the intensity of oxidative and nitrosative stress, to an increase in the concentration of reduced glutathione and an increase in the concentration of mitochondrial and cytosolic HSP70. In animals with carotid artery occlusion treated with these compounds, the concentrations of ATP and ADP in the cytosol and mitochondria of the brain were higher than in the control group (Belenichev et al., 2017; **Table 2**). Thus, the conducted experimental studies *in vitro* and *in vivo* established that positive modulation of the state of the TDS was manifested in a complex neuroprotective effect, which was provided by antioxidant, energy-modulating, mitoprotective action, as well as the ability to influence subtle mechanisms of endogenous neuroprotection and compensatory-adaptive reactions, aimed at the modulating action of HSP70 proteins. The combination of antioxidant properties and the ability to modulate gene transcription in the studied drugs leads to a more pronounced effect on the expression and synthesis of the studied protective proteins. The analysis of the obtained data showed that the possible

mechanisms of the neuroprotective effect of the studied drugs in the conditions of cerebral ischemia are as follows: Selenase – activates selenium-dependent GPO; serves as a "trap" of free radicals, thereby realizing its ability to reduce the level of peroxide compounds; limits the expression of iNOS and the production of cytotoxic NO derivatives. Glutoxim – protects mitochondrial membranes from the harmful effects of free radicals in the S-glutathionylation reaction; serves as a substrate for GR, γ-GT (in the synthesis of *de novo* reduced glutathione); suppresses the expression of pro-inflammatory interleukins – IL-1β, TNF-α, TNF-α – dependent expression of iNOS and thus indirectly prevents the formation of mitochondrial dysfunction (Kobeliatsky et al., 2021). Glutaredoxin makes a significant contribution to the regulation of signal transduction through the ratio of glutathionylation and deglutathionylation processes; is incorporated into the C-terminal segment of ASK-1, thereby inhibiting ASK-1 kinase activity and the subsequent signal transmission pathway (Kekulandara et al., 2018).

Summarizing the obtained data, it should be emphasized that the restoration of the thiol status of the neuron manifests itself in a pronounced neuroprotective activity, which consists in the prevention of cell death, reduction of neurological deficits and the death of experimental animals.

4.4. L-lysine 3-methyl-1,2,4-triazolyl-5-thioacetate

Angiolin (L-lysine 3-methyl-1,2,4-triazolyl-5-thioacetate) exhibits anti-ischemic, antioxidant properties. It is known that L-lysine can be transformed in the body into pipecolic acid, which increases the affinity of GABA-benzodiazepines-receptor complex and reduces glutamate excitotoxicity (Belenichev et al., 2015b; Nagornaya et al., 2015; Kucherenko et al., 2018a; **Figure 4**). The mechanism of this action of Angiolin may be associated with its effect on the level of HSP70. Angiolin at a course administration (50–100 mg/kg) to Mughal gerbils with irreversible occlusion of the common carotid artery and Wistar white rats with occlusion of the middle cerebral artery reduced the intensity of nitrosative stress in the ischemic brain (decrease in the level of nitrotyrosine) and increased the expression of endogenous neuroprotection agents – HSP70 in the cytosol and mitochondria of neurocytes (**Table 2**). Angiolin increases the survival of CA-1 neurons in the hippocampus zone, activates the expression of bcl-2, inhibits the formation of nitrotyrosine, carbonated proteins, increases the content of ATP, malate and pyruvate, an inhibitory transmitter GABA has a beneficial effect on behavioral responses, on the manifestations of neurological symptoms in animals with chronic alcohol intoxication (P McGraw scale). It has been established that the Angiolin protective effect is aimed at normalizing the thiol-disulfide balance of neurons under ischemia conditions – increasing the activity of glutathione-dependent enzymes against the background of an increase in the content of reduced thiol intermediates and a decrease in their oxidized forms (Belenichev et al., 2022). The course administration of Angiolin to animals with chronic cerebral ischemia leads to a decrease in mitochondria with signs of ultrastructural disorders in the CA1 zone of the hippocampus, which may indicate a mitoprotective link in the neuroprotective mechanism of action of the drug.

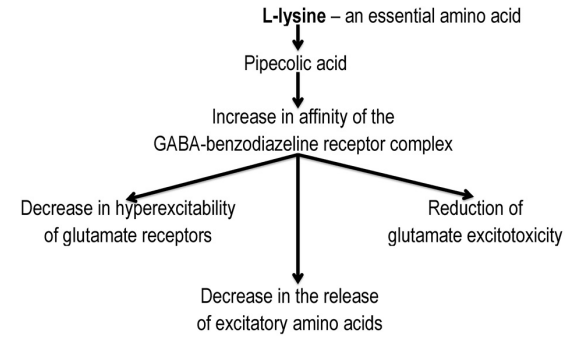

FIGURE 4
Mechanism of L-lysine action in cells damaged by ischemia/hypoxia.

The mechanism of this action is due to the ability of the L-lysine metabolite – pipecolic acid to limit transmitter autokoidosis and due to the properties of Angiolin to activate compensatory mechanisms, to inactivate cytotoxic forms of NO, to inhibit the NO-dependent mechanism of neuroapoptosis and to increase the bioavailability of this transmitter (Chekman et al., 2017). Also, due to its antioxidant properties, Angiolin is able to influence ROS- and SH-SS-dependent mechanisms of Red/Oxi regulation and transcription, which can lead to an increase in HSP70 expression.

5. Conclusion

Currently, the role of endogenous neuroprotection and its intermediate, HSP70, in the regulation of the mechanisms of neuron survival under conditions of cerebral ischemia is being considered. HSP70 performs a chaperone function and is involved in the regulation of growth, development, transfer of genetic material, signaling, and cell death. The neuroprotective properties of HSP70 have been confirmed in various models of ischemic injury *in vitro* and *in vivo*. The neuroprotective effect of HSP70 under conditions of ischemia is explained by its direct anti-apoptotic, antioxidant activity and influence on the TDS of the brain. The works devoted to the study of HSP70 under conditions of cerebral ischemia show its positive effect on the energy metabolism of the brain, which is implemented through a direct mitoprotective effect, as well as through an increase in ATP production in compensatory cytosolic-mitochondrial shunts (Turturici et al., 2011; Pavlov et al., 2017a; Andréasson et al., 2019; Belenichev and Bila, 2019). HSP70 stabilizes and prolongs the HIF-1α "lifetime," which in turn activates and regulates the malate-aspartate shuttle mechanism. It has been established that the HSP70 expression level in the brain determines the severity of neurological disorders in the modeling of stroke in laboratory animals.

We put forward a hypothesis that an increase in endogenous HSP70 through the use of pharmacological agents in ischemic neurodestruction may be a new direction in neuroprotection and treatment of cerebral strokes. The above-described properties of chaperone proteins in cellular reactions during cerebral ischemia raise the question of the development of new drugs capable of modulation/protection of genes encoding the synthesis of HSP

70 and HIF-1a proteins. Strategies aimed at pharmacological modulation of HSP70 require the maintenance and increase in HSP70 expression, thereby preventing progression toward a more severe course of a stroke and allowing to the mortality reduction. Thus, HSP70 is attractive as a therapeutic target in the treatment of cerebral strokes. The development of new approaches to neuroprotection by creating agents – positive HSP70 modulators is an important task of modern pharmacology. In this respect, drugs with a high neuroprotective potential – tamoxifen, melatonin, glutamine, HSF-1, as well as pharmacological agents that increase the expression of HSP70 by acting on the TDS – selenium compounds, glutaredoxin, glutoxim, and Angiolin are of particular interest.

The established mechanisms of action of HSP70 modulators can contribute to the creation of a new generation of effective drugs that have a targeted effect on the key target links of endogenous neuroprotection mechanisms in conditions of acute cerebrovascular disorders.

Data availability statement

The original contributions presented in this study are included in the article/supplementary material, further inquiries can be directed to the corresponding author.

Author contributions

IB designed the research. IB and OA wrote the original manuscript. OP and NB performed the literature search and revised the manuscript. OA made the illustrations. All authors contributed to the article and approved the submitted version.

Conflict of interest

The authors declare that the research was conducted in the absence of any commercial or financial relationships that could be construed as a potential conflict of interest.

Publisher's note

All claims expressed in this article are solely those of the authors and do not necessarily represent those of their affiliated organizations, or those of the publisher, the editors and the reviewers. Any product that may be evaluated in this article, or claim that may be made by its manufacturer, is not guaranteed or endorsed by the publisher.

References

Albensi, B. C. (2019). What Is nuclear factor kappa B (NF-κB) doing in and to the mitochondrion? *Front. Cell. Dev. Biol.* 7:154. doi: 10.3389/fcell.2019.00154

Albrecht, J., Sidoryk-Węgrzynowicz, M., Zielińska, M., and Aschner, M. (2010). Roles of glutamine in neurotransmission. *Neuron Glia Biol.* 6, 263–276.

Alderson, T. R., Kim, J. H., Cai, K., Frederick, R. O., Tonelli, M., and Markley, J. L. (2014). The specialized Hsp70 (HscA) interdomain linker binds to its nucleotide-binding domain and stimulates ATP hydrolysis in both cis and trans configurations. *Biochemistry* 53, 7148–7159. doi: 10.1021/bi5010552

An, R., Zhao, L., Xi, C., Li, H., Shen, G., Liu, H., et al. (2016). Melatonin attenuates sepsis-induced cardiac dysfunction via a PI3K/Akt-dependent mechanism. *Basic Res. Cardiol.* 111:8. doi: 10.1007/s00395-015-0526-1

Andréasson, C., Ott, M., and Büttner, S. (2019). Mitochondria orchestrate proteostatic and metabolic stress responses. *EMBO Rep.* 20:e47865. doi: 10.15252/embr.201947865

Aquilano, K., Baldelli, S., and Ciriolo, M. R. (2014). Glutathione: New roles in redox signaling for an old antioxidant. *Front. Pharmacol.* 5:196. doi: 10.3389/fphar.2014.00196

Arevalo, M. A., Santos-Galindo, M., Lagunas, N., Azcoitia, I., and Garcia-Segura, L. M. (2011). Selective estrogen receptor modulators as brain therapeutic agents. *J. Mol. Endocrinol.* 46, R1–R9. doi: 10.1677/JME-10-0122

Aufricht, C. (2005). Heat-shock protein 70: Molecular supertool? *Pediatr. Nephrol.* 20, 707–713. doi: 10.1007/s00467-004-1812-6

Ayrapetov, M. K., Xu, C., Sun, Y., Zhu, K., Parmar, K., D'Andrea, A. D., et al. (2011). Activation of Hif1α by the prolylhydroxylase inhibitor dimethyoxalyglycine decreases radiosensitivity. *PLoS One* 6:e26064. doi: 10.1371/journal.pone.0026064

Ballanyi, K. (2004). Protective role of neuronal KATP channels in brain hypoxia. *J. Exp. Biol.* 207, 3201–3212. doi: 10.1242/jeb.01106

Barreto, G. E., White, R. E., Xu, L., Palm, C. J., and Giffard, R. G. (2012). Effects of heat shock protein 72 (Hsp72) on evolution of astrocyte activation following stroke in the mouse. *Exp. Neurolexp. Neurol.* 238, 284–296. doi: 10.1016/j.expneurol.2012.08.015

Belenichev, I. F. (2013). The Role of heat shock proteins in realization of molecular biochemical mechanisms of neuroprotection. *Pharm. Drug Toxicol.* 36, 72–80.

Belenichev, I. F., Aliyeva, E. G., and Popazova, O. O. (2022). Experimental substantiation of new target links in complex therapy of prenatal cns damage. pharmacological modulation of HSP70 – dependent mechanisms of endogenous neuroprotection. *Neurotherapeutics* 19, 1414–1431. doi: 10.1007/s13311-022-01298-5

Belenichev, I. F., and Aliyeva, E. G. (2019). New targets for pharmacological correction of cognitive disorders in prenatal hypoxia action. *Pharm. Drug Toxicol.* 13, 235–248. doi: 10.33250/13.04.235

Belenichev, I. F., and Litvinenko, E. S. (2017). Neuroprotective action of glutathione system modulators in conditions of glutamate excitotoxicity modeling *in vitro*. *Pharm. Drug Toxicol.* 4–5, 20–26.

Belenichev, I. F., Cherniy, V. I., Nagornaya, E. A., Pavlov, S. V., and Cherniy, T. V. (2015a). *Neuroprotection and neuroplasticity*. Kyiv: Logos, 512.

Belenichev, I. F., Kucherenko, L. I., Nagornaya, E. A., Mazur, I. A., Bidnenko, A. S., Bukhtiyarova, N. V., et al. (2015b). Functional nitric oxide conjugate systems state/restored heart thiols of rats in modeling isadrine-pituitrin's myocardial infarction using metabolite-tropic cardioprotector "Angiolin". *Int. J. Basic Clin. Pharmacol.* 4, 15–19. doi: 10.5455/2319-2003.ijbcp20150238

Belenichev, I. F., Feroz, S., Chekman, I. S., Nagornaya, E. A., Gorbacheva, S. V., Gorchakova, N. A., et al. (2020). *Thiol-disulfide system: role in endogenous cyto - and organoprotection, pathways of pharmacological modulation*. Kyiv: Yuston Publishing House, 232.

Belenichev, I. F., Odnokoz, O. V., Pavlov, S. V., Belenicheva, O. I., and Polyakova, E. N. (2012). The neuroprotective activity of tamoxifen and tibolone during glutathione depletion *in vitro*. *Neurochem. J.* 6, 202–212. doi: 10.1134/S181971241203004X

Belenichev, I. F., Pavlov, S. V., Bukhtiayarova, N. V., Samura, I. B., Egorov, A. N., and Semenov, D. M. (2017). Expression of HSP70 in the brain of rats during experimental cerebral ischemia modeling and on the background of neuroprotection. *Biol. Mark. Guid. Ther.* 4, 105–111. doi: 10.12988/bmgt.2017.7911

Belenichev, I., and Bila, Y. (2019). The effect of the heat shock protein HSP70 modulators on the energy metabolism of the rats brain in acute cerebral ischemia. *Biol. Mark. Guid. Ther.* 6, 51–62. doi: 10.12988/bmgt.2019.949

Beni, S. M., Kohen, R., Reiter, R. J., Tan, D. X., and Shohami, E. (2004). Melatonin-induced neuroprotection after closed head injury is associated with increased brain antioxidants and attenuated late-phase activation of NF-kappaB and AP-1. *FASEB J.* 18, 149–151. doi: 10.1096/fj.03-0323fje

Bera, S., De Rosa, V., Rachidi, W., and Diamond, A. M. (2013). Does a role for selenium in DNA damage repair explain apparent controversies in its use in chemoprevention? *Mutagenesis* 28, 127–134. doi: 10.1093/mutage/ges064

Bouhamida, E., Morciano, G., Perrone, M., Kahsay, A. E., Della Sala, M., Wieckowski, MR, et al. (2022). The Interplay of hypoxia signaling on mitochondrial

dysfunction and inflammation in cardiovascular diseases and cancer: From molecular mechanisms to therapeutic approaches. *Biology* 11:300. doi: 10.3390/biology11020300

Brigelius-Flohé, R., and Maiorino, M. (2013). Glutathione peroxidases. *Biochim. Biophys. Acta* 1830, 3289–3303. doi: 10.1016/j.bbagen.2012.11.020

Brovedan, M. A., Molinas, S. M., Pisani, G. B., Monasterolo, L. A., and Trumper, L. (2018). Glutamine protection in an experimental model of acetaminophen nephrotoxicity. *Can. J. Physiol. Pharmacol.* 96, 366–371. doi: 10.1139/cjpp-2017-0423

Cardoso, B. R., Ong, T. P., Jacob-Filho, W., Jaluul, O., Freitas, M. I., Cominetti, C., et al. (2012). Glutathione peroxidase 1 pro198leu polymorphism in Brazilian Alzheimer's disease patients: Relations to the enzyme activity and to selenium status. *J. Nutrigenet. Nutrigenomics.* 5, 72–80. doi: 10.1159/000338682

Chekman, I. S., Kazakova, O. A., Mazur, I. A., Nagornaya, E. A., Belenichev, I. F., Gorchakova, N. A., et al. (2017). New original metabolitotropic endothelioprotector "Angiolin": Quantum-chemical parameters and peculiarities of pharmacological action. *Rep. NAS Ukraine* 8, 86–93. doi: 10.15407/dopovidi2017.08.086

Chen, G., Shi, J., Qi, M., Yin, H., and Hang, C. (2008). Glutamine decreases intestinal nuclear factor kappa B activity and pro-inflammatory cytokine expression after traumatic brain injury in rats. *Inflamm. Res.* 57, 57–64. doi: 10.1007/s00011-007-7101-7

Chen, J., Hao, L., Zhang, Z., Zhang, S., Zhang, Y., Dong, B., et al. (2022). Activation hypoxia inducible factor-1α gene affected the tumor microenvironment and induced recurrence and invasion of bladder cancer in vitro. *Cir. Cir.* 90, 588–595. doi: 10.24875/CIRU.22000027

Cioccari, L., Gautschi, M., Etter, R., Weck, A., and Takala, J. (2015). Further concerns about glutamine: A case report on hyperammonemic encephalopathy. *Crit. Care Med.* 43, e458–e460. doi: 10.1097/CCM.0000000000001151

Clerico, E. M., Meng, W., Pozhidaeva, A., Bhasne, K., Petridis, C., and Gierasch, L. M. (2019). Hsp70 molecular chaperones: Multifunctional allosteric holding and unfolding machines. *Biochem. J.* 476, 1653–1677. doi: 10.1042/BCJ20170380

Clerico, E. M., Tilitsky, J. M., Meng, W., and Gierasch, L. M. (2015). How hsp70 molecular machines interact with their substrates to mediate diverse physiological functions. *J. Mol. Biol.* 427, 1575–1588. doi: 10.1016/j.jmb.2015.02.004

Costa, N. A., Gut, A. L., Pimentel, J. A., Cozzolino, S. M., Azevedo, P. S., Fernandes, A. A., et al. (2014). Erythrocyte selenium concentration predicts intensive care unit and hospital mortality in patients with septic shock: A prospective observational study. *Crit. Care* 18:R92. doi: 10.1186/cc13860

Craig, E. A. (2018). Hsp70 at the membrane: Driving protein translocation. *BMC Biol.* 16:11. doi: 10.1186/s12915-017-0474-3

Cruzat, V., Macedo, R. M., Noel, K. K., Curi, R., and Newsholme, P. (2018). Glutamine: Metabolism and immune function, supplementation and clinical translation. *Nutrients* 10:1564. doi: 10.3390/nu10111564

Curi, R., Lagranha, C. J., Doi, S. Q., Sellitti, D. F., Procopio, J., Pithon-Curi, T. C., et al. (2005). Molecular mechanisms of glutamine action. *J. Cell Physiol.* 204, 392–401. doi: 10.1002/jcp.20339

Cyr, M., Thibault, C., Morissette, M., Landry, M., and Di Paolo, T. (2001). Estrogen-like activity of tamoxifen and raloxifene on NMDA receptor binding and expression of its subunits in rat brain. *Neuropsychopharmacology* 25, 242–257. doi: 10.1016/S0893-133X(01)00233-0

Deka, K., and Saha, S. (2018). "Regulation of Mammalian HSP70 Expression and Stress Response," in *Regulation of heat shock protein responses. heat shock proteins*, Vol. 13, eds A. Asea and P. Kaur (Cham: Springer), 3–25. doi: 10.1007/978-3-319-74715-6_1

Demyanenko, S., Nikul, V., Rodkin, S., Davletshin, A., Evgen'ev, M. B., and Garbuz, D. G. (2021). Exogenous recombinant Hsp70 mediates neuroprotection after photothrombotic stroke. *Cell Stress Chaper.* 26, 103–114. doi: 10.1007/s12192-020-01159-0

Dery, M. A., Michaud, M. D., and Richard, D. E. (2005). Hypoxia-inducible factor 1: Regulation by hypoxic and non-hypoxic activators. *Int. J. Biochem. Cell. Biol.* 37, 535–540. doi: 10.1016/j.biocel.2004.08.012

Dolgodilina, E., Imobersteg, S., Laczko, E., Welt, T., Verrey, F., and Makrides, V. (2016). Brain interstitial fluid glutamine homeostasis is controlled by blood–brain barrier SLC7A5/LAT1 amino acid transporter. *J. Cereb. Blood Flow Metab.* 36, 1929–1941. doi: 10.1177/0271678X15609331

Dukay, B., Csoboz, B., and Tóth, M. E. (2019). Heat-shock proteins in neuroinflammation. *Front. Pharmacol.* 10:920. doi: 10.3389/fphar.2019.00920

Dwaich, K. H., Al-Amran, F. G., Al-Sheibani, B. M., and Al-Aubaidy, H. A. (2016). Melatonin effects on myocardial ischemia-reperfusion injury: Impact on the outcome in patients undergoing coronary artery bypass grafting surgery. *Int. J. Cardiol.* 221, 977–986. doi: 10.1016/j.ijcard.2016.07.108

Evans, C. G., Chang, L., and Gestwicki, J. E. (2010). Heat shock protein 70 (hsp70) as an emerging drug target. *J. Med. Chem.* 53, 4585–4602. doi: 10.1021/jm100054f

Fimiani, V., Cavallaro, A., Ainis, T., Baranovskaia, G., Ketlinskaya, O., and Kozhemyakin, L. (2002). Immunomodulatory effect of glutoxim on some activities of isolated human neutrophils and in whole blood. *Immunopharmacol. Immunotoxicol.* 24, 627–638. doi: 10.1081/iph-120016039

Finney, C. A., Shvetcov, A., Westbrook, R. F., Morris, M. J., and Jones, N. M. (2021). The selective estrogen receptor modulator tamoxifen protects against subtle cognitive decline and early markers of injury 24 h after hippocampal silent infarct in male Sprague-Dawley rats. *Horm. Behav.* 134:105016. doi: 10.1016/j.yhbeh.2021.105016

Fischer, T. W., Kleszczyńsk, K., Hardkop, L. H., Kruse, N., and Zillikens, D. (2013). Melatonin enhances antioxidative enzyme gene expression (CAT, GPx, SOD), prevents their UVR-induced depletion, and protects against the formation of DNA damage (8-hydroxy-2'-deoxyguanosine) in ex vivo human skin. *J. Pineal Res.* 54, 303–312. doi: 10.1111/jpi.12018

Fisher, A. B. (2017). Peroxiredoxin 6 in the repair of peroxidized cell membranes and cell signaling. *Arch. Biochem. Biophys.* 617, 68–83. doi: 10.1016/j.abb.2016.12.003

Galano, A., Tan, D. X., and Reiter, R. J. (2011). Melatonin as a natural ally against oxidative stress: A physicochemical examination. *J. Pineal Res.* 51, 1–16. doi: 10.1111/j.1600-079X.2011.00916.x

Giffard, R. G., and Yenari, M. A. (2004). Many mechanisms for hsp70 protection from cerebral ischemia. *J. Neurosurg. Anesthesiol.* 16, 53–61. doi: 10.1097/00008506-200401000-00010

Ginsberg, M. (2016). Expanding the concept of neuroprotection for acute ischemic stroke: The pivotal roles of reperfusion and the collateral circulation. *Prog. Neurobiol.* 14, 46–77. doi: 10.1016/j.pneurobio.2016.09.002

Guo, S., Wharton, W., Moseley, P., and Shi, H. (2007). Heat shock protein 70 regulates cellular redox status by modulating glutathione-related enzyme activities. *Cell Stress Chaperones* 12, 245–254. doi: 10.1379/csc-265.1

Hacke, W., Kaste, M., Bluhmki, E., Brozman, M., Dávalos, A., Guidetti, D., et al. (2008). Thrombolysis with alteplase 3 to 4.5 hours after acute ischemic stroke. *N. Engl. J. Med.* 359, 1317–1329. doi: 10.1056/NEJMoa0804656

Hayashi, M. K. (2018). Structure-function relationship of transporters in the glutamate-glutamine cycle of the central nervous system. *Int. J. Mol. Sci.* 19:1177. doi: 10.3390/ijms19041177

Hernandez-Ontiveros, D. G., Tajiri, N., Acosta, S., Giunta, B., Tan, J., and Borlongan, C. V. (2013). Microglia activation as a biomarker for traumatic brain injury. *Front. Neurol.* 4:30. doi: 10.3389/fneur.2013.00030

Huang, Z., Rose, A. H., and Hoffmann, P. R. (2012). The role of selenium in inflammation and immunity: From molecular mechanisms to therapeutic opportunities. *Antioxid. Redox Signal.* 16, 705–743. doi: 10.1089/ars.2011.4145

Jo, S. K., Ko, G. J., Boo, C. S., Cho, W. Y., and Kim, H. K. (2006). Heat preconditioning attenuates renal injury in ischemic ARF in rats: Role of heat-shock protein 70 on NF-kappaB-mediated inflammation and on tubular cell injury. *J. Am. Soc. Nephrol.* 17, 3082–3092. doi: 10.1681/ASN.2005101077

Kadhim, H. J., Duchateau, J., and Sébire, G. (2008). Cytokines and brain injury: Invited review. *J. Intens. Care Med.* 23, 236–249. doi: 10.1177/0885066608318458

Kampinga, H. H., and Craig, E. A. (2010). The HSP70 chaperone machinery: J proteins as drivers of functional specificity. *Nat. Rev. Mol. Cell. Biol.* 11, 579–592. doi: 10.1038/nrm2941

Kaur, P., and Asea, A. (2019). "The Chaperokine Activity of Heat Shock Proteins," in *Chaperokine activity of heat shock proteins. heat shock proteins*, Vol. 16, eds A. Asea and P. Kaur (Cham: Springer), 3–22. doi: 10.1007/978-3-030-02254-9_1

Kekulandara, D. N., Nagi, S., Seo, H., Chow, C. S., and Ahn, Y. H. (2018). Redox-inactive peptide disrupting trx1-ask1 interaction for selective activation of stress signaling. *Biochemistry* 57, 772–780. doi: 10.1021/acs.biochem.7b01083

Kim, J. Y., Barua, S., Huang, M. Y., Park, J., Yenari, M. A., and Lee, J. E. (2020a). Heat Shock Protein 70 (HSP70) Induction: Chaperonotherapy for Neuroprotection after Brain Injury. *Cells* 9:2020. doi: 10.3390/cells9092020

Kim, J. Y., Kim, J. W., and Yenari, M. A. (2020b). Heat shock protein signaling in brain ischemia and injury. *Neurosci. Lett.* 715:134642. doi: 10.1016/j.neulet.2019.134642

Kim, J. Y., Han, Y., Lee, J. E., and Yenari, M. A. (2018). The 70-kDa heat shock protein (Hsp70) as a therapeutic target for stroke. *Expert Opin. Ther. Targets.* 22, 191–199. doi: 10.1080/14728222.2018.1439477

Kim, J. Y., Huang, M., Lee, J. E., and Yenari, M. A. (2019). "Role of Heat Shock Proteins (HSP) in Neuroprotection for Ischemic Stroke," in *Heat shock proteins in neuroscience. heat shock proteins*, Vol. 20, eds A. Asea and P. Kaur (Cham: Springer), doi: 10.1007/978-3-030-24285-5_6

Kityk, R., Vogel, M., Schlecht, R., Bukau, B., and Mayer, M. P. (2015). Pathways of allosteric regulation in Hsp70 chaperones. *Nat. Commun.* 6:8308. doi: 10.1038/ncomms9308

Kobeliatsky, Y., Maltseva, L., Mosentsev, M., and Lisnycha, V. (2021). Glutoxim as a modulator of glutathione redox state in septic patients with encephalopathy. *Emerg. Med.* 91, 104–109. doi: 10.22141/2224-0586.4.91.2018.137866

Koh, P. O. (2008). Melatonin attenuates the cerebral ischemic injury via the MEK/ERK/p90RSK/bad signaling cascade. *J. Vet. Med. Sci.* 70, 1219–1223. doi: 10.1292/jvms.70.1219

Koszta, G., Kacska, Z., Szatmári, K., Szerafin, T., and Fülesdi, B. (2012). Lower whole blood selenium level is associated with higher operative risk and mortality following cardiac surgery. *J. Anesth.* 26, 812–821. doi: 10.1007/s00540-012-1454-y

Kucherenko, L. I., Belenıchev, I., Mazur, I., Khromylova, O., and Parniuk, N. (2018a). Influence of the fixed combination of glycine with thiotriazoline on energy metabolism parameters in brain in conditions of experimental cerebral ischemia. *J. Fac. Pharm. Ankara* 42, 14–21. doi: 10.1501/Eczfak_0000000598

Kucherenko, L. I., Bidnenko, O. S., and Khromylova, O. V. (2018b). Validation of the spectrofotometric method for the determination ofquantitative composition of s-2,6-diagenoxic acid of 3-methyl-1,2,4-triazolyl-5-thioacetate. *Asian J. Pharm. Clin. Res.* 11, 91–94.

Lamont, K., Nduhirabandi, F., Adam, T., Thomas, D. P., Opie, L. H., and Lecour, S. (2015). Role of melatonin, melatonin receptors and STAT3 in the cardioprotective effect of chronic and moderate consumption of red wine. *Biochem. Biophys. Res. Commun.* 465, 719–724. doi: 10.1016/j.bbrc.2015.08.064

Lee, J. E., Kim, Y. J., Kim, J. Y., Lee, W. T., Yenari, M. A., and Giffard, R. G. (2004). The 70 kDa heat shock protein suppresses matrix metalloproteinases in astrocytes. *Neuroreport* 15, 499–502. doi: 10.1097/00001756-200403010-00023

Lee, J., Giordano, S., and Zhang, J. (2012). Autophagy, mitochondria and oxidative stress: Cross-talk and redox signalling. *Biochem. J.* 441, 523–540. doi: 10.1042/BJ20111451

Leite, J. S. M., Cruzat, V. F., Krause, M., and de Bittencourt, P. I. (2016). Physiological regulation of the heat shock response by glutamine: Implications for chronic low-grade inflammatory diseases in age-related conditions. *Nutrire* 41:17. doi: 10.1186/s41110-016-0021-y

Lener, M., Muszyńska, M., Jakubowska, A., Jaworska-Bieniek, K., Sukiennicki, G., Kaczmarek, K., et al. (2015). Selenium as a marker of cancer risk and of selection for control examinations in surveillance. *Contemp. Oncol.* 19, A60–A61. doi: 10.5114/wo.2014.47131

Leu, J. I., Barnoud, T., Zhang, G., Tian, T., Wei, Z., Herlyn, M., et al. (2017). Inhibition of stress-inducible HSP70 impairs mitochondrial proteostasis and function. *Oncotarget* 8, 45656–45669. doi: 10.18632/oncotarget.17321

Li, R. L., He, L. Y., Zhang, Q., Liu, J., Lu, F., Duan, H. X. Y., et al. (2020). HIF-1α is a potential molecular target for herbal medicine to treat diseases. *Drug Des. Devel. Ther.* 14, 4915–4949. doi: 10.2147/DDDT.S274980

Liu, B., Li, J., Zhou, P., Pan, W., Li, N., and Tang, B. (2021). Real-time *in situ* sequential fluorescence activation imaging of cyt c and caspase-9 with a gold–selenium-bonded nanoprobe. *Anal. Chem.* 93, 16880–16886. doi: 10.1021/acs.analchem.1c03872

Liu, J., Clough, S. J., Hutchinson, A. J., Adamah-Biassi, E. B., Popovska-Gorevski, M., and Dubocovich, M. L. (2016). MT1 and MT2 melatonin receptors: A therapeutic perspective. *Annu. Rev. Pharmacol. Toxicol.* 56, 361–383. doi: 10.1146/annurev-pharmtox-010814-124742

Liu, N., Ma, X., Luo, X., Zhang, Y., He, Y., Dai, Z., et al. (2018). l-Glutamine attenuates apoptosis in porcine enterocytes by regulating glutathione-related redox homeostasis. *J. Nutr.* 148, 526–534. doi: 10.1093/jn/nxx062

Liu, W., Xia, F., Ha, Y., Zhu, S., Li, Y., Folorunso, O., et al. (2019). Neuroprotective effects of hsf1 in retinal ischemia-reperfusion injury. *Invest. Ophthalmol. Vis. Sci.* 60, 965–977. doi: 10.1167/iovs.18-26216

Lochner, A., Huisamen, B., and Nduhirabandi, F. (2013). Cardioprotective effect of melatonin against ischaemia/reperfusion damage. *Front. Biosci.* 5, 305–315. doi: 10.2741/e617

Lu, J., and Holmgren, A. (2014). The thioredoxin antioxidant system. *Free Radic. Biol. Med.* 66, 75–87. doi: 10.1016/j.freeradbiomed.2013.07.036

Lu, S. C. (2013). Glutathione synthesis. *Biochim. Biophys. Acta* 1830, 3143–3153. doi: 10.1016/j.bbagen.2012.09.008

Luo, L. L., Li, Y. F., Shan, H. M., Wang, L. P., Yuan, F., Ma, Y. Y., et al. (2019). L-glutamine protects mouse brain from ischemic injury via up-regulating heat shock protein 70. *CNS Neurosci. Ther.* 25, 1030–1041. doi: 10.1111/cns.13184

Madeira, C., Vargas-Lopes, C., Brandão, C. O., Reis, T., Laks, J., Panizzutti, R., et al. (2018). Elevated glutamate and glutamine levels in the cerebrospinal fluid of patients with probable alzheimer's disease and depression. *Front. Psychiatry* 9:561. doi: 10.3389/fpsyt.2018.00561

Mayer, M. P., and Gierasch, L. M. (2019). Recent advances in the structural and mechanistic aspects of Hsp70 molecular chaperones. *J. Biol. Chem.* 294, 2085–2097. doi: 10.1074/jbc.REV118.002810

McRae, M. P. (2017). Therapeutic benefits of glutamine: An umbrella review of meta-analyses. *Biomed. Rep.* 6, 576–584. doi: 10.3892/br.2017.885

Mehta, S. L., Kumari, S., Mendelev, N., and Li, P. A. (2012). Selenium preserves mitochondrial function, stimulates mitochondrial biogenesis, and reduces infarct volume after focal cerebral ischemia. *BMC Neurosci.* 13:79. doi: 10.1186/1471-2202-13-79

Mendillo, M. L., Santagata, S., Koeva, M., Bell, G. W., Hu, R., Tamimi, R. M., et al. (2012). HSF1 drives a transcriptional program distinct from heat shock to support highly malignant human cancers. *Cell* 150, 549–562. doi: 10.1016/j.cell.2012.06.031

Nagai, Y., Fujikake, N., Popiel, H. A., and Wada, K. (2010). Induction of molecular chaperones as a therapeutic strategy for the polyglutamine diseases. *Curr. Pharm. Biotechnol.* 11, 188–197. doi: 10.2174/138920110790909650

Nagornaya, A. A., Magomedov, S., Gorchakova, N. A., Belenichev, I. F., Ghekman, I. S., and Kuzub, T. A. (2015). Influence of quinapril in combination with angioline on the connective tissue components in the rats serum with experimental hypertension. *Lik. Sprava* 5-6, 116–120.

Naka, K. K., Vezyraki, P., Kalaitzakis, A., Zerikiotis, S., Michalis, L., and Angelidis, C. (2014). Hsp70 regulates the doxorubicin-mediated heart failure in Hsp70-transgenic mice. *Cell Stress Chaperones* 19, 853–864. doi: 10.1007/s12192-014-0509-4

Neef, D. W., Jaeger, A. M., and Thiele, D. J. (2011). Heat shock transcription factor 1 as a therapeutic target in neurodegenerative diseases. *Nat. Rev. Drug Discov.* 10, 930–944. doi: 10.1038/nrd3453

Nitika, Porter, C. M., Truman, A. W., and Truttmann, M. C. (2020). Post-translational modifications of Hsp70 family proteins: Expanding the chaperone code. *J. Biol. Chem.* 295, 10689–10708. doi: 10.1074/jbc.REV120.011666

Okuyama, H., Langsjoen, P. H., Hamazaki, T., Ogushi, Y., Hama, R., Kobayashi, T., et al. (2015). Statins stimulate atherosclerosis and heart failure: Pharmacological mechanisms. *Expert. Rev. Clin. Pharmacol.* 8, 189–199. doi: 10.1586/17512433.2015.1011125

Ortan, P., Akan, O. Y., and Hosgorler, F. (2018). "Heat Shock Protein70 in Neurological Disease," in *HSP70 in human diseases and disorders. Heat shock proteins*, Vol. 14, eds A. Asea and P. Kaur (Cham: Springer), 57–69. doi: 10.1007/978-3-319-89551-2_3

Otsuka, S., Sakakima, H., Sumizono, M., Takada, S., Terashi, T., and Yoshida, Y. (2016). The neuroprotective effects of preconditioning exercise on brain damage and neurotrophic factors after focal brain ischemia in rats. *Behav. Brain Res.* 303, 9–18. doi: 10.1016/j.bbr.2016.01.049

Paul, S., and Mahanta, S. (2014). Association of heat-shock proteins in various neurodegenerative disorders: Is it a master key to open the therapeutic door? *Mol. Cell. Biochem.* 386, 45–61. doi: 10.1007/s11010-013-1844-y

Pavlov, S. V., and Belenichev, I. F. (2014). Molecular and biochemical aspects of the neuroprotective effect of the selective estrogen receptor modulator tamoxifen in a model of acute cerebral ischemia. *Neurochem. J.* 8, 28–32. doi: 10.1134/S1819712413040077

Pavlov, S. V., Belenichev, I. F., Nikitchenko, Y. V., and Gorbachova, S. V. (2017a). Molecular bio-chemical mechanisms of HSP 70-mediated cytoprotection in pathologies of ischemic origin. *Bull. Probl. Biol. Med.* 1, 61–67.

Pavlov, S. V., Levchenko, K. V., and Kamyshniy, O. M. (2017b). Influence of the selective esrogen receptor modulators on the expression and synthesis of HSP 70 proteins in cardiomyocytes of rats with acute myocardial infarction. *Pharm. Drug Toxicol.* 56, 59–65.

Pillai, R., Uyehara-Lock, J. H., and Bellinger, F. P. (2014). Selenium and selenoprotein function in brain disorders. *IUBMB Life* 66, 229–239. doi: 10.1002/iub.1262

Qu, Z., Titus, A. S. C. L. S., Xuan, Z., and D'Mello, S. R. (2018). Neuroprotection by Heat Shock Factor-1 (HSF1) and trimerization-deficient mutant identifies novel alterations in gene expression. *Sci. Rep.* 8:17255. doi: 10.1038/s41598-018-35610-1

Rahmanto, A. S., and Davies, M. J. (2012). Selenium-containing amino acids as direct and indirect antioxidants. *IUBMB Life* 64, 863–871. doi: 10.1002/iub.1084

Raizel, R., and Tirapegui, J. (2018). Role of glutamine, as free or dipeptide form, on muscle recovery from resistance training: A review study. *Nutrire* 43:28. doi: 10.1186/s41110-018-0087-9

Ramos, E., Patiño, P., Reiter, R. J., Gil-Martín, E., Marco-Contelles, J., Parada, E., et al. (2017). Ischemic brain injury: New insights on the protective role of melatonin. *Free Radic. Biol. Med.* 104, 32–53. doi: 10.1016/j.freeradbiomed.2017.01.005

Raznatovskaya, E. N. (2015). The evolution of the cytokine profile under the influence of immunomodulator glutamine-cystine-glycine disodium in patients with destructive multidrug-resistant lung tuberculosis. *Zap. Med. J.* 3, 95–98. doi: 10.14739/2310-1210.2015.3.44508

Reiter, R. J., Mayo, J. C., Tan, D. X., Sainz, R. M., Alatorre-Jimenez, M., and Qin, L. (2016). Melatonin as an antioxidant: Under promises but over delivers. *J. Pineal Res.* 61, 253–278. doi: 10.1111/jpi.12360

Ren, X., Zou, L., Zhang, X., Branco, V., Wang, J., Carvalho, C, et al. (2017). Redox signaling mediated by thioredoxin and glutathione systems in the central nervous system. *Antioxid. Redox Signal.* 27, 989–1010. doi: 10.1089/ars.2016.6925

Richie, J. P., Das, A., Calcagnotto, A. M., Sinha, R., Neidig, W., Liao, J., et al. (2014). Comparative effects of two different forms of selenium on oxidative stress biomarkers in healthy men: A randomized clinical trial. *Cancer Prev. Res.* 7, 796–804. doi: 10.1158/1940-6207.CAPR-14-0042

Rose, A. H., and Hoffmann, P. R. (2015). Selenoproteins and cardiovascular stress. *Thromb. Haemost.* 113, 494–504. doi: 10.1160/TH14-07-0603

Rosenzweig, R., Nillegoda, N. B., Mayer, M. P., and Bukau, B. (2019). The HSP70 chaperone network. *Nat. Rev. Mol. Cell. Biol.* 20, 665–680. doi: 10.1038/s41580-019-0133-3

Roth, E. (2008). Nonnutritive effects of glutamine. *J. Nutr.* 138, 2025S–2031S. doi: 10.1093/jn/138.10.2025S,

Ryu, E. J., Kim, D. W., Shin, M. J., Jo, H. S., Park, J. H., Cho, S. B, et al. (2018). PEP-1-glutaredoxin 1 protects against hippocampal neuronal cell damage from oxidative stress via regulation of MAPK and apoptotic signaling pathways. *Mol. Med. Rep.* 18, 2216–2228. doi: 10.3892/mmr.2018.9176

Sakakima, H. (2019). Endogenous neuroprotective potential due to preconditioning exercise in stroke. *Phys. Ther. Res.* 22, 45–52. doi: 10.1298/ptr.R0006

Santiago, A., and Morano, K. A. (2022). Redox regulation of yeast Hsp70 modulates protein quality control while directly triggering an Hsf1-dependent cytoprotective response. *bioRxiv* [Preprint]. doi: 10.1101/2022.04.08.487668v1.full

Sharp, F. R., Zhan, X., and Liu, D. Z. (2013). Heat shock proteins in the brain: Role of Hsp70, Hsp 27, and HO-1 (Hsp32) and their therapeutic potential. *Transl. Stroke Res.* 4, 685–692. doi: 10.1007/s12975-013-0271-4

Shen, J. (2013). Modeling the glutamate-glutamine neurotransmitter cycle. *Front. Neuroenerget.* 5:1. doi: 10.3389/fnene.2013.00001

Sheng, S., Huang, J., Ren, Y., Zhi, F., Tian, X., Wen, G., et al. (2018). Neuroprotection Against Hypoxic/Ischemic Injury: δ-Opioid Receptors and BDNF-TrkB Pathway. *Cell. Physiol. Biochem.* 47, 302–315. doi: 10.1159/000489808

Shulyatnikova, T. V., and Shavrin, V. A. (2012). Morphometric characteristics of acute swelling and induration of neurons in the critical zone of ischemic brain infarction. *Pathologia* 3, 93–95. doi: 10.14739/2310-1237.2012.3.17034

Song, Y. J., Zhong, C. B., and Wang, X. B. (2019). Heat shock protein 70: A promising therapeutic target for myocardial ischemia-reperfusion injury. *J. Cell. Physiol.* 234, 1190–1207. doi: 10.1002/jcp.27110

Sousa Fialho, M. D. L., Purnama, U., Dennis, K. M. J. H., Montes Aparicio, C. N., Castro-Guarda, M., Massourides, E., et al. (2021). Activation of HIF1α rescues the hypoxic response and reverses metabolic dysfunction in the diabetic heart. *Diabetes* 70, 2518–2531. doi: 10.2337/db21-0398

Srinivasan, V., Gobbi, G., Shillcut, S. D., and Suzen, S. (2015). *Melatonin: Therapeutic Value and Neuroprotectin*. Boca Raton: CRC Press/Taylor and Francis, 576. doi: 10.1201/b17448

Steurer, C., Kerschbaum, S., Wegrostek, C., Gabriel, S., Hallaj, A., Ortner, V., et al. (2022). Quantitative Comparison of HSF1 Activators. *Mol. Biotechnol.* 64, 873–887. doi: 10.1007/s12033-022-00467-3

Storr, M., Koppitz, P., Sibaev, A., Saur, D., Kurjak, M., Franck, H., et al. (2002). Melatonin reduces non-adrenergic, non-cholinergic relaxant neurotransmission by inhibition of nitric oxide synthase activity in the gastrointestinal tract of rodents in vitro. *J. Pineal Res.* 33, 101–108. doi: 10.1034/j.1600-079x.2002.02909.x

Su, K. H., Cao, J., Tang, Z., Dai, S., He, Y., Sampson, S. B., et al. (2016). HSF1 critically attunes proteotoxic stress sensing by mTORC1 to combat stress and promote growth. *Nat. Cell. Biol.* 18, 527–539. doi: 10.1038/ncb3335

Sun, X., Crawford, R., Liu, C., Luo, T., and Hu, B. (2015). Development-dependent regulation of molecular chaperones after hypoxia-ischemia. *Neurobiol. Dis.* 82, 123–131. doi: 10.1016/j.nbd.2015.06.001

Szyller, J., and Bil-Lula, I. (2021). Heat Shock Proteins in Oxidative Stress and Ischemia/Reperfusion Injury and Benefits from Physical Exercises: A Review to the Current Knowledge. *Oxid. Med. Cell. Longev.* 2021:6678457. doi: 10.1155/2021/6678457

Tajes, M., Ill-Raga, G., Palomer, E., Ramos-Fernández, E., Guix, F. X., Bosch-Morató, M., et al. (2013). Nitro-oxidative stress after neuronal ischemia induces protein nitrotyrosination and cell death. *Oxid. Med. Cell. Longev.* 2013:826143. doi: 10.1155/2013/826143

Tang, S., Chen, H., Cheng, Y., Nasir, M. A., Kemper, N., and Bao, E. (2016). The interactive association between heat shock factor 1 and heat shock proteins in primary myocardial cells subjected to heat stress. *Int. J. Mol. Med.* 37, 56–62. doi: 10.3892/ijmm.2015.2414

Tapieroa, H., Mathé, G., Couvreur, P., and Tew, K. D. (2002). II. Glutamine and glutamate. *Biomed. Pharmacother.* 56, 446–457. doi: 10.1016/s0753-3322(02)00285-8

Tordjman, S., Chokron, S., Delorme, R., Charrier, A., Bellissant, E., Jaafari, N., et al. (2017). Melatonin: Pharmacology, functions and therapeutic benefits. *Curr. Neuropharmacol.* 15, 434–443. doi: 10.2174/1570159X14666161228122115

Townsed, D. M., and Tew, K. D. (2009). Pharmacology of a mimetic of glutathione disulfide. NOV-002. *Biomed. Pharmacother.* 63, 75–78. doi: 10.1016/j.biopha.2008.08.019

Townsed, D. M., He, L., Hutchens, S., Garrett, T. E., Pazoles, C. J., and Tew, K. D. (2008). NOV-002, a glutathione disulfide mimetic, as a modulator of cellular redox balance. *Cancer Res.* 68, 2870–2877. doi: 10.1158/0008-5472.CAN-07-5957

Townsed, D. M., Manevich, Y., He, L., Hutchens, S., Pazoles, C. J., and Tew, K. D. (2009). Novel role for glutathione S-transferase pi. Regulator of protein S-Glutathionylation following oxidative and nitrosative stress. *J. Biol. Chem.* 284, 436–445. doi: 10.1074/jbc.M805586200

Tukaj, S. (2020). Heat Shock protein 70 as a double agent acting inside and outside the cell: Insights into autoimmunity. *Int. J. Mol. Sci.* 21:5298. doi: 10.3390/ijms21155298

Turturici, G., Sconzo, G., and Geraci, F. (2011). Hsp70 and its molecular role in nervous system diseases. *Biochem. Res. Int.* 2011:618127. doi: 10.1155/2011/618127

Verma, P., Pfister, J. A., Mallick, S., and D'Mello, S. R. (2014). HSF1 protects neurons through a novel trimerization- and HSP-independent mechanism. *J. Neurosci.* 34, 1599–1612. doi: 10.1523/JNEUROSCI.3039-13.2014

Vrienda, J., and Reiter, R. J. (2015). The Keap1-Nrf2-antioxidant response element pathway: A review of its regulation by melatonin and the proteasome. *Mol. Cell. Endocrinol.* 401, 213–220. doi: 10.1016/j.mce.2014.12.013

Wakade, C., Khan, M. M., De Sevilla, L. M., Zhang, Q. G., Mahesh, V. B., and Brann, D. W. (2008). Tamoxifen neuroprotection in cerebral ischemia involves attenuation of kinase activation and superoxide production and potentiation of mitochondrial superoxide dismutase. *Endocrinology* 149, 367–379. doi: 10.1210/en.2007-0899

Wang, B., Wu, G., Zhou, Z., Dai, Z., Sun, Y., Ji, Y., et al. (2015). Glutamine and intestinal barrier function. *Amino Acids.* 47, 2143–2154. doi: 10.1007/s00726-014-1773-4

Wang, Y. L., Lin, C. H., Chen, C. C., Chang, C. P., Lin, K. C., Su, F. C., et al. (2019). Exercise Preconditioning attenuates neurological injury by preserving old and newly formed HSP72-containing neurons in focal brain ischemia rats. *Int. J. Med. Sci.* 16, 675–685. doi: 10.7150/ijms.32962

Wang, Y., Gibney, P. A., West, J. D., and Morano, K. A. (2012). The yeast Hsp70 Ssa1 is a sensor for activation of the heat shock response by thiol-reactive compounds. *Mol. Biol. Cell.* 23, 3290–3298. doi: 10.1091/mbc.E12-06-0447

Wasinger, C., Hofer, A., Spadiut, O., and Hohenegger, M. (2018). Amino acid signature in human melanoma cell lines from different disease stages. *Sci. Rep.* 8:6245. doi: 10.1038/s41598-018-24709-0

Watanabe, Y., Cohen, R. A., and Matsui, R. (2016a). Redox regulation of ischemic angiogenesis - another aspect of reactive oxygen species. *Circ. J.* 80, 1278–1284. doi: 10.1253/circj.CJ-16-0317

Watanabe, Y., Murdoch, C. E., Sano, S., Ido, Y., Bachschmid, M. M., Cohen, R. A., et al. (2016b). Glutathione adducts induced by ischemia and deletion of glutaredoxin-1 stabilize HIF-1α and improve limb revascularization. *Proc. Natl. Acad. Sci. U.S.A.* 113, 6011–6016. doi: 10.1073/pnas.1524198113

Weekly, C. M., and Harris, H. H. (2013). Which form is that? The importance of selenium speciation and metabolism in the prevention and treatment of disease. *Chem. Soc. Rev.* 42, 8870–8894. doi: 10.1039/c3cs60272a

Welbourne, T., Routh, R., Yudkoff, M., and Nissim, I. (2001). The glutamine/glutamate couplet and cellular function. *News Physiol. Sci.* 16, 157–160. doi: 10.1152/physiologyonline.2001.16.4.157

Wischmeyer, P. E. (2003). Clinical applications of L-glutamine: Past, present, and future. *Nutr. Clin. Pract.* 18, 377–385. doi: 10.1177/0115426503018005377

Xi, P., Jiang, Z., Zheng, C., Lin, Y., and Wu, G. (2011). Regulation of protein metabolism by glutamine: Implications for nutrition and health. *Front. Biosci.* 16, 578–597. doi: 10.2741/3707

Xing, H., Mayhew, C. N., Cullen, K. E., Park-Sarge, O. K., and Sarge, K. D. (2004). HSF1 modulation of Hsp70 mRNA polyadenylation via interaction with symplekin. *J. Biol. Chem.* 279, 10551–10555. doi: 10.1074/jbc.M311719200

Yang, J., Zhang, H., Gong, W., Liu, Z., Wu, H., Hu, W., et al. (2020). S-Glutathionylation of human inducible Hsp70 reveals a regulatory mechanism involving the C-terminal α-helical lid. *J. Biol. Chem.* 295, 8302–8324. doi: 10.1074/jbc.RA119.012372

Yu, L., Sun, Y., Cheng, L., Jin, Z., Yang, Y., Zhai, M., et al. (2014). Melatonin receptor-mediated protection against myocardial ischemia/reperfusion injury: Role of SIRT1. *J. Pineal Res.* 57, 228–238. doi: 10.1111/jpi.12161

Zabot, G. P., Carvalhal, G. F., Marroni, N. P., Hartmann, R. M., da Silva, V. D., and Fillmann, H. S. (2014). Glutamine prevents oxidative stress in a model of mesenteric ischemia and reperfusion. *World J. Gastroenterol.* 20, 11406–11414. doi: 10.3748/wjg.v20.i32.11406

Zhang, H., Gong, W., Wu, S., and Perrett, S. (2022). HSP70 in Redox Homeostasis. *Cells* 11:829. doi: 10.3390/cells11050829

Zhang, Y., Milatovic, D., Aschner, M., Feustel, P., and Kimelberg, H. (2007). Neuroprotection by tamoxifen in focal cerebral ischemia is not mediated by an agonist action at estrogen receptors but is associated with antioxidant activity. *J. Exp. Neurol.* 204, 819–827. doi: 10.1016/j.expneurol.2007.01.015

Zhang, Z., Yan, J., Chang, Y., ShiDu, Y. S., and Shi, H. (2011). Hypoxia inducible factor-1 as a target for neurodegenerative diseases. *Curr. Med. Chem.* 18, 4335–4343. doi: 10.2174/092986711797200426

Zheng, Y., Hou, J., Liu, J., Yao, M., Li, L., Zhang, B., et al. (2014). Inhibition of autophagy contributes to melatonin-mediated neuroprotection against transient focal cerebral ischemia in rats. *J. Pharmacol. Sci.* 124, 354–364. doi: 10.1254/jphs.13220fp

Zheng, Z., Kim, J. Y., Ma, H., Lee, J. E., and Yenari, M. A. (2008). Anti-inflammatory effects of the 70 kDa heat shock protein in experimental stroke. *J. Cereb. Blood Flow Metab.* 28, 53–63. doi: 10.1038/sj.jcbfm.9600502

Zoidis, E., Seremelis, I., Kontopoulos, N., and Danezis, G. P. (2018). Selenium-dependent antioxidant enzymes: Actions and properties of selenoproteins. *Antioxidants* 7:66. doi: 10.3390/antiox7050066

Zou, W., Fang, C., Ji, X., Liang, X., Liu, Y., Han, C., et al. (2015). Estrogen Receptor (ER)-α36 Is Involved in Estrogen- and Tamoxifen-Induced Neuroprotective Effects in Ischemic Stroke Models. *PLoS One* 10:e0140660. doi: 10.1371/journal.pone.0140660

Zwolak, I., and Zaporowska, H. (2012). Selenium interactions and toxicity: A review. Selenium interactions and toxicity. *Cell. Biol. Toxicol.* 28, 31–46. doi: 10.1007/s10565-011-9203-9

frontiers | Frontiers in Cellular Neuroscience

TYPE Opinion
PUBLISHED 17 April 2023
DOI 10.3389/fncel.2023.1131653

OPEN ACCESS

EDITED BY
Rosa Maria Vitale,
National Research Council (CNR), Italy

REVIEWED BY
Guilherme Rapozeiro França,
Rio de Janeiro State Federal University, Brazil

*CORRESPONDENCE
Maksim V. Storozhuk
✉ maksim@biph.kiev.ua

SPECIALTY SECTION
This article was submitted to Cellular Neuropathology, a section of the journal Frontiers in Cellular Neuroscience

RECEIVED 25 December 2022
ACCEPTED 13 March 2023
PUBLISHED 17 April 2023

CITATION
Storozhuk MV (2023) Cannabidiol: potential in treatment of neurological diseases, flax as a possible natural source of cannabidiol. *Front. Cell. Neurosci.* 17:1131653. doi: 10.3389/fncel.2023.1131653

Cannabidiol: potential in treatment of neurological diseases, flax as a possible natural source of cannabidiol

Maksim V. Storozhuk *

Department of Cellular Membranology, Bogomoletz Institute of Physiology, National Academy of Sciences of Ukraine, Kyiv, Ukraine

KEYWORDS

cannabidiol, neurological diseases, epilepsy, anxiety, anxiolytic, $GABA_A$ receptors

Cannabidiol (CBD) is a non-psychoactive phytocannabinoid obtained from Cannabis (Jung et al., 2019). As a part of Cannabis-based medicinal preparation, CBD has been used for a long time; however, until recently, it has received far less attention as a single drug (Morales et al., 2017). Currently, CBD and its analogs receive growing attention because of their potential therapeutic benefits (Pisanti et al., 2017; Jung et al., 2019), including neuroprotective (Campos et al., 2016), anti-epileptic (Silvestro et al., 2019), anti-inflammatory (Couch et al., 2017), anxiolytic (Lee et al., 2017), and anti-cancer (Massi et al., 2013) properties. The clinical use of CBD is the most advanced in the treatment of epilepsy (WHO, 2018). Research in relation to other neurological disorders is substantially less advanced: for most indications, there is only pre-clinical evidence or a combination of pre-clinical and limited clinical evidence (WHO, 2018). Nevertheless, there is growing evidence suggesting the therapeutic potential of CBD for treating several neurological and neuropsychiatric disorders that affect millions of people worldwide (see Vitale et al., 2021; Bhunia et al., 2022 for a recent review).

At the same time, at least in several countries, the use of CBD for medicinal and even for research purposes is complicated or not possible due to legal restrictions that are mostly related to one source of CBD. Indeed, while Cannabis has been recently legalized for medicinal purposes in several countries, it is still illegal for these purposes in many others. Moreover, although the content of the psychoactive cannabinoid tetrahydrocannabinol (Δ9-THC) is substantially lower in hemp, the latter is also illegal for medicinal purposes in some countries. In addition, the usage of synthetic CBD can also be a subject of regulation or unclear (Appendino et al., 2022). Thus, the potential of CBD in the treatment of diseases (defined as the actual possibility of patients using CBD for treatment) is limited by restrictions related to the *source* of this cannabinoid. Indeed, concerns about the source of CBD were a reason for the recent ban (Yeung, 2023) on CBD-containing products in Hong Kong. Considering the above issues taken together, the idea of using CBD from non-cannabis plants seems to be interesting. In this context, the occurrence of cannabinoids in non-cannabis plants with a focus on CBD has recently been reviewed (Appendino et al., 2022). Flax (*Linum usitatissimum*) was considered a reasonable candidate with respect to the occurrence of a CBD-like compound, though levels of this compound were considered very low (Appendino et al., 2022).

In this study, (i) a brief outline of the therapeutic potential of CBD in relation to some neurological diseases and respective molecular targets of CBD is provided, and (ii) some details/concerns regarding flax as a potential natural source of CBD have been discussed with a focus on levels of the CBD-like compound in flax.

Therapeutic potential of cannabidiol in neurological diseases

The therapeutic potential of CBD in relation to neurological disorders has recently been reviewed in detail in many studies (Vitale et al., 2021; Bhunia et al., 2022). In the following paragraphs, some of these disorders and potential molecular targets of cannabidiol in relation to them are introduced.

Epilepsy is a neurological disorder characterized by unprovoked seizures, caused by abnormal brain activity. Epilepsy affects approximately 50 million people worldwide (WHO, 2022). Considering that 30–40% of patients develop drug-resistant epilepsy, the availability of novel treatments is of great importance. Recently, one pure CBD product (Epidiolex) has been approved for patients with rare forms of drug-resistant epilepsy (Vitale et al., 2021). The therapeutic effects of CBD in epilepsy are thought to be mediated by multiple molecular targets, including $GABA_A$ receptors, glycine receptors, TRPV1, TRPV2, TRPA1, and GPR55 (Vitale et al., 2021).

Parkinson's disease (PD) is a progressive neurodegenerative disorder caused by the degeneration of dopaminergic neurons in the *substantia nigra* of the midbrain and the development of neuronal Lewy bodies (Beitz, 2014). In PD animal models, CBD had neuroprotective effects, probably mediated by its antioxidant and anti-inflammatory properties (Moises Garcia-Arencibia et al., 2007). It was also shown that CBD counteracts non-motor symptoms of PD (Crippa et al., 2019). These works are just two examples see (Vitale et al., 2021; Bhunia et al., 2022) for detailed review. 5-HT3Rs and GPR6 are thought to be molecular targets mediating the therapeutic effects of CBD in PD (Vitale et al., 2021).

Alzheimer's disease (AD) is a progressive neurodegenerative disorder, affecting millions of people worldwide. Currently, only symptomatic treatments are available for this disease. Although the accumulation of β-amyloids is considered to be a major histopathological hallmark of AD, it is still debated whether this is the primary *cause* of the disease. Nevertheless, it is generally accepted that multiple factors, including oxidative stress and neuroinflammation, contribute to the progression of AD. Evidence suggesting the potential benefits of CBD in relation to AD has been discussed in detail in a recent review (Bhunia et al., 2022). Here, it will be just mentioned that deficits in hippocampal LTP in a model of AD are reversed by CBD (Hughes and Herron, 2019).

In addition, CBD is potentially useful in numerous other disorders and pathologies that affect the CNS. These include multiple sclerosis, schizophrenia, post-traumatic stress, depression, and anxiety (Campos et al., 2016; Scarante et al., 2020, for a review; see Vitale et al., 2021; Bhunia et al., 2022), and this is just to name a few. In relation to depression and anxiety, CBD has been considered due to its antidepressant- and anxiolytic-like effects observed in animal models (see Schier et al., 2014, for review). Interestingly, some effects of CBD may be gender-dependent (Franzen et al., 2023). Analysis of *clinical trials* suggests that while CBD seems to be effective as an anxiolytic, its efficacy for other non-seizure-related conditions is much more variable (Tang et al., 2022). 5-HT3AR, 5-HT1AR, and the two closely related G-protein coupled receptors, GPR3 and GPR6, are considered as main molecular targets mediating the antidepressive effects of CBD (Vitale et al., 2021). These receptors are also likely to be involved in anxiety disorders (Vitale et al., 2021).

Abbreviations: CNS, central nervous system; $GABA_A$, receptors, γ-aminobutyric acid (GABA) A receptors; 5-HT1AR, 5-hydroxytryptamine (5-HT) type 1 receptor; 5-HT3Rs, 5-hydroxytryptamine (5-HT) type 3 receptor; GPR3, G-protein coupled receptor 3 receptor; GPR6, G protein-coupled receptor 6; GPR55, G protein-coupled receptor 55; TRPV1, transient receptor potential cation channel subfamily V member 1; TRPV2, transient receptor potential cation channel subfamily V member 2; TRPA1, transient receptor potential cation channel, subfamily A, member 1.

Flax as a possible natural source of cannabidiol

As already mentioned, the potential of CBD in the treatment of diseases is limited by restrictions related to the source of this cannabinoid. In this context, the presence of a CBD-like compound in fibers and seeds of flax (Styrczewska et al., 2012), with at least several characteristics similar to that of CBD, seems to be important. In brief, while studying the extract from previously generated transgenic plants overproducing phenylpropanoids, Styrczewska et al. found a new terpenoid compound. Further analysis of this compound using UPLC and gaschromatography–mass spectrometry (GC-MS) revealed that this compound is similar to CBD (Styrczewska et al., 2012). In addition, the biological assays carried out on the CBD-like compound showed a similar bioactivity profile of CBD, though the bioactivity assays performed are not specific for CBD. Importantly, *nearly the same* levels of this compound were also found in *wild-type plants* (see Figure 2 in Styrczewska et al., 2012).

In contrast to Cannabis and hemp, the usage of flax is not subject to strict regulation. Indeed, flax is authorized as an addition to foods, in particular, by FDA (Goyal et al., 2014), and is used for the production of several dietary supplements. Thus, given that the CBD compound in flax is indeed CBD, it may be useful in countries with the abovementioned restrictions. Moreover, it should be mentioned that while the results of Styrczewska et al. (2012) are encouraging, further studies on this issue are certainly required. Specifically, the isolation of the CBD-like compound from flax and its firm identification as CBD would be necessary in relation to this issue.

An additional concern is the levels of CBD-like compounds in flax, but these are considered very low (Appendino et al., 2022). However, this issue is not as clear as it may seem. Although the reported levels of CBD in hemp leaves (~800 μg/g, see Knezevic et al., 2021) are definitely much higher than the levels of CBD-like compounds in flax leaves (~7 μg/g, see Styrczewska et al., 2012), strikingly, low levels of CBD were reported in some commercial hemp dietary products such as *dried plant material* (0.64 μg/g) (Meng et al., 2018). The level of the CBD-like compound detected in flax seeds (10 μg/g) is comparable to that in hemp seeds (0.32 to 25.55 μg/g, see Jang et al., 2020). It should be also mentioned that the levels of CBD-like compounds in flax flowers were not determined by Styrczewska et al. (2012). Considering that the levels of CBD in hemp flowers are much higher than in seeds, it cannot be excluded that, similarly, levels of CBD-like compounds in flax

flowers are also higher compared to seeds. However, this is not likely because the levels of CBD-like compounds in the seed buds of flax are comparable to those in flax seeds.

In addition, comparing the effects of CBD-like compound from flax with already known effects of CBD in models of neurological diseases may give some interesting results. Just as an example, would CBD-like compound mimic effects of CBD in reversing deficits in hippocampal LTP (Hughes and Herron, 2019)? On the one hand, an answer should hint at whether the biological activity of the CBD-like compound is similar to that of CBD in this pharmacological model. On the other hand, even in the case that a CBD-like compound is not actually CBD, still interesting and potentially useful effects may be found. In any case, given that the compound found in flax is CBD, its levels appear to be sufficient for CBD-containing dietary products.

In summary, CBD is already approved for treating some forms of epilepsy, and there is growing evidence suggesting the therapeutic potential of CBD in relation to many other diseases of the central nervous system. At the same time, at least in several countries, the use of CBD for medicinal and even research purposes is complicated or not possible due to legal restrictions that are mostly related to a source of CBD. In this context, though it is chancy, the results of addressing scientific questions related to the occurrence of CBD-like compounds in flax may have potentially important implications, including implications related to the treatment of diseases of the central nervous system. For instance, given that the CBD-like compound in flax is indeed CBD, it could be used for medicinal properties in countries with legal restrictions on cannabis/hemp. Other potentially useful implications also cannot be excluded. For instance, given that the compound found in flax is CBD, its levels appear to be sufficient for CBD-containing dietary products. At the same time it should be emphasized that the major concern regarding possibility to use flax as a natural source is the exact nature of CBD-like compound in flax. An additional but also important concern is the low levels of CBD-like compounds in flax.

Author contributions

The author confirms being the sole contributor of this work and has approved it for publication.

Conflict of interest

The author declares that the research was conducted in the absence of any commercial or financial relationships that could be construed as a potential conflict of interest.

Publisher's note

All claims expressed in this article are solely those of the authors and do not necessarily represent those of their affiliated organizations, or those of the publisher, the editors and the reviewers. Any product that may be evaluated in this article, or claim that may be made by its manufacturer, is not guaranteed or endorsed by the publisher.

References

Appendino, G., Taglialatela-Scafati, O., and Muñoz, E. (2022). Cannabidiol (CBD) from non-cannabis plants: myth or reality? *Nat. Prod. Commun.* 17, 1–5. doi: 10.1177/1934578X221098843

Beitz, J. M. (2014). Parkinson's disease: a review. *Front Biosci. (Schol.Ed).* 6, 65–74. doi: 10.2741/S415

Bhunia, S., Kolishetti, N., Arias, A. Y., Vashist, A., and Nair, M. (2022). Cannabidiol for neurodegenerative disorders: a comprehensive review. *Front. Pharmacol.* 13, 989717. doi: 10.3389/fphar.2022.989717

Campos, A. C., Fogaca, M. V., Sonego, A. B., and Guimaraes, F. S. (2016). Cannabidiol, neuroprotection and neuropsychiatric disorders. *Pharmacol.Res.* 112, 119–127. doi: 10.1016/j.phrs.2016.01.033

Couch, D. G., Tasker, C., Theophilidou, E., Lund, J. N., and O'Sullivan, S. E. (2017). Cannabidiol and palmitoylethanolamide are anti-inflammatory in the acutely inflamed human colon. *Clin. Sci. (Lond).* 131, 2611–2626. doi: 10.1042/CS20171288

Crippa, J. A. S., Hallak, J. E. C., Zuardi, A. W., Guimaraes, F. S., Tumas, V., and Dos Santos, R. G. (2019). Is cannabidiol the ideal drug to treat non-motor Parkinson's disease symptoms? *Eur.Arch. Psychiatry Clin. Neurosci.* 269, 121–133. doi: 10.1007/s00406-019-00982-6

Franzen, J. M., Werle, I., Vanz, F., de Oliveira, B. B., Martins Nascimento, L. M., Guimaraes, F. S., et al. (2023). Cannabidiol attenuates fear memory expression in female rats via hippocampal 5-HT(1A) but not CB1 or CB2 receptors. *Neuropharmacology.* 223, 109316. doi: 10.1016/j.neuropharm.2022.109316

Goyal, A., Sharma, V., Upadhyay, N., Gill, S., and Sihag, M. (2014). Flax and flaxseed oil: an ancient medicine & modern functional food. *J.Food Sci.Technol.* 51, 1633–1653 doi: 10.1007/s13197-013-1247-9

Hughes, B., and Herron, C. E. (2019). Cannabidiol reverses deficits in hippocampal LTP in a model of Alzheimer's disease. *Neurochem.Res.* 44, 703–713. doi: 10.1007/s11064-018-2513-z

Jang, E., Kim, H., Jang, S., Lee, J., Baeck, S., In, S., et al. (2020). Concentrations of THC, CBD, and CBN in commercial hemp seeds and hempseed oil sold in Korea. *Forensic Sci. Int.* 306, 110064. doi: 10.1016/j.forsciint.2019.110064

Jung, B., Lee, J. K., Kim, J., Kang, E. K., Han, S. Y., Lee, H. Y., et al. (2019). Synthetic strategies for (-)-cannabidiol and its structural analogs. *Chem.Asian J.* 14, 3749–3762. doi: 10.1002/asia.201901179

Knezevic, F., Nikolai, A., Marchart, R., Sosa, S., Tubaro, A., and Novak, J. (2021). Residues of herbal hemp leaf teas–How much of the cannabinoids remain? *Food Control.* 127, 108146. doi: 10.1016/j.foodcont.2021.108146

Lee, J. L. C., Bertoglio, L. J., Guimaraes, F. S., and Stevenson, C. W. (2017). Cannabidiol regulation of emotion and emotional memory processing: relevance for treating anxiety-related and substance abuse disorders. *Br. J. Pharmacol.* 174, 3242–3256. doi: 10.1111/bph.13724

Massi, P., Solinas, M., Cinquina, V., and Parolaro, D. (2013). Cannabidiol as potential anticancer drug. *Br.J.Clin.Pharmacol.*, 75, 303–312. doi: 10.1111/j.1365-2125.2012.04298.x

Meng, Q., Buchanan, B., Zuccolo, J., Poulin, M. M., Gabriele, J., and Baranowski, D. C. (2018). A reliable and validated LC-MS/MS method for the simultaneous quantification of 4 cannabinoids in 40 consumer products. *PLoS ONE.* 13, e0196396. doi: 10.1371/journal.pone.0196396

Moises Garcia-Arencibia, S., Gonzalez de, L. E., Ramos, J. A., Mechoulam, R., and Fernandez-Ruiz, J. (2007). Evaluation of the neuroprotective effect of cannabinoids in a rat model of Parkinson's disease: importance of antioxidant and cannabinoid receptor-independent properties. *Brain Res.* 1134, 162–170. doi: 10.1016/j.brainres.2006.11.063

Morales, P., Reggio, P. H., and Jagerovic, N. (2017). An overview on medicinal chemistry of synthetic and natural derivatives of cannabidiol. *Front. Pharmacol.* 8, 422. doi: 10.3389/fphar.2017.00422

Pisanti, S., Malfitano, A. M., Ciaglia, E., Lamberti, A., Ranieri, R., Cuomo, G., et al. (2017). Cannabidiol: state of the art and new challenges for therapeutic applications. *Pharmacol.Ther.* 175, 133–150 doi: 10.1016/j.pharmthera.2017.02.041

Scarante, F. F., Ribeiro, M. A., Almeida-Santos, A. F., GuimarÃ£es, F. S., and Campos, A. C. (2020). Glial cells and their contribution to the mechanisms of action of cannabidiol in neuropsychiatric disorders. *Front Pharmacol.* 11, 618065. doi: 10.3389/fphar.2020.618065

Schier, A. R., de Oliveira Ribeiro, N. P., Coutinho, D. S., Machado, S., Arias-Carrion, O., Crippa, J. A., et al. (2014). Antidepressant-like and anxiolytic-like effects of cannabidiol: a chemical compound of Cannabis sativa. *CNS.Neurol. Disord. Drug Targets.* 13, 953–960. doi: 10.2174/1871527313666140612114838

Silvestro, S., Mammana, S., Cavalli, E., Bramanti, P., and Mazzon, E. (2019). Use of cannabidiol in the treatment of epilepsy: efficacy and security in clinical trials. *Molecules.* 24, (8) doi: 10.3390/molecules24081459

Styrczewska, M., Kulma, A., Ratajczak, K., Amarowicz, R., and Szopa, J. (2012). Cannabinoid-like anti-inflammatory compounds from flax fiber. *Cell Mol. Biol. Lett.* 17, 479–499. doi: 10.2478/s11658-012-0023-6

Tang, Y., Tonkovich, K. L., and Rudisill, T. M. (2022). The Effectiveness and safety of cannabidiol in non-seizure-related indications: a systematic review of published randomized clinical trials. *Pharmaceut. Med.* 36, 353–385. doi: 10.1007/s40290-022-00446-8

Vitale, R. M., Iannotti, F. A., and Amodeo, P. (2021). The (Poly)pharmacology of cannabidiol in neurological and neuropsychiatric disorders: molecular mechanisms and targets. *Int J. Mol. Sci.* 22, 9. doi: 10.3390/ijms22094876

WHO (2018). *Cannabidiol (CBD) Critical Review Report, Expert Committee on Drug Dependence 40th Meeting Geneva 4-7 June 2018.* Available online at: https://www.who.int/docs/default-source/controlled-substances/whocbdreportmay2018-2.pdf?sfvrsn=f78db177_2 (accessed February 5, 2023).

WHO (2022). *Epilepsy*. Available online at: https://www.who.int/news-room/fact-sheets/detail/epilepsy (accessed February 5, 2023).

Yeung, J. (2023). *Hong Kong is criminalizing CBD as a 'dangerous drug' alongside heroin, CNN Updated 2:58 AM EST, Wed February 1, 2023.* Available online at: https://edition.cnn.com/2023/01/31/business/hong-kong-cbd-ban-businesses-intl-hnk/index.html (accessed February 5, 2023).

frontiers | Frontiers in Cellular Neuroscience

TYPE Original Research
PUBLISHED 20 April 2023
DOI 10.3389/fncel.2023.1131130

OPEN ACCESS

EDITED BY
Ulises Gomez-Pinedo,
Health Research Institute of the Hospital Clínico San Carlos, Spain

REVIEWED BY
Maria Victoria Sánchez-Gómez,
University of the Basque Country, Spain
Doddy Denise Ojeda-Hernández,
Complutense University of Madrid, Spain

*CORRESPONDENCE
Irina Labunets
✉ irina_labunets@ukr.net

SPECIALTY SECTION
This article was submitted to Cellular Neuropathology, a section of the journal Frontiers in Cellular Neuroscience

RECEIVED 24 December 2022
ACCEPTED 30 March 2023
PUBLISHED 20 April 2023

CITATION
Labunets I, Rodnichenko A, Savosko S and Pivneva T (2023) Reaction of different cell types of the brain on neurotoxin cuprizone and hormone melatonin treatment in young and aging mice.
Front. Cell. Neurosci. 17:1131130.
doi: 10.3389/fncel.2023.1131130

Reaction of different cell types of the brain on neurotoxin cuprizone and hormone melatonin treatment in young and aging mice

Irina Labunets[1,2]*, Anzhela Rodnichenko[1], Sergey Savosko[1] and Tetyana Pivneva[3,4]

[1]Cell and Tissue Technologies Department, Institute of Genetic and Regenerative Medicine, National Scientific Center "M.D. Strazhesko Institute of Cardiology", Clinical and Regenerative Medicine of the National Academy of Medical Sciences of Ukraine, Kyiv, Ukraine, [2]Laboratory of Pathophysiology and Immunology, D. F. Chebotarev Institute of Gerontology of the National Academy of Medical Sciences of Ukraine, Kyiv, Ukraine, [3]Department of Sensory Signaling, Bogomoletz Institute of Physiology, National Academy of Sciences of Ukraine, Kyiv, Ukraine, [4]Department of Biomedicine and Neuroscience, Kyiv Academic University, Kyiv, Ukraine

Introduction: The brain myelin and neurons destruction in multiple sclerosis may be associated with the production of neuroinflammatory cells (macrophages, astrocytes, T-lymphocytes) of pro-inflammatory cytokines and free radicals. The age-associated changes of the above cells can influence on the response of nervous system cells to toxic damaging and regulatory factors of humoral/endocrine nature, in particular pineal hormone melatonin. The study aim was (1) to evaluate changes of the brain macrophages, astrocytes, T-cells, neural stem cells, neurons, and central nervous system (CNS) functioning in the neurotoxin cuprizone-treated mice of different age; and (2) to assess in such mice the effects of exogenous melatonin and possible courses of its action.

Methods: A toxic demyelination and neurodegeneration model was induced in 129/Sv mice aged 3–5 and 13–15 months by adding cuprizone neurotoxin to their food for 3 weeks. From the 8th day of the cuprizone treatment, melatonin was injected intraperitoneally at 6 p.m. daily, at a dose of 1 mg/kg. The brain GFPA + -cells were evaluated by immunohistochemical method, the proportion of CD11b+, CD3+CD11b+, CD3+, CD3+CD4+, CD3+CD8+, Nestin+-cells was determined via flow cytometry. Macrophage activity was evaluated by their ability to phagocytose latex beads Morphometric analysis of the brain neurons and the behavioral reactions ("open field" and rotarod tests) were performed. To assess the involvement of the bone marrow and thymus in the action of melatonin, the amount of granulocyte/macrophage colony-forming cells (GM-CFC), and blood monocytes and thymic hormone thymulin were evaluated.

Results and discussion: The numbers of the GFAP+-, CD3+-, CD3+CD4+, CD3+CD8+, CD11b+, CD3+CD11b+, Nestin+-cells and macrophages phagocytic latex beads and malondialdehyde (MDA) content were increased in the brain of young and aging mice under cuprizone influence. The proportion of undamaged neurons within the brain, motor, affective, and exploratory activities, and muscle tone decreased in mice of both ages. Introducing melatonin to mice of any

age reduced the number of GFAP+-, CD3+- cells and their subpopulations, macrophage activation, and MDA content. At the same time, the percentage of brain neurons that were unchanged increased as the number of Nestin+ cells decreased. The behavioral responses were also improved. Besides, the number of bone marrow GM-CFC and the blood level of monocytes and thymulin increased. The effects of both neurotoxin and melatonin on the brain astrocytes, macrophages T-cells, and immune system organs as well as the structure and functioning of neurons were more pronounced in the young mice.

Conclusion: We have observed the involvement of the astrocytes, macrophages, T-cells, neural stem cells, and neurons in the brain reaction of mice different age after administration of neurotoxin cuprizone and melatonin. The brain cell composition reaction has the age features. The neuroprotective effects of melatonin in cuprizone-treated mice have been realized through an improvement of the brain cell composition and oxidative stress factors and functioning of bone marrow and thymus.

KEYWORDS

cuprizone, melatonin, age, brain neurons and neuroinflammatory cells, multiple sclerosis, oxidative stress, bone marrow, thymus

Introduction

Multiple sclerosis is one of the most common demyelinating pathologies of the central nervous system (CNS) (Mishchenko et al., 2014; Vaughn et al., 2019). This results in the loss of myelin in nerve fibers, disruption of nerve impulse transmission, and a decline in motor activity. Recently, the leading scientists consider multiple sclerosis as a neuro-degenerative pathology. Destruction of neurons in different areas of the CNS can lead to the changes of their functioning and, as a result, to the disorders not only in motor activity but also in emotions, memory, vegetative dysfunction, intellect, etc.

Multiple sclerosis usually affects younger people, but today it can be reported in people over the age of 45. In older patients, this disease has pre-dominantly infectious and toxic origin, progressive character and more severe clinical course (Vaughn et al., 2019).

The pathogenic links of neuronal and myelin destructions in multiple sclerosis can be the productions of oxidative stress and neuro-inflammation (Chen et al., 2020; Absinta et al., 2021; Murioz-Jurado et al., 2022). For example, the brain microglial cells and macrophages produce free radicals and pro-inflammatory cytokines (TNF-α, IFN-γ, and IL-1β) (Li and Barres, 2018). During neuro-inflammation the T-lymphocytes infiltrate the brain and become source of pro-inflammatory cytokines (Sonobe et al., 2007; Gonzalez and Pacheco, 2014).

In addition to microglia inflamed in multiple sclerosis, large populations of reactive astrocytes and stressed oligodendrocytes were present on the chronic active lesion area. As is known, astrocytes act a crucial role in the pathogenesis of multiple sclerosis. They take part in regulating the blood–brain barrier (BBB); in modulating T cell activity through the production of cytokines; in expressing toll-like receptors and major histocompatibility complex class I and II (Burda and Sofroniew, 2014; Liddelow and Barres, 2015; Sen et al., 2022).

Age-associated changes both in the amount of macrophages, microglial cells, T-cells, astrocytes and their relationships can influence not only on the efficiency of restoration of neurogenesis after its injury but also on the response of nervous system cells to regulatory factors of cellular/humoral nature (Gemechu and Bentivoglio, 2012; Hamilton et al., 2013; Moraga et al., 2015; Labunets et al., 2017a). Investigation of age aspects of nervous cells reaction on the neurotoxic and regulatory factors is impossible without the use of adequate experimental model of multiple sclerosis.

One of them is cuprizone toxic model. Neurotoxin cuprizone is a copper chelator that decreases cytochrome and monoamine oxidase activities in the mitochondria of mature oligodendrocytes and, as a result, leads to apoptosis in these cells and demyelination in CNS (Praet et al., 2014; Vega-Riquer et al., 2019; Zhan et al., 2020). According to our previous data, the cuprizone induced degeneration the neurons in cerebral cortex and cerebellum of experimental mice (Labunets et al., 2017a, 2018a,b; Labunets and Rodnichenko, 2020). According to the literature, neuroinflammation, and oxidative stress are important for oligodendrocyte and neuron damage in cuprizone-treated young animals (Gudi et al., 2014; Praet et al., 2014; Vega-Riquer et al., 2019).

Among the endocrine regulatory factors, the pineal gland hormone melatonin shows a wide range of biologic activity in the organism. This hormone acts on immune (thymus, bone marrow, macrophages, lymphocytes, etc.) and endocrine (pituitary, adrenal, gonadal glands, etc.) systems functions, regulates the biological rhythms in organism and reveals antiapoptotic, antioxidant, anti-inflammatory, and neurotrophic effects (Sarlak et al., 2013; Csaba, 2016; Wurtman, 2017; Murioz-Jurado et al., 2022). Melatonin

synthesis undergoes changes with age and in experimental demyelination (Hardeland, 2012; Wurtman, 2017). In contrast, the exogenous melatonin exhibits neuroprotective effects in animals of different age with experimental models of nervous system pathology (Hardeland, 2012; Murioz-Jurado et al., 2022). The aim of study was:(1) to evaluate changes of the brain macrophages, astrocytes, T-cells, neural stem cells, neurons and CNS functioning in the neurotoxin cuprizone-treated mice of different age; and (2) to assess in such mice the effects of exogenous melatonin and possible courses of its action.

Materials and methods

Animals

Experiments were performed on 3–5-month-old (young, $n = 79$) and 13–15-month-old (aging, $n = 79$) female 129/Sv mice (H-2b genotype) from experimental clinic of the Institute of Genetic and Regenerative Medicine. According to our investigations, the 129/Sv mice of both sexes are sensitive to the toxic action of neurotoxin cuprizone as well as C57Bl/6 mice where widely used in such experiments (Labunets et al., 2014a,b; Labunets, 2018). The animals were kept in standard vivarium conditions with a fixed light regimen 12:12 with food and water *ad libitum*. Biological tissues for studies were taken at 9 a.m. by ether anesthesia.

All experiments were carried out according to the European Convention for the Protection of Vertebrate Animals used for Experimental and other Scientific Purposes [European Union Directive of 22 September 2010 (2010/63/EU)] and Article 26 of the Law of Ukraine "On the Protection of Animals from Cruelty" (No.3447-IV, 2006) and were approved by the Bioethics Committee of Institute of Genetic and Regenerative Medicine.

Experimental groups of mice

Experimental animals were grouped (i) intact young ($n = 21$) and aging ($n = 21$) animals, receiving standard food; (ii) young ($n = 21$) and aging ($n = 21$) mice, receiving cuprizone-containing food for 3 weeks and injections of solvent; (iii) young ($n = 21$) and aging ($n = 21$) mice with cuprizone diet and melatonin injection; (iv) young mice ($n = 16$) and aging ($n = 16$) mice with standart food (intact mice) which received both melatonin and solvent. Experiments were conducted after completion of cuprizone diet on 7, 21, and 60 days.

Cuprizone-induced model of demyelination and neurodegeneration

The mice of both age groups received the neurotoxin cuprizone [bis(cyclohexylidenehydrazide)] (Sigma-Aldrich, USA). The animals were fed food mixed with cuprizone at 0.2% (w/w), daily for 3 weeks (Praet et al., 2014; Labunets et al., 2018a,b; Labunets and Rodnichenko, 2020; Zhan et al., 2020). Intact animals used regular food. The body weight of each mice was measured before and after cuprizone administration alone or in its combination with melatonin.

Weight loss is one of the signs of the toxic effects of cuprizone. After cuprizone treatment the young and aging mice lost weight. Before cuprizone treatment, body weights of young and aging mice were 22.0 ± 1.4 and 28.1 ± 1.9 g, respectively. After completion of the cuprizone diet, 18.0 ± 1.1 and 23.1 ± 1.2 g, respectively ($p < 0.05$). Weight of mice with cuprizone and melatonin treatment did not changed (data not shown).

Melatonin injections

Cuprizone-treated mice of both age groups received melatonin i.p. injections (Sigma-Aldrich, USA) in the dose of 1 mg/kg every day at 6 p.m. starting from the 8th to 21st day of the cuprizone diet. Melatonin was dissolved in solvent (0.9% sodium chloride). After 8–10 days of cuprizone diet the signs of both apoptosis of oligodendrocytes and structural changes of the brain neurons developed in mice of different strains, including 129/Sv (Praet et al., 2014; Labunets et al., 2018a; Zirngibl et al., 2022). In addition, we also evaluated the effects of melatonin alone on some parameters (thymus and bone marrow functions) in mice of both ages group ($n = 8$) with regular diet. Melatonin was administered according to the above scheme. Control groups of mice received solvent (sodium chloride) injections ($n = 8$).

Immunophenotyping of the brain cells

Immunophenotyping for CD3+, CD4+, CD8+ and CD11b+ (Mac-1) markers was performed using the mouse monoclonal antibodies conjugated to fluorochromes (BD Biosciences, USA): CD3 – PE-conjugated antibodies (cat. no. 555275), CD4 – APC-Cy^{TM} 7 conjugated antibodies (cat. no. 552051), CD8-APC conjugated antibodies (cat. no. 553035) and CD11b – FITC-conjugated antibodies (cat. no. 557396). The number of brain neural stem cells was determined by the expression of Nestin (Lendahl et al., 1990). To identify Nestin + cells, we used PE-conjugated mouse anti-nestin monoclonal antibodies (BD Biosciences, USA, cat. no. 561230). All antibodies used at a concentration of 0.5 μg/ml. The whole brain was homogenized; passed through the filter (70 μm); cells were fixed for 10 min at room temperature with 4% solution of paraformaldehyde in 0.1 M phosphate buffered saline (pH = 7.4); permeabilized and stained in Perm/Wash buffer (Becton Dickinson, USA) according to the manufacturer's instructions. Cell samples without antibodies were used as a control. The measurements of the percentage of labeled cells were performed using a flow cytometer-sorter BD FACSAria^{TM} I and BD FACS Diva 6.1 software (Becton Dickinson, Franklin Lakes, NJ, USA).

Functional activity of brain macrophages/phagocytic cells

Brain macrophages are heterogeneous population (Jordan and Thomas, 1988; Jordan et al., 1990). Among these cells, microglia,

and blood macrophages have a similar property, namely, the ability to phagocytose latex beads. The activity of macrophage/phagocytic brain cells in our experiments was determined according to Jordan et al. (1990) and in our modification (Labunets et al., 2017a). The method is based on the quantitative determination of the latex beads that are phagocytosed by activated macrophages after their incubation.

Whole-brain cell suspensions ($n = 5$ from each groups of mice) were first passed through a series of 100 μm and then 70 μm cell filters (Sigma-Aldrich, USA). Then cells were transferred to Petri dishes (100 mm diameter) in culture medium consisting of RPMI-1640, 10% fetal bovine serum, 2 mM L-glutamine, penicillin 100 U/ml, streptomycin 100 μg/ml (all reagents Sigma-Aldrich, USA). After cultivation for 1 h in CO_2 incubator in humidified atmosphere with 5% CO_2 at a temperature of 37°C the adherent cells were dissociated with 0.05% trypsin in 0.53 mM Na_2EDTA (Sigma-Aldrich, USA). Then 0.2 ml of cells suspension (2.5×10^6/ml) was placed on microscope slides and incubated for 1 h in the CO_2 incubator. After the cells incubation 0.2 ml suspension latex (2.5×10^8/ml) (Sigma-Aldrich, USA) was added and then incubated for 45 min. Then the cells were fixed and stained with Romanovsky-Gimsa (Macrochim, Ukraine). A total of 100 macrophages/phagocytes were counted and measured under a light microscope: (a) percentage of brain macrophages capable of phagocytosis of latex beads (phagocyte index) and (b) number of latex beads that phagocytose one macrophage (phagocyte number).

Immunohistochemistry

After decapitation, the removed brains ($n = 5$ from each groups of mice) were fixed in phosphate-buffered (PB) paraformaldehyde 4% in 0.1 M PB, pH 7.4. The sagittal sections of the brain (50 μm thick) were cut on a vibratome VT1000A (Leica, Wetzlar, Germany). Immunohistochemical staining of astrocytic cells was performed as previously described (Zabenko and Pivneva, 2016). Then hippocampus slices were washed with 0.1 M PB and blocked in 0.1 M PB containing 0.3% Triton X-100 and 0.5% bovine serum albumin. To identify the astrocytic cells the following primary antibody was used: polyclonal rabbit anti glial fibrillary acidic protein [GFAP, 1:1,500; Z0334[1] (GFAP) Dako cat z0334/product/Agilent technologies, DakoCytomation, Glostrup, Denmark]. On the next day sections were incubated with the secondary anti-rabbit antibody Alexa Fluor 594 (1:1,000, A-11012, Molecular Probes Inc., USA) diluted in 0.1 M PB, 0.5% bovine serum albumin, 0.3% Triton X-100. The slices were mounted on glass slides with fluorescent mounting medium Immu-Mount (Thermo Scientific, Waltham, MA, USA). Confocal images of glial cells were acquired with a laser-scanning microscope (FV1000-BX61WI, Olympus, Tokyo, Japan). For the evaluation of cells, the program Image J (NIH, USA) was used. The number of GFAP+ cells per 0.1 mm^2 area was counted in the CA1zone of the stratum radiatum of the hippocampus.

1 https://www.bioz.com/result/rabbitantiglialfibrillaryacidicprotein

Morphological studies of cerebral cortex neurons

Brain samples for morphological studies were obtained after transcardial perfusion of mice with 4% paraformaldehyde solution in 0.1 M PB (pH = 7.4). After dehydration in ascending alcohol solutions, brain samples were embedded in paraffin and sliced at 8 μm thickness in the frontal position of the brain. Paraffin sections were deparaffinized and rehydrated; were stained with toluidine blue for 10 min, were washed with tap water, differentiated with 1% glacial acetic acid, and washed again with tap water (Lu et al., 2022). After washing, the slices were cleared with ethanol and xylene for a few minutes, and mounted with Histofluid Mounting Media (Paul Marienfeld GmbH & Co. KG). Toluidine blue selectively stains acidic tissue components such as DNA in nuclei and RNA cytoplasm (Nissl bodies) of neuron and helps to analysis cell death and function (protein synthesis or functional degradation). Microphotographs of neurons were taking using a microscope Olympus BX-51.

Neurons were measured in layers III-V of cortex. The neurons were grouped into three categories: first – damaged neurons. Criteria for neuronal damage were the following: cytolysis, nucleolysis and nuclear pycnos, hydropic dystrophy, and/or deformed perikaryon. These neurons were considered as cuprizone-induced damage (destructive changes); second – neurons with moderate changes. These neurons were characterized by increased nucleus size, and the cytoplasm of the neurons was hypochrome (Labunets et al., 2017a, 2018a,b). Third group of neurons were with no signs of damage (no changes). The percentage of all neurons in the total number of neurons in layers III–V of the cortex was calculated from 10 histologically prepared images of mice from each experimental group, both young ($n = 5$) and aging ($n = 5$).

Malondialdehyde

The content of malondialdehyde (MDA) in whole brain homogenate was determined by the color intensity of the trimethine complex formed between thiobarbituric acid and MDA (Uchiyama and Mihara, 1978). The content of MDA was determined spectrophotometrically (μQuant Spectrophotometer, BioTek, USA) for $n = 5$ mice in each group.

Granulocyte/macrophage colony-forming cells

Granulocyte/macrophage colony-forming cells (GM-CFCs) were evaluated in the semi-agar cultures (Bradley and Metcalf, 1966; Labunets et al., 2017b). Bone-marrow cell suspensions were prepared by flushing from femur with R+PMI-1640 medium according to Anjos-Afonso and Bonnet (2008). 3×10^5 bone marrow cells in 0, 1 ml in RPMI-1640 were added to 1 ml medium McCoy 5A supplemented with 15% fetal bovine serum, 10 mM of L-glutamine, 1.6% sodium pyruvate, 0.94% of sodium bicarbonate, 20 mM of HEPES, 1% granulocyte/macrophage-colony-stimulating

factor (at a final concentration 0.5 ng/ml) (all reagents – Sigma-Aldrich, USA). Cultivation of bone-marrow cells was performed for 9 days in CO_2 incubator in humidified atmosphere with 5% CO_2 at a temperature of 37°C. On the 9th day of cultivation the number of GM-CFCs colonies consisting of at least 50 cells was counted. The types of colonies were following: granulocytic, mixed, and macrophage (Labunets et al., 2017b). The results were expressed as relative (per 10^6 bone marrow cells) and absolute number of GM-CFCs in the bone marrow of one femur in each experimental groups of mice ($n = 5$).

Peripheral blood monocytes

Calculation of the leukocyte formula of the peripheral blood of animals was carried out by the generally accepted method (Stephanov, 2001). This method is based on morphological recognition and counting of different cell types (neutrophils, eosinophils, basophils, lymphocytes, and monocytes) in stained peripheral blood smears. The smears were stained with Romanovsky-Gimsa stain (Macrochim, Ukraine). In the stained smears we found 200 leukocytes and individual cell types were expressed as a percentage.

The blood level of thymulin/thymic serum factor

Serum samples obtained by centrifugation of clotted blood were stored at −20°C. Thawed samples were filtered through Centriflo CF-50A ultrafilter (Amicon, USA) to remove the high molecular inhibitor of thymulin. The determination method of level thymulin is based on the its ability to restore the sensitivity of spontaneous rosette formation by splenocytes from thymectomized mice to inhibition with azathioprine (Sigma-Aldrich, USA), as described (Bach et al., 1978; Labunets et al., 2017b). Thymulin levels were evaluated at the last serum dilution, which reduced the number of rosette-forming cells by 50% compared to controls (cells without serum). The results were recorded as $\log_2$ thymulin titer.

Behavioral phenomena in animals

Behavioral reactions in mice were studied using the "open field" and rotarod tests. These tests provide adequate estimate of behavioral phenomena in young and aging animals (Franco-Pons et al., 2007; Gorina et al., 2017). The "open field" test allows to evaluate the locomotor activity (the number of crossed squares), the emotional activity (the number of fecal boluses) and the exploratory activity (the number of rearing and hole peeking). As shown, behavioral responses in mice are similar to human behavioral responses in neuropsychiatric disorders (Fisch, 2007). The duration of the "open field" test in mice ($n = 15$) in each groups was 3 min.

The rotarod test can assess an animal's coordination of movement, balance, and muscle tone. During the test (10 min), the rotation speed was changed sequentially from 10 rpm (3.0 V, 300 mA) to 20 rpm (5.0 V, 300 mA). Data were presented as total residence time (s) of mice ($n = 10$ in each groups) on the rod.

Statistical analysis

All data are presented as mean ± SEM. Statistical analysis was performed using StatSoft Statistica software 7.0 (StatSoft Inc., USA). Students two tailed t-test (paired or unpaired) was used to determine statistical differences between different experimental groups where appropriate. A $p < 0.05$ was considered as statistically significant.

Results

Changes in various cell types in brains of young and aging mice after treatment with cuprizone and melatonin

Brain T cells

One of early changes in the composition of the brain cells in cuprizone-treated mice (5–7 days of neurotoxin use) is the apoptosis of oligodendrocytes and structural changes in the neurons (Gudi et al., 2014; Labunets et al., 2018a).

We found that the amount of CD3+ T cells in the brain of mice of different group of age after 7 days of cuprizone diet (in each group $n = 4$) did not differ from that in intact animals (data not shown). As shown in **Figure 1**, the amounts of CD3+, CD3+CD4+ and CD3+CD8+ cells in the brain of young and aging cuprizone-treated mice (within 3 weeks) were significantly higher than in intact mice of the same age. Melatonin injection reduced the number of cell types in both age groups and their levels reached the values observed in the intact animals (except CD3+CD8+ cells in aging mice). The ratio of CD3+CD4+/CD3+CD8+ cells in the brains of young mice treated with cuprizone was reduced compared to intact animals and increased after melatonin administration to compare with cuprizone-treated mice (**Figure 1**). In aging mice, the cells ratio value did not change after cuprizone treatment but decreased after melatonin administration.

We have showed that 2 months after the completion of a 3-week cuprizone diet (period of remyelination and recovery of altered functions) the amount of CD3+ T cells and their subpopulations in the brain of young mice decreased but was still higher compared to intact mice (**Figure 1**). Two months after completion of cuprizone and melatonin treatment the amount of CD3+, CD3+CD4+ and CD3+CD8+ T cells corresponded the values in the intact animals.

In aging mice, 2 months after the completion of cuprizone treatment the amount of CD3+, CD3+CD4+ and CD3+CD8+ cells remained higher than in intact mice (**Figure 1**).

Two months after the end of cuprizone and melatonin treatment, the number of above cells did not differ from those immediately after using neurotoxin and hormone (**Figure 1**).

Thus, the number of T cell subpopulations in the brains of young and aging mice change in response to the effect of the cuprizone. Conversely, exogenous melatonin has a positive effect on these changes. The effect of melatonin on cuprizone-induced T cells changes persist for a long time. The influence of cuprizone and melatonin on T cells changes is more pronounced in young mice.

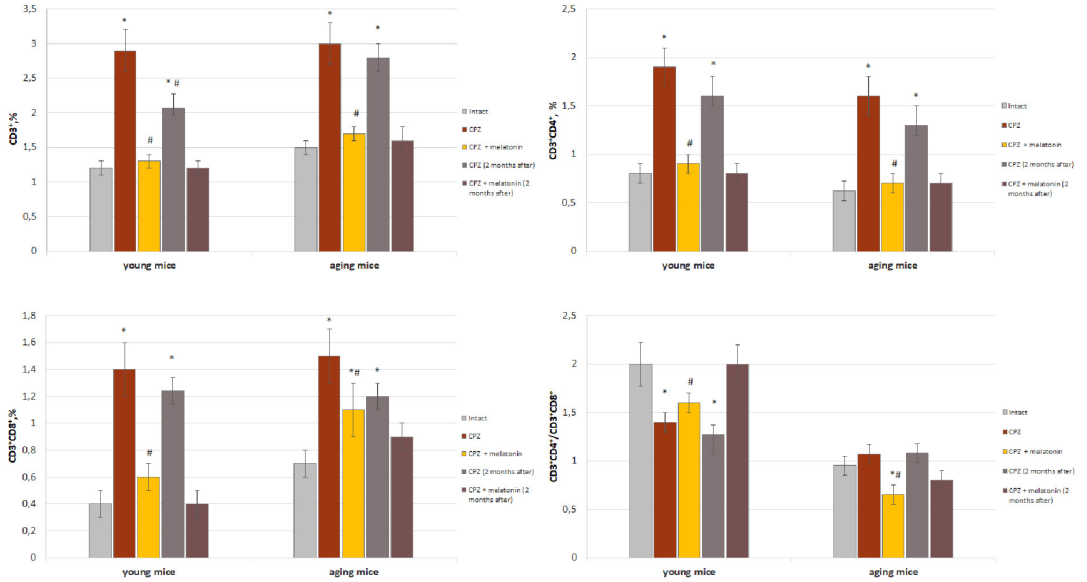

FIGURE 1
Percentage of CD3+, CD3+CD4+, and CD3+CD8+ T cells from total brain cells and cell ratio of CD3+CD4+/CD3+CD4+ in brain of young and aging mice of experimental groups ($n = 5$ in each group). Represented data are in 3 weeks of cuprizone (CPZ) diet and in 2 months after. Data are $M \pm$ SEM. $^{*}p < 0.05$ compared to intact group; $^{\#}p < 0.05$ compared to CPZ (t-test).

Brain macrophages

We found that both the index of latex beads phagocytic macrophages and of their phagocytic number in the brain of young mice after 7 days of taking cuprizone diet was higher than in the intact animals and remained that after 3 weeks of cuprizone diet (Figure 2). In the brain of aging mice, the index of latex beads phagocytic macrophages and their phagocytic number increased only after 3 weeks of cuprizone supplementation. After melatonin injections the values of the studied parameters decreased in mice of both age groups compare to cuprizone treated mice.

The amount of CD3+CD11b+ cells (activated macrophages) increased in both of young and aging neurotoxin-treated mice compare to intact groups of mice. After melatonin injections, the values of the studied indicators did not differ from those in the intact mice of both age groups (Figure 3).

Thus, we observed changes in both of the phagocytic index and phagocytic number of brain macrophages in response to cuprizone effect regardless of the age of mice. Exogenous melatonin reduced the values of the studied parameters in the cuprizone-treated mice.

Brain astrocytes

To study the reactivity of astrocytes after cuprizone and cuprizone + melatonin treatment, we carried out immunohistochemical labeling for the marker of astrocytes (GFAP). Our immunohistochemical studies have shown that the number of GFAP-positive astrocytes in the hippocampal CA1area was in both intact young and aging animals (21.40 ± 4.19, 21.50 ± 4.09), respectively. GFAP-positive astrocytes had non-enlarged soma with thin processes by their morphology (Figures 4A, D). After cuprizone use, the numbers of GFAP-positive astrocytes were markedly increased in all layers of the CA1 area in young and aging mice (37.63 ± 9.02 and 46.30 ± 6.67, respectively). The astrocytes acquired a hypertrophied form of both the soma and the processes (Figures 4B, E). It is known that the main manifestations of reactive gliosis are hypertrophy of astrocyte processes and upregulation of GFAP in their processes (Absinta et al., 2021).

After melatonin treatment the number of GFAP-positive astrocytes significantly decreased compared with those in cuprizone treatment and achieved 26.00 ± 5.81 in young and 28.70 ± 5.29 in aging animals but did not reach the control values (Figures 4C, F).

Thus, hormone melatonin significantly reduced astrocyte activation in the young and aging mice due to the antiapoptotic, antioxidant, anti-inflammatory, and neurotrophic effects (Wurtman, 2017).

Brain Nestin+ cells and neurons

We showed that the number of Nestin+ cells in the brains of young and aging mice treated with cuprizone was higher than in intact mice (Figure 5). After injections of melatonin, the number of Nestin+ cells decreased in mice of both ages compared to cuprizone-treated mice (Figure 5).

The percentage of unchanged neurons in cerebral cortex of cuprizone-treated mice of both ages decreased, while the percentage of neurons with destructive and moderate structural changes increased compared to the intact group (Figure 6). The percentage of neurons with destructive changes was higher in young cuprizone-treated mice than in aging mice. Injections of melatonin in both young and aging mice increased the percentage of unchanged neurons and decreased the percentage of neurons with destructive changes.

Thus, in the brains of young and aging mice, cuprizone changes the number and activity of neuroinflammatory cells (macrophages, astrocytes, and T cells) on the one hand and the structure of neurons on the other hand. This cellular imbalance was

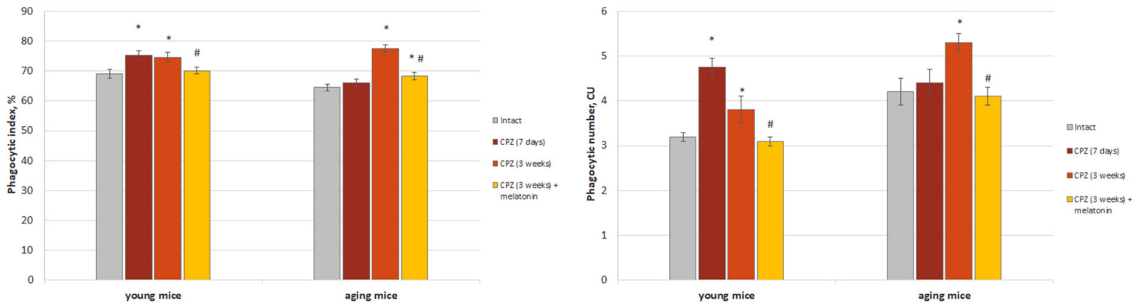

FIGURE 2
The amount (phagocytic index) and activity (phagocytic number) of macrophages phagocytic latex beads in the brain of young and aging mice of experimental groups ($n = 5$ in each group). Represented data are in 7 days and 3 weeks of cuprizone (CPZ) diet. Data are $M \pm SEM$. $^{*}p < 0.05$ compared to intact group; $^{\#}p < 0.05$ compared to 3 weeks of CPZ (t-test).

more pronounced in young cuprizone-treated animals. Exogenous melatonin has positive effects on T cells, macrophages, astrocytes and structurally altered neurons in the brains of cuprizone-treated mice of different ages. Effect was more pronounced in young mice.

Changes of behavioral reactions in young and aging mice after treatment with cuprizone and melatonin

An important manifestation of structural changes in neurons in the pathology of the nervous system was their dysfunction (Franco-Pons et al., 2007; Dutta and Trapp, 2011; Labunets et al., 2017a).

As shown in **Figure 7**, behavioral indicators in the "open field" test of young and aging mice treated with cuprizone were significantly lower than that of intact mice. The number of crossed squares increased after the injections of melatonin in mice of both ages. Moreover, values in aging mice reached values found in intact animals. Peeking and rearing activity increased after melatonin administration only in young cuprizone-treated mice. The number of boluses increased in mice of both age groups after administration of melatonin and did not differ from intact mice.

Rotarod test indicators were lower in young and aging mice treated with cuprizone compared to intact animals (**Figure 7**). After administration of melatonin, this behavioral parameter reached intact mice values only in young cuprizone-treated animals.

Thus, treatment with cuprizone reduces behavioral reactions in young and aging mice. Melatonin injections improve all behavioral parameters in young mice but only motor and emotional activity in aging mice.

Effects of cuprizone and melatonin treatment on brain oxidative stress and bone marrow and thymus function

Brain oxidative stress

One of the factors of oxidative stress is content of MDA. It is formed as a result of peroxidation of polyunsaturated fatty acids and can react with nucleic acids, phospholipids and amino acids.

Higher content of MDA was found in the brains of young and aging mice on the cuprizone diet compared to intact animals (**Figure 8**). After administration of melatonin, MDA content decreased to that of intact mice (**Figure 8**).

Thus, the results confirmed the antioxidant effect of melatonin on the brains of young and aging mice treated with cuprizone.

GM-CFCs in bone marrow and monocytes in the blood

It has been shown that the number of macrophages in the brain can be increased due to circulating monocytes derived from progenitor cells- bone marrow GM-CFCs (Zhao et al., 2018).

We found that, after 7 days of cuprizone administration, the amount of GM-CFCs in the bone marrow and monocytes in the blood of young ($n = 4$) and aging ($n = 4$) mice was not different from the intact animals (data not shown). After 3 weeks of cuprizone diet, the total number of nuclear cells and the absolute number of GM-CFCs were reduced in the bone marrow of young and aging mice compared to intact animals (**Figure 9**). Relative and absolute number of GM-CFCs in bone marrow in young mice after melatonin injections were higher than in cuprizone-treated mice (**Figure 9**). After administration of melatonin, the total number of nuclear cells and the absolute number of GM-CFCs in aging mice increased compared to cuprizone-treated mice, but remained at lower levels compared to intact animals.

Thus, under the influence of melatonin, the absolute number of GM-CFCs in the bone marrow of cuprizone-treated young mice changed due to an increase their colony-forming ability, but in cuprizone-treated aging mice, the absolute number of GM-CFCs increased due to elevation the total number of nuclear cells.

In addition, to confirm the positive effect only of melatonin on bone marrow function mice, the number of bone marrow GM-CFCs was measured in young and aging mice with regular diet after melatonin injections. Total number of nuclear cells in bone marrow of young mice treated with solvent ($n = 8$) or melatonin ($n = 8$) was $13.2 \pm 1.7.10^6$ and $13.4 \pm 1.5.10^6$, respectively; relative number of GM-CFCs was $21.0 \pm 1.1/10^6$ and $25.0 \pm 1.2/10^6$, respectively, ($p < 0.05$); absolute number of GM-CFCs was 275.1 ± 16.0/femur and 332.5 ± 23.0/femur, respectively, ($p < 0.05$). Total number of nuclear cells in bone marrow of aging mice treated with solvent ($n = 8$) or melatonin ($n = 8$) was $20.4 \pm 1.2.10^6$ and $25.4 \pm 1.8.10^6$, respectively ($p < 0.05$); relative

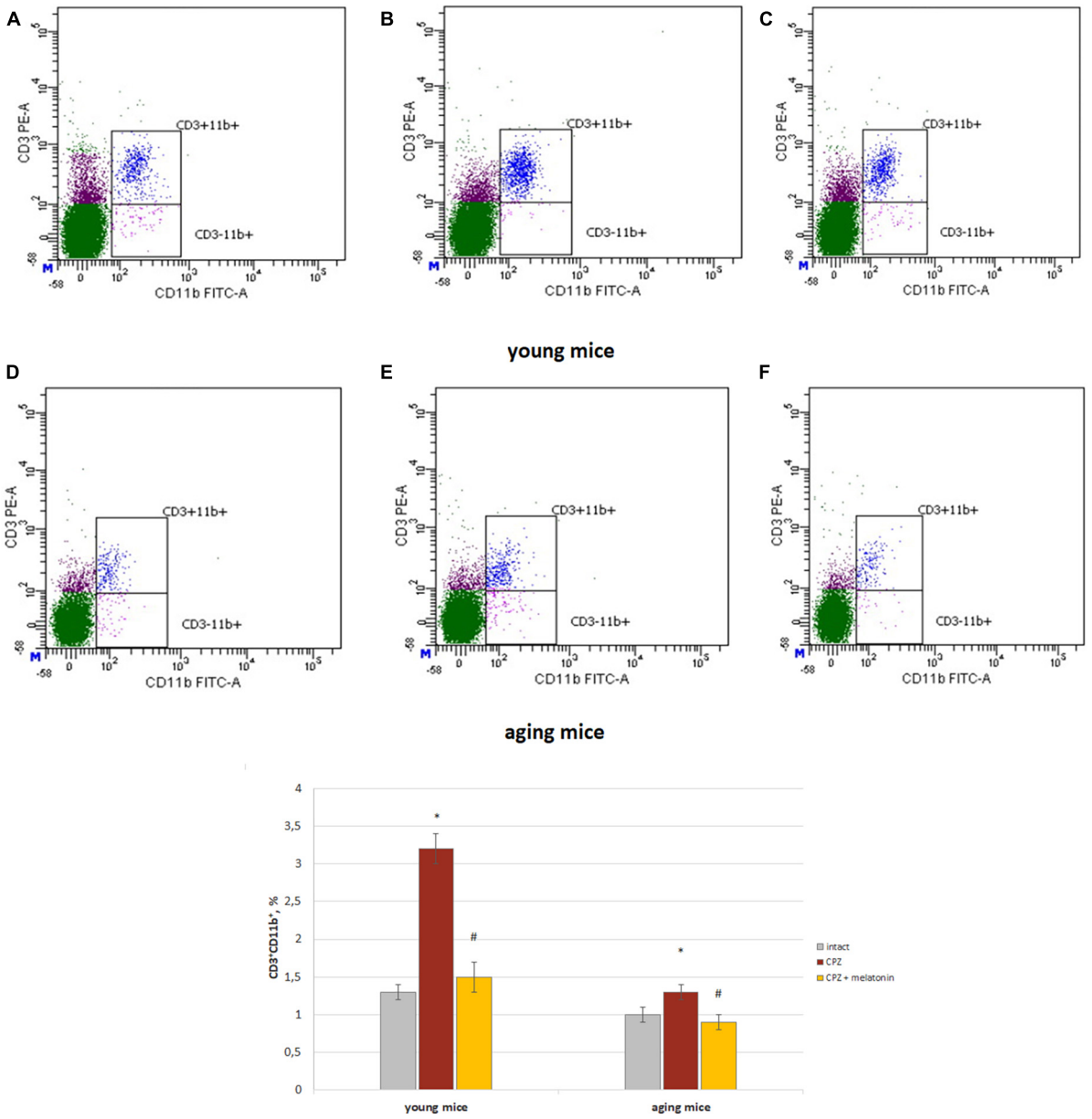

FIGURE 3
Histograms of expression of CD3 and CD11b markers in the whole brain cells according to flow cytometry and the percentages of CD3+CD11b+ cells in the brain of young and aging mice of experimental groups ($n = 5$ in each group). **(A,D)** Intact groups; **(B,E)** cuprizone treated groups; **(C,F)** cuprizone + melatonin groups. Represented data are in 3 weeks of cuprizone (CPZ) diet. Data are $M \pm$ SEM. $^{*}p < 0.05$ compared to intact group; $^{\#}p < 0.05$ compared to CPZ (*t*-test).

number of GM-CFCs was 28.5 ± 2.1/10^6 and 31.4 ± 3.2/10^6, respectively; absolute number GM-CFCs was 581.4 ± 25.2/femur and 796.5 ± 28.5/femur, respectively ($p < 0.05$). Thus, melatonin alone increases the colony-forming ability of GM-CFCs in young mice and total number nuclear cells of bone marrow in aging mice with regular diet.

The positive effect of melatonin on the reduced number of GM-CFCs in the bone marrow in cuprizone-treated mice of different ages can be explained by the effects of melatonin itself on bone marrow cells in mice with a regular diet.

After 3 weeks of the cuprizone diet, the number of blood monocytes was reduced in mice of both ages compared to intact animals (Figure 9). After melatonin injections, the number of blood monocytes in both age mice increased compared to cuprizone-treated mice and did not differ from that of intact animals (Figure 9). Thus, melatonin positively affects on the number of blood monocytes in young and aging mice treated with cuprizone.

Level of thymulin in the blood

Differentiation of T cell occurs in the thymus throughout life and is regulated by thymulin, one of the highly active thymic hormones (Bach et al., 1978; Csaba, 2016). We studied the dynamics of changes in level of thymulin in the blood of young

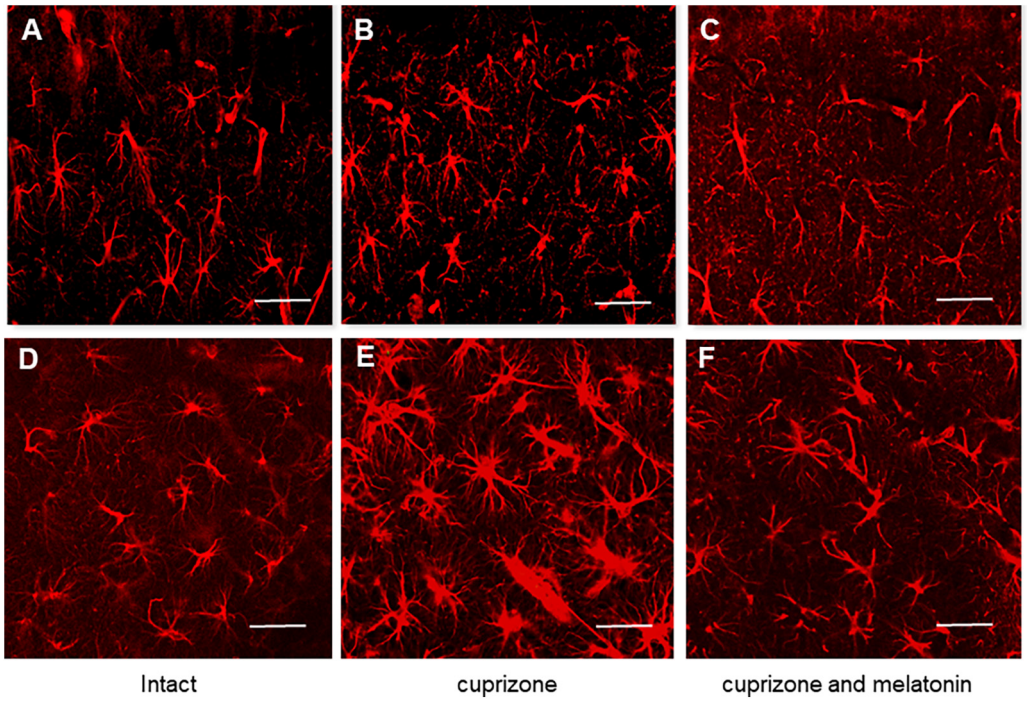

FIGURE 4
Confocal images of immunohistochemical staining of hippocampal CA1 area in intact **(A,D)**, cuprizone treated **(B,E)** and **(C,F)** cuprizone + melatonin treated mice. Immunohistochemical staining using the astrocyte marker GFAP in the hippocampal slices ($n = 10$) of mice ($n = 5$ in each group). **(A–C)** Young mice, **(D–F)** aging mice. Note a prominent outgrowth of GFAP-positive cells in panels **(B,E)** after cuprizone treatment (3 weeks). Scale bar, 50 μm.

and aging cuprizone-treated mice and after melatonin injection (Figure 10).

We found increased levels of thymulin in the blood of both young and aging mice after 7 days with cuprizone diet compared to intact animals. These increases were more pronounced in young mice than in aging mice treated with cuprizone. After 3 weeks of cuprizone diet in young mice level of thymulin was reduced compared to value after 7 days of application and also was lower than in intact ones in 2 months after completion of the cuprizone diet. Aging mice had higher blood thymulin level than intact mice after 3 weeks of the cuprizone diet and in 2 months after its completion. Thus, the dynamics of changes in levels of thymulin in aging mice is different from that in young mice during and after cuprizone administration.

Melatonin injections resulted in a significant increase levels of thymulin in blood in mice of both ages compared to mice treated with only cuprizone for 3 weeks. Two months after completion of administration of cuprizone and melatonin, levels of thymulin in blood of young mice decreased to those in intact animals but remained high in aging animals. Thereby, melatonin injection activates thymic function in cuprizone-treated mice of different ages, but only in young mice, thymic function is restored in 2 months after completion of cuprizone diet.

In addition, to confirm the positive effect only of melatonin on thymus function, level of thymulin in blood was measured in mice of both ages with a regular diet after melatonin injections. Levels of thymulin in blood in young mice treated with solvent ($n = 8$) or melatonin ($n = 8$) were 4.4 ± 0.4 and 6.2 ± 0.6, respectively ($p < 0.05$). Levels of thymulin in blood of aging mice treated with solvent ($n = 8$) or melatonin ($n = 8$) were 3.5 ± 0.3 and 6.0 ± 0.2, respectively ($p < 0.05$).

Thus, exogenous melatonin activated of thymus endocrine function in both young and aging mice with regular diet. The positive effect of melatonin on level thymulin in blood in cuprizone-treated mice of different ages can be explained by the effects of melatonin itself on thymus function in mice with regular diet.

Discussion

Reaction of different types of the brain cells on neurotoxin cuprizone in the young and aging mice

Brain cells of young mice

According to the authors, changes in the function of oligodendrocytes, their apoptosis and consequently the development of demyelination of nerve fibers occur in the brain of young mice during the early stages of cuprizone action (Praet et al., 2014; Vega-Riquer et al., 2019; Zirngibl et al., 2022). Demyelination pathology also refers to degenerative changes in brain neurons (Dutta and Trapp, 2011). Our previous study showed that after administration of cuprizone (within 3–4 weeks) in young 129/Sv mice, not only demyelination occurred, but also changes in the neuronal structure of the cerebral cortex, cerebellum, and hypocampus (increase the number of neurons

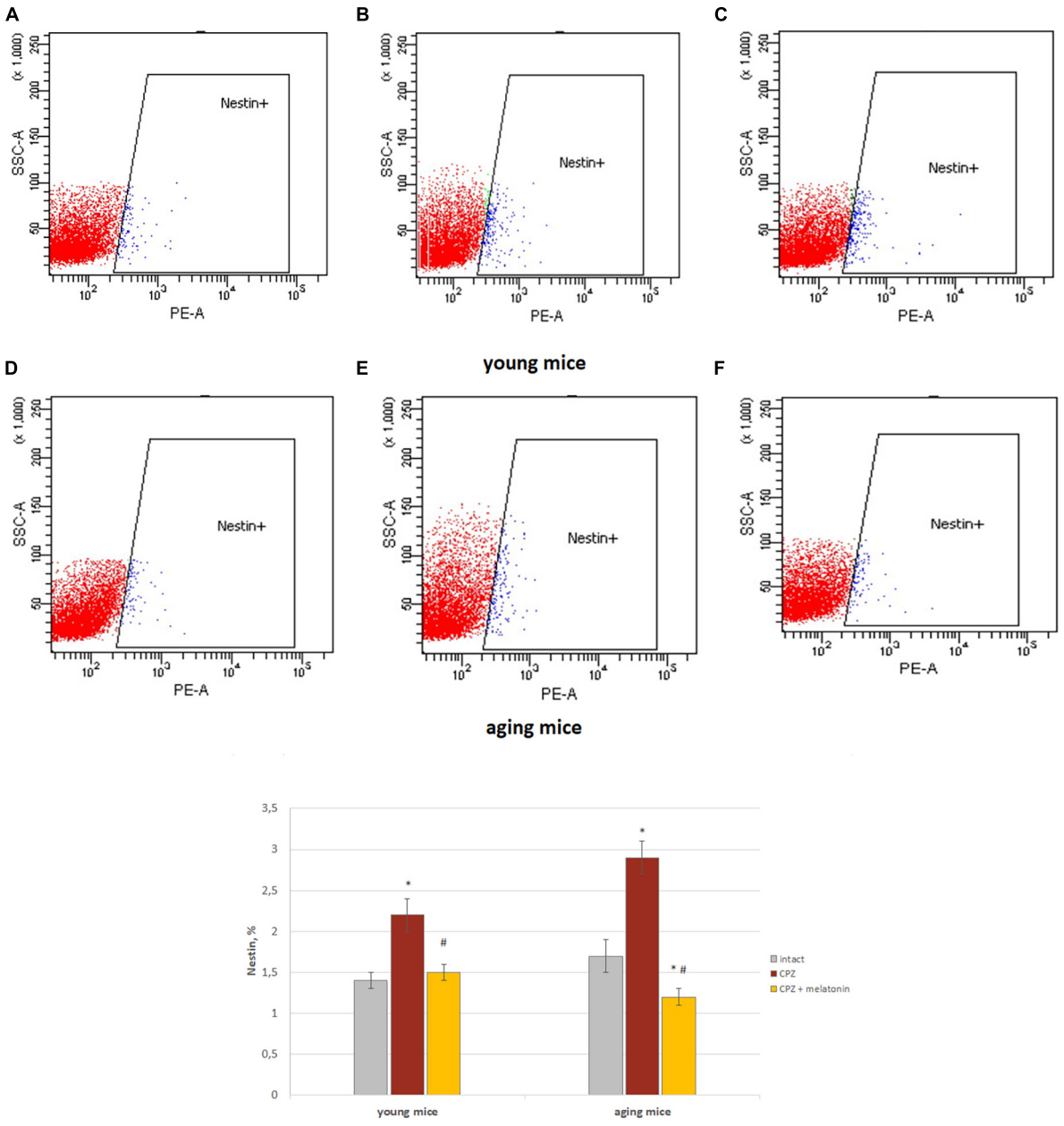

FIGURE 5
Histograms of Nestin marker expression in the total brain cells according to low cytometry and the percentage of Nestin+ cells in the brain of young and aging mice of each experimental groups ($n = 5$). **(A,D)** Intact groups; **(B,E)** cuprizone groups; **(C,F)** cuprizone + melatonin groups. Represented data are in 3 weeks of cuprizone (CPZ) diet. Data are $M \pm$ SEM. $^{*}p < 0.05$ compared to intact group; $^{\#}p < 0.05$ compared to CPZ (t-test).

with destructive and moderate changes) (Labunets et al., 2017a, 2018a,b, 2021).

The authors' studies have shown that in young animals, changes in the structure and functioning of nerve cells under the influence of cuprizone can be associated with the development of oxidative stress and an increased production of pro-inflammatory cytokines by neuroinflammatory cells (Gudi et al., 2014; Vega-Riquer et al., 2019; Zhan et al., 2020). Therefore, we found it necessary to study and compare the dynamics of changes in the neurons structure and the number of microglial/macrophage cells, T cells, astrocytes in the brain both young and aging cuprizone-treated mice. Previously we established that after 7 days of cuprizone taking, the number of neurons with moderate structural changes significantly increased in the cortex and cerebellum of young mice (Labunets et al., 2018a, 2021). As it turned out such changes in neurons coincide with an increased number and activity of phagocytic macrophages in the brain. The activating effect of neurotoxin on macrophages of young mice persisted even after 3 weeks of cuprizone diet, when the number of neurons with destructive changes in the brain sharply increased.

According to Praet et al. (2014), not only an increase in the number of activated microglial/macrophage cells but also in their interaction with T lymphocytes are important for the development of nerve cell damage in the brain. It has been shown that in the

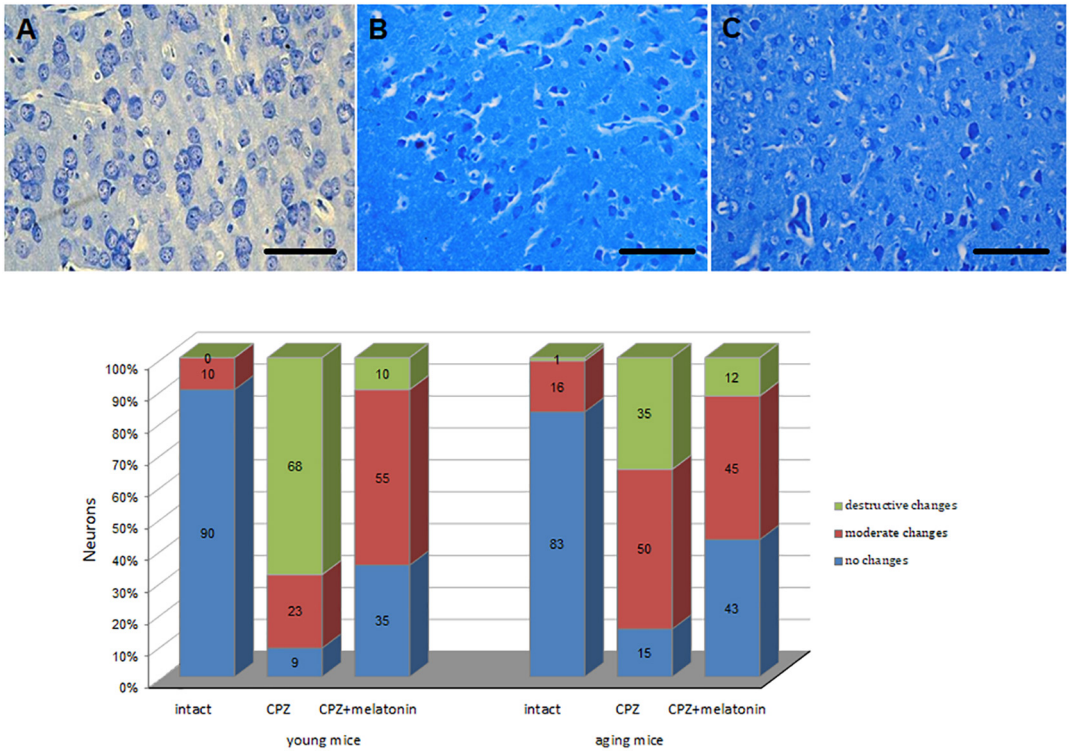

FIGURE 6
Microphotographs of histological sections of cerebral cortex ($n = 10$) and the percentages of different types of neurons in cerebral cortex of young and aging mice of experimental groups ($n = 5$ in each group): **(A)** intact group; **(B)** cuprizone group; **(C)** cuprizone + melatonin group (Labunets et al., 2018b). Toluidine blue staining. Scale bar, 50 μm.

CNS both CD4+ and CD8+ T cells are involved in the development of demyelination as a result of production by these cells of pro-inflammatory cytokines IFN-γ and TNF-α (Sonobe et al., 2007; Almuslehi et al., 2020). Besides, CD4+ T cells also produce IL-17, an important factor in the development of experimental demyelination, including cuprizone-induced (Sonobe et al., 2007; Kang et al., 2012). In our experiments, we have shown that the number of CD3+, CD3+CD4+ and CD3+CD8+ T cells significantly increased in the brain of young mice after 3 weeks of taking cuprizone. We do not rule out that such changes in the number of CD3+ T cells are the result of an increase in the number of activated macrophages during the early period of cuprizone treatment (in 7 days). Pro-inflammatory cytokines (TNF-α, IFN-γ, and IL-1β) produced by activated microglia/macrophages increase the expression of adhesion molecules in microvascular endothelial cells, leading to passage of T lymphocytes through the BBB (Gonzalez and Pacheco, 2014).

An important issue is the state of the BBB in mice with the cuprizone model of demyelination and the possibility of different origins cells penetrating through it into the brain. A number of researchers point to intact BBB in mice with the cuprizone diet, thereby excluding this possibility (Skripuletz et al., 2011; Tejedor et al., 2017). However, there are literature data supporting this possibility. The authors have shown that already at early stages of the development of multiple sclerosis, accompanied by neuroinflammation, the permeability of the BBB increases (Kamphuis et al., 2015). The increase of the permeability of the BBB was found already after three days of cuprizone diet (Shelestak et al., 2020). In addition, immune cells with a peripheral phenotype were found in the brains of the cuprizone-fed mice (McMahon et al., 2002).

Our experiments revealed a simultaneous significant increase in the number of CD3+CD4+ T lymphocytes as well as the development of reactive gliosis in young mice after 3 weeks of taking cuprizone. A study by Kang et al. (2012) showed that IL-17 produced by brain CD4+ T cells affects astrocytes and stimulates the synthesis of proinflammatory cytokines in astrocytes after 3–4 weeks of cuprizone diet. Other studies also point to the interaction of lymphocytes and astrocytes during the development of demyelination and neurodegeneration (Absinta et al., 2021).

Brain cells of aging mice

We found changes not only in the neurons, but also in neuroinflammatory cells in the brain of aging cuprizone-treated mice compared to young mice. Namely: a decrease in the percentage of neurons with destructive changes and, conversely, an increase in the proportion of neurons with moderate structural changes; delayed activation of macrophages and slightly increase in the number of CD3+CD8+ T lymphocytes.

The revealed features of the response of brain cells of aging mice to the damaging effects of cuprizone can be associated with age-related changes in both the cells themselves and in their interaction. It is known, that neurogenesis and the number of unchanged neurons in the mouse brain decrease with age, while increase the number of T lymphocytes; the proliferation and activity of

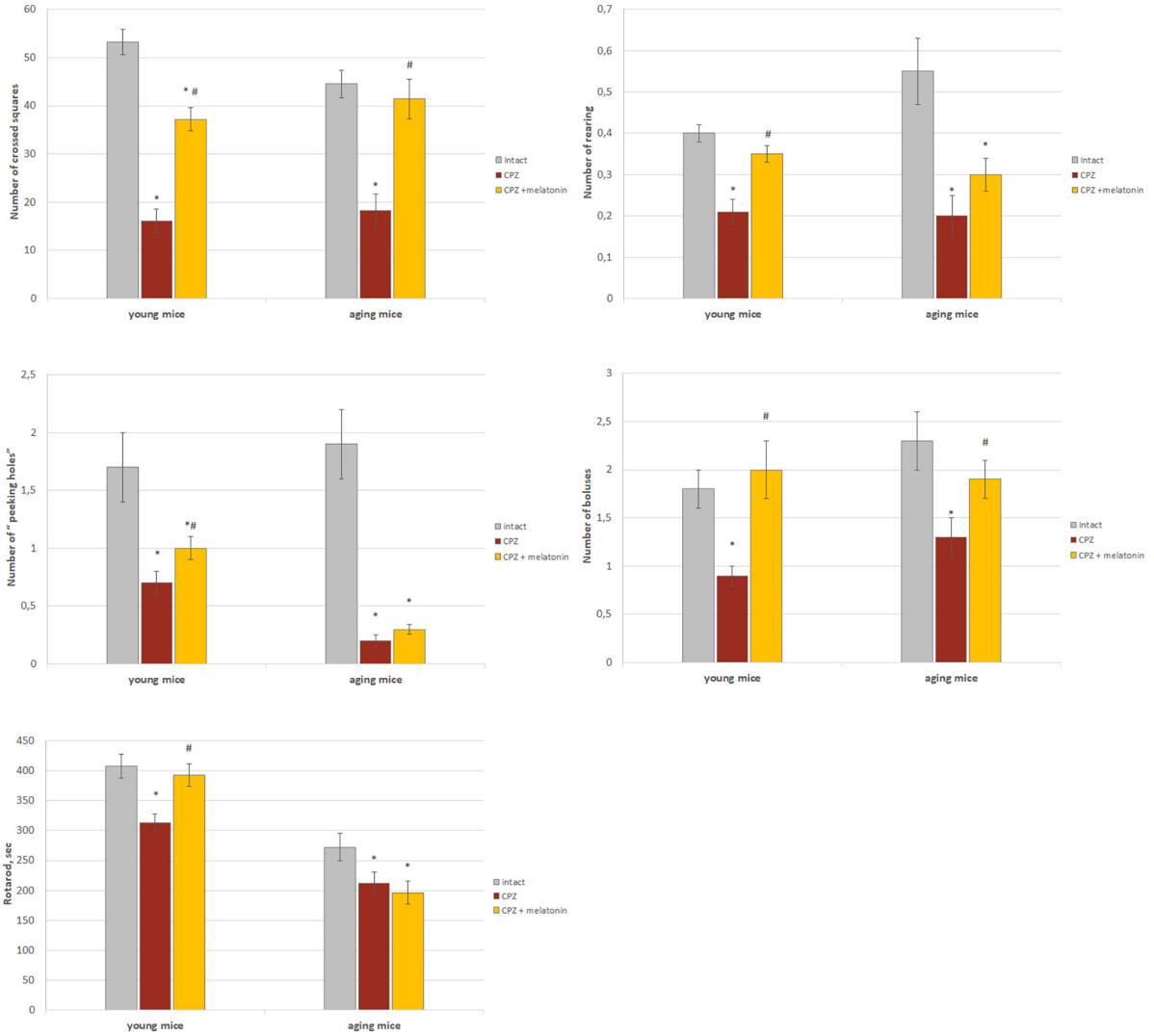

FIGURE 7
The effect of cuprizone (CPZ) and CPZ + melatonin on behavioral indicators ("open field" and rotarod tests) in young and aging mice of experimental groups ($n = 15$ in each group). Represented data are in 3 weeks of CPZ diet. Data are $M \pm$ SEM. $^{*}p < 0.05$ compared to intact group; $^{\#}p < 0.05$ compared to CPZ (t-test).

microglial cells; the expression of ICAM-1 and chemokines (MCP-1 and MIP1α) produced by astrocytes and the permeability of the BBB (Gemechu and Bentivoglio, 2012; Hamilton et al., 2013; Moraga et al., 2015; Labunets et al., 2017a).

We also observed decrease of the brain unchanged neurons in the intact aging mice versus young animals, increase of number of CD3+, CD3+CD8+ T cells, change in the balance of CD3+CD4+/CD3+CD8+ cells and a decrease in the number of activated macrophages (CD3+CD11b+). In addition, our experiments showed a delayed activation of macrophages in the brain of aging cuprizone-treated mice. It is possible that such response of macrophages in aging animals may be one of the reasons for a less pronounced increase in the number of CD3+ cells in mice after 3 weeks of cuprizone diet and, as a result, less significant disturbances in the structure of brain neurons compared to young animals with the same diet. In our studies we found that after cuprisone taking the number of neurons with destructive changes in the brain of aging animals was half that of young animals. Experiments of Xu et al. (2010) on old animals with an inflammation model confirmed the importance of initial activation of microglia/macrophage cells for subsequent infiltration of the brain by T cells.

Behavioral reactions

In our experiment, changes in the structure of neurons in mice with a cuprizone model of demyelination are accompanied with disturbance of behavioral responses. Disorders of motor, emotional, exploratory activities and muscle tone develop in young and aging cuprizone-treated mice. Manifestations of changes in behavior in such mice may be associated with the physiological characteristics of the CNS zones studied by us (cortex and hippocampus). The cerebral cortex together with cerebellum and the motor neurons of the spinal cord provide the nervous regulation of movement. In addition, the cerebral cortex together with the structures of the limbic system is an important component in the formation of emotional activity.

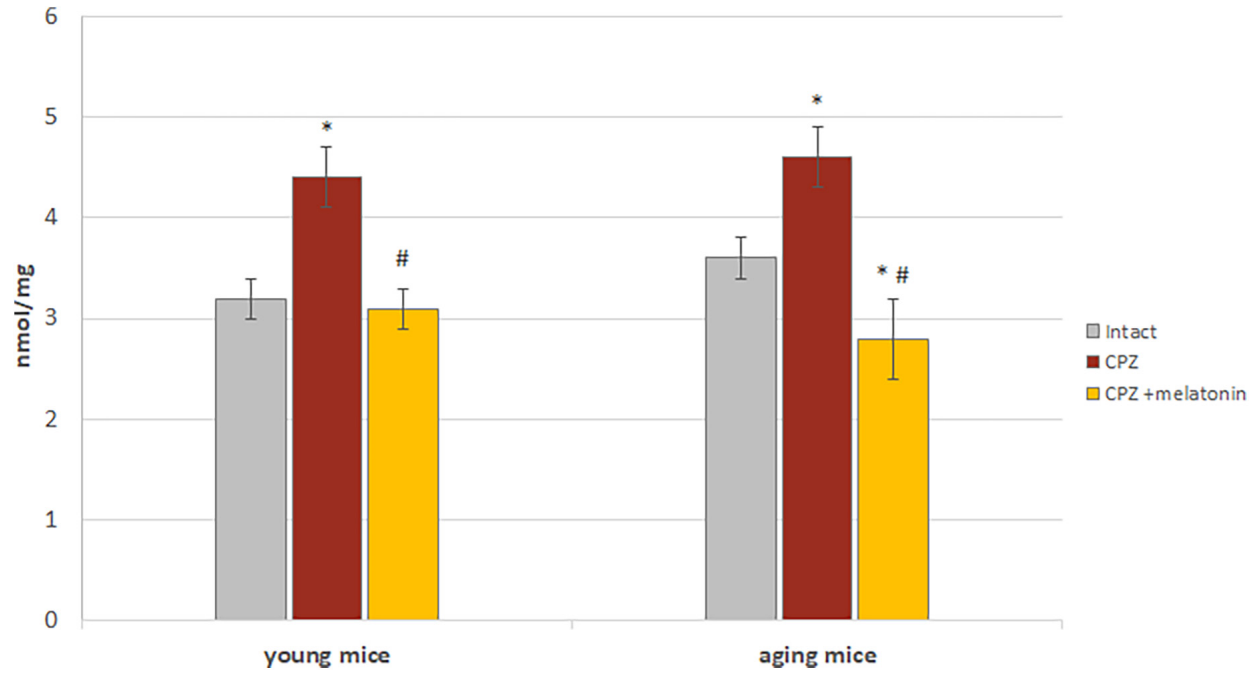

FIGURE 8
The effects of cuprizone (CPZ) and CPZ + melatonin on malondialdehyde content in the brain of young and aging mice of experimental groups ($n = 5$ in each group). Represented data are in 3 weeks of CPZ diet. Data are $M \pm$ SEM. $^{*}p < 0.05$ compared to intact group; $^{\#}p < 0.05$ compared to CPZ (t-test).

Reaction of different types of brain cells of young and aging mice with a cuprizone model of demyelination to melatonin administration

Neurons

We have found that exogenous melatonin had a positive effect on the structure of neurons in the cerebral cortex of cuprizone-treated mice of both age groups. For example, in the cerebral cortex of mice the proportion of neurons with destructive changes significantly decreased and the proportion of unchanged neurons increased. Similar changes in the structure of neurons under the influence of melatonin were previously found by us in the cerebellum and hippocampus of mice with a cuprizone diet (Labunets et al., 2018a, 2021).

The simultaneous decrease in the proportion of Nestin+ cells in the brain of such mice may be associated with their increased differentiation in the neurogenic direction. It is known ability of melatonin to penetrate the BBB, acting the viability, proliferation and differentiation of neural stem cells in neurogenic areas/niches of the brain and changes the synthesis of neurotrophic factors (BDNF and NGF) (Sarlak et al., 2013; Li et al., 2016; Kim et al., 2019).

The increase in the proportion of neurons with moderate changes in the cerebral cortex of cuprizone-treated mice under the influence of melatonin likely reflects the activation of regenerative processes in neurons that develop against on the background of neurotoxin intake. The authors Ng and Lee (2019) have shown that both the increase surface area of the nucleus and its swelling in neurons with moderate damage is associated with a compensatory reaction. These changes are necessary for the synthesis of group of proteins involved in the restoration of damaged brain structures. There are datà on the effect of melatonin on protein synthesis in cells (Liu et al., 2019).

In addition, the remyelinating effect of exogenous melatonin in the brain of mice with a cuprizone model of demyelination showed (Ghareghani et al., 2019; Kim et al., 2019; Vega-Riquer et al., 2019). Remyelinating action of melatonin *in vitro* in cuprizone-demyelinated brain culture was associated with an increased number of Olig2-cells and also with a change in the content of myelin basic protein (Rodnichenko and Labunets, 2018; Kim et al., 2019).

In our study, the less pronounced neuroprotective effect (structure of neurons and behavioral/functional reactions) of melatonin in aging mice with cuprizone model of demyelination can partly explain the age-related changes in the neurons themselves and their receptors to regulatory hormonal factors, in particular melatonin.

Neuroinflammatory cells

The protective effect of melatonin on the brain neurons and oligodendrocytes in demyelinating pathology is associated with its anti-inflammatory, anti-apoptotic and antioxidant effects (Vakilzadeh et al., 2016; Babaee et al., 2021; Murioz-Jurado et al., 2022).

The anti-inflammatory effect of melatonin is manifested in the inhibition of activation of NF-κB in cells, resulting to a decrease: (a) the synthesis of inflammatory mediators; (b) the level of adhesive molecules ICAM-1 and VCAM-1; (c) the production of pro-inflammatory cytokines (TNF-α, IL-1β, IFN-γ, IL-17, and IL-22) by T lymphocytes, macrophages and astrocytes and to

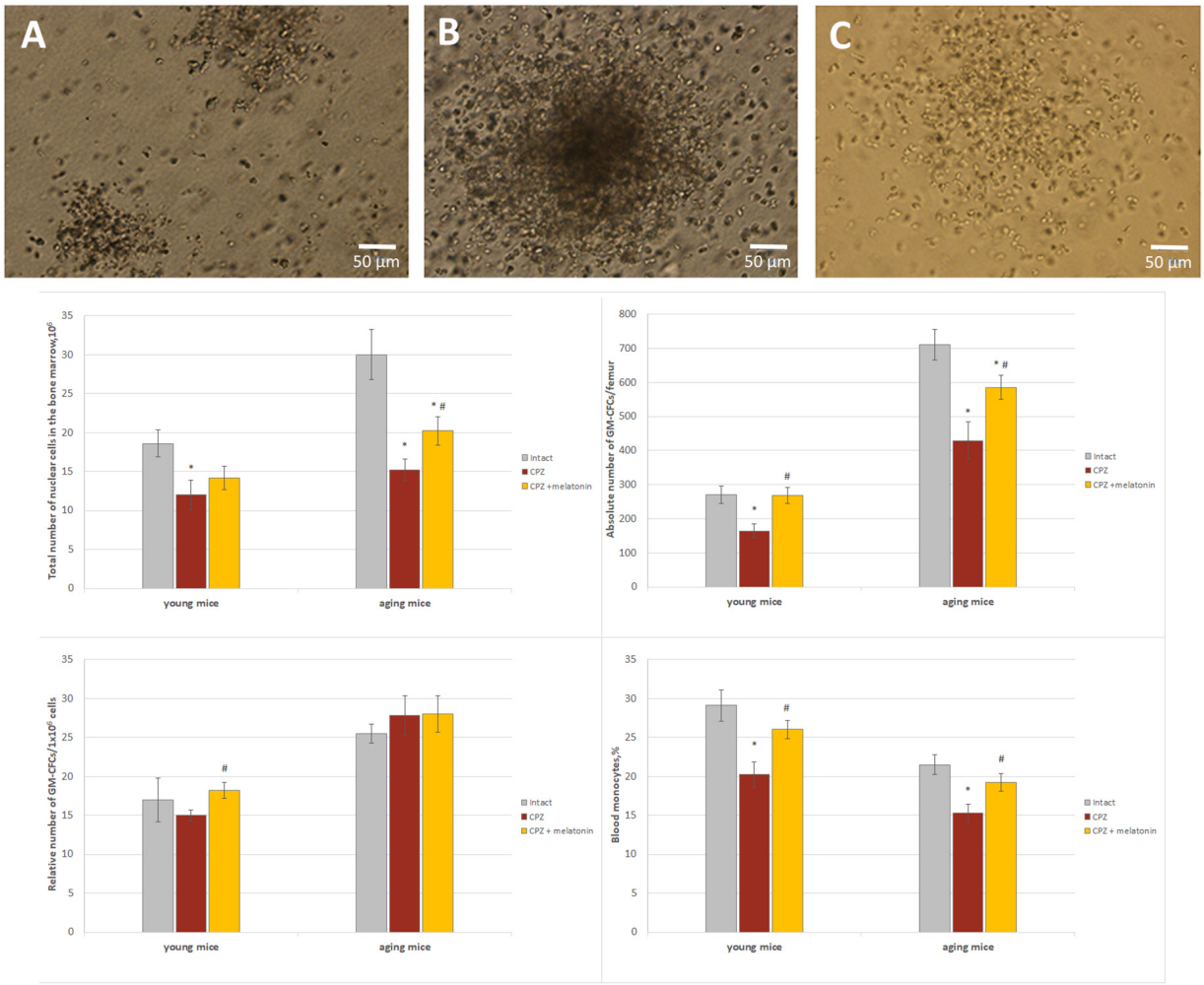

FIGURE 9
The number of GM-CFCs in bone marrow and the blood level of monocytes in young and aging mice of experimental groups. For GM-CFCs ($n = 5$) for monocytes ($n = 10$) from each group of mice. Types of GM-CFCs colonies: **(A)** granulocytic; **(B)** mixed; **(C)** macrophage. Phase contrast. Scale bar, 50 μm. Represented data are in 3 weeks of CPZ diet. Data are $M \pm$ SEM. $^{*}p < 0.05$ compared to intact group; $^{\#}p < 0.05$ compared to CPZ (*t*-test).

an increase the production of anti-inflammatory cytokines (IL-10 and IL-4) (Escribano et al., 2014; Alvarez-Sanchez et al., 2015, 2017; Farez et al., 2015; Xu et al., 2018; Babaee et al., 2021; Murioz-Jurado et al., 2022). Under melatonin influence activity of T-helpers, T-effectors, T-regulatory cells changes and the differentiation of Th17 inhibits in animals with an experimental model of multiple sclerosis (Alvarez-Sanchez et al., 2015; Farez et al., 2015).

We have shown that after melatonin administration in young cuprizone-treated mice the number of T cells decreased. In addition, the number of activated macrophages and the number of activated astrocytes also decreased.

Less pronounced effects of melatonin on the number T cells and activation of macrophages in the brain of aging cuprizone-treated mice may be associated with age-related changes in the above cells and their receptors for melatonin (Gemechu and Bentivoglio, 2012; Hardeland, 2012; Hamilton et al., 2013; Moraga et al., 2015; Gimenez et al., 2022).

Effects of cuprizone and melatonin on the oxidative stress, bone marrow, and thymus functions in young and aging mice

Oxidative stress of brain

It is known that oxidative stress products in demyelinating and neurodegenerative pathologies damage nerve cells (Chen et al., 2020; Murioz-Jurado et al., 2022). In cuprizone-induced demyelinating pathology, oxidative stress occurs in the brain, resulting in increased content of MDA and reactive oxygen species and decreased activity of antioxidant enzymes (Murioz-Jurado et al., 2022).

The properties of melatonin as a direct and indirect antioxidant in pathological processes of the CNS are described in reviews (Manchester et al., 2015; Chen et al., 2020). After melatonin injection the decrease in the content of oxidative stress biomarkers (including MDA) as well as an increase in the activity of antioxidant

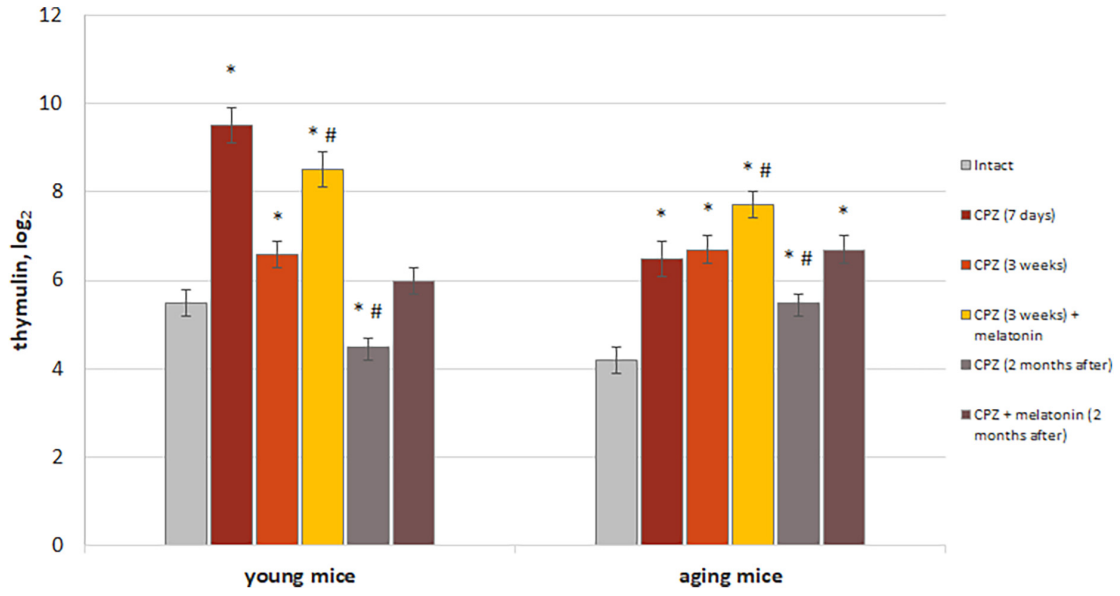

FIGURE 10
The effect of cuprizone (CPZ) and CPZ + melatonin on blood thymulin level in young and aging mice of experimental groups ($n = 5$ in each group). Represented data are in 7 days, 3 weeks of CPZ diet and 2 months after. Data are $M \pm$ SEM. $^{*}p < 0.05$ compared to intact group; $^{\#}p < 0.05$ compared to 3 weeks of CPZ (t-test).

enzymes (superoxide dismutase, catalase, glutathione peroxidase, and glutathione reductase) were observed in the tissues of young animals with experimental models of multiple sclerosis (Abo Taleb and Alghamdi, 2020; Murioz-Jurado et al., 2022).

In our experiments we observed a decrease in the level of MDA in the brain tissue not only in young but also in aging mice with cuprizone demyelination model and injection of melatonin.

We have previously shown that reduced activity of glutathione peroxidase and glutathione reductase in the brain of young and aging cuprizone treated mice increased after melatonin injection (Labunets et al., 2018b; Labunets and Rodnichenko, 2020). As is known, the redox cycle of glutathione plays an important role in the antioxidant protection of the brain.

Bone marrow and brain macrophages

It has been shown that brain macrophages are a heterogeneous population consisting of resident and blood-derived cells (Jordan and Thomas, 1988; Li and Barres, 2018). In pathological conditions the number of macrophages in the brain may be increased by to peripherally derived macrophages (Cronk et al., 2018). Increase of the pool of macrophages with a peripheral immunophenotype (CD45+, Mac1+ cells) was found in the brain of young mice in cuprizone diet during 2–6 weeks (McMahon et al., 2002). Besides, in the pathology of the CNS it is possible that monocytes circulating in the blood enter the brain and differentiating into tissue macrophages (Zhao et al., 2020).

Since cells of the monocyte-macrophage series are of bone marrow origin, we estimated the number of GM-CFCs in the bone marrow of mice with a cuprizone diet as well as their change after melatonin administration. We found that in young and aging mice with a cuprizone diet, the amount of GM-CFCc in the bone marrow and the number of monocytes in the blood significantly decreased compared to intact animals. At the same time, the number of macrophages in the brain of such mice significantly increased. After melatonin injections the number of GM-CFCs in the bone marrow and circulating monocytes increased and the number of macrophages in the brain of both age groups was less than in the control group.

Under melatonin influence the number of not only GM-CFCs, but also more committed precursors of granulocytes, monocytes, and macrophages increased in bone marrow of adult mice (Maestroni, 1998; Currier et al., 2000). The stimulating effect of melatonin on hematopoiesis is realized directly through receptors in the cells of the monocyte/macrophage line as well as by increasing sensitivity of these cells to the effect of cytokines stimulating hematopoiesis (IL-3,4,6, granulocyte/macrophage-colony stimulating factor) (Currier et al., 2000; Garcia-Maurino et al., 2000).

Thus, it can be assumed that one of the possible ways of the influence of the neurotoxin cuprizone and hormone melatonin on the brain macrophages is associated with change in the functioning of the bone marrow.

Thymulin, T cells, and macrophages in the brain

As we have previously shown, thymulin affects *in vivo* and *in vitro* the number of GM-CFCs in the bone marrow and the functioning of macrophages together in young in aging animals (Labunets et al., 2017b). In addition, thymulin affects the differentiation of T lymphocytes in the thymus to CD4+ T cells and CD8+ T cells (Bach et al., 1978; Reggiani et al., 2014; Csaba, 2016; Savino et al., 2016). We suggested activation of the endocrine function of the thymus in cuprizone-treated mice of different ages is one of the possible links in the changes number of macrophages and T lymphocytes in the brain.

We showed the increase the level thymulin in blood in both age group of mice with cuprizone diet. Age-related

differences in the dynamics of changes in thymulin level during cuprizone diet and remyelination period (in 2 months) may be associated with age-related dysfunction of the thymus as well as decreased number and/or affinity of receptors for glucocorticoids in the gland cells (Savino and Dardenne, 2000; Pazizandeh et al., 2004). It is known that glucorticoids, the level of which increases under the influence of damaging factors, have a depressing effect on the hormonal function of the thymus (Savino and Dardenne, 2000; Urbach-Ross and Kusnecov, 2007; Labunets, 2015).

Under the influence of melatonin, the level of thymulin was even higher in mice of both age groups compared with animals alone with cuprizone diet. Increasing of thymulin level in such mice seems to be aimed at enhancing the anti-inflammatory action of melatonin in the animal's brain. This assumption is based on literature data about thymulin ability to increase the synthesis of anti-inflammatory cytokines (IL-10) and reduce the synthesis of pro-inflammatory cytokines (IL-1β, IL-6, and TNF-α) in the brain of animals with an experimental model of neuroinflammation (Haddad and Hanball, 2013). We observed in aging animals with cuprizone diet and melatonin injection the prolonged activation of the endocrine function of the thymus and no changes in the number of T cells during remyelination period (in 2 months) compared to those in young animals.

Conclusion

The damaging effect of cuprizone on the structure and function of brain neurons of young and aging mice also accompanied with changes in the number and activity macrophages, T cells and astrocytes.

Neuroprotective effects of melatonin in the mice with cuprizone model of multiple sclerosis are associated with anti-inflammatory (decrease in the number and activity of macrophages, T lymphocytes and astrocytes) and antioxidant actions (decrease in MDA content). The anti-inflammatory effect of melatonin in the brain of mice with cuprizone diet is largely mediated by improving thymus and bone marrow functions.

The obtained results may be useful in the development of new biotechnological approaches to prevention and treatment of demyelinating pathology, in particular, multiple sclerosis.

Data availability statement

The original contributions presented in this study are included in the article/supplementary material, further inquiries can be directed to the corresponding author.

Ethics statement

This animal study was reviewed and approved by the Ethics Committee of the Institute of Genetic and Regenerative Medicine and performed in accordance with the European Union Directive of 22 September 2010 (2010/63/EU) for the protection of animals used for scientific purposes and Article 26 of the Law of Ukraine "On the Protection of Animals from Cruelty" (No. 3447-IV, 2006).

Author contributions

IL: research concept and conceiving the study. IL, TP, AR, and SS: data collection, analysis, and interpretation of data. IL and TP: manuscript preparation and improving final version of manuscript. All authors read and approved the final manuscript.

Funding

This study has been carried out within the project (No. 0116U000139) in the Institute of Genetic and Regenerative Medicine with financial support of the National Academy of Medical Sciences of Ukraine.

Acknowledgments

We are grateful to technic help Zoya Litochenko for animals care and behavioral tests and Vitalii Kyryk for help of histogram of low cytometry.

Conflict of interest

The authors declare that the research was conducted in the absence of any commercial or financial relationships that could be construed as a potential conflict of interest.

Publisher's note

All claims expressed in this article are solely those of the authors and do not necessarily represent those of their affiliated organizations, or those of the publisher, the editors and the reviewers. Any product that may be evaluated in this article, or claim that may be made by its manufacturer, is not guaranteed or endorsed by the publisher.

References

Abo Taleb, H. A., and Alghamdi, B. S. (2020). Neuroprotective effects of melatonin during demyelination and remyelination stages in a mouse model of multiple sclerosis. *J. Mol. Neurosci.* 70, 386–402. doi: 10.1007/s12031-019-01425-6

Absinta, M., Maric, D., Gharagozloo, M., Garton, T., Smith, M. D., Jin, J., et al. (2021). A lymphocyte-microglia-astrocyte axis in chronic active multiple sclerosis. *Nature* 597, 709–714. doi: 10.1038/s41586-021-03892-7

Almuslehi, M. S. M., Sen, M. K., Shortland, P. J., Mahns, D. A., and Coorssen, J. R. (2020). CD8+T-cells recruitment into the central nervous system of cuprizone-fed mice: relevance to modelling the etiology of multiple sclerosis. *Front. Cell. Neurosci.* 14:43. doi: 10.3389/fncel.2020.00043

Alvarez-Sanchez, N., Cruz-Chamorro, I., Diaz-Sanchez, M., Sarmiento-Soto, H., Medrano-Campillo, P., Martinez-Lopez, A., et al. (2017). Melatonin reduces inflammatory responses in peripheral T helper lymphocytes from relapsing-remitting multiple sclerosis patients. *J. Pineal Res.* 63. doi: 10.1111/jpi12442 [Epub ahead of print].

Alvarez-Sanchez, N., Cruz-Chamorro, I., Lopez-Gonzalez, A., Utrilla, J., Fernandez-Santos, J. M., Martinez-Lopez, A., et al. (2015). Melatonin controls experimental autoimmune encephalomyelitis by altering the T effector/regulatory balance. *Brain Behav. Immun.* 50, 101–114. doi: 10.1016/j.bbi.2015.06.021

Anjos-Afonso, F., and Bonnet, D. (2008). Isolation, culture, and differentiation potential of mouse marrow stromal cells. *Curr. Protoc. Stem Cell Biol.* Chapter 2:Units 2B.3. doi: 10.1002/978047-0151808.sc02b3s7

Babaee, A., Effekbar-Vaghefi, S. H., Dehghani Soltani, S., Asadi-Shekaari, M., Shahrokhi, N., and Basiri, M. (2021). Hippocampal astrocyte response to melatonin following neural damage induction in rats. *Basic Clin. Neurosci.* 12, 177–186. doi: 10.32598/bcn.122.986.1

Bach, J. F., Bach, M. A., and Blanot, D. (1978). Thymic serum factor (FTS). *Bull. Inst. Pasteur*. 76, 325–398.

Bradley, T. R., and Metcalf, D. (1966). The growth of mouse bone marrow cell in vitro. *Aust. J. Exp. Biol. Med. Sci.* 44, 287–299. doi: 10.1038/icb.1966.28

Burda, J. E., and Sofroniew, M. V. (2014). Reactive gliosis and the multicellular response to CNS damage and disease. *Neuron* 81, 229–248. doi: 10.1016/j.neuron.2013.12.034

Chen, D., Zhang, T., and Lee, T. H. (2020). Cellular mechanism of melatonin: insight from neurodegenerative deseases. *Biomolecules* 10:1158. doi: 10.3390/biom10081158

Cronk, J. C., Filiano, A. J., Louveau, A. L., Marin, I., Marsh, R., Ji, E., et al. (2018). Peripherally derived macrophages can engraft the brain independent of irradiation and maintain a indentify distinct from microglia. *J. Exp. Med.* 215, 1627–1647. doi: 10.1084/jem.20180247

Csaba, G. (2016). The immunoendocrine thymus as a pacemaker of lifespan. *Acta Microbiol. Immunol. Hung.* 63, 139–158. doi: 10.1556/030.63.2016.2.1

Currier, N. L., Sun, L. Z., and Miller, S. C. (2000). Exogenous melatonin: quantitative enhacement in vivo of cells mediating nonspecific immunity. *J. Neuroimmunol.* 104, 101–108. doi: 10.1016/s0165-5728(99)00271-4

Dutta, R., and Trapp, B. D. (2011). Mechanisms of neuronal dysfunction and degeneration in multiple sclerosis. *Prog. Neurobiol.* 93, 1–12. doi: 10.1016/j.pneurobio.2010.09.005

Escribano, B. M., Colin-Gonzalez, A., Santamaria, A. A., and Tunez, I. (2014). The role of melatonin in multiple sclerosis, Huntington's disease and cerebral ischemia. *CNS Neurobiol. Disord. Drug Targets.* 13, 1096–1119. doi: 10.2174/1871527313666140806160400

Farez, M. F., Mascanfroni, I. D., Mendez-Huergo, S. P., Yeste, A., Murugaiyan, G., Caro, L. P., et al. (2015). Melatonin contributes to the seasonality of multiple sclerosis relapses. *Cell* 162, 1338–1352. doi: 10.1016/j.cell.2015.08.025

Fisch, G. S. (2007). Animal models and human neuropsychiatric disorders. *Behav. Genet.* 37, 1–10. doi: 10.1007/s10519-006-9117-0

Franco-Pons, N., Torrente, M., Colomina, M. T., and Vilella, E. (2007). Behavioral deficits in the cuprizone-induced murine model of demyelination/remyelination. *Toxicol. Lett.* 169, 205–213. doi: 10.1016/j.toxlet.2007.01.010

Garcia-Maurino, S., Pozo, D., Calvo, J. R., and Guerrero, J. M. (2000). Correlation between nuclear melatonin receptor expression and enhanced cytokine production in human lymphocytic and monocytic cell lines. *J. Pineal Res.* 29, 129–137. doi: 10.1034/j.1600-079x.2000.290301.x

Gemechu, J. M., and Bentivoglio, M. (2012). T cell recruitment in the brain during normal aging. *Front. Ñell. Neurosci.* 6:38. doi: 10.3389/fncel.2012.00038

Ghareghani, M., Scavo, L., Jand, Y., Farhadi, N., Sadeghi, H., Ghanbari, A., et al. (2019). Melatonin therapy modulates cerebral metabolism and enhances remyelination by increasing PDK4 in a mouse model of multiple sclerosis. *Front. Pharmacol.* 10:147. doi: 10.3389/fphar.2019.00147

Gimenez, V. M. N., de las Heras, N., Lahera, V., Tresguerres, J. A. F., Reiter, R. J., and Manucha, W. (2022). Melatonin as an anti-aging therapy for age-related cardiovascular and neurodegenerative diseases. *Front. Aging Neurosci.* 14:888292. doi: 10.3389/fnagi.2022.888292

Gonzalez, H., and Pacheco, R. (2014). T-cell-mediated regulation of neuroinflammation involved in neurodegenerative diseases. *J. Neuroinflammation* 11:201. doi: 10.1186/s12974-014-0201-8

Gorina, Y. V., Komleva, Y. K., Lopatina, O. L., Volkova, V. V., Chernykh, A. I., Shabalova, A. A., et al. (2017). The battery of tests for experimental behavioral phenotyping of aging animals. *Adv. Gerontol.* 7, 137–142. doi: 10.1134/s2079057017020060

Gudi, V., Gingele, S., Skripuletz, T., and Stangel, M. (2014). Glial response during cuprizon-induced de- and remyelination in the CNS: lessons learned. *Front. Cell Neurosci.* 8:73. doi: 10.3389/fncel.2014.00073

Haddad, J. J., and Hanball, L. H. (2013). The anti-inflammatory and immunomodulatory activity of thymulin peptide is NF-kB dependent and involves the downregulation of IkB-α. *Am. J. Med. Biol. Res.* 1, 41–49. doi: 10.12691/ajmbr-1-2-2

Hamilton, L. K., Joppe, S. E., Cochard, L., and Fernandes, K. J. (2013). Aging and neurogenesis in the adult forebrain: what we havelearned and where we should go from here. *Eur. J. Neurosci.* 37, 1976–1986. doi: 10.1111/ejn.12207

Hardeland, R. (2012). Melatonin in aging and diseases-multiple consequences of reduced secretion. Options and limits of treatment. *Aging Dis.* 3, 194–225.

Jordan, F. L., and Thomas, W. E. (1988). Brain macrophages: questions of origin and interrelationship. *Brain Res.* 472, 165–178. doi: 10.1016/0165-0173(88)90019-7

Jordan, F. L., Wynder, H. J., Booth, P. L., and Thomas, W. E. (1990). Method for the identification of brain macrophages/phagocytic cells in vitro. *J. Neurosci. Res.* 26, 74–82. doi: 10.1002/jnr.4902601109

Kamphuis, W. W., Derada, T. C., Reijerkerk, A., Romero, I. A., and deVries, H. E. (2015). The blood-brain barrier in multiple sclerosis: microRNAs as key regulators. *CNS Neurol. Disord. Drug Targets* 14, 157–167. doi: 10.2174/1871527314666150116125246

Kang, Z., Liu, L., Spangler, R., Spear, C., Wang, C., Gulen, M. F., et al. (2012). IL-17-induced Act1-mediated signaling is critical for cuprizone-induced demyelination. *J. Neurosci.* 32, 8284–8292. doi: 10.1523/JNEUROSCI.0841-12.2012

Kim, W., Hahn, K. R., Jung, H., Kwon, H. J., Nam, S. M., Kim, J. W., et al. (2019). Melatonin ameliorates cuprizone-induced reduction of hippocampal neurogenesis, brain-derived neurotrophic factor, and phosphorylation cyclic AMP response element-binding protein in the mouse dentate gyrus. *Brain Behav.* 9:e01388. doi: 10.1002/brb3.1388

Labunets, I. F. (2015). Immune-neuroendocrine interactions involving thymus and pineal gland in stem cell therapy of age-related diseases. *Immunol. Endocr. Metab. Agents Med. Chem.* 15, 101–120. doi: 10.2174/1871522215666150831203443

Labunets, I. F. (2018). Possibilities and prospects of the application of the in vivo and in vitro toxic cuprizone model for demyelination in experimental and clinic neurology: literature review and own research results. *Ukr. Neurol. J.* 2, 63–68. doi: 10.30978/UNZ2018263

Labunets, I. F., and Rodnichenko, A. E. (2020). Melatonin effects in young and aging mice with the toxic cuprizone-induced demyelination. *Adv. Gerontol.* 10, 41–49.

Labunets, I. F., Melnyk, N. O., Kuzminova, I. A., and Butenko, G. M. (2014a). *Modeling structural changes of the central nervous system neurons in demyelinating diseases*. UA. Patent No 94458 (G09B 23/28 (2006.01)). Kyiv.

Labunets, I. F., Melnyk, N. O., Kuzminova, I. A., Pod'iachenko, O. V., and Butenko, G. M. (2014b). Effect of neurotoxin "cuprizone" on behavioral reactions and morphofunctional changes of cerebral and spinal cord neurons in mice. *J. NAMS Ukr.* 20, 402–408.

Labunets, I. F., Melnyk, N. O., Rodnichenko, A. E., Rymar, S. E., and Utko, N. A. (2017a). Cuprizone-induced disorders of central nervous system neurons, behavioral reactions, brain activity of macrophages and antioxidant enzymes in the mice of different ages: role of leukemia inhibitory factor in their improvement. *J. Aging Geriatr. Med.* 1:2. doi: 10.4172/AGM.1000104

Labunets, I. F., Rodnichenko, A. E., and Vasyliev, R. G. (2017b). Capacity of bone marrow granylocyte and macrophage precursors in mice of different strains for in vitro colony formation under changed thymuline level in the organism and cell cultures. *Genes Cells* 12, 97–103. doi: 10.23868/201707021

Labunets, I. F., Rodnichenko, A. E., Melnyk, N. O., Rymar, S. E., Utko, N. A., Gavrulyk-Skyba, G. O., et al. (2018a). Neuroprotective effect of the recombinant human leukemia inhibitory factor in mice with an experimental cuprizone model of multiple sclerosis: possible mechanisms. *Biopolym. Cell* 34, 350–360. doi: 10.7124/bc.000989

Labunets, I. F., Rodnichenko, A. E., Melnyk, N. O., and Utko, N. O. (2018b). Neuroprotective effect of melatonin in mice with toxic cuprizone model of demyelination and possible pathway of its realization. *Cell. Organ. Transpl.* 6, 145–151. doi: 10.22494/cot.v6i2.87

Labunets, I. F., Utko, N. A., Toporova, O. K., Savosko, S. I., Pokholenko, I., Panteleymonova, T. N., et al. (2021). Melatonin and fibroblast growth factor-2 potentiate the effects of human umbilical cord multipotent mesenchymal stromal cells in mice with cuprizone-induced demyelination. *Biopolym. Cell* 37, 369–378. doi: 10.7124/bc.000A62

Lendahl, U., Zimmerman, L. B., and McKay, R. D. (1990). CNS stem cells express a new class of intermediate filament protein. *Cell* 60, 585–595.

Li, Q., and Barres, B. A. (2018). Microglia and macrophages in brain homeostasis and disease. *Nat. Rev. Immunol.* 18, 225–239. doi: 10.1038/nri.2017.125

Li, X., Zheng, H., Ho, J., Ho, J., Chan, M. T., and Wu, W. K. K. (2016). Protective roles of melatonin in central nervous system disease by regulation of neural stem cells. *Cell Prolifer.* 50:e12323. doi: 10.1111/cpr.12323

Liddelow, S. A., and Barres, B. (2015). SnapShot: astrocytes in health and disease. *Cell* 162, 1170–1170.e1. doi: 10.1016/j.cell.2015.08.029

Liu, L., Labani, N., Cecon, E., and Jockers, R. (2019). Melatonin target proteins: too many or not enough? *Front. Endocrinol.* 10:791. doi: 10.3389/febdo.2019.00791

Lu, W., Li, J. P., Jiang, Z. D., Yang, L., and Liu, X. Z. (2022). Effects of targeted muscle reinnervation on spinal cord motor neurons in rats following tibial nerve transection. *Neural Regen. Res.* 17, 1827–1832. doi: 10.4103/1673-5374.332153

Maestroni, G. J. (1998). The photoperiod transducer melatonin and the immune-hematopoietic system. *J. Photochem. Photobiol. B.* 43, 186–192. doi: 10.1016/s1011-1344(98)00107-9

Manchester, L. C., Coto-Montes, A., Boga, J. A., Andersen, L. P. H., Vriend, J., Tan, D. X., et al. (2015). Melatonin: an ancient molecule that makes oxygen metabolically tolerable. *J. Pineal Res.* 59, 403–419. doi: 10.1111/jpi12267

McMahon, E. J., Suzuk, K., and Matsushima, G. K. (2002). Peripheral macrophage recruitment in cuprizone-induced CNS demyelination despite and intact blood-brain barrier. *J. Neuroimmunol.* 130, 32–45.

Mishchenko, E. S., Shul'ga, O. D., Bobrik, N. V., and Shul'lga, L. A. (2014). Multiple sclerosis: global perspectives. *Ukr. Med. J* 101, 84–87.

Moraga, A., Pradillo, J. M., Garcia-Culebras, A., Palma-Tortosa, S., Ballestero, S. J., Herhander-Jimenez, J., et al. (2015). Aging increases microglial proliferation, delays cell migration, and decreases cortical neurogenesis after focal ischemia. *J. Neuroinflammation* 12, 87. doi: 10.1186/s12974-015-0314-8

Murioz-Jurado, A., Escribano, B. M., Caballero-Villarraso, J., Galvan, A., Aquera, E., and Santamaria, A. (2022). Melatonin and multiple sclerosis: antioxidant, anti-inflammatory and immunomodulator mechanism of action. *Immunopharmacology* 30, 1569–1596. doi: 10.1007/s10787-022-01011-0

Ng, S. Y., and Lee, A. Y. W. (2019). Traumatic brain injuries: pathophysiology and potential therapeutic targets. *Front. Cell. Neurosci.* 13:528. doi: 10.3389/fncel.2019.00528

Pazizandeh, A., Jondal, M., and Okret, S. (2004). Glucocorticoids delay age-associated thymic involution through directly affecting the thymocytes. *Endocrinology* 145, 2392–2401. doi: 10.1210/en.2003-1660

Praet, J., Guglielmetti, C., Berneman, Z., van der Linden, A., and Ponsaerts, P. (2014). Cellular and molecular neuropathology of the cuprizone mouse model: clinical relevance for multiple sclerosis. *Neurosci. Biobehav. Rev* 47, 485–505. doi: 10.1016/j.neubiorev.2014.10.004

Reggiani, P. C., Schwedt, J. I., Console, G. M., Roggero, E. A., Dardenne, M., and Goya, R. G. (2014). Physiology and therapeutic potential of the thymic peptide thymulin. *Curr. Pharm. Des.* 20, 4690–4696. doi: 10.2174/1381612820666140130211157

Rodnichenko, A., and Labunets, I. (2018). The study of the remyelinating effect of leukemia-inhibitor factor and melatonin on the toxic cuprizone model of demyelination of murine cerebellar cells culture in vitro. *Cell. Organ. Transpl.* 6, 182–187. doi: 10.22494/cot.v6i2.90

Sarlak, G., Jenwitheesuk, A., Chetsawang, B., and Govitrapog, P. (2013). Effects of melatonin on nervous system aging: neurogenesis and neurodegeneration. *J. Pharmacol. Sci.* 123, 9–24.

Savino, W., and Dardenne, M. (2000). Neuroendocrine control of thymus physiology. *Endocr. Rev.* 21, 412–443. doi: 10.1210/er.21.4.412

Savino, W., Mendes-da-Cruz, D. A., Lepletier, A., and Dardenne, M. (2016). Hormonal control of T-cell development in health and disease. *Nat. Rev. Endocrinol.* 12, 77–89. doi: 10.1038/nrendo.2015.168

Sen, M. K., Mahns, D. A., Coorssen, J. R., and Shortland, P. J. (2022). The roles of microglia and astrocytes in phagocytosis and myelination: insights from the cuprizone model of multiple sclerosis. *Glia* 70, 1215–1250. doi: 10.1002/glia.24148

Shelestak, J., Singhal, N., Frankle, L., Tomor, R., Sternbach, S., McDonough, J., et al. (2020). Increased blood-brain barrier hyperpermability coincides with mast cell activation early under cuprizone administration. *PLoS One* 15:e0234001. doi: 10.1371/journal.pone.0234001

Skripuletz, T., Gudi, V., Hackstette, D., and Stangel, M. (2011). De- and remyelination in the CNS white and grey matter induced by cuprizone: the old, the new and the unexpected. *Histol. Histopathol.* 20, 1585–1597. doi: 10.14670/HH-26.1585

Sonobe, Y., Jin, S., Wang, J., Kawanokuchi, J., Takeuchi, H., Mizuno, T., et al. (2007). Chronobiological changes of CD4 (+) and CD 8(+) T cell subsets in the experimental autoimmune encephalomyelitis, a mouse model of multiple sclerosis. *Tohoku J. Exp. Med.* 213, 329–339. doi: 10.1620/tjem.213.329

Stephanov, O. V. (2001). *Preclinical studies of drugs (guidelines)*. Kiev: Avicenna.

Tejedor, L. A., Wosfradowski, T., Gingele, S., Skripuletz, T., Gudi, V., and Stangll, M. (2017). The effect of stereotactic injections on demyelination and remyelination: a study in the cuprizone model. *J. Mol. Neurosci.* 61, 479–488. doi: 10.1007/s12031-017-0888-y

Uchiyama, M., and Mihara, M. (1978). Determination of malonaldehyde precurcor in tissues by thiobarbituric acid test. *Anal. Biochem.* 86, 271–278. doi: 10.1016/0003-2697(78)90342-1

Urbach-Ross, D., and Kusnecov, A. W. (2007). Effects of acute and repeated exposure to lipopolysaccharide on cytokine and corticosterone production during remyelination. *Brain Behav. Immun.* 21, 962–974. doi: 10.1016/j.bbi.2007.03.010

Vakilzadeh, G., Khodagholi, F., Ghadiri, T., Ghaemi, A., Noorbakhsh, F., Sharifradeh, M., et al. (2016). The effect of melatonin on behavioral, molecular, and histopathological changes in cuprizone model of demyelination. *Mol. Neurobiol.* 53, 4675–4684. doi: 10.1007/s12035-015-9404-y

Vaughn, G. B., Jakimovski, D., and Weinstock-Guttman, B. (2019). Epidemiology and treatment of multiple sclerosis in elderly populations. *Nat. Rev. Neurol.* 15, 329–342. doi: 10.1038/s41582-019-0183-3

Vega-Riquer, J. M., Mendez-Victoriano, G., Morales-Luckie, R. A., and Gonzalez-Perez, O. (2019). Five decades of cuprizone, an updated model to replicate demyelinating diseases. *Curr. Neuropharmacol.* 17, 129–141. doi: 10.2174/1570159156661707171203 43

Wurtman, R. (2017). Multiple sclerosis, melatonin and neurobehavioral diseases. *Front. Endocrinol.* 8:280. doi: 10.3389/fendo.2017.00280

Xu, X., Wang, G., Ai, L., Shi, J., Zhang, J., and Chen, Y. X. (2018). Melatonin syppresses TLR9-triggered proinflammatory cytokine production in macrophages by inhibiting ERK1/2 and AKT activation. *Sci. Rep.* 8:15579. doi: 10.1038/s41598-018-34011-8

Xu, Y., Nygard, M., Kristensson, K., and Bentivoglio, M. (2010). Regulation of cytokine signaling and T-cell recruitment in the aging mouse brain in response to central inflammatory challenge. *Brain Behav. Immun.* 24, 138–152. doi: 10.1016/j.bbi.2009.09.006

Zabenko, Y. Y., and Pivneva, T. A. (2016). Flavonoid quercetin reduces gliosis after repetitive mild traumatic brain injury in mice. *Fiziol. Zh.* 62, 50–56.

Zhan, J., Mann, T., Joost, S., Behrangi, N., Frank, M., and Kipp, M. (2020). The cuprizone model: dos and do nots. *Cell* 9:843. doi: 10.3390/cells9040843

Zhao, M., Tuo, H., Wang, S., and Zhao, L. (2020). The roles of monocytes and monocyte and monocyte-derived macrophages in common brain disorders. *Biomed. Res. Int.* 2020:9396021. doi: 10.115512020/9396021

Zhao, Y., Zou, W., Du, J., and Zhao, Y. (2018). The origins and homeostasis of monocytes and tissue-resident macrophages in physiological situation. *J. Cell Physiol.* 233, 6425–6439. doi: 10.1002/jcp.26461

Zirngibl, M., Assinck, P., Sirov, A., Caprariello, A. V., and Plemel, J. (2022). Oligodendrocyte death and myelin loss in the cuprizone model: an updated overview of the intrinsic and extrinsic causes of cuprizone demyelination. *Mol. Neurodegen.* 17:34. doi: 10.1186/s13024-022-00538-8

frontiers | Frontiers in Cellular Neuroscience

TYPE Original Research
PUBLISHED 21 April 2023
DOI 10.3389/fncel.2023.1169980

OPEN ACCESS

EDITED BY
Satoshi Inoue,
Tokyo Metropolitan Institute of Gerontology, Japan

REVIEWED BY
Yanet Karina Gutierrez-Mercado,
University of Guadalajara, Mexico
Kaoru Sato,
Tokyo Metropolitan Institute of Gerontology, Japan

*CORRESPONDENCE
Victoria Vasilevna Sokolik
✉ v.sokolik67@gmail.com

RECEIVED 20 February 2023
ACCEPTED 06 April 2023
PUBLISHED 21 April 2023

CITATION
Sokolik VV and Berchenko OG (2023) The cumulative effect of the combined action of miR-101 and curcumin in a liposome on a model of Alzheimer's disease in mononuclear cells.
Front. Cell. Neurosci. 17:1169980.
doi: 10.3389/fncel.2023.1169980

The cumulative effect of the combined action of miR-101 and curcumin in a liposome on a model of Alzheimer's disease in mononuclear cells

Victoria Vasilevna Sokolik* and Olga Grigorievna Berchenko

Department of Neurophysiology, Immunology and Biochemistry, State Institution "Institute of Neurology, Psychiatry and Narcology of the National Academy of Medical Sciences of Ukraine", Kharkiv, Ukraine

The leading pathological mechanisms of Alzheimer's disease (AD) are amyloidosis and chronic inflammation. The study of new therapeutic drugs of the corresponding action, in particular miRNAs and curcominoids, as well as methods for their packaging, is topical. The aim of the work was to study the effect of miR-101 + curcumin in a single liposome in a cellular AD model. AD model was made by incubating a suspension of mononuclear cells with aggregates of beta-amyloid peptide 1–40 (Aβ40) for 1 h. The effect of the subsequent application of liposomal (L) preparations miR-101, curcumin (CUR), and miR-101 + CUR was analyzed over time of 1, 3, 6, and 12 h. A decrease in the level of endogenous Aβ42 under the influence of L(miR-101 + CUR) was revealed during the entire incubation period (1–12 h), the first part of which was overlapped due to inhibition of $mRNA^{APP}$ translation by miR-101 (1–3 h), and the second-by inhibition of $mRNA^{APP}$ transcription by curcumin (3–12 h), the minimum concentration of Aβ42 was recorded at 6 h. The cumulative effect of the combination drug L(miR-101 + CUR) was manifested in the suppression of the increase in the concentration of TNFα and IL-10 and a decrease in the concentration of IL-6 during the entire incubation period (1–12 h). Thus, miR-101 + CUR in one liposome enhanced each other's antiamyloidogenic and anti- inflammatory effects in a cellular AD model.

KEYWORDS

Alzheimer's disease, miR-101, curcumin, liposomes, mononuclear cells, cytokines

Introduction

The loss of neural connections in the Alzheimer's disease (AD) brain is mainly due to the disruption of signaling pathways that affect both synaptic plasticity and dendritic function, two critical regulators of cognitive processes (Abuelezz et al., 2021). At the molecular level, studies show that beta-amyloid peptide (Aβ) and Tau (τ) pathologies cause progressive axonal degeneration and severe disruption of downstream synaptic processes (Pereira et al., 2021). Moreover, Aβ and τ aggregates cause an increase in the immune response of microglia,

as well as a violation of the functionality of astrocytes, which ultimately contributes to cognitive decline in AD (Fakhoury, 2018).

Current treatments for AD currently focus on the use of acetylcholinesterase inhibitors designed to inhibit the enzyme acetylcholinesterase to increase acetylcholine levels (Mehta et al., 2012). However, these drugs can only relieve AD symptoms and have harmful side effects that limit success (Iqbal et al., 2010). Therefore, there is an urgent need for an effective therapeutic agent for the treatment of AD.

About 70% of experimentally detected miRNAs are expressed in the brain, where they regulate neurite outgrowth, dendritic spine morphology, and synaptic plasticity. A growing body of research shows that miRNAs are deeply involved in synaptic function and specific signals during memory formation (Reddy et al., 2017). This was a key point in considering the critical miRNAs that are being studied in AD. MicroRNA dysfunctions are increasingly recognized as a major factor influencing AD through deregulation of genes involved in the pathogenesis of AD. MiRNAs that directly target the APP support a role for miRNAs in the pathogenesis of AD. Reduced levels of miR-101 in the AD brain are reported, consistent with *in vitro* studies in which miR-101 inhibition increased APP levels (Siedlecki-Wullich et al., 2021). And vice versa: exogenous miR-101 caused inhibition of $mRNA^{APP}$ translation, reducing the level of endogenous Aβ42 and the inflammatory cytokine response (Sokolik et al., 2021).

Recent reports also suggest a therapeutic potential for CUR in the pathophysiology of Alzheimer's disease (Hamaguchi et al., 2010). CUR has been reported in *in vitro* studies to inhibit Aβ aggregation and Aβ-induced inflammation, as well as β-secretase and acetylcholinesterase activity (Ono et al., 2004; Ahmed and Gilani, 2009; Sokolik and Shulga, 2016). In *in vivo* studies, oral or nasal administration of CUR resulted in inhibition of Aβ deposition, Aβ oligomerization, and tau phosphorylation in the brain of AD animal models, as well as improvement in behavioral disturbances and cognitive characteristics (Garcia-Alloza et al., 2007; Sokolik and Shulga, 2015). These data suggest that CUR may be one of the most promising compounds for the development of AD treatments.

Another problem of AD therapy is the difficulty of effective and non-invasive drug delivery directly to the brain. However, growing advances in nanotechnology (Mageed et al., 2021) and targeted delivery of biological materials have been successfully reported in some animal AD models.

In our previous studies, the predominantly anti-amyloidogenic and/or anti- inflammatory effects of liposomal preparations of CUR and miR-101 have been established individually in animal and cellular models of Alzheimer's disease (Sokolik and Shulga, 2015, 2016; Sokolik et al., 2017, 2019, 2021). Therefore, it is logical that the aim of this study was to study the effect of miR-101 + CUR in a single liposome in an experimental AD model *in vitro*.

Abbreviations: 0.9% NaCl, saline τ, tau protein; Aβ, beta-amyloid peptide; Aβ40, beta-amyloid peptide 1–40; Aβ42, beta-amyloid peptide 1–42; AAPP, amyloid-β protein precursor; AMPs, antimicrobial peptides; BASE 1, beta-site APP cleaving enzyme 1; AD, Alzheimer's disease; CUR, curcumin; ELISA, enzyme-linked immunosorbent assay; IL-6, interleukin-6; IL-10, interleukin-10°L, liposomes; miR-101, micro ribonucleic acid-101; $mRNA^{APP}$, messenger ribonucleic acid of amyloid-β protein precursor; TNFα, tumor necrosis factor α; RPMI, Roswell Park Memorial Institute medium.

Materials and methods

A cellular Alzheimer's disease (AD) model was made *in vitro* on a suspension of human mononuclear cells (n = 3 samples). The ethics committee of the SI "Institute of Neurology, Psychiatry and Narcology of the National Academy of Medical Sciences of Ukraine," Kharkiv, Ukraine approved this study (Protocol no. 12-à, 12.12.2019). Written informed consent from volunteer donors was obtained at the time of blood sampling. Mononuclear cells were isolated using a Ficoll-Urografin density gradient, washed three times with 0.9% NaCl, and resuspended in RPMI medium to a concentration of 12,000 × 10^9 cells per liter.

Beta Amyloid Peptide (1–40) (Human), Abcam, Cambridge, UK was dissolved in double- distillate water to the concentration of 1.5 mmol/L and aggregated at 37°C during 24 h. Large conglomerates of Aβ40 were dispersed by ultrasound and sterilized intermediary before adding to the suspension of mononuclear cells. The suspension of Aβ40 aggregates was added to the incubation medium RPMI with mononuclear cells in a 1:17 dose.

The liposomal forms of miR-101 (miR-101-3p, SPF Sintol LLC, and RF), CUR (Sigma-Aldrich, St. Louis, MO, USA) and miR-101 + CUR was obtained using the lipid injection method. The diameter of liposomes (composed of phospholipid/cholesterol) was calibrated in an extruder using additional membranes with 100 nm openings. The concentration of microRNA in the suspension of liposomes was $12.5 \cdot 10^{18}$ molecules per liter, the CUR concentration was 0.7 g per liter. At the same time, liposomal preparations were added to the incubation medium at a ratio of 1:50. Nucleotide sequence of miR-101: UACAGUACUGUGAUAACUGAA.

Four experimental groups were created for each from three different samples of mononuclear suspensions:

Control: mononuclear cells + 0.9% NaCl (1 h) + 0.9% NaCl Group L(miR-101): mononuclear cells + Aβ40 (1 h) + L(miR-101).

Group L(miR-101 + CUR): mononuclear cells + Aβ40 (1 h) + L(miR-101 + CUR) Group L(CUR): mononuclear cells + Aβ40 (1 h) + L(CUR), Aβ40 aggregates (except for Control) were added to these cells, and after 1 h of incubation

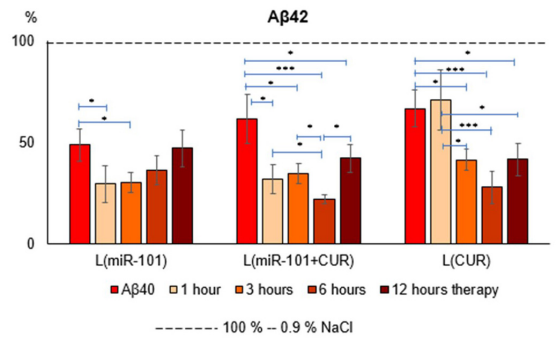

FIGURE 1
Diagrams of the relative content of Aβ42 in suspension of mononuclear cells after 1 h of incubation with aggregates of Aβ40 and subsequent incubation over time for 1, 3, 6 and 12 h with liposomal forms of miR-101, CUR, and miR-101 + CUR. The vertical axis is the concentration of Aβ42 in the target samples normalized to the corresponding concentration of this substance in the suspension of mononuclear cells incubated with saline, %. *$P < 0.05$, ***$P < 0.001$.

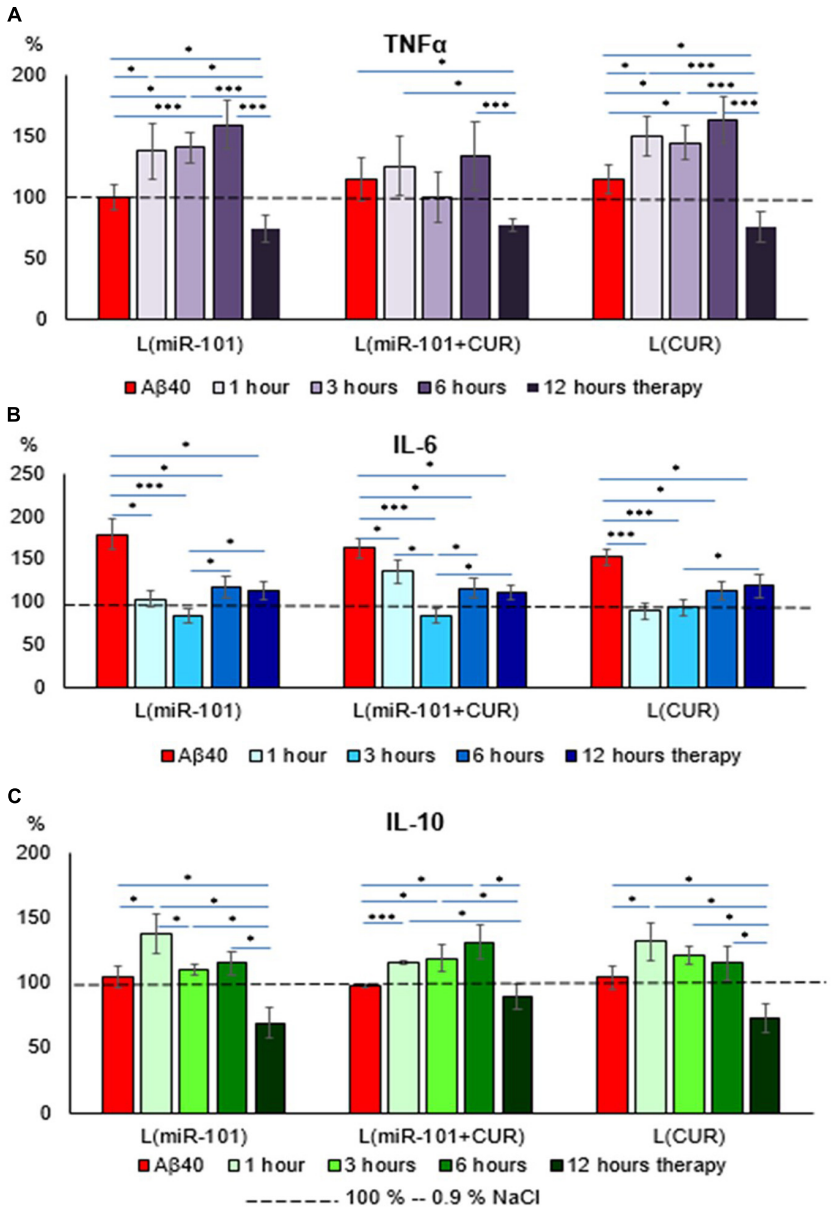

FIGURE 2
Diagrams of the relative content of cytokines: TNFα **(A)**, IL-6 **(B)**, and IL-10 **(C)** in mononuclear cell suspension after 1 h of incubation with Aβ40 aggregates and subsequent incubation over time 1, 3, 6, and 12 h with liposomal forms of miR-101, CUR, and miR-101 + CUR. The vertical axis is the concentration of the corresponding cytokine in the target samples normalized to the corresponding concentration of this substance in the suspension of mononuclear cells incubated with saline, %. $^{*}P < 0.05$, $^{***}P < 0.001$.

at 37°C, liposome suspensions miR-101, miR-101 + CUR, and CUR were added, respectively. Aliquots (V = 300 μl) for the determination of the concentration of Aβ42 and cytokines were taken at the beginning of the experiment, after 1 h of incubation with Aβ40 and atthe dynamics of the time after adding the suspension of liposomal reagents: on the 1st, 3rd, 6th, and 12th h. The control was given the corresponding volume of saline. Samples were negatively frozen and stored until ELISA simmered at −80°C.

Enzyme-linked immunosorbent assay for Aβ42 and cytokines (TNFα, IL-6, IL-10) concentration was performed according kit manuals for the Human Aβ 1–42 (Amyloid Beta 1–42) ELISA Kit Elabscience Bio-technology Inc., USA, α-TNF-EIA-BEST, Interleukin-6-EIA- BEST and Interleukin-10-EIA-BEST, RF. The absorbance of samples was read with a GBG Stat FAX 2,100 microplate analyzer (USA) at 450 nm with wavelength correction at 630 nm. The EIA data were represented in picograms per mL (pg/mL). To identify the specificity of the effect of Aβ40 and liposomal preparations miR-101, miR-101 + CUR, and CUR, the data of the L(miR-101), L(miR-101 + CUR), and L(CUR) groups were normalized to the corresponding indicators of the control group in dynamics research and are expressed in%.

Data are presented as mean ± standard deviation (SD). For comparison of non-parametric data sets the Mann-Whitney U-test. The results were considered statistically significant at $P < 0.05$.

Results

The liposomal form of miR-101 + CUR revealed the most effective (from the first hour of incubation by an average of 67% over the entire period) and long-term (within 12 h) suppression of the Aβ42 level in mononuclear suspension, caused by the preliminary administration of Aβ40 aggregates (**Figure 1**) according to compared with the action of miR-101 and CUR in liposomes individually. Thus, miR-101 in liposomes caused a decrease in the level of Aβ42 only during the first 3 h of incubation and, on average, by 70% during this time, while the effect of liposomal CUR actualized during 3–12 h of incubation, i.e., was more delayed.

The greatest effect of miR-101 + CUR liposomal preparation turned out to be at 6 h of incubation of mononuclear cells with the AD model (**Figure 1**). It was most compelling when compared to liposomal miR-101 or CUR individually in the same term. These data characterize the primary antiamyloidogenic action of miRNAs and only an indirect and delayed effect of CUR.

Liposomal preparations of miR-101 or CUR individually during the first 6 h of incubation failed to prevent an increase in TNFα concentration in the suspension of mononuclear cells activated by Aβ40 aggregates, in contrast to liposomes with miR-101 + CUR (**Figure 2A**). A decrease in the concentration of this cytokine by 12 h of incubation cannot be considered a specific anti-inflammatory effect of liposomes with microRNA and CUR, since TNFα is a cytokine of the first wave of the inflammatory cascade and its level decreases physiologically by this time, as well as IL-10 (**Figure 2C**). What cannot be said about the concentration dynamics of the ambivalent representative of the second wave of the cytokine cascade-IL-6 (**Figure 2B**). It was shown that all liposomal forms of reagents specifically reduced the concentration of IL-6 during the entire incubation period (1–12 h), which illustrates their anti-inflammatory effect. The dynamics of IL-10 concentration presented in **Figure 2C** shows that miR-101 + CUR in liposomes provides a stable increase in the level of this anti- inflammatory cytokine in the range of 1–6 h of incubation, while only miR-101 or only CUR in liposomes is effective only for the first hour of incubation.

Discussion

Alzheimer's disease is a multifactorial metabolic disorder of the central nervous system, so a single drug with a narrowly focused symptom-corrective action cannot be a panacea for it. From a large pool of miRNAs involved in the pathogenesis of AD (more than 40, 16 of which have diagnostic potential in humans), miR-101 was selected.

Deficiency of the latter leads to uncontrolled induction of APP synthesis, the excess of which is converted by beta-site APP cleaving enzyme 1 (BASE1) and γ- secretase into aggregate active Aβ (Vilardo et al., 2010). Altered expression of miR-101 was found in patients with AD. Two independent miRNA expression profiles (Hébert et al., 2008; Nunez-Iglesias et al., 2010) showed that miR-101 is down-regulated in the human cortex in AD, indicating that miR-101 down-regulation may play a role in the development of AD. This hypothesis is consistent with our previous results, which indicate a direct role for miR-101 in the control of APP translation and Aβ accumulation (Sokolik et al., 2021).

Liposomal miR-101 in mononuclear cell suspension caused a decrease in Aβ42 levels only for the first 3 h of incubation, while together with CUR, the effect lasted 12 h (**Figure 1**), since CUR came into play just starting from 3 h of incubation. This dynamic is since miR-101 has a direct inhibitory effect on the translation of $mRNA^{APP}$, while CUR affects indirectly: by inhibiting the inflammatory cytokine cascade. These data are consistent with previously published results that FAM-labeled miR-101 in liposomes is actively absorbed by mononuclear cells during the first 1–2 h of incubation, and then the intensity of the fluorescent signal decreases by half by 3 h of incubation (Sokolik et al., 2021).

Most likely, degradation of miR-101 occurs. Our other study revealed that CUR causes a decrease in $mRNA^{APP}$ expression precisely by 3 h of incubation (Sokolik and Shulga, 2016) and a corresponding decrease in Aβ concentration. Thus, miR-101 has a rapid and direct effect on $mRNA^{APP}$ translation, while CUR has a slow and indirect effect on its transcription. Therefore, their combined use in an experimental AD model had the most effective antiamyloidogenic effect.

Aβ is a representative of the ancient peptide defense system of the brain-antimicrobial peptides (AMPs), which can react faster and first of the cellular immunity systems and the cytokine cascade, activating the latter (Kumar et al., 2016; Moir et al., 2018; Pastore et al., 2020). In the present study, miR-101 in liposomes showed an indirect effect on the dynamics of the cytokine response (except for IL-6), which is most likely due to an inhibitory effect on the level of endogenous Aβ. CUR, in turn, is considered as a direct negative regulator of IL-6 inflammatory signaling pathways due to suppression of NF-kappaB activation (Ghandadi and Sahebkar, 2017). Therefore, of greatest interest is the revealed cumulative effect of their combined action miR-101 + CUR in one liposome on an experimental AD model. Namely: suppression of the increase in the concentration of TNFα and IL-10 and a decrease in the concentration of IL-6 during the entire incubation period (1–12 h). Undoubtedly, the subtle regulatory mechanisms of this effect require further detailed study, but the obtained fact inspires optimism regarding the advisability of using the liposomal form of miR-101 with CUR for the treatment of Thus, miR-101 + CUR in one liposome enhanced each other's antiamyloidogenic and anti-inflammatory effects in a cellular AD model.

Data availability statement

The original contributions presented in this study are included in the article/supplementary material, further inquiries can be directed to the corresponding author.

Ethics statement

The studies involving human participants were reviewed and approved by the Ethics Committee of the SI "Institute of

Neurology, Psychiatry and Narcology of the National Academy of Medical Sciences of Ukraine", Kharkiv, Ukraine (Protocol No. 12-à, 12.12.2019). The patients/participants provided their written informed consent to participate in this study.

Author contributions

VS carried out the entire experimental part of the work, statistical processing of the results, formulated the concept and task of the study, and prepared the manuscript for publication. OB took an active part in the discussion of the results and the formulation of the conclusions of the manuscript. Both authors contributed to the article and approved the submitted version.

Conflict of interest

The authors declare that the research was conducted in the absence of any commercial or financial relationships that could be construed as a potential conflict of interest.

Publisher's note

All claims expressed in this article are solely those of the authors and do not necessarily represent those of their affiliated organizations, or those of the publisher, the editors and the reviewers. Any product that may be evaluated in this article, or claim that may be made by its manufacturer, is not guaranteed or endorsed by the publisher.

References

Abuelezz, N. Z., Nasr, F. E., AbdulKader, M. A., Bassiouny, A. R., and Zaky, A. (2021). MicroRNAs as Potential Orchestrators of Alzheimer's Disease-Related Pathologies: Insights on Current Status and Future Possibilities. *Front. Aging Neurosci.* 13:743573. doi: 10.3389/fnagi.2021.743573

Ahmed, T., and Gilani, A. H. (2009). Inhibitory effect of curcuminoids on acetylcholinesterase activity and attenuation of scopolamine-induced amnesia may explain medicinal use of turmeric in Alzheimer's disease. *Pharmacol. Biochem. Behav.* 91, 554–559. doi: 10.1016/j.pbb.2008.09.010

Fakhoury, M. (2018). Microglia and Astrocytes in Alzheimer's Disease: Implications for Therapy. *Curr. Neuropharmacol.* 16, 508–518. doi: 10.2174/1570159X15666170720095240

Garcia-Alloza, M., Borrelli, L. A., Rozkalne, A., Hyman, B. T., and Bacskai, B. J. (2007). Curcumin labels amyloid pathology in vivo, disrupts existing plaques, and partially restores distorted neurites in an Alzheimer mouse model. *J. Neurochem.* 102, 1095–1104. doi: 10.1111/j.1471-4159.2007.04613.x

Ghandadi, M., and Sahebkar, A. (2017). Curcumin: An Effective Inhibitor of Interleukin-6. *Curr. Pharm. Des.* 23, 921–931. doi: 10.2174/1381612822666161006151605

Hamaguchi, T., Ono, K., and Yamada, M. (2010). Curcumin and Alzheimer's Disease. *CNS Neurosci. Therap.* 16, 285–297.

Hébert, S. S., Horré, K., Nicolaï, L., Papadopoulou, A. S., Mandemakers, W., Silahtaroglu, A. N., et al. (2008). Loss of microRNA cluster miR-29a/b-1 in sporadic Alzheimer's disease correlates with increased BACE1/β-secretase expression. *Proc. Natl. Acad. Sci. U.S.A.* 105, 6415–6420. doi: 10.1073/pnas.071026310

Iqbal, K., Liu, F., Gong, C.-X., and Grundke-Iqbal, I. (2010). Tau in Alzheimer disease and related tauopathies. *Curr. Alzheimer Res.* 7, 656–664. doi: 10.2174/156720510793611592

Kumar, D. K., Choi, S. H., Washicosky, K. J., Eimer, W. A., Tucker, S., Ghofrani, J., et al. (2016). Amyloid-β peptide protects against microbial infection in mouse and worm models of Alzheimer's disease. *Sci. Transl. Med.* 8:340ra72. doi: 10.1126/scitranslmed.aaf1059

Mageed, A. H., Emad, A., Mohamed, S. A., and Abuelezz, N. (2021). The tiny big world of solid lipid nanoparticles and nanostructured lipid carriers: An updated review. *J. Microencapsul.* 39, 1–42. doi: 10.1080/02652048.2021.2021307

Mehta, M., Adem, A., and Sabbagh, M. (2012). New acetylcholinesterase inhibitors for Alzheimer's disease. *Int. J. Alzheimers Dis.* 2012:728983. doi:10.1155/2012/728983

Moir, R. D., Lathe, R., and Tanzi, R. E. (2018). The antimicrobial protection hypothesis of Alzheimer's disease. *Alzheimer Dement.* 14, 1602–1614. doi: 10.1016/j.jalz.2018.06.3040

Nunez-Iglesias, J., Liu, C. C., Morgan, T. E., Finch, C. E., and Zhou, X. J. (2010). Joint genome-wide profiling of miRNA and mRNA expression in Alzheimer's disease cortex reveals altered miRNA regulation. *PLoS One* 5:e8898. doi: 10.1371/journal.pone.0008898

Ono, K., Hasegawa, K., Naiki, H., and Yamada, M. (2004). Curcumin has potent anti-amyloidogenic effects for Alzheimer's beta-amyloid fibrils in vitro. *J. Neurosci. Res.* 75, 742–750. doi: 10.1002/jnr.20025

Pastore, A., Raimondi, F., Rajendran, L., Temussi, PA. (2020). Why does the Aβ peptide of Alzheimer share structural similarity with antimicrobial peptides? *Commun. Biol.* 3:135. doi: 10.1038/s42003-020-0865-9

Pereira, J. B., Janelidze, S., Ossenkoppele, R., Kvartsberg, H., Brinkmalm, A., Mattsson-Carlgren, N., et al. (2021). Untangling the association of amyloid-β and tau with synaptic and axonal loss in Alzheimer's disease. *Brain* 144, 310–324. doi: 10.1093/brain/awaa395

Reddy, P. H., Tonk, S., Kumar, S., Vijayan, M., Kandimalla, R., and Kuruva, C. S. (2017). A Critical evaluation of neuroprotective and neurodegenerative MicroRNAs in Alzheimer's disease. *Biochem. Biophys. Res. Commun.* 483, 1156–1165. doi: 10.1016/j.bbrc.2016.08.067

Siedlecki-Wullich, D., Miñano-Molina, A. J., and Rodríguez-Álvarez, J. (2021). microRNAs as early biomarkers of Alzheimer's disease: A synaptic perspective. *Cells* 10:113. doi: 10.3390/cells10010113

Sokolik, V., Berchenko, O., Levicheva, N., and Shulga, S. (2019). Anti-amyloidogenic Effect of MiR-101 in Experimental Alzheimer's Disease. *Biotechnol. Acta* 12, 41–49. doi: 10.15407/biotech12.03.041

Sokolik, V., Berchenko, O. G., and Shulga, S. (2017). Comparative analysis of nasal therapy with soluble and liposomal forms of curcumin on rats with alzheimer's disease model. *J. Alzheimer Dis. Parkinson.* 7:1000357. doi: 10.4172/2161-0460.1000357

Sokolik, V. V., Berchenko, O. H., Kolyada, O. K., and Shulga, S. M. (2021). Direct and indirect action of liposomal form of MIR-101 on cells in the experimental model of alzheimer's disease. *Cytol. Genet.* 55, 499–509. doi: 10.3103/S0095452721060141

Sokolik, V. V., and Shulga, S. M. (2015). Effect of curcumin liposomal form on angiotensin converting activity, cytokines, and cognitive characteristics of the rats with Alzheimer's disease model. *Biotechnol. Acta* 8, 48–55. doi: 10.15407/biotech8.06.048

Sokolik, V. V., and Shulga, S. M. (2016). Effect of curcumin on accumulation in mononuclear cells and secretion in incubation medium of Àβ40 and cytokines under local excess of Àβ42-homoaggregates. *Ukr. Biochem. J.* 88, 83–91. doi: 10.15407/ubj88.03.083

Vilardo, E., Barbato, C., Ciotti, M., Cogoni, C., and Ruberti, F. (2010). MicroRNA-101 regulates amyloid precursor protein expression in hippocampal neurons. *J. Biol. Chem.* 285, 18344–18351. doi: 10.1074/jbc.M110.112664

frontiers | Frontiers in Cellular Neuroscience

TYPE Original Research
PUBLISHED 10 May 2023
DOI 10.3389/fncel.2023.1176676

OPEN ACCESS

EDITED BY
Dirk M. Hermann,
University of Duisburg-Essen, Germany

REVIEWED BY
Maryam Ardalan,
University of Gothenburg, Sweden
Stanislava Pankratova,
University of Copenhagen, Denmark

*CORRESPONDENCE
Dmytro Shepilov
✉ shepilov@biph.kiev.ua
Alexandru Movila
✉ amovila@iu.edu

†These authors have contributed equally to this work and share senior authorship

RECEIVED 28 February 2023
ACCEPTED 18 April 2023
PUBLISHED 10 May 2023

CITATION
Shepilov D, Osadchenko I, Kovalenko T, Yamada C, Chereshynska A, Smozhanyk K, Ostrovska G, Groppa S, Movila A and Skibo G (2023) Maternal antibiotic administration during gestation can affect the memory and brain structure in mouse offspring. *Front. Cell. Neurosci.* 17:1176676. doi: 10.3389/fncel.2023.1176676

Maternal antibiotic administration during gestation can affect the memory and brain structure in mouse offspring

Dmytro Shepilov[1]*, Iryna Osadchenko[1], Tetiana Kovalenko[1], Chiaki Yamada[2,3], Anastasiia Chereshynska[2], Kateryna Smozhanyk[1], Galyna Ostrovska[4], Stanislav Groppa[5,6], Alexandru Movila[2,3]*† and Galyna Skibo[1†]

[1]Department of Cytology, Bogomoletz Institute of Physiology, National Academy of Sciences of Ukraine, Kyiv, Ukraine, [2]Department of Biomedical Sciences and Comprehensive Care, School of Dentistry, Indiana University, Indianapolis, IN, United States, [3]Indiana Center for Musculoskeletal Health, Indiana University School of Medicine, Indianapolis, IN, United States, [4]Department of Cytology, Histology, and Reproductive Medicine, Institute of Biology and Medicine, Taras Shevchenko National University of Kyiv, Kyiv, Ukraine, [5]Department of Neurology, Institute of Emergency Medicine, Chişinău, Moldova, [6]Department of Neurology, State University of Medicine and Pharmacy "Nicolae Testemiţanu", Chişinău, Moldova

Maternal antibiotics administration (MAA) is among the widely used therapeutic approaches in pregnancy. Although published evidence demonstrates that infants exposed to antibiotics immediately after birth have altered recognition memory responses at one month of age, very little is known about *in utero* effects of antibiotics on the neuronal function and behavior of children after birth. Therefore, this study aimed to evaluate the impact of MAA at different periods of pregnancy on memory decline and brain structural alterations in young mouse offspring after their first month of life. To study the effects of MAA on 4-week-old offspring, pregnant C57BL/6J mouse dams (2–3-month-old; n = 4/group) were exposed to a cocktail of amoxicillin (205 mg/kg/day) and azithromycin (51 mg/kg/day) in sterile drinking water (daily/1 week) during either the 2nd or 3rd week of pregnancy and stopped after delivery. A control group of pregnant dams was exposed to sterile drinking water alone during all three weeks of pregnancy. Then, the 4-week-old offspring mice were first evaluated for behavioral changes. Using the Morris water maze assay, we revealed that exposure of pregnant mice to antibiotics at the 2nd and 3rd weeks of pregnancy significantly altered spatial reference memory and learning skills in their offspring compared to those delivered from the control group of dams. In contrast, no significant difference in long-term associative memory was detected between offspring groups using the novel object recognition test. Then, we histologically evaluated brain samples from the same offspring individuals using conventional immunofluorescence and electron microscopy assays. To our knowledge, we observed a reduction in the density of the hippocampal CA1 pyramidal neurons and hypomyelination in the *corpus callosum* in groups of mice *in utero* exposed to antibiotics at the 2nd and

3rd weeks of gestation. In addition, offspring exposed to antibiotics at the 2nd or 3rd week of gestation demonstrated a decreased astrocyte cell surface area and astrocyte territories or depletion of neurogenesis in the dentate gyrus and hippocampal synaptic loss, respectively. Altogether, this study shows that MAA at different times of pregnancy can pathologically alter cognitive behavior and brain development in offspring at an early age after weaning.

KEYWORDS

offspring mice, antibiotics, memory and learning, hippocampal structure, neurogenesis, myelination

1. Introduction

Since the COVID-19 pandemic was declared in December 2019, the World Health Organization and international statics, including those from Ukraine, have confirmed that pregnant women are a potentially vulnerable population to secondary bacterial co-infection (Emanoil et al., 2021; Januszek et al., 2022). Therefore, a significant increase in the maternal antibiotics administration (MAA) for therapeutic and prophylactic treatments of various secondary infections in pregnant women infected with COVID-19 (Ramírez-Lozada et al., 2022). However, a recently conducted population-based cohort study demonstrated increased severity of COVID-19 disease after treatment with antibiotics (Llor et al., 2021).

Maternal antibiotics often coincided with the perinatal period to prevent infectious morbidity and mortality (Cardetti et al., 2020; Thinkhamrop et al., 2021) and postpartum infection after post-surgical C-section complications (O'Connor et al., 2021). While the administration of antibiotics is maybe critical to maintaining maternal health during pregnancy, registry-based cohort studies demonstrated that maternal antibiotics exacerbate the risks of developing asthma and early-onset sepsis in their children (Stokholm et al., 2014; Zhou et al., 2020). Furthermore, the MAA can produce long-lasting effects on the neuroimmune responses of offspring in an experimental mouse model of dysbiosis (Madany et al., 2022a).

The normal gut microbiota is thought to be linked to physiological brain development, behavior, and stress response in a healthy lifespan (Heijtz et al., 2011; Dinan and Cryan, 2017). By contrast, dysbiosis of the gut microbiota plays a crucial role in the pathogenesis of several immunological diseases and neuroinflammation in adulthood (Carding et al., 2015; Cao et al., 2021). However, the *in utero* impact of antibiotics on the offspring begins to be explored. Accumulated lines of evidence indicate that MAA in pregnant women affects the gut microbiota and may cause endotoxemia (Madany et al., 2022a; Norooznezhad et al., 2022). Endotoxins are released from dead bacterial cells, which can cross the epithelial barrier ending up in the bloodstream (André et al., 2019). Recently published studies reported that bacterial-derived endotoxins promote neuroinflammation and affect cerebral circulation in pregnant mice (Cipolla et al., 2011; Kurita et al., 2020). Furthermore, endotoxemia mediates perinatal neuroinflammation in a murine model of preterm labor (Estrada et al., 2020). In addition, our recently published study demonstrated that bacterial-derived endotoxins influence hallmark findings in Alzheimer's disease (Yamada et al., 2020).

Although various published studies addressed the impact of MAA on gut microbiota during pregnancy (Kuperman and Koren, 2016; Madany et al., 2022a,b), it remains unclear whether widely used antibiotics in gynecological practice, *e.g.,* amoxicillin and azithromycin (Andrade et al., 2004; Bookstaver et al., 2015), elevate neuroinflammation and neurodegeneration in offspring after birth. Thus, this study assesses how an antibiotics cocktail containing amoxicillin and azithromycin used during the 2nd or the 3rd week of pregnancy alters offspring outcomes by investigating their behavioral defects and brain structure one month after birth.

Our results indicate that exposure of pregnant females to amoxicillin and azithromycin in drinking water during the 2nd week of pregnancy dramatically elevates intestinal barrier permeability and has a positive trend on the permeability of the blood–brain barrier (BBB) compared to the control group of dams. Furthermore, the density of the hippocampal CA1 pyramidal neurons in groups of offspring exposed to antibiotics at the 2nd and 3rd weeks of gestation was significantly reduced, and myelination in the corpus callosum was altered compared to the control group. In addition, offspring exposed to antibiotics *in utero* at the 2nd or the 3rd week of gestation demonstrated a decreased astrocyte cell surface area and astrocyte territories or depletion of neurogenesis in the dentate gyrus and hippocampal synaptic loss, respectively. Finally, we also confirmed that the administration of amoxicillin and azithromycin cocktail to dams affects spatial reference memory and hippocampus-related spatial learning in offspring.

2. Materials and methods

2.1. Mice and experimental cohorts

Dams and sires (2–3-month-old; C57BL/6J) mice were purchased from Charles River Laboratory (Czechia) and were exposed to the same sterile drinking water. The breeding protocol was started after one week of acclimatization to a new animal facility. The embryonic (E) day was determined by the presence of a vaginal plug marking E0.5 of pregnancy. Then, pregnant dams were placed individually and randomly divided into three experimental groups (n = 4 mice/group). Group I: *control*, no antibiotics in

sterile drinking water over the entire period of gestation. Group II (*2-w antibiotics)*, was exposed to an antibiotic pharmaceutic grade cocktail (Basalt, Ukraine) containing a mixture of amoxicillin (205 mg/kg bw/day) and azithromycin (51 mg/kg bw/day) in drinking water starting from the second week of pregnancy (E8-E14); pregnant dams were treated by the antibiotic cocktail in drinking water for 7 days followed by sterile drinking water until birth. Dams from the Group III: (*3-w antibiotics*) received antibiotics cocktail in drinking water from the third week of pregnancy to delivery (E15-P0). Experimental doses of antibiotics were selected according to the average clinical therapeutic doses for adult patients (Smith et al., 2020; Ahmadi et al., 2021) and converted to equivalent ones for adult mice (Nair and Jacob, 2016). Aqueous solutions of antibiotics were changed every other day.

All experimental groups of dams and sires as well as their offspring were kept on a 12-h light-dark cycle at a constant temperature, with free access to food and water. All procedures with experimental animals were carried out in compliance with NIH and Europe community (Directive 2010/63/EU) policies, and ethical approval was obtained from the Biomedical ethics committee at the Bogomoletz Institute of Physiology (protocol #1/22 from August 10, 2022).

The offspring mice were used to conduct behavioral tests during the 5th week of life followed by morphological analysis of their brains (n = 13–16 mice/group). In addition, we determined the BBB and intestinal barrier permeability (n = 4–5 mice/group) as demonstrated in the study design protocol (**Figure 1**).

2.2. Behavioral testing

Since previously published *in utero* pre-clinical observations recommended to at least 4-week-old offspring for behavioral alterations and brain histopathological studies (Zheng et al., 2013; Barnhart et al., 2015; Snow et al., 2015), we conducted our behavioral tests using 4-week-old mice born from experimental Groups I-III.

2.2.1. Novel object recognition test

The novel object recognition (NOR) test is a widely used cognitive task for assessing associative memory (Lueptow, 2017). The assay was conducted in a square plexiglass chamber (40 cm × 40 cm × 40 cm) and comprised three phases: habituation, familiarization, and test. During habituation, mice freely explored an empty room without objects for 5 min. After 24 h, two identical objects—sand-filled glass jars or rectangular wooden blocks—were placed in the device, and mice were allowed to examine them for 10 min (familiarization). Next, the object recognition memory was tested after 24 h. To do that, one of the familiar objects was replaced with a novel objective and explored for 10 min by offspring. To avoid any olfactory cues, the apparatus was cleaned with 70% ethanol between trials. In addition, object types in the familiarization phase and object positions (left/right) in the test phase were counterbalanced between mice. All trials of the familiarization and test phases were analyzed using ANY-maze software, version 7.15 (Stoelting Co., Ireland) using standard protocol. Briefly, the first 5 min of a trial were analyzed; if the mouse did not reach a 20s criterion of object exploration, the next 5 min of the video were also analyzed. Data from mice that failed to reach the standard for the whole 10-min trial were excluded. Preference of the 2nd object during familiarization (*(time with the 2nd object/total time exploring two things)* × *100%*) and Preference index (*(time with the novel object/total time exploring novel and familiar objects)* × *100%*) were calculated.

2.2.2. Morris water maze

The next day after NOR test, spatial reference memory was evaluated the by Morris water maze (MWM) test using an established protocol with minor modifications (Patil et al., 2009). Mice were trained in a water-filled pool (115 cm in diameter; 21–23°C), and adding dry milk was to make the water opaque. A drape surrounded the pool where spatial cues (geometric figures) were mounted. MWM consisted of three stages: pre-training (day 0), acquisition (days 1–4), and probe test (day 5). During pre-training, animals were habituated to the testing conditions. There were four trials of up to 120 s to find a visible platform (11 cm in diameter, 1 cm above the water) with a 60-min intertrial interval. The start point was fixed (E), while the position of the platform was changed between trials (S-E → S-W → N-W → N-E). After finding the platform, mice were allowed to explore it for the 30 s before returning to home cages. If a mouse did not see the platform for 120 s, it was sat there by the experimenter. The acquisition stage lasted for four consecutive days (4 trials/day, 60-min intertrial interval), during which animals found a hidden platform (0.5 cm below the water). The start point varied between trials (*e.g.,* E → N → W → S), however, the platform's position was fixed on all days of acquisition (N–W). If a mouse did not reach the platform for the 120 s, the investigator placed it there for the 30 s. On the last day of MWM, a probe test was carried out. The platform was removed from the pool, and animals were allowed to swim for the 60 s. Latency to find the hidden platform, path length, and mean speed during acquisition, as well as time in the target quadrant and heat maps with trajectories of movement in the probe task, were obtained using ANY-maze software, version 7.15 (Stoelting Co., Ireland).

2.3. Morphological analysis of the brain

2.3.1. Sample collection

Sample collections from the offspring was performed immediately after the MWM test using an established protocol (Goncharova et al., 2015; Marungruang et al., 2020). Briefly, mice were anesthetized with intramuscular injection of ketamine (100 mg/kg bw; Ketalar, Pfizer AB, Sweden) and xylazine (10 mg/kg bw; Sedazine, Biovet Pulawy, Poland). Then, anesthetized mice were transcardially perfused with a warm (+37°C) solution containing 0.1 M PBS (pH 7.4) + 0.3% heparin followed by ice-cold fixative solution containing 4% paraformaldehyde (PFA) + 0.25% glutaraldehyde (GA) (Sigma-Aldrich, USA) in 0.1M PBS. After that, the brains were dissected and split into two hemispheres. Finally, samples for immunohistochemistry (IF) were postfixed overnight in the fixative solution containing 4% PFA at + 4°C. The other brain hemisphere was postfixed in the solution containing 4% PFA + 2.5% GA for light and transmissional electron microscopy.

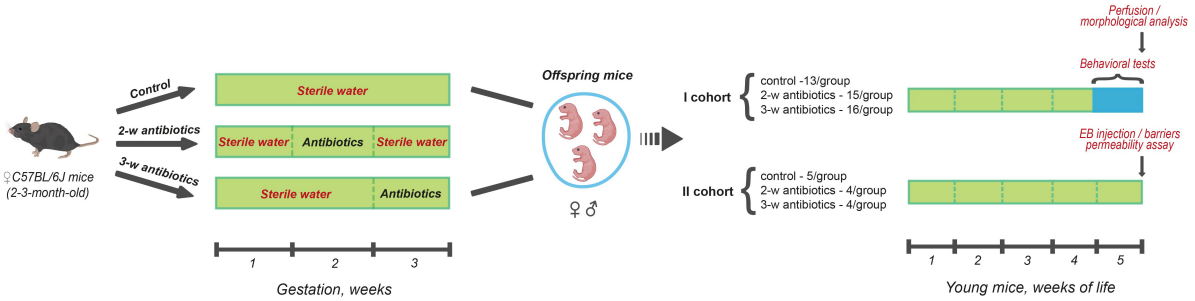

FIGURE 1
Scheme of the experiment. Pregnant C57BL/6J mice (between 2 and 3-month-old) were divided into three groups (4 females/group) according to the treatment procedure: (I) sterile drinking water over the entire gestation period (*control*); (II) sterile drinking water contained a cocktail of antibiotics (amoxicillin and azithromycin) during the 2nd week (8-14 days) of gestation (*2-w antibiotics*); (III) consumed antibiotics from the 15th day of gestation to delivery (*3-w antibiotics*). In the present study, offspring mice born from those dams were investigated. In doing so, the first cohort of the animals of all three experimental groups performed behavioral tests during the 5th week of life with further morphological analysis of their brains. There also assessed the permeability of the intestinal and blood-brain barriers in mice from the second cohort using Evans Blue extravasation method.

2.3.2. Immunohistochemistry and confocal microscopy

Altogether, 13–16 samples/treatment group were submitted for immunohistochemistry. The 40-μm-thick coronal sections of the dorsal hippocampus were obtained from the anatomical areas between 1.65 and 2.48 mm posterior to the bregma (Lein et al., 2007) using a vibratome Leica VT1000A (Leica Biosystems, Germany).

To visualize the hippocampal cellular structure, free-floating sections were placed in wells of 24-well plates, rinsed with 0.1M PBS, and treated with a blocking solution containing 1% BSA (Sigma-Aldrich, USA) and 0.3% Triton X-100 (Sigma-Aldrich, USA) for 1h at room temperature. The following primary antibodies were applied for immunostaining: anti-mouse monoclonal antibodies against neuronal nuclei marker (NeuN; 1:750, Abcam, UK), anti-rabbit polyclonal antibodies against the glial fibrillary acidic protein (GFAP, astrocyte marker; 1:1,500, Dako, USA), and anti-rabbit monoclonal antibodies against ionized calcium-binding adaptor molecule 1 (Iba1, microglia/macrophage-specific protein; 1:500, Wako, Japan). Incubation with primary antibodies lasted 16h at +4°C. After rinsing, sections were incubated with secondary antibodies for 1.5 h at room temperature in the dark: donkey anti-mouse Alexa Fluor 594, donkey anti-rabbit Alexa Fluor 647, and donkey anti-rabbit Alexa Fluor 488 (1:1,000, Invitrogen, USA). The sections were then rinsed, placed on histological slides, and mounted with Shandon Immu-Mount medium (Thermo Scientific, USA). Images of hippocampal tissue were taken with an FV1000-BX61WI confocal microscope at 20× (NA – 0.4) and 40× (NA – 0.65) objective magnifications (Olympus Corp., Japan).

To determine the intensity of postnatal neurogenesis, animals were intraperitoneally injected with 5-Bromo-2'-deoxyuridine in saline (BrdU, 50 mg/kg bw; Sigma-Aldrich, USA) two consecutive days before the perfusion (twice a day, at 10:00 and 17:00). 40-μm brain coronal sections (obtained as described above) were pre-treated with a 2N HCl for DNA denaturation during 1.5h at +37°C. After that, a standard immunohistochemical protocol was employed. Goat polyclonal antibodies against doublecortin (DCX, 1:250; Santa Cruz Biotechnology, USA) were used to detect neuroblasts. The proliferatively active cells were identified with rat monoclonal antibodies against BrdU (1:150; Bio-Rad AbD Serotec, UK). Donkey anti-goat Alexa Fluor 488 and goat anti-rat Alexa Fluor 546 secondary antibodies (1:1,000, Invitrogen, USA) were taken to display a marker-specific fluorescence. Confocal images of the dentate gyrus were obtained at 20× (NA – 0.4) objective magnification.

2.3.3. Light and transmission electron microscopy

As described above, collected hemispheres (n = 6 samples/condition) were postfixed overnight in a solution containing 4% PFA and 2.5% GA at +4°C. Next day, sample were histologically sliced into 300-μm-thick coronal sections using the vibratome Leica VT1000A (Leica Biosystems, Germany) on the levels of the hippocampus (bregma between −1.66 and −2.48 mm) and corpus callosum (bregma between 1.05 and −0.96 mm) (Lein et al., 2007). Samples were placed in 1% OsO_4 for 1 h, then dehydrated in an ascending series of ethanol, followed by dry acetone, and embedded in EPON resin (Sigma-Aldrich, Switzerland) according to a standard protocol (Weakley, 1972).

To quantify the hippocampal pyramidal neurons, semi-thin (1 μm) sections were prepared with an LKB 8800 ultramicrotome (LKB, Sweden), stained with methylene blue, embedded in a Pertex mounting medium (HistoLab Products AB, Sweden), and visualized using a Carl Zeiss Axiolab Re light microscope (Carl Zeiss AG, Germany) (objective magnification – 20×, NA – 0.40). For ultrastructural analysis, ultra-thin sections (60–70 nm) from the middle part of the CA1 *stratum radiatum* or corpus callosum were contrasted with uranyl acetate and lead citrate and examined using a JEM-100CX transmission electron microscope (Jeol, Japan) at magnifications of ×10,000 (hippocampal neuropil) or ×4,800 and ×6,400 (myelinated axons).

2.3.4. Quantifications and measurements

The brain morphology was performed using the ImageJ software, version 1.53k (https://imagej.nih.gov/ij/index.html; NIH, USA), and MyelTracer software (Kaiser et al., 2021) by a blind investigator. Quantitative parameters of the hippocampal neurons and glia – number density of neurons per mm^2 of the *stratum*

pyramidale, number densities of GFAP$^+$ astrocytes and Iba1$^+$ microglia per mm^2 of *stratum pyramidale* and *stratum radiatum*, glial cell surface area, astrocyte territory (area of brain tissue covered by individual astrocyte), the number of astrocytic and microglial base processes – were manually estimated in 3-5 sections/animal. The levels of postnatal neurogenesis in the dentate gyrus were assessed semi-automatically in 3-5 sections/mouse based on the integrated density of DCX$^+$ pixels per mm^2 of the subgranular zone and *stratum granulosum* and BrdU/DCX ratio. For this purpose, images were transformed to 8-bit, and a fixed background threshold was adjusted. Integrated density was calculated by multiplying the mean gray value of DCX$^+$ pixels above the background threshold with their total area within the region of interest (ROI). At the same time, BrdU/DCX ratio was obtained by dividing the overall area of BrdU$^+$ pixels by the total area of DCX$^+$ pixels within the ROI. Structural synaptic plasticity was manually evaluated on electron micrographs of the hippocampus (at least 20/animal) by such parameters: number density of synapses and their different morphological types – simple, perforated, and multiple ones per 100 μm^2 of the *stratum radiatum*, as well as the postsynaptic density length. Synapses were categorized into morphological groups as previously described (Shepilov et al., 2022), and their representative images are provided in **Supplementary Figure 1**. To characterize myelination in the *corpus callosum*, the density of myelinated axons was quantified on at least 20 micrographs/animal (magnification x4800). In addition, the diameter of myelinated axons (minimum 100/mouse) and G-ratio (minimum 50/mouse) were measured at magnification x6400. G-ratio, the ratio of the inner and outer radii of a myelinated axon (Mohammadi et al., 2015), is an inversely proportional indicator of the myelin sheath thickness. It was obtained using MyelTracer software as described elsewhere (Kaiser et al., 2021).

2.4. Evaluation of the intestinal barrier and blood-brain barrier (BBB) permeability

To study the physiological barrier permeability, a modified Evans Blue (EB) extravasation method was applied as described elsewhere (Uyama et al., 1988; Alves da Silva et al., 2011). Briefly, offspring mice were intravenously injected with 2% EB solution (4 mg/kg bw) in PBS. After 2 h, mice were anesthetized and perfused with an ice-cold 0.1M PBS. Then, brains and ileum tissue were isolated and homogenized in 0.5 ml of 0.1 M PBS, followed by adding 0.5 ml of 50% trichloroacetic acid. Specimens were vortexed for 2 min and left for 24 h at + 4°C to precipitate proteins. Next day, samples were centrifuged at 10,000 g in an Eppendorf 5415R refrigerated centrifuge (Eppendorf AG, Germany) for 20 min at +4°C. The EB absorbance was measured in supernatants at 610 nm and compared against a calibration curve (serial dilutions of the stock dye solution, concentration range is 0.1-50 μg/ml) using an LLG-uniSPEC2 spectrophotometer. Negative control values (homogenates of tissues from intact animals) normalized per unit mass were subtracted from sample values to obtain the final levels of EB leakage in the brain and intestine. The results were expressed as ng of EB/mg of tissue.

2.5. Statistical analysis

Statistical analysis was performed in the GraphPad Prism, version 8.0.2 (GraphPad Software, Inc., USA). The normality distribution of experimental data was evaluated using the Shapiro–Wilk normality test, and the equality of variances was determined with Levene's test. Data conformed to the Gaussian distribution were described as the Mean ± SEM and processed using the one-way ANOVA followed by Dunnett's *post hoc* test. Meanwhile, data with non-Gaussian distribution were presented as Median and interquartile range (IQR, 25th–75th percentile). Comparative statistics, in that case, was performed with the Kruskal–Wallis test, followed by Dunn's *post hoc* test. Relationship between variables was assessed using the Pearson correlation for data with normal distribution and the Spearman correlation for non-parametric variables. R value of 0–0.29, 0.3–0.49, and >0.5 indicates weak, moderate, and strong correlation, respectively. Differences between groups were considered statistically significant when $p < 0.05$.

3. Results

3.1. Long-term associative memory

First, we investigated associative recognition memory using the NOR test. During the familiarization phase, animals of all groups spent equal time with each identical object, as indicated by the exploratory preference for the 2nd object ranged between 49.2 and 52.9% (**Supplementary Figure 2A**). Nevertheless, a 24-h delay appeared to be a long period for maintaining a memory trace in young mice. The preference index, which characterizes a relative time exploring the novel object, stood at 49.4 ± 6.1, 46.4 ± 3.9, and 49.7 ± 4.7% for the control, 2-w antibiotics, and 3-w antibiotics groups in that order (**Supplementary Figure 2B**).

3.2. Spatial memory and learning

Next, we evaluated whether offspring exposed to antibiotics *in utero* demonstrated pathological changes in their spatial memory and learning alterations. Using the MWM test, we observed that the MAA significantly affected spatial reference memory and the hippocampus-related spatial learning in offspring mice (**Figure 2**). It was revealed that latency to find the hidden platform increased by 124% ($p < 0.001$) and 59% ($p < 0.05$) in the 2-w antibiotics group and by 57% ($p = 0.08$) and 77% ($p < 0.05$) in the 3-w antibiotics group on the 2nd and 3rd days of acquisition, respectively, compared with the control group. In addition, a tendency ($p = 0.08$) to extend the time necessary to reach the platform on the 4th day of testing was traced in 2-w antibiotics animals (**Figure 2A**). Similar to these results, 2-w antibiotics mice traveled 2.47 ($p < 0.001$) and 1.98 ($p < 0.01$) times longer distances on the 2nd and 3rd days of acquisition than their control peers. In contrast, 3-w antibiotics animals had 1.75 times greater ($p < 0.05$) path length on the 3rd day of the MWM test compared to controls (**Figure 2B**). Interestingly, 2-w antibiotics mice developed the highest speed in MWM, displaying a mean speed value during the 2nd day of testing 16% more ($p < 0.05$) than the same indicator in

control animals (Figure 2C). It should be also noted that offspring born form the 3-w antibiotics group dams memorized a location of the platform worse than others, spending 25% less time ($p = 0.06$) in the target quadrant during the probe test versus control animals (Figures 2D, E).

3.3. Functional integrity of physiological barriers

Because behavioral changes mediated by antibiotics often correlate with dysfunction of various blood-tissue barriers permeability (Kwon H. et al., 2020; Ray et al., 2021), we tested next the integrity of the intestinal barrier and blood-brain barrier (BBB) using the Evans blue (EB) leakage assay. It was detected that offspring born from the 2-w antibiotics group of dams had 2.45 times more EB concentration in the ileum tissue than those of the control group ($p < 0.05$; Supplementary Figure 3A). Furthermore, we also observed an elevated tendency for BBB disruption in offspring from the 2nd week of antibiotics exposure group ($p = 0.07$; Supplementary Figure 3B). In contrast, no or little effect on BBB leakage was observed in offspring collected from the group of dams exposed to antibiotics at the 3rd week of pregnancy (Supplementary Figure 3B).

3.4. Neuropathological changes in the hippocampal CA1 area

3.4.1. Hippocampal CA1 pyramidal neurons

Since dysbiosis-mediated inflammation in early life leads to increased dysfunction of CA1 pyramidal neurons in children and adults (Hagberg et al., 2012; Gomez et al., 2019), we tested next the $NeuN^+$ neuronal density in the CA1 *stratum pyramidale* using confocal microscopy assay (Figures 3A, B). To our knowledge, the density of $NeuN^+$ pyramidal neurons in offspring from the 2-w antibiotics and 3-w antibiotics groups was diminished ($p < 0.001$) compared to mice born from the control group of dams (Figure 3D).

Next, we evaluated the density of morphologically intact neurons, *i.e.,* neuronal cells with light blue nuclei, visible 1–3 nucleoli, thin normochromic cytoplasm, and clearly defined apical dendrites, using the light microscopy assay. To our knowledge, the density of morphologically intact neurons was also diminished in 2-w antibiotics ($p < 0.05$) and 3-w antibiotics ($p = 0.08$) compared to the control group (Figures 3C, E).

Finally, we aimed to find a possible correlation between MWM behavioral alterations and the number of $NeuN^+$ neurons in the hippocampus. Surprisingly, our data demonstrate a significant negative correlation between the diminished number of $NeuN^+$ neurons and average latency ($r = -0.39$; Figure 3F), and path length ($r = -0.42$; Figure 3G).

3.4.2. Morphological changes in astroglia and microglia in the hippocampus

Because a recently published study demonstrated that antibiotics promotes glial cells activation in adult mice (Çalışkan et al., 2022), we next aimed to evaluated whether MAA affects astroglia and microglia in 5-week-old offspring. The morphology and density of astrocytes and microglia in the CA1 hippocampal area was evaluated using GFAP and Iba1 markers, respectively (Figures 4A, B). There was a trend to reduce the density of astrocytes (by 12%; $p = 0.07$) in 3-w antibiotics mice (Figure 4C). In addition, the surface area of $GFAP^+$ cells and the size of astrocyte territories were significantly reduced by 21% ($p < 0.001$) and 18% ($p < 0.001$), respectively, in 2-w antibiotics offspring compared with that of the control offspring group (Figures 4D, E). In contrast, no significant differences in the density and surface area of $Iba1^+$ microglial cells were observed in antibiotic-treated and control groups of mice (Figures 4G, H). In addition, offspring also demonstrated a significant decrease in the number of astrocytic (2nd and 3rd-w antibiotics group) and microglial (3-w antibiotics group) base processes (Figures 4F, I), which is the evidence of de-ramification and glial cells activation (Schilling et al., 2004; Althammer et al., 2020).

3.5. Neurogenesis in the dentate gyrus

To further understand the impact of MAA on exacerbated neuropathological changes observed in offspring, the level of hippocampal neurogenesis was estimated by counting DCX^+ and $BrdU^+$ pixels in micrographs of the dentate gyrus (Figure 5A). The integrated density of DCX^+ pixels in the control group was $4.86 \pm 0.39 \times 10^6$ a.u. per mm^2 of the subgranular zone and *stratum granulosum*. By contrast, the DCX^+ density was significantly diminished by 13% and 23% ($p < 0.05$) in 2-w and 3-w antibiotics offspring, respectively, compared to control, indicating a decline in the number of neuroblasts and neurogenic potential (Figure 5B). Furthermore, the BrdU/DCX ratio in the 2-w antibiotics and 3-w antibiotics groups decreased by 24% ($p = 0.08$) and 44% ($p < 0.001$), respectively, compared to their control group (Figure 5C). These data indicated that the MAA is associated with diminished number of proliferatively active neuronal progenitors in offspring.

3.6. Structural synaptic plasticity

It is true that neurocognitive and emotional development is associated with synaptic structural and functional plasticity (Han et al., 2022). Therefore, we also evaluated the effects of MAA on the structural synaptic plasticity in offspring. All experimental groups were characterized by normal ultrastructure of the hippocampal neuropil, *i.e.,* synaptic contacts with clearly defined vesicles and postsynaptic density, as well as intact or moderately condensed mitochondria (Figure 6A). However, the total number of synapses and density of simple synapses in 3-w antibiotics offspring was reduced by 10% ($p < 0.05$) and 9% ($p < 0.05$), respectively, compared to control group (Figures 6B, C). No significant fluctuations in the density of perforated, multiple synaptic types, and postsynaptic density length between groups were observed (Figures 6D–F).

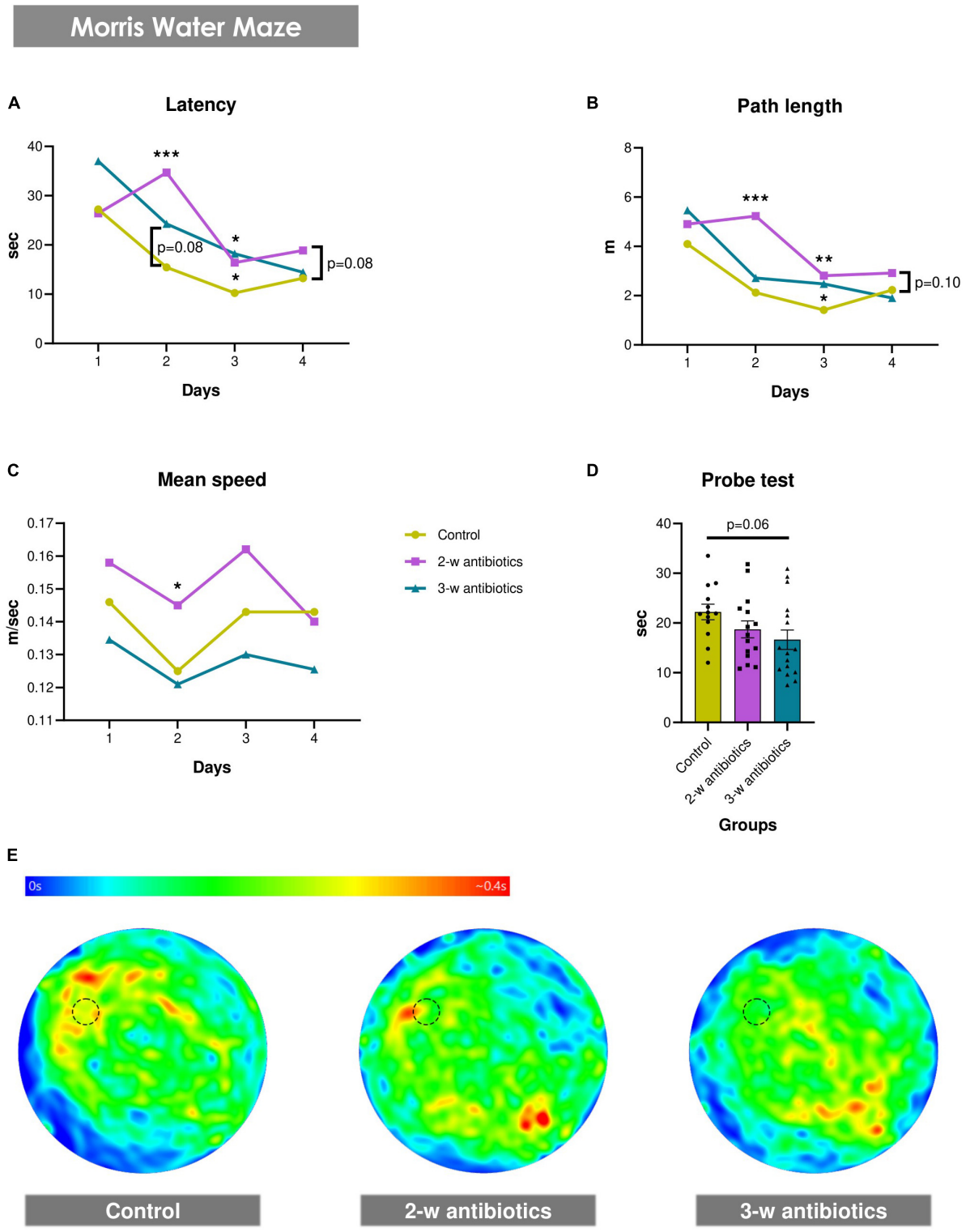

FIGURE 2
Spatial memory and learning in young mice born to antibiotic-treated C57BL/6J females. **(A–E)** Morris water maze test: **(A)** latency to find a hidden platform, **(B)** path length, and **(C)** mean speed during the acquisition task, as well as **(D)** time in the target quadrant of the water pool and **(E)** heat maps with animals' trajectories in the probe test. Dotted line circle on the heat map corresponds with the position of the hidden platform. Data on panels **(A–C)** are expressed as the Median with IQR, while data on graph 2D are expressed as the Mean ± SEM and presented in the form of dot plots (n = 13-16/group). Comparisons among groups were performed with either the one-way ANOVA followed by Dunnett's *post hoc* test (data with Gaussian distribution) or the Kruskal-Wallis test followed by Dunn's *post hoc* test (data with non-parametric distribution). *$p < 0.05$, **$p < 0.01$, and ***$p < 0.001$.

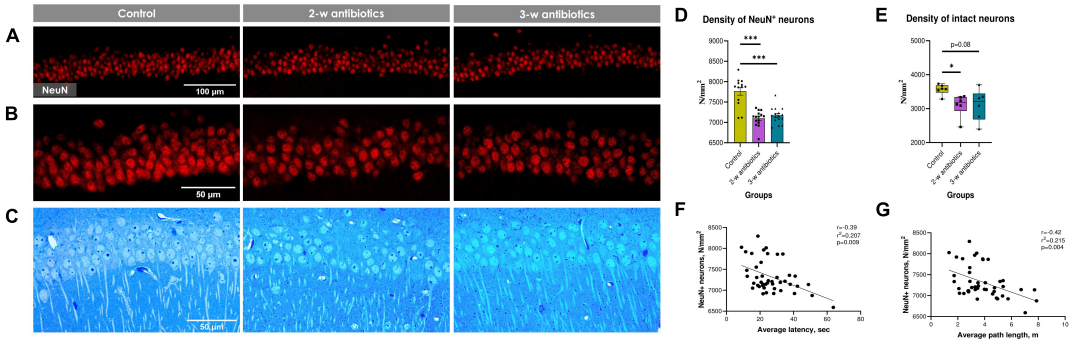

FIGURE 3
Hippocampal CA1 pyramidal neurons of the experimental mice. **(A,B)** Immunohistochemical images of NeuN$^+$ neurons in the CA1 *stratum pyramidale* at **(A)** 20× and **(B)** 40× objective magnifications. **(C)** Methylene blue-stained semi-thin sections of the *stratum pyramidale* used for light microscopic analysis (40x objective magnification). **(D)** The number of NeuN$^+$ cells per mm^2 of the pyramidal layer. **(E)** The number of intact (normochromic) neurons per mm^2 of the pyramidal layer on semi-thin sections. **(F,G)** Correlational analysis between the density of NeuN$^+$ cells and **(F)** average latency, **(G)** average path length during the acquisition task in MWM. Data on panel **(D)** are expressed as the Mean ± SEM and presented in the form of dot plots, whereas data on panel **(E)** are expressed as the Median with IQR and visualized using box and whisker plots (n = 6/group). Comparisons among groups were performed with either the one-way ANOVA followed by Dunnett's *post-hoc* test (data with Gaussian distribution) or the Kruskal–Wallis test followed by Dunn's *post hoc*-test (data with non-parametric distribution). *$p < 0.05$ and ***$p < 0.001$.

3.7. Myelination in the corpus callosum

Since our group and others demonstrated that intensive demyelination plays a critical role in the brain pathology (Pivneva et al., 2003; Chang et al., 2016; Yatsenko et al., 2020), we tested next myelination process in the corpus callosum. Morphological analysis revealed an altered myelination process in offspring exposed to antibiotics either at the 2nd or the 3rd week of gestation. This was structurally displayed in a stratification, curving, and vacuolization of myelin sheaths compared to control animals (**Figure 7A**). Furthermore, the density of myelinated axons decreased by 16% in 3-w antibiotics offspring (p = 0.07; **Figure 7B**), while 2-w antibiotics mice had 14% less diameter of axons ($p < 0.05$; **Figure 7C**) vs. control group of offspring. In addition, we detected statistically significant differences in the G-ratio values between the control (0.814 ± 0.005 a.u.) and 2-w antibiotics (0.856 ± 0.006 a.u.; $p < 0.001$) as well as 3-w antibiotics (0.844 ± 0.008 a.u.; $p < 0.01$) groups (**Figures 7D, E**). Therefore, these data indicate insufficient axonal myelination (hypo-myelination) in offspring under exposure to antibiotics cocktail at different time points of embryogenesis.

Finally, we tested whether hypo-myelination correlates with behavioral alterations and number of NeuN$^+$ cells in offspring. To our knowledge, we detected significant positive correlations between the G-ratio and MWM average latency (r = 0.66; **Figure 7F**) and path length (r = 0.71; **Figure 7G**). In contrast, G-ratio negatively correlates with the density of NeuN$^+$ pyramidal neurons in the hippocampus (r = −0.64; **Figure 7H**). Altogether, MAA affects the density and size of myelinated axons and the thickness of the myelin sheath, which correlates with behavioral and neuropathological alterations in offspring.

4. Discussion

Although pregnancy is considered a physiological state, most pregnant women frequently receive antibiotics to prevent maternal or neonatal complications (Siriwachirachai et al., 2014). Published clinical studies demonstrated the beneficial effects of MAA in the context of preterm labor, intrapartum fever, prevention of neonatal Group B *Streptococcus* fever, and cesarean section (de Tejada, 2014). In contrast, emerging evidence demonstrated that MAA unbalances women's vaginal microbiota, associated with establishing the newborn gut microbiota (Zhou et al., 2020). In addition, MAA influences neuro-immune response in children and teens, leading to neurobehavioral disorders, *e.g.,* altered recognition memory responses, early types of dementia, and autism (de Tejada, 2014; Kuperman and Koren, 2016; Makinson et al., 2017; Helaly et al., 2019; Cao et al., 2021; Hickey et al., 2021; Kim et al., 2022; Madany et al., 2022a). Furthermore, antibiotic abuse is a common health hazard in Low and Middle-income countries, including Ukraine (Helaly et al., 2019; Higgins et al., 2020; Jeżak and Kozajda, 2022). A study reported that leaky gut and endotoxemia exacerbate neuroinflammation in adulthood (Alhasson et al., 2017). In addition, concerns were reported regarding the safety of antibiotics in pregnancy (Taylor-Cousar et al., 2021). Surprisingly, a study reported that delayed azithromycin treatment of mice with spinal cord injury improves their recovery (Kopper et al., 2019), indicating that antibiotics may influence neuronal dysfunction and healing. It was also reported that maternal gut dysbiosis and subsequent imbalance of bacterial metabolites correlates with cognition and neurodevelopment observed in offspring (Fröhlich et al., 2016; Madany et al., 2022b). In addition, published studies demonstrated that amoxicillin and azithromycin cross the placental barrier of mammals within two hours after their oral administration (Sutton et al., 2015; Atli et al., 2016; Zareba-Szczudlik et al., 2017; Louchet et al., 2020) and have direct impact on fetal organogenesis (Lin et al., 2012; Louchet et al., 2020). Therefore, we aimed to examine whether widely used antibiotic in gynecological practice, including amoxicillin and azithromycin, affects behavior and neurodevelopment in offspring.

In the present study, we demonstrated that exposure of pregnant dams to a cocktail of antibiotics affected the spatial reference memory and hippocampus-related spatial learning in

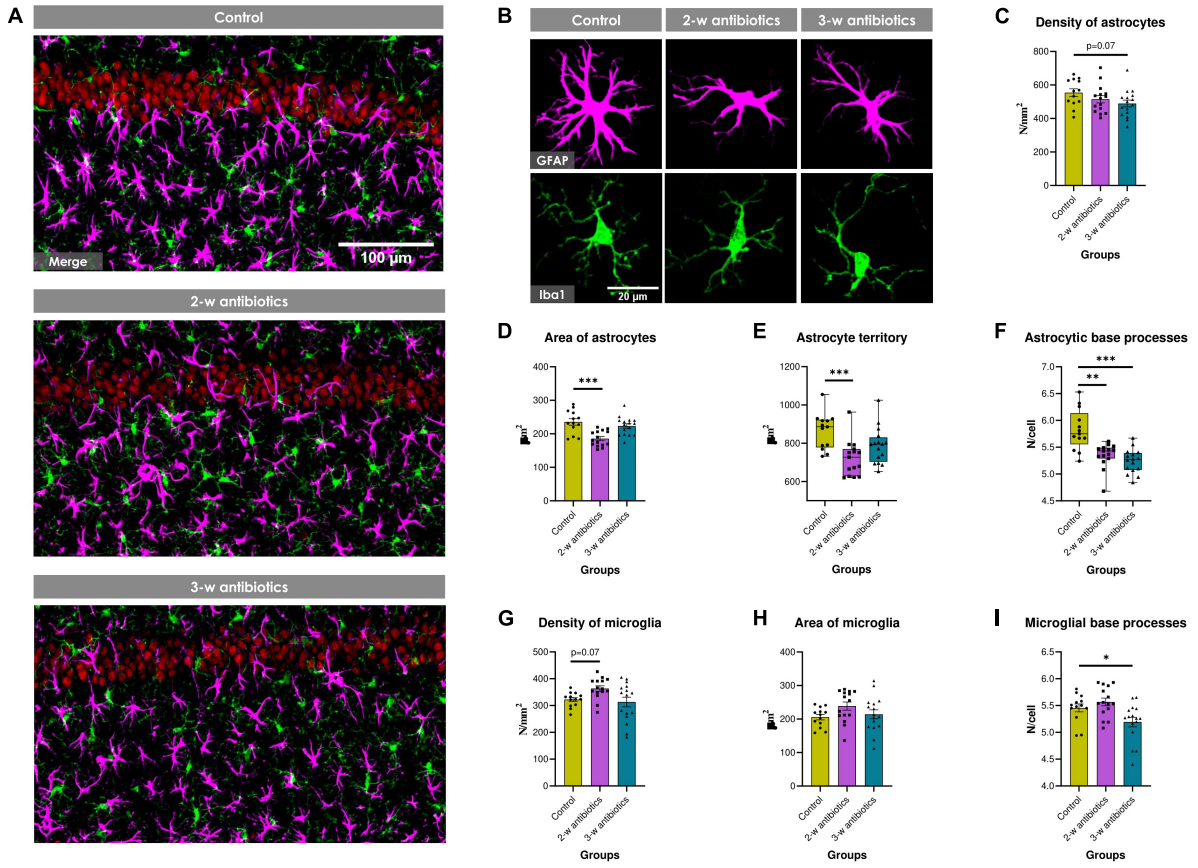

FIGURE 4
Glial cells in the hippocampus of young offspring animals. **(A)** Immunofluorescent-labeled images of the CA1 *stratum pyramidale* and *stratum radiatum* at 20× objective magnification: red—NeuN$^+$ neurons, green—Iba1$^+$ microglia, magenta—GFAP$^+$ astrocytes. **(B)** Images of individual glial cells at higher objective magnification (40×) displaying fine morphology of cellular somas and processes: magenta—GFAP$^+$ astrocytes, green—Iba1$^+$ microglia. **(C–I)** Morphometric indicators of hippocampal glia: the number density of **(C)** astrocytes and **(G)** microglial cells per mm^2 of brain tissue, the cell surface area of **(D)** astrocytes and **(H)** microglia, **(E)** astrocyte territory, as well as the mean number of **(F)** astrocytic and **(I)** microglial base processes. Data on graphs 4E/F are expressed as the Median with IQR and visualized using box and whisker plots, while data on other graphs are expressed as the Mean ± SEM and presented in the form of dot plots (n = 13–16/group). Comparisons among groups were performed with either the one-way ANOVA followed by Dunnett's *post-hoc* test (data with Gaussian distribution) or the Kruskal-Wallis test followed by Dunn's *post-hoc* test (data with non-parametric distribution). *$p < 0.05$, **$p < 0.01$, and ***$p < 0.001$.

offspring mice (Figure 2). Such results corresponded to the previously published studies showing that early-life exposure to the antibiotic in mice triggered mechanical allodynia, depressive-like behavior, and damaged spatial memory performance in MWM (Wang et al., 2021). Furthermore, it was demonstrated that antibiotics influenced the impairment of recognition memory and increased anxiety and depression in adult mice (Lurie et al., 2015; Kwon H. et al., 2020). Unfortunately, the major limitation of our findings is that no sex-specific data analysis was performed. Because antibiotic treatment during pregnancy alters offspring gut microbiota in a sex-dependent manner (Madany et al., 2022a), further studies are warranted.

In addition to behavioral changes, early published studies demonstrated that antibiotics promote gut dysbiosis-mediated intestinal hyperpermeability and BBB disruption (Fröhlich et al., 2016; Boutin et al., 2018; Lai et al., 2020). In this study, we also showed that exposure to pregnant dams during the 2nd week of pregnancy dramatically elevates intestinal permeability in offspring (Supplementary Figure 3A). Furthermore, a positive trend close to the statistical significance of the permeability of BBB was observed in those offspring (Supplementary Figure 3B). These findings corresponded to the previously published reports that both amoxicillin and azithromycin penetrate the blood brain barrier in healthy individuals even without CNS inflammation (Mingrino et al., 1981; Viaggi et al., 2022), and antibiotics may contribute to the BBB breakdown in offspring (O'Connor et al., 2021). Besides the role of BBB in central nervous protection, it also engaged in behavioral disorders (Dion-Albert et al., 2022). In addition, declined physiological barriers integrity observed under the direct impact of antibiotics and/or antibiotic-induced dysbiosis at the 2nd week of gestation may be associated with the terms of morphogenesis and formation of these barriers during embryogenesis. More specifically, the parenchyma of the murine fetal brain starts less permeable to infrared-labeled IgG2b at E15.5 to E17.5, evidencing the BBB development during this time (Braniste et al., 2014), while morphogenesis of the intestinal epithelium begins at E14.5 in mice (also the 3rd week of embryogenesis) (Kwon O. et al., 2020). Importantly, pathogen-free gut microbiota promotes healthy barriers establishment (Braniste et al., 2014). We assume that the 2nd week of pregnancy in

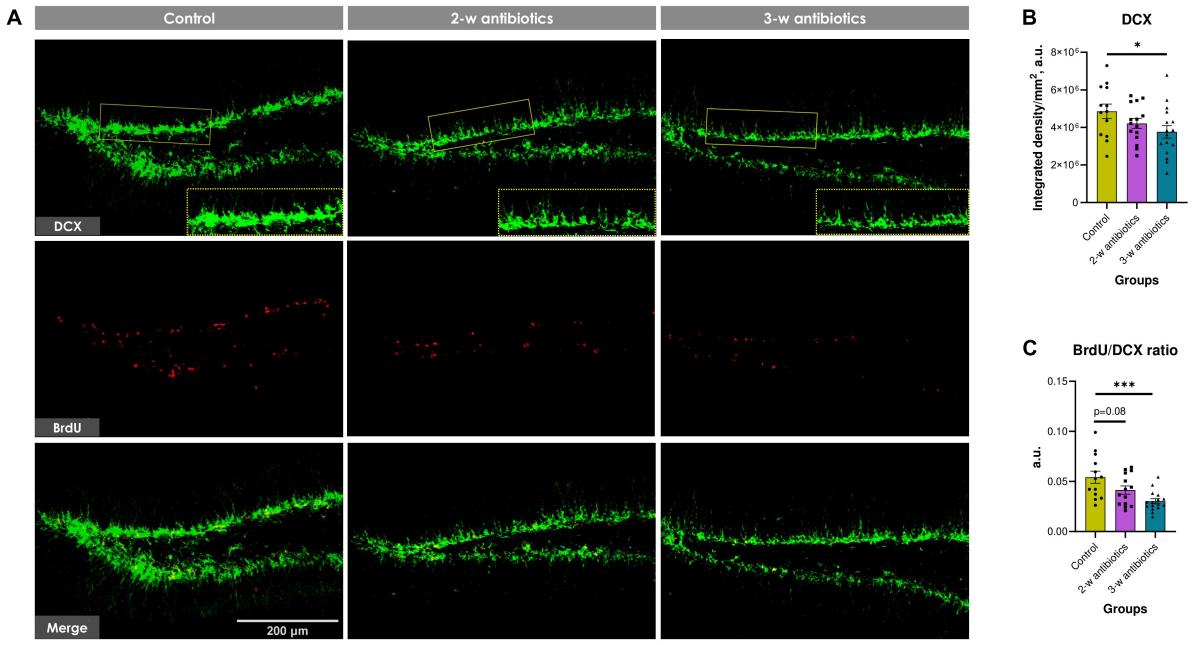

FIGURE 5
Neurogenesis in the dentate gyrus of C57BL/6J mice born to antibiotic-treated dams. **(A)** Immunofluorescent-labeled images of DCX$^+$ neuroblasts (green) and BrdU$^+$ proliferating cells (red) at 20× objective magnification. We used crops of DCX$^+$ cells denoted by the yellow dotted line for morphometric analysis. **(B)** The integrated density of DCX$^+$ pixels per mm^2 of the subgranular zone and *stratum granulosum*. **(C)** The relative proliferation rate of neuroblasts (BrdU/DCX ratio). Data are expressed as the Mean ± SEM (n = 13–16/group). Comparisons among groups were performed with the one-way ANOVA followed by Dunnett's *post-hoc* test. *$p < 0.05$ and ***$p < 0.001$.

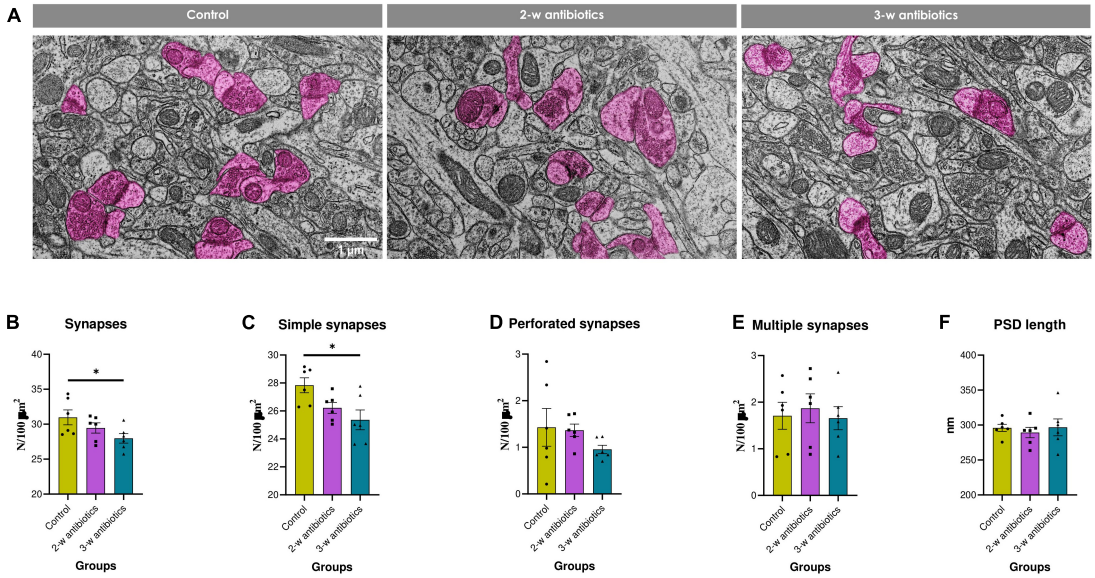

FIGURE 6
Structural synaptic plasticity in the hippocampal CA1 area of young offspring mice. **(A)** Electron micrographs of the *stratum radiatum* (×10,000). Synapses are marked in pink. **(B–F)** Morphometric characteristics of the neuropil: the number density of **(B)** synaptic contacts and their different morphological types—**(C)** simple, **(D)** perforated, and **(E)** multiple ones per 100 µm^2 of brain tissue, as well as the **(F)** postsynaptic density length. Data are expressed as the Mean ± SEM (n = 6/group). Comparisons among groups were performed with the one-way ANOVA followed by Dunnett's *post-hoc* test. *$p < 0.05$.

mice might be a critical window where microbiota-shifting factors, including antibiotics, can impact some cellular or molecular targets related to the subsequent formation of both the intestinal barrier and BBB in a fetus.

As supported by the current paradigm of behavioral biology and neuroinflammation, intestinal flora dysbiosis mediated by antibiotics may influence cerebral metabolites and cause morphological and functional rearrangements of neurons and

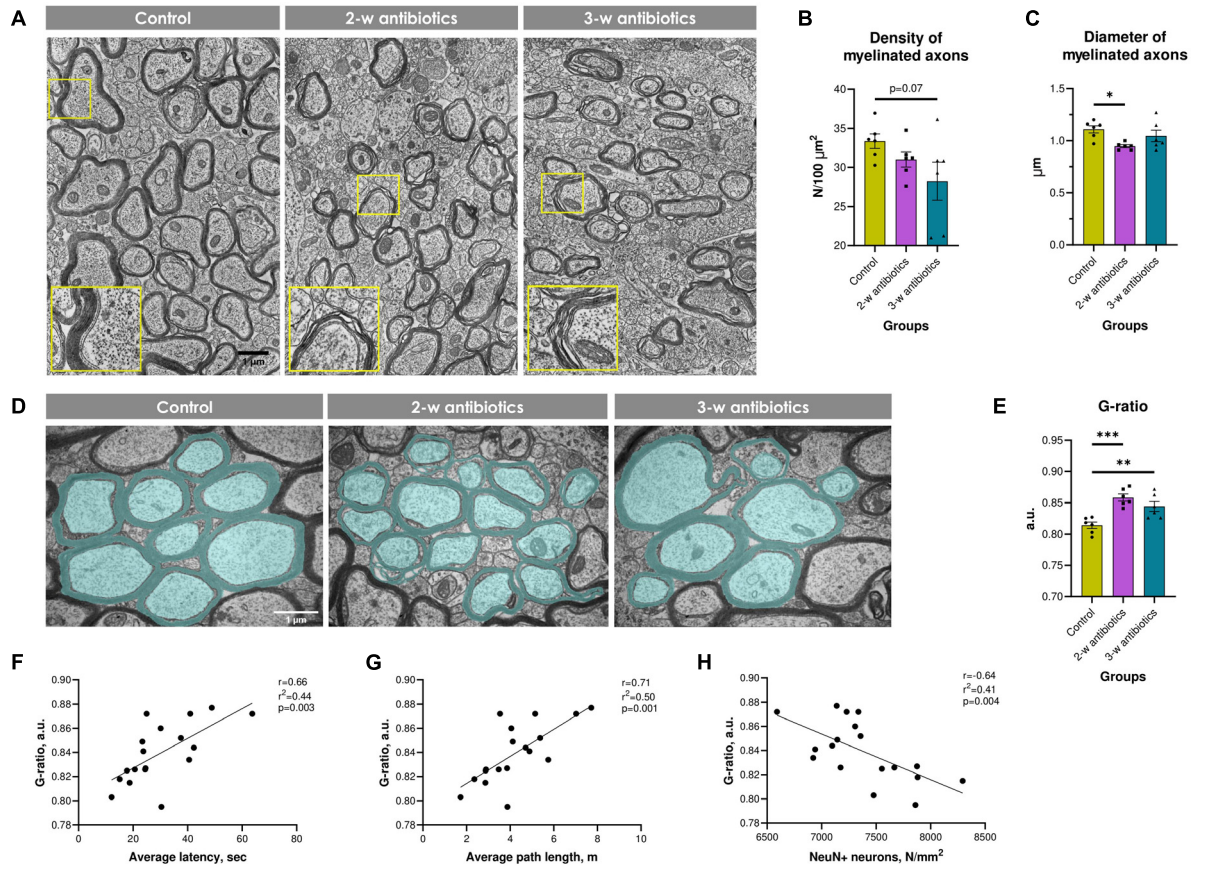

FIGURE 7
Myelination in the corpus callosum of experimental animals. **(A)** Electron micrographs of myelinated and unmyelinated axons in the corpus callosum (×4,800). Enlarged crops framed in yellow provide a more detailed morphology of myelin sheaths. **(B)** The density of myelinated axons per 100 μm^2 of brain tissue. **(C)** Mean diameter of myelinated axons. **(D)** Electron micrographs of the corpus callosum pseudocolorized in MyelTracer software for quantification of the G-ratio: light green—axons, dark green—myelin (×6,400). **(E)** G-ratio. **(F–H)** Correlational analysis between G-ratio and **(F)** average latency during the acquisition task in MWM, **(G)** average path length in MWM, **(H)** the density of $NeuN^+$ neurons in the hippocampus. Data are expressed as the Mean ± SEM (n = 6/group). Comparisons among groups were performed with the one-way ANOVA followed by Dunnett's *post-hoc* test. *$p < 0.05$, **$p < 0.01$, and ***$p < 0.001$.

glia in brain areas controlling behavior (Guida et al., 2018). Here, we observed that the density of CA1 pyramidal neurons was diminished in offspring born to dams exposed to antibiotics during the 2nd and 3rd week of pregnancy. Neuronal loss in the hippocampus corresponded with the deterioration of spatial reference memory found in the MWM test (**Figure 3**). Similar to our results, it was previously demonstrated the correlation between the reduction of hippocampal neuronal density and spatial memory loss in rats (Hagberg et al., 2012; Gomez et al., 2019). Lee et al. also reported a reduced $BDNF^+/NeuN^+$ cell population in the hippocampus of antibiotic-treated mice with global forebrain ischemia (Lee et al., 2020).

A large epidemiological study demonstrated the association between MAA and an increased risk of developing various CNS disorders in the offspring via dysregulation of microglia function and myelination (Kenyon et al., 2008; Dash et al., 2022). In this study, no notable changes were observed in microglial morphology that could be linked with neuroinflammation in offspring mice; however, cellular hypotrophy of the hippocampal astrocytes and reduction in astrocyte territories were detected in young animals born from 2nd-week antibiotic-treated dams (**Figure 4**) that may point to compromised homeostasis in the brain tissue (Verkhratsky et al., 2019).

Meanwhile, offspring from the 3-w antibiotics group were characterized by depletion of neurogenesis in the dentate gyrus (**Figure 5**) and synaptic loss in the hippocampal CA1 neuropil (**Figure 6**). It is commonly accepted that brain synaptogenesis in mice is the most prominent from the 3rd week of embryogenesis to the 2nd week after birth (Chen et al., 2017). In addition, the 3rd week of gestation (specifically, E14.5) is dentate precursors start to migrate from the ventricular zone, and the dentate gyrus becomes distinguishable (UrbÃin and Guillemot, 2014). It coincided with the most vulnerable time point to MAA we demonstrated for the postnatal hippocampal neurogenesis. Additionally, our data complement previous findings indicating a statistically significant decrease in DCX- and BrdU-labeled cells in the dentate gyrus of 4-week-old male germ-free mice (Scott et al., 2020).

Although myelination in the murine corpus callosum occurs postnatally between P14 and P45 (Sturrock, 1980), the production of oligodendrocyte precursor cells in the fetal brain begins on E12.5. It encompasses several waves till early post-embryogenesis (Chen et al., 2017). It could be partially correlated with our current

observations where MAA at both the 2nd and 3rd weeks of pregnancy-induced the impairments of myelination in the corpus callosum of offspring mice (**Figure 7**). Furthermore, published observations suggested that either antibiotics consumption or gut microbiota depletion affects the normal myelination process in the brain. For instance, oral administration of antibiotics was shown to enhance cuprizone-induced demyelination in C57BL/6J mice (Chen et al., 2019). Lu et al. reported that myelin quantity was significantly less in the corpus callosum of 4-week-old germ-free offspring than in specific-pathogen-free mice (Lu et al., 2018).

In sum, we discovered that MAA at different times of pregnancy could pathologically alter cognitive behavior and brain development in offspring at an early age after weaning. Thus, the results of this study may lay the groundwork for developing novel therapeutic regimens for pregnant women which will protect their offspring from the development of neuroinflammation and neurodegeneration in adulthood.

Data availability statement

The original contributions presented in this study are included in the article/**Supplementary material**, further inquiries can be directed to the corresponding authors.

Ethics statement

This animal study was reviewed and approved by the Biomedical Ethics Committee at the Bogomoletz Institute of Physiology, National Academy of Sciences of Ukraine.

Author contributions

GS, AM, and DS designed the study. DS, IO, TK, and AC performed procedures with experimental animals, behavioral tests, and sample collection. DS, IO, TK, KS, CY, SG, and GO conducted a morphological analysis of the brain. DS, AM, and GS interpreted the results. All authors contributed to the writing and revising of the manuscript.

Funding

This research was funded by a grant from the National Academy of Sciences of Ukraine 0122U002424 (GS) and NIH Grants R01AG-064003 and K02AG-068595 (AM).

Acknowledgments

We thank Andrii Khomiak for his help with animal maintenance, Dmytro Ilienko and Valerii Hryb for their assistance in behavioral testing, as well as Iryna Lushnikova for her involvement in morphometric analysis of immunofluorescent images.

Conflict of interest

The authors declare that the research was conducted in the absence of any commercial or financial relationships that could be construed as a potential conflict of interest.

Publisher's note

All claims expressed in this article are solely those of the authors and do not necessarily represent those of their affiliated organizations, or those of the publisher, the editors and the reviewers. Any product that may be evaluated in this article, or claim that may be made by its manufacturer, is not guaranteed or endorsed by the publisher.

Supplementary material

The Supplementary Material for this article can be found online at: https://www.frontiersin.org/articles/10.3389/fncel.2023.1176676/full#supplementary-material

References

Ahmadi, H., Ebrahimi, A., and Ahmadi, F. (2021). Antibiotic therapy in dentistry. *Int. J. Dent.* 2021, 1–10. doi: 10.1155/2021/6667624

Alhasson, F., Das, S., Seth, R., Dattaroy, D., Chandrashekaran, V., Ryan, C., et al. (2017). Altered gut microbiome in a mouse model of gulf war illness causes neuroinflammation and intestinal injury via leaky gut and TLR4 activation. *PLoS One* 12:e0172914. doi: 10.1371/journal.pone.0172914

Althammer, F., Ferreira-Neto, H., Rubaharan, M., Roy, R., Patel, A., Murphy, A., et al. (2020). Three-dimensional morphometric analysis reveals time-dependent structural changes in microglia and astrocytes in the central amygdala and hypothalamic paraventricular nucleus of heart failure rats. *J. Neuroinflam.* 17:221.

Alves da Silva, J. A., Oliveira, K., and Camillo, M. (2011). Gyroxin increases blood-brain barrier permeability to evans blue dye in mice. *Toxicon* 57, 162–167.

Andrade, S., Gurwitz, J., Davis, R., Chan, K., Finkelstein, J., Fortman, K., et al. (2004). Prescription drug use in pregnancy. *Am. J. Obstet. Gynecol.* 191, 398–407. doi: 10.1016/j.ajog.2004.04.025

André, P., Laugerette, F., and Féart, C. (2019). Metabolic endotoxemia: a potential underlying mechanism of the relationship between dietary fat intake and risk for cognitive impairments in humans? *Nutrients* 11:1887. doi: 10.3390/nu11081887

Atli, O., Demir-Ozkay, U., Ilgin, S., Aydin, T., Akbulut, E., and Sener, E. (2016). Evidence for neurotoxicity associated with amoxicillin in juvenile rats. *Hum. Exp. Toxicol.* 35, 866–876. doi: 10.1177/0960327115607948

Barnhart, C., Yang, D., and Lein, P. (2015). Using the morris water maze to assess spatial learning and memory in weanling mice. *PLoS ONE* 10:e0124521. doi: 10.1371/journal.pone.0124521

Bookstaver, P., Bland, C., Griffin, B., Stover, K., Eiland, L., and McLaughlin, M. A. (2015). Review of antibiotic use in pregnancy. *Pharmacotherapy* 35, 1052–1062. doi: 10.1002/phar.1649

Boutin, R., Dwyer, Z., Farmer, K., Rudyk, C., Forbes, M., and Hayley, S. (2018). Perinatal antibiotic exposure alters composition of murine gut microbiota and may influence later responses to peanut antigen. *Allergy Asthma Clin. Immunol.* 14:42. doi: 10.1186/s13223-018-0263-8

Braniste, V., Al-Asmakh, M., Kowal, C., Anuar, F., Abbaspour, A., Tóth, M., et al. (2014). The gut microbiota influences blood-brain barrier permeability in mice. *Sci. Trans. Med.* 6:263. doi: 10.1126/scitranslmed.3009759

Çalışkan, G., French, T., Enrile Lacalle, S., del Angel, M., Steffen, J., Heimesaat, M., et al. (2022). Antibiotic-induced gut dysbiosis leads to activation of microglia and impairment of cholinergic gamma oscillations in the hippocampus. *Brain Behav. Immunity* 99, 203–217. doi: 10.1016/j.bbi.2021.10.007

Cao, X., Liu, K., Liu, J., Liu, Y., Xu, L., Wang, H., et al. (2021). Dysbiotic gut microbiota and dysregulation of cytokine profile in children and teens with autism spectrum disorder. *Front. Neurosci.* 15:635925. doi: 10.3389/fnins.2021.635925

Cardetti, M., Rodríguez, S., and Sola, A. (2020). Use (and abuse) of antibiotics in perinatal medicine. *Anales de Pediatría* 93, .207.e1–e7. doi: 10.1016/j.anpedi.2020.06.010

Carding, S., Verbeke, K., Vipond, D., Corfe, B., and Owen, L. (2015). Dysbiosis of the gut microbiota in disease. *Microbial. Ecol. Health Dis.* 26:26191. doi: 10.3402/mehd.v26.26191

Chang, K., Redmond, S., and Chan, J. (2016). Remodeling myelination: implications for mechanisms of neural plasticity. *Nat. Neurosci.* 19, 190–197. doi: 10.1038/nn.4200

Chen, T., Noto, D., Hoshino, Y., Mizuno, M., and Miyake, S. (2019). Butyrate suppresses demyelination and enhances remyelination. *J. Neuroinflam.* 16:165. doi: 10.1186/s12974-019-1552-y

Chen, V., Morrison, J., Southwell, M., Foley, J., Bolon, B., and Elmore, S. (2017). Histology atlas of the developing prenatal and postnatal mouse central nervous system, with emphasis on prenatal days e7.5 to e18.5. *Toxicol. Pathol.* 45, 705–744. doi: 10.1177/0192623317728134

Cipolla, M., Houston, E., Kraig, R., and Bonney, E. (2011). Differential effects of low-dose endotoxin on the cerebral circulation during pregnancy. *Rep. Sci.* 18, 1211–1221. doi: 10.1177/1933719111410712

Dash, S., Syed, Y., and Khan, M. (2022). Understanding the role of the gut microbiome in brain development and its association with neurodevelopmental psychiatric disorders. *Front. Cell Dev. Biol.* 10:880544. doi: 10.3389/fcell.2022.880544

de Tejada, B. (2014). Antibiotic use and misuse during pregnancy and delivery: benefits and risks. *IJERPH* 11, 7993–8009. doi: 10.3390/ijerph110807993

Dinan, T., and Cryan, J. (2017). Brain–gut–microbiota axis — mood, metabolism and behaviour. *Nat. Rev. Gastroenterol. Hepatol.* 14, 69–70. doi: 10.1038/nrgastro.2016.200

Dion-Albert, L., Cadoret, A., Doney, E., Kaufmann, F., Dudek, K., Daigle, B., et al. (2022). Vascular and blood-brain barrier-related changes underlie stress responses and resilience in female mice and depression in human tissue. *Nat. Commun.* 13:164. doi: 10.1016/j.biopsych.2022.02.447

Emanoil, A., Stochino Loi, E., Feki, A., and Ben Ali, N. (2021). Focusing treatment on pregnant women with COVID disease. *Front. Glob. Womens Health* 2:590945. doi: 10.3389/fgwh.2021.590945

Estrada, S., Thagard, A., Dehart, M., Damicis, J., Dornisch, E., Ippolito, D., et al. (2020). The orphan nuclear receptor Nr4a1 mediates perinatal neuroinflammation in a murine model of preterm labor. *Cell Death Dis.* 11:11. doi: 10.1038/s41419-019-2196-7

Fröhlich, E., Farzi, A., Mayerhofer, R., Reichmann, F., Jaèan, A., Wagner, B., et al. (2016). Cognitive impairment by antibiotic-induced gut dysbiosis: analysis of gut microbiota-brain communication. *Brain Behav. Immunity* 56, 140–155. doi: 10.1016/j.bbi.2016.02.020

Gomez, C., Read, J., Acharjee, S., and Pittman, Q. (2019). Early life inflammation increases ca1 pyramidal neuron excitability in a sex and age dependent manner through a chloride homeostasis disruption. *J. Neurosci.* 39, 7244–7259. doi: 10.1523/JNEUROSCI.2973-18.2019

Goncharova, K., Skibo, G., Kovalenko, T., Osadchenko, I., Ushakova, G., Vovchanskii, M., et al. (2015). Diet-induced changes in brain structure and behavior in old gerbils. *Nutr. Diabet.* 5:e163. doi: 10.1038/nutd.2015.13

Guida, F., Turco, F., Iannotta, M., De Gregorio, D., Palumbo, I., Sarnelli, G., et al. (2018). Antibiotic-induced microbiota perturbation causes gut endocannabinoidome changes, hippocampal neuroglial reorganization and depression in mice. *Brain Behav. Immunity* 67, 230–245. doi: 10.1016/j.bbi.2017.09.001

Hagberg, H., Gressens, P., and Mallard, C. (2012). Inflammation during fetal and neonatal life: Implications for neurologic and neuropsychiatric disease in children and adults. *Ann. Neurol.* 71, 444–457. doi: 10.1002/ana.22620

Han, W., Pan, Y., Han, Z., Huang, D., Hong, S., Song, X., et al. (2022). Advanced maternal age impairs synaptic plasticity in offspring rats. *Behav. Brain Res.* 425:113830. doi: 10.1016/j.bbr.2022.113830

Heijtz, R., Wang, S., Anuar, F., Qian, Y., Björkholm, B., Samuelsson, A., et al. (2011). Normal gut microbiota modulates brain development and behavior. *Proc. Natl. Acad. Sci. U.S.A.* 108, 3047–3052. doi: 10.1073/pnas.1010529108

Helaly, A., El-Attar, Y., Khalil, M., Ahmed Ghorab, D., and El- Mansoury, A. (2019). Antibiotic abuse induced histopathological and neurobehavioral disorders in mice. *CDS* 14, 199–208. doi: 10.2174/1574886314666190612130921

Hickey, M., Miller, N., Haapala, J., Demerath, E., Pfister, K., Georgieff, M., et al. (2021). Infants exposed to antibiotics after birth have altered recognition memory responses at one month of age. *Pediatr. Res.* 89, 1500–1507. doi: 10.1038/s41390-020-01117-7

Higgins, P., Hagen, R., Podbielski, A., Frickmann, H., and Warnke, P. (2020). Molecular epidemiology of carbapenem-resistant *Acinetobacter baumannii* isolated from war-injured patients from the eastern ukraine. *Antibiotics* 9:579. doi: 10.3390/antibiotics9090579

Januszek, S., Siwiec, N., Januszek, R., Kluz, M., Lebed, R., Toś, P., et al. (2022). Approach of pregnant women from poland and the ukraine to COVID-19 vaccination—the role of medical consultation. *Vaccines* 10:255. doi: 10.3390/vaccines10020255

Jeżak, K., and Kozajda, A. (2022). Occurrence and spread of antibiotic-resistant bacteria on animal farms and in their vicinity in poland and ukraine—review. *Environ. Sci. Pollut. Res.* 29, 9533–9559. doi: 10.1007/s11356-021-17773-z

Kaiser, T., Allen, H., Kwon, O., Barak, B., Wang, J., He, Z., et al. (2021). MyelTracer: a semi-automated software for myelin g -ratio quantification. *eNeuro* 8:ENEURO.0558-20.2021. doi: 10.1523/ENEURO.0558-20.2021

Kenyon, S., Pike, K., Jones, D., Brocklehurst, P., Marlow, N., Salt, A., et al. (2008). Childhood outcomes after prescription of antibiotics to pregnant women with spontaneous preterm labour: 7-year follow-up of the ORACLE II trial. *Lancet* 372, 1319–1327. doi: 10.1016/S0140-6736(08)61203-9

Kim, M., Park, S., Choi, S., Chang, J., Kim, S., Jeong, S., et al. (2022). Association between antibiotics and dementia risk: a retrospective cohort study. *Front. Pharmacol.* 13:888333. doi: 10.3389/fphar.2022.888333

Kopper, T., McFarlane, K., Bailey, W., Orr, M., Zhang, B., and Gensel, J. (2019). Delayed azithromycin treatment improves recovery after mouse spinal cord injury. *Front. Cell Neurosci.* 13:490. doi: 10.3389/fncel.2019.00490

Kuperman, A., and Koren, O. (2016). Antibiotic use during pregnancy: how bad is it? *BMC Med.* 14:91. doi: 10.1186/s12916-016-0636-0

Kurita, N., Yamashiro, K., Kuroki, T., Tanaka, R., Urabe, T., Ueno, Y., et al. (2020). Metabolic endotoxemia promotes neuroinflammation after focal cerebral ischemia. *J. Cereb. Blood Flow Metab.* 40, 2505–2520. doi: 10.1177/0271678X19899577

Kwon, H., Mohammed, A., Eltom, K., Albrahim, J., and Alburae, N. (2020). Evaluation of antibiotic-induced behavioral changes in mice. *Physiol. Behav.* 223:113015. doi: 10.1016/j.physbeh.2020.113015

Kwon, O., Han, T., and Son, M. (2020). Intestinal morphogenesis in development, regeneration, and disease: the potential utility of intestinal organoids for studying compartmentalization of the crypt-villus structure. *Front. Cell. Dev. Biol.* 8:593969. doi: 10.3389/fcell.2020.593969

Lai, J., Svedin, P., Ek, C., Mottahedin, A., Wang, X., Levy, O., et al. (2020). Vancomycin is protective in a neonatal mouse model of staphylococcus epidermidis -potentiated hypoxic-ischemic brain injury. *Antim. Agents Chemother.* 64, e2003–e2019. doi: 10.1128/AAC.02003-19

Lee, K., Kim, J., and Kim, D. (2020). Orally administered antibiotics vancomycin and ampicillin cause cognitive impairment with gut dysbiosis in mice with transient global forebrain ischemia. *Front. Microbiol.* 11:564271. doi: 10.3389/fmicb.2020.564271

Lein, E., Hawrylycz, M., Ao, N., Ayres, M., Bensinger, A., Bernard, A., et al. (2007). Genome-wide atlas of gene expression in the adult mouse brain. *Nature* 445, 168–176. doi: 10.1038/nature05453

Lin, K., Mitchell, A., Yau, W., Louik, C., and Hernández-Díaz, S. (2012). Maternal exposure to amoxicillin and the risk of oral clefts. *Epidemiology* 23, 699–705. doi: 10.1097/EDE.0b013e318258cb05

Llor, C., Ouchi, D., Giner-Soriano, M., García-Sangenís, A., Bjerrum, L., and Morros, R. (2021). Correlation between previous antibiotic exposure and COVID-19 severity. A Population-Based Cohort Study. *Antibiotics* 10:1364. doi: 10.3390/antibiotics10111364

Louchet, M., Sibiude, J., Peytavin, G., Picone, O., Tréluyer, J., and Mandelbrot, L. (2020). Placental transfer and safety in pregnancy of medications under investigation to treat coronavirus disease 2019. *Am. J. Obstet. Gynecol. MFM* 2:100159. doi: 10.1016/j.ajogmf.2020.100159

Lu, J., Synowiec, S., Lu, L., Yu, Y., Bretherick, T., Takada, S., et al. (2018). Microbiota influence the development of the brain and behaviors in C57BL/6J mice. *PLoS One* 13:e0201829. doi: 10.1371/journal.pone.0201829

Lueptow, L. (2017). Novel object recognition test for the investigation of learning and memory in mice. *JoVE* 126:55718. doi: 10.3791/55718-v

Lurie, I., Yang, Y., Haynes, K., Mamtani, R., and Boursi, B. (2015). Antibiotic exposure and the risk for depression, anxiety, or psychosis: a nested case-control study. *J. Clin. Psychiatry* 76, 1522–1528. doi: 10.4088/JCP.15m09961

Madany, A., Hughes, H., and Ashwood, P. (2022a). Antibiotic treatment during pregnancy alters offspring gut microbiota in a sex-dependent manner. *Biomedicines* 10:1042. doi: 10.3390/biomedicines10051042

Madany, A., Hughes, H., and Ashwood, P. (2022b). Prenatal maternal antibiotics treatment alters the gut microbiota and immune function of post-weaned prepubescent offspring. *IJMS* 23:12879. doi: 10.3390/ijms232112879

Makinson, R., Lloyd, K., Rayasam, A., McKee, S., Brown, A., Barila, G., et al. (2017). Intrauterine inflammation induces sex-specific effects on neuroinflammation, white matter, and behavior. *Brain Behav. Immunity* 66, 277–288. doi: 10.1016/j.bbi.2017.07.016

Marungruang, N., Kovalenko, T., Osadchenko, I., Voss, U., Huang, F., Burleigh, S., et al. (2020). Lingonberries and their two separated fractions differently alter the gut microbiota, improve metabolic functions, reduce gut inflammatory properties, and improve brain function in ApoE-/- mice fed high-fat diet. *Nutr. Neurosci.* 23, 600–612. doi: 10.1080/1028415X.2018.1536423

Mingrino, S., Scanarini, M., and Magliulo, E. (1981). [Penetration of amoxicillin into the cerebrospinal fluid]. *Arch. Sci. Med.* 138, 33–35.

Mohammadi, S., Carey, D., Dick, F., Diedrichsen, J., Sereno, M., Reisert, M., et al. (2015). Whole-brain in-vivo measurements of the axonal g-ratio in a group of 37 healthy volunteers. *Front. Neurosci.* 9:441. doi: 10.3389/fnins.2015.00441

Nair, A., and Jacob, S. (2016). A simple practice guide for dose conversion between animals and human. *J. Basic Clin. Pharma.* 7:27. doi: 10.4103/0976-0105.177703

Norooznezhad, A., Anvari Aliabad, R., and Hantoushzadeh, S. (2022). Broad-spectrum antibiotics in pregnancy: role of inflammation in neonatal outcomes. *Am. J. Obstet. Gynecol.* 226, 284–285. doi: 10.1016/j.ajog.2021.09.044

O'Connor, R., Moloney, G., Fulling, C., O'Riordan, K., Fitzgerald, P., Bastiaanssen, T., et al. (2021). Maternal antibiotic administration during a critical developmental window has enduring neurobehavioural effects in offspring mice. *Behav. Brain Res.* 404:113156. doi: 10.1016/j.bbr.2021.113156

Patil, S., Sunyer, B., Höger, H., and Lubec, G. (2009). Evaluation of spatial memory of C57BL/6J and CD1 mice in the barnes maze, the multiple T-maze and in the morris water maze. *Behav. Brain Res.* 198, 58–68. doi: 10.1016/j.bbr.2008.10.029

Pivneva, T., Kolotushkina, E., and Skibo, G. (2003). Myelination and demyelination processes in the rat cerebellum cell culture: an electron microscopic study. *Fiziol* 49, 105–111.

Ramírez-Lozada, T., Loranca-García, M., Fuentes-Venado, C., Rodríguez-Cerdeira, C., Ocharan-Hernández, E., Soriano-Ursúa, M., et al. (2022). Does the fetus limit antibiotic treatment in pregnant patients with COVID-19? *Antibiotics* 11:252. doi: 10.3390/antibiotics11020252

Ray, P., Pandey, U., Das, D., and Aich, P. (2021). Vancomycin-induced changes in host immunity and behavior: comparative genomic and metagenomic analysis in C57BL/6 and BALB/c mice. *Dig. Dis. Sci.* 66, 3776–3791. doi: 10.1007/s10620-020-06729-x

Schilling, T., Lehmann, F., Rückert, B., and Eder, C. (2004). Physiological mechanisms of lysophosphatidylcholine-induced de-ramification of murine microglia: effects of LPC on microglia. *J. Physiol.* 557, 105–120. doi: 10.1113/jphysiol.2004.060632

Scott, G., Terstege, D., Vu, A., Law, S., Evans, A., and Epp, J. (2020). Disrupted neurogenesis in germ-free mice: effects of age and sex. *Front. Cell Dev. Biol.* 8:407. doi: 10.3389/fcell.2020.00407

Shepilov, D., Kovalenko, T., Osadchenko, I., Smozhanyk, K., Marungruang, N., Ushakova, G., et al. (2022). Varying dietary component ratios and lingonberry supplementation may affect the hippocampal structure of ApoE–/– mice. *Front. Nutr.* 9:565051. doi: 10.3389/fnut.2022.565051

Siriwachirachai, T., Sangkomkamhang, U., Lumbiganon, P., and Laopaiboon, M. (2014). Antibiotics for meconium-stained amniotic fluid in labour for preventing maternal and neonatal infections. *Syst. Rev.* 2014:7772. doi: 10.1002/14651858.CD007772.pub3

Smith, D., Du Rand, I., Addy, C., Collyns, T., Hart, S., Mitchelmore, P., et al. (2020). British thoracic society guideline for the use of long-term macrolides in adults with respiratory disease. *Thorax* 75, 370–404. doi: 10.1136/thoraxjnl-2019-213929

Snow, W., Pahlavan, P., Djordjevic, J., McAllister, D., Platt, E., Alashmali, S., et al. (2015). Morris water maze training in mice elevates hippocampal levels of transcription factors nuclear factor (erythroid-derived 2)-like 2 and nuclear factor kappa B p65. *Front. Mol. Neurosci.* 8:70. doi: 10.3389/fnmol.2015.00070

Stokholm, J., Sevelsted, A., Bønnelykke, K., and Bisgaard, H. (2014). Maternal propensity for infections and risk of childhood asthma: a registry-based cohort study. *Lancet Res. Med.* 2, 631–637. doi: 10.1016/S2213-2600(14)70152-3

Sturrock, R. (1980). Myelination of the mouse corpus callosum. *Neuropathol. Appl. Neurobiol.* 6, 415–420. doi: 10.1111/j.1365-2990.1980.tb00219.x

Sutton, A., Acosta, E., Larson, K., Kerstner-Wood, C., Tita, A., and Biggio, J. (2015). Perinatal pharmacokinetics of azithromycin for cesarean prophylaxis. *Am. J. Obstetr. Gynecol.* 212:812.e1. doi: 10.1016/j.ajog.2015.01.015

Taylor-Cousar, J., Jain, R., Kazmerski, T., Aitken, M., West, N., Wilson, A., et al. (2021). Concerns regarding the safety of azithromycin in pregnancy - relevance for women with cystic fibrosis. *J. Cyst. Fibr.* 20, 395–396. doi: 10.1016/j.jcf.2020.08.003

Thinkhamrop, J., Hofmeyr, G., Adetoro, O., and Lumbiganon, P. (2021). *Prophylactic antibiotic administration during second and third trimester in pregnancy for preventing infectious morbidity and mortality*. Available online at: https://doi.wiley.com/10.1002/14651858.CD002250 (accessed January 28, 2023).

UrbÃin, N., and Guillemot, F. (2014). Neurogenesis in the embryonic and adult brain: same regulators, different roles. *Front. Cell Neurosci.* 8:396. doi: 10.3389/fncel.2014.00396

Uyama, O., Okamura, N., Yanase, M., Narita, M., Kawabata, K., and Sugita, M. (1988). Quantitative evaluation of vascular permeability in the gerbil brain after transient ischemia using evans blue fluorescence. *J. Cereb Blood Flow Metab.* 8, 282–284. doi: 10.1038/jcbfm.1988.59

Verkhratsky, A., Parpura, V., Vardjan, N., and Zorec, R. (2019). Physiology of astroglia. *Adv. Exp. Med. Biol.* 1175, 45–91. doi: 10.1007/978-981-13-9913-8_3

Viaggi, B., Cangialosi, A., Langer, M., Olivieri, C., Gori, A., Corona, A., et al. (2022). Tissue penetration of antimicrobials in intensive care unit patients: a systematic review—part II. *Antibiotics* 11:1193. doi: 10.3390/antibiotics11091193

Wang, P., Tu, K., Cao, P., Yang, Y., Zhang, H., Qiu, X., et al. (2021). Antibiotics-induced intestinal dysbacteriosis caused behavioral alternations and neuronal activation in different brain regions in mice. *Mol Brain.* 14, 49. doi: 10.1186/s13041-021-00759-w

Weakley, B. (1972). *A beginner's handbook in biological electron microscopy*. Edinburgh: Churchill Livingstone, 228.

Yamada, C., Akkaoui, J., Ho, A., Duarte, C., Deth, R., Kawai, T., et al. (2020). Potential role of phosphoglycerol dihydroceramide produced by periodontal pathogen porphyromonas gingivalis in the pathogenesis of Alzheimer's disease. *Front. Immunol.* 11:591571. doi: 10.3389/fimmu.2020.591571

Yatsenko, K., Lushnikova, I., Ustymenko, A., Patseva, M., Govbakh, I., Kyryk, V., et al. (2020). Adipose-derived stem cells reduce lipopolysaccharide-induced myelin degradation and neuroinflammatory responses of glial cells in mice. *JPM* 10:66. doi: 10.3390/jpm10030066

Zareba-Szczudlik, J., Romejko-Wolniewicz, E., Lewandowski, Z., Rozanska, H., Malinowska-Polubiec, A., Dobrowolska-Redo, A., et al. (2017). Evaluation of the amoxicillin concentrations in amniotic fluid, placenta, umbilical cord blood and maternal serum two hours after oral administration. *Neuro. Endocrinol. Lett.* 38, 502–508.

Zheng, H., Dong, Y., Xu, Z., Crosby, G., Culley, D., Zhang, Y., et al. (2013). Sevoflurane anesthesia in pregnant mice induces neurotoxicity in fetal and offspring mice. *Anesthesiology* 118, 516–526. doi: 10.1097/ALN.0b013e3182834d5d

Zhou, P., Zhou, Y., Liu, B., Jin, Z., Zhuang, X., Dai, W., et al. (2020). Perinatal antibiotic exposure affects the transmission between maternal and neonatal microbiota and is associated with early-onset sepsis. *mSphere* 5:e984.

frontiers | Frontiers in Cellular Neuroscience

TYPE Mini Review
PUBLISHED 11 May 2023
DOI 10.3389/fncel.2023.1132114

OPEN ACCESS

EDITED BY
Dirk M. Hermann,
University of Duisburg-Essen, Germany

REVIEWED BY
Parimala Narne,
University of Hyderabad, India
Mina Borbor,
Essen University Hospital, Germany

*CORRESPONDENCE
Iryna Lushnikova
✉ li@biph.kiev.ua

RECEIVED 26 December 2022
ACCEPTED 24 April 2023
PUBLISHED 11 May 2023

CITATION
Lushnikova I, Kostiuchenko O, Kowalczyk M and Skibo G (2023) mTOR/α-ketoglutarate signaling: impact on brain cell homeostasis under ischemic conditions.
Front. Cell. Neurosci. 17:1132114.
doi: 10.3389/fncel.2023.1132114

mTOR/α-ketoglutarate signaling: impact on brain cell homeostasis under ischemic conditions

Iryna Lushnikova[1]*, Olha Kostiuchenko[1,2], Magdalena Kowalczyk[2] and Galyna Skibo[1]

[1]Department of Cytology, Bogomoletz Institute of Physiology, National Academy of Sciences of Ukraine, Kyiv, Ukraine, [2]Institute of Biochemistry and Biophysics, Polish Academy of Sciences, Warsaw, Poland

The multifunctional molecules mechanistic target of rapamycin (mTOR) and α-ketoglutarate (αKG) are crucial players in the regulatory mechanisms that maintain cell homeostasis in an ever-changing environment. Cerebral ischemia is associated primarily with oxygen-glucose deficiency (OGD) due to circulatory disorders. Upon exceeding a threshold of resistance to OGD, essential pathways of cellular metabolism can be disrupted, leading to damage of brain cells up to the loss of function and death. This mini-review focuses on the role of mTOR and αKG signaling in the metabolic homeostasis of brain cells under OGD conditions. Integral mechanisms concerning the relative cell resistance to OGD and the molecular basis of αKG-mediated neuroprotection are discussed. The study of molecular events associated with cerebral ischemia and endogenous neuroprotection is relevant for improving the effectiveness of therapeutic strategies.

KEYWORDS

mTOR, α-ketoglutarate (αKG), homeostasis, brain ischemia, autophagy, neuroprotection

1. Introduction

The brain is one of the most energy-consuming organs, so nutrient and oxygen deficiency is critical for cellular homeostasis. Complex signaling pathways and cooperation of molecular mechanisms ensure the homeostasis of brain cells, thus maintaining the viability and functioning of neurons with minor fluctuations in the extracellular environment. When

Abbreviations: ADP, adenosine diphosphate; AMP, adenosine monophosphate; ATP, adenosine triphosphate; αKG, α-ketoglutarate; Akt, protein kinase B (also known as PKB); AMPK, 5′-AMP-activated protein kinase; 4E-BP1, eukaryotic translation initiation factor 4E-binding protein 1; c-FOS, transcription factors; GDP/GTP, guanosine diphosphate/guanosine triphosphate; GTPases, family of hydrolase enzymes; GDH, glutamate dehydrogenase; HIF-1, hypoxia-inducible factor 1; HIF-1α, the alpha subunit of HIF-1; IDH, isocitrate dehydrogenase; IL-1, interleukin-1; KGDHC, α-ketoglutarate dehydrogenase complex; LC3, Microtubule-associated protein 1A/1B-light chain 3; LiCl, Lithium chloride; mTOR (mammalian/mechanistic target of rapamycin), serine/threonine protein kinase; mTORC1, mTOR complex 1; mTORC2, mTOR complex 2; mTORCs, mTOR complexes 1, 2; OGD, oxygen-glucose deficiency; p70 S6K1/2, p70 ribosomal S6 kinase 1 and 2; PHD, prolyl-4-hydroxylase; PI3K, phosphatidylinositol-3-kinase; PIKK, phosphatidylinositol-3-kinase-related kinase; REDD1, regulated DNA damage and development 1 protein; Rheb, Ras homolog enriched in brain; Rhes, a form of Rheb specifically expressed in the striatum; ROS, reactive oxygen species; SIAH2, ubiquitin-protein ligase; stat3, signal transducer and activator of transcription 3; Syt1, synaptotagmin 1; TCA, tricarboxylic acid; TSC, tuberous sclerosis complex; ULK1, unc-51-like kinase 1.

the threshold of ischemic resistance is exceeded, a metabolic imbalance in the brain tissue occurs, followed by progressive neuronal degradation. Oxygen-glucose deficiency (OGD) initiates ischemic injury as a result of energy-limiting and dysregulated signaling pathways (Cespedes et al., 2019; Datta et al., 2020; Fakih et al., 2022). However, functional failures can be reversible at the primary stage, and pharmacological correction at the molecular level could either prevent a destructive course or promote the restoration of tissue status and brain functions (Rosarda et al., 2021; Qin et al., 2022). Based on this, a comprehensive study of the molecular mechanisms of cellular adaptation, neurodegeneration, and neuroprotection in experimental models of cerebral ischemia is appropriate.

Oxygen-glucose deficiency-induced changes in the composition of the microenvironment transform intracellular metabolism, including events that are modulated by mTOR (mechanistic/mammalian target of rapamycin). This multifunctional molecule is one of the base elements for maintaining cellular homeostasis, while dysregulation of mTOR signaling is associated with many cerebral diseases, including ischemic stroke (Wong, 2013; Saxton and Sabatini, 2017). It is reported that under ischemic conditions, activation of autophagy induced by mTOR-suppression has a protective effect on cell survival, whereas excessive autophagy causes apoptosis and/or necrosis of neurons (Hou et al., 2019; Zhang et al., 2021). Exogenous or endogenous regulation of mTOR metabolism is reasonable in terms of possible correction of neurodegeneration. Numerous studies discuss the versatility of the properties of αKG (α-ketoglutarate) and its regulatory role in maintaining cellular metabolic balance (Zdzisińska et al., 2017; Wilson and Matschinsky, 2021; Hansen and Gibson, 2022). αKG is not only an intermediate of the tricarboxylic acid (TCA) cycle but also is involved in amino acid metabolism, regulation of signaling pathways, and the scavenging of reactive oxygen species (ROS), thereby ensuring cellular homeostasis and survival in adverse environmental conditions (Liu et al., 2018). Signaling cooperation between αKG and mTOR is often discussed in the context of metabolic regulation. There is conflicting evidence on whether αKG suppresses or activates mTOR function, and how it contributes to the protective effects of αKG.

Due to their heterogeneous functions and the constant availability in cells, both mTOR and αKG largely determine metabolic homeostasis under OGD conditions. The main patterns of mTOR/αKG-mediated mechanisms are widely described (Harrison and Pierzynowski, 2008; Kim et al., 2017; Zdzisińska et al., 2017; Bayliak and Lushchak, 2021; Kostiuchenko et al., 2022), however, data systematization is limited in the case of ischemic stress. Any correction of these signaling molecules' functioning could be complicated by the variety of regulatory mechanisms involved in the cellular metabolic scenario. A holistic view of mTOR and αKG-mediated interactions may contribute to finding more effective therapeutic strategies for cerebral ischemia. In this mini-review, we discuss the multifunctionality of mTOR and αKG and their collaboration in terms of metabolic homeostasis of neuronal cells under ischemic conditions with a focus on signaling mechanisms involved in endogenous neuroprotection.

2. Highlights of mTOR and αKG structure and functions

Mechanistic target of rapamycin is a serine/threonine protein kinase of the phosphatidylinositol-3-kinase-related kinase (PIKK) family that is the basis of two functionally distinct multiprotein complexes: rapamycin-sensitive complex 1 (mTORC1) and relatively rapamycin-insensitive complex 2 (mTORC2). Evolutionarily ancient and highly conserved, TOR is ubiquitously expressed in all eukaryotic cells from yeast to humans, and can be localized both in the nucleus and the cytoplasm (Saxton and Sabatini, 2017; Jhanwar-Uniyal et al., 2019). mTORCs act as convergence centers for incoming environmental stimuli and are important molecular sensors of cellular energy status. The canonical signaling pathway proceeds from extracellular and intracellular stimuli to mTOR via phosphatidylinositol 3-kinase (PI3K), protein kinase B (Akt), tuberous sclerosis complex (TSC), and GTPases, such as Ras homolog enriched in brain/striatum (Rheb/Rhes, respectively) (Bockaert and Marin, 2015). mTORC1 is induced predominantly by fluctuations in amino acids, oxygen, and glucose. At the same time, mTORC2 activity is promoted mainly by growth factors, hormones, and neurotransmitters. mTORs largely coordinate anabolism/catabolism and determine metabolic status and cellular viability (Switon et al., 2017; Schmidt and de Araujo, 2022; Simcox and Lamming, 2022).

Mechanistic target of rapamycin-signaling coordinates basic cell processes such as protein and lipid metabolism, energy homeostasis, mitochondrial and lysosomal biogenesis, proliferation, migration, autophagy, etc. Consistent with its role in coordinating anabolic and catabolic processes, constitutive mTOR activity ensures the adequacy of cellular functioning. In general, mTOR activation is associated with resource/energy sufficiency in the cells (specifically, glucose, oxygen, ATP, amino acids, growth factors, etc.), while mTOR suppression is related to a deficiency of the mentioned factors. Numerous recent studies have significantly deepened the understanding of both upstream mTOR pathways and downstream mTOR targets (Bockaert and Marin, 2015; Castellanos et al., 2016; Saxton and Sabatini, 2017). The main mTORCs-regulated downstream cellular functions are widely described in reviews for different organism systems (Switon et al., 2017; Kostiuchenko et al., 2022). However, many aspects of the molecular interactions that coordinate mTOR-mediated signaling in cerebral physiology and pathology have not yet been fully elucidated. In the brain, mTOR signaling, in addition to basic physiological functions, coordinates specific neuronal functions (e.g., axon regeneration/myelination, dendrite/spine formation, synaptic plasticity, ion channel expression, etc.) underlying cognitive processes (learning, memory, circadian rhythms, etc.) (Bockaert and Marin, 2015; Karalis and Bateup, 2021). Correct modulation of cellular metabolism in response to changing environmental conditions by mTOR signaling is critical to homeostasis.

α-ketoglutarate is a multifunctional molecule that is also actively involved in cellular metabolism as well as maintaining homeostasis in an ever-changing environment. αKG is highly water-soluble, non-toxic, and chemically stable. As a key intermediate in the TCA cycle, it is engaged in the ATP synthesis and balancing the anabolism and catabolism of products/substrates

of the TCA cycle (Wu et al., 2016; Kim et al., 2017; Hansen and Gibson, 2022). Endogenous αKG is mainly formed as a result of the oxidative decarboxylation of isocitrate catalyzed by NAD-dependent isocitrate dehydrogenase (IDH). In addition, it is produced through glutaminolysis as a result of glutamate oxidation initiated by transamination catalyzed by an aminotransferase, or oxidative deamination catalyzed by glutamate dehydrogenase (GDH) (Ugur et al., 2017; Andersen et al., 2021; Hinca et al., 2021). Passing further along the TCA cycle, the newly formed αKG increases the probability of ATP generation and thus contributes to the metabolic balance in OGD (Gul and Buyukuysal, 2021).

α-ketoglutarate is primarily present in the mitochondria and cytosol of any cell, besides it is also found in the bloodstream (Wagner et al., 2010). It can cross the blood-brain barrier both by simple diffusion and through a carrier-mediated process (oxoglutarate/malate antiporter, voltage-gated anion channels). This ketoacid exhibits functional features depending on localization, as well as on interactions with other bioactive molecules. Being a cofactor of numerous biochemical reactions in the cell, αKG is involved in multiple physiological processes such as growth, proliferation, neurotransmission, immunity, aging, etc. (Xiao et al., 2016; Zdzisińska et al., 2017; Hansen and Gibson, 2022). αKG contributes to the metabolism of a wide range of bioactive micro and macro molecules (namely, amino acids, proteins, lipids, nucleic acids, carbon, and nitrogen) and thereby modulates many signaling pathways and genes (Yao et al., 2012; Wu et al., 2016).

An important role in the regulation of αKG metabolism and maintenance of cellular homeostasis belongs to the α-ketoglutarate dehydrogenase complex (KGDHC), for which αKG is a substrate. KGDHC is made up of three functionally distinct subunits (E1k, E2k, and E3) that catalyze the conversion of α-ketoglutarate (KG) to succinyl-CoA. The three-step αKG/KGDHC interaction is the rate-limiting step in the TCA cycle. In cooperation with hypoxia-inducible factor 1 (HIF-1) and prolyl-4-hydroxylase (PHD), which controls HIF-1 synthesis/degradation, αKG/KGDHC regulates cellular responses to hypoxia through a feedback loop. In this case, when there is no oxygen present to activate PHD, HIF-1 is stable and activates the E3 ubiquitin-protein ligase SIAH2 which inhibits KGDHC, resulting in the accumulation of αKG that enters the reductive pathway of the TCA cycle and promotes lipid synthesis. αKG produced through glutaminolysis leaves the mitochondria and enters the cytosol leading to the activation of PHD which destabilizes HIF-1 (Kierans and Taylor, 2021; Hansen and Gibson, 2022).

In the brain, in addition to basic functions, αKG determines the balance of neurotransmitter metabolism and neuron-glia communications. This ketoacid can be both a precursor and a metabolite of glutamine and glutamate, according to the cell's needs (Andersen et al., 2021; Bodineau et al., 2021; Hansen and Gibson, 2022). During recycling between neurons and astroglia, part of the transmitter pool is lost as they are oxidized. The loss can be compensated by their synthesis using αKG as a substrate. Both the excitatory neurotransmitter glutamate and the inhibitory neurotransmitter γ-aminobutyric acid (GABA) can be produced. The increase in the amino acid pool during treatment with exogenous αKG has been shown in experimental models *in vivo* and *in vitro* (Zdzisińska et al., 2017; Bayliak and Lushchak, 2021; Hansen and Gibson, 2022). Although the glutamate-glutamine cycle is balanced under normal homeostatic conditions, αKG is a reliable buffer during critical fluctuations (McKenna et al., 2016; Schousboe, 2019; Rose et al., 2020; Meng et al., 2022). In addition, αKG treatment has been shown to intensify the spatial redistribution of synaptic vesicles, as well as increase the sensitivity of synaptotagmin 1 (Syt1) to Ca^{2+}, thereby promoting vesicle fusion with the presynaptic membrane and neurotransmitter release. Along with this, an increase in neurogenesis and an improvement in cognitive functions were observed (Ugur et al., 2017). Thus, in the brain, αKG is a key player in the regulation of both basic neuronal function and the quality/efficiency of synaptic transmission.

3. mTOR and αKG signaling in the brain under ischemic conditions

The cellular response to OGD is initiated primarily through oxygen- and AMP/ATP-sensitive molecules-sensors–HIF-1, and 5′AMP-activated protein kinase (AMPK), respectively. In close cooperation with mTOR/αKG-mediated mechanisms, these molecules are responsible for an adequate cellular response to OGD. In normoxia, when O_2 and AMP/ATP are balanced (**Figure 1**), HIF-1 and AMPK are predominantly inactive. In brain hypoxia/ischemia, PHD is downregulated, followed by upregulation of HIF-1 expression and HIF-mediated induction of transcription of multiple target genes to rearrange metabolism for adaptation. In parallel, AMPK is activated as a result of an increase in the AMP/ATP and ADP/ATP ratios, indicating an energy deficit caused by ischemia. Moreover, HIF-1 can also upregulate AMPK through REDD1 (REDD1–regulated DNA damage and development 1 protein). Activation of both mentioned sensor molecules (HIF and AMPK) triggers compensatory mechanisms programming brain cells to provide homeostasis and/or recovery processes.

Many data indicate that ischemia-induced neurodegenerative processes are associated with the dysregulation of mTOR- and αKG-signaling involving AMPK and HIF-1 intermediates (Stegen et al., 2016; Saxton and Sabatini, 2017; Kierans and Taylor, 2021; Li et al., 2021; Villa-González et al., 2022). OGD induces mTOR suppression and αKG accumulation, followed by an increase in autophagy and compensatory activation of ATP production due to the incorporation of excess αKG into the TCA cycle (Hansen and Gibson, 2022; Villa-González et al., 2022). It is known that under normoxic conditions, mTOR mainly blocks autophagy, but does not exclude it. The functional relationship between the mTOR pathway and autophagy involves complex regulatory signaling loops aimed at maintaining metabolic balance (Deleyto-Seldas and Efeyan, 2021). It has been shown that autophagy activation may result not only from AMPK-mediated mTOR suppression but also from direct phosphorylation of ULK1, a serine/threonine protein kinase involved in autophagy (Mo et al., 2020). At a certain stage, these processes are adaptive-protective, however, excessive autophagy can exacerbate brain damage. Treatment of animals with the mTOR inhibitor rapamycin after ischemia has shown neuroprotective effects and autophagy activation, but studies of its effects in other models of cerebral ischemia/reperfusion describe conflicting results (Beard et al., 2019). In the case of

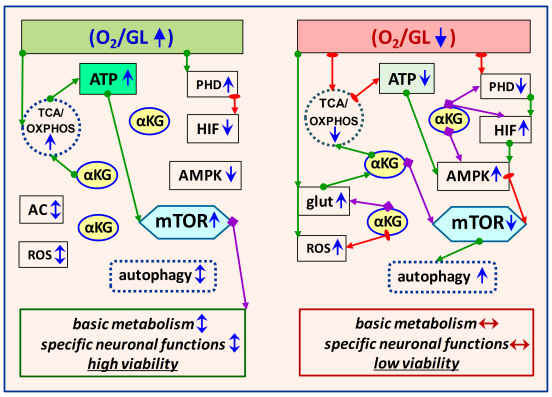

FIGURE 1
Schematic illustration of key signaling pathways involved in metabolic homeostasis of brain cells in physiological and OGD conditions. The left panel corresponds to normoxia when metabolism is balanced to ensure adequate brain cell functions. The right panel shows the OGD-induced mechanisms involved in equilibrating the metabolic imbalance. Modulatory effects of the molecules are marked with purple arrows, activation–with green arrows, and inhibitory effects–with red. Short arrows near the molecule or process indicate its functional activity (blue sharp–high or low, blue/red double-edged–balance/imbalance) under normoxia or OGD. GL, glucose; TCA, tricarboxylic acid cycle; OXPHOS, oxidative phosphorylation; AC, amino acids; glut, glutamate; AMPK, 5′AMP-activated protein kinase; PHD, oxygen-sensing prolyl hydroxylase domain enzymes; HIF, hypoxia-inducible factor; ROS, reactive oxygen species.

hyperactivation, the autophagy inhibitor LiCl activated mTOR signaling, promoting repair processes and improving neuronal viability (Hadley et al., 2019; Hou et al., 2019; Zhang et al., 2021). Thus, in the context of metabolic homeostasis, mTOR activation or suppression is appropriate at different stages of OGD. Besides, let us note that the effects of ischemia are determined both by the intensity and duration of ischemia/reperfusion and cell type, as well as by individual cell specificity and resistance. For example, in a focal ischemia model, mTORC1 is downregulated in the ischemic nucleus, but mTORC1 is upregulated in the ischemic penumbra (Wu et al., 2017; Villa-González et al., 2022). mTOR signaling dynamics vary widely across neuronal and glial cell types (McKenna et al., 2016; Cespedes et al., 2019; Schousboe, 2019; Rose et al., 2020). To maintain cellular homeostasis under OGD conditions, coordination of functional interactions of HIF/AMPK/mTOR/αKG molecules is required. Such signaling cooperation manifests itself according to the physiological expediency for a particular cell type under specific OGD conditions. It should be noted that the mobility and versatility of αKG allow it to provide metabolic plasticity at the cellular level.

Although the protective properties of exogenous αKG have been widely described in the treatment of brain diseases including cerebral ischemia (Zdzisińska et al., 2017; Meng et al., 2022), the molecular bases of these effects are still being studied. Stabilization of metabolic homeostasis in OGD involving mTOR/αKG signaling can be achieved by multidirectional events that become relevant at different stages during/after ischemia. Generally, metabolic transformations are oriented on the balance of ATP, glutamate, mTOR, and ROS in brain cells. In experimental ischemia models *in vivo* and *in vitro*, it was noted that conversion of glutamate into αKG can contribute to both the activation of ATP production and the reduction of glutamate excitotoxic effect, preserving viability and function of neurons in OGD (Kim et al., 2017; Ferrari et al., 2018; Andersen et al., 2021; Hinca et al., 2021). In addition, αKG has been shown to promote the synthesis of the amino acid L-carnitine, which is critical for the efficient metabolism of fatty acids into ATP (Thomas et al., 2015). These events are most relevant during and immediately after the OGD, which corresponds to OGD1 in **Figure 2**.

In the context of αKG/mTOR cooperation to maintain homeostasis under OGD conditions, many studies have shown that αKG indirectly inhibits mTOR with subsequent activation of autophagy. The effects of αKG may be mediated by the activation of HIF-1 and AMPK, as well as the inhibition of ATP synthase, which is a direct target of αKG (Chin et al., 2014; Su et al., 2019; Kostiuchenko et al., 2022). This may be an additional or alternative mechanism for the downregulation of mTOR functions by αKG that promotes cell survival in OGD. Such a scenario is most appropriate in the subsequent ischemic period, which corresponds to OGD2 in **Figure 2**.

When cells acquire resilience as a result of oxygen and glucose stabilization (Reperfusion) and ATP saturation in the environment, mTOR activation becomes relevant, which can also be mediated by αKG via HIF-1 and AMPK downregulation. αKG is a cofactor of many oxygenases that provide oxidation reactions involving molecular oxygen and determine oxygen homeostasis in cells (Hansen and Gibson, 2022). In particular, αKG activates PHD with subsequent suppression of PHD-dependent HIF signaling, thereby indirectly stabilizing the effects of HIF-1 (Stegen et al., 2016; Kierans and Taylor, 2021; Li et al., 2021). It should be noted that this variant of the event, taking into account the αKG excess in the cytoplasm, suggests the possibility of a metabolic shift toward the activation of the mTOR signaling pathway even under OGD conditions. In the post-ischemic period, mTOR-mediated synthetic processes are of great importance for ensuring homeostasis and restoring neuronal functions. There are results indicating activation of the mTOR signaling pathway by αKG as a biosynthetic precursor for amino acids such as glutamate, glutamine, leucine, and proline. αKG treatment increases the levels of phosphorylation of mTOR, 4E-BP1, and p70 S6K1, thereby promoting the initiation of protein synthesis. In addition, glutamine-derived αKG has been reported to activate mTORC1 via GDP/GTP-mediated signaling (Yao et al., 2012; Simcox and Lamming, 2022).

Moreover, αKG has been found to inhibit the inflammatory response and oxidative damage in the brain during ischemic injury. The authors point out that these effects may be mediated by the c-Fos/IL-10/stat3 signaling pathway (Hua et al., 2022). Thus, the antioxidant properties of αKG also may explain its protective effects. It contributes to ROS scavenging, as it can directly neutralize hydrogen peroxide, superoxide, and other reactive species, as well as increase the enzymatic activity of superoxide dismutase, catalase, and glutathione peroxidase (Liu et al., 2018).

Multiple neurodegenerative diseases accompanied by ischemic phenomena are associated with a decrease in KGDHC activity and accumulation of αKG, which may contribute to the implementation of αKG multifunctionality (Johnson et al., 2020; Gul and Buyukuysal, 2021; Hansen and Gibson, 2022; Meng et al., 2022). Thus, αKG is critical for metabolic plasticity, homeostasis, and viability of brain cells during ischemia through its involvement

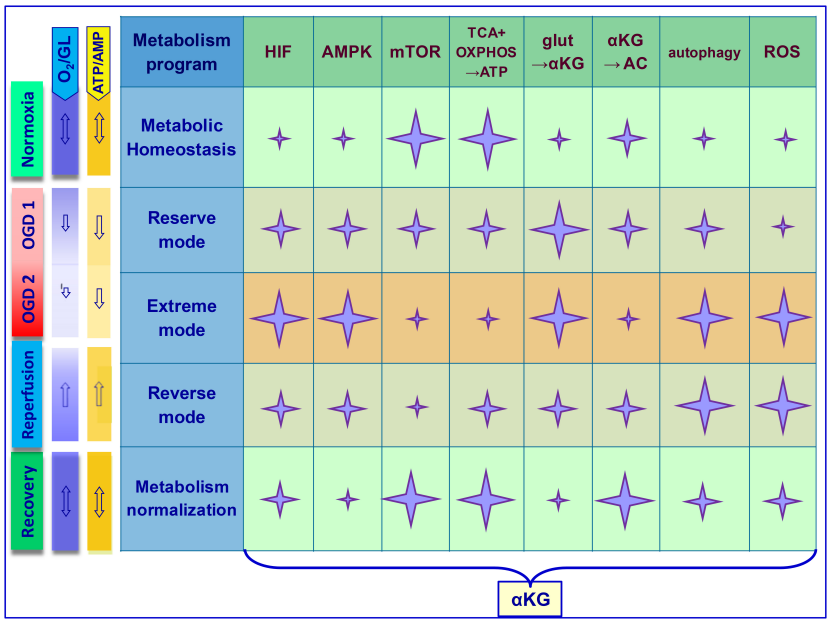

FIGURE 2
Multifunctional molecules in the metabolic dynamics of brain cells under ischemic exposure and recovery of homeostasis during reperfusion. The scheme shows key OGD-induced cellular events. Stages–Normoxia, OGD 1 (O_2, ATP–reduced), OGD 2 (O_2, ATP–depleted), reperfusion, recovery. Metabolism programs–Metabolic homeostasis, reserve mode, extreme mode, reverse mode, metabolism normalization. Involvement of basic functional molecules and mechanisms in the cellular response to OGD (marked with a star). Star size correlates with activity level. Note that at different stages, αKG can directly or indirectly contribute to the equalization of metabolic homeostasis through opposite mechanisms. In OGD, αKG promotes ATP synthesis, glutamate metabolism (glut→αKG), mTOR suppression, autophagy activation, and ROS neutralization. During the recovery stage after OGD, αKG promotes additional ATP synthesis, amino acid metabolism (αKG→AC), mTOR activation, and normalization of autophagy and ROS. Correspondence of arrows (double-edged–balance, sharp–decrease or increase in the indicator). GL, glucose; TCA, tricarboxylic acid cycle; OXPHOS, oxidative phosphorylation; AC, amino acids; glut, glutamate; AMPK, 5′AMP-activated protein kinase; PHD, oxygen-sensing prolyl hydroxylase domain enzymes; HIF, hypoxia-inducible factor; ROS, reactive oxygen species.

in the regulation of key metabolic processes (namely, energy production, amino acid metabolism, modulation of signaling pathways, and antioxidant defense).

4. Discussion

The status of brain cell homeostasis has been shaped evolutionally. Although the structure of biologically active molecules is conserved, their functional efficiency in cellular metabolism is determined by the plasticity of intermolecular communications. The involvement of numerous intermediates in ischemia-induced signaling processes can make cellular responses ambiguous, and the consequences for cells and the organism as a whole can be uncontrollable. However, the inherent cellular programs of self-regulation can maintain metabolic homeostasis within certain limits of OGD fluctuations. Neuronal metabolism is most sensitive to OGD compared to more resistant glial cells. In cerebral ischemia, the degree of OGD and individual metabolic programs of neuronal and/or glial cells determine the triggering of efficient molecular events that determine tissue homeostasis. mTOR and αKG signaling substantially mediate these processes, which manifest themselves according to the specificity of metabolism in various cell types. Under conditions of transient and reversible ischemia, metabolic dynamics can hypothetically be divided into several stages and characterized in the context of the mentioned signaling molecules. Namely, normoxia corresponds to metabolic homeostasis, OGD begins with a "reserve mode" using internal resources (OGD1), moving on to an "extreme mode" (OGD2) in case of energy depletion. It is assumed that when the disturbances can still be reversible, autophagy is activated, but cell damage/death becomes inevitable when the homeostatic threshold is exceeded. Oxygen-glucose stabilization of the extracellular environment (otherwise, reperfusion) corresponds to the "reverse mode" followed by the "metabolism normalization." The mechanistic model of metabolic dynamics in OGD and the involvement of the key molecules considered in this mini-review are presented in Figure 2.

The coordinated interaction of molecules, including mTOR and αKG, is of great importance for ensuring the gradual transition of cellular metabolism from a normal state to an extreme one, and then to a reverse one, followed by a return to metabolic homeostasis when the environment stabilizes.

Based on the available data, we hypothesize that the maintenance of metabolic homeostasis involves the support of ATP synthesis, the suspension of basic normoxic programs (anabolism/catabolism, etc.), the removal of critical consequences (glutamate metabolism, activation of autophagy, and ROS scavenging), the activation of stabilization/recovery programs due to existing cellular resources and expediency. In the context of ischemia-induced events, the multifunctional molecules mTOR and αKG can be mechanically defined as cellular "integrator" and "equalizer," respectively, which implement programs of endogenous neuroprotection. Taking into account

the multifunctionality and mobility of αKG, its abundance should increase the survival of brain cells in OGD. An integrated approach to understanding ischemia-induced molecular mechanisms of regulation of the mTOR signaling pathway, including the involvement of αKG, can increase the effectiveness of exogenous neuroprotection in ischemia-induced disorders.

Author contributions

IL: conceptualization and drafting the manuscript. OK: literature analysis and revising the manuscript. MK: reviewing the manuscript. GS: supervision and reviewing the manuscript. All authors read and agreed to the published version of the manuscript.

Funding

This work was funded by the National Academy of Sciences of Ukraine. State registration number of work is 0118U007350. This review study was supported by NAWA scholarship program "Solidarni z Ukrainą" and "IBB START" scholarship of the Institute of Biochemistry and Biophysics, Polish Academy of Sciences.

Conflict of interest

The authors declare that the research was conducted in the absence of any commercial or financial relationships that could be construed as a potential conflict of interest.

Publisher's note

All claims expressed in this article are solely those of the authors and do not necessarily represent those of their affiliated organizations, or those of the publisher, the editors and the reviewers. Any product that may be evaluated in this article, or claim that may be made by its manufacturer, is not guaranteed or endorsed by the publisher.

References

Andersen, J. V., Markussen, K. H., Jakobsen, E., Schousboe, A., Waagepetersen, H. S., Rosenberg, P. A., et al. (2021). Glutamate metabolism and recycling at the excitatory synapse in health and neurodegeneration. *Neuropharmacology* 196:108719. doi: 10.1016/j.neuropharm.2021.108719

Bayliak, M. M., and Lushchak, V. I. (2021). Pleiotropic effects of alpha-ketoglutarate as a potential anti-ageing agent. *Ageing Res. Rev.* 66:101237. doi: 10.1016/j.arr.2020.101237

Beard, D. J., Hadley, G., Thurley, N., Howells, D. W., Sutherland, B. A., and Buchan, A. M. (2019). The effect of rapamycin treatment on cerebral ischemia: a systematic review and meta-analysis of animal model studies. *Int. J. Stroke* 14, 137–145. doi: 10.1177/1747493018816503

Bockaert, J., and Marin, P. (2015). mTOR in brain physiology and pathologies. *Physiol. Rev.* 95, 1157–1187. doi: 10.1152/physrev.00038.2014

Bodineau, C., Tomé, M., Courtois, S., Costa, A. S. H., Sciacovelli, M., Rousseau, B., et al. (2021). Two parallel pathways connect glutamine metabolism and mTORC1 activity to regulate glutamoptosis. *Nat. Commun.* 12:4814. doi: 10.1038/s41467-021-25079-4

Castellanos, M., Gubern, C., and Kadar, E. (2016). "Chapter 7–mTOR: exploring a new potential therapeutic target for stroke," in *Molecules to medicine with mTOR*, ed. K. Maiese (Boston, MA: Academic Press), 105–122. doi: 10.1016/B978-0-12-802733-2.00012-8

Cespedes, A., Villa, M., Benito-Cuesta, I., Perez-Alvarez, M. J., Ordoñez, L., and Wandosell, F. (2019). Energy-sensing pathways in ischemia: the counterbalance between AMPK and mTORC. *Curr. Pharm. Des.* 25, 4763–4770. doi: 10.2174/1381612825666191210152156

Chin, R. M., Fu, X., Pai, M. Y., Vergnes, L., Hwang, H., Deng, G., et al. (2014). The metabolite α-ketoglutarate extends lifespan by inhibiting ATP synthase and TOR. *Nature* 510, 397–401. doi: 10.1038/nature13264

Datta, A., Sarmah, D., Mounica, L., Kaur, H., Kesharwani, R., Verma, G., et al. (2020). Cell death pathways in ischemic stroke and targeted pharmacotherapy. *Transl. Stroke Res.* 11, 1185–1202. doi: 10.1007/s12975-020-00806-z

Deleyto-Seldas, N., and Efeyan, A. (2021). The mTOR-autophagy axis and the control of metabolism. *Front. Cell Dev. Biol.* 1:655731. doi: 10.3389/fcell.2021.655731

Fakih, W., Zeitoun, R., AlZaim, I., Eid, A. H., Kobeissy, F., Abd-Elrahman, K. S., et al. (2022). Early metabolic impairment as a contributor to neurodegenerative disease: mechanisms and potential pharmacological intervention. *Obesity (Silver Spring)* 30, 982–993. doi: 10.1002/oby.23400

Ferrari, F., Gorini, A., Hoyer, S., and Villa, R. F. (2018). Glutamate metabolism in cerebral mitochondria after ischemia and post-ischemic recovery during aging: relationships with brain energy metabolism. *J. Neurochem.* 146, 416–428. doi: 10.1111/jnc.14464

Gul, Z., and Buyukuysal, R. L. (2021). Glutamate-induced modulation in energy metabolism contributes to protection of rat cortical slices against ischemia-induced damage. *Neuroreport* 32, 157–162. doi: 10.1097/WNR.0000000000001572

Hadley, G., Beard, D. J., Alexopoulou, Z., Sutherland, B. A., and Buchan, A. M. (2019). Investigation of the novel mTOR inhibitor AZD2014 in neuronal ischemia. *Neurosci. Lett.* 706, 223–230. doi: 10.1016/j.neulet.2019.05.023

Hansen, G. E., and Gibson, G. E. (2022). The α-ketoglutarate dehydrogenase complex as a hub of plasticity in neurodegeneration and regeneration. *Int. J. Mol. Sci.* 23:12403. doi: 10.3390/ijms232012403

Harrison, A. P., and Pierzynowski, S. G. (2008). Biological effects of 2-oxoglutarate with particular emphasis on the regulation of protein, mineral and lipid absorption/metabolism, muscle performance, kidney function, bone formation and cancerogenesis, all viewed from a healthy ageing perspective state of the art–review article. *J. Physiol. Pharmacol.* 59 (Suppl. 1), 91–106.

Hinca, S. B., Salcedo, C., Wagner, A., Goldeman, C., Sadat, E., Aibar, M. M. D., et al. (2021). Brain endothelial cells metabolize glutamate via glutamate dehydrogenase to replenish TCA-intermediates and produce ATP under hypoglycemic conditions. *J. Neurochem.* 157, 1861–1875. doi: 10.1111/jnc.15207

Hou, K., Xu, D., Li, F., Chen, S., and Li, Y. (2019). The progress of neuronal autophagy in cerebral ischemia stroke: mechanisms, roles and research methods. *J. Neurol. Sci.* 400, 72–82. doi: 10.1016/j.jns.2019.03.015

Hua, W., Zhang, X., Tang, H., Li, C., Han, N., Li, H., et al. (2022). AKG attenuates cerebral ischemia-reperfusion injury through c-Fos/IL-10/Stat3 signaling pathway. *Oxid. Med. Cell. Longev.* 2022:6839385. doi: 10.1155/2022/6839385

Jhanwar-Uniyal, M., Wainwright, J. V., Mohan, A. L., Tobias, M. E., Murali, R., Gandhi, C. D., et al. (2019). Diverse signaling mechanisms of mTOR complexes: mTORC1 and mTORC2 in forming a formidable relationship. *Adv. Biol. Regul.* 72, 51–62. doi: 10.1016/j.jbior.2019.03.003

Johnson, S. C., Kayser, E.-B., Bornstein, R., Stokes, J., Bitto, A., Park, K. Y., et al. (2020). Regional metabolic signatures in the Ndufs4(KO) mouse brain implicate defective glutamate/α-ketoglutarate metabolism in mitochondrial disease. *Mol. Genet. Metab.* 130, 118–132. doi: 10.1016/j.ymgme.2020.03.007

Karalis, V., and Bateup, H. S. (2021). Current approaches and future directions for the treatment of mTORopathies. *Dev. Neurosci.* 43, 143–158. doi: 10.1159/000515672

Kierans, S. J., and Taylor, C. T. (2021). Regulation of glycolysis by the hypoxia-inducible factor (HIF): implications for cellular physiology. *J. Physiol.* 599, 23–37. doi: 10.1113/JP280572

Kim, A. Y., Jeong, K.-H., Lee, J. H., Kang, Y., Lee, S. H., and Baik, E. J. (2017). Glutamate dehydrogenase as a neuroprotective target against brain ischemia and reperfusion. *Neuroscience* 340, 487–500. doi: 10.1016/j.neuroscience.2016.11.007

Kostiuchenko, O., Lushnikova, I., Kowalczyk, M., and Skibo, G. (2022). mTOR/α-ketoglutarate-mediated signaling pathways in the context of brain neurodegeneration and neuroprotection. *BBA Adv.* 2:100066. doi: 10.1016/j.bbadva.2022.100066

Li, K., Zheng, Y., and Wang, X. (2021). The potential relationship between HIF-1α and amino acid metabolism after hypoxic ischemia and dual effects on neurons. *Front. Neurosci.* 15:676553. doi: 10.3389/fnins.2021.676553

Liu, S., He, L., and Yao, K. (2018). The antioxidative function of alpha-ketoglutarate and its applications. *Biomed Res. Int.* 2018:3408467. doi: 10.1155/2018/3408467

McKenna, M. C., Stridh, M. H., McNair, L. F., Sonnewald, U., Waagepetersen, H. S., and Schousboe, A. (2016). Glutamate oxidation in astrocytes: roles of glutamate dehydrogenase and aminotransferases. *J. Neurosci. Res.* 94, 1561–1571. doi: 10.1002/jnr.23908

Meng, X., Liu, H., Peng, L., He, W., and Li, S. (2022). Potential clinical applications of alpha-ketoglutaric acid in diseases (Review). *Mol. Med. Rep.* 25, 1–8. doi: 10.3892/mmr.2022.12667

Mo, Y., Sun, Y.-Y., and Liu, K.-Y. (2020). Autophagy and inflammation in ischemic stroke. *Neural Regen. Res.* 15, 1388–1396. doi: 10.4103/1673-5374.274331

Qin, C., Yang, S., Chu, Y. H., Zhang, H., Pang, X. W., Chen, L., et al. (2022). Signaling pathways involved in ischemic stroke: molecular mechanisms and therapeutic interventions. *Signal Transduct. Target. Ther.* 7:215. doi: 10.1038/s41392-022-01064-1

Rosarda, J. D., Baron, K. R., Nutsch, K., Kline, G. M., Stanton, C., Kelly, J. W., et al. (2021). Metabolically activated proteostasis regulators protect against glutamate toxicity by activating NRF2. *ACS Chem. Biol.* 16, 2852–2863. doi: 10.1021/acschembio.1c00810

Rose, J., Brian, C., Pappa, A., Panayiotidis, M. I., and Franco, R. (2020). Mitochondrial metabolism in astrocytes regulates brain bioenergetics, neurotransmission and redox balance. *Front. Neurosci.* 14:536682. doi: 10.3389/fnins.2020.536682

Saxton, R. A., and Sabatini, D. M. (2017). mTOR signaling in growth, metabolism, and disease. *Cell* 168, 960–976. doi: 10.1016/j.cell.2017.02.004

Schmidt, O., and de Araujo, M. E. G. (2022). Establishing spatial control over TORC1 signaling. *J. Cell Biol.* 221:e202203136. doi: 10.1083/jcb.202203136

Schousboe, A. (2019). Metabolic signaling in the brain and the role of astrocytes in control of glutamate and GABA neurotransmission. *Neurosci. Lett.* 689, 11–13. doi: 10.1016/j.neulet.2018.01.038

Simcox, J., and Lamming, D. W. (2022). The central moTOR of metabolism. *Dev. Cell* 57, 691–706. doi: 10.1016/j.devcel.2022.02.024

Stegen, S., van Gastel, N., Eelen, G., Ghesquière, B., D'Anna, F., Thienpont, B., et al. (2016). HIF-1α promotes glutamine-mediated redox homeostasis and glycogen-dependent bioenergetics to support postimplantation bone cell survival. *Cell Metab.* 23, 265–279. doi: 10.1016/j.cmet.2016.01.002

Su, Y., Wang, T., Wu, N., Li, D., Fan, X., Xu, Z., et al. (2019). Alpha-ketoglutarate extends Drosophila lifespan by inhibiting mTOR and activating AMPK. *Aging (Albany NY)* 11, 4183–4197. doi: 10.18632/aging.102045

Switon, K., Kotulska, K., Janusz-Kaminska, A., Zmorzynska, J., and Jaworski, J. (2017). Molecular neurobiology of mTOR. *Neuroscience* 341, 112–153. doi: 10.1016/j.neuroscience.2016.11.017

Thomas, S. C., Alhasawi, A., Appanna, V. P., Auger, C., and Appanna, V. D. (2015). Brain metabolism and Alzheimer's disease: the prospect of a metabolite-based therapy. *J. Nutr. Health Aging* 19, 58–63. doi: 10.1007/s12603-014-0511-7

Ugur, B., Bao, H., Stawarski, M., Duraine, L. R., Zuo, Z., Lin, Y. Q., et al. (2017). The krebs cycle enzyme isocitrate dehydrogenase 3A couples mitochondrial metabolism to synaptic transmission. *Cell Rep.* 21, 3794–3806. doi: 10.1016/j.celrep.2017.12.005

Villa-González, M., Martín-López, G., and Pérez-Álvarez, M. J. (2022). Dysregulation of mTOR signaling after brain ischemia. *Int. J. Mol. Sci.* 23:2814. doi: 10.3390/ijms23052814

Wagner, B. M., Donnarumma, F., Wintersteiger, R., Windischhofer, W., and Leis, H. J. (2010). Simultaneous quantitative determination of alpha-ketoglutaric acid and 5-hydroxymethylfurfural in human plasma by gas chromatography-mass spectrometry. *Anal. Bioanal. Chem.* 396, 2629–2637. doi: 10.1007/s00216-010-3479-0

Wilson, D. F., and Matschinsky, F. M. (2021). Metabolic homeostasis in life as we know it: its origin and thermodynamic basis. *Front. Physiol.* 12:658997. doi: 10.3389/fphys.2021.658997

Wong, M. (2013). Mammalian target of rapamycin (mTOR) pathways in neurological diseases. *Biomed. J.* 36, 40–50. doi: 10.4103/2319-4170.110365

Wu, M., Zhang, H., Kai, J., Zhu, F., Dong, J., Xu, Z., et al. (2017). Rapamycin prevents cerebral stroke by modulating apoptosis and autophagy in penumbra in rats. *Ann. Clin. Transl. Neurol.* 5, 138–146. doi: 10.1002/acn3.507

Wu, N., Yang, M., Gaur, U., Xu, H., Yao, Y., and Li, D. (2016). Alpha-ketoglutarate: physiological functions and applications. *Biomol. Ther. (Seoul)* 24, 1–8. doi: 10.4062/biomolther.2015.078

Xiao, D., Zeng, L., Yao, K., Kong, X., Wu, G., and Yin, Y. (2016). The glutamine-alpha-ketoglutarate (AKG) metabolism and its nutritional implications. *Amino Acids* 48, 2067–2080. doi: 10.1007/s00726-016-2254-8

Yao, K., Yin, Y., Li, X., Xi, P., Wang, J., Lei, J., et al. (2012). Alpha-ketoglutarate inhibits glutamine degradation and enhances protein synthesis in intestinal porcine epithelial cells. *Amino Acids* 42, 2491–2500. doi: 10.1007/s00726-011-1060-6

Zdzisińska, B., Żurek, A., and Kandefer-Szerszeń, M. (2017). Alpha-ketoglutarate as a molecule with pleiotropic activity: well-known and novel possibilities of therapeutic use. *Arch. Immunol. Ther. Exp. (Warsz)* 65, 21–36. doi: 10.1007/s00005-016-0406-x

Zhang, X., Wei, M., Fan, J., Yan, W., Zha, X., Song, H., et al. (2021). Ischemia-induced upregulation of autophagy preludes dysfunctional lysosomal storage and associated synaptic impairments in neurons. *Autophagy* 17, 1519–1542. doi: 10.1080/15548627.2020.1840796

frontiers | Frontiers in Physiology

TYPE Perspective
PUBLISHED 18 May 2023
DOI 10.3389/fphys.2023.1174655

OPEN ACCESS

EDITED BY
Dirk M. Hermann,
University of Duisburg-Essen, Germany

REVIEWED BY
Jiusheng Yan,
University of Texas MD Anderson Cancer Center, United States

*CORRESPONDENCE
Alexander V. Zholos,
avzholos@knu.ua

†These authors have contributed equally to this work

RECEIVED 28 February 2023
ACCEPTED 09 May 2023
PUBLISHED 18 May 2023

CITATION
Zholos AV, Dryn DO and Melnyk MI (2023), General anaesthesia-related complications of gut motility with a focus on cholinergic mechanisms, TRP channels and visceral pain.
Front. Physiol. 14:1174655.
doi: 10.3389/fphys.2023.1174655

General anaesthesia-related complications of gut motility with a focus on cholinergic mechanisms, TRP channels and visceral pain

Alexander V. Zholos[1]*, Dariia O. Dryn[2†] and Mariia I. Melnyk[1,2†]

[1]ESC "Institute of Biology and Medicine", Taras Shevchenko National University of Kyiv, Kyiv, Ukraine, [2]O.O. Bogomoletz Institute of Physiology, National Academy of Sciences of Ukraine, Kyiv, Ukraine

General anesthesia produces multiple side effects. Notably, it temporarily impairs gastrointestinal motility following surgery and causes the so-called postoperative ileus (POI), a multifactorial and complex condition that develops secondary to neuromuscular failure and mainly affects the small intestine. There are currently limited medication options for POI, reflecting a lack of comprehensive understanding of the mechanisms involved in this complex condition. Notably, although acetylcholine is one of the major neurotransmitters initiating excitation-contraction coupling in the gut, cholinergic stimulation by prokinetic drugs is not very efficient in case of POI. Acetylcholine when released from excitatory motoneurones of the enteric nervous system binds to and activates M2 and M3 types of muscarinic receptors in smooth muscle myocytes. Downstream of these G protein-coupled receptors, muscarinic cation TRPC4 channels act as the major focal point of receptor-mediated signal integration, causing membrane depolarisation accompanied by action potential discharge and calcium influx via L-type Ca^{2+} channels for myocyte contraction. We have recently found that both inhalation (isoflurane) and intravenous (ketamine) anesthetics significantly inhibit this muscarinic cation current (termed mI_{CAT}) in ileal myocytes, even when G proteins are activated directly by intracellular GTPγS, i.e., bypassing muscarinic receptors. Here we aim to summarize Transient Receptor Potential channels and calcium signalling-related aspects of the cholinergic mechanisms in the gut and visceral pain, discuss exactly how these may be negatively impacted by general anaesthetics, while proposing the receptor-operated TRPC4 channel as a novel molecular target for the treatment of POI.

KEYWORDS

smooth muscles, DRG neurons, visceral pain/visceral nociception/visceral hypersensitivity, TRP channels, G proteins, neurotransmission, intracellular calcium, patch-clamp

Abbreviations: CNS, central nervous system; DRG, dorsal root ganglia; EA, (–)-englerin A; ENS, enteric nervous system; GI, gastrointestinal; IBS, irritable bowel syndrome; mAChR, muscarinic acetylcholine receptor; mI_{CAT}, muscarinic receptor cation current; POI, postoperative ileus; PTSD, post-traumatic stress disorder; SM, smooth muscle; TRP, Transient Receptor Potential.

1 Introduction

Postoperative ileus (POI) remains one of the most common and costly for the healthcare system complications of surgery, in particular abdominal surgery. POI is a multifactorial problem, whereby administration of general anaesthetics and anxiolytics is certainly one of the multiple risk factors, and is likely especially important during the first neurological phase of POI involving sympathetic and enteric nervous systems (Venara et al., 2016; Wattchow et al., 2021).

General anaesthetics are primarily aimed at targeting specific receptors of the central nervous system (CNS), but these drugs can also affect other molecular off-targets, such as receptors and ion channels outside of the CNS. Understanding how general anaesthetics can negatively affect gut motility would seem to require, in the first place, knowledge of their effects within the enteric nervous system (ENS), as well as on the pacemaker cells of the gastrointestinal (GI) tract - Interstitial Cells of Cajal (ICC cells), which coordinate and regulate the sensory, secretory and motor functions of the gut (Spencer and Hu, 2020). Indeed, one of the pioneer studies in this area has demonstrated that phencyclidine and related drugs including ketamine decreased neurogenic contractions of guinea-pig ileum and shifted the dose-response curve to acetylcholine to higher agonist concentrations. The authors have thus suggested that these drugs interact with both enteric neurones and smooth muscle myocytes (Gintzler et al., 1982). However, there has not been much subsequent progress towards delineating specific molecular and/or cellular pathways involved. On the other hand, among various prokinetic drugs used for POI treatment (Venara et al., 2016), low concentrations of neostigmine, which is an inhibitor of acetylcholinesterase, may be beneficial (results of the recent systematic review and meta-analysis performed by Liao et al., 2021), which calls for a better understanding of the possible dysfunction of the acetylcholine-mediated signal transduction during the impairment of GI motility by general anaesthetics.

Strong evidence has been accumulated over the recent years indicating a major functional role of various subtypes of Transient Receptor Potential (TRP) channels in smooth muscles and sensory neurons (Venkatachalam and Montell, 2007; Tsvilovskyy et al., 2009). Recent studies (Matta et al., 2008; Abeele et al., 2013; Dryn et al., 2018; Wang et al., 2019; Melnyk et al., 2020) have shown that TRP channels could interact with general anesthetics at subclinical doses, which makes them highly likely primary candidates for the development of side effects produced by local and general anaesthetics. Thus, in recent years we focused our research on the problem of how general anaesthetics, such as isoflurane and ketamine, affect acetylcholine-activated TRPC4 channels, which mediate muscarinic cation current in ileal myocytes, termed mI_{CAT} (Tsvilovskyy et al., 2009). Since TRPC4 channels are widely expressed in the CNS, ENS, ICC and GI smooth muscle myocytes they are increasingly proposed as promising pharmacological targets (Boesmans et al., 2011), but their role in GI pathophysiology in general, and specifically in the pathogenesis of POI, remains to be better elucidated, prompting us to summarize the current status of this research in this Perspective.

1.1 TRP channels and pain

Chronic pain significantly impairs quality of life. As reviewed by Julius (2013), TRP channels play a significant role in pain signalling (Julius, 2013). TRP channels are known as polymodal sensors of various stimuli, including chemical modulators, reactive oxygen species, changes in pH and temperature, and mechanical forces (Wu et al., 2010). Being a vital protective mechanism, pain perception could be a considerable problem under some pathological conditions, such as inflammation, when chronic pain develops. Among multiple other co-morbidities, severe pain also correlates with POI. Recent studies have highlighted the involvement of several members of the TRP superfamily of ion channels in producing pain. The cold receptor TRPM8 is expressed in various sensory neurons and is involved in cold nociception (Knowlton et al., 2013). Notably, these channels perceive noxious cold, innocuous cooling and TRPM8-mediated analgesia differently (Laing and Dhaka, 2016). These channels are implicated in inflammatory and neuropathic cold allodynia and other cold hypersensitivity (Bautista et al., 2007; Colburn et al., 2007; Moran and Szallasi, 2018). A recent study has identified the efficacy of novel TRPM8 antagonists in treating both inflammatory and neuropathic pain (De Caro et al., 2018). Different pharmaceutical companies have been developing novel TRPM8 antagonists as pharmacological treatment for chronic or inflammatory pain, migraine and chemotherapeutic-induced allodynia (Weyer and Lehto, 2017). However, as of yet there are no ongoing clinical trials of these compounds.

The other member of the TRP superfamily which is expressed in neuronal, smooth muscles cells and other non-neuronal cells is TRPV4, a multimodal sensor which underlies regulation of several important physiological functions such as osmotic, mechanical and warm temperature sensation (Everaerts et al., 2010; Moore et al., 2018). Recent studies revealed the involvement of this channel in nociception, in particular in joint- and skin-mediated inflammatory pain, neuropathic pain and visceral pain (Alessandri-Haber et al., 2004; Brierley et al., 2008; Moore et al., 2013; O'Conor et al., 2016; Qu et al., 2016). These data indicate that TRP channels are promising therapeutic targets for chronic pain relief. Better understanding of the underlying molecular mechanisms of the TRP channels' role in nociception could promote the search for chemical compounds as prospective and novel pharmacological approaches targeting these channels for effective pain relief.

1.2 The role of TRP channels in visceral pain generation triggered by smooth muscle spasm

The GI tract has differentiated sensory afferent innervation, with sensory neurones located in the dorsal root ganglia (DRGs), nodose ganglia and the inferior ganglion of the vagus nerve (Brookes et al., 2013; Spencer and Hu, 2020). Visceral pain can be associated with smooth muscle (SM) spasms, in turn causing irritable bowel syndrome (IBS). Abdominal pain is a primary symptom of IBS (Keszthelyi et al., 2012a; 2012b). Several of the TRP channels (most notably TRPA1, TRPC4, TRPV1 and TRPV4) are expressed in the gut, where they play important roles in multiple pathophysiological

processes, including visceral nociception and pain (Boesmans et al., 2011; Holzer, 2011). Thus, TRPC4 channels opened secondary to muscarinic acetylcholine receptor activation trigger excitation and contraction of small intestinal smooth muscles (Bolton et al., 1999; Tsvilovskyy et al., 2009). TRPV4 senses local pressure that can become painful when it exceeds certain threshold level (Liedtke, 2005). Moreover, TRPV4 in afferent nerves can be sensitized *via* protease-activated receptor 2 thus evoking visceral hyperalgesia (Sipe et al., 2008). The molecular pathophysiology of IBS is not completely understood (Shah et al., 2020), but among other ion channels, TRPV4 and TRPA1 have been suggested as important sensory channels in IBS (Yang et al., 2022).

Currently, three main agent classes are used for SM antispasmodic action: antimuscarinic agents (Tobin et al., 2009), calcium channel inhibitors (Evangelista, 2004), and direct smooth muscle relaxants (Subissi et al., 1983), but their efficiency is less than optimal, making these compounds questionable for their clinical use. There is thus an urgent need to develop other therapies for treating chronic abdominal pain, such as TRP channels modulators.

1.3 The mechanism of general anaesthesia action on TRP channels

Inhaled anesthetics rapidly equilibrate between air in the alveoli and capillary blood. Small hydrophobic molecules like anesthetics can first of all affect the membrane lipid bilayer, thus nonspecifically altering the functions of multiple, if not all, transmembrane proteins (Tsuchiya and Mizogami, 2013). The second, much better understood group of their molecular targets includes plasma membrane receptors and ion channels. Among the latter, both voltage-gated (Ca^{2+}, Na^+ and K^+ channels of different types) and ligand-activated (such as nicotinic acetylcholine receptors, serotonin, glycine and $GABA_A$ receptors) received considerable attention in this context (Jenkins et al., 1996; Tassonyi et al., 2002; Hara and Sata, 2007; Alberola-Die et al., 2011; Germann et al., 2016; Liu et al., 2019; Mathie et al., 2021). For example, the inhalational anaesthetic isoflurane, which is a halogenated ether, targets $GABA_A$, glutamate and glycine receptors, while ketamine is best characterised as an antagonist of NMDA receptors, which determines its strong analgesic action (Franks, 2006; Franks, 2008).

The TRP channels discussed above represent yet another group of such targets. There is indeed growing evidence in this area of research showing that, for example, halothane, chloroform, and propofol can inhibit TRPC5 channels (Bahnasi et al., 2008), isoflurane can activate TRPA1 channels in sensory DRG neurones (Matta et al., 2008), while propofol affects TRPA1 and TRPV1 channels as became evident from observing propofol-induced vasorelaxation of coronary arterioles (Wang et al., 2015).

Acetylcholine, a major neurotransmitter that plays multiple important roles in the central and peripheral nervous system, activates muscarinic acetylcholine receptors (mainly of M2 and M3 subtypes), which are the main excitatory receptor subtypes expressed in GI smooth muscles (Bolton, 1972; 1979; Zholos, 2006). This, in turn, results in the openings of two receptor-operated cation channels, TRPC4 and TRPC6, of which TRPC4 is of main importance since it mediates about 85% of mI_{CAT} (Tsvilovskyy et al., 2009). Signal transduction pathways leading to TRPC4 are complex, since two receptor subtypes, which are differentially coupled to Gi/o and Gq/11 proteins, are involved (M2 and M3 receptors, respectively). These have been previously extensively studied and reviewed (Zholos and Bolton, 1997; Bolton et al., 1999; Zholos et al., 2004; Zholos, 2006; Sakamoto et al., 2007; Tanahashi et al., 2020), as summarised schematically in Figure 1. In brief, these receptors systems act in synergy, whereby the $M_2/G_{i/o}$ is of primary nature, while the M_3/G_q/PLC system and the increase in intracellular Ca^{2+} concentration it produces by $InsP_3$-evoked Ca^{2+} release play both permissive (at least in part via PIP_2 depletion) and potentiating (via $[Ca^{2+}]_i$ elevation) roles. We therefore reasoned that inhibition of mI_{CAT} generation as the primary mechanism of cholinergic excitation-contraction coupling in the gut (Bolton et al., 1999) can occur at different levels, ranging from muscarinic receptors and the G-proteins that are coupled to them, and to Ca^{2+} signalling and TRPC4 channels themselves.

We have addressed these possibilities using a range of experimental techniques, from patch-clamp recordings to *in vitro* contractile recordings, in our recent studies of isoflurane and ketamine effects on mI_{CAT} and spontaneous as well as carbachol-stimulated contractions of ileal smooth muscles (Dryn et al., 2018; Melnyk et al., 2020). To bypass the receptor activation step, GTPγS infusion via patch-pipette was employed for direct activation of all trimeric G-proteins. Intriguingly, both isoflurane and ketamine strongly inhibited both carbachol- and GTPγS-induced mI_{CAT} at clinically relevant concentrations, and the inhibitory effects had much in common. Thus, muscarinic receptors are not the major targets of their action, and hence any strategy aimed at the upregulation of mACh receptor activity, such as inhibitors of acetylcholinesterase, would be, in theory, not very efficient. At the same time the effect of ketamine was effectively opposed by the direct TRPC4 agonist (−)-englerin A (EA) indicating that the function of the channel itself was preserved (Melnyk et al., 2020) (Figure 1). We thus concluded that TRPC4 agonists may be used for the correction of GI motility suppression induced by general anesthesia. It is worth noting that there has recently been significant progress in developing nontoxic analogue of EA (Seenadera et al., 2022).

1.4 Post-traumatic stress disorder and antidepressants

Currently, the most effective and widely used treatments for post-traumatic stress disorder (PTSD) are antidepressants and anxiolytics, but other novel treatments are being considered, especially for the treatment of more refractory and disabling cases of PTSD (Ipser and Stein, 2012; Liriano et al., 2019). Thus, ketamine is not only a widely used anesthetic, but has recently been considered as a potential antidepressant (Duman et al., 2012; Zanos and Gould, 2018; Jeong et al., 2022), in particular as a promising and novel pharmacotherapeutic agent for PTSD patients, especially in more complex cases (Liriano et al., 2019).

Recent studies have shown that some novel modulators of TRP channels possess antidepressant action. A recently identified inhibitor of TRPC4/C5 channels, M084, has demonstrated antidepressant and anxiolytic effects (Yang et al., 2015). HC-070, a new small molecule antagonist of these channels, also possess antidepressant effects and may be proposed as a treatment for a

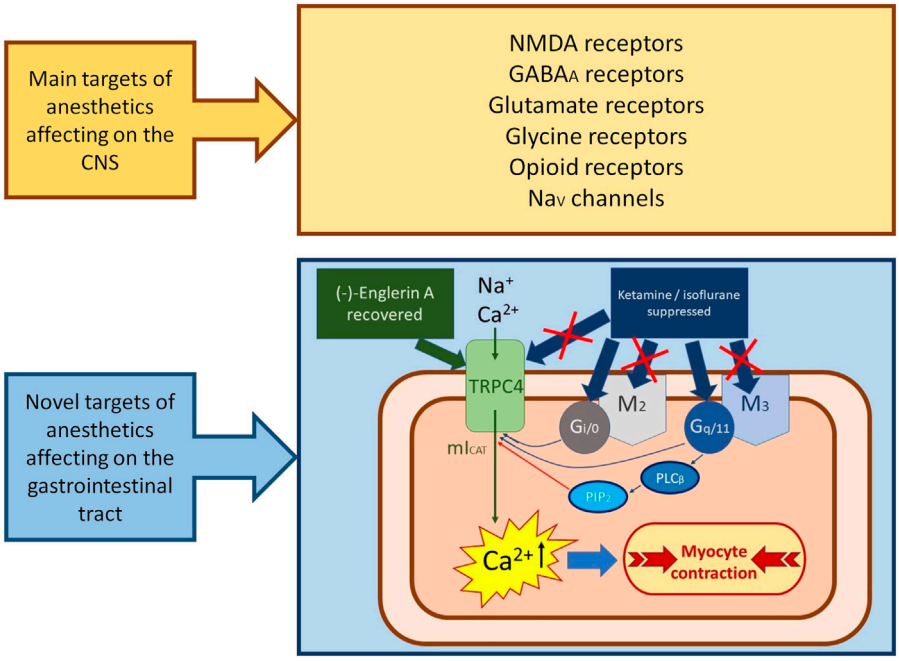

FIGURE 1
The schematic illustration of the possible mechanism of anaesthetics side-effects action on the novel molecular targets in intestinal myocytes. Acting in synergy with muscarinic M2 and M3 receptors coupled to $G_{i/o}$- and $G_{q/11}$-proteins, respectively, TRPC4 channels are the main molecular component of depolarizing inward current mI_{CAT}, which is the principal regulator of cholinergic excitation-contraction coupling in intestinal smooth muscles. Anaesthetics (ketamine and isoflurane) strongly suppressed mI_{CAT}, acting more likely on G-proteins, but minimally on M2/M3 receptors. TRPC4 channels direct agonist (–)-englerin A recovered ketamine-induced inhibition of mI_{CAT}, suggesting that this anaesthetic is targeting G-proteins rather than TRPC4 channels.

number of symptoms of psychiatric disorders (Just et al., 2018). Antidepressants, in turn, affect TRP channels, and not only in the nervous system, but also in other systems and organs, where they can produce side effects. It was shown that tricyclic antidepressants, which are also used for treating IBS, inhibited TRPC4 channels in colonic myocytes, resulting in suppression of GI motility (Jeong et al., 2022). These results well correlate with our recent studies of the inhibitory action of ketamine and isoflurane on the TRPC4 channel-mediated mI_{CAT} in mouse small intestinal myocytes (Dryn et al., 2018; Melnyk et al., 2020). Thus, antidepressants and anxiolytics can modulate the TRP channels function, which in turn could lead to intestinal complications.

2 Conclusion and further research

Currently, continuation of the studies of the side effects of anaesthetics and antidepressants on TRP channels, in particular in intestinal myocytes, remains an important task. War and military actions are the most significant factors of PTSD development, and also of the increase in the number and complexity of surgical interventions. According to the latest medical reports from the Ministry of Health of Ukraine, as a result of the Russian invasion of Ukraine in 2022 and the ongoing war, the risk of PTSD occurrence can be very high and will amount from 4.5 to 15 million people, including both military personnel and civilians (Bryant et al., 2022; Cai et al., 2022; Chaaya et al., 2022; Zaliska et al., 2022). The results of such studies as outlined in this Perspective can propose some recommendations for optimizing protocols for the use and dosage of certain types of anaesthetics and antidepressants in medical practice, in particular in the treatment of PTSD. Thus, our own future studies will be aimed at revealing ion channel mechanisms of side effects of other widely used anaesthetics, as well as anxiolytics and antidepressants, and their combinations. Moreover, other members of the TRP family, in particular TRPV4 and TRPM8 channels, which are important for the regulation of blood vessel tone, need to be more fully characterized in this context (Melanaphy et al., 2016; Dryn et al., 2018). There is accumulating evidence that some anaesthetics can affect these two types of channels (Abeele et al., 2013; Wang et al., 2019), as well as vascular tone (Liu et al., 2009; Gille et al., 2012; Sakai et al., 2014), therefore this research area is also relevant and promising.

Data availability statement

The original contributions presented in the study are included in the article/Supplementary Material, further inquiries can be directed to the corresponding author.

Ethics statement

The animal study was reviewed and approved. This Perspective refers to some results in our two papers published

previously. These are referenced, and the original papers include relevant Ethics information (Dryn et al., 2018; Melnyk et al., 2020).

Author contributions

AZ supervised the project; AZ, DD, and MM designed the studies outlined in this paper; DD, MM drafted the manuscript; AZ, DD, and MM finalized and approved the final version of the manuscript. All authors listed have made a substantial, direct, and intellectual contribution to the work and approved it for publication.

Funding

Supported by the Ministry of Education and Science of Ukraine (Grant No. 0122U001535 to AZ and MM) and National Academy of Sciences of Ukraine (Grant No. 0122U002126 to DD and MM).

Acknowledgments

We are grateful to Professor David J. Beech for a gift of (−)-englerin A and to Dmytro O. Dziuba for his consultations and discussion of the clinical significance/implications of our research findings.

Conflicts of interest

The authors declare that the research was conducted in the absence of any commercial or financial relationships that could be construed as a potential conflict of interest.

Publisher's note

All claims expressed in this article are solely those of the authors and do not necessarily represent those of their affiliated organizations, or those of the publisher, the editors and the reviewers. Any product that may be evaluated in this article, or claim that may be made by its manufacturer, is not guaranteed or endorsed by the publisher.

References

Abeele, F. V., Kondratskyi, A., Dubois, C., Shapovlov, G., Gkika, D., Busserolles, J., et al. (2013). Complex modulation of the cold receptor TRPM8 by volatile anaesthetics and its role in complications of general anaesthesia. *J. Cell Sci.* 126, 4479–4489. doi:10.1242/JCS.131631

Alberola-Die, A., Martinez-Pinna, J., González-Ros, J. M., Ivorra, I., and Morales, A. (2011). Multiple inhibitory actions of lidocaine on *Torpedo* nicotinic acetylcholine receptors transplanted to *Xenopus* oocytes. *J. Neurochem.* 117, 1009–1019. doi:10.1111/J.1471-4159.2011.07271.X

Alessandri-Haber, N., Dina, O. A., Yeh, J. J., Parada, C. A., Reichling, D. B., and Levine, J. D. (2004). Transient receptor potential vanilloid 4 is essential in chemotherapy-induced neuropathic pain in the rat. *J. Neurosci.* 24, 4444–4452. doi:10.1523/JNEUROSCI.0242-04.2004

Bahnasi, Y. M., Wright, H. M., Milligan, C. J., Dedman, A. M., Zeng, F., Hopkins, P. M., et al. (2008). Modulation of TRPC5 cation channels by halothane, chloroform and propofol. *Br. J. Pharmacol.* 153, 1505–1512. doi:10.1038/SJ.BJP.0707689

Bautista, D. M., Siemens, J., Glazer, J. M., Tsuruda, P. R., Basbaum, A. I., Stucky, C. L., et al. (2007). The menthol receptor TRPM8 is the principal detector of environmental cold. *Nature* 448, 204–208. doi:10.1038/NATURE05910

Boesmans, W., Owsianik, G., Tack, J., Voets, T., and Vanden Berghe, P. (2011). TRP channels in neurogastroenterology: Opportunities for therapeutic intervention. *Br. J. Pharmacol.* 162, 18–37. doi:10.1111/j.1476-5381.2010.01009.x

Bolton, T. B. (1979). Mechanisms of action of transmitters and other substances on smooth muscle. *Physiol. Rev.* 59, 606–718. doi:10.1152/PHYSREV.1979.59.3.606

Bolton, T. B., Prestwich, S. A., Zholos, A. V., and Gordienko, D. V. (1999). Excitation-contraction coupling in gastrointestinal and other smooth muscles. *Annu. Rev. Physiol.* 61, 85–115. doi:10.1146/annurev.physiol.61.1.85

Bolton, T. B. (1972). The depolarizing action of acetylcholine or carbachol in intestinal smooth muscle. *J. Physiol.* 220, 647–671. doi:10.1113/JPHYSIOL.1972.SP009728

Brierley, S. M., Page, A. J., Hughes, P. A., Adam, B., Liebregts, T., Cooper, N. J., et al. (2008). Selective role for TRPV4 ion channels in visceral sensory pathways. *Gastroenterol* 134, 2059–2069. doi:10.1053/J.GASTRO.2008.01.074

Brookes, S. J. H., Spencer, N. J., Costa, M., and Zagorodnyuk, V. P. (2013). Extrinsic primary afferent signalling in the gut. *Nat. Rev. Gastroenterol. Hepatol.* 10, 286–296. doi:10.1038/NRGASTRO.2013.29

Bryant, R. A., Schnurr, P. P., and Pedlar, D.5-Eyes Mental Health Research and Innovation Collaboration in military and veteran mental health (2022). Addressing the mental health needs of civilian combatants in Ukraine. *Lancet. Psychiatry* 9, 346–347. doi:10.1016/S2215-0366(22)00097-9

Cai, H., Bai, W., Zheng, Y., Zhang, L., Cheung, T., Su, Z., et al. (2022). International collaboration for addressing mental health crisis among child and adolescent refugees during the Russia-Ukraine war. *Asian J. Psychiatr.* 72, 103109. doi:10.1016/J.AJP.2022.103109

Chaaya, C., Thambi, V. D., Sabuncu, Ö., Abedi, R., Osman, A. O. A., Uwishema, O., et al. (2022). Ukraine – Russia crisis and its impacts on the mental health of Ukrainian young people during the COVID-19 pandemic. *Ann. Med. Surg.* 79, 104033. doi:10.1016/J.AMSU.2022.104033

Colburn, R. W., Lubin, M. L., Stone, D. J., Wang, Y., Lawrence, D., D'Andrea, M. R. R., et al. (2007). Attenuated cold sensitivity in TRPM8 null mice. *Neuron* 54, 379–386. doi:10.1016/J.NEURON.2007.04.017

De Caro, C., Russo, R., Avagliano, C., Cristiano, C., Calignano, A., Aramini, A., et al. (2018). Antinociceptive effect of two novel transient receptor potential melastatin 8 antagonists in acute and chronic pain models in rat. *Br. J. Pharmacol.* 175, 1691–1706. doi:10.1111/BPH.14177

Dryn, D., Luo, J., Melnyk, M., Zholos, A., and Hu, H. (2018). Inhalation anaesthetic isoflurane inhibits the muscarinic cation current and carbachol-induced gastrointestinal smooth muscle contractions. *Eur. J. Pharmacol.* 820, 39–44. doi:10.1016/j.ejphar.2017.11.044

Duman, R. S., Li, N., Liu, R. J., Duric, V., and Aghajanian, G. (2012). Signaling pathways underlying the rapid antidepressant actions of ketamine. *Neuropharmacol* 62, 35–41. doi:10.1016/J.NEUROPHARM.2011.08.044

Evangelista, S. (2004). Quaternary ammonium derivatives as spasmolytics for irritable bowel syndrome. *Curr. Pharm. Des.* 10, 3561–3568. doi:10.2174/1381612043382972

Everaerts, W., Nilius, B., and Owsianik, G. (2010). The vanilloid transient receptor potential channel TRPV4: From structure to disease. *Prog. Biophys. Mol. Biol.* 103, 2–17. doi:10.1016/J.PBIOMOLBIO.2009.10.002

Franks, N. P. (2008). General anaesthesia: From molecular targets to neuronal pathways of sleep and arousal. *Nat. Rev. Neurosci.* 9, 370–386. doi:10.1038/NRN2372

Franks, N. P. (2006). Molecular targets underlying general anaesthesia. *Br. J. Pharmacol.* 147 (1), S72–S81. doi:10.1038/SJ.BJP.0706441

Germann, A. L., Shin, D. J., Manion, B. D., Edge, C. J., Smith, E. H., Franks, N. P., et al. (2016). Activation and modulation of recombinant glycine and $GABA_A$ receptors by 4-halogenated analogues of propofol. *Br. J. Pharmacol.* 173, 3110–3120. doi:10.1111/BPH.13566

Gille, J., Seyfarth, H. J., Gerlach, S., Malcharek, M., Czeslick, E., and Sablotzki, A. (2012). Perioperative anesthesiological management of patients with pulmonary hypertension. *Anesthesiol. Res. Pract.* 2012, 356982. doi:10.1155/2012/356982

Gintzler, A. R., Zukin, R. S., and Zukin, S. R. (1982). Effects of phencyclidine and its derivatives on enteric neurones. *Br. J. Pharmacol.* 75, 261–267. doi:10.1111/j.1476-5381.1982.tb08782.x

Hara, K., and Sata, T. (2007). The effects of the local anesthetics lidocaine and procaine on glycine and gamma-aminobutyric acid receptors expressed in *Xenopus* oocytes. *Anesth. Analg.* 104, 1434–1439. doi:10.1213/01.ANE.0000261509.72234.A6

Holzer, P. (2011). TRP channels in the digestive system. *Curr. Pharm. Biotechnol.* 12, 24–34. doi:10.2174/138920111793937862

Ipser, J. C., and Stein, D. J. (2012). Evidence-based pharmacotherapy of post-traumatic stress disorder (PTSD). *Int. J. Neuropsychopharmacol.* 15, 825–840. doi:10.1017/S1461145711001209

Jenkins, A., Franks, N. P., and Lieb, W. R. (1996). Actions of general anaesthetics on 5-HT_3 receptors in N1E-115 neuroblastoma cells. *Br. J. Pharmacol.* 117, 1507–1515. doi:10.1111/J.1476-5381.1996.TB15314.X

Jeong, B., Sung, T. S., Jeon, D., Park, K. J., Jun, J. Y., So, I., et al. (2022). Inhibition of TRPC4 channel activity in colonic myocytes by tricyclic antidepressants disrupts colonic motility causing constipation. *J. Cell. Mol. Med.* 26 (19), 4911–4923. doi:10.1111/JCMM.17348

Julius, D. (2013). TRP channels and pain. *Annu. Rev. Cell Dev. Biol.* 29, 355–384. doi:10.1146/ANNUREV-CELLBIO-101011-155833

Just, S., Chenard, B. L., Ceci, A., Strassmaier, T., Chong, J. A., Blair, N. T., et al. (2018). Treatment with HC-070, a potent inhibitor of TRPC4 and TRPC5, leads to anxiolytic and antidepressant effects in mice. *PLoS One* 13 (1), e0191225. doi:10.1371/JOURNAL.PONE.0191225

Keszthelyi, D., Troost, F. J., and Masclee, A. A. (2012a). Irritable bowel syndrome: Methods, mechanisms, and pathophysiology. Methods to assess visceral hypersensitivity in irritable bowel syndrome. *Am. J. Physiol. Gastrointest. Liver Physiol.* 303 (2), G141–G154. doi:10.1152/AJPGI.00060.2012

Keszthelyi, D., Troost, F. J., Simrén, M., Ludidi, S., Kruimel, J. W., Conchillo, J. M., et al. (2012b). Revisiting concepts of visceral nociception in irritable bowel syndrome. *Eur. J. Pain* 16, 1444–1454. doi:10.1002/J.1532-2149.2012.00147.X

Knowlton, W. M., Palkar, R., Lippoldt, E. K., McCoy, D. D., Baluch, F., Chen, J., et al. (2013). A sensory-labeled line for cold: TRPM8-expressing sensory neurons define the cellular basis for cold, cold pain, and cooling-mediated analgesia. *J. Neurosci.* 33, 2837–2848. doi:10.1523/JNEUROSCI.1943-12.2013

Laing, R. J., and Dhaka, A. (2016). ThermoTRPs and pain. *Neuroscientist* 22, 171–187. doi:10.1177/1073858414567884

Liao, Y., Li, Y., and Ouyang, W. (2021). Effects and safety of neostigmine for postoperative recovery of gastrointestinal function: A systematic review and meta-analysis. *Ann. Palliat. Med.* 10, 12507–12518. doi:10.21037/apm-21-3291

Liedtke, W. (2005). TRPV4 as osmosensor: A transgenic approach. *Pflugers Arch.* 451, 176–180. doi:10.1007/S00424-005-1449-8

Liriano, F., Hatten, C., and Schwartz, T. L. (2019). Ketamine as treatment for post-traumatic stress disorder: A review. *Drugs Context* 8, 212305. doi:10.7573/DIC.212305

Liu, Q. Z., Hao, M., Zhou, Z. Y., Ge, J. L., Wu, Y. C., Zhao, L. L., et al. (2019). Propofol reduces synaptic strength by inhibiting sodium and calcium channels at nerve terminals. *Protein Cell* 10, 688–693. doi:10.1007/S13238-019-0624-1

Liu, Y., Chang, H., Niu, L., Xue, W., Zhang, X., Liang, Y., et al. (2009). Effects of propofol on responses of rat isolated renal arteriole to vasoactive agents. *Vasc. Pharmacol.* 51, 182–189. doi:10.1016/J.VPH.2009.06.003

Mathie, A., Veale, E. L., Cunningham, K. P., Holden, R. G., and Wright, P. D. (2021). Two-pore domain potassium channels as drug targets: Anesthesia and beyond. *Annu. Rev. Pharmacol. Toxicol.* 61, 401–420. doi:10.1146/ANNUREV-PHARMTOX-030920-111536

Matta, J. A., Cornett, P. M., Miyares, R. L., Abe, K., Sahibzada, N., and Ahern, G. P. (2008). General anesthetics activate a nociceptive ion channel to enhance pain and inflammation. *Proc. Natl. Acad. Sci. U. S. A.* 105, 8784–8789. doi:10.1073/PNAS.0711038105

Melanaphy, D., Johnson, C. D., Kustov, M. V., Watson, C. A., Borysova, L., Burdyga, T. V., et al. (2016). Ion channel mechanisms of rat tail artery contraction-relaxation by menthol involving, respectively, TRPM8 activation and L-type Ca^{2+} channel inhibition. *Am. J. Physiol. Heart Circ. Physiol.* 311, H1416–H1430. doi:10.1152/AJPHEART.00222.2015

Melnyk, M. I., Dryn, D. O., Al Kury, L. T., Dziuba, D. O., and Zholos, A. V. (2020). Suppression of mI_{CAT} in mouse small intestinal myocytes by general anaesthetic ketamine and its recovery by TRPC4 agonist (-)-englerin A. *Front. Pharmacol.* 11, 594882. doi:10.3389/fphar.2020.594882

Moore, C., Cevikbas, F., Pasolli, H. A., Chen, Y., Kong, W., Kempkes, C., et al. (2013). UVB radiation generates sunburn pain and affects skin by activating epidermal TRPV4 ion channels and triggering endothelin-1 signaling. *Proc. Natl. Acad. Sci. U. S. A.* 110 (34), E3225–E3234. doi:10.1073/PNAS.1312933110

Moore, C., Gupta, R., Jordt, S. E., Chen, Y., and Liedtke, W. B. (2018). Regulation of pain and itch by TRP channels. *Neurosci. Bull.* 34, 120–142. doi:10.1007/S12264-017-0200-8

Moran, M. M., and Szallasi, A. (2018). Targeting nociceptive transient receptor potential channels to treat chronic pain: Current state of the field. *Br. J. Pharmacol.* 175, 2185–2203. doi:10.1111/BPH.14044

O'Conor, C. J., Ramalingam, S., Zelenski, N. A., Benefield, H. C., Rigo, I., Little, D., et al. (2016). Cartilage-specific knockout of the mechanosensory ion channel TRPV4 decreases age-related osteoarthritis. *Sci. Rep.* 6, 29053. doi:10.1038/SREP29053

Qu, Y. J., Zhang, X., Fan, Z. Z., Huai, J., Teng, Y. B., Zhang, Y., et al. (2016). Effect of TRPV4-p38 MAPK pathway on neuropathic pain in rats with chronic compression of the dorsal root ganglion. *Biomed. Res. Int.* 2016, 6978923. doi:10.1155/2016/6978923

Sakai, Y., Kawahito, S., Takaishi, K., Mita, N., Kinoshita, H., Hatakeyama, N., et al. (2014). Propofol-induced relaxation of rat aorta is altered by aging. *J. Med. Invest.* 61, 278–284. doi:10.2152/JMI.61.278

Sakamoto, T., Unno, T., Kitazawa, T., Taneike, T., Yamada, M., Wess, J., et al. (2007). Three distinct muscarinic signalling pathways for cationic channel activation in mouse gut smooth muscle cells. *J. Physiol.* 582, 41–61. doi:10.1113/jphysiol.2007.133165

Seenadera, S. P. D., Long, S. A., Akee, R., Bermudez, G., Parsonage, G., Strope, J., et al. (2022). Biological effects of modifications of the englerin A glycolate. *ACS Med. Chem. Lett.* 13, 1472–1476. doi:10.1021/ACSMEDCHEMLETT.2C00258

Shah, A., Talley, N. J., Jones, M., Kendall, B. J., Koloski, N., Walker, M. M., et al. (2020). Small intestinal bacterial overgrowth in irritable bowel syndrome: A systematic review and meta-analysis of case-control studies. *Am. J. Gastroenterol.* 115, 190–201. doi:10.14309/AJG.0000000000000504

Sipe, W. E. B., Brierley, S. M., Martin, C. M., Phillis, B. D., Cruz, F. B., Grady, E. F., et al. (2008). Transient receptor potential vanilloid 4 mediates protease activated receptor 2-induced sensitization of colonic afferent nerves and visceral hyperalgesia. *Am. J. Physiol. Gastrointest. Liver Physiol.* 294 (5), G1288–G1298. doi:10.1152/AJPGI.00002.2008

Spencer, N. J., and Hu, H. (2020). Enteric nervous system: Sensory transduction, neural circuits and gastrointestinal motility. *Nat. Rev. Gastroenterol. Hepatol.* 17, 338–351. doi:10.1038/s41575-020-0271-2

Subissi, A., Brunori, P., and Bachi, M. (1983). Effects of spasmolytics on K^+-induced contraction of rat intestine *in vivo*. *Eur. J. Pharmacol.* 96, 295–301. doi:10.1016/0014-2999(83)90320-5

Tanahashi, Y., Katsurada, T., Inasaki, N., Uchiyama, M., Sakamoto, T., Yamamoto, M., et al. (2020). Further characterization of the synergistic activation mechanism of cationic channels by M 2 and M 3 muscarinic receptors in mouse intestinal smooth muscle cells. *Am. J. Physiol. Cell Physiol.* 318, C514–C523. doi:10.1152/AJPCELL.00277.2019

Tassonyi, E., Charpantier, E., Muller, D., Dumont, L., and Bertrand, D. (2002). The role of nicotinic acetylcholine receptors in the mechanisms of anesthesia. *Brain Res. Bull.* 57, 133–150. doi:10.1016/S0361-9230(01)00740-7

Tobin, G., Giglio, D., and Lundgren, O. (2009). Muscarinic receptor subtypes in the alimentary tract. *J. Physiol. Pharmacol.* 60 (3–21), 3–21. PMID: 19439804.

Tsuchiya, H., and Mizogami, M. (2013). Interaction of local anesthetics with biomembranes consisting of phospholipids and cholesterol: Mechanistic and clinical implications for anesthetic and cardiotoxic effects. *Anesthesiol. Res. Pract.* 2013, 297141. doi:10.1155/2013/297141

Tsvilovskyy, V. V., Zholos, A. V., Aberle, T., Philipp, S. E., Dietrich, A., Zhu, M. X., et al. (2009). Deletion of TRPC4 and TRPC6 in mice impairs smooth muscle contraction and intestinal motility *in vivo*. *Gastroenterol* 137, 1415–1424. doi:10.1053/j.gastro.2009.06.046

Venara, A., Neunlist, M., Slim, K., Barbieux, J., Colas, P. A., Hamy, A., et al. (2016). Postoperative ileus: Pathophysiology, incidence, and prevention. *J. Visc. Surg.* 153, 439–446. doi:10.1016/J.JVISCSURG.2016.08.010

Venkatachalam, K., and Montell, C. (2007). TRP channels. *Annu. Rev. Biochem.* 76, 387–417. doi:10.1146/ANNUREV.BIOCHEM.75.103004.142819

Wang, B., Wu, Q., Liao, J., Zhang, S., Liu, H., Yang, C., et al. (2019). Propofol induces cardioprotection against ischemia-reperfusion injury via suppression of Transient Receptor Potential Vanilloid 4 channel. *Front. Pharmacol.* 10, 1150. doi:10.3389/FPHAR.2019.01150

Wang, Y., Zhou, H., Wu, B., Zhou, Q., Cui, D., and Wang, L. (2015). Protein kinase C isoforms distinctly regulate propofol-induced endothelium-dependent and endothelium-independent vasodilation. *J. Cardiovasc. Pharmacol.* 66, 276–284. doi:10.1097/FJC.0000000000000275

Wattchow, D., Heitmann, P., Smolilo, D., Spencer, N. J., Parker, D., Hibberd, T., et al. (2021). Postoperative ileus—an ongoing conundrum. *Neurogastroenterol. Motil.* 33, e14046. doi:10.1111/nmo.14046

Weyer, A. D., and Lehto, S. G. (2017). Development of TRPM8 antagonists to treat chronic pain and migraine. *Pharm. (Basel)* 10 (2), 37. doi:10.3390/PH10020037

Wu, L. J., Sweet, T. B., and Clapham, D. E. (2010). International Union of Basic and Clinical Pharmacology. LXXVI. Current progress in the mammalian TRP ion channel family. *Pharmacol. Rev.* 62, 381–404. doi:10.1124/PR.110.002725

Yang, H., Hou, C., Xiao, W., and Qiu, Y. (2022). The role of mechanosensitive ion channels in the gastrointestinal tract. *Front. Physiol.* 13, 904203. doi:10.3389/fphys.2022.904203

Yang, L. P., Jiang, F. J., Wu, G. S., Deng, K., Wen, M., Zhou, X., et al. (2015). Acute treatment with a novel TRPC4/C5 channel inhibitor produces antidepressant and anxiolytic-like effects in mice. *PLoS One* 10 (8), e0136255. doi:10.1371/journal.pone.0136255

Zaliska, O., Oleshchuk, O., Forman, R., and Mossialos, E. (2022). Health impacts of the Russian invasion in Ukraine: Need for global health action. *Lancet* 399, 1450–1452. doi:10.1016/S0140-6736(22)00615-8

Zanos, P., and Gould, T. D. (2018). Mechanisms of ketamine action as an antidepressant. *Mol. Psychiatry* 23, 801–811. doi:10.1038/MP.2017.255

Zholos, A. V., and Bolton, T. B. (1997). Muscarinic receptor subtypes controlling the cationic current in Guinea-pig ileal smooth muscle. *Br. J. Pharmacol.* 122, 885–893. doi:10.1038/SJ.BJP.0701438

Zholos, A. V. (2006). Regulation of TRP-like muscarinic cation current in gastrointestinal smooth muscle with special reference to PLC/$InsP_3$/Ca^{2+} system. *Acta Pharmacol. Sin.* 27, 833–842. doi:10.1111/J.1745-7254.2006.00392.X

Zholos, A. V., Tsytsyura, Y. D., Gordienko, D. V., Tsvilovskyy, V. V., and Bolton, T. B. (2004). Phospholipase C, but not $InsP_3$ or DAG, -dependent activation of the muscarinic receptor-operated cation current in Guinea-pig ileal smooth muscle cells. *Br. J. Pharmacol.* 141, 23–36. doi:10.1038/SJ.BJP.0705584

frontiers | Frontiers in Cellular Neuroscience

TYPE Original Research
PUBLISHED 01 June 2023
DOI 10.3389/fncel.2023.1192780

OPEN ACCESS

EDITED BY
Alexander V. Zholos,
Taras Shevchenko National University of Kyiv, Ukraine

REVIEWED BY
Matthew McMillin,
The University of Texas at Austin, United States
Kalliopi Pitarokoili,
St Josef Hospital, Germany

*CORRESPONDENCE
Olena A. Petrushenko
✉ petrushenko@biph.kiev.ua

RECEIVED 29 March 2023
ACCEPTED 09 May 2023
PUBLISHED 01 June 2023

CITATION
Petrushenko OA, Stratiievska AO, Petrushenko MO and Lukyanetz EA (2023) Resensitization of TRPV1 channels after the P2 receptor activation in sensory neurons of spinal ganglia in rats.
Front. Cell. Neurosci. 17:1192780.
doi: 10.3389/fncel.2023.1192780

Resensitization of TRPV1 channels after the P2 receptor activation in sensory neurons of spinal ganglia in rats

Olena A. Petrushenko*, Anastasiiya O. Stratiievska, Mariia O. Petrushenko and Elena A. Lukyanetz

Department of Biophysics of Ion Channels, Bogomoletz Institute of Physiology, Kyiv, Ukraine

Introduction: TRPV1 channels are responsible for detecting noxious stimuli such as heat (>43°C), acid, and capsaicin. P2 receptors are involved in numerous functions of the nervous system, including its modulation and specific response to the application of ATP. In our experiments, we investigated the dynamics of calcium transients in DRG neurons associated with TRPV1 channel desensitization and the effect of activation of P2 receptors on this process.

Methods: We used DRG neurons from rats P7–8 after 1–2 days of culture to measure calcium transients by microfluorescence calcimetry using the fluorescent dye Fura-2 AM.

Results: We have shown that DRG neurons of small (d < 22 μm) and medium (d = 24–35 μm) sizes differ in TRPV1 expression. Thus, TRPV1 channels are mainly present in small nociceptive neurons (59% of the studied neurons). Short-term sequential application of the TRPV1 channel agonist capsaicin (100nM) leads to the desensitization of TRPV1 channels by the type of tachyphylaxis. We identified three types of sensory neurons based on responses to capsaicin: (1) desensitized 37.5%, (2) non-desensitized 34.4%, and (3) insensitive 23.4% to capsaicin. It has also been shown that P2 receptors are present in all types of neurons according to their size. So, the responses to ATP were different in different-sized neurons. Applying ATP (0.1 mM) to the intact cell membrane after the onset of tachyphylaxis caused recovery of calcium transients in response to the addition of capsaicin in these neurons. The amplitude of the capsaicin response after reconstitution with ATP was 161% of the previous minimal calcium transient in response to capsaicin.

Discussion: Significantly, the restoration of the amplitude of calcium transients under the ATP application is not associated with changes in the cytoplasmic pool of ATP because this molecule does not cross the intact cell membrane, thus, our results show the interaction between TRPV1 channels and P2 receptors. It is important to note that the restoration of the amplitude of calcium transients through TRPV1 channels after application of ATP was observed mainly in cells of 1–2 days of cultivation. Thus, the resensitization of capsaicin transients following P2 receptor activation may be associated with the regulation of the sensitivity of sensory neurons.

KEYWORDS

P2 receptor, TRPV1 channel, capsaicin, ATP, DRG neurons, desensitization, resensitization, calcium ions

1. Introduction

TRPV1 (transient receptor potential vanilloid 1) channels belong to the receptor-controlled cationic channels of transient receptor potential, which are activated by vanilloids, and provide thermoreception in the range of 33–39°C and nociception. The most well-known activator of TRPV1 receptors is capsaicin (Caterina et al., 1997). Long-term use of capsaicin leads to almost complete desensitization of the TRPV1 channel. An increase in the intracellular concentration of Ca^{2+} ions facilitates this desensitization (Koplas et al., 1997; Mandadi et al., 2004; Liu et al., 2005).

Desensitization of TRPV1 channels to the action of capsaicin can be acute when the receptor loses its ability to respond to the application of an agonist after its long-term application, and tachyphylaxis, which is manifested in a gradual decrease in the maximum amplitude of calcium transients during successive short-term additions of the same concentrations of capsaicin (Petrushenko et al., 2018, 2020). TRPV1 desensitization is, at least in part, a Ca^{2+-}dependent process and is reportedly enhanced by dephosphorylation of the receptor by calmodulin-dependent phosphatase 2B (calcineurin; Docherty et al., 1996; Numazaki et al., 2002; Mohapatra and Nau, 2005; Lukacs et al., 2007; Szallasi et al., 2007; Petrushenko et al., 2021).

The process of increased activity (sensitization) of the nociceptor is called hyperalgesia. Sensitization of TRPV1 receptors in the cytoplasm is mediated by various plasma agents (Lopshire and Nicol, 1998; Tominaga et al., 2001; Mandadi et al., 2004; Liu et al., 2005; Petrushenko et al., 2020). On the other hand, some works show the role of the application of agonists for metabotropic receptors on the cell membrane in the sensitization of TRPV1 receptors (Lopshire and Nicol, 1998; Zhang et al., 2005; Petrushenko et al., 2021). The study (Shimizu et al., 2022) shows that intracellular ATP regulates the basal activity of TRPV1 channels in the absence of capsaicin. These results suggest that intracellular ATP functions as a modifier of TRPV1 channel gating.

Application ATP on the plasma membrane activates ionotropic P2X and metabotropic P2Y receptors. This division is based on the molecular structure and mechanism of signal transmission (Roberts et al., 2006; Evans, 2009; Burnstock, 2012; Petrushenko, 2012). ATP, acting on P2 receptors, leads to significant changes in cell membrane permeability (Nicke et al., 1998; Burgard et al., 1999; MacKenzie et al., 1999; Torres et al., 1999).

We hypothesize that activation of P2 receptors has a regulatory effect on TRPV1 channels in rat sensory neurons.

2. Methods

2.1. Obtaining cultures of DRG neurons

An 8-day-old female rat (P8) was used to obtain a culture of DRG neurons. The rat was sedated with ether, decapitated, and the spinal cord was removed. In total, 15–18 dorsal ganglia were sequentially isolated from the cleaned spinal canal. Freshly isolated cells were placed in a solution of MEM with the addition of HEPES-NaOH (pH 7.4). Ganglion bodies were separated from nerve fibers and placed in a solution containing the enzymes trypsin 2 mM and collagenase 1 mM, which was incubated in a thermostat for 30–35 min at $t = 37°C$. Next, the ganglia were moved into a medium solution containing fetal serum and incubated in a CO_2 incubator for 10 min to inactivate enzymes. The bodies of the ganglia were freed from the connective tissue sheath, and each was cut into several parts with the help of scissors. After that, 0.5 ml of the medium solution was homogenized with a glass pipette with a hole <0.5 mm in diameter until the solution became cloudy. A drop of the resulting cell suspension was placed in a Petri dish containing 5–7 glass slides with a diameter of 10 mm and 2 ml of medium solution. After that, the glass with the neuron suspension was kept in a CO_2 incubator for 24 h to 7 days, with periodic replacement of the culture medium every 3–5 days.

2.2. Experimental solutions and media for cell cultivation

The isolation solution is aqueous on MEM with (mM) 10HEPES and a pH of 7.4.

The culture medium containing 90% DMEM liquid medium and 10% inactivated fetal calf serum, 2 mM $NaHCO_3$, 2 mM glutamine, 5 mM sodium pyruvate, 0.6 μM dry bovine insulin, and a penicillin/streptomycin mixture (0.03%) was added to the resulting solution.

The base solution for the experiments is an aqueous Tyrode solution containing (in mmol/l) 125 NaCl; 2.5 KCl; 2 $CaCl_2$, 1 $MgCl_2$, 10 glucose, and 20 HEPES. The required concentration of $CaCl_2$ (1–3 mM) was added under the experimental conditions. The pH of the solution was adjusted to 7.35–7.40.

Extracellular solution with an increased concentration of KCl contained (in mmol/l) 78 NaCl; 50 KCl; 2 $CaCl_2$, 1 $MgCl_2$, 10 glucose, and 20 HEPES. The pH of the solution was adjusted to 7.35–7.40.

The ATP and capsaicin solutions used in the experiments were prepared based on Tyrode's basic solution and contained 100 μM ATP and 1 μM capsaicin, respectively.

All reagents used to prepare the above solutions were purchased from Sigma, USA.

2.3. Measurement of intracellular Ca^{2+} level (calcium imaging)

Intracellular calcium concentration was measured using an experimental setup consisting of an optical microscope (Olympus IX70 Tokyo, Japan), an experimental camera fixed on the microscope platform, image recording and data logging software (Cell M Imaging Software, Olympus, Tokyo, Japan), local application system, a monochromator, and a light source (Illumination System MT10, Olympus, Tokyo, Japan).

To measure the intracellular concentration of calcium ($[Ca^{2+}]i$), we used the common calcium-sensitive dye Fura-2, which was loaded into the DRG cells using the lipophilic form of the Fura-2 AM dye (Molecular Probes, USA), which can penetrate the cell membrane. After Fura-2 AM enters the cell, the dye is cleaved by intracellular esterases and converted into a hydrophilic,

calcium-sensitive form (Fura-2), which no longer penetrates the cell membrane.

Freshly isolated DRG neurons were incubated for 30 min at 37°C in a base solution containing 1–2 μm Fura-2 AM. After that, the cells were washed with a pure basic solution and left in the dark at 37°C for 30–40 min for the final de-esterification of Fura-2 AM. A Petri dish with glass on the surface of which the cells were attached was placed in the field of view of an Olympus IX70 inverted microscope (Tokyo, Japan) with a short-focus objective with a magnification of x20. The measurement and data recording processes were managed using the Cell M Imaging Software (Olympus, Tokyo, Japan). A local application system changed the extracellular solution around the selected cell. The experimental setup allowed working in two modes. Thus, the object was illuminated in the setting mode by a visible light source. In registration mode, the installation was set to illuminate the object using a xenon lamp. In this mode, the fluorescent probe is excited at 340 and 380 nm wavelengths using appropriate filters. The emission of the probe was recorded in the ranges of 395–415 nm (F1) and 470–490 nm (F2) using two photomultipliers. The signals from the photomultipliers were fed to the input (DIV100, Burr Broun, USA), which in real time calculated the ratio of fluorescent probe signals at two wavelengths of excitation light: Ratio = F1/F2 = F340/F380. The obtained experimental data were digitized and stored on the computer's hard disk for further processing.

2.4. Statistical processing of the obtained results

The analysis of experimental data was carried out using the program Microcal™ Origin Pro™, version 8.5 (Microcal Software Inc., USA). Based on the obtained values, histograms of the distribution of the "Microcal™ Origin Pro™" program, version 8.5, were constructed. Finding the most probable values was carried out by the standard method of approximating the obtained histograms with the Gaussian distribution. Data groups were assessed for normality using the "Origin Pro™" software as the Shapiro–Wilk normality test. Statistical hypotheses were assessed using the Student's *t*-test.

3. Results

3.1. The role of purinoreceptors in generating ATP-induced calcium transients in DRG cells

Our studies by the method of microfluorescence calcimetry showed that the sequential injection of ATP (5 s) with an interval of 60 s into neurons of the dorsal ganglion causes a rapid and short-term increase in the concentration of cytosolic calcium $[Ca^{2+}]i$. The concentration of $[Ca^{2+}]i$ reaches a maximum of 2–4 s after 3–5 s of ATP application and returns to the basal level after ATP was removed from the solution.

To study the dynamics of calcium entry into neurons, we applied ATP several times with an interval of 60 s.

The first type of response developed if the successive application of ATP caused a gradual decrease in the amplitude of Ca^{2+} transients (by 30 ± 4%) compared to the first (control) application. Continuation of such applications every 20–25 s led to a decrease in the amplitude of transients almost to zero in some neurons. This decrease occurred as a result of the desensitization of Ca transients by the type of tachyphylaxis.

The second type of response was characterized by the preservation of the amplitude of calcium transients in the conditions of several consecutive applications of ATP and the non-availability of desensitization of P2 receptors.

Our results show that P2 receptors are expressed in DRG neurons of different diameters. In most cells of medium and large diameters, consecutive applications of ATP with an interval of 60 s did not cause a noticeable decrease in the amplitude of $[Ca^{2+}]i$ transients. Thus, we conclude that P2 receptors that do not show desensitization are predominantly present in most medium- and large-diameter cells.

A typical graph of calcium transients in cells of medium and large diameters in response to a standard depolarizing agent—KCl and to the studied substance—ATP is presented in Figure 1.

In small-diameter cells, a decrease in the amplitude of transients was observed in response to ATP applications with an interval of 20–25 s starting from the second application until the transients completely disappeared. A typical graph of such transients obtained experimentally is presented in Figure 2.

Thus, we conclude that P2 receptors that show clear desensitization are present in the small-diameter cells.

3.2. Investigation of capsaicin-induced calcium transients through TRPV1 channels in the membrane of DRG neurons

Cultivated cells of DRG ganglia used in the experiment showed a relationship between the activity of neurons in response to the application of an agonist and their size. We measured the largest cell diameter in linear dimensions. Small neurons were considered d < 22 μm (8% of total cells), medium-sized neurons had d = 24–32 μm (22%), and large neurons had d = 32–48 μm (63%).

Desensitization of TRPV1 channels is called acute when the receptor loses its ability to respond to the application of an agonist after its long-term application, and tachyphylaxis, which is manifested in a gradual decrease in the maximum amplitude of calcium transients during successive short-term additions of the same concentrations of capsaicin (Koplas et al., 1997; Liu et al., 2005). As it was shown earlier, there is a specific heterogeneity of the studied DRG cells in terms of the dynamics of activation and desensitization of calcium transients of TRPV1 channels under the action of capsaicin (Petrushenko et al., 2020). This study also identified three types of sensory neurons maintained in a primary culture based on responses to capsaicin: (1) desensitized 37.5%, (2) non-desensitized 34.4%, and (3) insensitive 23.4%. When applying capsaicin (after 2 min), desensitization of TRPV1 channels was observed in 37.5% of neurons, which lasted until the complete cessation of calcium entry.

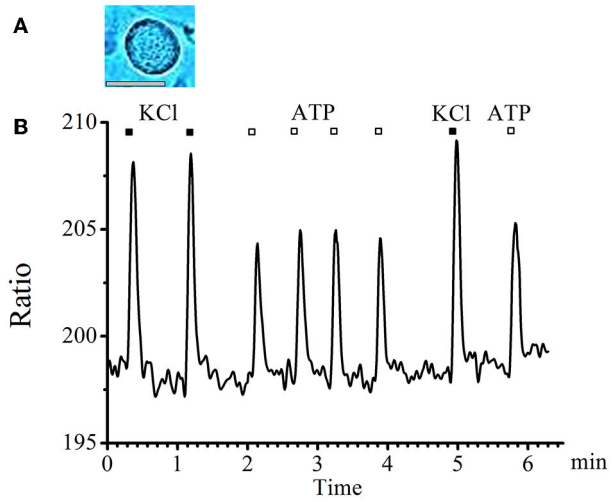

FIGURE 1
Absence of tachyphylaxis of calcium transients in response to ATP applications in large- and medium-diameter neurons. **(A)** Image of a typical neuron with an medium diameter (scale bar 25 μM long). **(B)** Recording of calcium transients in medium-diameter cells in response to the standard depolarizing agent —50mM KCl (black rectangles) and to the tested substance —0.1 mM ATP (white rectangles).

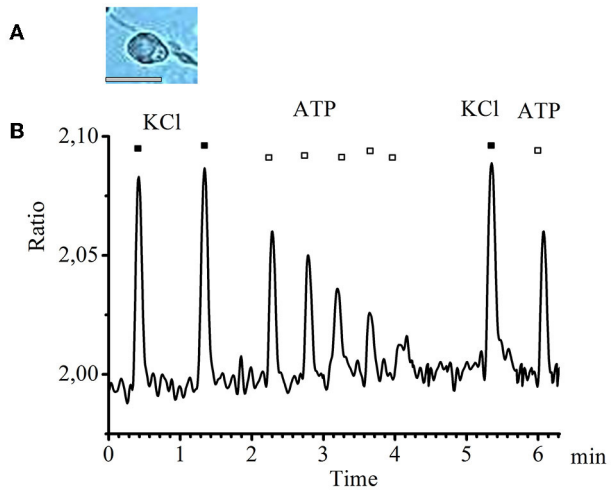

FIGURE 2
Desensitization of calcium transients in response to ATP application in small-diameter neurons. **(A)** Image of a typical neuron with a small diameter (scale bar 25 μM long). **(B)** Recording of calcium transients in cells of small diameter in response to the standard depolarizing agent —50 mM KCl (black rectangles) and to the investigated substance —0.1 mM ATP (white rectangles).

Figure 3 shows the development of desensitization of TRPV1 channels by the type of tachyphylaxis. Successive short-term application of Caps (100 nM, 5 s) to the neuron membrane with a 2-min washout after each application activated TRPV1 channels and led to their desensitization. As shown in Figure 3, repeated use of Caps at a low concentration leads to a clear desensitization of TRPV1 channels, manifested in a gradual decrease in the maximum amplitude of calcium transients.

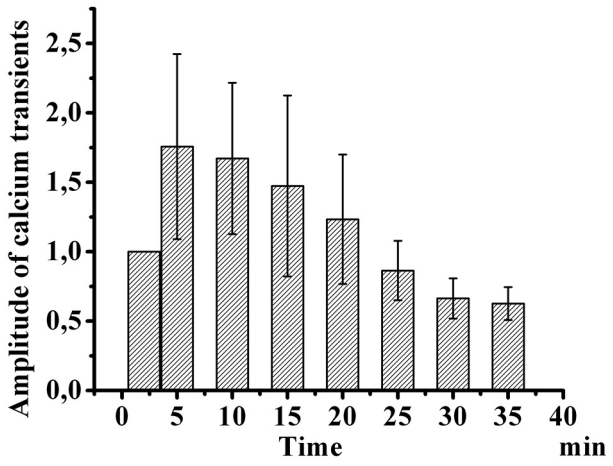

FIGURE 3
Desensitization of calcium transients in response to capsaicin application in small-diameter neurons. The diagram shows changes in the amplitude of successive short-term applications of capsaicin over time (100 nM, 5 s). The y-axis illustrates normalized averaged amplitudes of calcium transients in response to capsaicin application. Means and S.E. shown data groups were assessed for normality using the software "Origin Pro™" as the Shapiro–Wilk normality test.

3.3. Interaction between TRPV1 and ATP receptors in DRG neurons

Capsaicin activates ligand-gated TRPV1 channels, which leads to an increase in the concentration of intracellular ionized calcium. When capsaicin was added (after 2 min), desensitization of TRPV1 channels was observed in 37.5% of neurons by the type of tachyphylaxis until the complete cessation of calcium entry. At the same time, the addition of ATP (100 μM, 10–20 s) 5 min after the onset of desensitization, immediately before the next capsaicin application, caused an increase in calcium transients in response to capsaicin application in 35.7% of desensitized neurons. The calcium transient amplitude after sequential application of ATP and capsaicin was 161% of the previous minimal calcium transient in response to capsaicin of the same neuron. A comparison of the normalized values of the amplitudes of the responses to capsaicin before and after the application of ATP is shown in Figure 4.

It should be noted that not all neurons showed resensitization of calcium transients in response to activation of P2 receptors. The number of cells that showed an increase in calcium transients under conditions of simultaneous application of ATP and capsaicin was 29% of the total number of cells that showed desensitization to the action of capsaicin (Figure 5).

4. Discussion

TRPV1 and purine receptors play a significant role in nerve cell activity. Interaction between the two has been observed in a variety of processes, including pain sensation, synaptic plasticity, and synaptic transmission (Yu et al., 2021). TRPV1 is a non-selective cation channel that is found throughout the central and peripheral

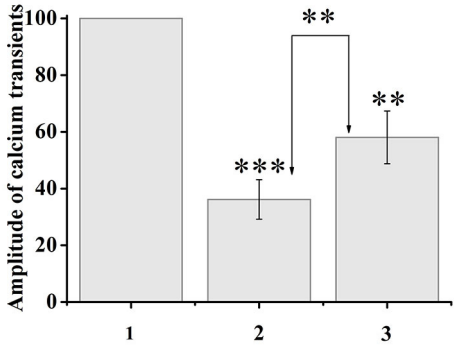

FIGURE 4
Application of ATP (100 μM, 20 s) to capsaicin-desensitized neurons caused resensitization of TRPV1 channels. The y-axis illustrates normalized to the maximal peak averaged amplitudes of calcium transients in response to capsaicin application. (1) Maximal peak at the start of the experiment, (2) minimum amplitude during desensitization, (3) resensitization of calcium transients after ATP application. The numbers in the second and third columns of the chart indicate the percentage increase. Data sets were evaluated for normality by the Shapiro–Wilk normality test. Statistical hypotheses were evaluated by Student's *t*-test. ***$p \leq 0.001$ (2) vs. (2) between desensitization transients; **$p \leq 0.01$ (2) vs. (3) between desensitization transients and resensitization transients; **$p < 0.01$ (3) vs. (3) between resensitization transients.

nervous systems. It has been linked to a variety of processes and has been widely studied due to its involvement in pain sensation. Activation of TRPV1 receptors can lead to the release of a variety of neurotransmitters, such as calcitonin gene-related peptide (CGRP) and substance P.

Regulation of TRPV1 channels can also occur through modulation by intracellular molecules such as Ca^{2+} ions (Koplas et al., 1997), phosphatidylinositol 4,5 bisphosphate (PIP2; Prescott and Julius, 2003), or calmodulin (Rosenbaum et al., 2004). TRPV1 channels are inactivated upon binding to PIP2 and re-sensitized through PKC-mediated hydrolysis of PIP2 (Prescott and Julius, 2003). Due to the activation of protein kinase C (PKC) and phosphorylation of TRPV1 channel proteins, the channels can participate in interaction with other receptors, for example, P2Y1 (Tominaga et al., 2001) or P2Y2 (Lakshmi and Joshi, 2005; Wang et al., 2010). Malin et al. (2008) showed that P2Y2 receptors found in sensory neurons can be co-expressed with TRPV1 receptors.

Purine receptors are another important player in nerve cell activity. They are involved in synaptic plasticity, the ability of neurons to change their response to a stimulus (Ren and Bertrand, 2008). Purine signaling has been linked to the release of neurotransmitters, such as glutamate and GABA, and has been shown to modulate synaptic transmission.

The interaction between TRPV1 and purine receptors has been observed in many processes (Tominaga and Moriyama, 2007). In pain sensation and synaptic plasticity, TRPV1 activation leads to the release of CGRP, which can then activate purine receptors, leading to the release of glutamate and GABA.

ATP activation of P2Y2 receptors leads to activation of Gq-proteins of the mediated metabolic pathway (Erb and Weisman, 2012) with subsequent phosphorylation of channel proteins and resensitization of TRPV1 channels.

Overall, the interaction between TRPV1 and purine receptors is essential for normal nerve cell activity.

In the study (Khmyz et al., 2008), it was found that the P2X3 receptor is responsible for temperature sensitivity. It is shown that the development of desensitization of the P2X3 receptor does not depend on the temperature in the range of 25.40°C; at the same time, recovery after desensitization is significantly accelerated with increasing temperature. The authors conclude that the unusual combination of sensitivity/insensitivity of P2X3 receptors may be related to the key role of these receptors in thermosensitivity. It should be noted that TRPV1 channels are also associated with hot temperature perception (>43°C). Thus, resensitization of TRPV1 channels after P2X receptor activation may be associated with increased sensitivity regulation.

In the work (Glaser et al., 2013), the authors conclude the participation of purinergic receptors in controlling metabolic activities and many physiological functions but in different ways: while most P2Y receptors induce transient elevations of intracellular calcium as waves, P2X receptors produce fast calcium spikes.

Among DRG neurons, nociceptive C-fiber neurons belong to a subset of small cells. In small sensory neurons of rats, two populations of nociceptors were isolated – functional homomeric P2X3 and heteromeric P2X2/3 receptors (Nicke et al., 1998; MacKenzie et al., 1999; Torres et al., 1999). The time of the open state of the ion channel depends on the subunit composition of the receptors. For example, P2X3 receptor channels desensitize rapidly in the presence of ATP (several hundred milliseconds), while the P2X2 receptor channel remains open as long as ATP is associated with it (Torres et al., 1999). Another study showed that ATP elicits P2X receptor-mediated responses in rat DRG neurons with different desensitization kinetics - slow non-desensitizing kinetics, fast desensitizing kinetics, or a combination of fast and slow kinetics. The authors conclude that rapid desensitization responses were similar to P2X3 receptor responses, and responses without desensitization had properties indicative of P2X2 or P2X2/3 receptor activation (MacKenzie et al., 1999).

In our experiments, the majority of medium- and large-diameter cells did not show a significant decrease in the amplitude of calcium transients through P2 receptors after successive applications of ATP. Thus, we concluded that P2 receptors, which do not show desensitization, are present mainly in cells of medium and large diameters. In small-diameter DRG neurons, observed calcium transitions through P2 receptors in response to ATP application demonstrate pronounced desensitization. Thus, P2 receptors with desensitization are expressed in these neurons.

It should be noted that when comparing the responses of the studied cells on days 1-2 and 5-7 of cultivation, differences were found in the number of each of the groups of cells in terms of sensitivity to capsaicin. On the 5-7th days of cultivation, changes occur in neurons associated with their adaptation to the conditions of cultivation. Accordingly, there is a significant reduction in the number of cells that respond to capsaicin. It is important to note that the restoration of the amplitude of calcium transients under the influence of ATP was observed mainly in cells on the 1st to 2nd days of cultivation. Thus, under the conditions of a short cultivation time, neurons retain the properties of freshly isolated cells and there

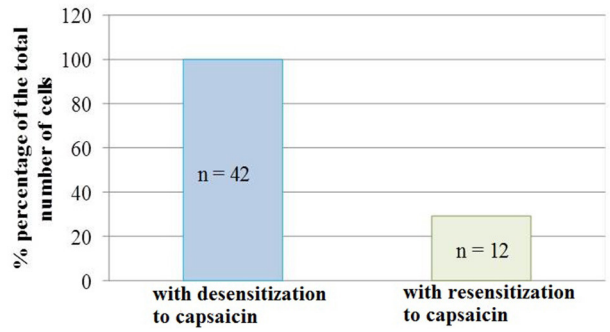

FIGURE 5
Diagram showing the ratio of cell number which demonstrated the desensitization to capsaicin (100%, $n = 42$) and resensitization (29%, $n = 12$) of calcium transients in conditions of co-application of capsaicin and ATP. Data sets were evaluated for normality by the Shapiro–Wilk normality test.

are no transformations associated with adaptation to cultivation conditions.

In conclusion, we found that when DRG neurons are desensitized to capsaicin, activation of P2 purinoceptors can restore calcium transients. The amplitude of calcium transients in response to capsaicin after the application of ATP was 161% of the desensitized calcium transient in response to capsaicin.

It is known that the activation of P2 receptors under the influence of ATP is an important factor affecting the formation of inflammation or visceral pain (Chizh and Illes, 2000). Thus, we have shown that ATP-induced resensitization of TRPV1 channels makes them possible participants in elevated calcium responses and the development of these disease states.

Data availability statement

The original contributions presented in the study are included in the article/supplementary material, further inquiries can be directed to the corresponding author.

Ethics statement

The animal study was reviewed and approved by Committee for Biomedical Ethics.

Author contributions

All authors listed have made a substantial, direct, and intellectual contribution to the work and approved it for publication.

Conflict of interest

The authors declare that the research was conducted in the absence of any commercial or financial relationships that could be construed as a potential conflict of interest.

Publisher's note

All claims expressed in this article are solely those of the authors and do not necessarily represent those of their affiliated organizations, or those of the publisher, the editors and the reviewers. Any product that may be evaluated in this article, or claim that may be made by its manufacturer, is not guaranteed or endorsed by the publisher.

References

Burgard, E. C., Niforatos, W., van Biesen, T., Lynch, K. J., Touma, E., Metzger, R. E., et al. (1999). P2X receptor-mediated ionic currents in dorsal root ganglion neurons. *J. Neurophysiol.* 82, 1590–1598. doi: 10.1152/jn.1999.82.3.1590

Burnstock, G. (2012). "Purinergic neurotransmission and nucleotide receptors" in *Primer on the Autonomic Nervous System, 3rd Edn*, ed P. A. Low (Academic Press), 87–93. doi: 10.1016/B978-0-12-386525-0.00018-4

Caterina, M. J., Schumacher, M. A., Tominaga, M., Rosen, T. A., Levine, J. D., and Julius, D. (1997). The capsaicin receptor: A heat-activated ion channel in the pain pathway. *Nature* 389, 816–824. doi: 10.1038/39807

Chizh, B., and Illes, P. (2000). 2X receptors and nociception. *Pharmacol. Rev.* 53, 553–568.

Docherty, R. J., Yeats, J. C., Bevan, S., and Boddeke, H. W. (1996). Inhibition of calcineurin inhibits the desensitization of capsaicin-evoked currents in cultured dorsal root ganglion neurons from adult rats. *Pflugers Arch.* 431, 828–837. doi: 10.1007/s004240050074

Erb, L., and Weisman, G. A. (2012). Coupling of P2Y receptors to G proteins and other signaling pathways. *Wiley Interdiscip. Rev. Membr. Transp. Signal.* 1, 789–803. doi: 10.1002/wmts.62

Evans, R. J. (2009). Orthosteric and allosteric binding sites of P2X receptors. *Eur. Biophys. J.* 38, 319–327. doi: 10.1007/s00249-008-0275-2

Glaser T., Resende, R. R., and Ulrich, H. (2013). Implications of purinergic receptor-mediated intracellular calcium transients in neural differentiation. *Cell Commun. Signal.* 11, 12. doi: 10.1186/1478-811X-11-12

Khmyz, V., Maximyuk, O., Teslenko, V., Verkhratsky, A., and Krishtal O. (2008). P2X3 receptor gating near normal body temperature. *Pflügers Arch.* 456, 339–347. doi: 10.1007/s00424-007-0376-2

Koplas, P. A., Rosenberg, R. L., and Oxford, G. S. (1997). The role of calcium in the desensitization of capsaicin responses in rat dorsal root ganglion neurons. *J. Neurosci.* 17, 3525–3537. doi: 10.1523/JNEUROSCI.17-10-03525.1997

Lakshmi, S., and Joshi, P. G. (2005). Co-activation of P2Y2 receptor and TRPV channel by ATP: Implications for ATP induced pain. *Cell Mol. Neurobiol.* 25, 819–832. doi: 10.1007/s10571-005-4936-8

Liu, B., Zhang, C., and Qin, F. (2005). Functional recovery from desensitization of vanilloid receptor TRPV1 requires resynthesis of phosphatidylinositol 4,5-bisphosphate. *J. Neurosci.* 25, 4835–4843. doi: 10.1523/JNEUROSCI.1296-05.2005

Lopshire, J. C., and Nicol, G. D. (1998). The cAMP transduction cascade mediates the prostaglandin E2 enhancement of the capsaicin-elicited current in rat sensory neurons: Whole-cell and single-channel studies. *J. Neurosci.* 18, 6081–6092. doi: 10.1523/JNEUROSCI.18-16-06081.1998

Lukacs, V., Thyagarajan, B., Varnai, P., Balla, A., Balla, T., and Rohacs, T. (2007). Dual regulation of TRPV1 by phosphoinositides. *J. Neurosci.* 27, 7070–7080. doi: 10.1523/JNEUROSCI.1866-07.2007

MacKenzie, A. B., Surprenant, A., and North, R. A. (1999). Functional and molecular diversity of purinergic ion channel receptors. *Ann. N. Y. Acad. Sci.* 868, 716–729. doi: 10.1111/j.1749-6632.1999.tb11351.x

Malin, S. A., Davis, B. M., Koerber, H. R., Reynolds, I. J., Albers, K. M., and Molliver, D. C. (2008). Thermal nociception and TRPV1 function are attenuated in mice lacking the nucleotide receptor P2Y2. *Pain* 138, 484–496. doi: 10.1016/j.pain.2008.01.026

Mandadi, S., Numazaki, M., Tominaga, M., Bhat, M. B., Armati, P. J., and Roufogalis, B. D. (2004). Activation of protein kinase C reverses capsaicin-induced calcium-dependent desensitization of TRPV1 ion channels. *Cell Calcium* 35, 471–478. doi: 10.1016/j.ceca.2003.11.003

Mohapatra, D. P., and Nau, C. (2005). Regulation of Ca^{2+}-dependent desensitization in the vanilloid receptor TRPV1 by calcineurin and cAMP-dependent protein kinase. *J. Biol. Chem.* 280, 13424–13432. doi: 10.1074/jbc.M410917200

Nicke, A., Bäumert, H. G., Rettinger, J., Eichele, A., Lambrecht, G., Mutschler, E., et al. (1998). P2X1 and P2X3 receptors form stable trimers: A novel structural motif of ligand-gated ion channels. *Embo J.* 17, 3016–3028. doi: 10.1093/emboj/17.11.3016

Numazaki, M., Tominaga, T., Toyooka, H., and Tominaga, M. (2002). Direct phosphorylation of capsaicin receptor VR1 by protein kinase C epsilon and identification of two target serine residues. *J. Biol. Chem.* 277, 13375–13378. doi: 10.1074/jbc.C200104200

Petrushenko, M., Petrushenko, O., and Lukyanetz, E. (2021). Effect of calcium ions and chlorpromazine on TRPV1 channels of rat DRG neurons. *Scient. Heritage.* 75, 7–10. Available online at: https://cyberleninka.ru/article/n/effect-of-calcium-ions-and-chlorpromazine-on-trpv1-channels-of-rat-drg-neurons

Petrushenko, M. O., Petrushenko, E. A., and Lukyanetz, E. A. (2018). Properties of vanilloid receptor type 1. *Fiziol zh* 64, 91–102. doi: 10.15407/fz64.01.091

Petrushenko, M. O., Petrushenko, E. A., and Lukyanetz, E. A. (2020). Activation and desensitization of TRPV1 channels under the influence of capsaicin. *Neurophysiology* 52, 256–260. doi: 10.1007/s11062-021-09880-x

Petrushenko, Y. A. (2012). P2X receptors: Peculiarities of the structure and modulation of the functions. *Neurophysiology* 44, 163–173. doi: 10.1007/s11062-012-9284-y

Prescott, E. D., and Julius, D. (2003). A modular PIP2 binding site as a determinant of capsaicin receptor sensitivity. *Science* 300, 1284–1288. doi: 10.1126/science.1083646

Ren, J., and Bertrand, P. P. (2008). Purinergic receptors and synaptic transmission in enteric neurons. *Purinergic Signal.* 4, 255–266. doi: 10.1007/s11302-007-9088-5

Roberts, J. A., Vial, C., Digby, H. R., Agboh, K. C., Wen, H., Atterbury-Thomas, A., et al. (2006). Molecular properties of P2X receptors. *Pflugers Arch.* 452, 486–500. doi: 10.1007/s00424-006-0073-6

Rosenbaum, T., Gordon-Shaag, A., Munari, M., and Gordon, S. E. (2004). Ca^{2+}/calmodulin modulates TRPV1 activation by capsaicin. *J. Gen. Physiol.* 123, 53–62. doi: 10.1085/jgp.200308906

Shimizu, T., Yanase, N., Fujii, T., Sakakibara, H., and Sakai, H. (2022). Regulation of TRPV1 channel activities by intracellular ATP in the absence of capsaicin. *Biochim. Biophys. Acta Biomembr.* 1864, 183782. doi: 10.1016/j.bbamem.2021.183782

Szallasi, A., Cortright, D. N., Blum, C. A., and Eid, S. R. (2007). The vanilloid receptor TRPV1: 10 years from channel cloning to antagonist proof-of-concept. *Nat. Rev. Drug Discov.* 6, 357–372. doi: 10.1038/nrd2280

Tominaga, M., and Moriyama, T. (2007). "Functional interaction between ATP and TRPV1 receptors," in *Molecular Sensors for Cardiovascular Homeostasis*, ed D. H. Wang (Boston, MA: Springer), 133–140. doi: 10.1007/978-0-387-47530-1_7

Tominaga, M., Wada, M., and Masu, M. (2001). Potentiation of capsaicin receptor activity by metabotropic ATP receptors as a possible mechanism for ATP-evoked pain and hyperalgesia. *Proc. Natl. Acad. Sci. U. S. A.* 98, 6951–6956. doi: 10.1073/pnas.111025298

Torres, G. E., Egan, T. M., and Voigt, M. M. (1999). Hetero-oligomeric assembly of P2X receptor subunits. Specificities exist with regard to possible partners. *J. Biol. Chem.* 274, 6653–6659. doi: 10.1074/jbc.274.10.6653

Wang, H., Wang, D. H., and Galligan, J. J. (2010), 2Y.2 receptors mediate ATP-induced resensitization of TRPV1 expressed by kidney projecting sensory neurons. *Am. J. Physiol. Regul. Integr. Comp. Physiol.* 298, R1634–R1641. doi: 10.1152/ajpregu.00235.2009

Yu, J., Du, J., Fang, J., Liu, Y., Xiang, X., Liang, Y., et al. (2021). The interaction between P2X3 and TRPV1 in the dorsal root ganglia of adult rats with different pathological pains. *Mol. Pain* 17, 17448069211011315. doi: 10.1177/17448069211011315

Zhang, X., Huang, J., and McNaughton, P. A. (2005). NGF rapidly increases membrane expression of TRPV1 heat-gated ion channels. *EMBO J.* 24, 4211–4223.

frontiers | Frontiers in Cellular Neuroscience

TYPE Brief Research Report
PUBLISHED 03 July 2023
DOI 10.3389/fncel.2023.1202083

OPEN ACCESS

EDITED BY
Dirk M. Hermann,
University of Duisburg-Essen, Germany

REVIEWED BY
Alexander V. Zholos,
Taras Shevchenko National University of Kyiv, Ukraine
Fusheng Tang,
National Institutes of Health (NIH), United States
Henrique Prado von Gersdorff,
Oregon Health and Science University, United States
Ulisse Bocchero,
National Institutes of Health (NIH), United States

*CORRESPONDENCE
Hanna Dumanska
✉ doomannya@gmail.com
Mariia Telka
✉ mariyka.t@gmail.com

RECEIVED 07 April 2023
ACCEPTED 08 June 2023
PUBLISHED 03 July 2023

CITATION
Dumanska H, Telka M and Veselovsky N (2023) Inhibition of high-voltage-activated calcium currents by acute hypoxia in cultured retinal ganglion cells.
Front. Cell. Neurosci. 17:1202083.
doi: 10.3389/fncel.2023.1202083

Inhibition of high-voltage-activated calcium currents by acute hypoxia in cultured retinal ganglion cells

Hanna Dumanska*, Mariia Telka* and Nikolai Veselovsky

Department of Neuronal Network Physiology, Bogomoletz Institute of Physiology, National Academy of Science of Ukraine, Kyiv, Ukraine

Hypoxia is a common factor of numerous ocular diseases that lead to dysfunctions and loss of retinal ganglion cells (RGCs) with subsequent vision loss. High-voltage-activated calcium channels are the main source of calcium entry into neurons. Their activity plays a central role in different signaling processes in health and diseases, such as enzyme activation, gene transcription, synaptic transmission, or the onset of cell death. This study aims to establish and evaluate the initial effect of the early stage of acute hypoxia on somatic HVA calcium currents in cultured RGCs. HVA calcium currents were recorded in RGCs using the whole-cell patch-clamp technique in the voltage-clamp mode. The fast local superfusion was used for a brief (up to 270 s) application of the hypoxic solution (pO_2 < 5 mmHg). The switch from normoxic to hypoxic solutions and vice versa was less than 1 s. The HVA calcium channel activity was inhibited by acute hypoxia in 79% of RGCs (30 of 38 RGCs) in a strong voltage-dependent manner. The level of inhibition was independent of the duration of hypoxia or repeated applications. The hypoxia-induced inhibition of calcium currents had a strong correlation with the duration of hypoxia and showed the transition from reversible to irreversible at 75 s of hypoxia and longer. The results obtained are the first demonstration of the phenomena of HVA calcium current inhibition by acute hypoxia in RGCs and provide a conceptual framework for further research.

KEYWORDS

retinal ganglion cells, somatic calcium channels, high-voltage-activated calcium currents, acute hypoxia, reversible and irreversible inhibition

1. Introduction

Hypoxia in terms of its duration is divided into acute, sustained, cyclic, and many other types. Each type has different dynamics, molecular mechanisms, and effects on cells and tissues (Weir and Olschewski, 2006; Kaur et al., 2008; Saxena and Jolly, 2019; Liu et al., 2022). Several ocular diseases and sight-threatening disorders including glaucoma, diabetic retinopathy, optic nerve atrophy, central retinal artery occlusion, and ischemic central retinal vein thrombosis are accompanied by retinal hypoxia of different durations (Tezel and Wax, 2004; Arden and Sivaprasad, 2011; Chidlow et al., 2017; Lazzara et al., 2020). In the pathogenesis of these diseases, the common issue is the degeneration of retinal ganglion cells (RGCs) and their axons, leading to vision loss and blindness (Osborne et al., 2001; Kuehn et al., 2005; Munemasa and Kitaoka, 2013; Potilinski et al., 2020; Tezel, 2021). Retinal ganglion cells (RGCs) are the output neurons of the retina that collect, process, and transmit signals to the visual centers of the brain. Changes in electrophysiological characteristics and activity parameters of RGCs induced by sustained and long-lasting hypoxia were previously

investigated (Kaur et al., 2008; Chidlow et al., 2017; Lee et al., 2022; Warwick et al., 2022). However, there is very limited information about the early effects induced by acute hypoxia in RGCs (Gross et al., 1999). Such an initial cellular response might be targeted to prevent further development of RGCs degeneration.

Among all cellular regulatory mechanisms, cytosolic calcium plays a key role in the regulation of retinal homeostasis (Shahulhameed et al., 2020). Voltage-gated calcium channels are the main transducers of membrane depolarization into intracellular calcium transients (Simms and Zamponi, 2014). These channels are transmembrane multiprotein complexes and are classified into high-voltage-activated (HVA) and low-voltage-activated (LVA) based on their voltage-dependent activation. HVA calcium channels are known to play a vital role in numerous physiological processes such as synaptic transmission, cell excitability, gene transcription, and initiation of several intracellular signaling events (Clapham, 2007; Catterall, 2011; Dolphin, 2021). The dysfunction of different types of HVA calcium channels appears to be involved in several neurological and psychiatric disorders (Zamponi, 2016). The effect of sustained hypoxia on intracellular calcium concentration in RGCs has been investigated in the modeling studies of glaucoma and optic neuritis (Yamada et al., 2006; Sasaki and Kaneko, 2007). Obviously, calcium plays a dual role in healthy and injured cells, and investigating the very early effects induced by acute hypoxia on HVA calcium channels might provide the necessary electrophysiological basis to increase their capacity for functional recovery and survival. In this study, we focused on identifying and evaluating the initial effect of acute hypoxia on somatic HVA calcium channels and their recovery during reoxygenation in cultured RGCs.

2. Materials and methods

All procedures involving animals were reviewed and approved by the Ethics Committee of Bogomoletz Institute of Physiology National Academy of Science of Ukraine.

2.1. Primary culture of retinal cells

Primary retinal cell cultures were prepared from Wistar rat pups of both sexes from postnatal day 0 to day 1, as previously described (Dumanska and Veselovsky, 2019). Briefly, after the decapitation and eye enucleation, retinal tissue was enzymatically and mechanically dissociated into single cells. Suspensions with cell densities of 10^4 cells/cm^2 were placed on the coverslip coated with poly-L-ornithine (Sigma-Aldrich) in Petri dishes. Furthermore, cells were maintained in the incubator in a humidified atmospheric air with ~21% O_2 enriched by 5 ± 0.5% CO^2 at 37 ± 0.5°C. We added 10 μM cytosine-α-D arabinofuranoside (AraC, Sigma, USA) on the fourth day of cultivation to suppress glia proliferation and completely replaced culture media on the fifth day. During cultivation, we partially replaced culture media every 4–5 days to maintain a stable nutrition supply. The culture medium was composed of Minimum Essential Medium Eagle with Hepes supplemented with 26 mM $NaHCO_3$, 1.25% insulin (Insulin from bovine pancreas, Sigma-Aldrich), and 10% horse serum (Gibco).

2.2. Electrophysiological recordings

We recorded HVA calcium currents in RGCs using the whole-cell patch-clamp technique in voltage-clamp mode. The extracellular solution contained the following: NaCl, 130 mM; $MgCl_2$, 2 mM; $CaCl_2$, 2 mM; TEA-Cl, 20 mM; 4-aminopyridine, 3 mM; glucose, 15 mM, HEPES 20 mM, (Sigma-Aldrich); and pH 7.4 (by adding NaOH). We added 1 μM of tetrodotoxin (TTX) to the extracellular solution to block sodium currents. The patch pipettes with internal tip diameters 1.0–1.5 μm were filled with intracellular solution containing Cesium acetate, 90 mM; CsCl, 20 mM; TEA-Cl, 20 mM; $MgCl_2$, 4 mM; Na_2ATP, 3 mM; NaADP, 0.5 mM; NaGTP, 0.5 mM; EGTA, 10 mM; HEPES, 20 mM (Sigma-Aldrich); and pH 7.4 (by adding CsOH). After the gigaomic contact formation, the pipette capacitance was compensated by using compensation adjustment on the amplifier. We recorded HVA calcium currents in response to a rectangular voltage pulse of 200 ms stimuli from −70 to 0 mV. The current–voltage relationships were elicited from holding potential of −70 mV using 100 ms steps to test potentials over the range of −50 to +50 mV in 10 mV increments every 10 s. Potentials were corrected for a junction potential of −10 mV. In the experiments, we used Ca^{2+} as the charge carrier; therefore, to avoid calcium-dependent inactivation, the intervals between stimuli were set to 10–15 s.

We monitored the quality parameters of voltage clamping, such as leakage current (I_{leak}) and the time constant of capacitive current (τ_{cap}), using applications of short (10 ms) small-amplitude hyperpolarizing rectangular stimuli (−10 mV). We analyzed the obtained data if the I_{leak} and τ_{cap} values varied within 5% of the mean values. The average series resistance was 16.6 ± 3.2 MΩ and was not electronically compensated. All experiments were performed at room temperature of 20–24°C. All data were recorded and digitized at 10 kHz using an Axopatch-1D amplifier, DigiData 1322A, and Clampex 9.0 software (Axon Instruments).

2.3. Acute hypoxia *in vitro*

We mimicked acute hypoxia during electrophysiological recordings by applying the hypoxic solution to the recorded RGCs using the fast local superfusion technique (Veselovsky et al., 1996). This method allows us to control the speed and area of the application and quick exchange (<1 s) of multiple solutions. The hypoxic solution was obtained by saturating the extracellular solution with nitrogen for 20 min. The duration of the hypoxia application was 45–270 s.

2.4. Polarographic measurements

The concentration of oxygen in the extracellular solution was measured by the polarographic method using a platinum microelectrode and Ag–AgCl reference electrode. The indicator

microelectrode was made from a borosilicate glass pipette, into the tip of which we soldered a platinum wire with a diameter of about 0.3 mm and a length of the open area of about 30–40 μm. We recorded the diffusion current at an applied potential of −700 mV. Such a potential corresponds to the middle of the diffusion plateau of the electrode polarogram. For the calibration of pO_2, we used two points by recording the diffusion current in solutions with defined and fixed oxygen concentrations. First, to obtain the zero point, we used a saturated sodium sulfite solution (8 mM). For the second point, we recorded the diffusion current in the control normoxic solution that was equilibrated with air. The pO_2 in the normoxic control solution was set in the range of 150–155 mmHg. After 20 min of saturation of extracellular solution with nitrogen, the pO_2 value was <5 mmHg. All measurements of oxygen concentration were performed in a laminar flow of applied normoxic and hypoxic solutions.

2.5. Data analysis

Conductance was calculated as follows:

$$G = \frac{I_{peak}}{(V - V_{rev})} \quad (1)$$

where I_{peak} is the peak current at each test potential, V is the test potential, and V_{rev} is the reversal potential. The relative conductance (G/G_{max})–voltage (V) curves, hereinafter referred to as G–V curves, were plotted and fit using the Boltzmann equation:

$$\frac{G}{G_{max}} = G_{max} + \frac{(G_{min} - G_{max})}{\left[1 + e^{(V - V_{1/2})/k}\right]}, \quad (2)$$

where G_{max} is the maximal conductance, G_{min} is the minimal conductance, V is the test potential, $V_{1/2}$ is the voltage at half-maximal conductance, and k is the slope factor.

To trace whether hypoxia-induced inhibition is associated with changes in current kinetics, we normalized currents during the control, hypoxia, and reoxygenation periods.

As the level of hypoxia-induced inhibition varied in a quite wide range, we calculated the recovery index (η) as follows:

$$\eta = \frac{I_{wash} - I_{N2}}{I_{control} - I_{N2}}, \quad (3)$$

where $I_{control}$, I_{N2}, and I_{wash}, are mean amplitudes of calcium currents during control, hypoxia, and reoxygenation, respectively.

We calculated the confidence interval (CI) for each hypoxia duration to verify the recovery index switch from reversible to irreversible. We defined the recovery process as reversible if the value 1 was within the calculated confidence interval.

2.6. Statistical analysis

We used Origin 8.5 Pro and Clampfit 9.0 for data analysis and graphic presentation. The normality of data was checked with the Shapiro-Wilk test, and the difference between two sets of values was determined using a two-sample *t*-test. Spearman's rank coefficient of correlation was used as a non-parametric measure of statistical dependence of ranking between two variables. The results of Spearman's rank correlation were presented in the text as correlation coefficient (r_s), *p*-values (*p*), and number of cells (*n*). All data in the text were presented as mean ± SD.

3. Results

In the culture, RGCs (Figure 1A) were easily identified initially by their morphological characteristics—soma diameters (Guenther et al., 1994). The diameters of RGC somata were 20–25 μm and calculated as the mean of the measurements by two perpendicular axes. Then, after establishing whole-cell configuration and before the HVA calcium currents recording, we confirmed RGCs identification by observing sodium currents with magnitudes ranging between 1 and 3 nA (Figures 1B, C). To observe sodium current, RGCs were first superfused with the normoxic extracellular solution without TTX. All further recordings in identified RGCs were performed in the presence of TTX.

We examined 38 RGCs from 11 to 32 days *in vitro*. All neurons exhibited HVA calcium currents with a peak magnitude ranging between 180 and 698 pA and the mean value is −316 ±137 pA, $n = 38$. The inactivation of currents developed extremely slowly. It was difficult to measure their time constants precisely because of the harmful effect of prolonged depolarization, but estimated values varied from 100 ms to 1 s. The I–V relationships of calcium currents have a clear single peak at a maintained potential of −10 mV. They do not have any low voltage-activated components, resulting in a plateau or peak at maintained potentials close to −40 mV (Figure 2D). Thus, the characteristics of HVA calcium currents in cultured RGCs were consistent with those previously described in the retina of the rat (Schmid and Guenther, 1999; Wanaverbecq et al., 2003).

We evaluated the initial effect of acute hypoxia on HVA calcium currents channels in cultured RGCs. The application of a hypoxic solution during 45–270 s led to the inhibition of HVA calcium current in most of the RGCs (79%, $n = 30$), in 10.5% of cells ($n = 4$) to augmentation, and 10.5% of RGCs ($n = 4$) remained insensitive to hypoxia. The evaluated level of effects induced by hypoxia of different durations and morphological and electrophysiological parameters of RGCs from these three distinct groups are shown in Table 1. Here, we did not observe any statistically significant differences in the parameters of recorded RGCs to classify them according to observed hypoxia-induced effects. The correlation analyses revealed that the level of inhibition was independent of the duration of hypoxia application ($rs = -0.24$, $p = 0.2$, $n = 30$), and the mean value was 27 ± 18% (varied from 8 to 77%; Figure 2A; Table 1). The representative recordings of inhibition of HVA calcium currents induced by 60 s of hypoxia are shown in Figure 2B. The normalized currents above the recordings represented the general tendency of hypoxia to decrease current amplitudes without any changes in current kinetics. The time course of HVA calcium current amplitudes showed that inhibition started to develop and reversed very quickly, within 15 s of application of the hypoxic and normoxic solutions, respectively (Figure 2C, $n = 4$). We also assessed the inhibitory effect of hypoxia over a broad range of membrane

10.3389/fncel.2023.1202083

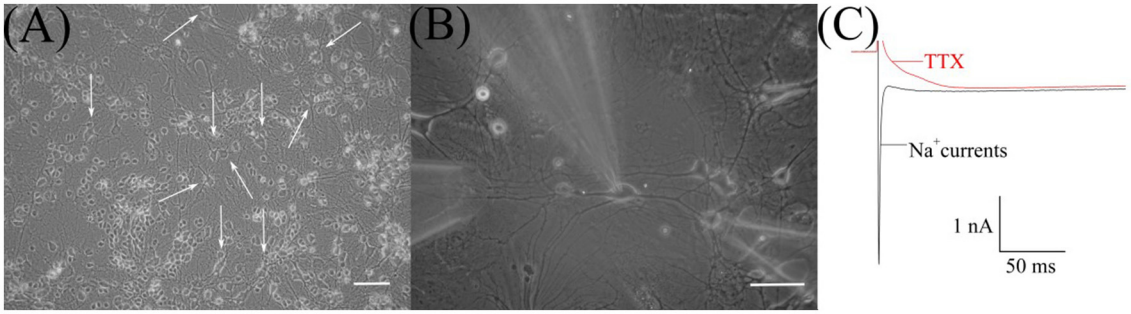

FIGURE 1
Microphotograph of cultured retinal ganglion cells (RGCs). **(A)** Primary culture of rat retinal cells on 19th day *in vitro*: white arrows indicate RGCs, scale marker corresponds to 100 μm. **(B)** Cultured RGCs during patch-clamp recording and fast local superfusion application on the 22nd day *in vitro*; the scale marker corresponds to 50 μm. **(C)** Representative recordings of sodium current before and after TTX application during electrophysiological identification of cultured RGCs.

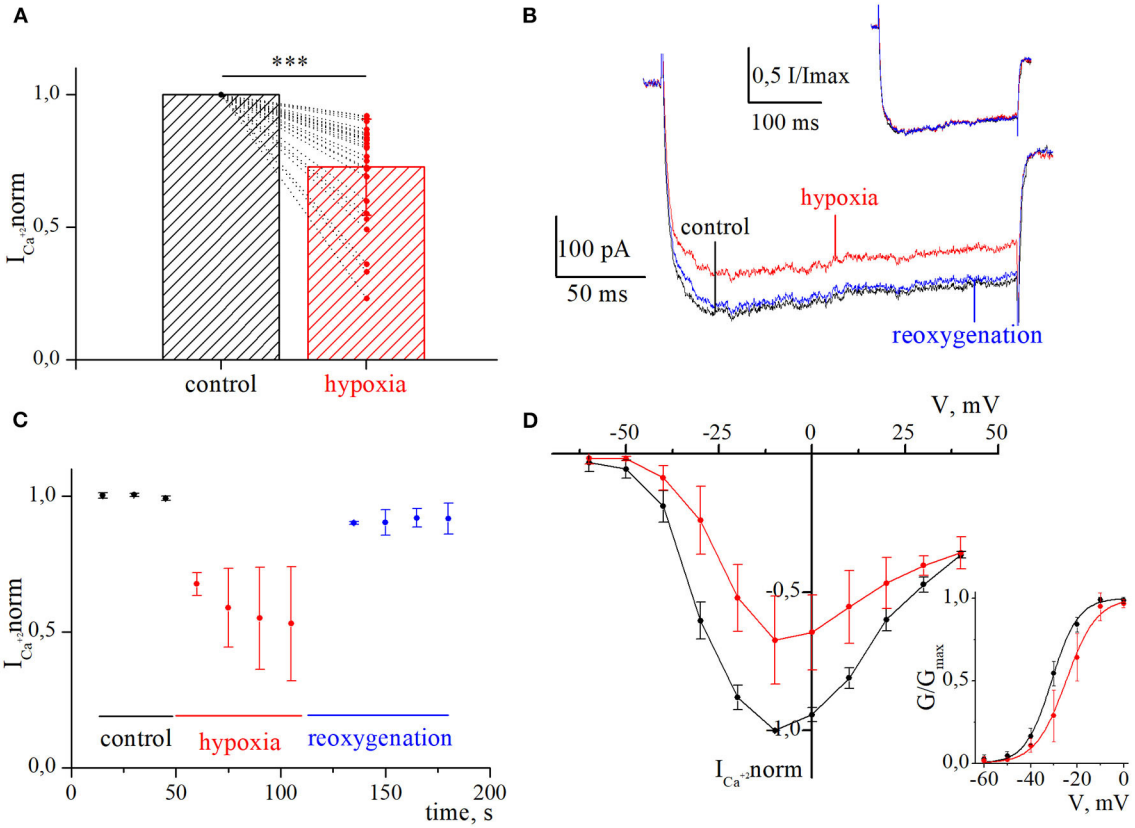

FIGURE 2
Inhibition of currents through high-voltage-activated calcium channels by acute hypoxia in retina ganglion cells. **(A)** The bar graph of the mean normalized values of calcium currents in control (black) and during the hypoxia (red); ***$p < 0.001$ compare to control. **(B)** Representative recordings of calcium currents under control, 60 s of hypoxia, and reoxygenation. The corresponding normalized currents are plotted above the recording. **(C)** The dynamic of averaged, normalized calcium currents amplitudes during control, 60 s of hypoxia (red), and reoxygenation (blue). **(D)** I–V relationships of averaged normalized calcium current amplitudes in control (black) and during hypoxia (red). The corresponding G–V curve of HVA calcium channels was built for control (black) and hypoxia (red). The solid lines are fitted with the Boltzmann curve.

potentials and built an I–V relationship (Figure 2D; $n = 3$). Hypoxia-induced inhibition was strongly voltage dependent. The average hypoxic inhibition of HVA calcium currents was around 60% at −30 mV and 15% at +30 mV. Moreover, G–V plots revealed that hypoxia-induced a shift in the midpoint of the relative conductance curve to more depolarizing membrane potentials compared to control ($V_{1/2control} = -31 \pm 1.4$ mV, $V_{1/2hypoxia} = -24.8 \pm 1.4$ mV, $p = 0.005$). The slope factor remains unchanged ($k_{control} = 5.7 \pm 0.5$, $k_{hypoxia} = 6.4 \pm 0.9$, $p = 0.53$).

TABLE 1 Summary of the characteristics of hypoxia-induced effects on HVA calcium currents and corresponding electrophysiological parameters of RGCs.

Hypoxia-induced effect on HVA Ca^{+2} currents	Inhibition				Augmentation	Insensitivity
Hypoxia duration	40–50 s	60–70 s	75–85 s	≥100 s	40–270 s	40–270 s
Number of cells	$n = 7$	$n = 7$	$n = 7$	$n = 9$	$n = 4$	$n = 4$
Level of hypoxia-induced effect	27 ± 19	33 ± 15	21 ± 12	26 ± 18	15 ± 5	–
η	0.8 ± 0.16	0.69 ± 0.2	0.24 ± 0.16	0.04 ± 0.01		
	$n = 7$	$n = 5$	$n = 4$	$n = 5$		
	$CI^{99\%}$ 0.57–1.02	$CI^{99\%}$ 0.27–1.1	$CI^{99\%}$ −0.22 to 0.71	$CI^{99\%}$ 0.02–0.06		
I_{Ca}, pA	−307 ± 109	−406 ± 194	−292 ± 109	−281 ± 114	−297 ± 154	−283 ± 65
R_{in}, GOm	0.68 ± 0.32	0.77 ± 0.32	0.81 ± 0.41	0.7 ± 0.28	0.84 ± 0.36	0.86± 0.37
C_m, pF	48 ± 13	56 ± 12	57 ± 13	50 ± 12	54 ± 12	57 ± 13
I_{Na}, nA	∼1.5	∼1.8	∼1.6	∼1.7	∼1.6	∼1.8
Somata Ø, μm	23.3 ± 1.7	22.3 ± 1.9	22.8 ± 2	22.6 ± 2.2	22.8 ± 2.2	23.3 ± 1.7

The mean ± SD is given for each parameter. η, recovery index; $CI^{99\%}$, 99% confidence interval for given η; I_{Ca}, magnitude of calcium current; R_{in}, input resistance; C_m, membrane capacity; I_{Na}, magnitude of sodium current; Somata Ø, diameter of somata.

We were interested in estimating not only the effect of hypoxia-induced inhibition of HVA calcium currents but also the recovery process during reoxygenation. The representative time courses of normalized HVA calcium current amplitudes with hypoxia application of different durations are shown in Figure 3A. As can be seen, the recovery during reoxygenation was dependent on the duration of hypoxia application, and the longer the hypoxia application, the less recovery during reoxygenation was observed. For quantitative evaluation of the recovery process and reversibility of hypoxia-induced inhibition, we calculated the recovery index (η). The dependency between the recovery index and the duration of hypoxia application (Figure 3B; Table 1) reflects the transition of inhibition from reversible to irreversible ($r_s = -0.87$, $p = 8^{*}10^{-7}$, $n = 21$). The inhibition of HVA calcium currents induced by 40–70 s of hypoxia was reversible, and the recovery index ranged between 0.53 and 1 with a mean value of 0.76 ± 0.2 ($n = 12$), whereas inhibition induced by 75 s of hypoxia or longer became irreversible, with the recovery index ranging between 0.03 and 0.36 with a mean value 0.13 ± 0.15 ($n = 9$).

We also tested the effect of repetitive application of hypoxia (Figures 3C, D, $n = 4$). The secondary application of hypoxia did not change the level of hypoxia inhibition ($hypoxia_1$ 18.4 ± 2.1%; $hypoxia_2$ 17.8 ± 1.1%; $p = 0.6308$) but decreased the recovery index during the second reoxygenation ($reoxygenation_1$ 0.87 ± 0.03%; $reoxygenation_2$ 0.4 ± 0.15%; $p = 0.001$).

4. Discussion

In this study, we investigated the initial effect of acute hypoxia ($pO_2 < 5$ mmHg, up to 270 s) on somatic HVA calcium currents in cultured RGCs. In the majority of RGCs (79%), hypoxia led to the inhibition of HVA calcium currents. The level of inhibition was strongly voltage dependent but independent of the duration of hypoxia or repeated applications. The recovery index had a strong correlation with hypoxia duration and showed the transition of inhibition from reversible to irreversible.

To the best of our knowledge, this is the first demonstration of the phenomena of HVA calcium current inhibition by acute hypoxia in RGCs, which could contribute to the cellular compensatory response, preventing cells from hypoxic injury and improving neuronal survival (Kaur et al., 2008; Shimoda and Polak, 2011; Lange and Bainbridge, 2012).

The effect of calcium currents inhibition by hypoxia is not as commonly observed as hypoxia-induced augmentation. Hypoxia-induced inhibition of calcium currents is shown in taenia caeci smooth muscle cells (Rekalov et al., 1997) and in glomus cells (Montoro et al., 1996). Both these structures are involved in the oxygen-sensory body system due to their quick reaction to the direct action of hypoxia on oxygen-sensitive ion channels (Lahiri et al., 2005). The retina, as part of the visual system, has extremely high oxygen and energy demands (Cohen and Noell, 1965) and a unique O_2 profile (Wangsa-Wirawan and Linsenmeier, 2003). It has been reported that the retina responds differently to acute and sustained hypoxia, from promoting blood flow to quick changes in transmembrane ion permeability and generation of vasoactive molecules to maintain oxygen homeostasis (Lange and Bainbridge, 2012). RGCs appeared to be particularly sensitive to different types of hypoxic stress (Kergoat et al., 2006), but what mechanisms mediate such a rapid reaction to changes in oxygen concentration is still unclear. For now, there is no confirmed evidence of the presence of oxygen-sensitive calcium channels in RGCs.

Previously, it has been shown that long-term hypoxia led to an increase in intracellular calcium ions concentration in RGCs (Yamada et al., 2006; Sasaki and Kaneko, 2007). Such an increase with subsequent cellular calcium overload can cause certain types of cellular death (Charriaut-Marlangue et al., 1996; Nicotera and Orrenius, 1998; Joo et al., 1999). On the other hand, brief periods of hypoxia, also called hypoxic preconditioning, can be adaptive for tissue and cells and show the neuroprotective effect on RGCs in a model of glaucoma and ischemic damage (Whitlock et al.,

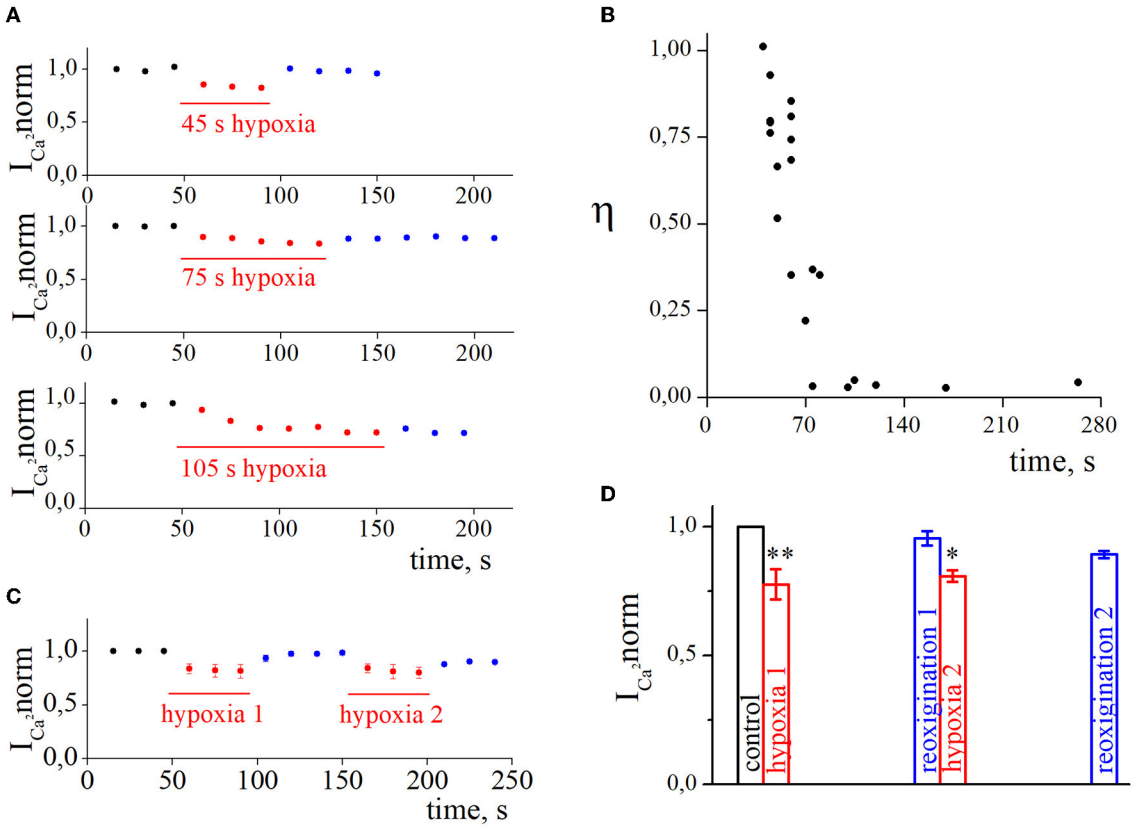

FIGURE 3
The recovery of high-voltage-activated calcium currents after acute hypoxia in retina ganglion cells. **(A)** The dynamic of normalized calcium currents amplitudes during control, 45 s/75 s/105 s of hypoxia (red), and reoxygenation (blue). **(B)** The dependence between the recovery index and the duration of hypoxia application. **(C)** The dynamic of averaged, normalized calcium currents amplitudes with repetitive 45 s of hypoxia application: control (black), hypoxia (red), reoxygenation (blue). **(D)** Bar graph of the mean normalized values of calcium currents with repetitive hypoxia application presented in **(C)**; $*p < 0.05$ $**p < 0.01$ compare to control.

2005; Zhu et al., 2007, 2012, 2013). A strong dependence has been observed between hypoxia-induced effects on calcium channels and experimental conditions in terms of ionic compositions, duration of hypoxia, pO_2 values and speed of its decrease, and the activity of voltage-dependent potassium channels (Montoro et al., 1996; Summers et al., 2000; Shkryl et al., 2001; Lukyanetz et al., 2003). Moreover, the activity of calcium currents by hypoxia might be modulated by several mechanisms. Hypoxia may lead to depolarization by the decrease of the potassium channels' activity (Montoro et al., 1996; López-Barneo et al., 2004); by ATP depletion (Hansen, 1985; Erecińska and Silver, 1994; Allen et al., 2005) and by the direct influence of hypoxia on calcium channels (Montoro et al., 1996; López-Barneo et al., 2004). Also, hypoxia-induced activation of NMDAR leads to an increase in intracellular calcium levels (Sucher et al., 1990; Siliprandi et al., 1992; Dumanska and Veselovsky, 2019).

In this study, we were able to record the initial effect induced by acute hypoxia, as the switch of pO_2 from 150 to 5 mmHg was in <1 s during electrophysiological recordings of HVA calcium currents. According to our experimental conditions, detected inhibition of calcium currents by hypoxia was not dependent on changes in potassium channel activity, as these channels were blocked. Also, the hypoxia-induced inhibition was not associated with depolarization, as RGCs were voltage clamped. Furthermore, we observed that the inhibition of HVA calcium currents by acute hypoxia is strongly voltage dependent. Such a phenomenon has been previously observed in oxygen-sensitive potassium and calcium channels in glomus cells (Ganfornina and López-Barneo, 1992; Montoro et al., 1996) and arterial myocytes (Franco-Obregón et al., 1995). According to the literature, voltage dependence of hypoxia-induced inhibition is a characteristic feature of oxygen-sensitive channels. Moreover, the depolarizing shift of channel conductance, observed on the G–V plot, reflects that hypoxia-induced inhibition is associated with the reduction of voltage sensitivity of HVA calcium channels and the mechanisms of such a reduction should be investigated more closely. Whether calcium channels in RGCs might be oxygen-sensitive should be examined further, but all these together suggest the possibility that hypoxia directly inhibited calcium currents or was mediated by second messengers.

We also presented the transitions of hypoxia-induced inhibition of calcium currents from reversible to irreversible depending on the hypoxia duration. The inhibition appeared to become irreversible when the duration of hypoxia was 75 s or longer. It may reflect the involvement of different enzyme activation in time such as nitric oxide synthase (NOS) and nitric

oxide (NO) synthesis. One of the NOS isoforms is calcium-independent iNOS. It has been reported that in hypoxic retina RGCs expressed iNOS and nNOS. The synthesized NO contributes to cytotoxicity, RGCs death, and axonal damage (Mishra et al., 2002; Zubrow et al., 2002; Kaur et al., 2006).

It is interesting that with the same parameters of hypoxia application, in 10.5% of recorded RGCs, we observed augmentation of HVA calcium currents and 10.5% of the cells remain insensitive to hypoxia. Such a diversity of responses to acute hypoxia might reflect the diversity of RGCs. There are various types of RGCs with specific gene expression, retinorecipient targets, morphological and physiological characteristics, and functions (Baden et al., 2021; Kim et al., 2021). Previous studies showed selective vulnerability of RGCs (Luo et al., 2009; Ou et al., 2016; Mayer et al., 2018) and type-specific survival and regeneration in response to different injuries (Tran et al., 2019; Tapia et al., 2022). Identification and classification of the general cellular mechanisms that either contribute to or inhibit type-specific RGC survival and regeneration are critical for the development of effective neuroprotective strategies.

We demonstrated that the diversity of hypoxia-induced effects in RGCs might also be associated with the type-specific composition of HVA calcium currents in different RGCs. Here we did not observe any difference in morphological or electrophysiological parameters of recorded RGCs to classify them according to observed hypoxia-induced effects, but the results obtained provide the platform for further research.

We also want to show that hypoxia, depending on its duration and magnitude, may cause a wide range of acid–base consequences such as alkalosis or acidosis (Swenson, 2016). In the presence of severe hypoxia, metabolic and hypercapnic acidosis develops with a high level of lactate formation and a fall in pH. Conventionally, acidosis is considered an additional injury that affects cell function and survival. However, sometimes it may also be cytoprotective to limit hypoxic injury. Mild extracellular acidosis, as a physiological consequence of oxygen deprivation, initiates mitochondrial metabolic pathway reprogramming to maintain the necessary level of ATP production in cortical neurons (Khacho et al., 2014). Some acidosis-induced effects were also shown in retinal cells. Activity-dependent drop in the pH, associated with exocytosis, inhibits HVA L-type calcium currents in bipolar cell terminals of goldfish retina (Palmer et al., 2003). Acidosis can also trigger a chain of intracellular processes, such as increasing the production of reactive oxygen species (ROS) by mitochondria (Riemann et al., 2011). It has been shown that ROS produced by RGCs' mitochondria modulate ion channel gating and excitability (Smith et al., 2023). It is also important to remember that RGCs can directly sense pH changes with TWIK-related acid-sensitive K+ (TASK) channels (Zhong et al., 2013; Wen et al., 2022) and to consider this in planning the research and interpretation of the results. In our research, we isolated hypoxia-induced effects using such a strong buffer as HEPES to maintain stable pH. In bicarbonate-based buffers, the hypoxia often leads to acidosis and it might cause a distortion of the investigating effects.

Summarizing the results obtained, we conclude that the inhibition of somatic HVA calcium currents in cultured RGCs induced by acute hypoxia reflects the initial compensatory reaction to the drop in oxygen level. It is not clear for now whether hypoxia affects calcium currents directly or due to the activation of some intracellular system. Taking into account the role of RGCs dysfunctions in blinding disorders, the mechanisms mediating detected inhibition should be investigated in further experiments.

Data availability statement

The raw data supporting the conclusions of this article will be made available by the authors, without undue reservation.

Ethics statement

The animal study was reviewed and approved by the Ethics Committee of Bogomoletz Institute of Physiology National Academy of Science of Ukraine.

Author contributions

HD conceptualized the research ideas, prepared retinal cell cultures, and prepared the manuscript. MT designed and performed the electrophysiological experiments, analyzed data, and prepared the plots for further scientific interpretation. MT and HD contributed to research design creation, literature search, and interpretation of the obtained results with comments and suggestions from NV. All authors read and approved the final manuscript.

Funding

This study was supported by basic financial support from the National Academy of Science of Ukraine, 0118U007353.

Acknowledgments

Partially, the data were presented in abstracts at the FENS Forum 2022, 9–13 July, Paris, France. Since the presentation, we added more than 30% of the original data in this study. We thank Dr. Captain Lee V. Hensley for the excellent editing of the English language of this manuscript.

Conflict of interest

The authors declare that the research was conducted in the absence of any commercial or financial relationships that could be construed as a potential conflict of interest.

Publisher's note

References

Allen, N. J., Káradóttir, R., and Attwell, D. (2005). A preferential role for glycolysis in preventing the anoxic depolarization of rat hippocampal area CA1 pyramidal cells. *J. Neurosci*. 25, 848–859. doi: 10.1523/JNEUROSCI.4157-04.2005

Arden, G. B., and Sivaprasad, S. (2011). Hypoxia and oxidative stress in the causation of diabetic retinopathy. *Curr. Diabetes Rev*. 7, 291–304. doi: 10.2174/157339911797415620

Baden, T., Berens, P., Franke, K., Roson, M. R., Bethge, M., and Euler, T. (2021). The functional diversity of retinal ganglion cells in the mouse. *Nature* 529, 345–350. doi: 10.1038/nature16468

Catterall, W. A. (2011). Voltage-gated calcium channels. *Cold Spring Harb. Perspect. Biol*. 3, a003947. doi: 10.1101/cshperspect.a003947

Charriaut-Marlangue, C., Pollard, H., and Ben-Ari, Y. (1996). Is ischemic cell death of the apoptotic type? *Adv. Neurol*. 71, 425–430.

Chidlow, G., Wood, J. P. M., and Casson, R. J. (2017). Investigations into hypoxia and oxidative stress at the optic nerve head in a rat model of glaucoma. *Front. Neurosci*. 11, 478. doi: 10.3389/fnins.2017.00478

Clapham, D. E. (2007). Calcium signaling. *Cell* 131, 1047–1058. doi: 10.1016/j.cell.2007.11.028

Cohen, L. H., and Noell, W. K. (1965). "Relationships between visual function and metabolism," in *Biochemistry of the Retina*, ed C. N. Graymore (Orlando, FL: Academic Press Inc.), 36–50.

Dolphin, A. C. (2021). Functions of presynaptic voltage-gated calcium channels. *Function* 2, zqaa027. doi: 10.1093/function/zqaa027

Dumanska, H., and Veselovsky, N. (2019). Short-term hypoxia induces bidirectional pathological long-term plasticity of neurotransmission in visual retinocollicular pathway. *Exp. Eye Res*. 179, 25–31. doi: 10.1016/j.exer.2018.10.014

Erecińska, M., and Silver, I. A. (1994). Ions and energy in mammalian brain. *Prog. Neurobiol*. 43, 37–71. doi: 10.1016/0301-0082(94)90015-9

Franco-Obregón, A., Ureña, J., and López-Barneo, J. (1995). Oxygen-sensitive calcium channels in vascular smooth muscle and their possible role in hypoxic arterial relaxation. *Proc. Natl. Acad. Sci. U. S. A*. 92, 4715–4719. doi: 10.1073/pnas.92.10.4715

Ganfornina, M. D., and López-Barneo, J. (1992). Gating of O2-sensitive K+ channels of arterial chemoreceptor cells and kinetic modifications induced by low PO2. *J. Gen. Physiol*. 100, 427–455. doi: 10.1085/jgp.100.3.427

Gross, R. L., Hensley, S. H., Gao, F., and Wu, S. M. (1999). Retinal ganglion cell dysfunction induced by hypoxia and glutamate: Potential neuroprotective effects of β-blockers. *Survey Ophthalmol*. 43, S162–S170. doi: 10.1016/s0039-6257(99)00054-5

Guenther, E., Schmid, S., Grantyn, R., and Zrenner, E. (1994). *In vitro* identification of retinal ganglion cells in culture without the need of dye labeling. *J. Neurosci. Methods* 51, 177–181. doi: 10.1016/0165-0270(94)90008-6

Hansen, A. J. (1985). Effect of anoxia on ion distribution in the brain. *Physiol. Rev*. 65, 101–148. doi: 10.1152/physrev.1985.65.1.101

Joo, C. K., Choi, J. S., Ko, H. W., Park, K. Y., Sohn, S., Chun, M. H., et al. (1999). Necrosis and apoptosis after retinal ischemia: involvement of NMDA-mediated excitotoxicity and p53. *Invest. Ophthalmol. Vis. Sci*. 40, 713–720.

Kaur, C., Foulds, W. S., and Ling, E. A. (2008). Hypoxia-ischemia and retinal ganglion cell damage. *Clin. Ophthalmol*. 2, 879–889. doi: 10.2147/OPTH.S3361

Kaur, C., Sivakumar, V., and Foulds, W. S. (2006). Early response of neurons and glial cells to hypoxia in the retina. *Invest. Ophthalmol. Vis. Sci*. 47, 1126–1141. doi: 10.1167/iovs.05-0518

Kergoat, H., Hérard, M. E., and Lemay, M. (2006). RGC sensitivity to mild systemic hypoxia. *Invest. Ophthalmol. Vis. Sci*. 47, 5423–5427. doi: 10.1167/iovs.06-0602

Khacho, M., Tarabay, M., Patten, D., Khacho, P., MacLaurin, J. G., Guadagno, J., et al. (2014). Acidosis overrides oxygen deprivation to maintain mitochondrial function and cell survival. *Nat. Commun*. 5, 3550. doi: 10.1038/ncomms4550

Kim, U. S., Mahroo, O. A., Mollon, J. D., and Yu-Wai-Man, P. (2021). Retinal ganglion cells-diversity of cll types and clinical relevance. *Front. Neurol*. 12, 661938. doi: 10.3389/fneur.2021.661938

Kuehn, M. H., Fingert, J. H., and Kwon, Y. H. (2005). Retinal ganglion cell death in glaucoma: mechanisms and neuroprotective strategies. *Ophthalmol. Clin. North Am*. 18, 383–395, vi. doi: 10.1016/j.ohc.2005.04.002

Lahiri, S., Roy, A., Baby, S. M., Hoshi, T., Semenza, G. L., and Prabhakar, N. R. (2005). Oxygen sensing in the body. *Prog. Biophys. Mol. Biol*. 91, 249–286. doi: 10.1016/j.pbiomolbio.2005.07.001

Lange, C. A., and Bainbridge, J. W. (2012). Oxygen sensing in retinal health and disease. *Ophthalmologica* 227, 115–131. doi: 10.1159/000331418

Lazzara, F., Trotta, M. C., Platania, C. B. M., D'Amico, M., Petrillo, F., Galdiero, M., et al. (2020). Stabilization of HIF-1α in human retinal endothelial cells modulates expression of miRNAs and proangiogenic growth factors. *Front. Pharmacol*. 11, 1063. doi: 10.3389/fphar.2020.01063

Lee, D., Kunimi, H., Negishi, K., and Kurihara, T. (2022). Degeneration of retinal ganglion cells in hypoxic responses: hypoxia-inducible factor inhibition, a new therapeutic insight. *Neural Regen. Res*. 17, 2230–2231. doi: 10.4103/1673-5374.335801

Liu, Q., Palmgren, V. A. C., Danen, E. H., and Le Dévédec, S. E. (2022). Acute vs. chronic vs. intermittent hypoxia in breast cancer: a review on its application in in vitro research. *Mol. Biol. Rep*. 49, 10961–10973. doi: 10.1007/s11033-022-07802-6

López-Barneo, J., del Toro, R., Levitsky, K. L., Chiara, M. D., and Ortega-Sáenz, P. (2004). Regulation of oxygen sensing by ion channels. *J. Appl. Physiol*. 96, 1187–1195. doi: 10.1152/japplphysiol.00929.2003

Lukyanetz, E. A., Shkryl, V. M., Kravchuk, O. V., and Kostyuk, P. G. (2003). Effect of hypoxia on calcium channels depends on extracellular calcium in CA1 hippocampal neurons. *Brain Res*. 980, 128–134. doi: 10.1016/S0006-8993(03)02951-2

Luo, X. G., Chiu, K., Lau, F. H., Lee, V. W., Yung, K. K., and So, K. F. (2009). The selective vulnerability of retinal ganglion cells in rat chronic ocular hypertension model at early phase. *Cell. Mol. Neurobiol*. 29, 1143–1151. doi: 10.1007/s10571-009-9407-1

Mayer, C., Bruehl, C., Salt, E. L., Diem, R., Draguhn, A., and Fairless, R. (2018). Selective vulnerability of αOFF retinal ganglion cells during onset of autoimmune optic neuritis. *Neuroscience* 393, 258–272. doi: 10.1016/j.neuroscience.2018.07.040

Mishra, O. P., Ashraf, Q. M., and Delivoria-Papadopoulos, M. (2002). Phosphorylation of cAMP response element binding (CREB) protein during hypoxia in cerebral cortex of newborn piglets and the effect of nitric oxide synthase inhibition. *Neuroscience* 115, 985–991. doi: 10.1016/S0306-4522(02)00275-0

Montoro, R. J., Ureña, J., Fernández-Chacón, R., Alvarez de Toledo, G., and López-Barneo, J. (1996). Oxygen sensing by ion channels and chemotransduction in single glomus cells. *J. Gen. Physiol*. 107, 133–143. doi: 10.1085/jgp.107.1.133

Munemasa, Y., and Kitaoka, Y. (2013). Molecular mechanisms of retinal ganglion cell degeneration in glaucoma and future prospects for cell body and axonal protection. *Front. Cell. Neurosci*. 6, 60. doi: 10.3389/fncel.2012.00060

Nicotera, P., and Orrenius, S. (1998). The role of calcium in apoptosis. *Cell Calcium* 23, 173–180. doi: 10.1016/S0143-4160(98)90116-6

Osborne, N. N., Melena, J., Chidlow, G., and Wood, J. P. (2001). A hypothesis to explain ganglion cell death caused by vascular insults at the optic nerve head: possible implication for the treatment of glaucoma. *Br. J. Ophthalmol*. 85, 1252–1259. doi: 10.1136/bjo.85.10.1252

Ou, Y., Jo, R. E., Ullian, E. M., Wong, R. O., and Della Santina, L. (2016). Selective vulnerability of specific retinal ganglion cell types and synapses after transient ocular hypertension. *J. Neurosci*. 36, 9240–9252. doi: 10.1523/JNEUROSCI.0940-16.2016

Palmer, M. J., Hull, C., Vigh, J., and von Gersdorff, H. (2003). Synaptic cleft acidification and modulation of short-term depression by exocytosed protons in retinal bipolar cells. *J. Neurosci*. 23, 11332–11341. doi: 10.1523/JNEUROSCI.23-36-11332.2003

Potilinski, M. C., Lorenc, V., Perisset, S., and Gallo, J. E. (2020). Mechanisms behind retinal ganglion cell loss in diabetes and therapeutic approach. *Int. J. Mol. Sci*. 21, 2351. doi: 10.3390/ijms21072351

Rekalov, V., Juránek, I., Málekov,á, L., and Bauer, V. (1997). Hypoxia-induced inhibition of calcium channels in guinea-pig taenia caeci smooth muscle cells. *J. Physiol*. 505, 107–119. doi: 10.1111/j.1469-7793.1997.107bc.x

Riemann, A., Schneider, B., Ihling, A., Nowak, M., Sauvant, C., Thews, O., et al. (2011). Acidic environment leads to ROS-induced MAPK signaling in cancer cells. *PLoS ONE* 6, e22445. doi: 10.1371/journal.pone.0022445

Sasaki, T., and Kaneko, A. (2007). Elevation of intracellular ca(2+) concentration induced by hypoxia in retinal ganglion cells. *Jpn. J. Ophthalmol*. 51, 175–180. doi: 10.1007/s10384-006-0426-x

Saxena, K., and Jolly, M. K. (2019). Acute vs. chronic vs. cyclic hypoxia: their differential dynamics, molecular mechanisms, and effects on tumor progression. *Biomolecules* 9, 339. doi: 10.3390/biom9080339

Schmid, S., and Guenther, E. (1999). Voltage-activated calcium currents in rat retinal ganglion cells in situ: changes during prenatal and postnatal development. *J. Neurosci*. 19, 3486–3494. doi: 10.1523/JNEUROSCI.19-09-03486.1999

Shahulhameed, S., Swain, S., Jana, S., Chhablani, J., Ali, M. J., Pappuru, R. R., et al. (2020). A robust model system for retinal hypoxia: live imaging of calcium dynamics and gene expression studies in primary human mixed retinal culture. *Front. Neurosci*. 13, 1445. doi: 10.3389/fnins.2019.01445

Shimoda, L. A., and Polak, J. (2011). Hypoxia. 4. Hypoxia and ion channel function. *Am. J. Physiol. Cell Physiol*. 300, C951–967. doi: 10.1152/ajpcell.00512.2010

Shkryl, V. M., Kostyuk, P. G., and Lukyanetz, E. A. (2001). Dual action of cytosolic calcium on calcium channel activity during hypoxia in hippocampal neurones. *Neuroreport* 12, 4035–4039. doi: 10.1097/00001756-200112210-00036

Siliprandi, R., Canella, R., Carmignoto, G., Schiavo, N., Zanellato, A., Zanoni, R., et al. (1992). N-methyl-D-aspartate-induced neurotoxicity in the adult rat retina. *Vis. Neurosci*. 8, 567–573. doi: 10.1017/S0952523800005666

Simms, B. A., and Zamponi, G. W. (2014). Neuronal voltage-gated calcium channels: structure, function, and dysfunction. *Neuron* 82, 24–45. doi: 10.1016/j.neuron.2014.03.016

Smith, B. J., McHugh, C. F., Hirano, A. A., Brecha, N. C., and Barnes, S. (2023). Transient and sustained ganglion cell light responses are differentially modulated by intrinsically produced reactive oxygen species acting upon specific voltage-gated Na^+ channel isoforms. *J. Neurosci*. 43, 2291–2304. doi: 10.1523/JNEUROSCI.1723-22.2023

Sucher, N. J., Wong, L. A., and Lipton, S. A. (1990). Redox modulation of NMDA receptor-mediated Ca2+ flux in mammalian central neurons. *Neuroreport* 1, 29–32. doi: 10.1097/00001756-199009000-00009

Summers, B. A., Overholt, J. L., and Prabhakar, N. R. (2000). Augmentation of L-type calcium current by hypoxia in rabbit carotid body glomus cells: evidence for a PKC-sensitive pathway. *J. Neurophysiol*. 84, 1636–1644. doi: 10.1152/jn.2000.84.3.1636

Swenson, E. R. (2016). Hypoxia and its acid-base consequences: from mountains to malignancy. *Adv. Exp. Med. Biol*. 903, 301–323. doi: 10.1007/978-1-4899-7678-9_21

Tapia, M. L., Nascimento-Dos-Santos, G., and Park, K. K. (2022). Subtype-specific survival and regeneration of retinal ganglion cells in response to injury. *Front. Cell Dev. Biol*. 10, 956279. doi: 10.3389/fcell.2022.956279

Tezel, G. (2021). Multifactorial pathogenic processes of retinal ganglion cell degeneration in glaucoma towards multi-target strategies for broader treatment effects. *Cells* 10, 1372. doi: 10.3390/cells10061372

Tezel, G., and Wax, M. B. (2004). Hypoxia-inducible factor 1α in the glaucomatous retina and optic nerve head. *Arch. Ophthalmol.* 122, 1348–1356. doi: 10.1001/archopht.122.9.1348

Tran, N. M., Shekhar, K., Whitney, I. E., Jacobi, A., Benhar, I., Hong, G., et al. (2019). Single-cell profiles of retinal ganglion cells differing in resilience to injury reveal neuroprotective genes. *Neuron* 104, 1039–1055.e12. doi: 10.1016/j.neuron.2019.11.006

Veselovsky, N. S., Engert, F., and Lux, H. D. (1996). Fast local superfusion technique. *Pflugers Arch*. 432, 351–354. doi: 10.1007/s004240050143

Wanaverbecq, N., Marsh, S. J., Al-Qatari, M., and Brown, D. A. (2003). The plasma membrane calcium-ATPase as a major mechanism for intracellular calcium regulation in neurones from the rat superior cervical ganglion. *J. Physiol*. 550, 83–101. doi: 10.1113/jphysiol.2002.035782

Wangsa-Wirawan, N. D., and Linsenmeier, R. A. (2003). Retinal oxygen: fundamental and clinical aspects. *Arch. Ophthalmol.* 121, 547–557. doi: 10.1001/archopht.121.4.547

Warwick, A. M., Bomze, H. M., Wang, L., Klingeborn, M., Hao, Y., Stinnett, S. S., et al. (2022). Continuous hypoxia reduces retinal ganglion cell degeneration in a mouse model of mitochondrial optic neuropathy. *Invest. Ophthalmol. Vis. Sci*. 63, 21. doi: 10.1167/iovs.63.13.21

Weir, E. K., and Olschewski, A. (2006). Role of ion channels in acute and chronic responses of the pulmonary vasculature to hypoxia. *Cardiovasc. Res.* 71, 630–641. doi: 10.1016/j.cardiores.2006.04.014

Wen, X., Liao, P., Luo, Y., Yang, L., Yang, H., Liu, L., et al. (2022). Tandem pore domain acid-sensitive K channel 3 (TASK-3) regulates visual sensitivity in healthy and aging retina. *Sci. Adv*. 8, eabn8785. doi: 10.1126/sciadv.abn8785

Whitlock, N. A., Agarwal, N., Ma, J. X., and Crosson, C. E. (2005). Hsp27 upregulation by HIF-1 signaling offers protection against retinal ischemia in rats. *Invest. Ophthalmol. Vis. Sci*. 46, 1092–1098. doi: 10.1167/iovs.04-0043

Yamada, H., Chen, Y. N., Aihara, M., and Araie, M. (2006). Neuroprotective effect of calcium channel blocker against retinal ganglion cell damage under hypoxia. *Brain Res*. 1071, 75–80. doi: 10.1016/j.brainres.2005.11.072

Zamponi, G. W. (2016). Targeting voltage-gated calcium channels in neurological and psychiatric diseases *Nat. Rev. Drug Discov*. 15, 19–34 doi: 10.1038/nrd.2015.5

Zhong, Y. S., Wang, J., Liu, W. M., and Zhu, Y. H. (2013). Potassium ion channels in retinal ganglion cells (review). *Mol. Med. Rep*. 8, 311–319. doi: 10.3892/mmr.2013.1508

Zhu, Y., Zhang, L., and Gidday, J. M. (2013). Role of hypoxia-inducible factor-1α in preconditioning-induced protection of retinal ganglion cells in glaucoma. *Mol. Vis*. 19, 2360–2372.

Zhu, Y., Zhang, L., Schmidt, J. F., and Gidday, J. M. (2012). Glaucoma-induced degeneration of retinal ganglion cells prevented by hypoxic preconditioning: a model of glaucoma tolerance. *Mol. Med*. 18, 697–706. doi: 10.2119/molmed.2012.00050

Zhu, Y., Zhang, Y., Ojwang, B. A., Brantley, M. A. Jr., and Gidday, J. M. (2007). Long-term tolerance to retinal ischemia by repetitive hypoxic preconditioning: role of HIF-1alpha and heme oxygenase-1. *Invest. Ophthalmol. Vis. Sci*. 48, 1735–1743. doi: 10.1167/iovs.06-1037

Zubrow, A. B., Delivoria-Papadopoulos, M., Ashraf, Q., Ballesteros, J. R., Fritz, K. I., and Mishra, O.P. (2002). Nitric oxide-mediated expression of Bax protein and DNA fragmentation during hypoxia in neuronal nuclei from newborn piglets. *Brain Res*. 954, 60–67. doi: 10.1016/S0006-8993(02)03342-5

frontiers | Frontiers in Cellular Neuroscience

TYPE Original Research
PUBLISHED 12 July 2023
DOI 10.3389/fncel.2023.1131661

OPEN ACCESS

EDITED BY
Xiaodi Chen,
Women & Infants Hospital of Rhode Island,
United States

REVIEWED BY
Ari-Pekka Koivisto,
Orion Corporation, Finland
Melissa Anne Tadros,
The University of Newcastle, Australia

*CORRESPONDENCE
Yurii Tkachenko
✉ tkachenko@biph.kiev.ua

RECEIVED 25 December 2022
ACCEPTED 26 June 2023
PUBLISHED 12 July 2023

CITATION
Tkachenko Y, Khmyz V, Buta A, Isaev D, Maximyuk O and Krishtal O (2023) Acid-sensing ion channel blocker diminazene facilitates proton-induced excitation of afferent nerves in a similar manner that Na^+/H^+ exchanger blockers do. *Front. Cell. Neurosci.* 17:1131661. doi: 10.3389/fncel.2023.1131661

Acid-sensing ion channel blocker diminazene facilitates proton-induced excitation of afferent nerves in a similar manner that Na^+/H^+ exchanger blockers do

Yurii Tkachenko*, Volodymyr Khmyz, Andrii Buta, Dmytro Isaev, Oleksandr Maximyuk and Oleg Krishtal

Bogomoletz Institute of Physiology, National Academy of Sciences of Ukraine, Kyiv, Ukraine

Tissue acidification causes sustained activation of primary nociceptors, which causes pain. In mammals, acid-sensing ion channels (ASICs) are the primary acid sensors; however, Na^+/H^+ exchangers (NHEs) and TRPV1 receptors also contribute to tissue acidification sensing. ASICs, NHEs, and TRPV1 receptors are found to be expressed in nociceptive nerve fibers. ASIC inhibitors reduce peripheral acid-induced hyperalgesia and suppress inflammatory pain. Also, it was shown that pharmacological inhibition of NHE1 promotes nociceptive behavior in acute pain models, whereas inhibition of TRPV1 receptors gives relief. The murine skin-nerve preparation was used in this study to assess the activation of native polymodal nociceptors by mild acidification (pH 6.1). We have found that diminazene, a well-known antagonist of ASICs did not suppress pH-induced activation of CMH-fibers at concentrations as high as 25 μM. Moreover, at 100 μM, it induces the potentiation of the fibers' response to acidic pH. At the same time, this concentration virtually completely inhibited ASIC currents in mouse dorsal root ganglia (DRG) neurons (IC_{50} = 17.0 ± 4.5 μM). Non-selective ASICs and NHEs inhibitor EIPA (5-(N-ethyl-N-isopropyl)amiloride) at 10 μM, as well as selective NHE1 inhibitor zoniporide at 0.5 μM induced qualitatively the same effects as 100 μM of diminazene. Our results indicate that excitation of afferent nerve terminals induced by mild acidification occurs mainly due to the NHE1, rather than acid-sensing ion channels. At high concentrations, diminazene acts as a weak blocker of the NHE. It lacks chemical similarity with amiloride, EIPA, and zoniporide, so it may represent a novel structural motif for the development of NHE antagonists. However, the effect of diminazene on the acid-induced excitation of primary nociceptors remains enigmatic and requires additional investigations.

KEYWORDS

skin-nerve preparation, primary afferent nociceptors, acidic pH, diminazene, zoniporide, 5-(N-ethyl-N-isopropyl)amiloride (EIPA), Na^+/H^+ exchangers (NHEs)

Introduction

Virtually all proteins, including enzymes and ion channels, depend on pH to maintain their function (Whitten et al., 2005). Proteins gain proton sensitivity by changing the charge of amino acids by protonation or deprotonation. Only a few amino acids, such as histidine, aspartic acid, arginine, lysine, and glutamic acid, are protonated at pH values ranging from 5 to 7.4. Histidine has pKa $\approx$ 6–7 making it the most prominent candidate for sensing slight changes in pH. Histidine is thought to be uncharged at neutral pH and doubly protonated and positively charged at pH 6 and lower, while the effective pKa of a single histidine varies on its local environment. Tight control of both extra- and intracellular pH is essential for maintaining cellular biochemical reactions and tissue homeostasis (Casey et al., 2010). Despite the efficient pH control mechanisms, various pathological conditions, such as inflammation, injury, or solid tumors, are associated with the development of local acidosis. In the normal state, pH values in tissue ranged from 7.35 to 7.45. However, inflammation could reduce the pH in the injury place down to 6–6.5 units (Rajamaki et al., 2013). The value of extracellular pH decreases to 6.69–6.89 in fractures (Berkmann et al., 2020), intra-abdominal infections cause a drop in pH to values less than 7.1 (Simmen et al., 1994), and in various tumors, the pH ranges from 6.4 to 7.0 (Engin et al., 1995). The metabolic decrease in pH in pathological conditions is thought to be due to the accumulation of lactic acid and carbon dioxide in the affected tissues.

Intracellular pH (pHi) is a fundamental parameter of cell function that requires tight homeostasis (Casey et al., 2010). Mammalian cells constantly have to eliminate internal acidification. This task is mainly performed by Na^+/H^+ antiporters, which exchange extracellular Na^+ for intracellular H^+, which activates when cells become acidic. NHEs are widespread in neuronal and non-neuronal cells. Of the 9 NHE isoforms identified, NHE1 is the most ubiquitous and expressed in nerve cells (Slepkov et al., 2007; Torres-Lopez et al., 2013). NHE inhibitors concentration-dependently produce intracellular acidosis and can even cause cell death (Schneider et al., 2004). By using the *in vitro* electrophysiological skin-nerve preparation recording method, it was shown that intracellular proton release by photolysis from NPE-caged proton compounds caused the same irritation and transient heat sensitization of sensory endings in skin sensory neurons as extracellular acidification by phosphate buffered solution (pH 5.4) and CO_2-gassed solution (pH 6.1) (Guenther et al., 1999). While, the membrane-permeable proton buffer SNARF-AM, which was used to prevent changes in intracellular pH, prevented pH-induced heat sensitization. Studies using fluorescent indicators have shown that depolarization with high K^+, as well as extracellular acidification of sensory neurons, causes a decrease in intracellular pH (Werth and Thayer, 1994; Zeilhofer et al., 1997). Due to the widespread expression of NHE1 in nerve cells, including nociceptors, it is probable that NHE1 could affect the excitability of neurons and the transmission of pain by altering the pH levels within the cells. However, the experimental data on the effect of NHE blockers on the activity of nerve cells obtained using various models are somewhat contradictory. Administration of amiloride derivatives as non-selective NHE inhibitors, and zoniporide, a selective NHE1 inhibitor, significantly increased formalin-induced startle in a dose-dependent manner in rats (Castaneda-Corral et al., 2011). But, experiments performed on dorsal root ganglia (DRG) cells have shown that NHE1 inhibitor zoniporide reduces the amplitude of the compound action potential (Liu and Somps, 2008).

Pain stimuli (chemical, mechanical, and thermal) are first detected by the nerve endings of specialized peripheral primary sensory neurons called nociceptors. These nerve fibers arise from small-diameter pseudounipolar neurons located in the DRG. Endings of primary sensory neurons detect local changes in pH and respond to these changes with a depolarization response, which is thought to be the initial trigger for pain sensation. The tissue acidification causes the excitation of cutaneous nociceptors without signs of desensitization or adaptation (Steen et al., 1995). The subpopulation of polymodal nociceptive mechanoheat-sensitive C-fibers (CMH-fibers) possesses the highest sensitivity to a decrease in pH. Its threshold levels were found within the range from pH 6.9 to 6.1, and the mean maximum discharge level was at pH 5.2 (Steen et al., 1992). To detect changes in pH, nociceptors are equipped with an assortment of different acid sensors, some of which can detect mild changes in pH, such as the acid-sensing ion channels, proton-sensing G protein-coupled receptors, and several two-pore potassium channels, whereas others, such as the transient receptor potential vanilloid 1 ion channel (TRPV1), require larger shifts in pH (Pattison et al., 2019). In many species, nociceptors are polymodal, i.e., they respond to multiple noxious stimuli (e.g., heat, pressure, and chemicals such as acid), owing to the expression of different receptors (Boscardin et al., 2016).

Acid-sensing ion channels (ASICs) and TRPV1 receptors have been proposed as the main acid sensors (Ugawa et al., 2002) in nociceptors. ASIC1a, ASIC1b, ASIC3, and TRPV1 receptors are mainly expressed in small-diameter DRG neurons with a high level of co-expression. ASIC1a transcripts were found in 20–25% of DRG neurons; ASIC1b and ASIC3 transcripts are expressed in approximately 10 and 30–35% of DRG neurons, respectively (Ugawa et al., 2005). Half-maximal activation (pH_{50}) for ASIC1a occurs at pH 6.2–6.6; for ASIC1b, pH_{50} is 5.9–6.3; and pH_{50} for ASIC3 is 6.4–6.7 (Boscardin et al., 2016). Severe extracellular acidosis (acidification to pH $\leq$ 6.4) activates the whole repertoire of ASIC subtypes. TRPV1 is expressed in 35–40% of DRG neurons (Ugawa et al., 2005). TRPV1 is a polymodal ion channel activated by capsaicin and a number of other stimuli including noxious heat ($>$42°C) and protons (Caterina et al., 1997; Mickle et al., 2015). TRPV1-mediated sustained currents due to acidification have a pH_{50} of ~5.4. Thus, TRPV1 and ASICs ion channels expressed in small-diameter DRG neurons are very important extracellular acid sensors, contributing to acid-induced nociception within the physiological pH range (below pH 7.3 for ASICs and below pH 6.0 for TRPV1) (Blanchard and Kellenberger, 2011).

The high sensitivity of ASICs to acidosis and their distribution in primary sensory neurons point to a significant role of these channels in acid-induced nociception (Kellenberger and Schild, 2002; Krishtal, 2003). Local administration of ASIC1 and ASIC3 channel activators induces pain behavior (Yu et al., 2010; Bohlen et al., 2011), while the administration of ASIC channel inhibitors has an analgesic effect (Jones et al., 2004; Diochot et al., 2012). These data indicate that ASICs are promising targets for antinociceptive drugs. However, a well-known blocker of ASICs amiloride demonstrates some controversial effects on different

experimental models (Steen et al., 1999; Ugawa et al., 2002). In this study, we examined the effect of the non-amiloride ASICs receptor antagonist, diminazene, on acid-evoked responses of mouse cutaneous nociceptors *ex vivo*.

Materials and methods

Animals

Adult (6–7 weeks old) BALB/c mice weighing 22–30 g were used in the *ex vivo* skin-nerve preparation experiments. For patch-clamp studies, mice aged 8–12 days were selected. To avoid potential sex-specific effects (Riley et al., 1998; Ross et al., 2018) only male subjects were used in all the experiments. Animals were bred in the vivarium of the Bogomoletz Institute of Physiology, where they were housed on a 12-h light-dark cycle and given food and water *ad libitum*. All experiments were performed in accordance with the guidelines of the Bogomoletz Institute Animal Care and Use Committee. A total of 34 mice were used in this study.

Skin-nerve preparation

Murine skin-nerve preparation has been used for electrophysiology recording from single primary afferents, as described earlier (Tkachenko et al., 2023). Under deep anesthesia by urethane (2 g per kg, i.p.), the saphenous nerve and its innervating territory on the hairy hind paw skin were subcutaneously dissected and excised. After dissection, the animals were euthanized with an intraperitoneal injection of a lethal dose of urethane. Next, the skin was gently stretched and pinned corium side up in the organ bath for pharmacological application to the receptive fields of single sensory units. The end of the nerve was gently threaded through a hole into a separate recording chamber for fiber teasing and single-unit recording. The tissue and recording chambers were separately superfused with a modified Krebs–Henseleit solution composed of (in mM): NaCl 118, KCl 5.4, NaH_2PO_4 1.0, $MgSO_4$ 1.2, $CaCl_2$ 1.9, $NaHCO_3$ 25.0, and dextrose 11.1, and gassed with 95% O_2–5% CO_2, pH 7.4, at a flow rate of 8 ml $\times$ min^{-1} and 3 ml $\times$ min^{-1}, respectively. The temperature in the organ bath and recording chamber was maintained at 32 $\pm$ 0.1°C.

Single fiber activity recordings

The recordings of single fiber activity were performed using a suction glass microelectrode. The microelectrodes were pulled using a Flaming-Brown micropipette puller (Model P-97, Sutter Instrument CO., USA). The recording signal was amplified (Model 3000, A-M Systems, Inc., Carlsborg, WA, USA) and filtered (low cut-off, 0.3 kHz; high cut-off, 1 kHz). Nerve fiber activities were recorded to a PC via a Digidata 1200 analog-to-digital converter (Axon Instruments, USA). Single units were characterized as follows: conduction latency in milliseconds was determined by electrical stimulation inside the receptive field with a fine steel electrode using an A-M Systems analog stimulus isolator model 2200, and the conduction distance was assessed to calculate conduction velocity. A cutoff of 1.0 m/s was used to distinguish between myelinated and unmyelinated fibers. Extracellular recordings were obtained only from single fibers that could be easily discriminated according to amplitude and shape (**Figure 1A**). We limited our investigation to the CMH subpopulation of nerve fibers since this group of mechano-heat sensitive "polymodal" C-units is significantly more responsive to acidic pH (Steen et al., 1992). Other types of fibers, including the A-fiber population with higher conduction velocities, were not investigated. The CMH nerve fibers that did not respond to chemical stimulation were not taken into account. The recorded signal was stored on a computer using WinEDR v 3.3.1 software.

Chemical stimulation of the nerve endings

To boost the rate of solution exchange, the receptive field was isolated from its surroundings using a tiny glass ring (inner diameter: 6 mm; volume: 0.3 ml). The ring was separately perfused at 4 ml/min, providing a rapid exchange of the fluid. The nerve fiber's receptive field was superfused with the same modified Krebs-Henseleit solution, continuously gassed with 100% CO_2, triggering a pH drop to 6.1 (Steen et al., 1992). The experimental series consisted of three subsequent acidic stimuli of a 5-min duration. After a 5-min pre-application, the tested reagents were applied together with the second acid stimulus. Each chemical stimulation was followed by a washout period lasting more than 10 min. The temperature of the buffer solutions in the glass ring was maintained at 32 $\pm$ 0.1°C unless otherwise indicated.

Primary culture of mouse DRG neurons

Dorsal root ganglia neurons were isolated using a standard procedure (Maximyuk et al., 2015). In brief, after animal decapitation, ganglia were rapidly removed and placed in an Eagle's minimal essential medium (MEM) solution containing 4 mg/mL trypsin and 2 mg/mL collagenase for 25 min. The solution was held at 35°C during the enzymatic treatment and constantly saturated with a gas mixture of 95% oxygen and 5% carbon dioxide to maintain a pH of 7.4. The ganglia were then rinsed out and dissociated in a MEM solution containing 7.4 pH HEPES-NaOH. Finally, the isolated neurons were suspended in a mixture of 90% Dulbecco's modified Eagle's medium (DMEM), 0.3% penicillin, 10 μg/ml insulin, and 10% fetal calf serum and maintained at 37°C for 5–48 h before being used in electrophysiological experiments.

Patch-clamp experiments

The whole-cell patch clamp recordings were done using an EPC8 amplifier and LIH 1600 acquisition system (HEKA, Germany). The recordings were taken at a holding potential of −60 mV. The current traces were sampled at 10–20 kHz and filtered online at 7 kHz. The patch electrodes, having a resistance of 2–3 MΩ, were filled with a solution containing 120 mM CsF and 20 mM Tris-Cl, pH 7.3. The extracellular solution had the

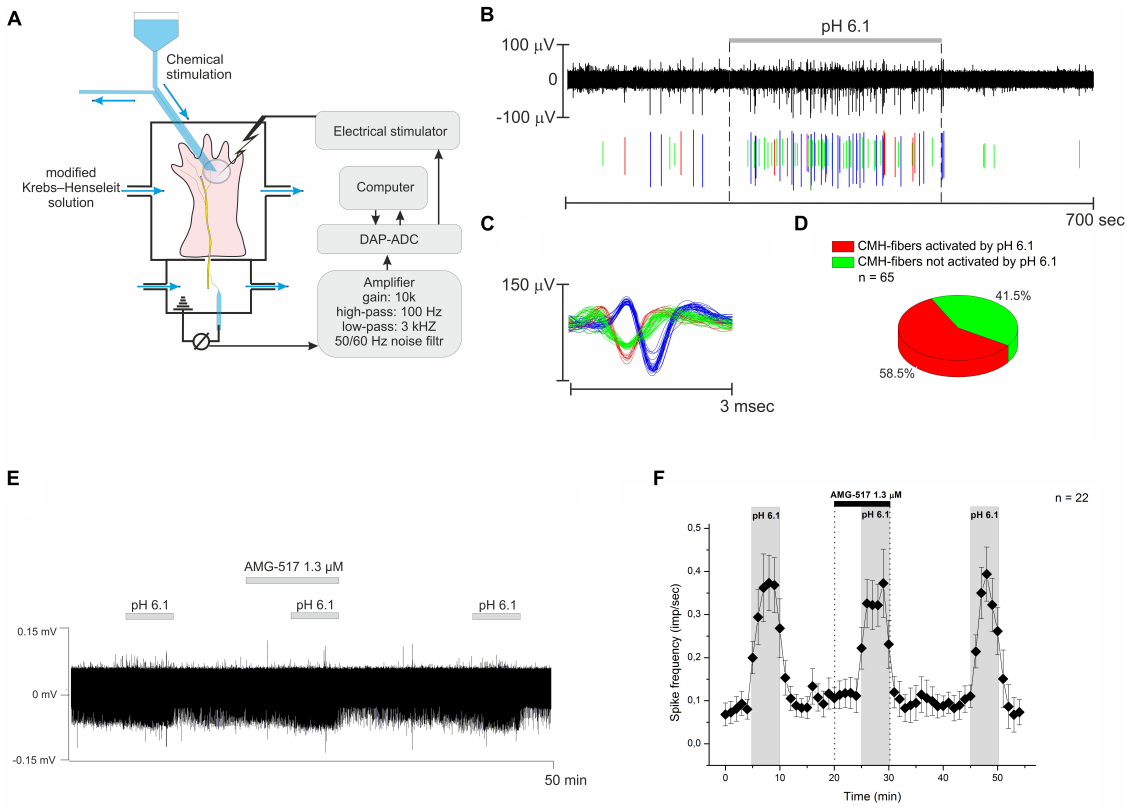

FIGURE 1
(A) The simplified experiment diagram shows the process of identifying the receptive fields of nerve fibers using electrical, mechanical, and temperature stimulation. Next, the skin area with the receptive field was isolated using a small glass ring for chemical stimulation and drug testing. **(B)** Example recording from three nervous CMH-fibers upon stimulation of their receptive field using a modified Krebs–Henseleit solution with pH 6.1. **(C)** Action potentials from the same nerve filament are displayed as their superimposed waveforms. **(D)** Summary data for activation of CMH-fibers by pH 6.1. **(E)** Representative recording of CMH-fiber activity under the TRPV1 receptor antagonist AMG-517. AMG-517 was applied at a concentration of 1.3 µM before and during the activation of nerve fibers by pH 6.1 at 40°C. **(F)** Descriptive statistics: CMH-fiber activity (imp/s) was averaged at 60-s intervals (mean ± SEM). AMG-517 did not alter the activity of CMH-fibers by itself, nor did it cause any changes in low pH-induced discharge.

following composition: 130 mM NaCl, 5 mM KCl, 2 mM $MgCl_2$, 2 mM $CaCl_2$, and 20 mM HEPES/NaOH, pH 7.4 (adjusted with NaOH). A rapid pH decrease from 7.4 to 6.0 caused a transient transmembrane ionic current, which is mediated by activation of ASICs, in around 30% of the DRG neurons examined. PatchMaster v.2 × 69 software (HEKA, Germany) was used to record and store the experimental data. A fully automated "jumping table" setup (PharmaRobot in Kyiv, Ukraine) was used for solution exchange, allowing for approximately 90% solution exchange in about 10 ms. The experiments were made at room temperature (20°C).

Data analysis

Single-fiber recordings were analyzed offline with a template-matching function of Spike 2 software (CED, Cambridge, UK). The PatchMaster v.2 × 69 (HEKA, Germany) software was used for the initial analysis of patch-clamp data. Origin Pro 8.5 software (Origin Lab. Corp., Northampton, MA, USA) was used for conducting all statistical tests. All experimental data are presented as mean ± SEM. A paired Student's *t*-test was used to determine the significance of the differences in nerve fiber activity and for the comparison of current amplitudes in patch-clamp experiments. The level of significance was chosen at 0.05 unless otherwise indicated.

Chemicals

All chemicals were purchased from Sigma-Aldrich Chemie GmbH (Taufkirchen, Germany).

Results

Single-unit recordings were made from a total of 87 CMH-fibers of polymodal nerve afferents from 32 animals. All tested CMH-fibers demonstrate the spontaneous basal activity with a corresponding instantaneous frequency of 0.034 ± 0.0083 imp/s at 32°C.

In response to the stimulation of the receptive field by pH 6.1, an increase in spontaneous activity to 0.449 ± 0.099 imp/s ($n = 52$, $p = 0.000073$, Figures 1B, C) was observed in 58.5% (38/65, Figure 1D) of nerve fibers. Further decreasing pH promoted an

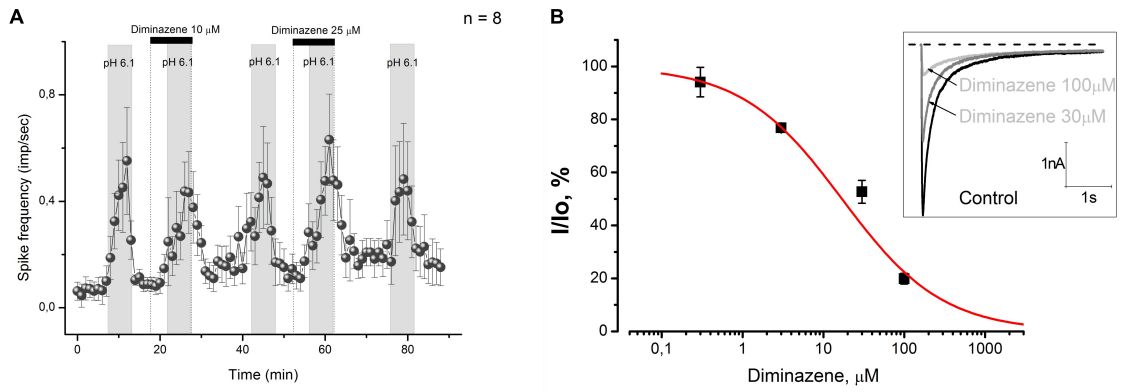

FIGURE 2
(A) Diminazene at concentrations of 10 and 25 μM did not excite CMH-fibers by itself and did not cause changes in low pH-induced discharge. **(B)** Diminazene inhibits native ASIC currents in primary cultured mouse DRG neurons at micromolar concentrations. Currents were elicited by a rapid pH drop from 7.4 to 6.0 at a holding voltage of −60 mV. The dose-response fit of the data gives IC_{50} = 16.9 ± 4.4 μM and k = 0.7 ± 0.1.

increase in CMH-fiber activity as well as the percent of responding fibers (data not shown). However, TRPV1 receptors are also sensitive to extracellular pH and may induce the firing of nerve fibers in response to low pH (Tominaga et al., 1998; Blanchard and Kellenberger, 2011). We have checked the effect of a selective antagonist of TRPV1 channels, AMG-517, on the response of CMH-fibers to pH 6.1 at 40°C. The tested CMH-fibers (n = 22) demonstrated spontaneous basal activity with a corresponding instantaneous frequency of 0.08 ± 0.025 imp/s in control conditions at the beginning of the experiment. AMG-517 1.3 μM by itself did not affect the basal activity of nerve fibers during pre-application (n = 22, p = 0.096, **Figures 3E, F**). Stimulation by pH 6.1 increased spike frequency to 0.51 ± 0.084 imp/s (n = 22, p = 0.000009), while AMG-517 at a concentration of 1.3 μM did not produce any feasible effect on this increase (0.483 ± 0.074; n = 22; p = 0.298).

Diminazene does not inhibit the acid-induced activity of CMH-fibers at 10 and 25 μM

Acid-sensing ion channels are shown to be the most sensitive effectors to protons (Ugawa et al., 2002; Blanchard and Kellenberger, 2011) in sensory nerve endings, while diminazene has been proven to be an efficient blocker of them [pIC50 ∼ 6.5, see Chen et al. (2010)]. Therefore, the diminazene should effectively antagonize the response of the CMH-fibers to acidic pH. We examined the effect of diminazene in concentrations of 10 and 25 μM on the response of CMH-fibers to pH 6.1. The tested CMH-fibers (n = 8) demonstrated spontaneous basal activity with a corresponding instantaneous frequency of 0.063 ± 0.031 imp/s in control conditions at the beginning of the experiment. Diminazene by itself did not affect the basal activity of nerve fibers during pre-application (n = 8, p = 0.291, and p = 0.14, correspondingly, **Figure 2A**). Stimulation by an acidic pH increased spike frequency to 0.683 ± 0.17 imp/s (n = 8, p = 0.00416, **Figure 2A**). Coadministration of acidic solution with diminazene at concentrations as high as 10 and 25 μM did not produce any feasible effect on this increase (0,533 ± 0.117; n = 8; p = 0.157, and 0.679 ± 0.174 imp/s n = 8; p = 0.972, correspondingly).

Since diminazene at concentrations as high as 10 and 25 μM did not affect the acid-induced response of skin nociceptors, we used the patch-clamp technique to evaluate its activity on native acid-sensing ion channels expressed in mouse DRG neurons, because we could not find any data on its activity on these channels. We have found that diminazene causes a dose-dependent inhibition (**Figure 2B**) of the ASIC currents in mouse DRG neurons with a corresponding IC_{50} = 16.9 ± 4.4 μM, which is substantially higher than previously reported for various ASIC subunits (Chen et al., 2010).

So, diminazene effectively decreased native ASICs expressed in the cell bodies of mouse DRG neurons at high micromolar concentrations. The ASIC currents in these neurons were almost completely suppressed by 100 μM diminazene.

Diminazene facilitates acid-induced activity of CMH-fibers at 100 μM

Our findings on diminazene activity on native ASICs expressed in mouse DRG neurons prompted us to increase its concentration in the skin-nerve preparation experiments. In this series of experiments, the tested CMH-fibers (n = 13) demonstrated spontaneous baseline activity with a corresponding instantaneous frequency of 0.046 ± 0.02 imp/s in control conditions. Stimulation by the acidic pH statistically significantly increased the average spike frequency to 0.398 ± 0.106 imp/s (n = 13, p = 0.00265). Diminazene at a concentration of 100 μM did not excite nociceptors by itself while applied alone (n = 13, p = 0.281, **Figure 3A**), while its coadministration with a low-pH solution increased the low pH-induced activity to 1.806 ± 0.416 imp/s (n = 13, p = 0.000337, **Figures 3A, D**). Our data indicate that diminazene at a concentration of 100 μM increased the responsiveness of CMH-fibers to pH 6.1 by 453.8%.

The above, together with the patch-clamp data, pointed us to the hypothesis that the enhancement of acid-induced nerve

10.3389/fncel.2023.1131661

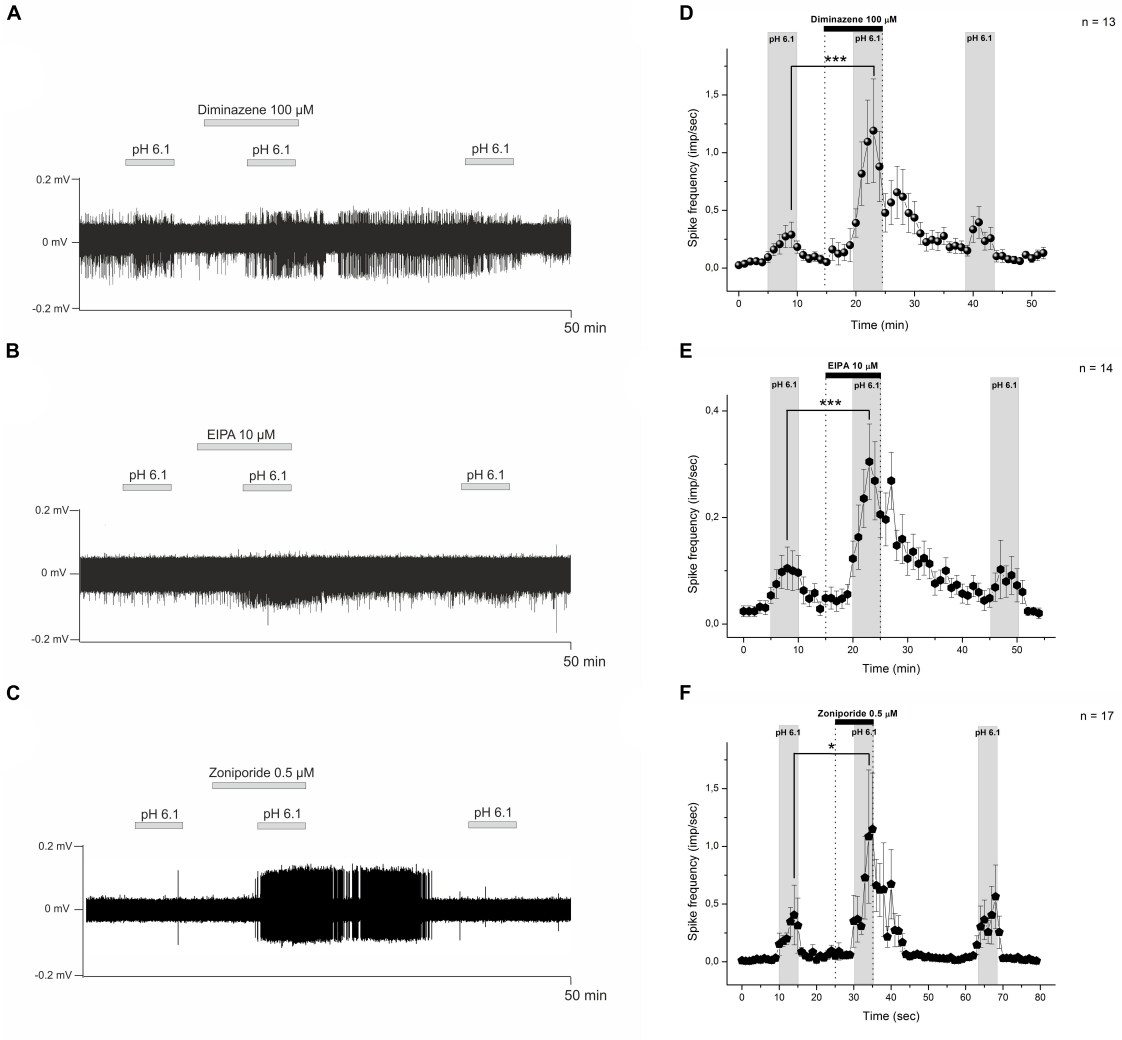

FIGURE 3
Sample recordings from nerve fibers show the influence of diminazene 100 μM **(A)**, EIPA 10 μM **(B)**, and zoniporide 0.5 μM **(C)** on the low pH-induced nociceptor discharge. The test drugs were applied with an acidic solution (pH 6.1) to the receptive field of nerve fibers. Descriptive statistics **(D–F)**. The graphs show averaged CMH-fiber activity (imp/s) at 60-s intervals (mean ± SEM). **(D)** Diminazene 100 μM did not excite the nociceptors at pH 7.4, while low pH-induced discharge increased under diminazene. Polymodal C-fibers also show an increase in low pH-induced discharge under EIPA 10 μM **(E)** and zoniporide 0.5 μM **(F)**. *$p < 0.05$, ***$p < 0.001$.

fibers responses by diminazene involves excitation mechanisms not associated with the activation of ASICs located on nerve endings. It was reported that the ASIC and NHE blocker amiloride increases the pH response of rat skin nociceptors in a dose-dependent manner (Steen et al., 1999). One would suggest that in our experiments, diminazene acts similarly to amiloride, enhancing the response of mouse skin nociceptors to low pH. To verify this hypothesis we tested the effect of well-known NHE1 antagonists on acid-induced responses.

Facilitation of acid-induced activity of CMH-fibers by NHE blockers EIPA and zoniporide

Recently, it was shown that EIPA acts as a non-specific ASIC and NHEs inhibitor (Leng et al., 2016). In these experiments, 14 tested CMH-fibers demonstrated spontaneous activity with a corresponding instantaneous frequency of 0.027 ± 0.01 imp/s in control conditions. Similarly to diminazene, EIPA at 10 μM did affect nociceptors by itself during pre-application ($p = 0.14$, Figures 3B, E). Stimulation by the acidic pH statistically significantly increased the spike frequency to 0.11 ± 0.028 imp/s ($n = 14$, $p = 0.023$). Application of EIPA at 10 μM together with a low-pH solution increased the acid-induced activity to 0.414 ± 0.064 imp/s ($n = 14$; $p = 0.00003$; Figures 3B, E). Four nerve fibers were totally insensitive to both low pH and low pH supplemented with 10 μM (22%). In summary, EIPA at a concentration of 10 μM causes increased sensitivity to low pH of CMH-fibers by 376.4%.

Unlike EIPA, zoniporide is a selective and potent sodium-hydrogen exchanger isoform 1 (NHE1) inhibitor. All tested CMH-fibers demonstrate basal spontaneous activity with corresponding instant frequency of 0.017 ± 0.0057 imp/s ($n = 17$) in control

conditions. Stimulation by the acidic pH statistically significantly, increased spike frequency to 0.661 ± 0.272 imp/s ($n = 17$, $p = 0.029$). Zoniporide at 0.5 μM did not affect the spontaneous activity of primary nerve afferents during pre-application by itself ($n = 17$, $p = 0.154$). Whereas, an application of 0.5 μM zoniporide together with the low pH solution increased the acid-induced activity to 1.678 ± 0.58 imp/s ($n = 17$, $p = 0.0118$, **Figures 3C, F**). So, zoniporide at a concentration of 0.5 μM causes an increase in sensitivity to the low pH of CMH-fibers of 253.8%. Thus, the combination of zoniporide 0.5 μM with low pH induces significantly higher excitation of cutaneous afferent nerve endings than EIPA, but not diminazene.

Discussion

The decrease in pH to the threshold level of 6.9 to 6.1 causes the excitation of cutaneous nociceptors without signs of desensitization or adaptation (Steen et al., 1992). In our experiments, lowering the pH of the superfusion solution from 7.4 to 6.1 induced an approximately 13-fold increase in the spontaneous activity of CMH-fibers in 58.5% (**Figures 1B, D**) cases. While ASICs are described as the most sensitive sensors of protons in nociceptors (Lee and Chen, 2018), their activation is suspected to be the main mechanism for sensing the elevated concentration of protons by nociceptors. However, TRPV1 receptors are also sensitive to extracellular hydrogen ions and may cause the firing of nerve fibers in response to low pH [below 6.0 (Blanchard and Kellenberger, 2011)], especially at elevated temperatures (Tominaga et al., 1998; Tkachenko et al., 2023). To exclude this hypothesis, we used AMG-517, a selective antagonist of TRPV1 channels. At the concentration of 1.3 μM, AMG-517 did not affect the described acid sensitivity of the skin nerve fibers (**Figure 1F**), indicating that TRPV1 channels are not involved in the observed excitation of nerve fibers.

Diminazene was previously known as an anti-protozoal drug in veterinary medicine, but it is now one of the most potent commercially available low-molecular-weight inhibitors of ASIC. It is a non-amiloride-derived ASIC that inhibits ASIC currents at submicromolar concentrations via an open channel and subtype-dependent mechanism and, unlike amiloride, does not have an effect on ENaC (Chen et al., 2010; Lee et al., 2018). The highest potency of diminazene was found to be for ASIC1b and ASIC3, both of which are highly expressed in peripheral sensory neurons and implicated in peripheral nociception. Consistent with this, it was found that diminazene induces peripheral antihyperalgesia in Freund's complete adjuvant rat model of unilateral inflammatory pain, but substantial inter-individual heterogeneity in the antihyperalgesic efficacy of ASIC inhibition was also revealed: some animals (more than 50%) were totally insensitive to the blockade of ASICs (Lee et al., 2018). We found that the blockade of ASICs by diminazene in concentrations as high as 10 and 25 μM did not affect the low pH-induced responses in sensory nerve fibers (**Figure 2A**). The blocking effect of diminazene was described in ASICs heterologously expressed in CHO cells, *X. laevis* oocytes, and native rat channels (Chen et al., 2010; Lee et al., 2018), but not for mouse channels. Consequently, we decided to test the sensitivity of native mouse ASICs expressed in DRG neurons to diminazene. In our experiments, mouse ASICs were found to be at least 20-fold less sensitive to diminazene: $IC_{50} \sim 320$ and 864 nM for rASIC3 and rASIC2a correspondingly (Lee et al., 2018) vs. $IC_{50} = 16.9 \pm 4.4$ μÌ (**Figure 2B**). Respectively, we have decided to increase its concentration in sensory nerve excitation experiments but found an unpredictable result: the low pH-induced activity of nerve fibers was significantly increased under 100 μM of diminazene (0.398 ± 0.106 vs. 1.806 ± 0.416 imp/s; $n = 13$, $p = 0.000337$, **Figures 3A, D**). So, diminazene at a concentration of 100 μM increased the responsiveness of CMH-fibers to pH 6.1 by 453.8%. The described action of diminazene was qualitatively the same as that previously described for amiloride (Steen et al., 1999).

Amiloride and its analogs, such as EIPA, are non-specific blockers of ASICs and Na^+/H^+ exchangers (Kleyman and Cragoe, 1988; Maidorn et al., 1993; Leng et al., 2016). Amiloride is well-known blocker of ASICs (Leng et al., 2016). On the other hand, amiloride causes a dose-dependent increase and prolongation of low pH-induced responses in rat skin-nerve preparation (Steen et al., 1999). Inhibition of the Na^+/H^+ antiporter by replacing external sodium with sucrose induces the same effect on the onset of the response as its blocking by amiloride. The authors conclude that in both cases, blockade of the Na^+/H^+ antiporter increased intracellular acidosis in nerve endings and, as a consequence, increased nociceptive activity (Steen et al., 1999). Peripheral and spinal administration of the non-selective NHE inhibitors amiloride, 5-(N,N-dimethyl)amiloride (DMA), EIPA, and the selective NHE1 inhibitor zoniporide significantly increased formalin-induced nociceptive behavior in a dose-dependent manner (Rocha-Gonzalez et al., 2009; Castaneda-Corral et al., 2011). This data suggests that the sodium-proton exchangers, especially their first isoform (NHE1), play a role in pain processing at peripheral and spinal levels in formalin-induced long-lasting nociceptive behaviors.

Our data indicate that the application of 10 μM EIPA and 0.5 μM of the selective NHE1 blocker zoniporide produces qualitatively the same effects as we described for diminazene. The instantaneous frequency of the response to low pH rose in response to the application of 10 μM EIPA from 0.11 ± 0.028 to 0.414 ± 0.064 imp/s ($n = 14$; $p = 0.00003$; **Figures 3B, E**). Thus, EIPA at a concentration of 10 μM causes increased sensitivity to low pH of CMH-fibers by 376.4%. EIPA is a derivative of amiloride and is not the selective antagonist of Na^+/H^+ antiporter. It is known that the amiloride derivative EIPA also acts as a weak blocker of ASIC receptors (Leng et al., 2016).

Therefore we used a selective blocker of a widely distributed first isoform of Na^+/H^+ antiporter (NHE1) zoniporide. Zoniporide at a concentration of 1 μM is sufficient for the effective inhibition of NHE1 (Kleyman and Cragoe, 1988). Moreover, at this concentration, it did not induce any changes in the activity of ASIC channels endogenously expressed in DRG neurons of mice and rats as well as on hASIC1a in HEK293 cells (**Supplementary Figure 1**). Here we show that in the concentration of 0.5 μM zoniporide facilitates the low pH-induced response from 0.661 ± 0.272 to 1.678 ± 0.58 imp/s ($n = 17$; $p = 0.0118$; **Figure 3F**) providing the increase in sensitivity of CMH-fibers to low pH by 253.8%. Taken together these data suggest that diminazene may act as a weak blocker of Na^+/H^+ antiporter.

Our data support previous studies and demonstrate that blockers of sodium/hydrogen exchangers (NHEs) increase the nociceptive response of nerve fibers. NHEs are expressed in various

tissues of the body in many species. According to a widely accepted model, NHEs located on the gill epithelium of fish play a crucial role in sodium uptake. It was shown that amiloride and diminazene dose-dependently reduce Na^+ uptake in adult rainbow trout at micromolar concentrations (Dymowska et al., 2014). In our study, diminazene enhanced the response to low pH stimulation in mouse nerve fibers. This suggests that diminazene may also influence proton transport out of the nerve endings. It is worth noting that certain drugs can bind to multiple molecular targets or receptors, resulting in a broad range of side effects (Frantz, 2005). So we can speculate that diminazene acts as a weak blocker of the NHE. It lacks chemical similarity with amiloride, EIPA, and zoniporide, so it may represent a novel structural motif for the development of HNE antagonists. But we could not exclude that the effect of diminazene in high concentrations is totally unspecific between different effectors due to the presence of two amidine functional groups. These highly charged groups can provide non-specific effects, and novel designs of ASICs antagonists should consider this issue. In summary, the effect of diminazene on the acid-induced excitation of primary nociceptors remains enigmatic and requires additional investigations.

Data availability statement

The original contributions presented in the study are included in the article/**Supplementary material**, further inquiries can be directed to the corresponding author.

Ethics statement

The animal study was reviewed and approved by the Bogomoletz Institute Animal Care and Use Committee.

Author contributions

YT conducted experimental research using the method of skin-nerve preparation, experimental data processing, and analysis of experimental data. VK conducted experimental research using the method of patch-clamp, analysis, and interpretation of experimental data. AB conducted experimental research using the method of patch-clamp. DI substantial contribution to the conception and design of experiments. OM conception of research, wrote the manuscript, data analysis, and interpretation. OK project management and critical review of the relevance of experimental research. All authors contributed to the article and approved the submitted version.

Funding

This study was supported by the National Research Foundation of Ukraine (https://nrfu.org.ua/) under the project "Enzymes of posttranslational modifications of microtubules proteins, as targets for excitability inhibition of primary nociceptive neurons of peripheral nervous system," State Registration No. 0120U104883.

Conflict of interest

The authors declare that the research was conducted in the absence of any commercial or financial relationships that could be construed as a potential conflict of interest.

Publisher's note

Supplementary material

The Supplementary Material for this article can be found online at: https://www.frontiersin.org/articles/10.3389/fncel.2023.1131661/full#supplementary-material

References

Berkmann, J. C., Herrera, M. A. X., Ellinghaus, A., Schlundt, C., Schell, H., Lippens, E., et al. (2020). Early pH Changes in Musculoskeletal Tissues upon Injury-Aerobic Catabolic Pathway Activity Linked to Inter-Individual Differences in Local pH. *Int. J. Mol. Sci.* 2020:21. doi: 10.3390/ijms21072513

Blanchard, M. G., and Kellenberger, S. (2011). Effect of a temperature increase in the non-noxious range on proton-evoked ASIC and TRPV1 activity. *Pflugers Arch.* 461, 123–139. doi: 10.1007/s00424-010-0884-3

Bohlen, C. J., Chesler, A. T., Sharif-Naeini, R., Medzihradszky, K. F., Zhou, S., King, D., et al. (2011). A heteromeric Texas coral snake toxin targets acid-sensing ion channels to produce pain. *Nature* 479, 410–414. doi: 10.1038/nature10607

Boscardin, E., Alijevic, O., Hummler, E., Frateschi, S., and Kellenberger, S. (2016). The function and regulation of acid-sensing ion channels (ASICs) and the epithelial Na(+) channel (ENaC): IUPHAR Review 19. *Br. J. Pharmacol.* 173, 2671–2701. doi: 10.1111/bph.13533

Casey, J. R., Grinstein, S., and Orlowski, J. (2010). Sensors and regulators of intracellular pH. *Nat. Rev. Mol. Cell Biol.* 11, 50–61. doi: 10.1038/nrm2820

Castaneda-Corral, G., Rocha-Gonzalez, H. I., Godinez-Chaparro, B., Jimenez-Andrade, J. M., and Granados-Soto, V. (2011). Role of the spinal Na+/H+ exchanger in formalin-induced nociception. *Neurosci. Lett.* 501, 4–9. doi: 10.1016/j.neulet.2011.06.048

Caterina, M. J., Schumacher, M. A., Tominaga, M., Rosen, T. A., Levine, J. D., and Julius, D. (1997). The capsaicin receptor: a heat-activated ion channel in the pain pathway. *Nature* 389, 816–824. doi: 10.1038/39807

Chen, X., Qiu, L., Li, M., Durrnagel, S., Orser, B. A., Xiong, Z. G., et al. (2010). Diarylamidines: high potency inhibitors of acid-sensing ion channels. *Neuropharmacology* 58, 1045–1053. doi: 10.1016/j.neuropharm.2010.01.011

Diochot, S., Baron, A., Salinas, M., Douguet, D., Scarzello, S., Dabert-Gay, A. S., et al. (2012). Black mamba venom peptides target acid-sensing ion channels to abolish pain. *Nature* 490, 552–555. doi: 10.1038/nature11494

Dymowska, A. K., Schultz, A. G., Blair, S. D., Chamot, D., and Goss, G. G. (2014). Acid-sensing ion channels are involved in epithelial Na+ uptake in the rainbow trout Oncorhynchus mykiss. *Am. J. Physiol. Cell Physiol.* 307, C255–C265. doi: 10.1152/ajpcell.00398.2013

Engin, K., Leeper, D. B., Cater, J. R., Thistlethwaite, A. J., Tupchong, L., and Mcfarlane, J. D. (1995). Extracellular pH distribution in human tumours. *Int. J. Hyperthermia* 11, 211–216. doi: 10.3109/02656739509022457

Frantz, S. (2005). Drug discovery: playing dirty. *Nature* 437, 942–943. doi: 10.1038/437942a

Guenther, S., Reeh, P. W., and Kress, M. (1999). Rises in [Ca2+]i mediate capsaicin- and proton-induced heat sensitization of rat primary nociceptive neurons. *Eur. J. Neurosci.* 11, 3143–3150. doi: 10.1046/j.1460-9568.1999.00734.x

Jones, N. G., Slater, R., Cadiou, H., Mcnaughton, P., and Mcmahon, S. B. (2004). Acid-induced pain and its modulation in humans. *J. Neurosci.* 24, 10974–10979. doi: 10.1523/JNEUROSCI.2619-04.2004

Kellenberger, S., and Schild, L. (2002). Epithelial sodium channel/degenerin family of ion channels: a variety of functions for a shared structure. *Physiol. Rev.* 82, 735–767. doi: 10.1152/physrev.00007.2002

Kleyman, T. R., and Cragoe, E. J. Jr. (1988). Amiloride and its analogs as tools in the study of ion transport. *J Membr Biol* 105, 1–21. doi: 10.1007/BF01871102

Krishtal, O. (2003). The ASICs: signaling molecules? Modulators? *Trends Neurosci.* 26, 477–483. doi: 10.1016/S0166-2236(03)00210-8

Lee, C. H., and Chen, C. C. (2018). Roles of ASICs in Nociception and Proprioception. *Adv. Exp. Med. Biol.* 1099, 37–47. doi: 10.1007/978-981-13-1756-9_4

Lee, J. Y. P., Saez, N. J., Cristofori-Armstrong, B., Anangi, R., King, G. F., Smith, M. T., et al. (2018). Inhibition of acid-sensing ion channels by diminazene and APETx2 evoke partial and highly variable antihyperalgesia in a rat model of inflammatory pain. *Br. J. Pharmacol.* 175, 2204–2218. doi: 10.1111/bph.14089

Leng, T. D., Si, H. F., Li, J., Yang, T., Zhu, M., Wang, B., et al. (2016). Amiloride Analogs as ASIC1a Inhibitors. *CNS Neurosci. Ther.* 22, 468–476. doi: 10.1111/cns.12524

Liu, C. N., and Somps, C. J. (2008). Na+/H+ exchanger-1 inhibitors reduce neuronal excitability and alter na+ channel inactivation properties in rat primary sensory neurons. *Toxicol. Sci.* 103, 346–353. doi: 10.1093/toxsci/kfn045

Maidorn, R. P., Cragoe, E. J. JR., and Tannock, I. F. (1993). Therapeutic potential of analogues of amiloride: inhibition of the regulation of intracellular pH as a possible mechanism of tumour selective therapy. *Br. J. Cancer* 67, 297–303. doi: 10.1038/bjc.1993.56

Maximyuk, O., Khmyz, V., Lindskog, C. J., Vukojevic, V., Ivanova, T., Bazov, I., et al. (2015). Plasma membrane poration by opioid neuropeptides: a possible mechanism of pathological signal transduction. *Cell Death Dis.* 6, e1683. doi: 10.1038/cddis.2015.39

Mickle, A. D., Shepherd, A. J., and Mohapatra, D. P. (2015). Sensory TRP channels: the key transducers of nociception and pain. *Prog. Mol. Biol. Transl. Sci.* 131, 73–118. doi: 10.1016/bs.pmbts.2015.01.002

Pattison, L. A., Callejo, G., and St, J. S. E. (2019). Evolution of acid nociception: ion channels and receptors for detecting acid. *Philos. Trans. R. Soc. Lond. B Biol. Sci.* 374:20190291. doi: 10.1098/rstb.2019.0291

Rajamaki, K., Nordstrom, T., Nurmi, K., Akerman, K. E., Kovanen, P. T., Oorni, K., et al. (2013). Extracellular acidosis is a novel danger signal alerting innate immunity via the NLRP3 inflammasome. *J. Biol. Chem.* 288, 13410–13419. doi: 10.1074/jbc.M112.426254

Riley, J. L. 3rd, Robinson, M. E., Wise, E. A., Myers, C. D., and Fillingim, R. B. (1998). Sex differences in the perception of noxious experimental stimuli: a meta-analysis. *Pain* 74, 181–187. doi: 10.1016/S0304-3959(97)00199-1

Rocha-Gonzalez, H. I., Castaneda-Corral, G., Araiza-Saldana, C. I., Ambriz-Tututi, M., Caram-Salas, N. L., Torres-Lopez, J. E., et al. (2009). Identification of the Na+/H+ exchanger 1 in dorsal root ganglion and spinal cord: its possible role in inflammatory nociception. *Neuroscience* 160, 156–164. doi: 10.1016/j.neuroscience.2009.02.033

Ross, J. L., Queme, L. F., Lamb, J. E., Green, K. J., and Jankowski, M. P. (2018). Sex differences in primary muscle afferent sensitization following ischemia and reperfusion injury. *Biol. Sex Differ.* 9:2. doi: 10.1186/s13293-017-0163-5

Schneider, D., Gerhardt, E., Bock, J., Muller, M. M., Wolburg, H., Lang, F., et al. (2004). Intracellular acidification by inhibition of the Na+/H+-exchanger leads to caspase-independent death of cerebellar granule neurons resembling paraptosis. *Cell Death Differ.* 11, 760–770. doi: 10.1038/sj.cdd.4401377

Simmen, H. P., Battaglia, H., Giovanoli, P., and Blaser, J. (1994). Analysis of pH, pO2 and pCO2 in drainage fluid allows for rapid detection of infectious complications during the follow-up period after abdominal surgery. *Infection* 22, 386–389. doi: 10.1007/BF01715494

Slepkov, E. R., Rainey, J. K., Sykes, B. D., and Fliegel, L. (2007). Structural and functional analysis of the Na+/H+ exchanger. *Biochem. J.* 401, 623–633. doi: 10.1042/BJ20061062

Steen, K. H., Reeh, P. W., Anton, F., and Handwerker, H. O. (1992). Protons selectively induce lasting excitation and sensitization to mechanical stimulation of nociceptors in rat skin, in vitro. *J. Neurosci.* 12, 86–95. doi: 10.1523/JNEUROSCI.12-01-00086.1992

Steen, K. H., Steen, A. E., and Reeh, P. W. (1995). A dominant role of acid pH in inflammatory excitation and sensitization of nociceptors in rat skin, in vitro. *J. Neurosci.* 15, 3982–3989. doi: 10.1523/JNEUROSCI.15-05-03982.1995

Steen, K. H., Wegner, H., and Reeh, P. W. (1999). The pH response of rat cutaneous nociceptors correlates with extracellular [Na+] and is increased under amiloride. *Eur. J. Neurosci.* 11, 2783–2792. doi: 10.1046/j.1460-9568.1999.00695.x

Tkachenko, Y., Khmyz, V., Isaev, D., Maximyuk, O., and Krishtal, O. (2023). Temperature increase significantly enhances nociceptive responses of C-fibers to ATP, high K(+), and acidic pH in mice. *Front. Cell Neurosci.* 17:1131643. doi: 10.3389/fncel.2023.1131643

Tominaga, M., Caterina, M. J., Malmberg, A. B., Rosen, T. A., Gilbert, H., Skinner, K., et al. (1998). The cloned capsaicin receptor integrates multiple pain-producing stimuli. *Neuron* 21, 531–543. doi: 10.1016/S0896-6273(00)80564-4

Torres-Lopez, J. E., Guzman-Priego, C. G., Rocha-Gonzalez, H. I., and Granados-Soto, V. (2013). Role of NHE1 in Nociception. *Pain Res. Treat.* 2013:217864. doi: 10.1155/2013/217864

Ugawa, S., Ueda, T., Ishida, Y., Nishigaki, M., Shibata, Y., and Shimada, S. (2002). Amiloride-blockable acid-sensing ion channels are leading acid sensors expressed in human nociceptors. *J. Clin. Invest.* 110, 1185–1190. doi: 10.1172/JCI0215709

Ugawa, S., Ueda, T., Yamamura, H., and Shimada, S. (2005). In situ hybridization evidence for the coexistence of ASIC and TRPV1 within rat single sensory neurons. *Brain Res. Mol. Brain Res.* 136, 125–133. doi: 10.1016/j.molbrainres.2005.01.010

Werth, J. L., and Thayer, S. A. (1994). Mitochondria buffer physiological calcium loads in cultured rat dorsal root ganglion neurons. *J. Neurosci.* 14, 348–356. doi: 10.1523/JNEUROSCI.14-01-00348.1994

Whitten, S. T., Garcia-Moreno, E. B., and Hilser, V. J. (2005). Local conformational fluctuations can modulate the coupling between proton binding and global structural transitions in proteins. *Proc. Natl. Acad. Sci. U. S. A.* 102, 4282–4287. doi: 10.1073/pnas.0407499102

Yu, Y., Chen, Z., Li, W. G., Cao, H., Feng, E. G., Yu, F., et al. (2010). A nonproton ligand sensor in the acid-sensing ion channel. *Neuron* 68, 61–72. doi: 10.1016/j.neuron.2010.09.001

Zeilhofer, H. U., Kress, M., and Swandulla, D. (1997). Fractional Ca2+ currents through capsaicin- and proton-activated ion channels in rat dorsal root ganglion neurones. *J. Physiol.* 503, 67–78. doi: 10.1111/j.1469-7793.1997.067bi.x

Frontiers in
Cellular Neuroscience

Leading research in cellular mechanisms underlying brain function and development

Part of the world's most cited neuroscience journal series that advances our understanding of the cellular mechanisms underlying cell function in the nervous system across all species.

Discover the latest Research Topics

See more →

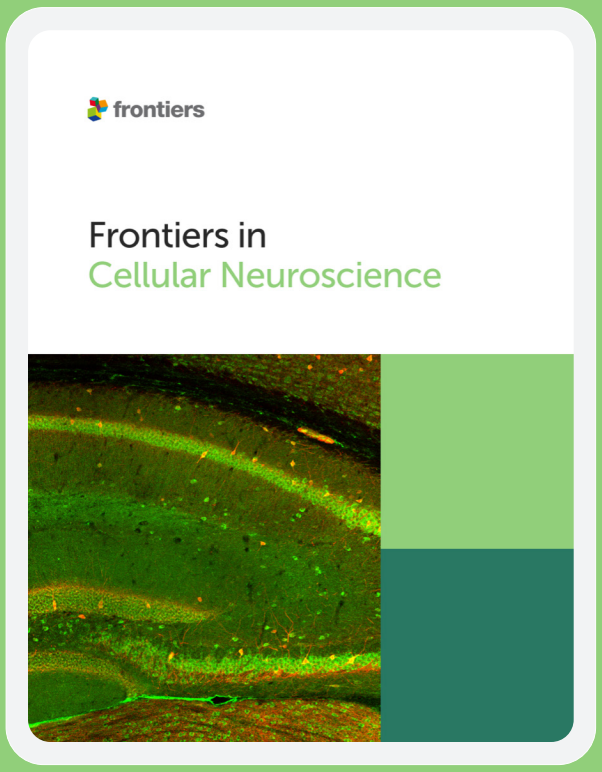

Frontiers

Avenue du Tribunal-Fédéral 34
1005 Lausanne, Switzerland
frontiersin.org

Contact us

+41 (0)21 510 17 00
frontiersin.org/about/contact